Field measurement and numerical modelling of infiltration and matric suctions within slopes.

Ilias Tsaparas

Field Measurements and Numerical Modelling of Infiltration and Matric Suctions within Slopes

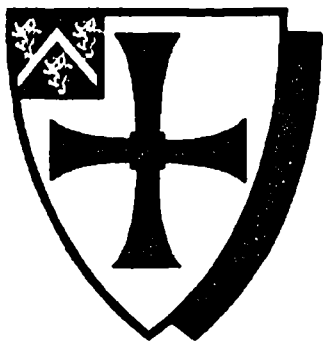

University of Durham

Ilias Tsaparas

Ph.D. Thesis

2002

DECLARATION

I hereby declare that the work in this thesis has not been previously submitted for any degree. All material in this thesis is original except where indicated by reference to other work.

STATEMENT OF COPYRIGHT

Dedicated to my parents

Polykarpos and Alice Tsaparas

in gratitude for their love and support.

Field Measurements and Numerical Modelling of Infiltration and Matric Suctions within Slopes

Ilias Tsaparas

Abstract

This work presents an analysis of the pore-water pressures and seepage conditions within two residual soil slopes in Singapore. The analysis is based on field measurements and on numerical modelling using a finite element software capable of modelling transient unsaturated flow.

The field measurements consist of rainfall data, runoff data of rainfall events and pore-water pressure changes during infiltration at several depths and locations on the two slopes. The field measurements indicated that the infiltration mechanism is complex. Pore-water pressure changes could not be explained purely in terms of the amount or intensity of rainfall. The initial values of the pore-water pressures had a significant effect on the pore-water pressure changes resulted from rainfall.

The objective of the numerical modelling of the field measurements was to couple all the available field information into one complete model that could describe the seepage conditions within a residual soil slope during infiltration. The numerical analysis reflects the complexity of the mechanism of how rain water infiltrates the slope and produces the pore-water pressure changes. The results from the numerical model confirm that infiltration is controlled by the initial conditions within a slope. It was seen that a slope appears to have a limiting capacity for how much rainfall water can penetrate the slope surface to become infiltration. When pore-water pressures near the ground surface are highly negative the permeability with respect to water is low and this restricts infiltration. When the pore-water pressures near the ground surface are highly positive then the hydraulic gradient is low and the water flow potential is also small (even though the permeability to water is higher), leading to low infiltration rates. That means that large amounts of rainfall do not automatically lead to high infiltration.

Acknowledgements

This research was completed under the supervision of Dr. D.G. Toll, Senior Lecturer of the School of Engineering, University of Durham. I am grateful to Dr. D.G. Toll for inviting me initially as an exchange student to Durham from the National Technical University of Athens (NTUA) and afterwards to offer me the opportunity to do my Ph.D. in Durham. I would like to extend my heartfelt thanks to Dr. D.G. Toll for his unlimited interest in my research during the past three years. Without his valuable comments and his continuing support from start to finish, I would not be in this position today.

A significant part of this work was undertaken in Singapore which would not have been possible had I not been given the special opportunity to work at Nanyang Technological University (NTU), under the exchange agreement that exists with the University of Durham. This research was supported by a research grant from the National Science and Technology Board of Singapore (NSTB Grant 17/6/16: Rainfall-Induced Slope Failures). Particular thanks are due to Associate Professor H. Rahardjo, Vice Dean of the School of Civil and Structural Engineering (CSE) of NTU for his valuable help and constant encouragement.

I would also like to acknowledge the important role of Professor P. Marinos of NTUA, who warmly encouraged in pursuing a Ph.D. in Durham. I would also like to thank Professor N. Markatos of NTUA for his support and friendship all these years. Special thanks are also due to Professor D. Davies of the University of Durham, who as a Principal of the College of St. Hild and St. Bede offered me a position as a resident tutor in the College. The contribution of Dr. S.M. White, Lecturer of the University of Durham, and Associate Professor E.C. Leong of NTU are also greatly appreciated. Special thanks are also due to the technicians of the Geotechnics Laboratory and to the countless others in CSE for their assistance and friendship.

Last but by no means least, the moral support of my family and Ms. C. de Souza during the last few years in Durham has been tremendous. I am greatly indebted to my parents for their unfailing support and encouragement.

Table of Contents

List of Figures

List of Tables

CHAPTER 1

Introduction

1.1 Background

Rainfall-induced slope failures are a common geotechnical problem in tropical and subtropical areas. In such areas the climate is warm and humid and soil slope retain unsaturated zones near the ground surface during long dry periods and negative pore-water pressures (suctions) develop. A large number of steep, natural and engineered slopes in tropical and subtropical areas remain stable for a long time and then fail during heavy rainstorms. In many cases these failures cause loss of life and economic losses. Past research studies suggested that conventional methods, based on the assumption of saturated behaviour, for the design and construction of saturated soil slopes cannot be applied successfully for slopes under unsaturated conditions.

In tropical and subtropical areas, the phenomenon of rainfall-induced slope failures is closely related to the properties of the local soils. Due to the warm and humid climatic conditions and the occurrence of intense rainfall in these geographical areas, the parent rock formations decompose by weathering to produce residual soils. Residual soils have properties that vary considerably from one geographical area to another and behave differently to transported soils that are common in temperate regions.

Slope stability analysis of unsaturated residual slopes requires an extensive and detailed seepage analysis, because slope failures in unsaturated conditions are closely related to heavy rainfall. The main parameters that are identified as affecting the seepage characteristics of a slope are the rainfall pattern (i.e. total rainfall and rainfall intensity), the initial conditions within the slope (expressed either as initial pore-water pressure distribution within the slope or as antecedent rainfall) and the hydrological parameters of the slopes. The main hydrological parameters of the slope are the saturated coefficient of permeability of the soil and the soil-water characteristic curve of the soil (i.e. the relationship between suctions and water

content). For a better understanding of the mechanism of how rainfall causes slope failures it is important to identify the way in which all these parameters affect the seepage characteristics of an unsaturated residual slope.

Past experiences in Singapore show that landslides may occur due to long heavy rainfall. For Singapore, a better understanding of the mechanism of rainfall-induced slope failures is needed, in order to produce appropriate guidance for the design of slopes against rainfall.

1.2 Objectives

The main objectives of the present research study are:

- a field study of pore-water pressure changes at various depths within residual soil slopes.

- the numerical investigation of the effect of various parameters on the stability of a residual slope during infiltration

- the numerical modelling of the seepage characteristics of a slope, based on available field measurements, to better understand the mechanism of how rainfall water infiltrates an unsaturated slope.

1.3 Methodology

The objectives of the present research study were achieved with field monitoring of two residual soil slopes in Singapore, with laboratory testing of soil samples from the two research slopes and with numerical analysis using a finite element software package.

1.3.1 Field monitoring

Two residual soil slopes in the west part of Singapore were instrumented for the field monitoring. The field instrumentation consisted of tensiometers installed at various locations and depths within the two slopes, measuring pore-water pressure changes

during rainfall and during dry periods to depths of 3.2m. The field instrumentation also included piezometers for observing changes in the ground water table at greater depth and rainfall gauges for recording rainfall. In one of the two slopes a rainfall simulator was built that was able to evenly distribute water on the slope with controlled intensities. With the rainfall simulator it was possible to study the pore-water pressure response during controlled rainfall of constant intensity. On the same slope, a device was also installed for the measurement of runoff produced by natural and simulated rainfall events. The field instrumentations of the two slopes were linked to data acquisition systems for the automatic collection and storage of the measurements.

1.3.2 Laboratory testing

The laboratory testing included the production of several soil-water characteristic curves of soil samples from the two research slopes. The hysterisis of the soil-water characteristic curves between the wetting and drying phase was also identified.

1.3.3 Numerical analysis

The numerical analysis consisted of a parametric study and the numerical modelling of the field measurements. For the numerical analysis the finite element software Seep/W was used, which is capable of modelling unsaturated transient flow in two dimensions. For both parts of the numerical analysis, attention was given in building a finite element mesh that would overcome possible numerical instabilities.

The objective of the parametric study was to identify the effect of several hydrological parameters on the seepage conditions of a typical residual soil slope in Singapore. The soil properties adopted in the parametric study were obtained from laboratory testing of samples on one of the two research slopes. The variables of the parametric study were the antecedent rainfall, the distribution of a rainfall, the initial conditions of the slope and the saturated coefficient of permeability of the soil with respect to water. The parametric study also included a slope stability analysis. The slope stability analysis was conducted using Slope/W.

The numerical analysis also included the modelling of the field measurements of one of the two research slopes. In this part of the numerical analysis it was attempted to incorporate all the available information from the field and the laboratory into one complete numerical model. The results of the numerical model were used to describe the infiltration mechanism of the slope, and provide useful information on the effect of rainfall on the pore-water pressure changes.

1.4 Overview of the thesis

Chapter 1 presents the general background of rainfall-induced slope failures. Chapter 1 also presents the objectives and the methodology of the study, as well as an overview of the thesis.

Chapter 2 presents the theoretical background that is related to seepage analysis and stability analysis of unsaturated soil slopes. Chapter 2 also presents recent research studies on rainfall-induced slope failures.

Chapter 3 presents a description of the two research sites. Chapter 3 also includes a detailed description of all the instruments and equipment used for the field monitoring and laboratory testing. The calibration of the instruments and the field testing procedures are also included in Chapter 3.

The presentation of all the field measurements and lab testing can be found in Chapter 4. In Chapter 4, the results are presented separately for the two research slopes. Chapter 5 provides the discussion and analysis on the field measurements. The discussion and analysis of the field measurements is made separately for each research slope. In addition, the last section of Chapter 5 is dedicated on the comparison between the findings from the field measurements of the two slopes.

Chapter 6 presents the results of the parametric study. Chapter 7 presents the results and discussion of the numerical modelling of the field measurements.

Finally, Chapter 8 presents the final conclusions of the present research work and some recommendations for future research works on rainfall-induced slope failures.

CHAPTER 2

Literature Review

This chapter presents the basic terms and definitions, which are related to unsaturated soil mechanics. The main concepts of seepage analysis and stability analysis of unsaturated soil slopes is also presented. Finally, this chapter also presents recent research works in the field of rainfall-induced slope failures.

2.1 Phases of unsaturated soils

A soil is generally a system of three phases: the solid phase (i.e. the soil particles of different minerals), the water phase and the air phase. The water and the air phase are also called the fluid phase. The water and the air are filling the spaces between the soil particles, which are defined as pores of the soil. A soil mass is considered saturated when the pores are filled completely with water, and therefore a saturated soil is considered as a two phase system (solids and water). A soil mass is considered unsaturated (or partially saturated) when water and air coexist within the pores. For unsaturated soils, Fredlund and Morgenstern (1977), introduced a fourth phase in order to describe the stress state of a soil element. The fourth phase of an unsaturated soil is called the contractile skin, which exists at the air-water interface.

In the following sections it will be seen that the existence of air and water in the unsaturated soil mass, has a great impact on the behaviour of the unsaturated soil, as it affects its shear strength, and the permeability of the soil with respect to water.

2.2 Shear strength equation of unsaturated soils

All frameworks that describe unsaturated soil behaviour, use stress state variables, which are based on combinations of the total stress σ, the pore-air pressure u_a and the pore-water pressure u_w. The combination of stress state variables $(\sigma-u_a)$ and (u_a-u_w) is generally recognised as the most useful (Fredlund et al. 1978) for two reasons. The first reason is that when the pore-water pressure changes, then only one of the two variables is affected. The second reason is that in the field the pore-air pressure

becomes atmospheric and then (σ-u_a) is equal to the total stress (σ) and u_a-u_w is equal to the negative pore-water pressure (-u_w). The variable (σ-u_a) is called net stress and the variable (u_a-u_w) is called matrix- or matric-suction (Fredlund and Morgenstern, 1977).

Bishop (1959) first developed a framework to describe unsaturated soil behaviour using an effective stress concept. The constitutive Equation 2.1 presents the relationship between the effective normal stress with the net stress state variable and the matric suction.

$$\sigma' = (\sigma - u_a) + \chi(u_a - u_w) \tag{2.1}$$

where, σ'= effective normal stress,

σ= total stress,

u_a= pore-air pressure,

u_w= pore-water pressure,

u_a-u_w= negative pore pressure or matric suction,

and χ=a factor, which is related to the degree of saturation of the soil.

Fredlund et al. (1978) suggested that due to difficulties in combing stress states into a single 'effective stress' it was better to deal with two stress states independently. They introduced a constitutive equation to describe the relationship between the shear strength and the stress state variables (σ-u_a) and (u_a-u_w). Equation 2.2 presents the constitutive equation, proposed by Fredlund et al. (1978), which is based on independence of the stress state variables.

$$\tau = c' + (\sigma - u_a)\tan\varphi' + (u_a - u_w)\tan\varphi^b \tag{2.2}$$

where, τ= shear strength,

c'= effective cohesion of the soil,

σ= total stress,

u_a= pore-air pressure,

u_w= pore-water pressure,

φ'= the angle of internal friction with respect to changes of $(\sigma-u_a)$ when (u_a-u_w) is held constant,

and φ^b= the angle of internal friction with respect to changes of (u_a-u_w) when $(\sigma-u_a)$ is kept constant.

In Equation 2.2, φ' is taken to be constant for any changes of the pore pressures and is assumed to be equal to the angle of internal friction at saturation. Fredlund et al. (1978) initially assumed that the φ^b component was also constant with pore pressure changes. The two assumptions, that $\varphi'$and φ^b angles remain constant with pore pressure changes, meant that Equation 2.2 gave a linear relationship between the shear strength τ and the pore pressures (u_a-u_w). Later works by Escario and Saez (1986) and Gan et al. (1988) proved that the φ^b value changes in a non-linear manner for different matric suction values. From the shear strength results with a direct shear apparatus, which Gan et al. (1988) presented, it was seen that φ^b angle was close to the φ' angle when the soil is saturated. As pore pressures start to decrease and becoming negative (i.e. matric suction increases) then φ^b starts to decrease towards a constant value.

Equation 2.2 can also determine the shear strength of a saturated soil, as a special case where the matric suction is zero (u_a-u_w=0). That means that for a near saturated soil, the pore-air pressure comes in equilibrium with the pore-water pressure (u_a=u_w). Therefore, for a saturated soil Equation 2.2 becomes:

$$\tau = c'+(\sigma - u_w)\tan\varphi' \qquad (2.3)$$

Equation 2.3 is the Mohr-Coulomb failure criterion for saturated soils. The failure criterion for unsaturated soils, expressed in Equation 2.2, is also referred to as the extended Mohr-Coulomb failure criterion for unsaturated soils (Fredlund and Rahardjo, 1993), because it can describe the behaviour of a saturated soil as a

special case. The graphical presentation of the extended Mohr-Coulomb failure criterion for unsaturated soils, is shown in Figure 2.1. In the three-dimensional graph of Figure 2.1, the Mohr circles defined by the shear stress (τ) axis and the effective normal stress (σ-u_a) are extended to the third axis of matric suction (u_a-u_w). The failure envelope, which defines the shear strength of the unsaturated soil, is the surface tangent to the Mohr circles.

The Mohr-Coulomb failure criterion of Equation 2.3, including the extended failure envelope for unsaturated soils (Equation 2.2) only represents the stress state at failure. The approach of Fredlund et al. (1978) cannot be used to model behaviour prior to failure. Although Bishop's (1959) approach, based on an effective stress concept, could be used for pre-failure stress states, it has been shown that the χ factor used in the effective stress equation (Equation 2.1) is different whether one is considering shear behaviour or volume change (Jennings and Burland, 1962). Khallili and Khabbaz (1998) do suggest that such an approach can be used if χ is defined in terms of matric suction rather than degree of saturation. However, this is still subject to discussion with the research community.

More complete representations of unsaturated soil behaviour have been put forward by Toll (1990), Alonso et al. (1990), Wheeler and Sivakumar (1995) by using generalized stress states:

$$p = \frac{\sigma_1 + \sigma_2 + \sigma_3}{3} \tag{2.4}$$

$$q = \sigma_1 - \sigma_3 \tag{2.5}$$

However, for the purposes of this thesis (slope stability analysis) the extended Mohr-Coulomb failure criterion, given in Equation 2.2, is sufficient to represent the shear strength that can be mobilized on a defined failure surface.

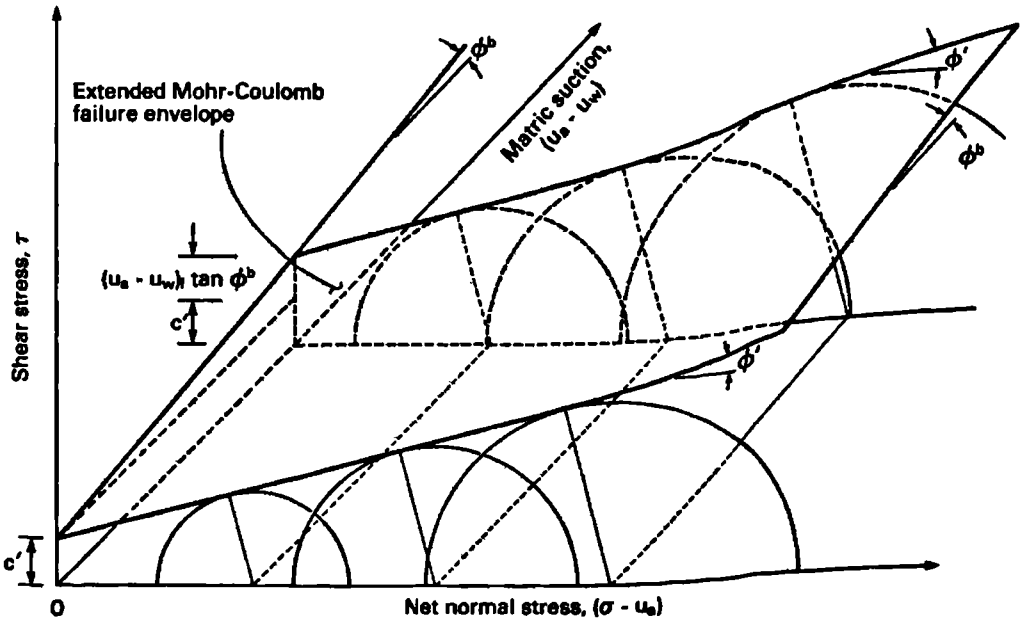

Figure 2.1 Extended Mohr-Coulomb failure envelope for unsaturated soils (from Fredlund and Rahardjo 1993).

2.3 Physics of groundwater flow

2.3.1 Groundwater potential

Groundwater flows in response to differences in pressure and elevation between two points. Hubert (1940) defines the groundwater potential at a given point as the required energy to transport a mass of water from one point to another. Groundwater will flow from a high potential to a lower potential. For water flow it is more convenient to express the potential in terms of head (i.e. energy per unit of mass). The groundwater potential is divided into the potential energy per unit mass of water (or elevation head), the pressure energy per unit mass of water (or pressure head) and the kinetic energy per unit mass of water (or velocity head). The total groundwater potential or the total head (h) at a point can be expressed as follows:

$$h = h_e + h_w + h_v \tag{2.6}$$

where, h is the total head, h_e is the elevation head, h_w is the pressure head and h_v is the velocity head.

The elevation head h_e is equal to the elevation (y) and the pressure head h_w and the velocity head h_v are expressed as follows:

$$h_w = \frac{u_w}{\rho_w g} \tag{2.7}$$

$$h_v = \frac{v^2}{2g} \tag{2.8}$$

where, u_w is the pore-water pressure,

ρ_w is the density of water,

g is the acceleration of gravity,

and v is the flow velocity

In general, groundwater flows with very small velocities, and therefore the velocity head of Equation 2.6 can safely be omitted. Incorporating Equations 2.7 and 2.8 into Equation 2.6, the total head at a point can be expressed as follows:

$$h = y + \frac{u_w}{\rho_w g} \tag{2.9}$$

2.3.2 Flow law through a porous media

During the 19th century Darcy found experimentally the factors that control groundwater flow through a sand. By a series of experiments Darcy concluded, that for a given type of sand, the volume discharge rate Q is directly proportional to the head drop h_2-h_1 and to the cross-sectional area A, but it is inversely proportional to the length difference L_2-L_1. Darcy's law for groundwater flow between two points, through a given porous media is expressed in Equation 2.10.

$$Q = -k \cdot A \frac{h_2 - h_1}{L_2 - L_1} \tag{2.10}$$

where, Q is the volume rate of flow,

k is the hydraulic conductivity or permeability of the porous media with respect to water,

A is the cross-sectional area, through which groundwater flow takes place,

h_2-h_1 is the drop of head between two points,

and L_2-L_1, is the distance between the two points.

The negative sign in Equation 2.10 indicates that groundwater flows from a high to a low head. Darcy's law (Equation 2.10) is only valid for laminar flow (i.e. no turbulence takes place). However, because groundwater flow through a soil occurs almost always with very small velocities, it can be assumed that Darcy's law can be applied in the majority of the studies of groundwater flow. As the drop of head (h_2-h_1) occurs to a smaller and smaller length (L_2-L_1), then Equation 2.10 can be written in a differential form as follows:

$$Q = -k \cdot A \frac{dh}{dL} \tag{2.11}$$

where dh/dL is the rate of change of head with position and is called as the hydraulic gradient (i):

$$i = \frac{dh}{dL} \tag{2.12}$$

Finally, if we call q the specific discharge (also called as the Darcy velocity), defined as the volume rate of flow per unit area, then:

$$q = \frac{Q}{A} \tag{2.13}$$

Incorporating Equations 2.12 and 2.13 into the Equation 2.11, then Darcy's law gets its final form:

$$q = -k \cdot i \tag{2.14}$$

In order for Darcy's law, as expressed in Equation 2.14, to be generalised for two

dimensional flow, Equation 2.14 must be valid for both x- and y- components of the flow:

$$q_x = -k_x \cdot i_x \quad q_y = -k_y \cdot i_y \tag{2.15}$$

where, q_x and q_y are the specific discharges along the x- and y- coordinate system, respectively

k_x and k_y are the permeability of the porous media with respect to water along the x- and y- coordinate system, respectively,

and i_x and i_y are the hydraulic gradients along the x- and y- coordinate system, respectively.

2.4 Soil-water characteristic curve and permeability function with respect to water of unsaturated soil

The soil-water characteristic curve (swcc) is the graphical relationship between the water content of the soil and the matric suction. Figure 2.2 presents an example of a soil-water characteristic curve of a sandy sample. From Figure 2.2 can be seen that the volumetric water content (θ_w) of the soil is dependent on the matric suction in a non-linear and sigmoid fashion. Figure 2.2 also shows that the soil-water characteristic curve is not unique for the drying and wetting phase, but hysteresis is shown between the drying and the wetting phases. From the soil-water characteristic curve a few parameters can be defined:

- the saturated volumetric water content (θ_{sat}), which is the volumetric water content at saturation

- the air-entry value (a), which is the minimum value of matric suction above which the volumetric water content starts to decrease

- and the residual volumetric water content (θ_r), which is defined as the maximum volume of water in the soil that will not contribute in water flow,

because of blockage from the flow channels (Luckner et al. 1989).

There is a number of equations available in the literature that can be used to describe a soil-water characteristic curve (van Genuchten et al. 1991, Fredlund and Xing 1994 and Leong and Rahardjo 1997a). Leong and Rahardjo (1997a) suggest that the most of these equations can be derived from the following general expression:

$$a_1\Theta^{b_1} + a_2 \exp(a_3\Theta^{b_1}) = a_4\psi^{b_2} + a_5 \exp(a_6\psi^{b_2}) + a_7 \tag{2.16}$$

where, a_1, a_2, a_3, a_4, a_5, a_6, a_7, b_1 and b_2 are constants

ψ is the matric suction

and Θ is the normalized volumetric water content (Equation 2.17):

$$\Theta = \frac{\theta_w - \theta_r}{\theta_{sat} - \theta_r} \tag{2.17}$$

where, (θ_w) is the volumetric water content.

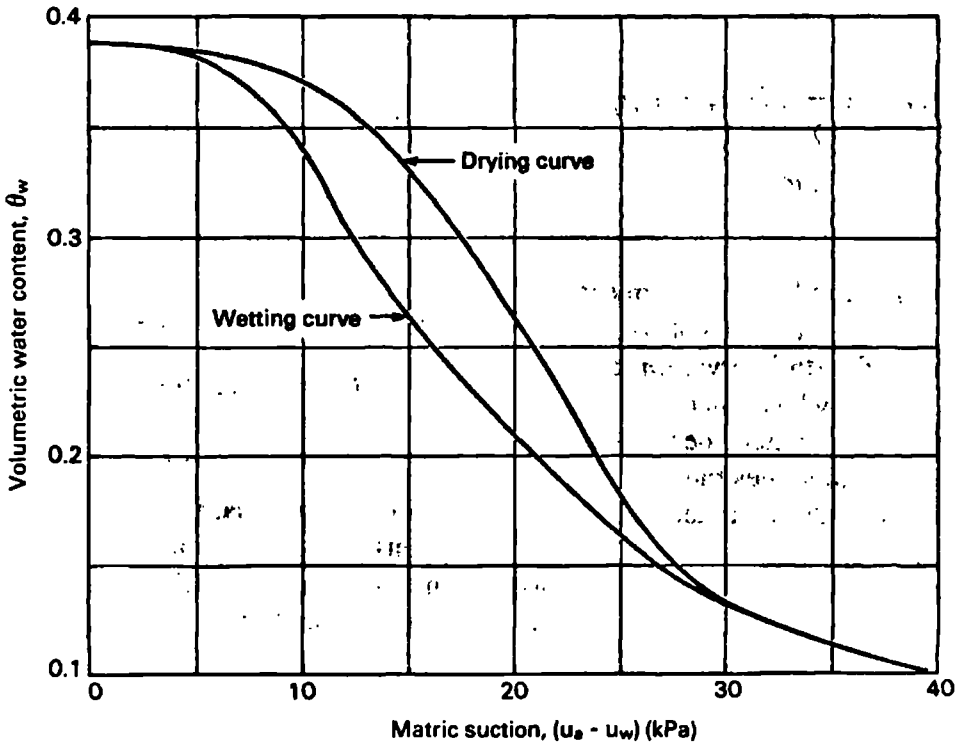

Figure 2.2 Example of a soil water-characteristic curve (from Fredlund and Rahardjo 1993).

Two well-known versions of the equations that describe the soil-water characteristic curve of a soil, are given by Brooks and Corey (1964) and van Genuchten (1980). Brooks and Corey (1964) suggested the following formula for soil-water characteristic curves:

$$\theta = \begin{cases} \theta_r + (\theta_{sat} - \theta_r) \cdot (a \cdot \psi)^{-\lambda} & if\ a \cdot \psi > 1 \\ \theta_{sat} & if\ a \cdot \psi \leq 1 \end{cases} \tag{2.18}$$

where, λ is a parameter related to the pore-size distribution of the soil and affects the inclination of the soil-water characteristic curve.

The van Genuchten (1980) expression for the soil-water characteristic curve is shown in Equation 2.19.

$$\Theta = \frac{1}{\left[1 + (a \cdot \psi)^n\right]^m} \tag{2.19}$$

where, a, n and m are empirical parameters.

The mathematical expressions of Equations 2.18 and 2.19 are relatively simple. However, the Brook and Corey (1964) equation is not a continuous function, but has a break at the air-entry value (a) in soil-water characteristic curves of finely graded soils. Therefore using the Equation 2.18 the predicted soil-water characteristic does not have a sigmoid shape (Leong and Rahardjo 1997a). On the other hand, van Genuchten (1980) incorporates the air-entry value in his model and therefore the sigmoid shape of the soil-water characteristic of finely graded soils is preserved.

The permeability of a soil with respect to water (hydraulic conductivity) is the capability of the soil to transfer volumes of water through its pores. Groundwater does not flow through the soil mass in a straight line, but through the interconnected pores of the soil mass. That means that groundwater flow is taking place through non-linear channels, created by the pores of the soil. For a saturated soil, where the pores of the soil are filled with water, the interconnected pores create continuous channels that allow groundwater to flow. For an unsaturated soil, where the pores are partially filled with water and partially with air, the permeability of the soil with

respect to water is reduced. This is because the air-filled pores are non-conductive channels to the groundwater flow. Therefore, it is expected that the permeability of a soil with respect to water is highly affected by the porosity of the soil (i.e. the percentage of the total volume of the soil that is occupied by pores) and the degree of saturation or the volumetric water content of the soil.

The permeability function with respect to water of a soil is the relationship between the coefficient of permeability with the water content or the matric suction. Under unsaturated conditions, the coefficient of permeability with respect to water of a soil is a non-linear function of the volumetric water content of the soil. Only when the soil approaches saturation does the permeability with respect to water become constant and equal to the saturated coefficient of permeability.

The available methods for the direct measurement of the permeability function with respect to water in the laboratory or in the field are costly, time consuming and their application face great difficulties, which may affect the accuracy of the results (van Genuchten et al. 1991 and Leong and Rahardjo 1997b). As an alternative to the direct measurement of the coefficient of permeability with respect to water there is a large number of theoretical models that predict the relationships between the coefficient of permeability with respect to water with the degree of saturation, the volumetric content or the matric suction (Mualem 1986, Leong and Rahardjo 1997b and Huang et al. 1998). These theoretical models are indirect methods but they give a fast and reasonably accurate prediction of the permeability function with respect to water of a soil. These indirect methods to estimate the permeability function with respect to water of a soil, are based on the soil-water characteristic curve.

The indirect methods for estimating the permeability function with respect to water are categorised as empirical or semi-empirical, macroscopic and statistical models (Leong and Rahardjo 1997b). Empirical and semi-empirical models are developed from fitting curves to direct measurements of the coefficient of permeability with respect to water with the volumetric water content (e.g. Gardner 1958, Campbell 1974, Dane and Klute 1977, Hillel 1982) or the matric suction (e.g. Richards 1931, Gardner 1958, Barden 1965 Philip 1986).

The macroscopic models of permeability functions with respect to water are based on the assumption that water flows through cylindrical pores and incorporate Darcy's law (Equation 2.14). An example of a macroscopic model is Brooks and Corey (1964), with the following expression:

$$k_r = \frac{k(\psi)}{k_{sat}} \tag{2.20}$$

where, k_r is the coefficient of relative permeability with respect to water,

$k(\psi)$ is the permeability function with respect to water,

ψ is the matric suction

and k_{sat} is the coefficient of permeability with respect to water at saturation

The relative coefficient of relative permeability with respect to water (k_r) is a function of the effective degree of saturation (S_e) as follows:

$$k_r = S_e^2 \frac{\int_0^S \frac{1}{\psi^2} dS}{\int_0^1 \frac{1}{\psi^2} dS} \tag{2.21}$$

where the effective degree of saturation (S_e) is expressed as follows (Corey 1954):

$$S_e = \frac{S - S_r}{1 - S_r} \tag{2.22}$$

where S_r is the residual degree of saturation.

The statistical models for the indirect prediction of the permeability function with respect to water are considered more sophisticated models than the empirical or semi-empirical and macroscopic models (Huang et al. 1998 and Leong and Rahardjo 1997b). The statistical models are based on the assumption that the water flow through a porous media is simulated as a set of interconnected, randomly distributed pores with a frequency function $f(r)$ and that the soil-water characteristic curve

represents the pore-size distribution function based on the capillary model (Mualem 1986). The statistical models also assume that the Hagen-Poiseuille equation, which is shown in Equation 2.23, is valid at the level of a singular pore (Mualem 1986).

$$v_{av} = -\left(\frac{r^2 \cdot g}{C \cdot v}\right) \cdot i \tag{2.23}$$

where, v_{av} is the average flow velocity,

i is the hydraulic gradient,

r is the hydraulic radius,

v is the kinematic coefficient of viscosity,

C is the shape constant of the flow system,

and g is the gravitational acceleration.

Green and Corey (1971) proposed the following statistical approach for the prediction of the permeability function with respect to water of a soil:

$$k_w(\theta)_i = \frac{k_{sat}}{k_{satc}} \frac{T_s^2 \rho_w g}{2\mu_w} \frac{\theta_{sat}^p}{N^2} \sum_{j=1}^{m} \left\{(2j+1-2i)(u_a - u_w)_j^{-2}\right\} \tag{2.24}$$

where, $k_w(\theta)_i$ is the calculated coefficient of permeability with respect to water (m/s) for a specified volumetric water content $(\theta)_i$, that corresponds to the i^{th} interval,

m is the total number of intervals between the saturated volumetric water content (θ_{sat}) and the lowest volumetric water content of the soil-water characteristic curve (θ_{lowest}).

i is the interval number, which increases with the decreasing volumetric water content (i.e. for the saturated volumetric water content: (θ_{sat}) i=1 and for the lowest volumetric water content of the soil-water characteristic curve (θ_{lowest}):

i=m,

j is a counter, which ranges from i to m,

k_{sat} is the measured saturated coefficient of permeability with respect to water (m/s),

k_{satc} is the calculated saturated coefficient of permeability with respect to water (m/s),

T_s is the surface tension of water (kN/m),

ρ_w is the water density (kg/m^3),

g is the gravitational acceleration (m/s^2),

μ_w is the absolute viscosity of water (N s/m^2),

θ_{sat} is the volumetric water content at saturation,

and p is a constant which accounts for the interaction of pores of various sizes.

For the constant (p) of Equation 2.24 the following estimations are proposed:

- p=2.0 by Marshall (1958)
- p=1.3 by Millington and Quirk (1961)
- p=1.0 by Kunze et al. (1968).

2.5 Governing equations for seepage through unsaturated soil

Groundwater flow can be either steady state or transient. In steady-state conditions there is no change in the hydraulic head at any point with time. In transient flow the hydraulic head changes as a function of time. The governing equation for flow in either case combines Darcy's law (Equation 2.14) and the continuity equation. In

general, the continuity or conservation equation requires that no loss of water that flows into an element of soil may occur. Due to the different characteristics of flow between steady-state and transient flow, the continuity equation is expressed differently.

2.5.1 Steady-state flow

For steady state conditions, where no hydraulic head changes with time occur, the continuity equation requires that the amount of water that flows into an elemental volume of soil is equal to the amount of water that is flowing out. For two dimensional steady-state conditions the continuity equation is expressed as follows:

$$\frac{\partial q_x}{\partial x} + \frac{\partial q_y}{\partial y} = 0 \tag{2.25}$$

where, q_x and q_y are the specific discharge rate along the x- and y- coordinates.

The continuity equation, expressed in Equation 2.25, is based on two simplifying assumptions. The first assumption is that water is incompressible. If water was compressible, then it could be compressed and stored in the elemental volume of the soil. This assumption is important as the mass of a fluid is always conserved, while its volume is conserved only when the fluid is incompressible. The second assumption is that there are no additions or withdrawals of water in the whole soil domain.

Combining Darcy's law (Equation 2.15) and the continuity equation (Equation 2.25), with the help of Equation 2.12, gives the derivation of Laplace's equation:

$$\frac{\partial}{\partial x}\left(-k_x \frac{\partial h}{\partial x}\right) + \frac{\partial}{\partial y}\left(-k_y \frac{\partial h}{\partial y}\right) = 0 \tag{2.26}$$

where h is the hydraulic head,

and k_x, k_y are the coefficients of permeability of the soil with respect to water along the x and y coordinate accordingly.

Equation 2.26 is the governing equation of the two-dimensional flow under steady-state conditions through anisotropic and heterogeneous soil, where no amount of water is added or removed from the domain. If additions or withdrawals of water in the soil domain, such as precipitation or evaporation, respectively, are considered to occur, then Laplace's equation (Equation 2.26) is no longer the governing equation. Since the left-hand side of Equation 2.28 represents the net changes of volume rate of flow per unit area, then if q is the volume rate of flow of water added in the domain or removed from the domain per unit area then:

$$\frac{\partial q_x}{\partial x}+\frac{\partial q_y}{\partial y}=q \tag{2.27}$$

Substituting Darcy's law into Equation 2.27, then Equation 2.27 becomes:

$$\frac{\partial}{\partial x}\left(-k_x\frac{\partial h}{\partial x}\right)+\frac{\partial}{\partial y}\left(-k_y\frac{\partial h}{\partial y}\right)=q \tag{2.28}$$

Equation 2.28 is called Poisson's equation and is the governing equation for two-dimensional, steady-state flow within a domain composed of heterogeneous and anisotropic soil.

2.5.2 Transient flow

For the case of transient flow where the hydraulic head is no longer independent of time (i.e. the volumetric water content is changing with time) the continuity equation is not satisfied unless the change with time of the volumetric water content at a point is included. Therefore, Equation 2.28 has to be adapted for unsteady-state flow and takes the following form (Equation. 2.29) known as Richard's equation:

$$\frac{\partial}{\partial x}\left(k_x\frac{\partial h}{\partial x}\right)+\frac{\partial}{\partial y}\left(k_y\frac{\partial h}{\partial y}\right)+q=\frac{\partial \theta_w}{\partial t} \tag{2.29}$$

where θ_w is the volumetric water content.

The right hand side of Equation 2.29 can be written as:

$$\frac{\partial \theta_w}{\partial t} = m_w^2 \frac{\partial u_w}{\partial t} = m_w^2 \rho_w g \frac{\partial h}{\partial t} \tag{2.30}$$

where, m_w^2 is the coefficient of volumetric water change with respect to a change in negative pore-water pressure ($-u_w$) and is equal to the slope of the soil-water characteristic curve,

and ρ_w is the density of water and g is gravitational acceleration.

Combining Equations 2.29 and 2.30, the final form of the governing equation of water flow through an unsaturated media is obtained and presented as Equation 2.31.

$$\frac{\partial}{\partial x}\left(k_x \frac{\partial h}{\partial x}\right) + \frac{\partial}{\partial y}\left(k_y \frac{\partial h}{\partial y}\right) + q = m_w^2 \rho_w g \frac{\partial h}{\partial t} \tag{2.31}$$

From the above it can be concluded that Equation 2.31 is highly non-linear since the hydraulic head and also the coefficient of permeability with respect to water of the soil are functions of the volumetric water content of the soil. To solve a non-linear equation like Equation 2.31 requires a numerical method like the finite element method. For the numerical solution of Equation 2.31, the soil-water characteristic curve, the permeability function and the boundary flux q are required. Finally the initial condition of the problem (initial hydraulic head at any point of the initial time step) must also be defined.

2.6 Weathering process and residual soils

Weathering is the process during which the composition and structure of rocks is altered. Weathering is divided into chemical weathering and mechanical weathering. Chemical weathering produces chemical changes in the minerals of the rock, while mechanical weathering is associated with the decomposition of the rock material into smaller fragments. Weathering is highly dependent on the climatic conditions (precipitation, temperature and humidity) (Townsend 1985). Townsend (1985) states: 'Rainfall controls the supply of moisture for chemical reactions and the leaching of soluble constituents of the minerals, while temperature influences reaction rates'. Thus in tropical and subtropical areas, with high temperatures, humid

atmosphere and heavy rainfall, weathering is accelerated leading to highly weathered soil materials that extend to great depths.

The mineral composition of the parent rock is a controlling parameter for the resistance of the material against weathering. The weathering plays the major role in altering the fabric of the parent rock for the production of residual soils. Different kinds of rock do not have the same resistance against weathering. Rocks, which contain basic minerals, are less resistant to weathering than those of acid rocks (Townsend 1985). Therefore basic igneous rocks tend to weather more rapidly into soils compared to acid rocks, such as granite.

Little (1969) suggested a description system of soils according to their degree of weathering in a typical soil profile (Figure 2.3). According to this description system the degree of weathering starts from grade I (fresh rock) and finishes at grade VI (residual soil). It is very useful on a localised basis, where the description and classification of soil properties of a particular formation is required. However, Little's (1969) classification system does not provide sufficient information for comparing completely different formations (Wesley 1988). Another limitation identified by Wesley (1988) is that Little (1969) material description by the degree of weathering, assumes a series of zones of similar thickness, although there are often cases where the transition from rock to soil is not gradual, but very abrupt. However, soil description using the degree of weathering as proposed by Little (1969) is very commonly used.

Residual soil is the final product of the in-situ mechanical and chemical weathering of underlying rocks, which has lost its original rock fabric (Wesley 1990). The most important characteristic of residual soils is the decreasing strength because of the destruction of the bonds and the cementation of the material as the weathering processes.

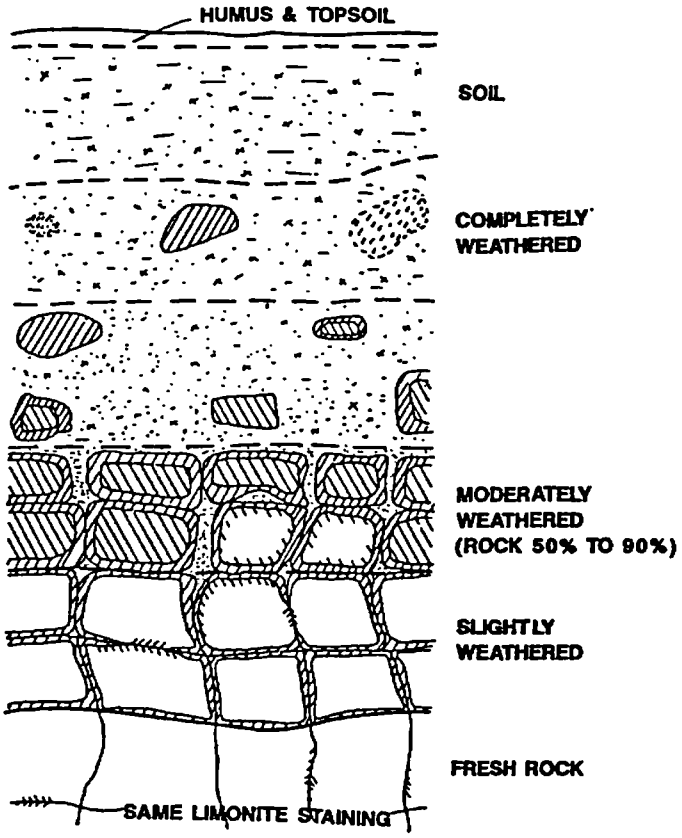

Figure 2.3 Classification of residual soil by degree of weathering (from Little 1969).

The factors that mainly affect the behaviour of a residual soil are the composition and the structure (Wesley 1990). The composition of the material is related to the nature of the soil particles (size, shape, and mineralogical composition) and the structure with the particular state in which these particles exist in the soil (interparticle bonding and cementation). The structure of a residual soil results from the weathering process. In general, the behaviour of residual soils is very complex and residual soils are characterised by their heterogeneity (Lumb 1965, Wesley 1990, Faisal 2000). The characteristics tend to vary at different depths due to the different degree of weathering and predictability is very difficult. Residual soils are usually found unsaturated, in which case they appear to have high shear strength, but as they reach saturation the shear strength reduces significantly with zero or very small effective cohesion (Lumb 1965). Residual soils also tend to have high porosity, in comparison to their parental rock materials and therefore they also appear to be permeable. These characteristics of residual soils cause major problems in the stability of slopes during infiltration especially in tropical areas where severe rainfall

events are common (Lumb 1965, 1975, Brand 1984, Chinniah et al. 1994).

2.7 Geology of Singapore

Four main rock types can be found in Singapore (Public Works Department 1976 and Pitts 1984). Figure 2.4 presents the geological map of Singapore. The main rock types are the Gombak Norite of the Upper Palaeozoic age, the Bukit Timah Granite of the Lower and Middle Triassic age, the Sahajat Formation of the Lower Palaeozoic formation and finally the Jurong Formation of the Upper Triassic, Lower and Middle Jurassic ages.

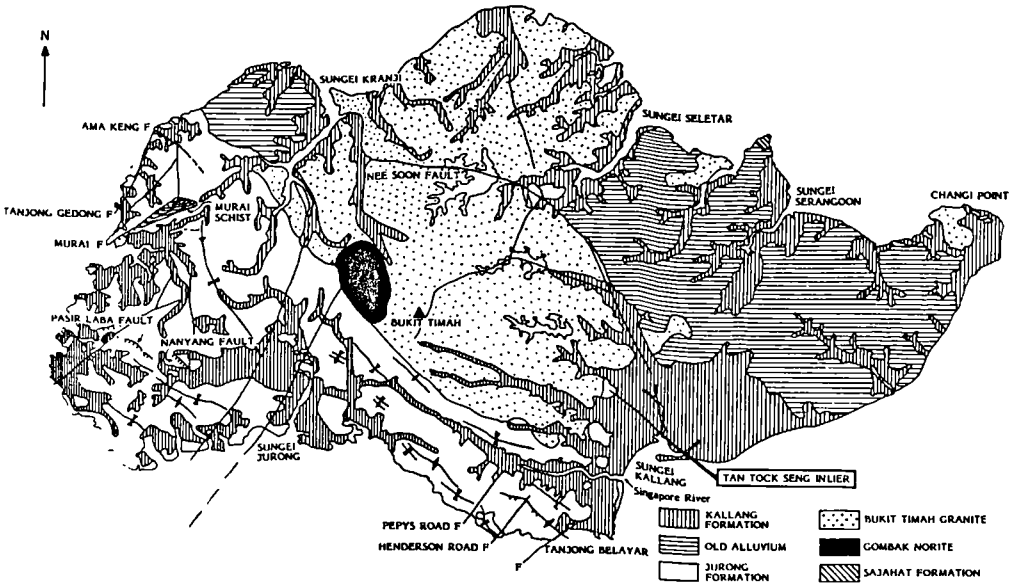

Figure 2.4 Geological map of Singapore (from Pitts 1984).

The Gombak Formation is a series of basic igneous rocks of gabbroic and noritic composition. The Gombak Norite formation exists in a small area at the centre of Singapore and is altered by the intrusion of the Bukit Timah Granite (Pitts 1984). The Bukit Timah Granite is one of the predominant formations in Singapore, mainly covering the central part of the island. Bukit Timah Granite is composed mainly from acid igneous rocks and some mixtures of less acidic formation from the Gombak Intrusives. The Sahajat Formation of the Lower Palaeozoic age covers only a small part in the eastern part of Singapore. The Sahajat Formation is composed of hard quartzite, sandstones and mudrocks, which are covered by younger deposits

(Pitts, 1984).

The Jurong Formation covers a significant area of the western part of Singapore and is composed of a variety of sedimentary rocks. These sedimentary rocks can be conglomerates, sandstones or mudrocks. The weathering process is the main reason for the great variability in the engineering properties of the rocks of the Jurong Formation. These variations can be significant even in small areas of single sites.

The weathering process in the Jurong Formation has produced highly heterogeneous and variable residual soils that can extend to great depths (Chang 1988). Residual soils originated from rocks of the Jurong Formation have mainly clayey particles with sand or less commonly silt size material (Pitts 1984). The residual soils of the Jurong Formation are usually medium to high plasticity (Chang 1988 and Rahardjo et al. 1995). Rahardjo et al. (1995) state that the shear strength parameters of residual soil produced from the Jurong Formation usually vary between 30 and 45kPa for the effective cohesion (c') and 26±1° for the effective angle of internal friction (φ') with respect to changes of effective stress. Rahardjo et al. (1995) also concluded that the angle of internal friction with respect to changes of negative pore-water pressure (φ^b) is usually equal to 26° for negative pore-water pressure up to -400kPa (i.e. equal to φ'). The in-situ measurements of the saturated coefficient of permeability with respect to water for residual soils of the Jurong Formation vary between 10^{-7} to 10^{-9}m/s (Agus et al. 1999).

Hillslopes composed of residual soils of the Jurong Formation usually have a piezometric line that lies at great depth and a perched water table, which is usually developed near to the ground surface due to precipitation (Pitts 1984, Rahardjo et al. 1995 and Lim et al. 1996). The effect of precipitation on the stability of residual soil slopes can be significant, as the pore-water pressures increase from initially negative values and become positive within the wetting front (i.e. the zone from the ground surface down to the perched water table).

2.8 Rainfall-induced slope failures in residual soils

A large number of steep, natural and engineered slopes in tropical and subtropical

areas remain stable for a long time and then fail during heavy rainstorms (Brand 1984 and Toll 2001). In many cases these failures cause loss of life and economic losses. Landslides induced by rainfall are usually shallow (Krahn et al. 1989, Day and Axten 1989), due to the fact that infiltration alters the pore-water pressures at shallow depths (Section 2.10). However, depending on the rainfall patterns and for very permeable residual soil slopes, like those of Hong Kong, slope failures may be disastrous (Lumb 1975).

There is a large number of research studies on the correlation between total rainfall and landslides occurring for various geographical areas. Brand et al. (1984) related the occurrence of landslides with total rainfall for Hong Kong. Brand et al. (1984) concluded that rainfall intensities of 70mm/h and above can be an indication that landslides may occur and the higher the rainfall intensity, the more severe the consequences will be. Brand et al. (1984) also concluded that a 24-hour rainfall of less than 100mm is unlikely to produce any slope failures. Premchitt et al. (1994) reviewed Brand et al.'s conclusions and suggested that after a 20-year review of landslides events in Hong Kong, the 70mm/h rainfall intensity is clearly a threshold for severe landslides to occur. For Singapore, Toll (2001) reviewed the available data from slope failures and concluded that major slope failures may occur after a 24-hour rainfall of over 110mm.

Although rainfall is recognised to have a major negative effect on the stability of slopes, there is a debate on the effect of the initial conditions on the slope stability during infiltration. Initial conditions can be expressed as the water content or the pore-water pressure distributions within the slope at the time the rainfall event starts. Another way to express initial conditions is the antecedent rainfall, i.e. the rainfall that falls on the slope over a period prior to the major rainfall event. Wolle and Hachichi (1989) studied landslides caused by rainfall in Brazil and concluded that intense rainfall does not cause slope instability by itself and that antecedent rainfall that will have increased the initial moisture of the soil must be incorporated in the analysis. McDonell (1990) also suggested that slope failures in New Zealand, which occurred in 1988, were subjected to high antecedent rainfall over a long period. Lumb (1975) studied the slope failures that took place in Hong Kong during the

period from 1950 to 1973 and concluded that an antecedent period plays a major role in the likelihood of slope failure occurring. Lumb (1975) adopted a combination of a 15-day period of antecedent rainfall with a 24-hour period of rainfall for his analysis. However Kay and Chen (1995) showed that for Hong Kong the choice of these time-periods are not the optimum, and instead they suggested the use of 1-day rainfall period with peak hourly rainfall. Kay and Chen (1995) based their analysis on Brand et al.'s (1984) conclusion that for Hong Kong the controlling parameter for rainfall-induced slope failures is the peak hour rainfall intensity and the 24-hour rainfall and that antecedent rainfall is not of a particular interest. For Singapore, Pitts (1985) came to a similar conclusion regarding the effect of the antecedent rainfall on slope failures. However later works on rainfall-induced landslides for Singapore showed that antecedent plays a major role (Wei et al. 1991, Rahardjo et al. 1998, Toll 2001 and Rahardjo et al. 2001). Toll (2001) states that in Singapore it is possible for minor landslides to occur after significant amounts of antecedent rainfall. Rahardjo et al. (2001) and Toll (2001) adopted a 5-day period of antecedent rainfall for their analysis. Also, Chatterjea (1989) studying the effect of antecedent rainfall on slope failures in Singapore concluded that a 5-day period of antecedent rainfall should be sufficient.

2.9 Slope stability for residual soils

Many authors (Lumb 1975, Fredlund 1979, Brand 1984, Chinniah et al. 1994, Fourie 1996) suggested that conventional methods, based on the assumption of saturated behaviour, for the design and construction of saturated soil slopes cannot be applied successfully for slopes under unsaturated conditions, which are subjected to intense rainfalls.

A simplified mechanism of how rainfall may induce slope failures was proposed by Brand (1981). According to Brand (1981), the negative pore-water pressures start to increase when water starts to infiltrate the unsaturated soil, and the loss of negative pore-water pressures decreases the shear strength of the soil below the mobilised shear strength along the potential slip surface. For the stability analysis of unsaturated soil slopes it is necessary for the effect of the negative pore-water

pressure to be incorporated. This is possible by deriving the factor of safety (FoS) of the unsaturated slope using the extended Mohr-Coulomb criterion for unsaturated soils (Equation 2.2). For this case the mobilised shear strength (S_m) at the base of a slice (Figure 2.5) is expressed as follows:

$$S_m = \frac{\beta}{FoS}\left\{c' + (\sigma - u_a)\tan\varphi' + (u_a - u_w)\tan\varphi^b\right\} \tag{2.32}$$

where β is the length across the base of each slice.

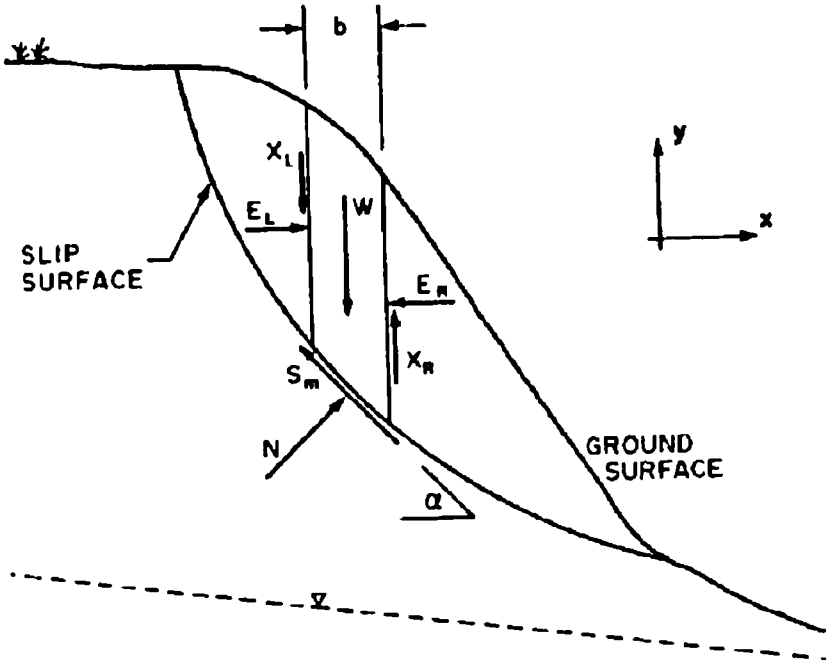

Figure 2.5 Forces acting on each slice of the slope for the slope stability analysis using the method of slices.

With the assumption of zero pore-air pressure (u_a=0), the moment equilibrium factor of safety $(FoS)_m$ is expressed as follows (Fredlund and Barbour 1992):

$$(FoS)_m = \frac{\sum\left(c' \cdot \beta \cdot R + \left(N - u_w \cdot \beta \frac{\tan\varphi^b}{\tan\varphi'}\right) R\tan\varphi'\right)}{\sum W \cdot x - \sum N \cdot f} \tag{2.33}$$

where W is the total weight of each slice,

N is the normal force acting at the base of each slice

X_R and X_L are the right and left vertical interslice forces,

and a is the inclination of the base of the slice.

R is the radius of the potential slip surface,

x is the horizontal distance from the centre of each slice to the centre of moments,

and f is the offset distance from the force to the centre of moments.

The force equilibrium factor of safety $(FoS)_f$ is expressed as follows:

$$(FoS)_f = \frac{\sum\left(c' \cdot \beta \cos a + \left(N - u_w \cdot \beta \frac{\tan \varphi^b}{\tan \varphi'}\right) \tan \varphi' \cos a\right)}{\sum N \sin a} \tag{2.34}$$

In order to determine a realistic pore-water pressure distribution within the unsaturated slope, so that it can be used in the slope stability analysis, an extensive and detailed seepage analysis is required.

2.10 Infiltration and seepage analysis for residual soils

During a rainfall event, the rainwater will partially infiltrate the ground surface, and the excess will disappear as runoff. The amount of rainwater that infiltrates the slope is a function of the rainfall intensity, the coefficient of permeability of the soil with respect to water and the vegetation at the ground surface of the slope. In theory, rainwater will infiltrate the slope at a rate equal to the rainfall intensity, provided that the rainfall intensity is lower than the permeability of the soil with respect to water. If the average rainfall intensity is greater than the permeability of the soil with respect to water, then the infiltration will be taking place at a rate, which is controlled by the coefficient of permeability of the soil with respect to water. Part of the infiltrated rainwater is held at the ground surface as initial abstraction. Initial abstraction is the sum of interception by vegetation and depression storage at the

ground surface (Premchitt et al. 1986). Interception by vegetation is dependent on the type of vegetation, the antecedent rainfall and total rainfall and usually is considered small for slopes covered with grass (Penman 1963). Depression storage depends on the type of soil and Overton and Meadows (1976) suggest that depression storage usually ranges between 2.5 and 5mm for various types of soils. Figure 2.6 presents a qualitative development with time of the infiltration rate, runoff rate and initial abstraction rate during a rainfall event. From Figure 2.6 can be observed that the rate of the initial abstraction is very high at the start of the rainfall event and rapidly reduces to an insignificant rate. The infiltration rate increases from zero at the start of the rainfall to maximum rate and then starts to decrease with time, causing the runoff to increase. The decrease of infiltration is caused by the slow movement of infiltrated water towards larger depths where the permeability of the soil with respect to water is significantly lower than the permeability of the soil with respect to water at the ground surface, which very soon after the start of the rainfall event becomes maximum and equal to the saturated coefficient of permeability with respect to water.

The model of infiltration, which is presented in Figure 2.6, is verified with measurements of runoff of several rainfall events by Premchitt et al. (1986), and Lee et al. (1999). Similar behaviour of infiltration during a rainfall event was also predicted by Gasmo et al. (2000) using a numerical model. Premchitt et al. (1986) and Lee et al. (1999), also showed that there is a good relationship between total rainfall and total runoff, and as total rainfall increases then total runoff increases. Lee et al. (1999) estimate that for a residual soil slope in Singapore the total runoff is approximately equal to 50% of the total rainfall. Premchitt et al. (1986) concluded that there is a poor relationship between total rainfall and total infiltration.

Premchitt et al. (1986) also concluded that the existence of grass cover at the ground surface of the slopes caused total infiltration to reach up to 70% of the total rainfall at particular rainfall events. The existence of vegetation on the ground surface produces cracks and macropores in the soil and thus increases the permeability of the soil with respect to water (Collison et al. 1995). Anderson et al. (1996), concluded that the increase of the saturated coefficient of permeability with respect to water of

surficial residual soils, caused by vegetation, is linearly related to the root area ratio (i.e. area of roots per unit area).

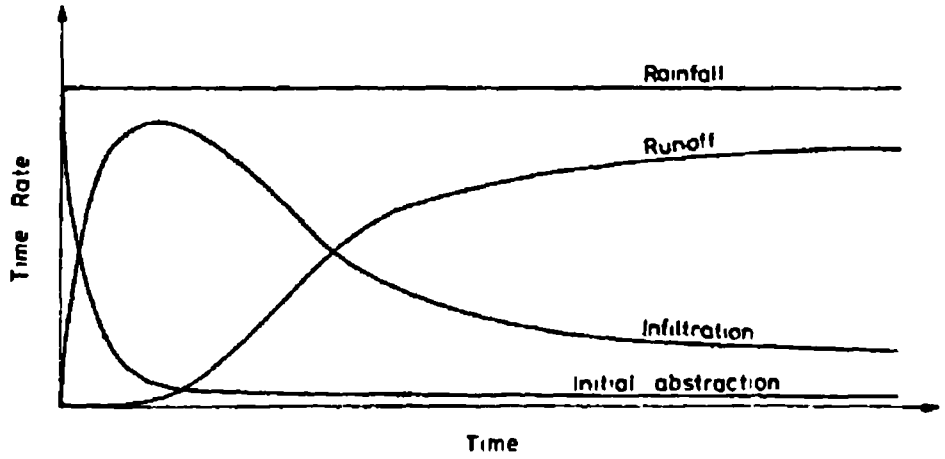

Figure 2.6 Development with time of infiltration rate, runoff rate and initial abstraction rate during a rainfall event (Premchitt et al. 1986).

The infiltrated water seeps into the slope, wetting the soil and thus increasing the pore-water pressures towards positive values, creating a zone of saturation. The lower limit of the zone of saturation is called a wetting front. The progression of the zone of saturation with time from the ground surface ends either at the end of the rainfall event or until is reaches large depths where the permeability is considerably lower. Lumb (1975) established a relationship between the depth of the wetting front, the coefficient of permeability of the soil with respect to water and the degree of saturation, which is presented in Equation 2.35.

$$h = \frac{k \cdot t}{n(S_f - S_o)} \tag{2.35}$$

where h is the depth of the wetting front,

t is the duration of the rainfall event,

k is the saturated coefficient of permeability of the soil with respect to water,

n is the porosity of the soil,

S_f is the final degree of saturation,

and S_o is the initial degree of saturation.

Equation 2.35 was established with the simplification that the saturated coefficient of permeability of the soil with respect to water is constant throughout the wetting front, which in reality may not be true (Vaughan 1985 and Fourie 1996). In addition, Brand (1984) suggests that the depth of the wetting front (h) in Equation 2.35 is directly related to the initial and final degrees of saturation (S_o and S_f), which in practice are speculative.

Several research studies, based on field measurements, describe aspects of the way seepage processes in residual soil slopes during infiltration cause redistribution in the pore-water pressures. Lim et al. (1996) measured the pore-water pressure changes in a residual soil slope of Singapore, with different conditions at the ground surfaces: bare soil, grass cover and canvas covered surface. They concluded from the field data that different soil covers at the ground surface had a large impact on the way pore-water pressure changes during infiltration. More specifically Lim et al. (1996) found that vegetation prevented the advancement of the developing perched water table from reaching large depths due to the evapotranspiration. At the same time, for the case of a bare slope, the wetting front extended to larger depths, causing the pore-water pressures to increase to 1.5m deep. Lim et al. (1996) also showed that during dry periods pore-water pressures near the ground surface could drop below –80kPa. Field measurements by Bao and Ng. (2000) also showed that pore-water pressures during dry periods could go towards very low negative values and become positive during wet periods, building a deep wetting front. Other similar results from field monitoring on the effect of rainfall on the seepage conditions and the pore-water pressures are presented by Macari et al. (1992), Fourie (1996), Gasmo et al. (1999), Deutcher et al. (2000), Low et al. (2000) and Dykes and Thornes (2000). All these research studies present general trends of the way rainfall causes pore-water pressure changes within the slope and the development of a perched water table and reflect the complexity of the whole mechanism.

From the above analysis it is obvious that infiltration works in a complex way and

prediction of the response of the pore-water pressures within a residual soil slope due to rainfall is difficult and any analysis is always limited to the very localised cases. However, field measurements serve as indicators for better modelling using numerical methods.

2.11 Numerical modelling of the seepage conditions of unsaturated slopes during infiltration

In earlier sections an analysis is presented of the relationship between rainfall and landslides using statistical approaches. Such approaches serve as good indications as to when a slope failure may occur and is used broadly in landslides warning systems (Premchitt et al. 1994). However, statistical approaches do not provide information on the mechanism of how rainfall causes the pore-water pressures to increase and as a consequence produce slope instability. A statistical approach like the ones presented by Brand et al. (1984) or by Toll (2001) cannot explain how the soil properties of the slope influence the seepage conditions within the slope. A better approach for the description of the infiltration mechanism on slopes is provided with the use of numerical models. A numerical model is a tool designed to represent a simplified version of reality (Wang and Anderson 1982). Numerical models for the seepage conditions within a slope are based on the governing equations for seepage within a soil (Equations 2.26 to 2.31).

2.11.1 Limitations in numerical modelling of seepage

Modelling infiltration in unsaturated soil slopes is a difficult task and past studies show a great number of limitations. One of the first attempts to illustrate the effect of the seepage conditions within a residual slope on the stability of the slope was presented with the model of Hodge and Freeze (1977). Hodge and Freeze (1977) presented a parametric study using a two-dimensional steady state analysis with a finite element model, where the slope was considered fully saturated. However, steady-state analyses are not of particular interest as the response of the seepage conditions within a slope to a rainfall event is rapid and therefore transient analysis must be adopted (Leach and Herbert 1982).

Leach and Herbert (1982) composed a preliminary analysis using a two dimensional finite-difference model and compared their results with available field data. They concluded that generally the numerical model overestimated the head at a particular point and the magnitude of error decreased with depth. Leach and Herbert (1982) also identified the need to decrease the mesh dimensions near the ground surface where rapid changes in head occur.

Vargas et al. (1990) conducted a two-dimensional transient flow analysis using a finite element code. Vargas et al. (1990) concentrated their analysis on the wetting process of the slope and excluded the effect of vegetation and evaporation at the ground surface. In reality, evaporation takes place in a complex way and is a function of the water content and negative pore-water pressure of the soil and the soil type (Wilson et al. 1995). Thus the effect of evaporation on the pore-water pressure changes during drying periods is very often excluded from analyses as its modelling is very difficult to handle. Gasmo et al. (2000) also attempted to incorporate evaporation in their numerical analysis, defining it in a more simplistic way as a negative flux at the ground surface and concluded that the decrease of the negative pore-water pressures at the ground surface was too fast in comparison with available field data. Vargas et al. (1990) also assumed that no runoff takes place on the slope (i.e. all the rainfall water infiltrates the slope) and finally no hysteresis of the soil-water characteristic curve was considered in the analysis. The hysteresis of the soil-water characteristic curve is also difficult to model, because at the end of a rainfall event the soil near the ground surface starts to drain and therefore the drying part of the soil-water characteristic curve has to be used, while at larger depths the slope is still in the wetting process, and for that reason the wetting part of the soil-water characteristic curve has to be used for that area.

The limitations in the numerical modelling of seepage in an unsaturated residual soil slope, as were described above, are important for the analysis of the ground water flow conditions during infiltration and must be taken into account while interpreting the results of such analyses. However, the numerical models are useful tools for a better understanding of the controlling parameters for rainfall-induced landslides.

2.11.2 Review of numerical analyses for rainfall-induced slope failures

Neuman (1973) identified the need for the definition of proper boundary conditions when carrying out a saturated-unsaturated flow analysis using the finite element method. Neuman (1973) proposed the following procedure for the definition of the boundary conditions:

- Initial position of seepage was guessed and the head pressure was set to zero along the seepage face.
- flux Q was set to zero along the unsaturated portion of the slope.
- the new Q that was calculated would indicate that flow was directed out of the slope only along the prescribed zero pressure head and the newly calculated value of pressure head would be negative where Q was zero.
- If these expectations were not met, then the boundary conditions at the errant nodes were redefined to agree with the new solution.
- This procedure continued until the solution converged.

Hodge and Freeze (1977) illustrated that a highly weathered soil profile near the ground surface, with high permeability with respect to water due to fractures, cracks and vegetation, has an important effect on the pore-water pressure distribution and highly positive pore-water pressures are developed near the ground surface. According to their analysis the slope failure would normally be shallow.

Rulon and Freeze (1984) carried out a two-dimensional steady state analysis of saturated-unsaturated flow in a layered heterogeneous slope, by assuming that the average annual rate of precipitation would be close to steady state conditions. The results of their analysis were verified with laboratory measurements of a two-layered sand box. They showed that ignoring the unsaturated zone within the slope may result in the overdesign of a stable slope angle. They also identified the importance of the hydraulic properties of the soil layers for the developments of the wetting front

and the perched water table near the ground surface during precipitation.

Vargas et al. (1990) showed that during infiltration a wetting front develops near the ground surface and pore-water pressures in the slope are either negative or null. The decrease of the negative pore-water pressure brings about a decrease in the cohesion that leads to instability and shallow superficial slides. Vargas et al. (1990) also identified the importance of the development of positive pore-water pressures at the toe of the slope.

Pradel and Raad (1993) investigated the influence of the surficial coefficient of permeability with respect to water (k_{sat}) on the seepage conditions within slopes, subjected to rainfall and concluded that there is a threshold of the k_{sat} above which the soil may not become saturated. This threshold in k_{sat} is a function of the rainfall pattern and the depth of the wetting front that is required to produce instability of the slope, which is under investigation.

Alonso et al. (1995) carried out a parametric study using the NOSAT code, and highlighted that the permeability and the soil-water characteristic curve of the soil control the stability of an unsaturated slope, when the slope is subjected to rainfall infiltration. For soils with low k_{sat} the time to a significant reduction in safety factor is related to the time duration of isolated rainfalls. Alonso et al. (1995) also showed that specific combinations of rainfall intensity and k_{sat} may lead to a decrease of safety factor after the end of the rainfall, and this fact may explain the delayed failure of some slopes.

McDougall and Pyrah (1998) also investigated the effect of the rainfall intensity and the saturated coefficient of permeability of a soil with respect to water (k_{sat}) and their results showed that if the ratio of rainfall to k_{sat} is the same between two cases, then the same seepage pattern occurs in each cases but at a time separated according to the relative saturated hydraulic conductivities. Spierenburg et al. (1995) also concluded that the time needed for a slope to saturate under constant infiltration rate is similar but the time required for saturation is a function of the k_{sat} of the surficial soil.

Ng and Shi (1998a) and (1998b) investigated the influence of the rainfall duration, the initial conditions, the antecedent rainfall and the soil parameters on the seepage

conditions of a residual soil slope in Hong Kong. They concluded that for a initially low level of the ground water table the infiltration reduces the negative pore-water pressures by an amount depending on the rainfall intensity, but infiltration does not produce a significant rise in the ground water table. Ng and Shi also concluded that initial conditions and antecedent rainfall also influences the stability of the slope. Rahardjo et al. (2001) also studied numerically the influence of antecedent rainfall on the stability of residual soil slopes in Singapore and concluded that antecedent rainfall is a parameter that may lead to slope instability. However, in Rahardjo et al.'s (2001) analysis a significant rise of the ground water table was predicted.

Gasmo et al. (2000) studied the infiltration rates of a residual slope in Singapore, using the Seep/W (Geo-Slope Int. Ltd 1998a) finite element software and showed that infiltration rates may momentarily exceed the surficial coefficient of permeability with respect to water (k_{sat}), if the rainfall intensity is significantly higher that k_{sat}. Gasmo et al. (2000) attempted to calculate the infiltration rates of the slope, but concluded that this is a difficult task as a better definition of the hydraulic properties of the slope is required.

The numerical analyses as described above, reflect the complexity of the infiltration process and how this influences the stability of an unsaturated slope. From the research work mentioned above, it can be seen that the rainfall intensity and duration is not the only controlling factor that leads to slope instability. Antecedent rainfall, initial conditions and the hydraulic properties of the soil (permeability function and soil-water characteristic curve) also influence the seepage conditions of a residual soil slope. More attention must be given on these parameters in order to explain the infiltration mechanism. In addition, from the above research work in numerical modelling it is seen that realistic modelling of the seepage process is possible, despite several limitations.

CHAPTER 3

Description of the Research Slopes, Instrumentation and Equipment

3.1 Location and general description of the study areas

Field monitoring took place on two slopes in the west of Singapore. The slopes are called NTU-CSE and NTU-ANX and are located on the campus of Nanyang Technological University (NTU). Figure 3.1 presents the location of the NTU campus on the map of Singapore and Figure 3.2 shows the exact location of the two instrumented slopes on the campus of NTU.

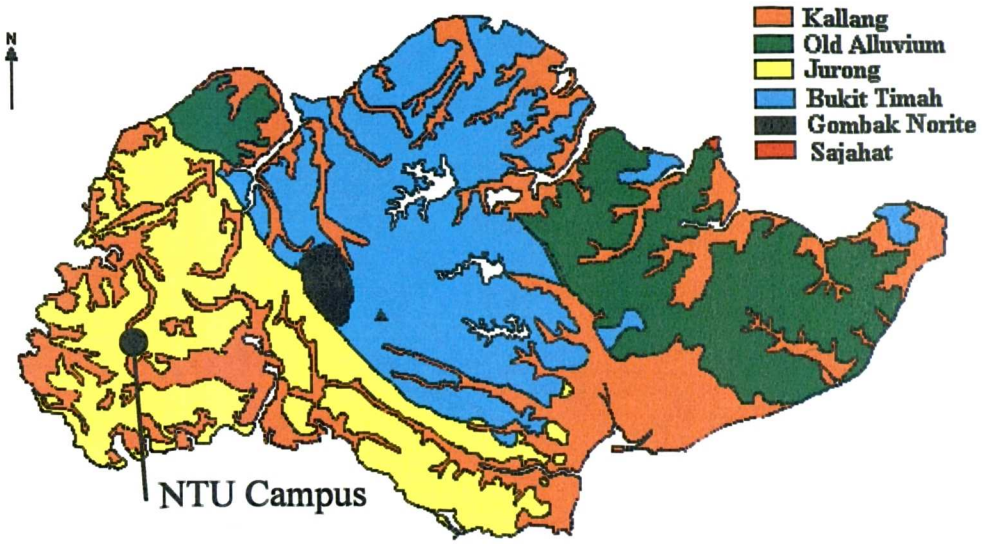

Figure 3.1 Geology map of Singapore with the location of NTU campus.

The inclination of the NTU-CSE slope is 27° and its height is 7m (Figure 3.3). Along the middle of the NTU-CSE slope is a berm with a ditch for drainage purposes. An 11m high rain tree, of the Samanea saman type (Rao and Wee 1989), exists at the toe of the NTU-CSE slope and 2m from the instrumentation. The branches of that tree cover the lower quarter of the slope and it is assumed that its roots may extend for a large area around it. The NTU-CSE slope was covered by grass.

The inclination of the NTU-ANX slope is 29°. The length of the study area on the NTU-ANX slope is relatively small in comparison to the length of the whole slope

(Figure 3.4). The crest of the slope is more than 20m in distance from the study area. The slope below the study area is cut and a retaining wall is present. However this retaining wall stands at an adequate distance from the instrumentation so that it can safely be assumed that it does not have any effect on the measurements that were collected on the NTU-ANX slope. For these reasons the study area of the NTU-ANX slope is assumed not to be affected by the crest or the toe of the slope. The NTU-ANX slope is also covered by grass. Table 3.1 presents the geometric details of the two slopes.

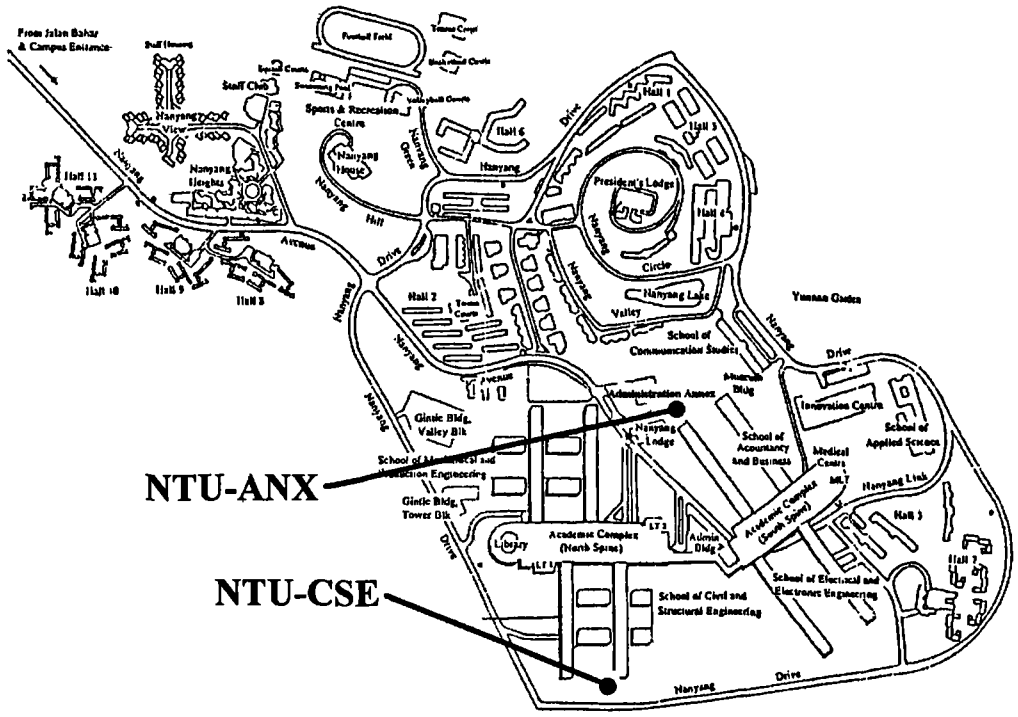

Figure 3.2 Map of the campus of Nanyang Technological University with the location of the two slopes.

Table 3.1 Summary of the geometry of the instrumented slopes.

Slope	Height	Angle
NTU-CSE	7.1m	27°
NTU-ANX	Infinite slope	29°
NTU-ANX (research area)	3.3m	29°

Figure 3.3 Photograph of the NTU-CSE slope.

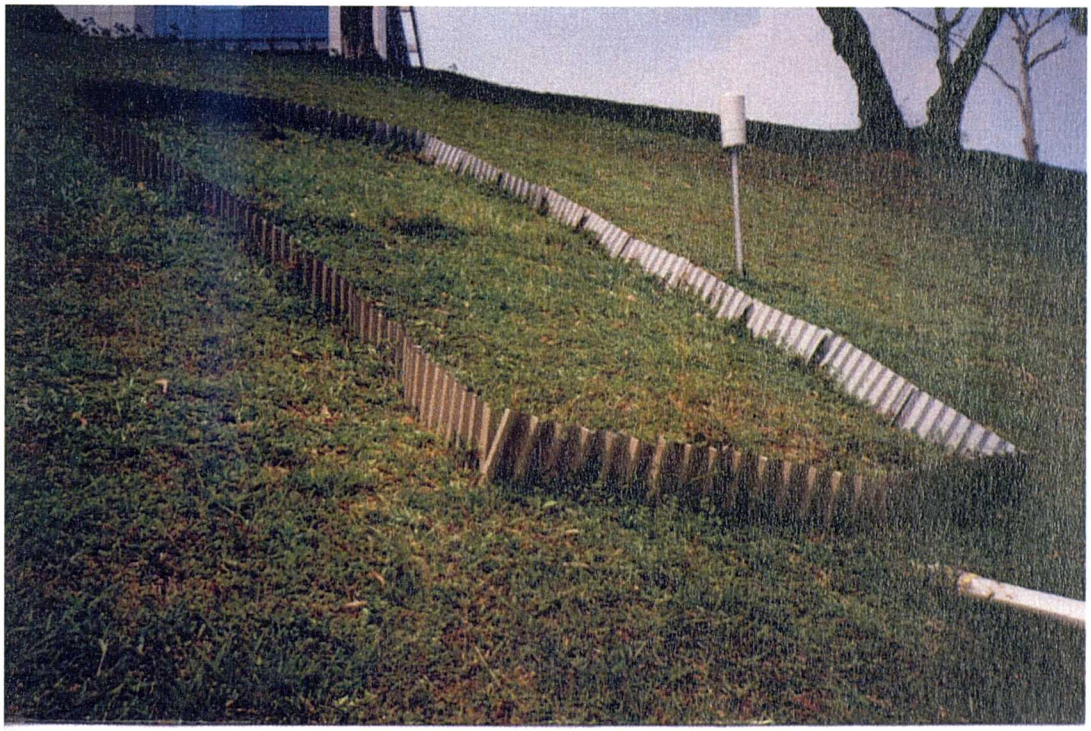

Figure 3.4 Photograph of the of the NTU-ANX slope. The picture also shows the catchment, created by corrugated sheets, for the runoff measurement and the rainfall gauge.

3.2 Geology of the research slopes and soil properties

Five boreholes were drilled in the NTU-CSE slope as part of the site investigation (Gasmo et al. 1999 and Rahardjo et al. 2000). The results of the site investigation showed that the geology of the NTU-CSE slope is complicated and the soil properties vary considerably with depth. Nearby construction activities required the removal of part of the slope, in adequate distance from the research area. The excavation works revealed the soil profile of the slope (Figure 3.5) and the great variations of the soil materials over a very small distance were evidenced. The information from the site investigation at the NTU-CSE slope and the laboratory tests of samples from the NTU-CSE slope were combined to produce a simplified slope profile. Figure 3.6 presents this simplified slope profile of the NTU-CSE slope.

Figure 3.5 The soil profile of the NTU-CSE slope as it was revealed from nearby excavation works.

The simplified slope profile, presented in Figure 3.6, consists of 3 soil-layers and the bedrock (Sedimentary Jurong Formation). The properties of the three soil layers are presented in Table 3.2. At the crest of the slope is a soil layer (Layer 1) that extends to 1m depth. Layer 1 is silt and clay with moderate to high plasticity, with an orange

colour and with 94% fines. Layer 2 is the surficial soil layer of the slope except from the area close to the crest and covers the slope to 2m depth. Layer 2 is silt and clay with low plasticity, has orange colour and 74% fines. Layer 3 is classified as hard silty sand with fines of low plasticity and with purple colour. Layer 3 is characterised by variations in the degree of weathering with distance and depth.

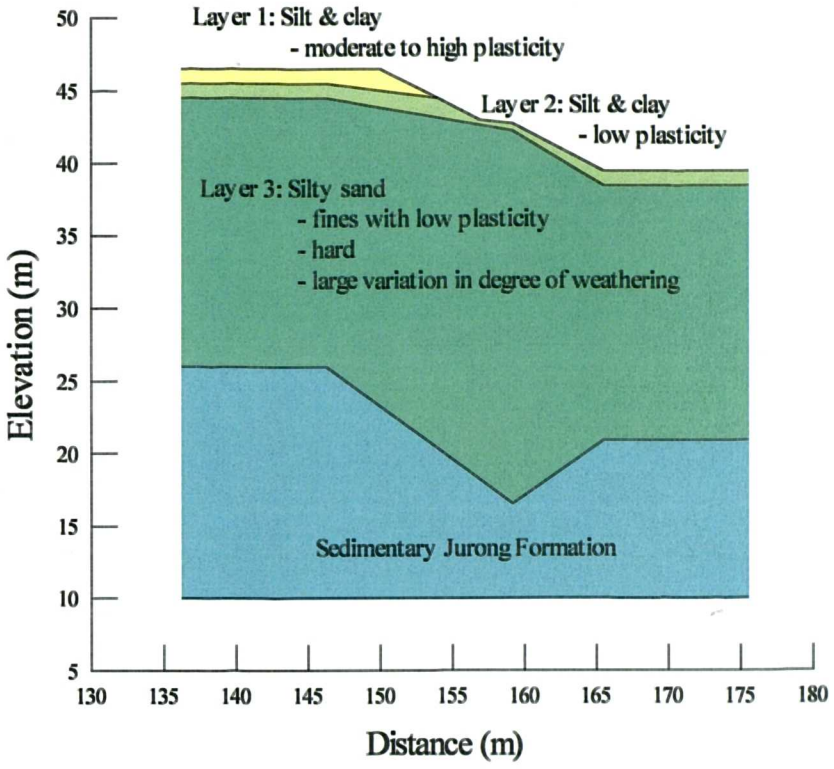

Figure 3.6 Simplified soil profile of the NTU-CSE slope.

The results of several permeability tests on samples of the NTU-CSE slope reflect the variability in the soil properties across the slope, especially for the orange soil (Layers 1 and 2). Laboratory tests conducted by Rahardjo (2000) with an oedometer ring using the falling head method, showed that the coefficient of permeability with respect to water of soil samples from 2.5m deep at the crest of the NTU-CSE slope could be as high as $5x10^{-4}$m/s. Gasmo (1997) measured the coefficient of saturated permeability with respect to water (in the laboratory with a triaxial permeameter) of the near surface soil samples of Layers 1 and 2 at the middle of the slope to be equal to $8x10^{-7}$m/s. Also, in-situ permeability tests (using a Guelph permeameter) on the surface of NTU-CSE slope determined the saturated coefficient of permeability with respect to water equal to $2x10^{-7}$m/s (Agus et al. 1999). The saturated coefficient of

permeability to water of Layer 3 was measured in the laboratory with a triaxial permeameter to be equal to $3x10^{-9}$m/s (Hritzuk 1997).

For the site investigation of the NTU-ANX slope two boreholes were drilled close to the study area. Using the information from the two boreholes, a simplified soil profile was produced. Figure 3.7 shows the simplified profile for the NTU-ANX slope and the properties of the two soil-layers are summarised in Table 3.3. Layer 1, which is the surficial soil layer and extends to 10m deep, is silty to sandy clay, hard, has orange colour, moderate plasticity and 58% fines. Layer 2 is clayey silt with siltstone and sandstone fragments. The fines of Layer 2 of NTU-ANX slope were measured to be 32%.

Table 3.2 Engineering properties of the soil-layers of the simplified profile of NTU-CSE slope.

Layer no.	Description	Properties	
1	Silt and clay, moderate to high plasticity	Classification (USCS)	CH-MH
		w (%)	30
		LL	65
		PL	35
		PI	30
		fines (%)	94
2	Silt and clay, low plasticity	Classification (USCS)	CL to SC-CL
		w(%)	19
		LL	36
		PL	23
		PI	14
		fines (%)	74
3	Hard silty sand, with fines of low plasticity and large variations in degree of weathering	Classification (USCS)	SM-ML
		w(%)	13
		LL	29
		PL	23
		PI	6
		fines (%)	27
4	Hard sand, silt and clay, low plasticity and variations in degree of weathering	Classification (USCS)	SM-ML to SC-CL
		w(%)	15
		LL	10
		PL	10
		PI	10
		fines (%)	15

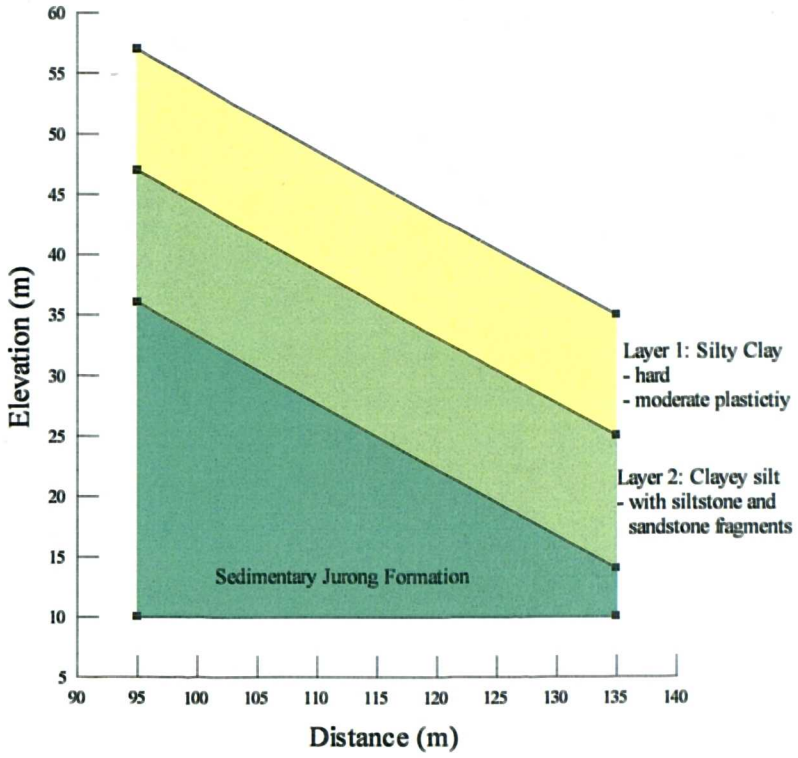

Figure 3.7 Simplified soil profile of the NTU-ANX slope.

Table 3.3 Engineering properties of the soil-layers of the simplified profile of NTU-ANX slope.

Layer no.	Description	Properties	
1	Hard, silty clay with moderate plasticity	Classification (USCS)	CL-ML
		w(%)	22
		LL	45
		PL	26
		PI	19
		fines (%)	58
2	Silt and clay, low plasticity	Classification (USCS)	ML-CL
		w(%)	16
		LL	46
		PL	29
		PI	18
		fines (%)	32

3.3 Description of the field instrumentation

3.3.1 Description of equipment for field monitoring

Jet-Fill tensiometers

The in-situ measurements of negative pore-water pressures were achieved with the use of tensiometers. Tensiometers are usually capable of measuring up to –100kPa (1 bar) of negative pore-water pressures in the field. The tensiometers installed on the NTU-CSE and NTU-ANX slopes were Jet-Fill tensiometers (Figure 3.8), manufactured by Soilmoisture™ Equipment Corp. Santa Barbara, California, model 2725 (Soilmoisture™ Equipment Corp. 1997).

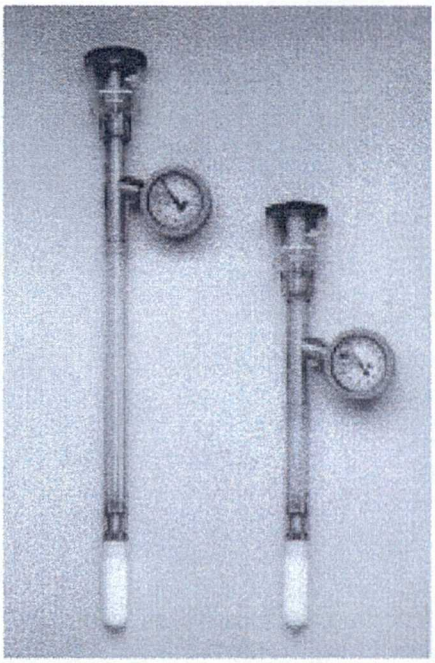

Figure 3.8 The 2725 Jet-Fill tensiometer manufactured by Soilmoisture™ Equipment (after Soilmoisture™ Equipment Corp. 1997).

The tensiometer has a high-air entry porous ceramic tip at the bottom and at the top a reservoir cap (Figure 3.9). The plastic tube and the reservoir cap at the top of the tensiometers are filled with water. Once the tensiometer is installed in the field and the ceramic tip at the bottom of the instrument comes in contact with the soil, water flows through the ceramic tip and into the soil, until equilibrium of pressure is achieved between the water in the tube of the tensiometer and the soil. Once the equilibrium between the water in the tube of the tensiometer and the soil is

established the negative pore-water pressure can be measured with a pressure gauge, which is installed at the top of the tensiometer (Figure 3.9). As will be shown below, the pressure gauges in the tensiometers, which were installed on the NTU-CSE and NTU-ANX slopes, were replaced with pressure transducers.

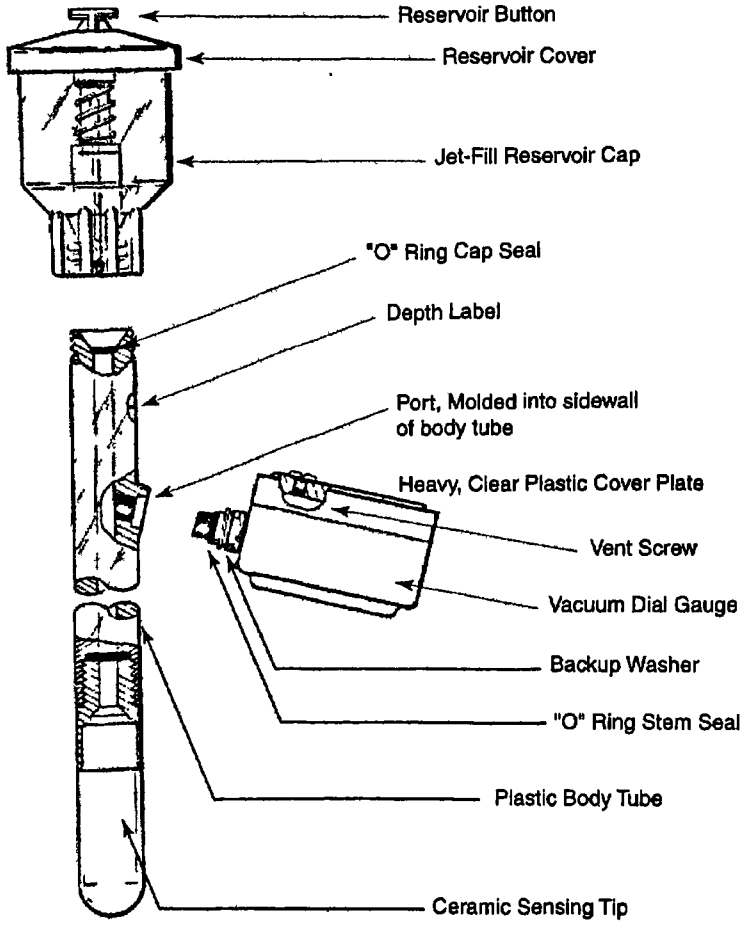

Figure 3.9 The Jet-Fill tensiometer (after Soilmoisture^{TM} Equipment Corp. 1997).

The quality of the negative pore-water pressure measurements in the field with the use of tensiometers is depended on good contact of the ceramic tip with the soil. In addition, regular maintenance of the installed tensiometers is required to avoid cavitation and air diffusion through the ceramic tip. Air diffusion takes place under very low negative pore-water pressures when dissolved air diffuses from the soil into the ceramic tip and comes into the water within the tensiometer's tube. Cavitation takes place when the water pressure reaches the vapour pressure and then amounts of water in the tube become vapour. The removal of the air bubbles from the water within the tensiometer tube is achieved with the reservoir button of the jet fill cap at

the top of the tensiometer (Figure 3.9).

Rainfall Gauge

Rainfall is measured with rainfall gauges. The rainfall gauge that was used at the NTU-CSE slope was the double tipping-bucket type, model Handar 444A, manufactured by Vaisala Inc., California. The rainfall gauge that was used at the NTU-ANX slope was the single tipping-bucket type, model Rain-o-matic, manufactured by Pronamic Co. Ltd.

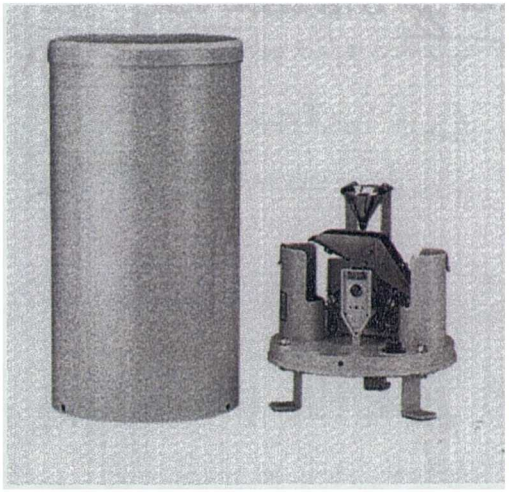

Figure 3.10 The Handar 444A rainfall gauge, manufactured by Vaisala Inc.

The Handar 444A rainfall gauge (Figure 3.10) is composed of a 20cm diameter funnel where water is collected and then directed to a tipping mechanism. The tipping mechanism is adjusted to tip and dump when 0.25mm of rainwater is collected. With each tip of the bucket, a magnet passes over a reed switch, which causes a momentary contact closure. The contact closure is counted by the circuitry in a data acquisition system. Each tip also causes a second bucket to come into position below the funnel, ready to be filled and repeat the cycle. The measured rainfall is discharged through a drain tube at the bottom of the rainfall gauge.

The Rain-o-matic rainfall gauge, which was installed on the NTU-ANX slope operated in a similar fashion to the Handar 444A. Rainwater was collected by a 20cm diameter funnel and directed to the tipping mechanism. Each tipping occurs when 0.25mm of rainwater are collected. The Rain-o-matic rainfall gauge has two

reed switches (the one is normally closed and the second is open) and can be connected to an LCD counter and to a data logger.

Piezometers

The fluctuations of the groundwater level during wet and dry periods were monitored with the piezometers. The piezometers on the NTU-CSE and NTU-ANX slope were installed during the site investigations (Rahardjo 2000) and were the Casagrande type with a ceramic tip and PVC riser tubing (Figure 3.11). The ceramic tip of the piezometer was sealed at a particular depth with a bentonite seal.

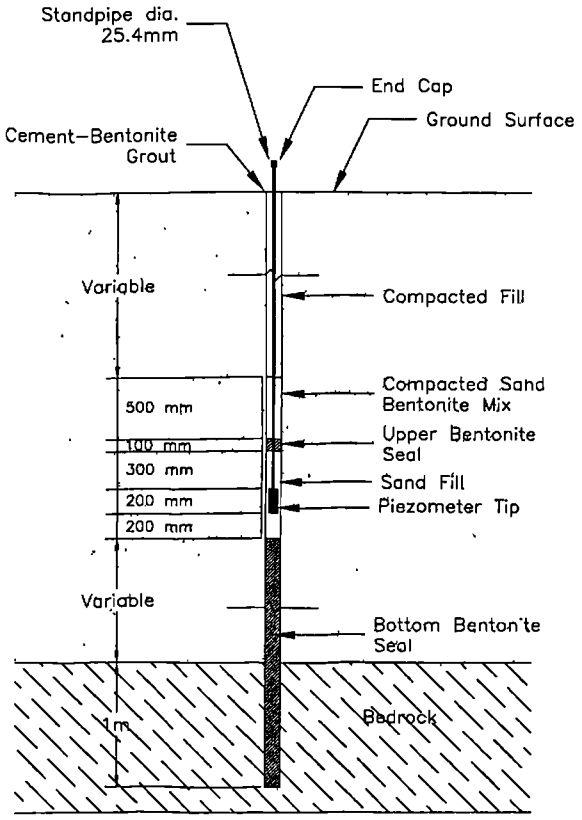

Figure 3.11 The Casagrande piezometer installed on the NTU-CSE and NTU-ANX slopes (after Rahardjo 2000).

The piezometers were fitted with depth transducers to allow automated measurements with data acquisition systems. The description of the depth transmitters is presented in the following paragraphs.

Pressure and depth transducers

Pressure transducers were used to measure the pressure at the top of each tensiometer. The pressure transducers that were used in the NTU-CSE and NTU-ANX slopes had a 2-wire technique in order to give current output. That means that the pressure transducers had only a pair of wires from which the current signal was measured. The pressure transducers, which were used in the NTU-CSE slope were manufactured by VDO™ (VDO Industrie-Messtechnik Gmbh, Germany), had a signal range between 4 and 20mA and measured absolute pressure within a range from -100 to 100kPa. The required power supply for the VDO pressure transducers was 12V. The pressure transducers that were used to measure at the top of the each tensiometer on the NTU-ANX slope were manufactured by Kristal™ (Kristal Instrumente A.G., Switzerland), type Ceraline-S. The output range of the transducers was 4mA to 20mA with an accuracy of ±0.5% of the full scale (output) and the instruments were able to measure absolute pressures from -175kPa to 175kPa. The pressure transducers operated with 12V power supply.

The depth transducers, installed in the Casagrande piezometers, were Druck™ Industrial Depth Transmitters, model no. PTX-161/D. The current output range was from 4 to 20mA with a maximum error of 0.3% of the full scale (output) and the depth transducers could measure up to 20m high water level.

Data acquisition systems

Two different data acquisition systems operated in the NTU-CSE and NTU-ANX slopes. The choice of the acquisition system for each research slopes was made according to the needs of the instrumentation and the general conditions on each slope. The NTU-CSE slope was in a close distance to the Geotechnics laboratory of the School of Civil and Structural Engineering (CSE) and therefore the acquisition system of the NTU-CSE slope could be housed in the laboratory. That meant that it was possible to install and operate a data acquisition system with more sophisticated data loggers that were able to be connected with PCs and record and store a large amount of data, which could be displayed in real-time fashion. On the other hand, the NTU-ANX slope was in a remote area and therefore there were several

restrictions on the way the data logger would be supplied with power and on the way the data logger would be stored. In addition, the installed data logger for NTU-ANX slope should be a stand-alone data logger that could store a large number data over a long period of time.

The collection of pressure measurements from the tensiometers of the NTU-CSE slope was made with two Hydra 2635A Data Buckets, manufactured by Fluke® Co., USA (Fluke® 1997), which were stored and powered in the Geotechnics Laboratory of CSE. The configuration and communication software for the Hydra 2635A Data Bucket was designed by Fluke® Co. The Hydra 2635A Data Bucket receives the current output signal with a two-wire connection from the pressure transducers and translates it into voltage. The Hydra 2635A Data Bucket has an auto-ranging mode, which means that the instrument chooses the appropriate measuring scale automatically in order to obtain the best resolution (i.e. the incremental input signal that yields the smallest distinguishable reading or output). When the slow scanning rate is used, the Hydra 2635A Data Bucket provides a resolution of 1mV for measurement range up to 30V. In addition, for measurement range up to 30V the data logger has an accuracy of ±(0.24%+2mV) with a slow scanning rate. The two data loggers were connected to a PC via an RS-232 communication link between the data logger RS-232 port and the PC serial COM port. In that way, the configuration and operation in real time of the data loggers was done using the supplied PC application software. At the same time the data loggers returned scanned measurement data, which could be viewed through the application software. The measurements took place every 20 minutes and the data were stored in a memory card in the Hydra 2635A Data Bucket. On a weekly basis, the data were saved on the hard disk of the PC and the memory cards of the data loggers were cleared.

The collection and storage of the rainfall data on the NTU-CSE slope was done with a Handar 555 data collection platform, manufactured by Vaisala Inc., California. The Handar 555A accommodates a switch closure input for the tipping bucket. The Handar 555A was 24 hours on-line with the rainfall gauge and monitored in a real-time fashion the momentary contact closure of the reed switch of the rainfall gauge, each time the bucket tipped. Vaisala Inc. also provided with the configuration and

communication software for the Handar 555A.

The collection of the field measurements from the NTU-ANX slope was achieved with a data acquisition system manufactured by Grayhill Inc., model MicroDac Optomux (Grayhill 1995). The MicroDac consists of a stand-alone controller, an I/O mounting rack and single point I/O modules. Figure 3.12 presents the MicroDac controller with the module rack, which were installed on the NTU-ANX slope. The controller was used to control the rate of measurements and for storing the data. The mounting rack with the modules was connected to the pressure transducers, the rainfall gauge, and the piezometer. Rahardjo (2000) made the software for the configuration of the MicroDac. The main advantage of the MicroDac was that it was possible to connect all the instruments on one system. In addition, the MicroDac could be configured to take measurements under different intervals during the wet and dry periods and thus it was more efficient in the number of stored data. However, the configuration was not an easy task and several problems were encountered with establishing communication between a portable PC and the controller for uploading of the data.

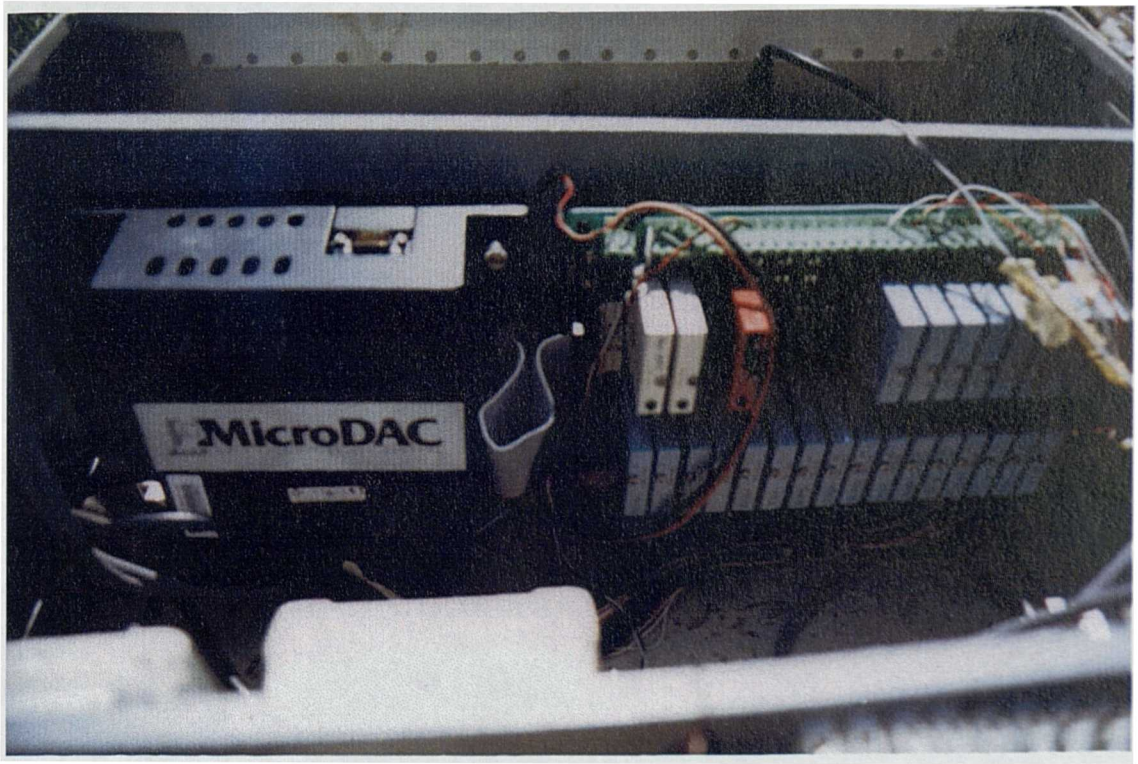

Figure 3.12 The MicroDac controller with its module rack installed on the NTU-ANX slope.

The resolution of the acquisition system depends on the I/O modules. The I/O modules, which were used for the depth and pressure transducers were the analog current input modules, manufactured by Grayhill Inc., model 73G-II420. The resolution of the 73G-II420 analog current input modules was 3.91μA, with a measuring range from 4 to 20mA and an accuracy of ±0.2% of the full scale. The MicroDac recorded the rainfall data through a DC input module, manufactured by Grayhill Inc., model 70G-IDC. During a rainfall event and as the reed switches of the rainfall gauge were changing positions (open and closed) the DC input module was switched on momentarily. The controller measured the number of times the DC input module was switched on during the rainfall event. The MicroDac controller and the mounting rack were powered with 5V.

The MicroDac received measurements every four hours during dry periods. When a rainfall event started, the rainfall gauge "triggered" the controller, through the DC input module, and during the rainfall event the controller received measurements every 10 minutes. The feature of triggering the MicroDac through the rainfall gauge as soon as the rainfall bucket was tipped by the rainfall proved efficient as it reduced the number of data points to be stored. The stored data could be downloaded every three weeks. However, during a rainfall event the MicroDac could save only cumulative rainfall over a period of 10 minutes and the real time that each tip of the rainfall gauge occurred could not be recorded. That meant that the hyetograph of each rainfall event (i.e. the development with time of the rainfall intensity of a rainfall event) could only be produced with a 10 minutes average intensity.

Protection and maintenance and troubleshooting of the instrumentation

The instruments as described above needed regular maintenance and protection. The tensiometers needed regular flushing using the flushing button of the jet-fill reservoir cap, in order to remove the air bubbles that developed from cavitation and air diffusion through the ceramic tip of the tensiometers. The flushing of the tensiometers was done at least every three weeks. In addition, the level of the water in the tube of the tensiometers needed to be checked during flushing. In order to slow down the development of fungus and algae, the tensiometers were filled with a sulphate solution. The regular maintenance of the instrumentation also included

thorough cleaning of the rainfall gauges. It was very often found that leaves from trees could fall inside the funnel of the rainfall gauges and prevent the free movement of the collected rainwater to the tipping bucket.

Figure 3.13 Example of a corroded pressure transducer, which were installed in the slopes, from left to right: new transducer, transducer used for 2 months and transducer used for more than 5 months.

During the operation of the data acquisition systems several problems were encountered due to the harsh environment of the field. These problems were usually related to corrosion of the pressure transducers (Figure 3.13) and to water seeping into the junction boxes and damaging connections and the data cables. Such problems with the acquisition system caused the occasional appearance of erroneous readings in the measured data. Such misleading readings usually included sudden changes in the measured data ('spikes') to very high absolute values of pressure (usually ±180 kPa). In addition, technical faults (corrupted files of data) in the NTU-CSE slope caused the loss of rainfall data during two weeks of February 2000. In order to minimise such electrical problems the data cables that were connecting the transducers with the data loggers were run within a rubberised conduit on the ground surface. The junction boxes were sealed carefully with a combination of silicon rubber and hard sealing tapes. Finally, all cables that were connected to the

two data loggers were first connected to fuses in order to protect the data loggers from lightning.

3.3.2 Instrumentation layout of the NTU-CSE slope

At the NTU-CSE slope 6 rows each containing 5 tensiometers were used to measure the pore-water pressures within the slope during the monitoring period. The rows of tensiometers were at a distance of 3m from each other and the tensiometers of each row were drilled at 0.5m from each other. The 5 tensiometers of each row at the NTU-CSE slope measured the pore-water pressures at 0.5m, 1.1m, 1.4m, 2.3m and 3.2m deep. Figure 3.14 presents the layout of the instrumentation that was installed and operated on the slope of the NTU-CSE slope. The rainfall was measured with a double tipping bucket rainfall gauge (Figure 3.15). The tensiometers and the rainfall gauge were installed at earlier time by Rahardjo (2000), while the acquisition system was installed and operated for the needs of the present work.

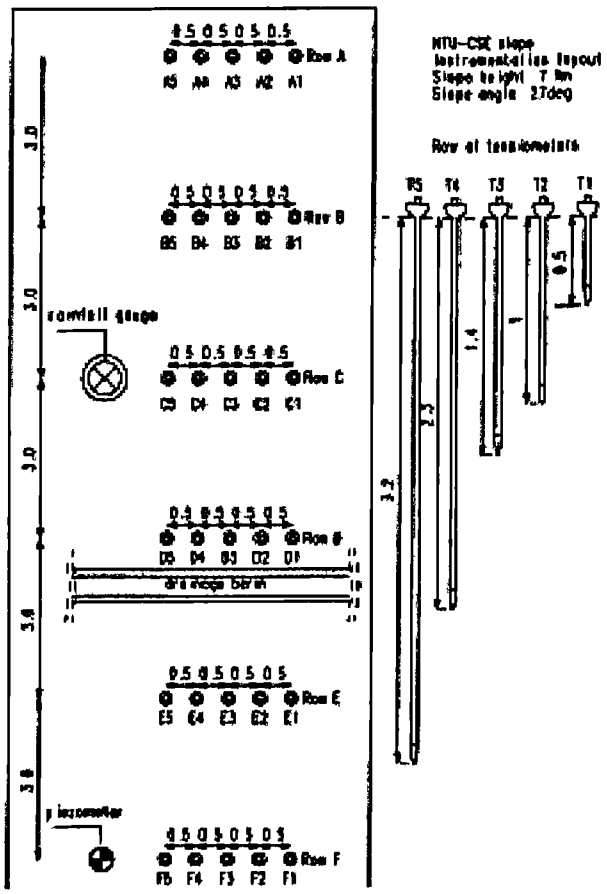

Figure 3.14 Layout of the instrumentation installed on the NTU-CSE slope.

The piezometer installed at the NTU-CSE site was not fitted with a depth transmitter. The water table at the NTU-CSE is relatively deep, and earlier work (Gasmo 1997) showed that the ground water table was not affected by rainfall.

Figure 3.15 Handar double tipping bucket rainfall gauge that is installed on the NTU-CSE slope.

3.3.3 Instrumentation layout of the NTU-ANX slope

The main instrumentation for the NTU-ANX slope consists of three rows, each containing 5 tensiometers, a rainfall gauge and a piezometer. Additionally to this instrumentation, a rainfall simulator was built and a device for measuring the runoff was also installed. Figure 3.16 presents the instrumentation installed on the NTU-ANX slope, where the layout of the tensiometers and the location of the

rainfall gauge, the piezometer and the storage box for the data acquisition system is shown. The spacing between each row was 3m and the tensiometers within each row were drilled at 0.5m distance from each other, measuring the pore-water pressures at 0.5m, 1.1m, 1.7m, 2.3m and 2.9m deep. The type of the tensiometer used in the NTU-ANX slope was the Jet-Fill tensiometer, model 2725 manufactured by Soilmoisture™ Equipment Corp. Santa Barbara, California. The rainfall gauge installed on the NTU-ANX slope was a tipping bucket with a single tip event of 0.25mm each (Figure 3.4). Rahardjo (2000) installed the tensiometers and the rainfall gauge at earlier time. The data acquisition system was housed next to the instrumentation area in a special storage box that protected the controller from the rainfall.

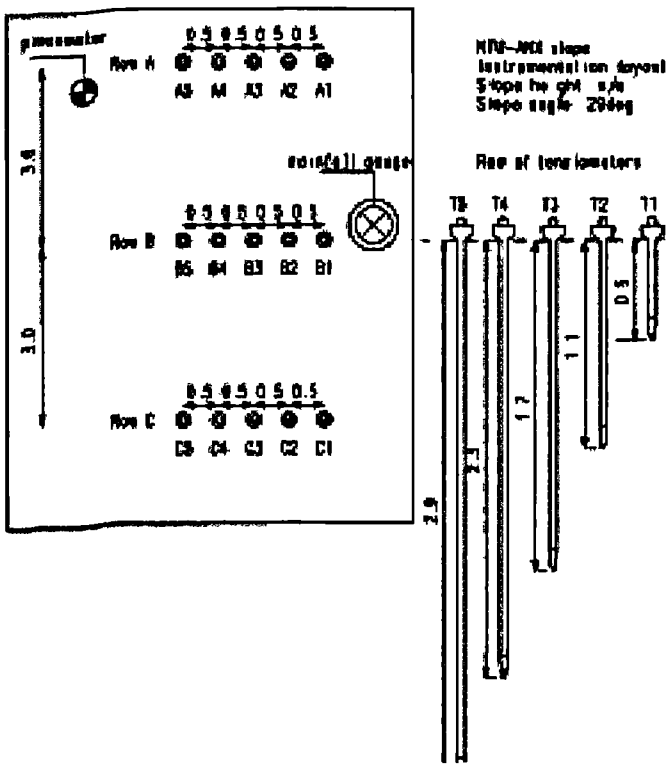

Figure 3.16 Layout of the instrumentation installed on the NTU-ANX slope.

3.3.4 Instrumentation for runoff measurements

Measurements of runoff of natural and simulated rainfall were also achieved on the NTU-ANX slope. Along the perimeter of the study area of the NTU-ANX slope corrugated sheets were driven 30 cm deep into the soil in order to create a small

catchment for the runoff (Figure 3.4). The rainfall water that ran off the slope was collected at the lowest point of the catchment. The measurement of runoff was achieved with the use of a Perspex flume and a capacitive water level probe (Figure 3.17). The flume was an in-house design (Lee et al. 1999) and had two points where the height of the water flow could be measured manually. For automating the measurement of the runoff a capacitive water level probe was installed in the flume. The probe was manufactured by UNIDATA^{TM}, model Starlog 6521J, is 0.5m high and made from strong PVC (UNIDATA 1990). The probe could measure water level in a range from 0m to 0.5m. The output range of the transducer was from 0V to 2.55V and required 5V power supply. The probe was connected with a Fluke Hydra 2635A data bucket, which was stored in the housing box of the acquisition system of the main instrumentation (Figure 3.18).

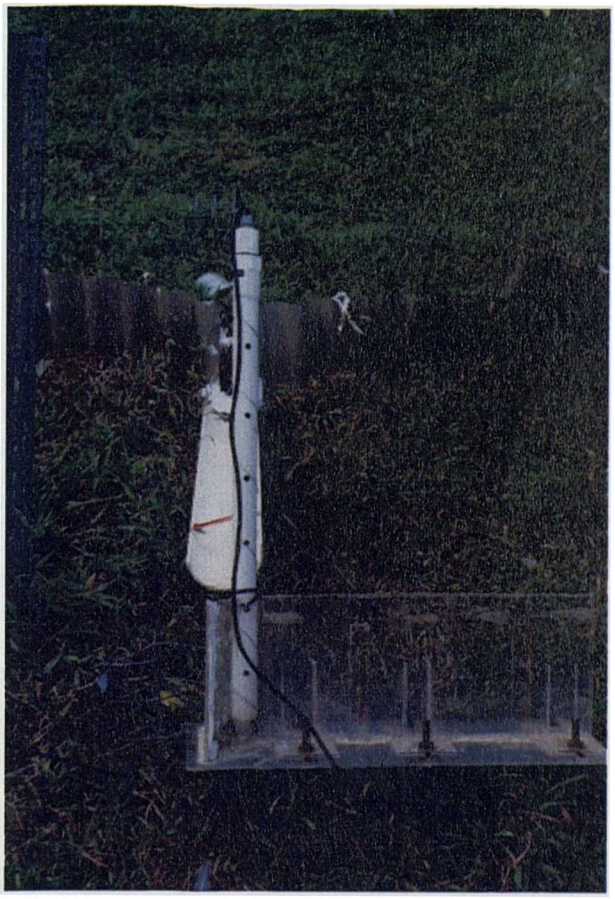

Figure 3.17 The Perspex flume with the capacitive water level probe, which was installed at that lower point of the catchment of NTU-ANX slope for the measurements of runoff.

The whole system of the probe and the Perspex flume was first calibrated in the

laboratory (Figure 3.19) and then installed carefully on the slope. The calibration procedure consisted of two parts. In the first part the probe was calibrated for different depths of water. This was achieved by inserting the probe vertically into a bucket of water. The height of the water level was measured and then the signal of the probe, expressed in volts, was monitored. The procedure was repeated for different heights of water level in the bucket. Figure 3.20 shows the linear changes of the probe's signal, expressed in volts for different heights of water level. It has to be noted that the calibration of the probe was done using an extension to the manufacturers cable, as was required for installation in the field. The extension of the data cable meant an increase in the resistance of the cable and thus an increase in the voltage signal, which the data logger could measure. For that reason for zero height of water level the signal of the probe was slightly greater than zero volts and for 0.5m height of water level the maximum signal of the probe was greater than 2.5V. In both cases the increase was 14mV. That meant, that with the use of the extension of the data cable, the capacitive water level probe could not measure any water level lower than 1cm (i.e. the resolution of the instrument was reduced from zero cm to 1cm of water level).

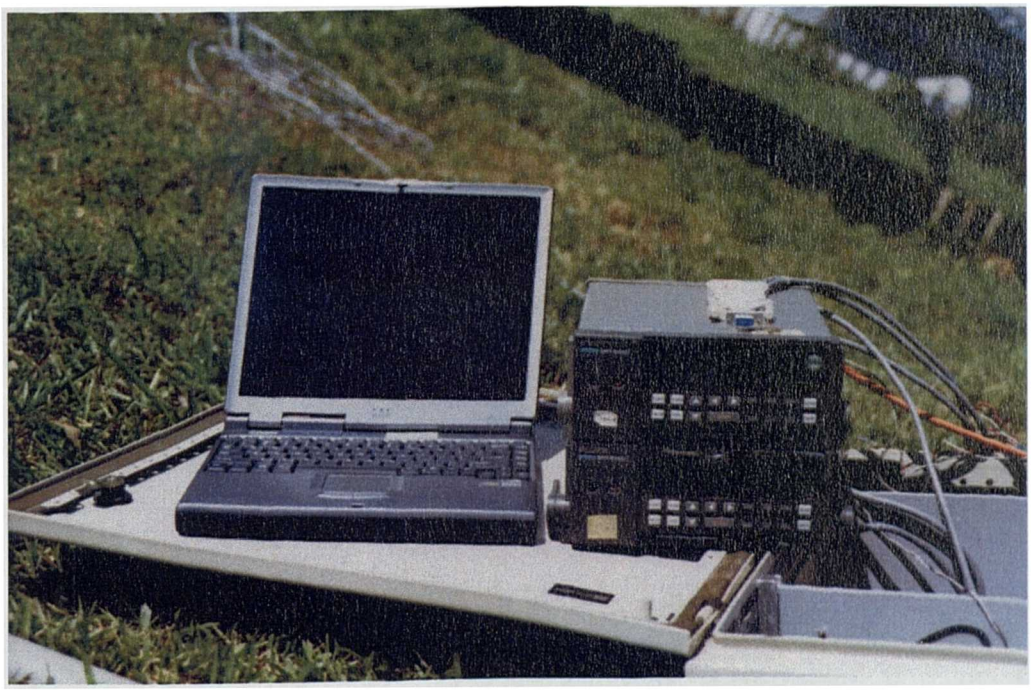

Figure 3.18 The set of two Hydra data bucket controllers (Fluke^{TM}) that were used for collecting the measurements of the capacitive water level probe and the additional rainfall gauge.

The second part of the calibration was to calibrate the Perspex flume and the capacitive water level probe for different water flows. For this part a flowmeter was used to measure the flow rate of the water coming into the flume. During this procedure the signal of the probe was monitored and the height of the water in the flume was also measured by reading the two rules in the flume, where the flow pattern was smooth (Lee et al. 1999). Figure 3.21 shows the non-linear changes of the probe's signal with different flow rates. Figure 3.22 presents the non-linear relation between the measured height of water in the flume and the water flow. The same figure shows the changes of water height in the flume, as measured using the probe with different water flow rates. From Figure 3.22 can be seen that for small flow rates the differences between the two curves are very small. However, as the flow rate in the flume increases the maximum error between the manual readings and the readings using the probe increases. The maximum error is less than 4% of the manual reading for flow rate equal to $3x10^{-4}m^3/s$ (i.e. 1100l/h).

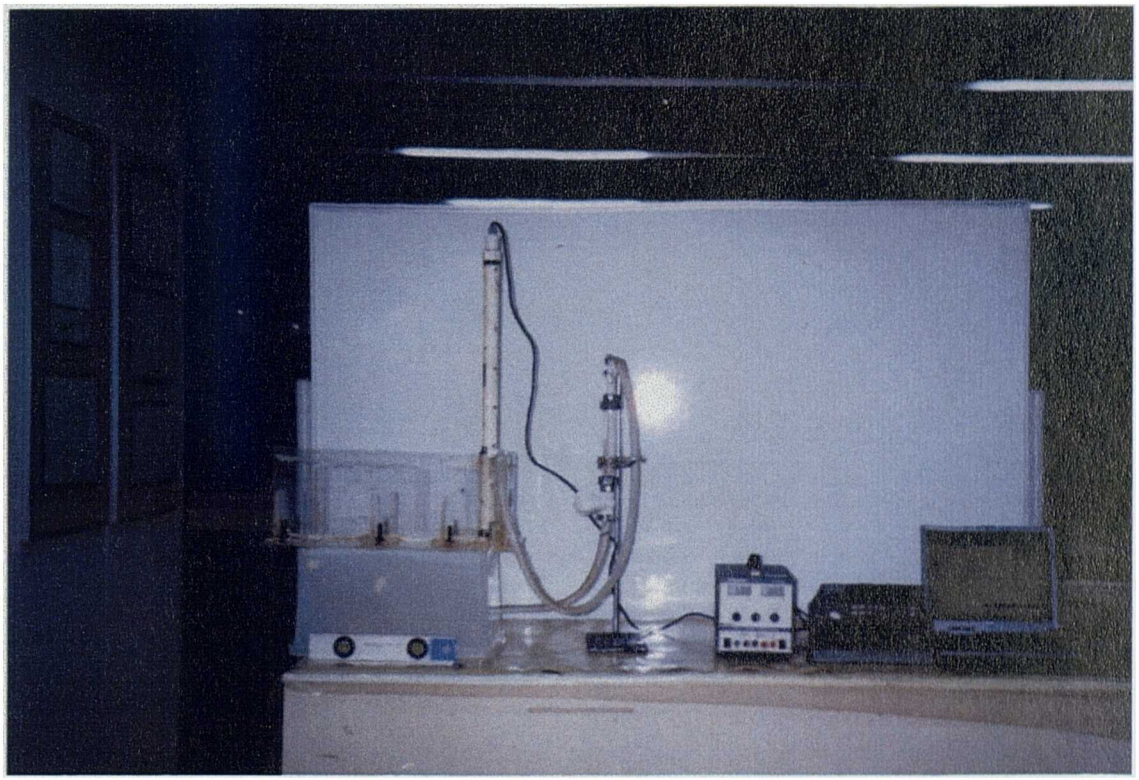

Figure 3.19 Calibration in the lab of the flume and the capacitive water level probe.

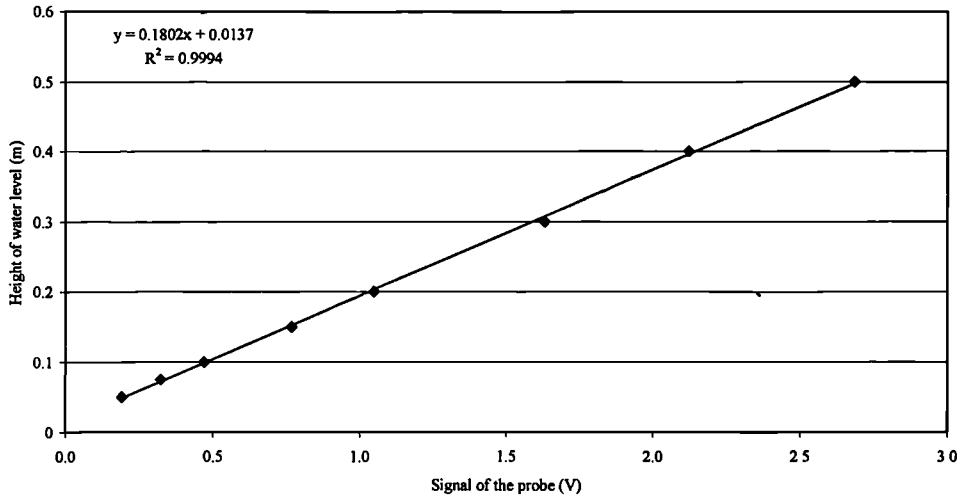

Figure 3.20 Calibration curve of the water level capacitive probe with height of water level.

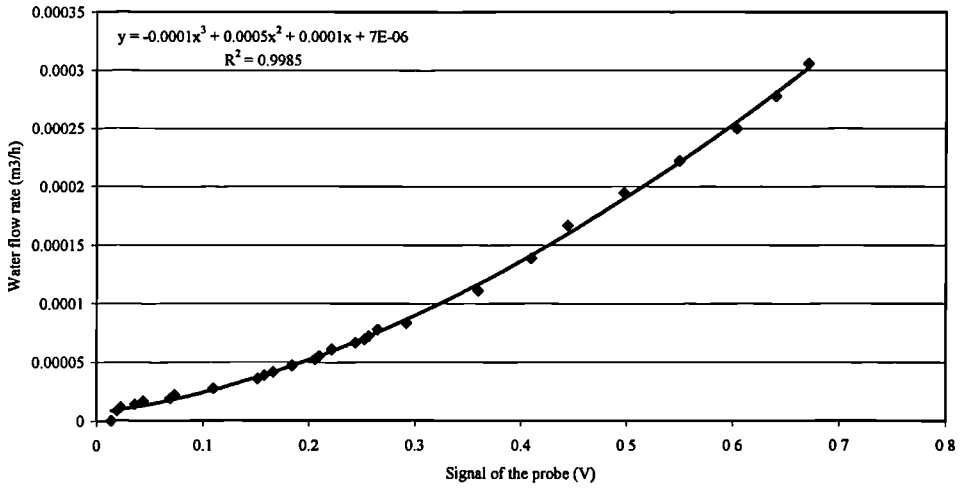

Figure 3.21 Calibration curve of the capacitive water level probe with rate of water flow in the Perspex flume.

The use of the capacitive water level probe in the flume proved to be a more accurate and consistent method than reading the indicator of the flume manually. Using the probe also made it possible to monitor the runoff of natural rainfall as automated data logging could be used. However, because of the cable extension of the probe that connects with the Hydra 2635A data bucket, very small flows of runoff could not be measured. The calibration of the probe with water level and with flow rate as these

are presented in Figure 3.20 to Figure 3.22, shows that the probe cannot measure water flow rates in the flume, which are smaller than $4x10^{-6}m^3/s$ (i.e. 14.4l/h). For the catchment of the NTU-ANX slope, a flow rate $4x10^{-6}m^3/s$ is equivalent to 1.1mm/h of runoff production. The Hydra 2635A data bucket was configured to take readings every 5 seconds. The data from the Hydra 2635A data bucket had to be downloaded very frequently, every 2 or 3 days.

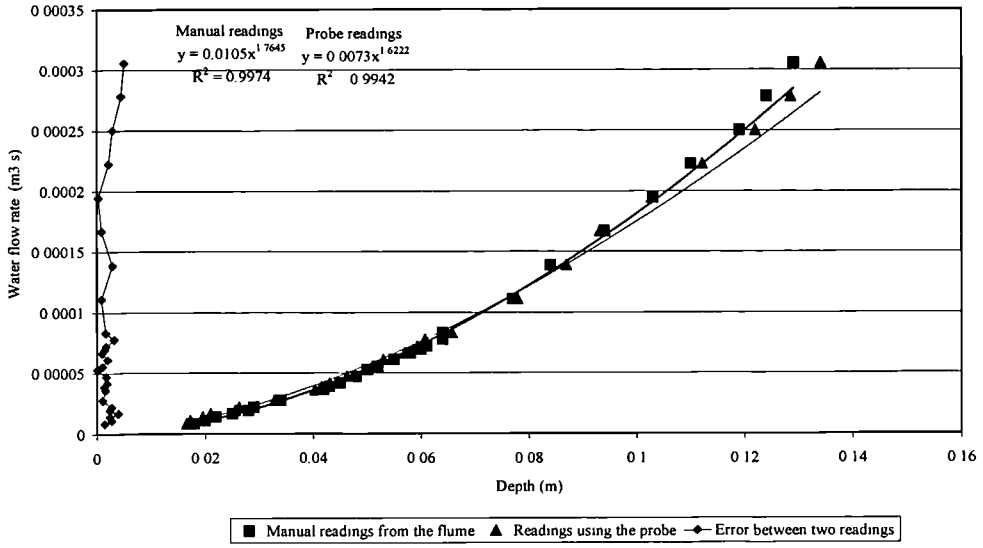

Figure 3.22 Flume calibration curve (manual and using the capacitive water level probe) with rate of water flow in the Perspex flume.

3.3.5 Rainfall simulator

A rainfall simulator was built in order to spray water with a controlled intensity on the study area of the NTU-ANX slope (Figure 3.23). The device was approximately 6m long, 3m wide and 2m high. The pipe system consisted of a combination of PVC pipes with internal diameter 16mm, 20mm, and 40mm. Three frames of slotted angle bars supported the pipe system. The three frames were connected to each other in order to ensure that the structure was stable.

A water tank, with dimensions 1.0x1.5x2.0m, was installed at the toe of the slope of the NTU-ANX slope. A fully submersible pump, model NOVA 600, delivered the water to the spraying sources with an adequate pressure. The output capacity of the pump was from $1m^3/h$ to $14.5m^3/h$ with a hydraulic head between 3.5m and 12m.

Two flowmeters of different measuring flow capacities were installed along the pipe system in order to measure the flow rate running into the system. The flowmeters were manufactured by Ryutai Kogyo Co. Ltd. and their measuring range of flow was from $0.25m^3/h$ to $2.5m^3/h$ for the big flowmeter and from $0.03m^3/h$ to $0.3m^3/h$ for the small flowmeter. Valves were also installed along the pipe system for adjusting the flow.

Figure 3.23 The rainfall simulator device installed on the NTU-ANX slope. Note the additional rainfall gauge installed on the research slope for measuring the intensity of the sprayed water.

The required rainfall intensity was achieved by a combination of microsprays of different capacities, manufactured by Netafim (Figure 3.24). The pipe system has 5 source-points with microsprays where water was sprayed on the study area. It was found that if the microsprays operated at a height of 1.8m then they could spray the water evenly over a circle of 2m diameter. The capacities that were used were between $0.04m^3/h$ and $0.14m^3/h$. Each combination of microsprays was calibrated to determine the exact rainfall intensity that could be produced. The calibration was made by covering the study area with PVC sheets (Figure 3.25) and collecting all the sprayed water in the flume. In addition, a second rainfall gauge was installed on the research slope measuring the rainfall intensity during each test.

Figure 3.24 Microsprays manufactured by Netafim that were used in the rainfall simulator.

Periodically, the rainfall gauge was moved to several points within the research slope to ensure that an even distribution of water was achieved. During each simulated rainfall PVC sheets from all sides covered the frame in order to minimise the influence on the outcome of the test from external factors such as wind or natural rainfall. The collection of runoff was done at the lower point of the slope using the same device used for the runoff measurements of natural rainfall.

Figure 3.25 Calibration of the rainfall simulator for different sets of sprinklers for the production of different rainfall intensities.

3.4 Field permeability measurements in the NTU-ANX slope

The in-situ coefficient of permeability of the surficial soil in the NTU-ANX slope was measured with a constant head well permeability test, using the Guelph permeameter method developed by Reynolds and Elrick (1986). Total hydraulic head is maintained constant during the test using the mariotte bottle principle (Figure 3.26). When a constant well height is established in the borehole, a saturated bulb develops around the borehole with a size depending on the soil type, the radius of the borehole and the water head in the borehole. Water infiltrates from this bulb in three dimensions.

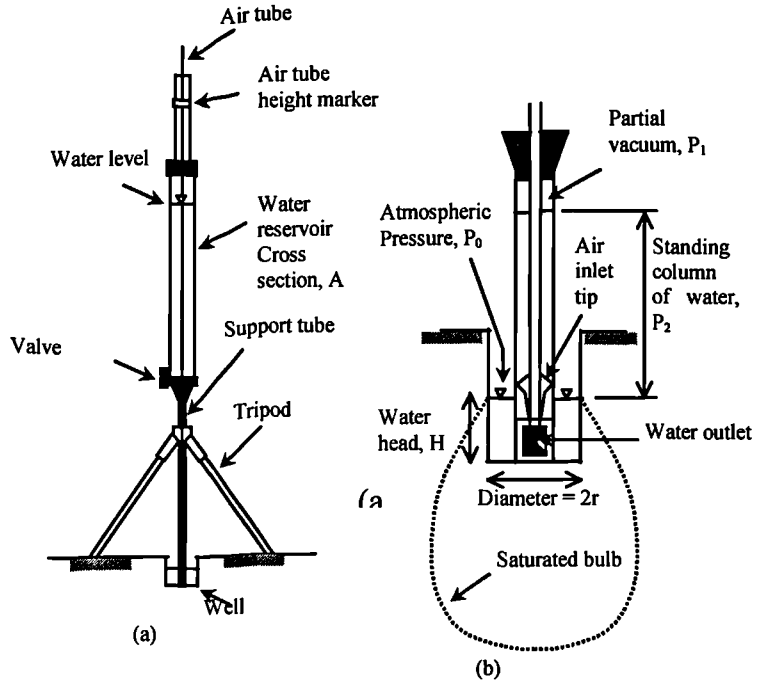

Figure 3.26 CHWP test (a) Guelph permeameter (b) Mariotte principle (after Agus et al. 1999).

The Guelph permeameter, which was used for the in-situ measurement of the saturated coefficient of permeability with respect to water of the soil was manufactured by Soilmoisture^{TM} Equipment Corp. Santa Barbara, California, model 2800 (Figure 3.27). The 6cm diameter borehole was drilled very close to the ground surface, about 30cm (i.e. just below the roots of the grass cover of the slope), using a hand auger and sizing auger. In addition, the smear layer that is usually produced from augering was removed with a brush. After the preparation of the borehole, the Guelph permeameter was inserted into the borehole and the reservoir of the permeameter was filled up with water. First a 10cm constant hydraulic head was developed, by monitoring the drop of the water level in the reservoir tube with time. When the drop of the water level in the tube (R) becomes constant with time, then it is assumed that steady-state flow conditions under 10cm constant hydraulic head are established. The same procedure is repeated for 15cm of constant hydraulic head.

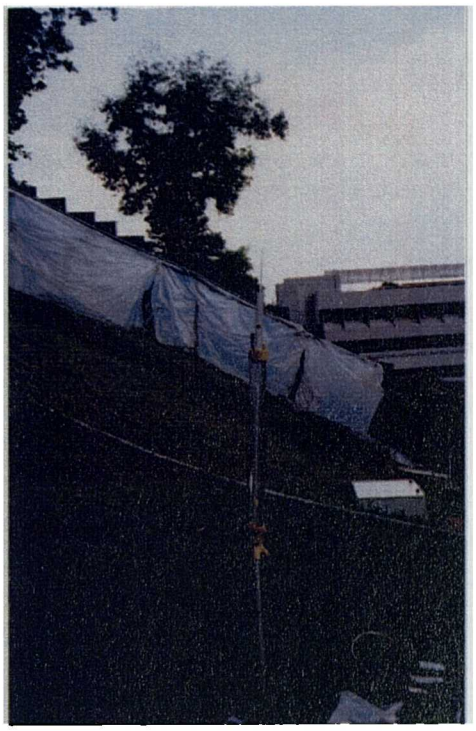

Figure 3.27 The Guelph permeameter, manufactured by Soilmoisture™ Equip. Barbara, California, model 2800.

Assuming that by the time the steady-state conditions in the borehole are established the soil has become fully saturated, then the saturated coefficient of permeability of the soil with respect to water (k_{sat}) can be determined from Equation (3.1), developed by Elrick and Reynolds (1992):

$$k_{sat} = \frac{CAR}{\left(2\pi H^2 + C\pi r^2\right)} \tag{3.1}$$

where; C is a dimensionless shape factor, which is given in Figure 3.28,

A is the cross-sectional area of the water reservoir,

R is the steady-state rate of fall of the water level in the water reservoir

H is the water level in the borehole or well head,

and r is the radius of the drilled borehole

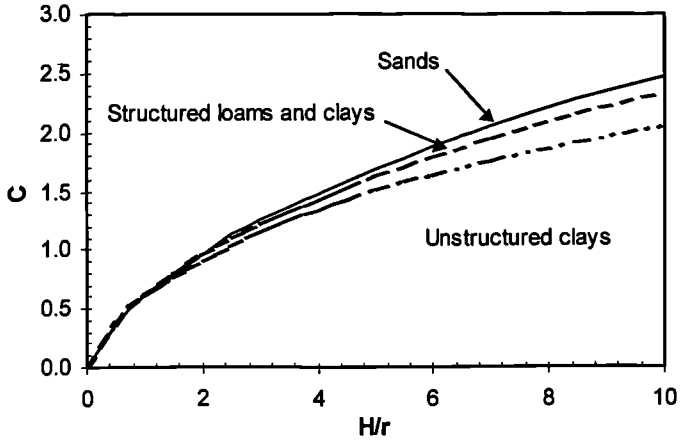

Figure 3.28 The dimensionless shape factor (C) for the calculation of the in-situ coefficient of permeability of the soil with respect to water (after Reynolds and Elrick, 1986).

3.5 Laboratory determination of soil-water characteristic curves

The soil-water characteristic curves of one soil sample from the NTU-CSE slope and two soil samples from the NTU-ANX slope were determined in the laboratory using a pressure plate apparatus. The pressure plate apparatuses, which were used were manufactured by Soilmoisture^{TM} Equipment Corp., Santa Barbara, California, models 1250 (Figure 3.29) and 1600 (Figure 3.30).

A cross section diagram of a pressure plate apparatus is shown in Figure 3.31. A pressure plate apparatus consists of a chamber, within which a fully saturated porous ceramic plate is installed. Below the porous ceramic plate exists a rubber membrane, called a bladder, filled with water. The soil specimens are put on top of the porous ceramic plate and air pressure is applied in the chamber. The applied air pressure in the chamber causes volumes of water, contained in the soil specimen, to flow through the porous ceramic stone towards the water, which is contained in the bladder. The water in the bladder is connected to an external burette through an outflow tube (Figure 3.31), thus the water in the bladder is under atmospheric pressure and can be assumed equal to zero (u_w=0). That means that once the soil specimen comes to equilibrium and no further reduction in the weight of the specimen takes place, the established suction in the soil specimen will be equal to the applied air pressure in the chamber.

Figure 3.29 The 1250 model pressure plate, manufactured by Soilmoisture™ Equip., Santa Barbara, California.

The accurate determination of the soil-water characteristic curve of a soil sample requires water flow from the soil specimen to the water in the bladder through the porous ceramic plate. In order to establish this flow the porous ceramic plate must be fully saturated, which means that no air exists within the pores of the ceramic plate. In practice, the porous ceramic plates have an air-entry value, which is the maximum air pressure above which air will start penetrating into the porous ceramic plate causing the desaturation of the plate. Therefore, during a test for the determination of the soil-water characteristic curve the applied air pressure in the chamber should not exceed the air-entry value of the porous ceramic stone.

Figure 3.30 The 1600 model pressure plate, manufactured by Soilmoisture™ Equip., Santa Barbara, California.

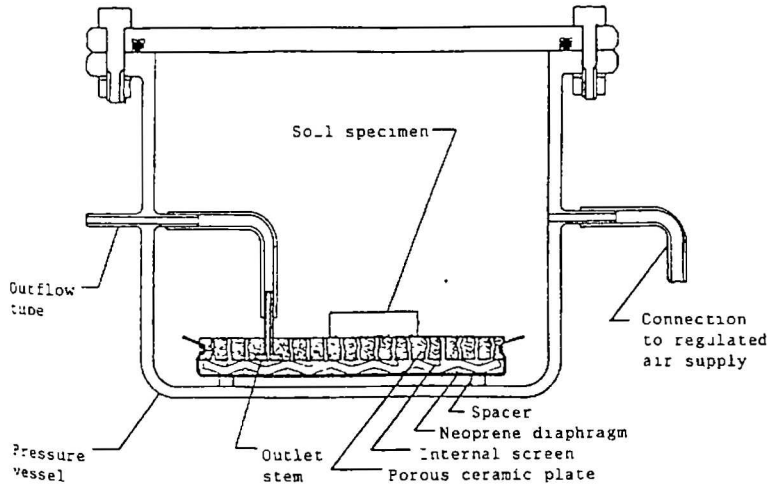

Figure 3.31 Cross section diagram of a pressure plate apparatus.

The 1250 and the 1600 pressure plate models of Soilmoisture™ Equip. in Figure

3.29 and Figure 3.30 were supplied with 2-bar and a 5-bar porous ceramic stones respectively (i.e. the air-entry values of the porous ceramic stones were 200kPa and 500kPa, respectively). That meant that with the 1250 pressure plate model the highest suction that could successfully be established was 200kPa, while with the 1600 pressure plate model the highest suction that could be established was 500kPa. The 2-bar porous ceramic plate has larger porosity than the 5-bar porous ceramic plate and therefore the 2-bar plate will have greater saturated permeability than the 5-bar plate. That means that water will flow at a higher rate from the soil specimen through the 2-bar pressure plate than it would through the 5-bar pressure plate. Therefore the equilibrium in the soil specimen at a specific negative pore-water pressure will be established faster with the use of the 1250 pressure plate model (carrying a 2-bar porous ceramic stone) than it will with the 1600 pressure plate model (carrying a 5-bar porous ceramic stone). Another advantage of the 1250 pressure plate model to the 1600 pressure plate model is that due to the small size of its chamber the effect of evaporation is very small. On the contrary the effect of evaporation in the 1600 pressure plate model must also be monitored during a test. However, due to the ability of the 1600 pressure plate model to apply suctions up to 500kPa a more realistic assumption for the residual water content of the soil specimen can be made.

The procedure of the test for the determination of the soil-water characteristic curves was as follows:

Preparation of the pressure plate

Before a test for the determination of the soil-water characteristic curve could begin it was important to saturate the porous ceramic plate. This was achieved by filling the chamber of the pressure plate with water and applying a high air pressure (e.g. 150kPa) in the chamber. Water would start flowing through the porous ceramic plate and gradually saturating it. When no air bubbles could be seen coming out of the outflow tube (Figure 3.31), then it was ensured that the pressure plate was fully saturated. The saturation of the porous ceramic plates lasted between 2 to 4 days.

Table 3.4 Summary of the soil specimens used for the determination of soil-water characteristic curves.

Specimen no	Slope	Depth (m)	Description	Dimensions of cylindrical samples (diameter x height)
1 & 2	NTU-ANX	1.50-2.30	Silty to sandy clay, brown to light orange.	6.5cm x 2cm
3	NTU-CSE	3.00-4.00	Sandy clay, purple, hard.	7.6cm x 4cm

Preparation of the soil specimens

Three soil specimens were used for the production of a series of soil-water characteristic curves. Table 3.4 presents a summary of the soil specimens. The soil specimens were trimmed carefully to retain their undisturbed properties. Before the soil specimens were placed in the pressure plate apparatus, they were saturated. The saturation of the soil specimens was achieved by placing a piece of wet cotton on top of the soil specimen. The soil specimens with the wet cotton remained in the humidator for at least 48 hours, or until their weight (without the cotton) was not increasing any further, indicating that they could not absorb any more water from the cotton.

Procedure of test and determination of the gravimetric water content

After the soil specimens were saturated they were weighed and placed on the saturated porous ceramic plate. The chamber of the pressure plate was closed and sealed with vacuum grease and air pressure was applied in the chamber. The weight of the soil specimens was monitored two times a day using a balance. When no decrease in the weight of the soil specimens was noticed for 24 hours, then it was assumed that the desired suctions were established in the soil specimens. Then the applied air pressure in the chamber was increased and the next step of the soil-water characteristic curve was started. The procedure was continued until the soil specimens reached the highest matric suction (i.e. 200kPa or 500kPa). Then the wetting phase was starting by decreasing the air pressure towards zero, following the same procedure as that described for the drying phase.

The selection of the pressure steps was carefully made in order to produce soil-water

characteristic curves with a sigmoid shape. This meant that initially small pressure steps were chosen in order to identify the air-entry value of the soil specimens and as the suctions were increasing, then the chosen pressure steps were also increased. The pressure steps that were chosen for the drying phase with the 2-bar pressure plate were from 0kPa to 10kPa, 20kPa, 40kPa, 60kPa, 80kPa, 100kPa, 150kPa to 200kPa and for the wetting phase from 200kPa to 100kPa, 60kPa, 20kPa, 10kPa and then back to 0kPa. A soil-water characteristic curve from sample 1 (Table 3.4) was determined in the 5-bar pressure plate. For this test the pressure steps that were selected for the drying phase were from 0kPa to 10kPa, 20kPa, 40kPa, 60kPa, 80kPa, 100kPa, 150kPa, 200kPa, 300kPa to 500kPa. In each pressure step the gravimetric water content (w) was calculated.

CHAPTER 4

Presentation of the Laboratory and Field Measurements

This chapter presents the laboratory tests and the field monitoring data from the NTU-CSE and NTU-ANX slopes. The data from the two slopes are presented in sections 4.1 and 4.2 respectively. The analysis period varies between the two slopes. The analyses period for each slope is summarized in Table 4.1. This chapter presents the pore-water pressure readings and the rainfall data for the total duration of the analyses period of the two slopes. Monthly changes of pore-water pressures and rainfall data of the NTU-CSE and NTU-ANX slopes can be found in Appendices A and B, respectively. The description of the instrumentation of the research slopes and of all the equipment used is presented in Chapter 3. Gaps in the record occur because of non-availability of data due to occasional instrument malfunction, as described in Chapter 3. Occasional 'spikes' in the record were observed indicating spurious readings from the transducers. These 'spikes' were removed to avoid obscuring the real behaviour.

Table 4.1 Analysis period for the field monitoring results from the research sites.

Site	Start of the Monitoring Period	Finish of the Monitoring Period	Duration (approximately in. months)
NTU-CSE	14-Aug-99	18-Aug-00	12
NTU-ANX	17-Mar-00	18-Aug-00	6

4.1 NTU-CSE slope

The field measurements at the instrumented NTU-CSE slope were pore-water pressures and rainfall data. The development of pore-water pressures with time was monitored using the several tensiometers installed at the site, while the rainfall data was obtained using the rainfall gauge. In addition, a soil-water characteristic curve was produced in the laboratory using a pressure plate. The soil-water characteristic curve is from a soil specimen from layer 3 (purple sand clay) of the NTU-CSE slope (Sections 3.2 and 3.5).

4.1.1 Soil-water characteristic curve

A gravimetric soil-water characteristic curve was produced from a sample of Layer 3 using the 2-bar pressure plate (Section 3.5). The soil specimen had a 7.6cm diameter and 4cm height. Table 4.2 presents a summary of the data points of the gravimetric soil-water characteristic curve and Figure 4.1 presents in a logarithmic scale the plot of the gravimetric soil-water characteristic curve. The gravimetric water content of the sample at saturation was measured 13% and when -100kPa of pore-water pressure was established in the sample its gravimetric water content was reduced from 13% to 10%. The air entry value of the gravimetric soil-water characteristic curve in Figure 4.1 is approximately 2kPa.

Table 4.2 Data points of the soil-water characteristic curve of a soil specimen from the NTU-CSE slope.

Pore-water pressure (kPa)	Gravimetric water content (%)
0 (saturation)	13.5
-10	12.8
-15	12.6
-20	12.5
-30	12.2
-40	11.7
-60	11.1
-100	10.0

4.1.2 Rainfall gauge

The total rainfall that was recorded in NTU-CSE slope was 1552mm over the one-year period. This gives an average monthly total rainfall of 119mm. The wettest period of the year was from October to December 1999 with 615mm of total rainfall and the driest period of the year was from April to June 2000 with 279mm of total rainfall. Figure 4.2 presents a summary of the rainfall distribution from the data collected by the rainfall gauge. The data in this graph is presented as the daily rainfall (i.e. the total amount of rainfall captured in a 24-hour period).

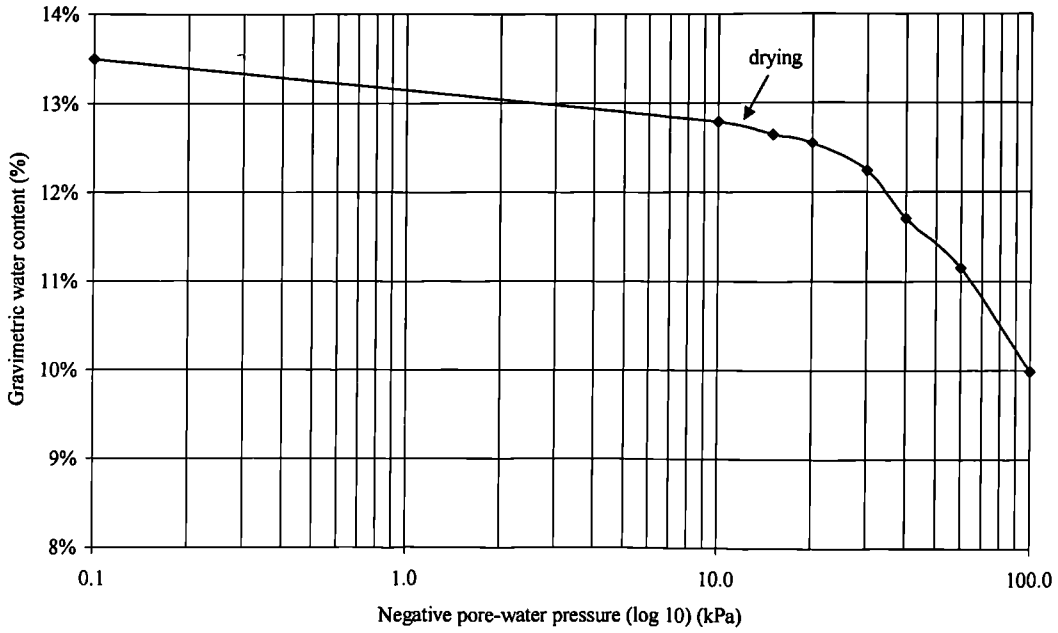

Figure 4.1 Soil-water characteristic curve from the NTU-CSE slope.

In addition to the daily rainfall, the rainfall data has been analysed to identify rainfall events (i.e. periods of significant rainfall separated by periods of no rain). A rainfall event is considered that ends after a time period of 20 minutes, during which no tip on the rainfall gauge occurred. All rainfall events with a total rain above 5mm that were measured on NTU-CSE slope during the studied period are summarised in Table 4.3. Out of the 1552mm annual rainfall, the 1348mm was precipitated during 70 rainfall events having a total rainfall greater than 5mm. The rainfall of each of those 70 rainfall events was ranging from 5 to 125mm with an average of 19mm. The average rainfall intensity of each individual event was ranging from 1mm/h to 31mm/h with an average of 11mm/h. Table 4.3 also presents the related details such as the time that each rainfall event took place, the duration and the average intensity.

In Table 4.4 the monitoring period is divided into sub-periods of significant rainfall and of low rainfall. This subdivision of the monitoring period takes into account the average daily rainfall over each period. A wet period has an average daily rainfall that exceeds the 10mm per day, while a dry period has an average daily rainfall smaller than 2mm per day.

Table 4.3 Summary of significant rainfall events in the NTU-CSE slope for the analysis period.

Event No.	Event start time	Event finish time	Rainfall (mm)	Duration (hours)	Average intensity (mm/h)
1	24-Aug-99 14:12	24-Aug-99 15:40	5.75	1.47	3.9
2	25-Aug 99 15:31	25-Aug-99 19:40	22.75	4.15	5.5
3	29-Aug-99 10:18	29-Aug-99 13:30	56.25	3.20	17.6
4	09-Sept-99 15:12	09-Sept-99 17:30	5.25	2.30	2.3
5	10-Sept-99 05:19	10-Sept-99 05:43	6.75	0.40	16.9
6	10-Sept-99 16:19	10-Sept-99 16:44	6.75	0.42	16.2
7	25-Sept-99 14:16	25-Sept-99 16:03	13.75	1.78	7.7
8	27-Sept-99 11:07	27-Sept-99 12:36	9.25	1.48	6.2
9	29-Sept-99 09:31	29-Sept-99 10:42	33.25	1.18	28.1
10	30-Sept-99 05:24	30-Sept-99 08:06	10.25	2.70	3.8
11	02-Oct-99 13:06	02-Oct-99 13:42	7.50	0.60	12.5
12	04-Oct-99 00:49	04-Oct-99 03:30	40.00	2.68	14.9
13	06-Oct-99 16:04	06-Oct-99 17:53	38.50	1.82	21.2
14	11-Oct-99 14:57	11-Oct-99 15:46	9.75	0.82	11.9
15	12-Oct-99 12:05	12-Oct-99 16:05	10.00	4.00	2.5
16	13-Oct-99 22:18	13-Oct-99 23:58	5.25	1.67	3.2
17	21-Oct-99 06:38	21-Oct-99 07:28	5.25	0.83	6.3
18	23-Oct-99 04:53	23-Oct-99 07:31	13.75	2.63	5.2
19	24-Oct-99 01:24	24-Oct-99 04:00	28.25	2.60	10.9
20	25-Oct-99 02:03	25-Oct-99 03:57	9.25	1.9	4.9
21	27-Oct-99 12:09	27-Oct-99 13:16	5.25	1.12	4.7
22	28-Oct-99 14:39	28-Oct-99 17:37	12.75	2.97	4.3
23	03-Nov-99 03:36	03-Nov-99 06:03	18.50	2.45	7.6
24	11-Nov-99 13:06	11-Nov-99 16:18	46.00	3.20	14.4
25	12-Nov-00 16:52	12-Nov-00 17:16	6.00	0.40	15.0
26	16-Nov-99 16:30	16-Nov-99 19:06	11.00	2.60	4.2
27	17-Nov-99 13:20	17-Nov-99 15:18	45.00	1.97	22.9
28	18-Nov-99 15:01	18-Nov-99 16:10	9.75	1.15	8.5
29	20-Nov-99 04:42	20-Nov-99 05:13	9.75	0.52	18.9
30	29-Nov-99 19:13	29-Nov-99 22:16	5.75	3.05	1.9
31	03-Dec-99 06:29	03-Dec-99 09:46	6.00	3.25	1.9
32	03-Dec-99 21:22	03-Dec-99 22:24	11.75	1.03	11.4
33	04-Dec-99 00:37	04-Dec-99 04:56	75.50	4.31	17.5
34	06-Dec-99 00:10	06-Dec-99 06:59	86.25	6.82	12.7
35	18-Dec-99 22:06	18-Dec-99 23:58	15.25	1.87	8.2
36	19-Dec-99 00:06	19-Dec-99 03:10	5.50	3.06	1.8
37	19-Dec-99 16:34	19-Dec-99 19:34	9.75	3.00	3.3
38	12-Jan-00 16:31	12-Jan-00 17:27	8.25	0.93	8.8
39	17-Jan-00 14:16	17-Jan-00 17:24	36.25	3.13	11.6
40	17-Jan-00 18:59	17-Jan-00 22:58	5.00	3.98	1.3
41	18-Jan-00 18:02	18-Jan-00 18:51	5.50	0.82	6.7
42	19-Jan-00 13:08	19-Jan-00 15:09	28.50	2.02	14.1
43	22-Jan-00 15:09	22-Jan-00 15:24	6.25	0.25	25.0
44	23-Mar-00 20:02	23-Mar-00 21:08	17.75	1.10	16.1
45	24-Mar-00 06:20	24-Mar-00 08:13	22.25	1.88	11.8
46	28-Mar-00 16:14	28-Mar-00 21:27	23.75	5.22	4.6
47	30-Mar-00 15:57	30-Mar-00 16:51	11.00	1.07	10.3

Event No.	Event start time	Event finish time	Rainfall (mm)	Duration (hours)	Average intensity (mm/h)
48	03-Apr-00 03:20	03-Apr-00 04:03	5.25	0.72	7.3
49	06-Apr-00 13:16	06-Apr-00 16:05	37.00	2.82	13.1
50	20-Apr-00 16:53	20-Apr-00 17:35	17.25	0.70	24.6
51	21-Apr-00 13:46	21-Apr-00 15:22	26.25	1.60	16.4
52	27-Apr-00 09:22	27-Apr-00 09:39	8.75	0.28	30.9
53	18-May-00 09:22	18-May-00 10:22	15.75	1.00	15.7
54	24-May-00 14:52	24-May-00 16:56	9.25	2.07	4.5
55	25-May-00 17:04	25-May-00 18:17	14.25	1.22	11.7
56	27-May-00 16:04	27-May-00 18:36	20.25	2.53	8.0
57	02-Jun-00 10:30	02-Jun-00 14:12	6.75	3.70	1.8
58	05-Jun-00 14:19	05-Jun-00 16:03	5.25	1.73	3.0
59	11-Jun-00 05:13	11-Jun-00 11:50	41.25	5	8.3
60	28-Jun-00 06:06	28-Jun-00 07:17	7.75	1.25	6.2
61	24-Jul-00 04:59	24-Jul-00 13:12	125.5	9	13.9
62	15-Aug-00 22:17	15-Aug-00 23:50	41.75	1.5	27.8
63	16-Aug-00 00:16	16-Aug-00 03:37	15.75	3	5.3

Table 4.4 Summary of wet and dry periods in the NTU-CSE and NTU-ANX sites for the analysis periods.

Period start	Period finish	Period description	Rainfall (mm)
14-Aug-99	24-Aug-99	Dry period 1	18.00
24-Aug-99	29-Aug 99	Wet period 1	84.25
30-Aug-99	23-Sept-99	Dry period 2	28.25
24-Sept-99	13-Oct-99	Wet period 2	194.00
14-Oct-99	22-Oct-99	Dry period 3	13.00
23-Oct-99	02-Nov-99	Wet period 3	104.00
03-Nov-99	10-Nov-99	Dry period 4	0.50
11-Nov-99	20-Nov-99	Wet period 4	139.75
21-Nov-99	02-Dec-99	Dry period 5	12.50
03-Dec-99	06-Dec-99	Wet period 5	180.75
07-Dec-99	30-Dec-99	Dry period 6	41.75
10-Jan-00	16-Jan-00	Dry period 7	21.00
17-Jan-00	24-Jan-00	Wet period 6	84.00
24-Jan-00	13-Feb-00	Dry period 8	3.25
29-Feb-00	16-Mar-00	Dry period 9	2.75
17-Mar-00	30-Mar-00	Wet period 7	106.00
31-Mar-00	05-Apr-00	Dry period 10	6.00
06-Apr-00	10-Apr-00	Wet period 8	45.00
11-Apr-00	19-Apr-00	Dry period 11	3.00
20-Apr-00	21-Apr-00	Wet period 9	44.00
22-Apr-00	17-May-00	Dry period 12	12.25
18-May-00	18-May-00	Wet period 10	15.75
19-May-00	23-May-00	Dry period 13	0.00
24-May-00	27-May-00	Wet period 11	43.75
28-May-00	01-Jun-00	Dry period 14	2.75
02-Jun-00	05-Jun-00	Wet period 12	22.00
06-Jun-00	10-Jun-00	Dry period 15	3.00
11-Jun-00	19-Jun-00	Wet period 13	75.75

Period start	Period finish	Period description	Rainfall (mm)
20-Jun-00	27-Jun-00	Dry period 16	0.50
28-Jun-00	05-Jul-00	Wet period 14	28.00
06-Jul-00	11-Jul-00	Dry period 17	0.00
12-Jul-00	31-Jul-00	Wet period 15	141.25
01-Aug-00	06-Aug-00	Dry period 18	14.50
07-Aug-00	10-Aug-00	Wet period 16	3.50
11-Aug-00	14-Aug-00	Dry period 19	2.75
15-Aug-00	18-Aug-00	Wet period 17	57.5
		Total:	1551.75

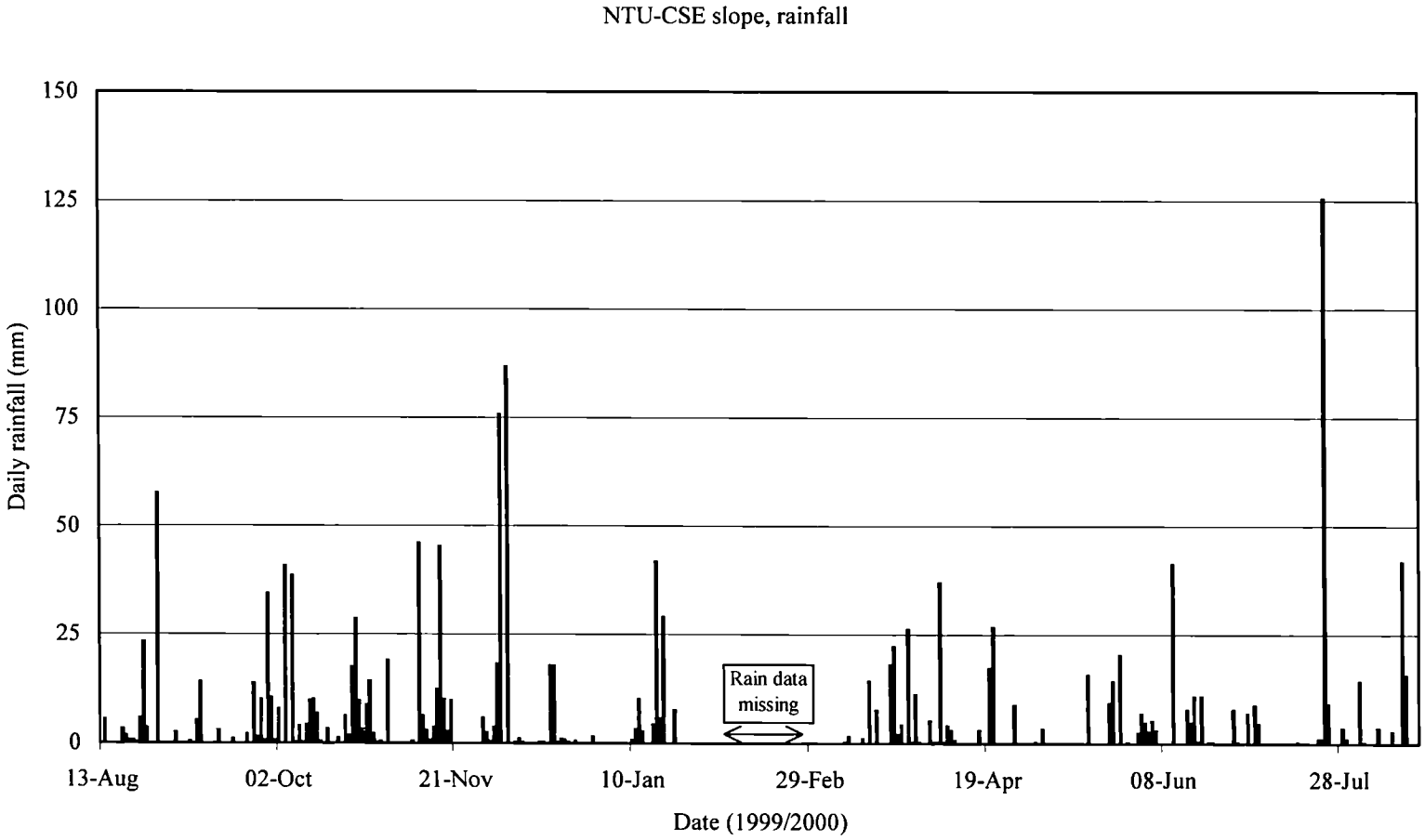

Figure 4.2 Summary of rainfall gauge data at the NTU-CSE slope for the analysis period.

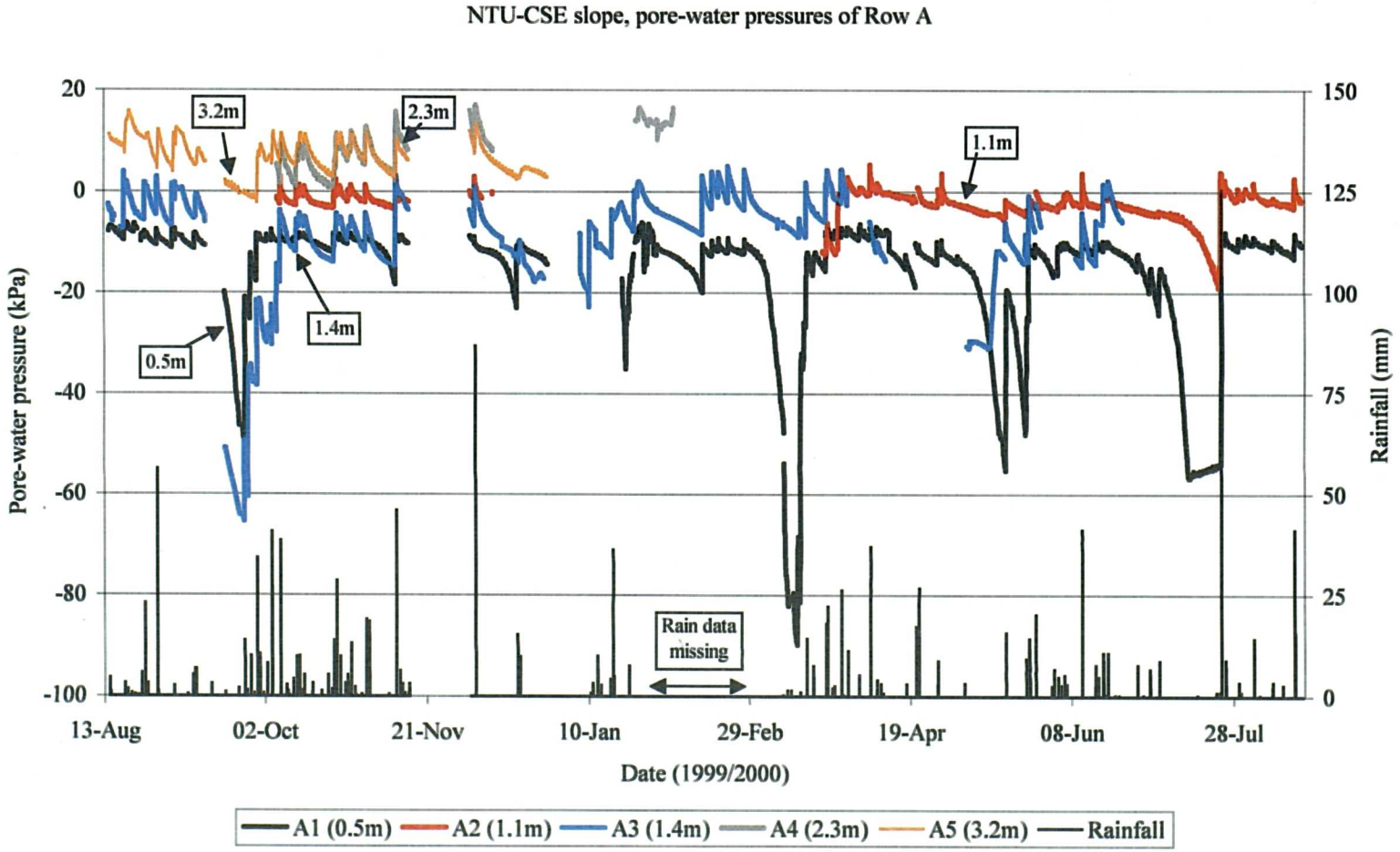

Figure 4.3 Tensiometer readings from Row A at the NTU-CSE slope for the studied period.

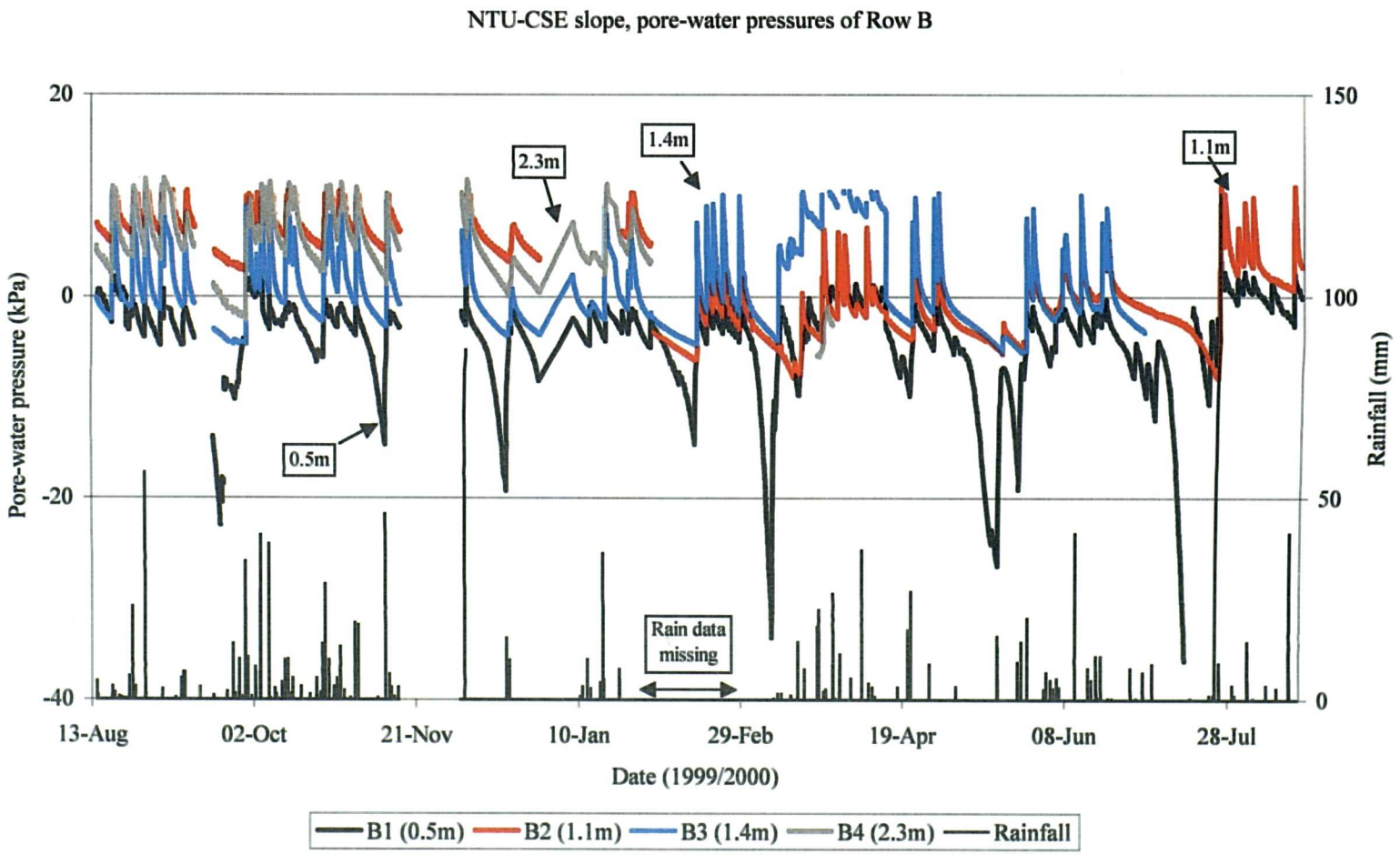

Figure 4.4 Tensiometer readings from Row B at the NTU-CSE slope for the studied period.

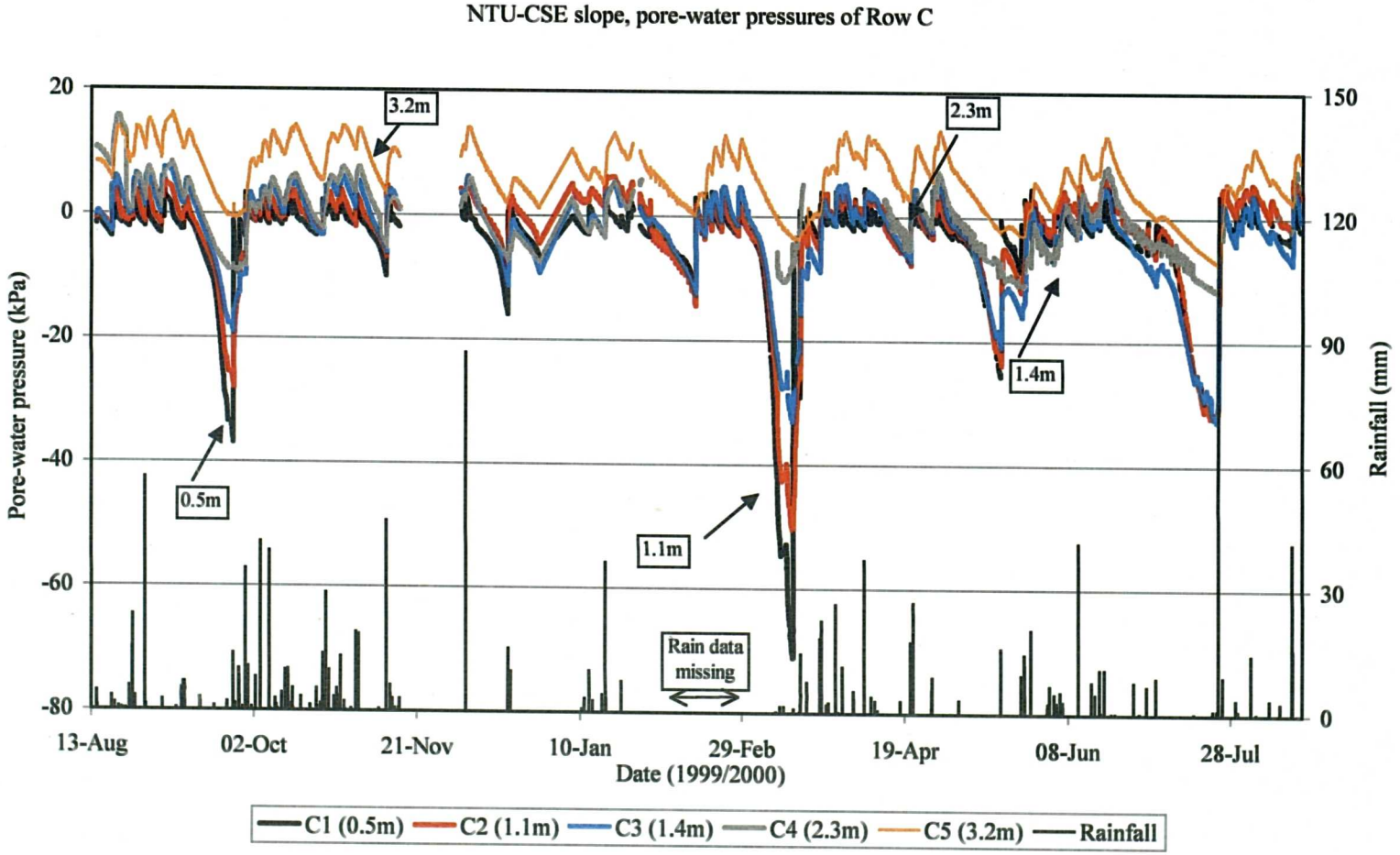

Figure 4.5 Tensiometer readings from Row C at the NTU-CSE slope for the studied period.

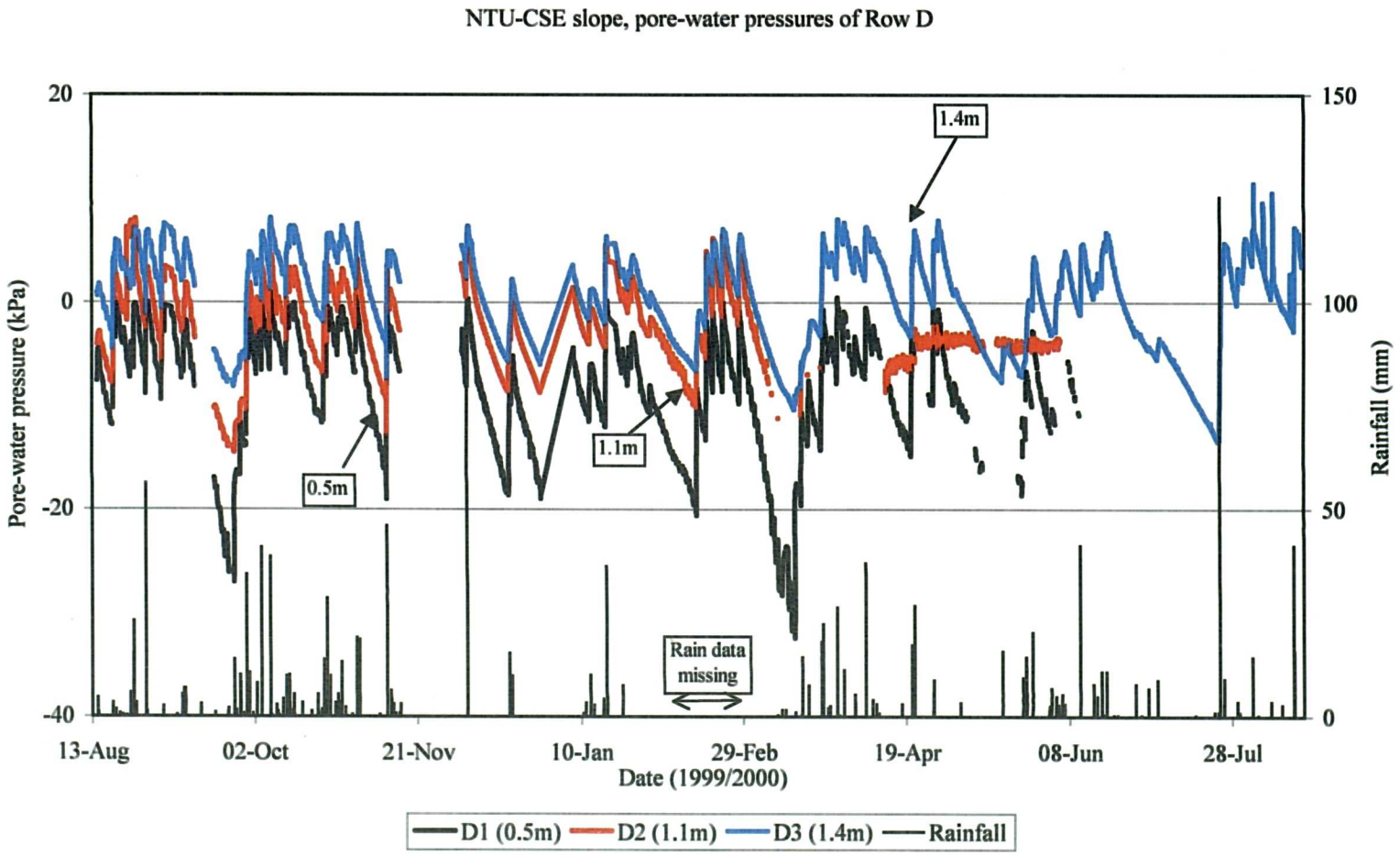

Figure 4.6 Tensiometer readings from Row D at the NTU-CSE slope for the studied period.

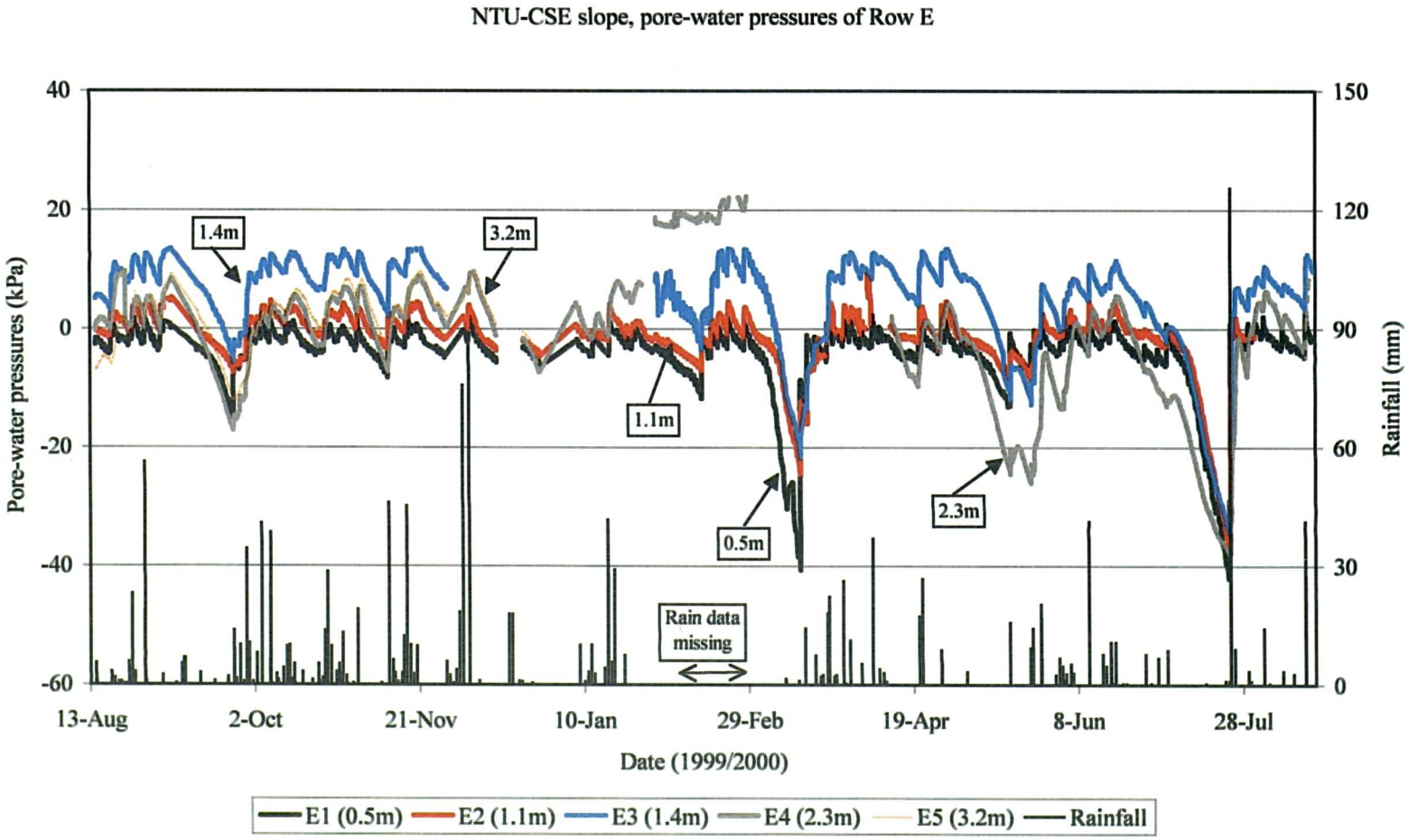

Figure 4.7 *Tensiometer readings from Row E at the NTU-CSE slope for the studied period.*

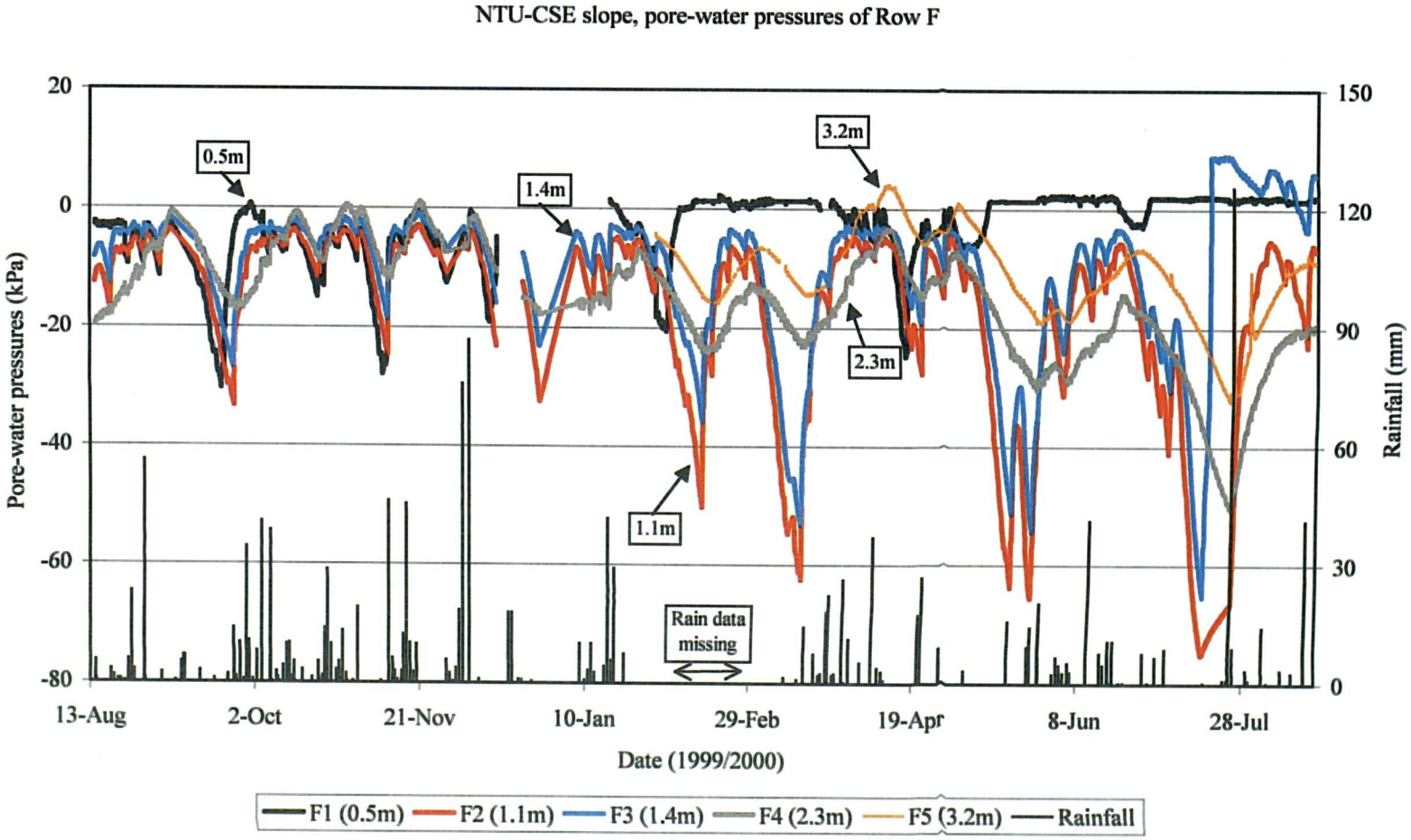

Figure 4.8 Tensiometer readings from Row F at the NTU-CSE slope for the studied period.

4.1.3 Tensiometers

The development of the pore-water pressures with time for the instrumented slope of NTU-CSE site are presented in Figure 4.3 through Figure 4.8 as they were measured by the tensiometers of rows A (crest) through F (toe) accordingly (Figure 3.15). The same figures present the available rainfall data in order to study the development of the pore-water pressures at each depth due to infiltration. Table 4.5 summarises the minimum and maximum measurements of all tensiometers for the studied period in the NTU-CSE slope. It has to be noted that as the studied period is relatively long (12 continuous months) the pressure transducers that were connected on the tensiometers failed or were damaged periodically due to the harsh environment that they were exposed to. Those erroneous readings were excluded from the data presented. The range of readings for each depth in the NTU-CSE slope, provided in Table 4.5 is also presented in Figure 4.9.

Table 4.5 Summary of tensiometer readings at the NTU-CSE slope.

Tensiometer	Depth (m)	Maximum (kPa)	Date of maximum	Minimum (kPa)	Date of minimum
A1	0.5	-6.0	19-Aug-99 07:40	-89.8	14-Mar-00 16:25
A2	1.1	8.9	08-Dec-99 10:23	-12.7	23-Mar-00 17:54
A3	1.4	5.1	22-Feb-00 16:51	-65.3	25-Sep-99 10:17
A4	2.3	16.5	05-Feb-00 5:29	0.7	22-Oct-99 22:30
A5	3.2	15.9	20-Aug-00 16:20	-2.2	29-Sep-99 10:30
B1	0.5	2.9	19-Aug-99 07:40	-33.9	09-Mar-00 17:16
B2	1.1	10.5	06-Sep-00 18:33	-8.0	15-Mar-00 16:05
B3	1.4	10.5	01-Apr-00 06:48	-5.6	24-May-00 15:05
B4	2.3	11.8	04-Sep-99 11:02	-6.0	23-Mar-00 10:54
B5	3.2	-	-	-	-
C1	0.5	5.0	06-May-00 19:29	-71.2	15-Mar-00 14:45
C2	1.1	6.3	18-Jan-00 4:57	-50.5	15-Mar-00 09:45
C3	1.4	7.4	04-Sep-99 08:42	-33.4	15-Mar-00 15:45
C4	2.3	22.4	27-Mar-00 04:54	-11.1	25-May-00 08:05
C5	3.2	16.1	06-Sep-99 16:53	-3.8	15-Mar-00 23:45
D1	0.5	1.0	07-Oct-99 01:19	-32.0	15-Mar-00 15:25
D2	1.1	8.1	26-Aug-99 08:34	-14.5	25-Sep-99 14:37
D3	1.4	8.2	07-Oct-99 01:19	-10.3	15-Mar-00 13:05
D4	2.3	-	-	-	-
D5	3.2	-	-	-	-
E1	0.5	2.9	02-Nov-99 06:00	-40.6	15-Mar-00 15:45
E2	1.1	10.0	05-Apr-00 00:43	-24.9	15-Mar-00 16:05
E3	1.4	13.5	06-Sep-99 16:33	-21.7	15-Mar-00 16:45
E4	2.3	22.4	28-Feb-00 23:10	-25.9	24-May-00 15:40
E5	3.2	9.75	21-Nov-99 16:10	-12.2	25-Sep-99 16:37
F1	0.5	2.4	29-May-00 22:37	-30.7	21-Sep-99 22:37

Tensiometer	Depth (m)	Maximum (kPa)	Date of maximum	Minimum (kPa)	Date of minimum
F2	1.1	-2.9	21-Nov-99 02:30	-65.5	24-May-00 15:00
F3	1.4	-0.7	20-Nov-99 16:50	-54.3	24-May-00 16:00
F4	2.3	1.1	21-Nov-99 07:50	-30.4	24-May-00 17:20
F5	3.2	4.2	10-Apr-00 17:23	-19.2	27-May-00 16:40

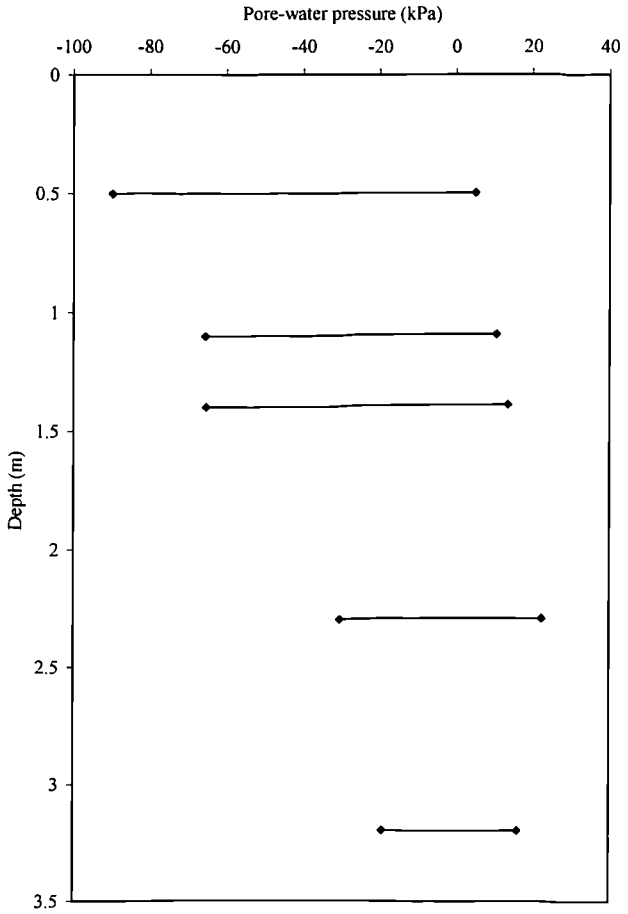

Figure 4.9 Recorded range of pore-water pressure with depth at the NTU-CSE slope (i.e., all rows combined).

4.2 NTU-ANX slope

The field measurements at the instrumented NTU-ANX slope were pore-water pressures, depth of the piezometric line, rainfall data and measurements of the coefficient of permeability with respect to water of soil Layer 1 (Section 3.2). The development of pore-water pressures with time was monitored using several tensiometers installed on the site, while the depth of the piezometric line was monitored using a Casagrande piezometer, fitted with a depth transducer. The

rainfall data were obtained from a rainfall gauge. Finally, three gravimetric soil-water characteristic curves of two soil-specimens (Section 3.5) were produced using a 2-bar and a 5-bar pressure plate. The equipment and the instrumentation of the NTU-ANX slope are presented in Chapter 3.

4.2.1 Soil-water characteristic curves

Four gravimetric soil-water characteristic curves of two soil specimens from the surficial soil Layer 1 of NTU-ANX slope were produced in the laboratory with pressure plates. The two soil specimens (specimens 1 and 2) had a 6.5cm diameter and were 2cm high. Figure 4.10Figure 4.11 present the gravimetric soil-water characteristic curves of soil specimen 1 and 2, respectively. Table 4.6 and Table **4.7** present the data points of the gravimetric characteristic curves of the soil specimens 1 and 2, respectively. The gravimetric soil-water characteristic curve no. 1 of soil specimen 1 (Figure 4.10) has a drying and wetting phase. A hysteresis may be observed between the drying and wetting phase for negative pore-water pressure range from –100 to –20kPa. The gravimetric water content at saturation of the two soil specimens is between 40 and 43% (Figure 4.10Figure 4.11). The air entry value of the two specimens has a value close to zero. When the negative pore-water pressure in the soil specimens were equal to –200kPa the gravimetric water content for both samples was 31%. For the soil specimen 1, when the negative pore-water pressures were increased further to –500kPa then the gravimetric water content was measured to be 28% (Figure 4.10).

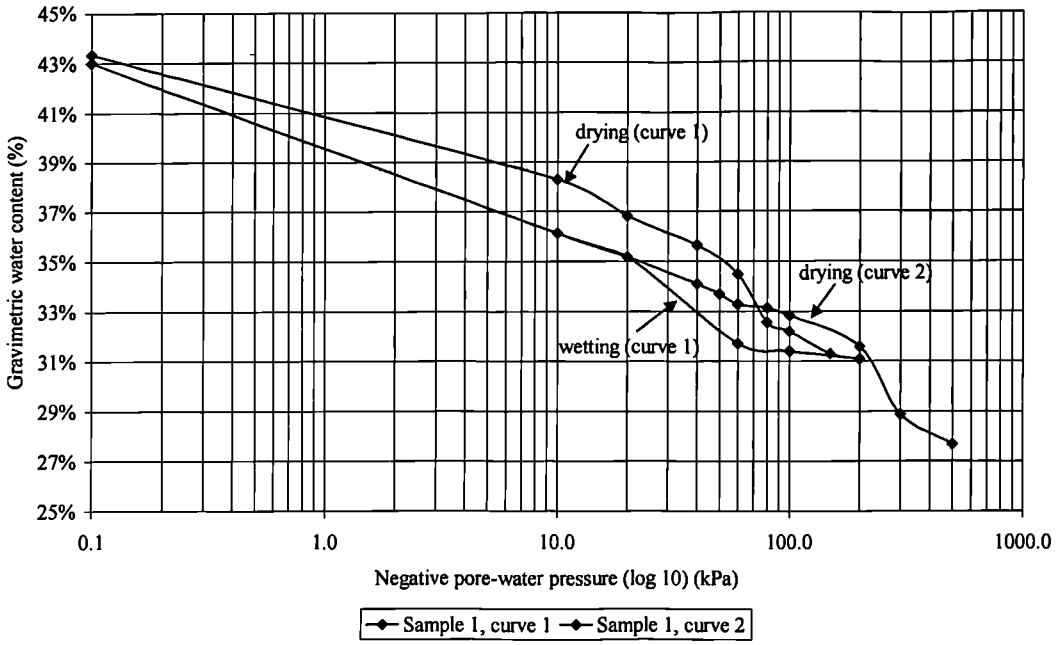

Figure 4.10 Soil-water characteristic curves of soil specimen 1 from the NTU-ANX slope.

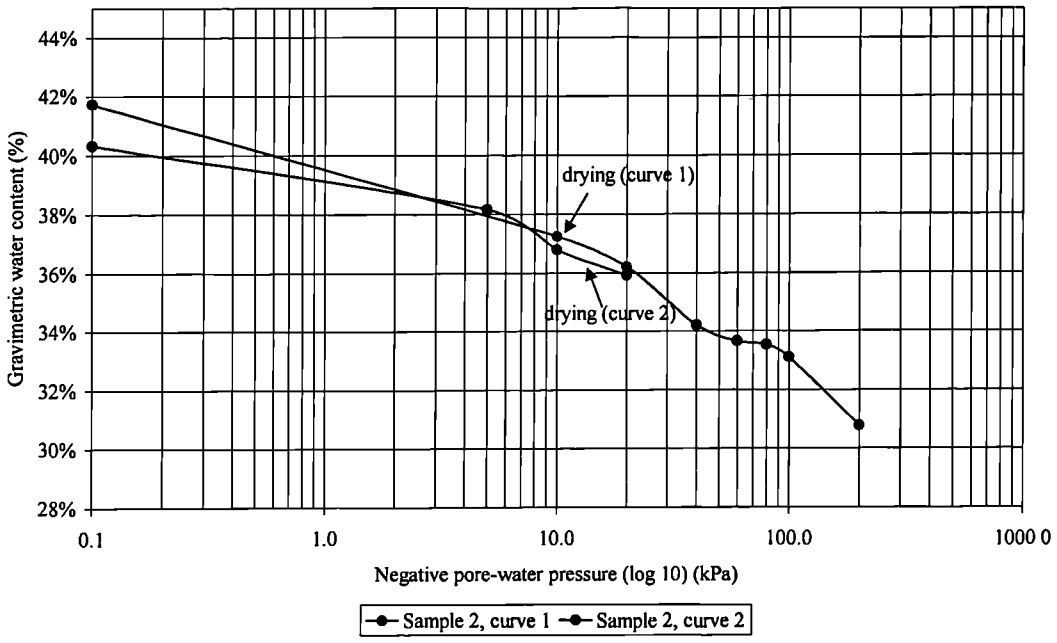

Figure 4.11 Soil-water characteristic curves of soil specimen 2 from the NTU-ANX slope.

Table 4.6 Data points of the soil-water characteristic curves of soil specimen 1 from the NTU-ANX slope.

Curve 1		Curve 2	
Pore-water pressure (kPa)	Gravimetric water content (%)	Pore-water pressure (kPa)	Gravimetric water content %
0 (saturation)	43.3	0 (saturation)	43.0
-10	38.3	-10	36.1
-20	36.8	-20	35.2
-40	35.6	-40	34.1
-60	34.5	-50	33.7
-80	32.6	-60	33.3
-100	32.2	-80	33.1
-150	31.3	-100	32.8
-200	31.1	-200	31.6
-100	31.4	-300	28.9
-60	31.7	-500	27.7
-20	35.2		
-10	36.1		
0	43.0		

Table 4.7 Data points of the soil-water characteristic curves of soil specimen 2 from the NTU-ANX slope.

Curve 1		Curve 2	
Pore-water pressure (kPa)	Gravimetric water content (%)	Pore-water pressure (kPa)	Gravimetric water content %
0 (saturation)	41.7	0 (saturation)	40.3
-10	37.2	-5	38.2
-20	36.2	-10	36.8
-40	34.2	-20	35.9
-60	33.7		
-80	33.5		
-100	33.1		
-200	30.8		

4.2.2 Rainfall gauge

At the NTU-ANX slope 942mm of natural rainfall was recorded over the 6-month monitoring period. During the monitoring period the average monthly rainfall was 157mm. Figure 4.12 presents a summary of the rainfall distribution from the data collected by the rainfall gauge. The data in this graph are shown as the total daily rainfall and include the simulated rainfalls that were applied on the research area of NTU-ANX slope, they will be presented in Section 4.2.6.

During the monitoring period 39 rainfall events were recorded having a total rainfall above 5mm. The total rainfall of these 39 events was 792mm. The total rainfall for

each of the rainfalls ranged from 5mm to 135mm with an average of 20mm. The rainfall intensity of those events ranged from 2 to 40mm/h with an average intensity of 11mm/h. All rainfall events with a total rain above 5mm that were measured at the NTU-ANX slope during the studied period are summarised in Table 4.8. The same table also presents the date and time that each rainfall event took place, the duration and the average intensity. In Table 4.9 the monitoring period is divided into dry and wet sub-periods. In the same table the simulated rainfalls, applied on the NTU-ANX slope are also shown.

Table 4.8 Summary of significant natural rainfall events at the NTU-ANX slope for the analysis period.

Event No.	Event start time	Event finish time	Rainfall (mm)	Duration (hours)	Average intensity (mm/h)
1	19-Mar-00 19:09	20-Mar-00 00:17	11.00	5.13	2.1
2	23-Mar-00 19:58	23-Mar-00 21:01	28.25	1.05	26.9
3	24-Mar-00 06:21	24-Mar-00 10:31	34.00	4.17	8.2
4	28-Mar-00 16:33	28-Mar-00 21:27	39.25	4.90	8.0
5	30-Mar-00 15:07	30-Mar-00 17:18	17.75	2.18	8.1
6	03-Apr-00 03:11	03-Apr-00 04:24	11.50	1.21	9.4
7	06-Apr-00 13:16	06-Apr-00 16:13	48.75	2.95	16.5
8	07-Apr-00 17:28	07-Apr-00 17:59	20.50	0.51	39.7
9	08-Apr-00 12:39	08-Apr-00 14:41	5.25	2.03	2.6
10	20-Apr-00 16:52	20-Apr-00 19:18	27.50	2.43	11.3
11	21-Apr-00 13:52	21-Apr-00 15:30	32.25	1.63	19.7
12	18-May-00 09:22	18-May-00 10:24	23.00	1.03	22.3
13	24-May-00 14:52	24-May-00 16:56	13.75	2.07	6.6
14	25-May-00 17:04	25-May-00 18:17	19.00	1.22	15.6
15	27-May-00 16:04	27-May-00 18:36	29.00	2.53	11.4
16	01-Jun-00 17:58	01-Jun-00 19:21	7.50	1.38	5.4
17	02-Jun-00 10:30	02-Jun-00 14:12	10.00	3.70	2.7
18	03-Jun-00 16:23	03-Jun-00 19:05	8.25	2.70	3.1
19	05-Jun-00 14:19	05-Jun-00 16:03	8.00	1.73	4.6
20	06-Jun-00 09:11	06-Jun-00 11:05	5.50	1.90	2.9
21	11-Jun-00 05:09	11-Jun-00 06:22	11.75	1.22	9.7
22	11-Jun-00 08:51	11-Jun-00 11:59	43.50	3.13	13.9
23	15-Jun-00 07:20	15-Jun-00 08:12	10.00	0.87	11.5
24	16-Jun-00 05:15	16-Jun-00 05:46	7.50	0.52	14.5
25	17-Jun-00 17:57	17-Jun-00 19:00	12.50	1.05	11.9
26	19-Jun-00 03:55	19-Jun-00 06:31	15.75	2.60	6.1
27	28-Jun-00 06:06	28-Jun-00 07:48	11.00	1.70	6.47
28	02-Jul-00 02:44	02-Jul-00 03:16	5.25	0.53	9.84
29	04-Jul-00 23:37	05-Jul-00 01:50	16.75	2.22	7.56
30	23-Jul-00 15:13	23-Jul-00 16:57	24.50	1.73	14.13
31	24-Jul-00 04:44	24-Jul-00 13:28	134.75	8.72	15.46
32	25-Jul-00 10:33	25-Jul-00 11:15	8.50	0.78	10.85

Event No.	Event start time	Event finish time	Rainfall (mm)	Duration (hours)	Average intensity (mm/h)
33	25-Jul-00 12:07	25-Jul-00 13:52	9.00	1.75	5.14
34	25-Jul-00 15:51	25-Jul-00 16:33	5.50	0.87	6.35
35	29-Jul-00 12:23	29-Jul-00 14:20	11.00	1.95	5.64
36	31-Jul-00 13:49	31-Jul-00 17:05	9.75	4.10	2.38
37	03-Aug-00 05:26	03-Aug-00 05:58	10.75	0.53	20.16
38	08-Aug-00 23:20	08-Aug-00 23:52	5.25	0.53	9.84
39	15-Aug-00 22:26	16-Aug-00 04:30	43.5	6.07	7.17

Table 4.9 Summary of wet and dry periods at the NTU-ANX slope for the analysis periods.

Period start	Period finish	Period description	Natural Rainfall (mm) NTU-ANX	Simulated Rainfall (mm) NTU-ANX
17-Mar-00	30-Mar-00	Wet period 7	187.5	-
31-Mar-00	05-Apr-00	Dry period 10	25.75	-
06-Apr-00	10-Apr-00	Wet period 8	81.75	-
11-Apr-00	19-Apr-00	Dry period 11	7.50	-
20-Apr-00	21-Apr-00	Wet period 9	60.50	-
22-Apr-00	17-May-00	Dry period 12	35.50	26.00
18-May-00	18-May-00	Wet period 10	23.00	-
19-May-00	23-May-00	Dry period 13	0.50	-
24-May-00	27-May-00	Wet period 11	63.75	-
28-May-00	01-Jun-00	Dry period 14	7.50	-
02-Jun-00	05-Jun-00	Wet period 12	41.50	-
06-Jun-00	10-Jun-00	Dry period 15	6.00	-
11-Jun-00	19-Jun-00	Wet period 13	107.50	13.61
20-Jun-00	27-Jun-00	Dry period 16	1.25	19.29
28-Jun-00	05-Jul-00	Wet period 14	35.00	-
06-Jul-00	11-Jul-00	Dry period 17	0.00	-
12-Jul-00	31-Jul-00	Wet period 15	216.25	164.06
01-Aug-00	06-Aug-00	Dry period 18	18.00	-
07-Aug-00	10-Aug-00	Wet period 16	5.50	129.33
11-Aug-00	14-Aug-00	Dry period 19	4.25	-
15-Aug-00	18-Aug-00	Wet period 17	44.75	-
		Total:	973.25	352.29

4.2.3 Piezometer

The location of the Casagrande-type piezometer was at the next to Row A of tensiometers, at the centre of the NTU-ANX slope (Figure 3.16). Figure 4.13 presents the measurements of the depth of water in the piezometer. The same graph also presents the rainfall data for the study of the effect of rainfall on the level of the groundwater table. Table 4.10 presents a summary of the piezometric readings

including the lowest, highest as well as the average depth of water in the piezometer. The depth of the piezometric readings is referenced to the ground level (Figure 3.16), where the piezometer was installed.

Table 4.10 Average, highest and lowest piezometric levels with respect to ground elevation in the NTU-ANX slope for the studied period.

Average depth (m)	Date of highest level (m)	Highest level (m)	Date of lowest level (m)	Lowest level (m)
-16.25	02-May-00 18:24	-15.22	05-Jun-00 12:00	-17.03

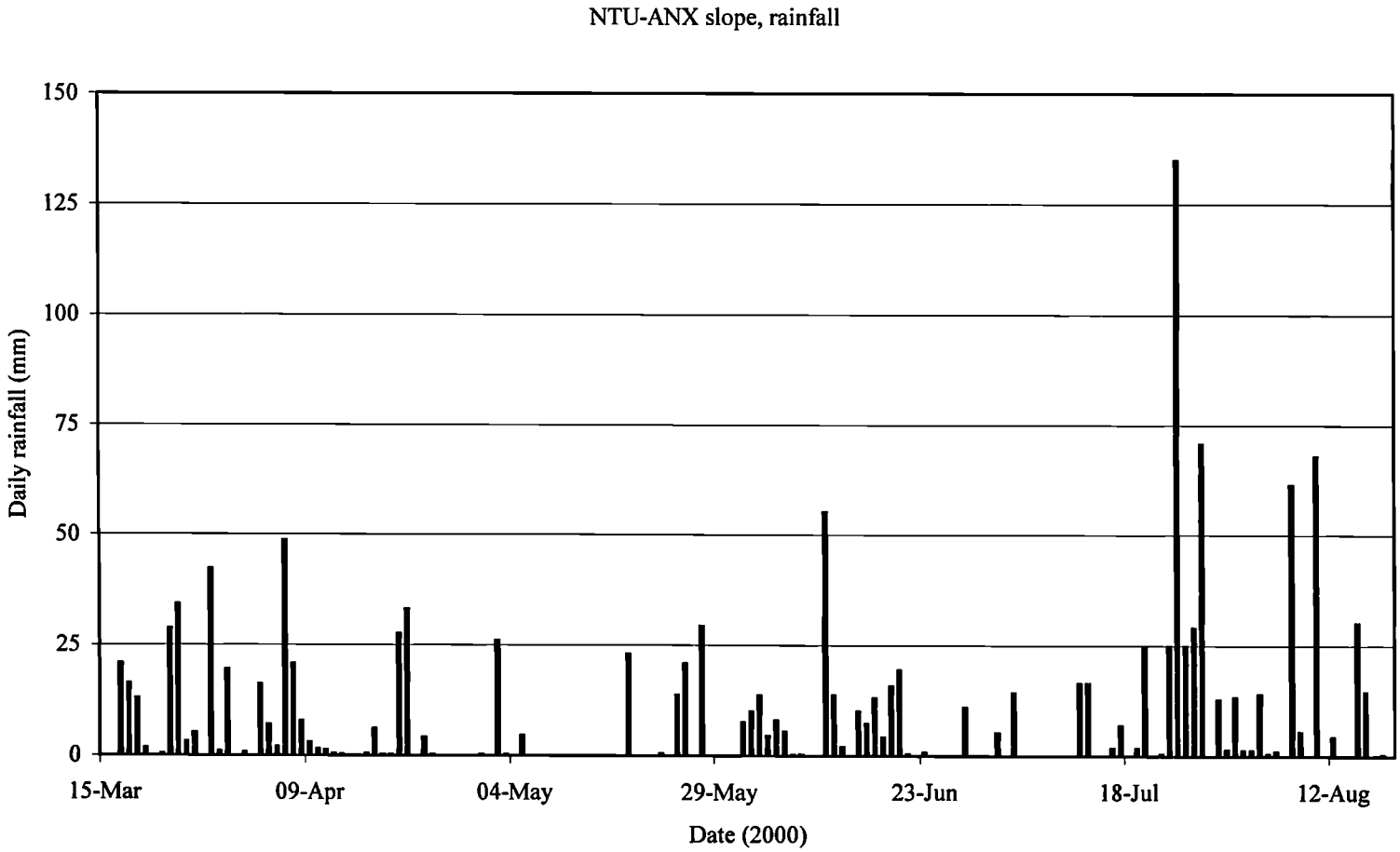

Figure 4.12 Summary of rainfall gauge data at the NTU-ANX slope for the analysis period.

4.2.4 Tensiometers

The developments of the pore-water pressures with time for the instrumented slope at NTU-ANX slope are presented in Figure 4.14 through Figure 4.16 as they were measured by the tensiometers of rows A through C (Figure 3.16). The same figures present the available rainfall data in order to study the development of the pore-water pressures at each depth due to infiltration.

Table 4.11 presents the summary of the minimum and maximum measurements of all tensiometers for the studied period at the NTU-ANX site. It has to be noted that as the studied period is relatively long (6 months) the pressure transducers that were connected on the tensiometers failed or were damaged periodically due to the harsh environment that they were exposed to. Those erroneous readings were excluded from the data presented. Figure 4.17 presents the range of readings for all depths as they are provided in Table 4.11.

Table 4.11 Summary of readings for tensiometers at the NTU-ANX slope for the analysis period.

Tensiometer	Depth (m)	Maximum (kPa)	Date of maximum	Minimum (kPa)	Date of minimum
A1	0.5	4.7	28-Mar-00 23:35	-52.6	18-Apr-00 08:00
A2	1.1	11.2	12-Aug-00 04:48	-26.4	17-Mar-00 19:13
A3	1.7	11.4	23-Mar-00 20:40	-11.7	17-Mar-00 00:00
A4	-	-	-	-	-
A5	2.9	18.7	10-Aug-00 17:27	-3.5	03-Jun-00 18:03
B1	0.5	4.9	23-Mar-00 20:19	-67.6	18-May-00 09:22
B2	1.1	8.3	11-Jun-00 09:33	-36.2	17-Mar-00 16:00
B3	1.7	-	-	-	-
B4	2.3	23.7	12-Aug-00 04:59	-7.2	17-Mar-00 16:00
B5	2.9	15.7	13-Jul-00 18:00	-19.9	21-Jun-00 16:00
C1	-	-	-	-	-
C2	1.1	10.6	06-Apr-00 13:47	-25.0	17-Mar-00 16:00
C3	1.7	17.15	11-Apr-00 00:00	-16.9	17-Mar-00 16:00
C4	2.3	-	-	-	-
C5	2.9	33.6	13-Jul-00 17:16	-0.8	23-Jul-00 15:54

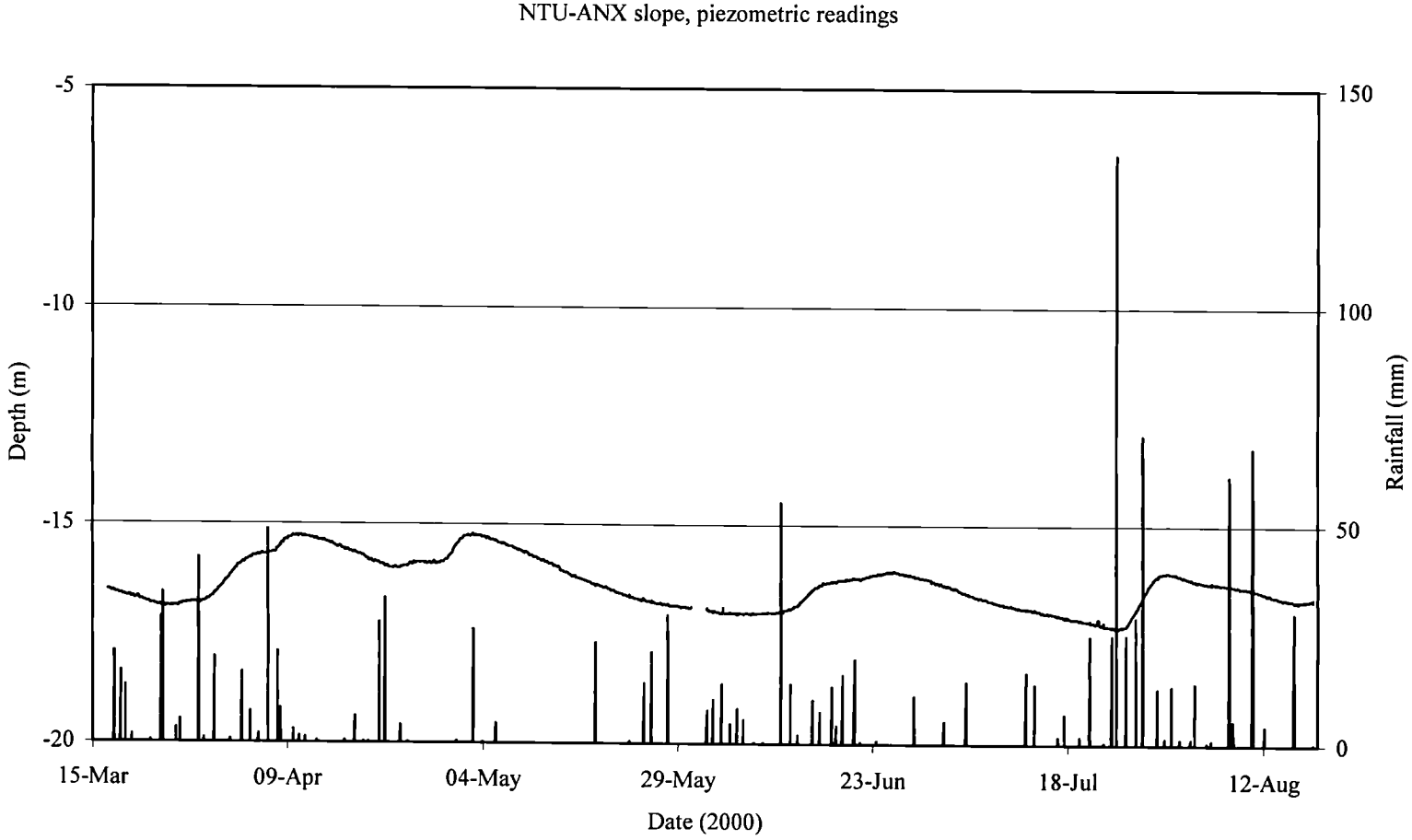

Figure 4.13 Piezometric levels with respect to ground elevation for the piezometer at the NTU-ANX slope.

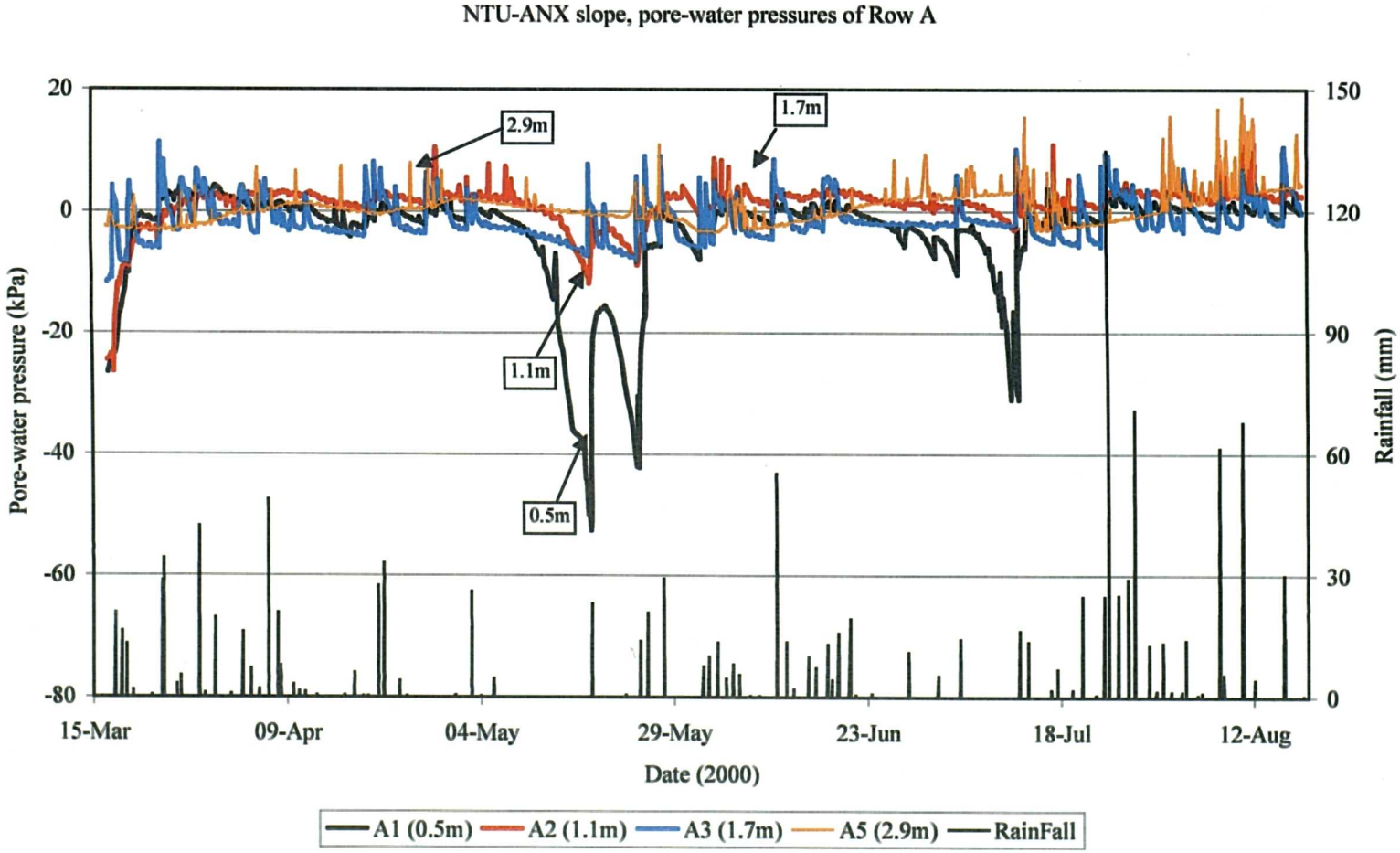

Figure 4.14 Tensiometer readings from Row A at the NTU-ANX slope for the studied period.

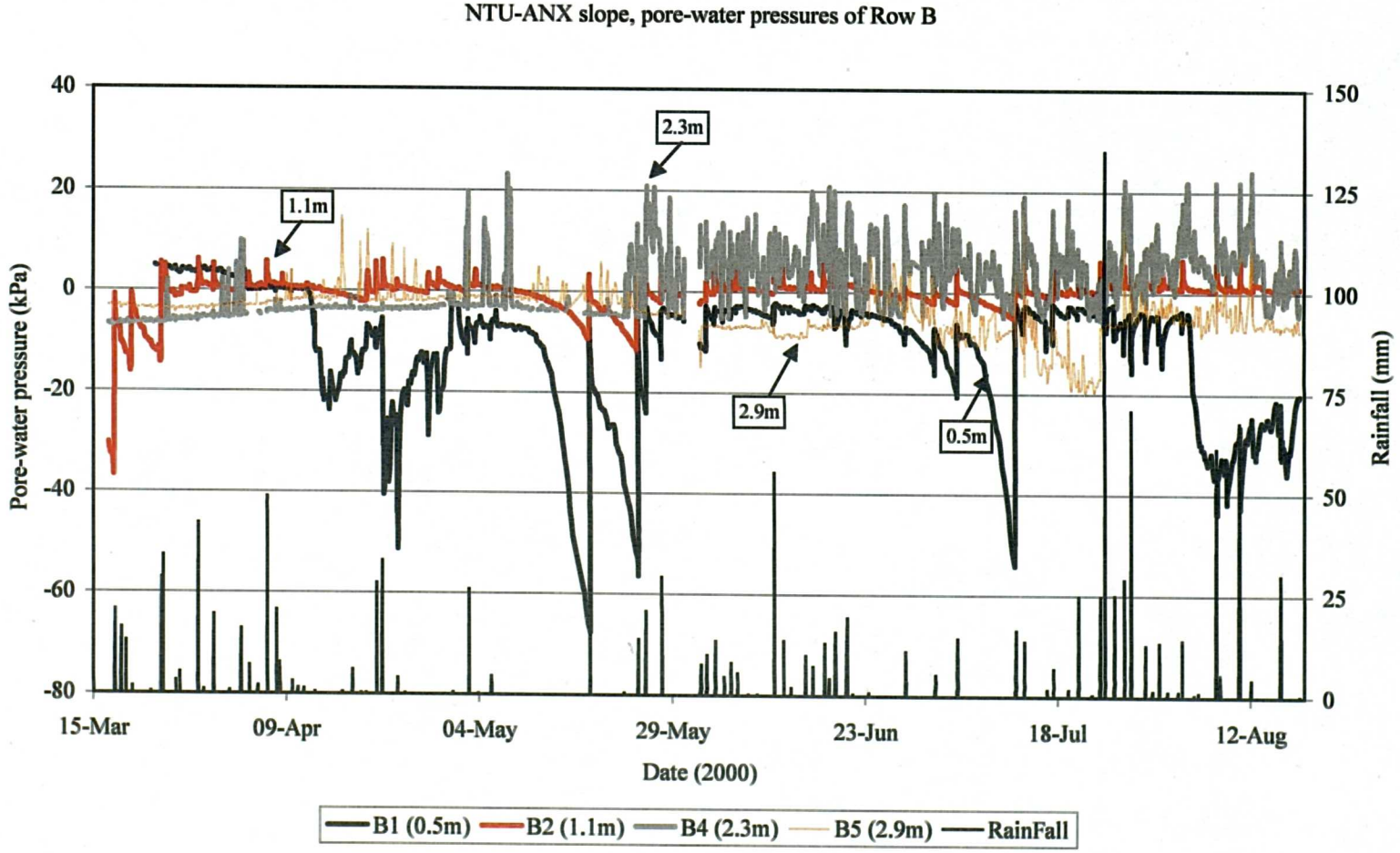

Figure 4.15 Tensiometer readings from Row B at the NTU-ANX slope for the studied period.

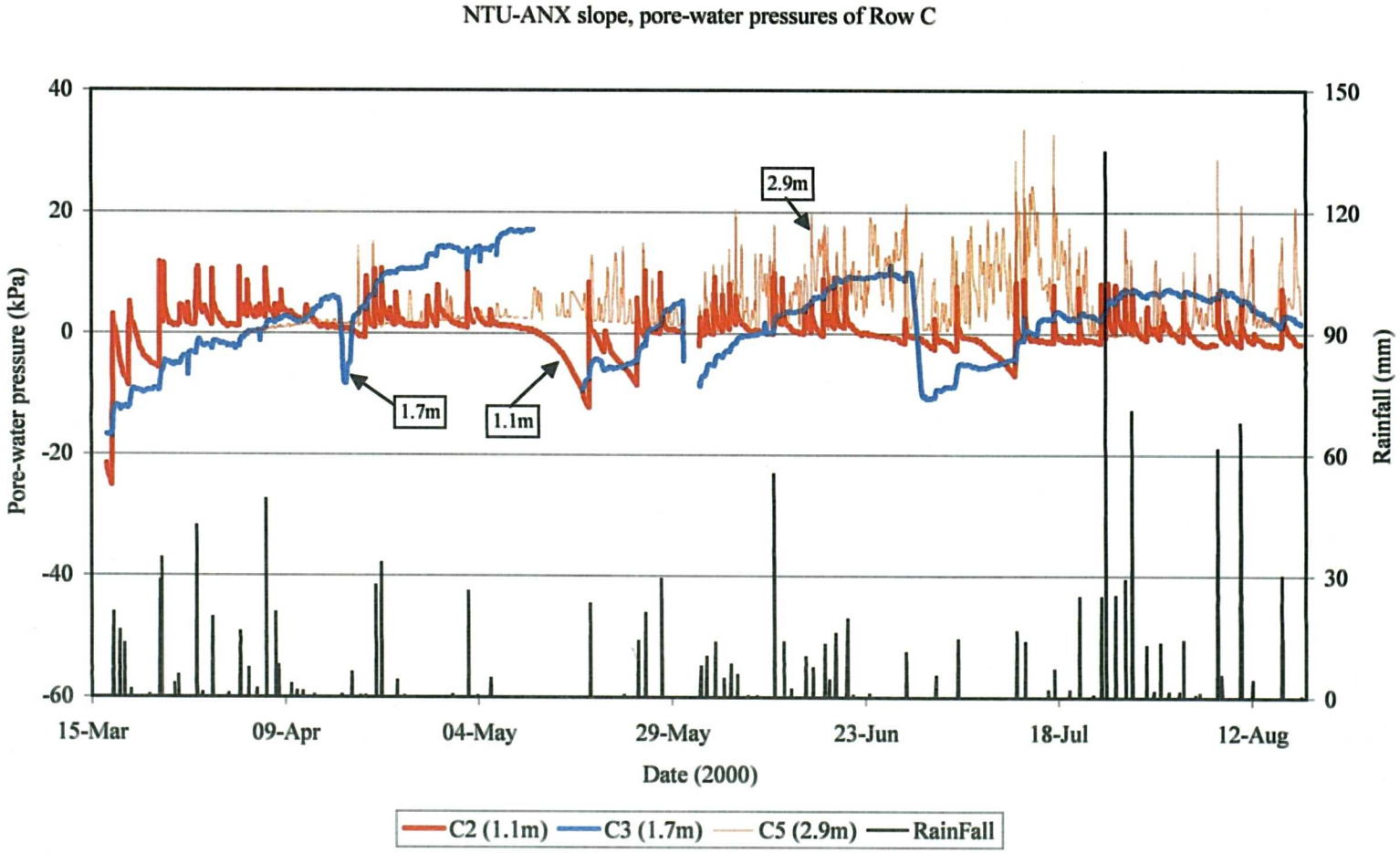

Figure 4.16 Tensiometer readings from Row C at the NTU-ANX slope for the studied period.

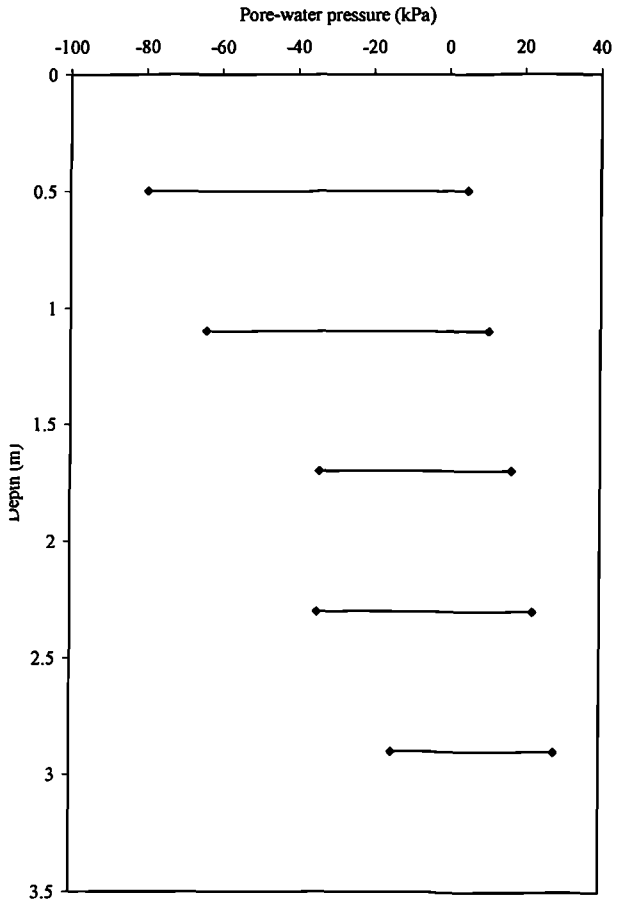

Figure 4.17 Recorded range of pore-water pressures with depth at the NTU-ANX slope (i.e. all rows combined).

4.2.5 Runoff measurement of natural rainfall

The measurements of runoff of natural rainfall at the NTU-ANX site are presented in this section. The instrumentation consisted of a rainfall gauge for the rainfall measurements and a water level capacitive probe with a flume for the measurement of the runoff during each rainfall. Section 3.3.4 provides a detailed description of the instrumentation that was used for the measurements of runoff. The analysis periods are summarised in Table 4.12. During the first week of April the capacitance water level probe as well as the data logger and the power supply box of the two devices were brought back to the laboratory, because there were problems encountered with the measurements. It was found that the power supply box was not operating properly and had to be changed.

Table 4.12 Analysis period for runoff of natural rainfall measurements at the NTU-ANX research site.

Period no.	Date started	Date finished
1	17-Mar-00	30-Mar-00
2	06-Apr-00	13-Apr-00
3	01-May-00	04-May-00
4	30-May-00	27-Jun-00
5	04-Jul-00	18-Aug-00

Natural rainfall events of total rainfall less than 5mm were excluded in the analysis of the runoff measurements as only small amount of runoff could be expected for such small rainfall events. During the studied period, 23 natural rainfall events took place, of total rainfall greater than 5mm (Table 4.13). The total rainfall for each of these events was between 5 and 57.75mm. Unfortunately, due to technical problems there are no runoff measurements available of the 24 July 2000, when rainfall with a maximum total rainfall of 134.75mm took place. The average intensity of these rainfall events was from 2.6mm/h to 39.7mm/h.

From the 23 natural rainfall events, 14 natural rainfall events produced measurable runoff and another 9 natural rainfall events did not produce any runoff. Table 4.14 presents a summary of the significant rainfall events that produced runoff during the studied periods. Table 4.14 also presents the characteristics of the runoff measurements. The same table gives the amount of the measured runoff as a percentage of the total rainfall. The range of the measured runoff was from 8% to 94% of the total rainfall, with an average of 56%. Runoff usually started reaching the collection point after 4 to 79 minutes (for long rainfall events of low intensity) from the start of the rainfall event, depending on the rainfall intensity. A typical delay was close to 25min from the start of the rainfall event.

Figure 4.20 and Figure 4.21 present the hyetographs of the natural rainfall events of the 06 April 2000 and 11 June 2000 with the runoff measurements. In these figures the rainfall readings were taken every 10 minutes, while runoff readings were taken every 5 seconds. The difference in the time intervals between the rainfall and runoff readings was due to the use of different acquisition systems (Sections 3.3.1 and 3.3.4). On the 06 April 2000 48.75mm of rainfall were distributed in nearly 3hours with an average intensity of 16.5mm/h. The runoff produced for that event was

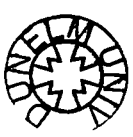

45.9mm or 94% of the total rainfall. The total rainfall of the 11 June 2000 event was 43.5mm, with a duration of 2.63 hours. The average rainfall intensity of that event was 16.5mm/h and the runoff produced was 33.8mm, or 77.7% of the total rainfall. All runoff measurements of natural rainfall can be found in Appendix C.

Table 4.13 Summary of the significant rainfall events during the studied periods.

Event No.	Event start time	Event finish time	Rainfall (mm)	Duration (hours)	Average intensity (mm/h)	Produced runoff
1	23-Mar-00 19:58	23-Mar-00 21:01	28.25	1.05	26.9	yes
2	24-Mar-00 06:21	24-Mar-00 10:31	34.00	4.17	8.2	yes
3	06-Apr-00 13:16	06-Apr-00 16:13	48.75	2.95	16.5	yes
4	07-Apr-00 17:28	07-Apr-00 17:59	20.50	0.51	39.7	no
5	08-Apr-00 12:39	08-Apr-00 14:41	5.25	2.03	2.6	no
6	01-Jun-00 17:58	01-Jun-00 19:21	7.50	1.38	5.4	no
7	02-Jun-00 10:30	02-Jun-00 14:12	10.00	3.70	2.7	no
8	03-Jun-00 16:23	03-Jun-00 19:05	8.25	2.70	3.1	yes
9	05-Jun-00 14:19	05-Jun-00 16:03	8.00	1.73	4.6	no
10	06-Jun-00 09:11	06-Jun-00 11:05	5.50	1.90	2.9	no
11	11-Jun-00 05:09	11-Jun-00 06:22	11.75	1.22	9.7	no
12	11-Jun-00 08:51	11-Jun-00 11:59	43.50	3.13	13.9	yes
13	15-Jun-00 07:20	15-Jun-00 08:12	10.00	0.87	11.5	no
14	16-Jun-00 05:15	16-Jun-00 05:46	7.50	0.52	14.5	no
15	17-Jun-00 17:57	17-Jun-00 19:00	12.50	1.05	11.9	yes
16	19-Jun-00 03:55	19-Jun-00 06:31	15.75	2.60	6.1	yes
17	25-Jul-00 10:33	25-Jul-00 11:15	8.50	0.78	10.9	yes
18	25-Jul-00 11:47	25-Jul-00 13:53	9.00	1.75	5.1	yes
19	25-Jul-00 15:51	25-Jul-00 16:33	5.50	0.87	6.4	yes
20	29-Jul-00 12:23	29-Jul-00 14:20	11.00	1.95	5.6	yes
21	03-Aug-00 04:08	03-Aug-00 05:58	13.75	1.83	7.5	yes
22	08-Aug-00 23:20	08-Aug-00 23:52	5.25	0.53	9.8	yes
23	15-Aug-00 22:26	16-Aug-00 03:25	57.50	5.2	11.1	yes

Table 4.14 Summary of the significant rainfall events during the studied periods which produced runoff.

Event		Rainfall				Runoff			
No.	Date (2000)	Start time	Finish time	Total rain (mm)	Average intensity (mm/h)	Start time	Finish time	Total (mm)	Percentage of total rain (%)
1	23-Mar	19:58	21:01	28.25	26.9	20:26	20:59	18.2	64
2	24-Mar	06:21	10:31	34.00	8.2	07:22	10:36	18.3	54
3	06-Apr	13:16	16:13	48.75	16.5	13:36	14:32	45.9	94
8	03-Jun	16:23	19:05	8.25	3.1	17:29	17:34	0.7	9
12	11-Jun	08:51	11:29	43.50	16.5	09:06	10:15	32.7	75
15	17-Jun	17:57	19:00	12.50	12.3	18:21	18:37	4.1	33
16	19-Jun	03:55	6:31	15.75	6.1	05:00	05:21	4.4	28

Event No.	Date (2000)	Rainfall Start time	Finish time	Total rain (mm)	Average intensity (mm/h)	Runoff Start time	Finish time	Total (mm)	Percentage of total rain (%)
17	25-Jul	10:33	11:15	8.50	12.1	10:47	11:27	5.9	69
18	25-Jul	11:47	13:53	9.00	5.1	12:07	13:26	7.7	85
19	25-Jul	15:51	16:33	5.50	7.9	16:16	16:44	1.9	35
20	29-Jul	12:23	14:20	11.00	5.6	12:35	12:46	2.6	23
21	03-Aug	04:08	05:58	13.75	25.8	05:37	06:19	12.4	90
22	08-Aug	23:20	23:52	5.25	9.8	23:24	23:39	0.6	12
23	15-Aug	22:26	03:25	57.5	10.6	23:11	03:32	54.5	95

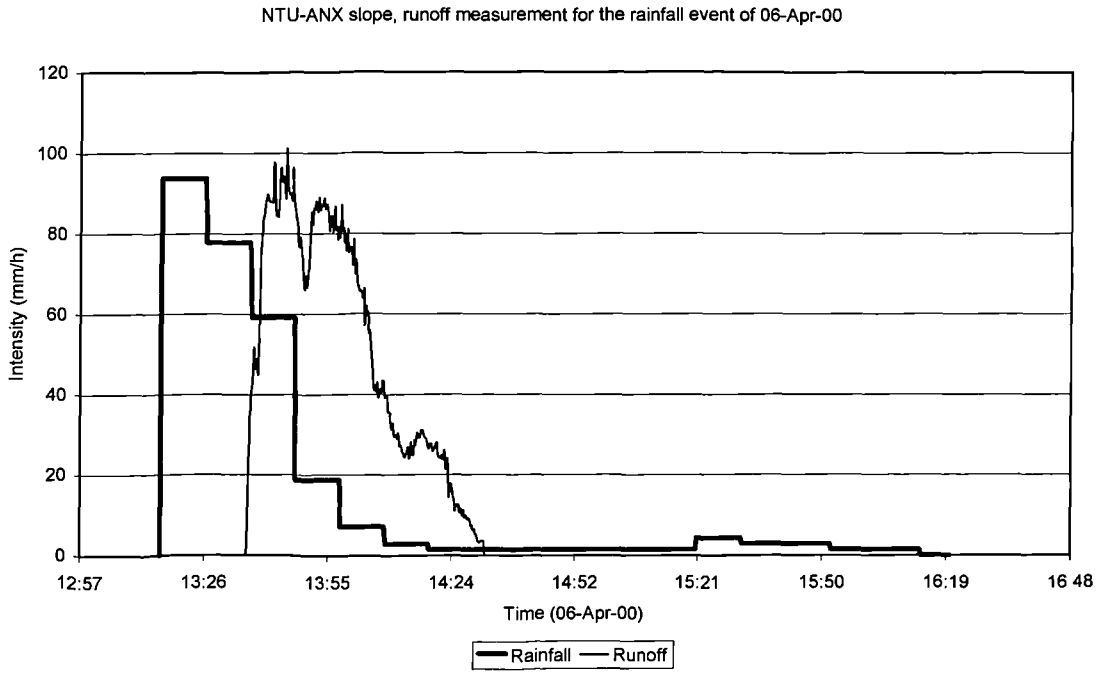

Figure 4.18 Hyetograph for 06-Apr-00 with the runoff measurement.

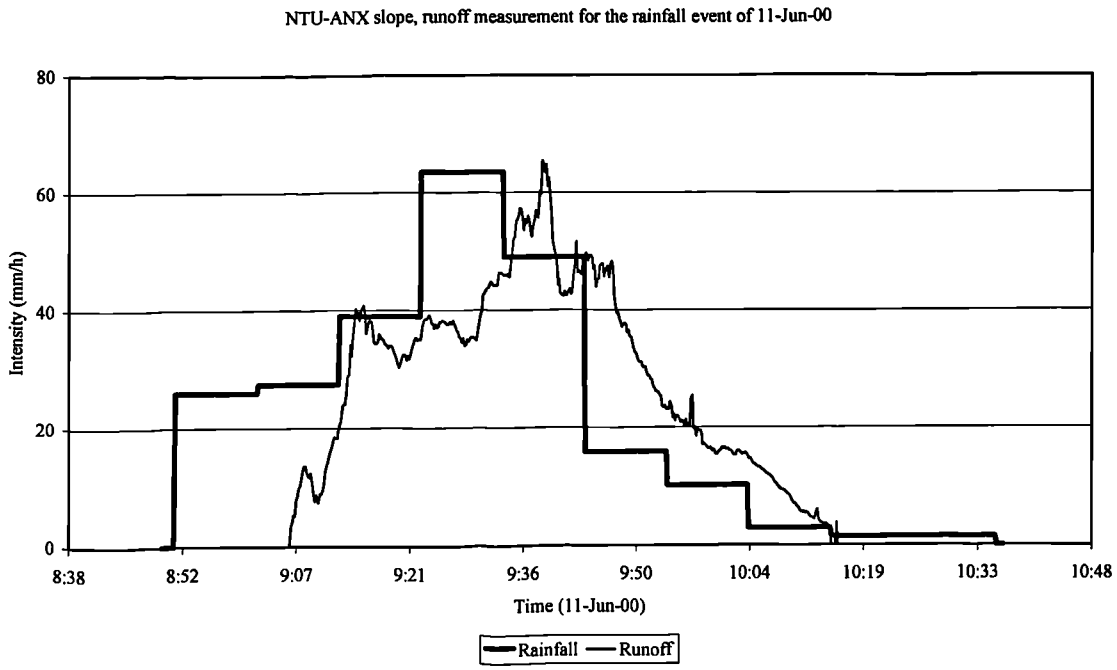

Figure 4.19 Hyetograph for 11-Jun-00 with the runoff measurement.

4.2.6 Runoff measurements of simulated rainfall

The measurements of runoff of simulated rainfall at the NTU-ANX slope are presented in this section. The instrumentation consisted of a rainfall gauge for the rainfall measurements and a water level capacitive probe with a flume for the measurement of the runoff during each rainfall and the rainfall simulator as described in Section 3.3.5.

During days of no natural rainfall events, 14 simulated rainfall events of various intensities and with different total rainfalls were applied on the NTU-ANX slope. The simulated rainfall events as well as comments on the runoff measurements are presented in Table 4.15. Table 4.16 summarises the characteristics of the rainfall and the measured runoff of the events presented in Table 4.15. The simulated rainfall intensity was constant for each test and varied from 8.2mm/h to 67.2mm/h. The total rainfall of each simulated rainfall varied from 6.8mm to 35.1mm. Of the 14 simulated rainfalls, only one rainfall did not produce runoff. The range of the rainfall produced was from 7% to 89%, with an average of 52%.

Table 4.15 Summary of the simulated rainfall events.

Event No.	Event start time	Event finish time	Rainfall (mm)	Duration (hours)	Average intensity (mm/h)	Produced runoff
1	02-May-00 17:01	02-May-00 17:46	33.5	0.75	44.7	yes
2	12-Jun-00 10:50	12-Jun-00 11:40	10.9	0.67	16.4	yes
3	20-Jun-00 15:48	20-Jun-00 16:33	19.3	0.75	25.7	yes
4	12-Jul-00 15:48	12-Jul-00 17:48	16.4	2.00	8.18	no
5	13-Jul-00 17:26	13-Jul-00 19:26	16.4	2.00	8.18	yes
6	17-Jul-00 12:15	17-Jul-00 13:05	6.8	0.83	8.18	yes
7	20-Jul-00 18:13	20-Jul-00 19:13	24.7	1.00	24.75	yes
8	26-Jul-00 17:05	26-Jul-00 18:05	29.0	1.00	29.00	yes
9	27-Jul-00 14:54	27-Jul-00 15:54	34.0	1.00	34.00	yes
10	27-Jul-00 16:48	27-Jul-00 17:33	36.82	0.75	49.10	yes
11	07-Aug-00 15:30	07-Aug-00 16:00	26.3	0.50	52.70	yes
12	07-Aug-00 17:19	07-Aug-00 17:59	35.2	0.67	52.70	yes
13	10-Aug-00 16:35	10-Aug-00 17:05	33.5	0.50	67.20	yes
14	10-Aug-00 18:00	10-Aug-00 18:30	33.2	0.50	66.30	yes

Figure 4.20 presents the runoff measurements of the simulated rainfall that was applied on the slope on 12 June 2000. The rainfall intensity achieved during that test was 16.4mm/h and the test lasted for 0.65 hours. The total rainfall of the event was 10.9mm and the runoff produced was 5.99mm or 54.8% of the total rainfall.

Table 4.16 Summary of the rainfall and runoff characteristics of the studied period.

Event No.	Rainfall			Runoff	
	Total rain (mm)	Duration (hours)	Average Intensity mm/h	Total mm	Percentage of total rain (%)
1	33.53	0.75	44.7	8.0	23.9
2	10.93	0.67	16.4	6.0	54.8
3	19.27	0.75	25.7	1.3	6.7
4	16.4	2.00	8.18	0.0	0.0
5	16.4	2.00	8.18	12.3	75.2
6	6.8	0.83	8.18	1.4	20.2
7	24.7	1.00	24.75	10.8	43.7
8	29.0	1.00	29.00	21.3	73.6
9	34.0	1.00	34.00	28.2	83.0
10	36.82	0.75	49.10	32.8	89.0
11	26.3	0.50	52.70	11.6	44.1
12	35.2	0.67	52.70	21.9	62.3
13	33.5	0.50	67.20	16.0	47.6
14	33.2	0.50	66.30	20.1	60.7

Figure 4.21presents the runoff measurement of the simulated rainfall, which was conducted on 7 August 2000. The simulated rainfall intensity was 52.7mm/h and the duration of the test was 0.5 hours (i.e. the total rainfall was 26.35mm). For that

simulated rainfall event the runoff produced was 44% of the total simulated rainfall. All runoff measurements of the simulated rainfalls can be found in Appendix D. The observed delay in the production of runoff from the start of each simulation was usually 4 to 10 minutes.

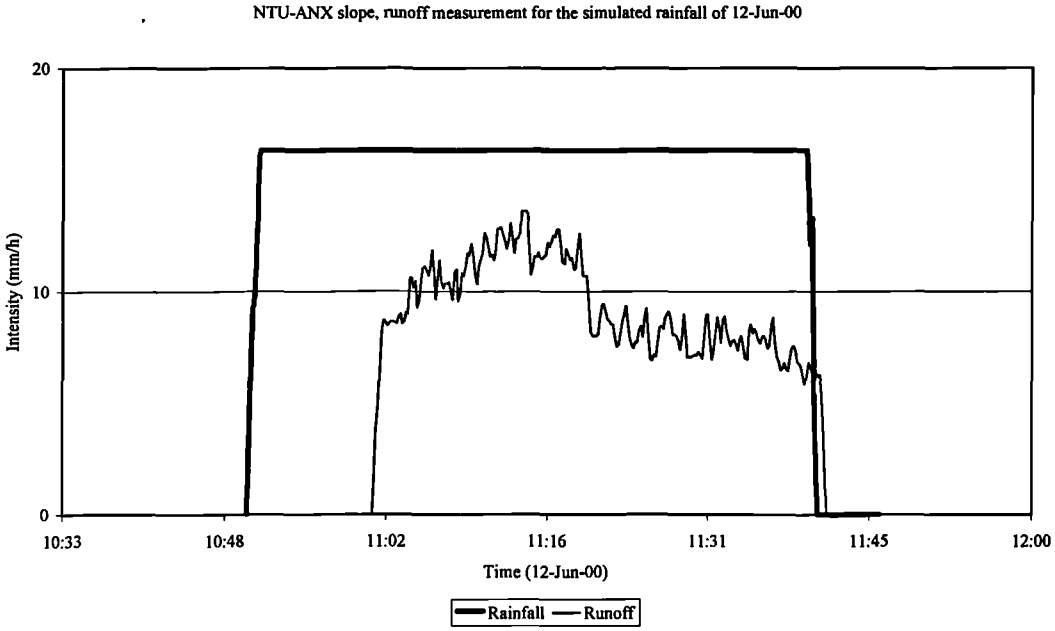

Figure 4.20 Hyetograph of the simulated rainfall on 12-Jun-00 with the runoff measurement.

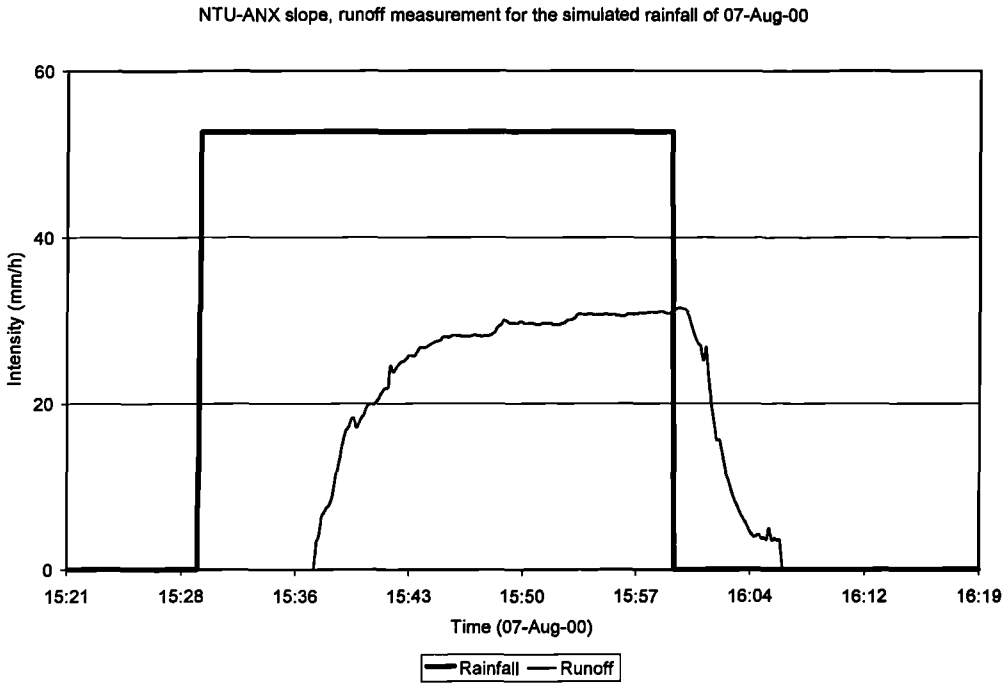

Figure 4.21 Hyetograph of the simulated rainfall on 07-Aug-00 with the runoff measurement.

4.2.7 In situ permeability measurements

Three in-situ permeability tests were conducted at the NTU-ANX slope. The tests were conducted using the Guelph permeameter, model 2800 manufactured by Soilmoisture™ Equipment Corp. Santa Barbara, California. Details of the test procedure and the equipment are given in Section 3.4. From the three tests in total, the two were successful while the last one failed (the drilled borehole was blocked during the test). The depth of the borehole was 30cm (just below the roots of the grass cover of the slope). Table 4.17 presents the summary of the two successful tests for the measurements of the saturated coefficient of permeability with respect to water of the surficial layer (Layer 1) of the NTU-ANX slope (Section 3.2). The results show that the soil Layer 1 of NTU-ANX slope has a saturated coefficient of permeability with respect to water equal to $6x10^{-7}$m/s.

Table 4.17 Summary of the in-situ measurements of the saturated coefficient of permeability with respect to water (k_{sat}) of the surficial Layer 1 of NTU-ANX slope.

Test no	Date	Borehole depth (m)	Well head (m)	k_{sat} (m/s)
1	07-Aug-00	0.30	0.10	$1.3x10^{-7}$
			0.15	$8.7x10^{-7}$
2	10-Aug-00	0.30	0.10	$9.8x10^{-7}$
			0.15	$5.4x10^{-7}$
			Average:	$6.3x10^{-7}$

CHAPTER 5

DISCUSSION OF THE FIELD MEASUREMENTS AND FIELD TESTING

5.1 NTU-CSE slope

This section presents the analysis of the field measurements for the NTU-CSE slope. The field measurements of the NTU-CSE slope consist of pore-water pressures and rainfall over a period of 12 months (from August 1999 to August 2000). Detailed description of the field measurements of the NTU-CSE slope can be found in Chapter 4. It has to be noted that the groundwater level was measured close to the toe of the slope to be at depth, greater than 10m (Rahardjo, 2000). Finally, it should be remembered that a big tree exists at the toe of the NTU-CSE slope and the tree roots are expected to cover a big area close to the toe of the slope.

5.1.1 Magnitude and distribution of pore-water pressures during rainfall for the NTU-CSE slope

In order to illustrate the effects of rainfall on the pore-water pressure changes in the NTU-CSE slope, the extreme conditions (i.e. the moistest and driest conditions) of the slope are considered. The NTU-CSE slope was at its moistest conditions on 06 December 1999, when a major rainfall event of 86mm took place, after a 5-day period of heavy rainfall. The 5-day antecedent rainfall (i.e. the rainfall precipitated on the slope prior to the major rainfall event) prior to the rainfall event of 06 December 1999 was 98mm. The NTU-CSE slope was at its driest on 15 March 2000 after a long dry period. On 15 March 2000 a minor rainfall event of 1mm took place, after a 5-day antecedent rainfall of 1mm.

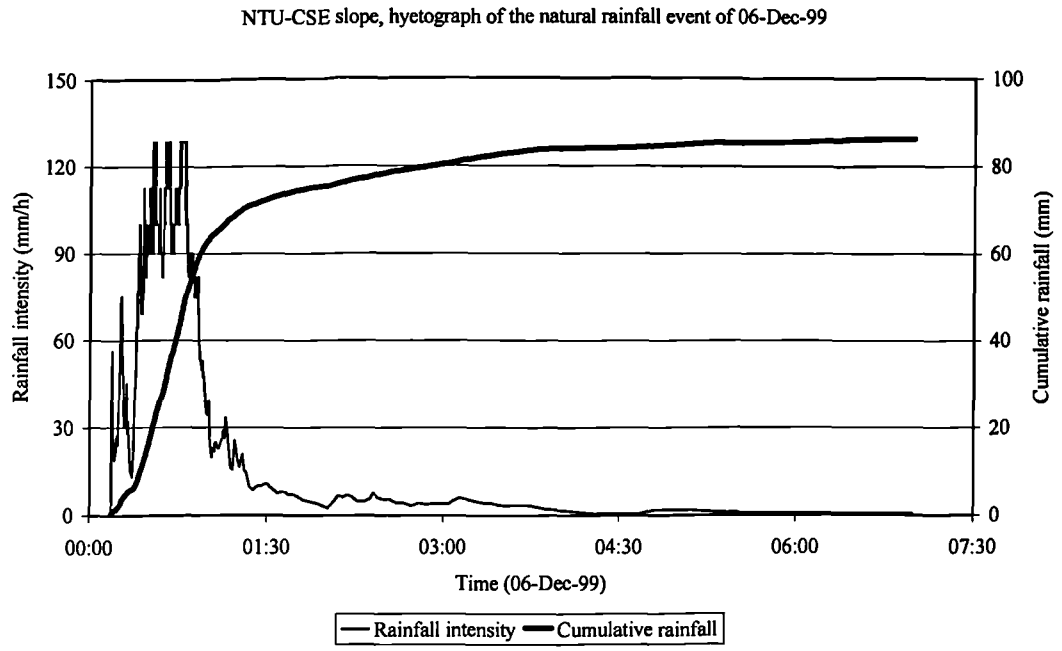

Figure 5.1 Hyetograph of the rainfall event of 06-Dec-99, measured on the NTU-CSE slope.

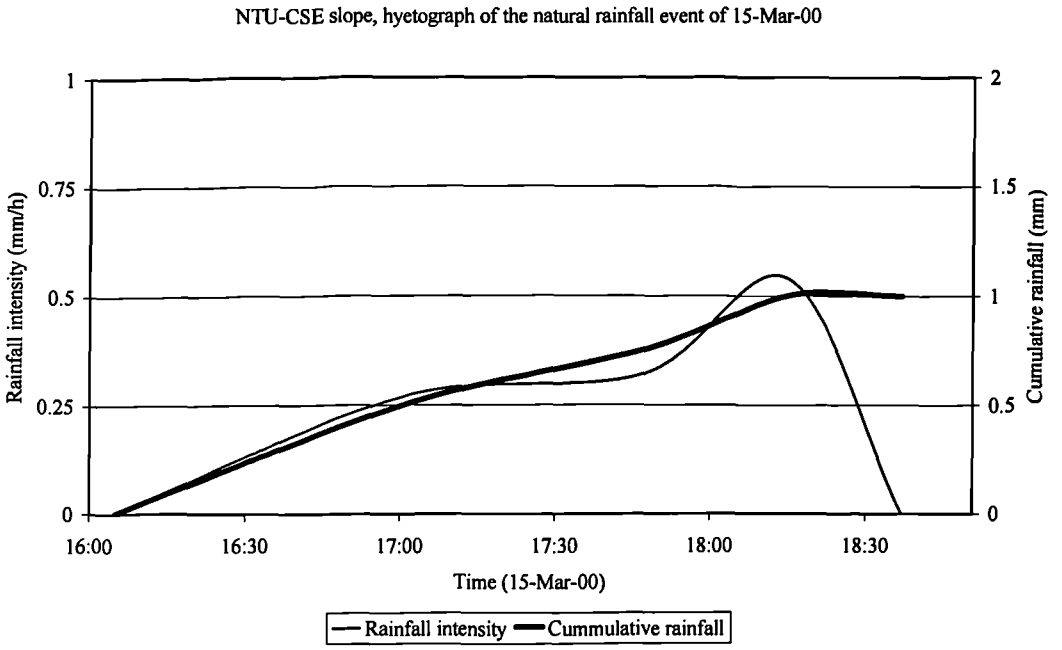

Figure 5.2 Hyetograph of the rainfall event of 15-Mar-00, measured on the NTU-CSE slope.

On 06 December 1999, the total amount of rainfall that was precipitated was 86mm and was distributed over 6.5 hours. Figure 5.1 presents the hyetograph of the rainfall event that took place on 06 December 1999. The average intensity of this rain event was 13mm/h. The peak intensity of the rainfall event was 129mm/h measured at 00:45 and lasted for approximately 2 minutes. After that the intensity decreased

rapidly to 90mm/h, 50mm/h, 10mm/h and from 01:45 decreased gradually from 5mm/h to zero at 06:59. The rainfall event of 15 March 2000 analysis started at 16:27 and was terminated at 18:37 (i.e. duration 2.17hours). The total amount of the 15-Mar-00 rainfall event was 1mm with an average intensity of 0.5mm/h. Figure 5.2 presents the hyetograph of the 15 March 2000 minor rainfall event.

Analysis of the worst (wettest) conditions

The measurements of pore-water pressures at the NTU-CSE slope show maximum values on 06-Dec-99. For the analysis of the pore-water pressure changes during the rainfall event of 06-Dec-99, the following time steps were chosen:

1. 06-Dec-99 00:10, at the start of the long heavy rainfall recorded that day.
2. 06-Dec-99 01:03, when the pore-water pressures near the ground surface were at maximum.
3. 06 Dec-99 06:59, when the rainfall stopped.
4. 07 Dec-99 06:59, 24 hours after the end of the rainfall of 06-Dec-99.

Figure 5.3 presents the pore-water pressure distributions with depth at rows A to F (Section 3.3.2) for the chosen time steps of the analysis. Figure 5.4 present the pore-water pressure changes with time for all depths at the crest of the slope (row A), middle of the slope (row C) and at the toe of the slope (row F). Figure 5.5 presents the pressure contours of the slope and Figure 5.6 presents the total head contours of the slope for the analysis time steps. The pressure and total head contours of the NTU-CSE slope were drawn based on the data presented in the pore-water pressure profiles of Figure 5.3. The contours were drawn with the commercial software Surfer for Windows (Golden Software Inc.) and will be discussed below.

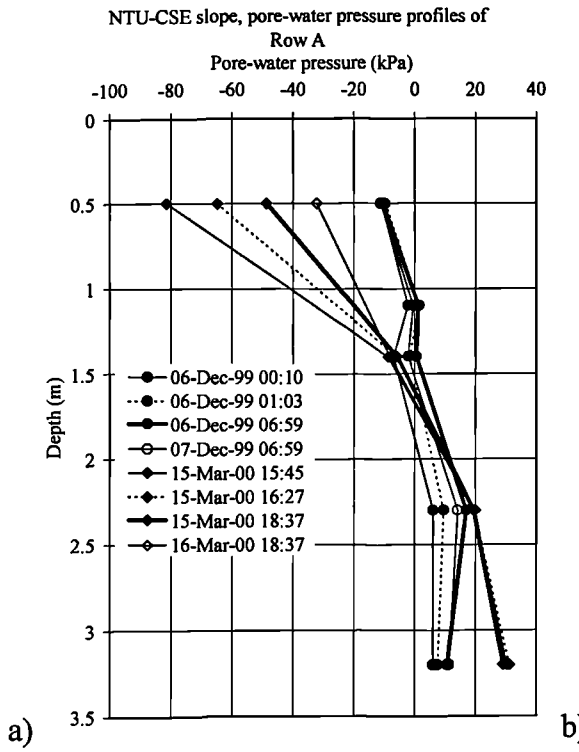
NTU-CSE slope, pore-water pressure profiles of
Row A
Pore-water pressure (kPa)
-100 -80 -60 -40 -20 0 20 40
Depth (m)
0 0.5 1 1.5 2 2.5 3 3.5
06-Dec-99 00:10
06-Dec-99 01:03
06-Dec-99 06:59
07-Dec-99 06:59
15-Mar-00 15:45
15-Mar-00 16:27
15-Mar-00 18:37
16-Mar-00 18:37

a)

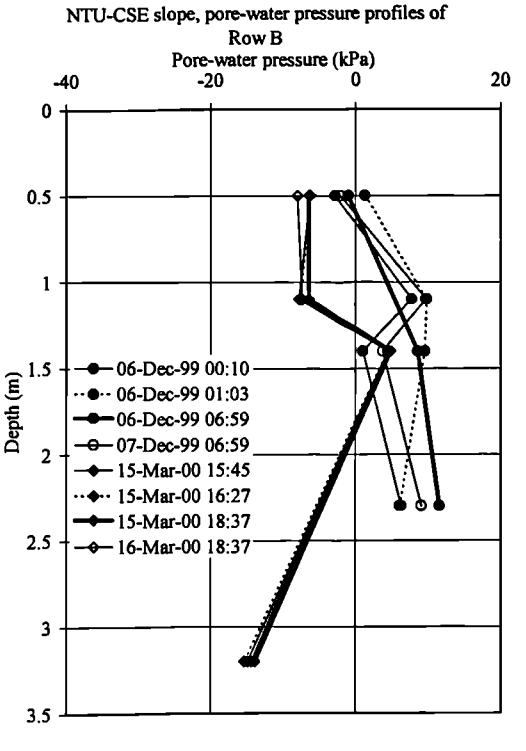
NTU-CSE slope, pore-water pressure profiles of
Row B
Pore-water pressure (kPa)
-40 -20 0 20
Depth (m)
0 0.5 1 1.5 2 2.5 3 3.5
06-Dec-99 00:10
06-Dec-99 01:03
06-Dec-99 06:59
07-Dec-99 06:59
15-Mar-00 15:45
15-Mar-00 16:27
15-Mar-00 18:37
16-Mar-00 18:37

b)

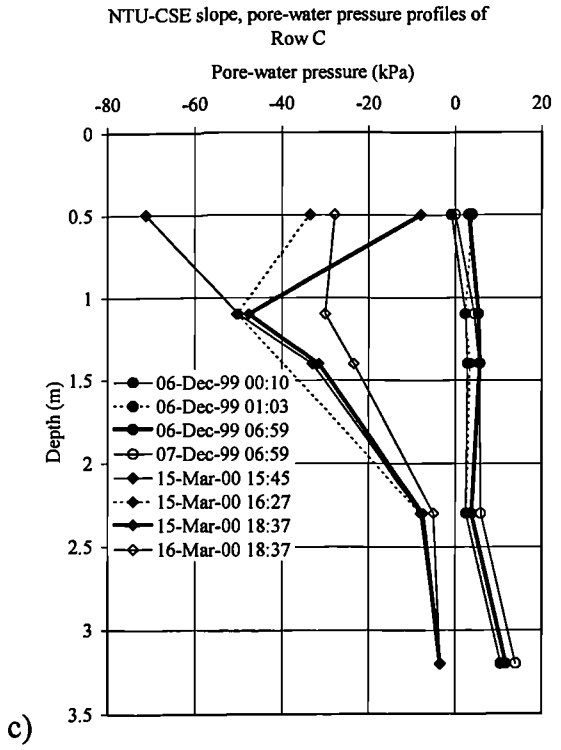
NTU-CSE slope, pore-water pressure profiles of
Row C
Pore-water pressure (kPa)
-80 -60 -40 -20 0 20
Depth (m)
0 0.5 1 1.5 2 2.5 3 3.5
06-Dec-99 00:10
06-Dec-99 01:03
06-Dec-99 06:59
07-Dec-99 06:59
15-Mar-00 15:45
15-Mar-00 16:27
15-Mar-00 18:37
16-Mar-00 18:37

c)

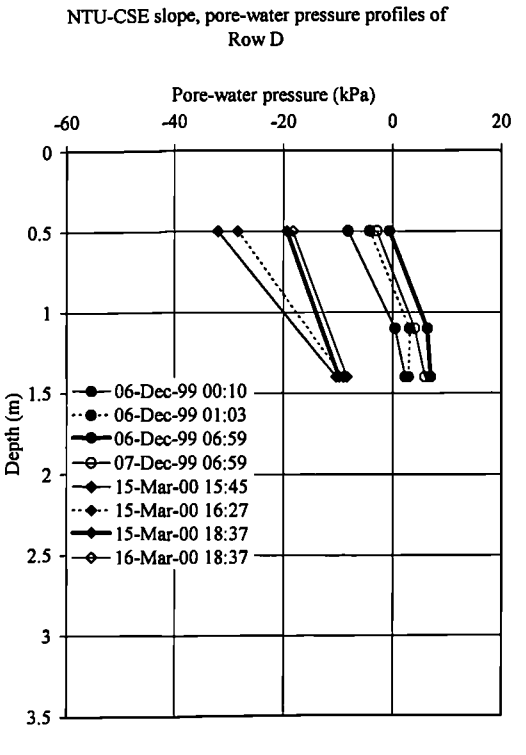
NTU-CSE slope, pore-water pressure profiles of
Row D
Pore-water pressure (kPa)
-60 -40 -20 0 20
Depth (m)
0 0.5 1 1.5 2 2.5 3 3.5
06-Dec-99 00:10
06-Dec-99 01:03
06-Dec-99 06:59
07-Dec-99 06:59
15-Mar-00 15:45
15-Mar-00 16:27
15-Mar-00 18:37
16-Mar-00 18:37

d)

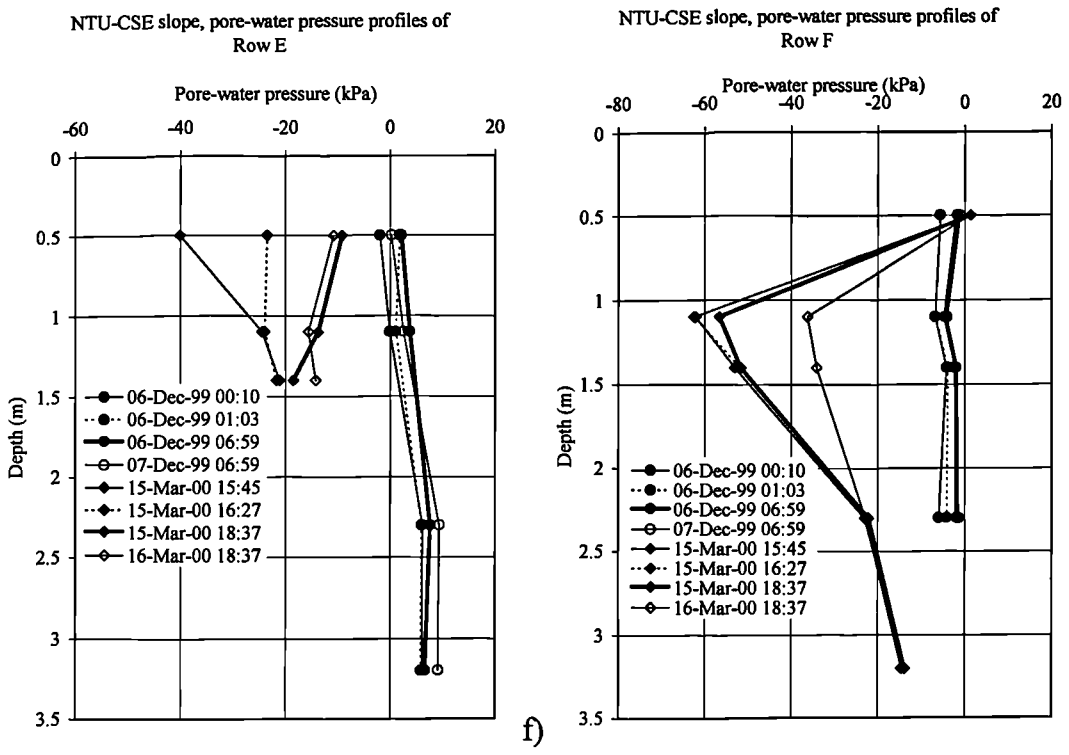

Figure 5.3 Pore-water pressure profiles of the NTU-CSE slope at the analysis time steps during 06-Dec-99 and 15-Mar-00: a) row A (crest of the slope), b) row B, c) row C (middle of the slope), d) row D, e) row E and f) row F (toe of the slope).

At the start of the rainfall event (06-Dec-99 00:10) the pore-water pressures near the ground surface (0.5m deep) are negative (Figure 5.3). At the crest of the slope the pore-water pressures at 0.5m deep was measured to be –10kPa and in the rest of the slope the pore-water pressures at 0.5m deep were slightly lower, about -5kPa. At larger depths the pore-water pressures were measured to be higher and below the 2.3m deep the pore-water pressures were positive (Figure 5.3). However, near the toe of the slope, at row F (Figure 5.3f), pore-water pressures were negative for all depths, due to the existence of the tree roots (see also Section 3.1) that kept the soil relatively dry in comparison with other locations of the slope.

The pore-water pressure profiles of Figure 5.3 show that the pore-water pressures near the ground surface (at 0.5m deep) increase soon after the rainfall of 06 December 1999 started. Pore-water pressures at larger depths started to increase long after the rainfall started but their increase lasted for longer than at smaller depths. The behaviour of the pore-water pressures at various will be discussed below in more detail considering pore-water changes with time (Figure 5.4).

Figure 5.4 shows that the pore-water pressures near the surface (0.5m deep) increased as soon as the rainfall started. The pore-water pressures at 0.5m deep initially increased, but soon reached a maximum and then remained constant or even slightly decreased before the end of the rainfall. The decrease started after the rainfall intensity started to decrease. By 01:03, when the maximum pore-water pressures near the ground surface were recorded, 65mm out of the 86mm of total rainfall had been precipitated (Figure 5.1). However, the negative pore-water pressures were retained near the ground surface of the crest of the slope (in row A the pore-water pressures at 0.5m deep have increased from –11 to –10kPa) (Figure 5.4a). At the middle of the slope (row C in Figure 5.4b) the pore-water pressure at 0.5m deep have increased from –1kPa to 4kPa and at the toe of the slope (row F in Figure 5.4c) the pore-water pressure remained almost unchanged and equal to –5kPa possibly due to the existence of the tree roots. At 1.1m and 1.4m deep the pore-water pressures did not change significantly at all the measuring points (Figure 5.4).

In the time period between 01:03 (when the maximum pore-water pressures at 0.5m deep were recorded) and the end of the rainfall event at 06:59, the pore-water pressures changes near the ground surface remained almost constant (Figure 5.4). However, during the same time period the pore-water pressure at the crest of the slope, at 1.1, and 1.4m deep increased by 3 and 4 kPa respectively and at the middle of the slope the pore-water pressures increased by 2kPa (Figure 5.4).

The deeper tensiometers (2.3 and 3.2m deep) showed that the increase of the pore-water pressures took place at a lower rate but for much longer (Figure 5.4). That led to a build-up of highly positive pore-water pressures between 2.3m and 3.2m that lasted for long after the end of the rainfall event. At the crest of the slope (Figure 5.4a), the total increase of the pore-water pressures at 2.3m and 3.2m was 11kPa and 6kPa respectively. At the middle of the slope (Figure 5.4b) the increase of the pore-water pressures at 2.3m and 3.2m deep was 4kPa for both depths. On 07 December 1999 06:59 (i.e. 24 hours after the end of the rainfall event) the pore-water pressures near the ground surface have recovered some of their initially negative values, while the pore-water pressures at 2.3m and 3.2m deep have further increased (Figure 5.4).

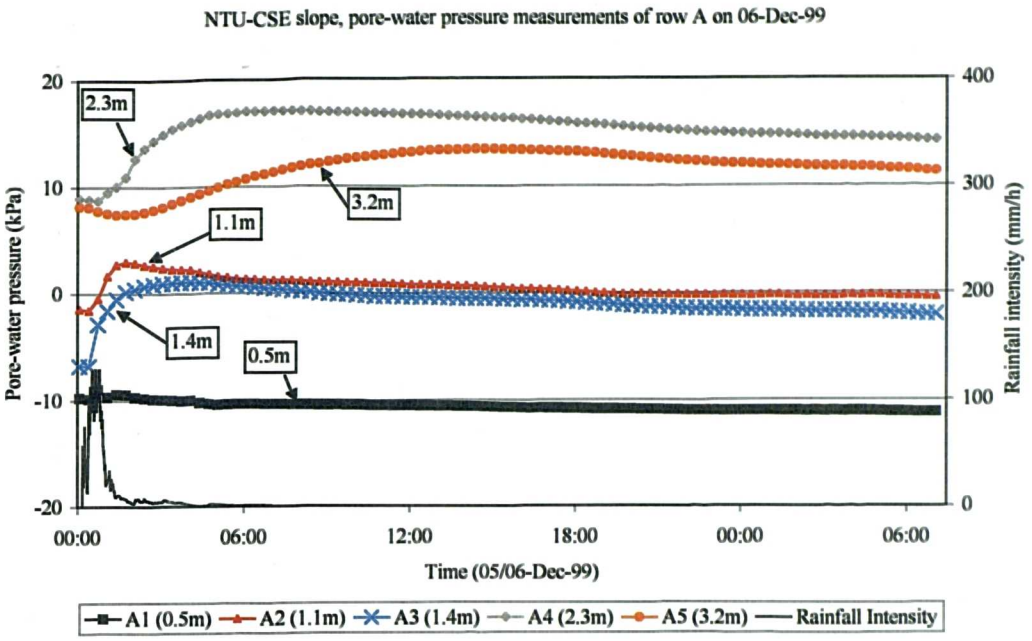
NTU-CSE slope, pore-water pressure measurements of row A on 06-Dec-99
Pore-water pressure (kPa)
Rainfall intensity (mm/h)
Time (05/06-Dec-99)
2.3m
3.2m
1.1m
1.4m
0.5m
A1 (0.5m)
A2 (1.1m)
A3 (1.4m)
A4 (2.3m)
A5 (3.2m)
Rainfall Intensity

a)

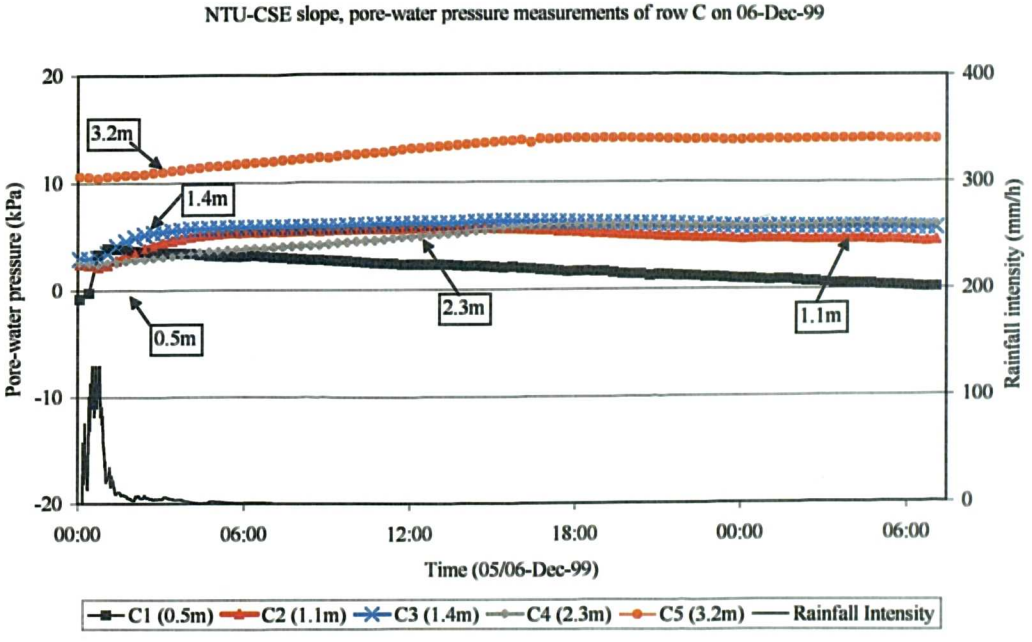
NTU-CSE slope, pore-water pressure measurements of row C on 06-Dec-99
Pore-water pressure (kPa)
Rainfall intensity (mm/h)
Time (05/06-Dec-99)
3.2m
1.4m
2.3m
1.1m
0.5m
C1 (0.5m)
C2 (1.1m)
C3 (1.4m)
C4 (2.3m)
C5 (3.2m)
Rainfall Intensity

b)

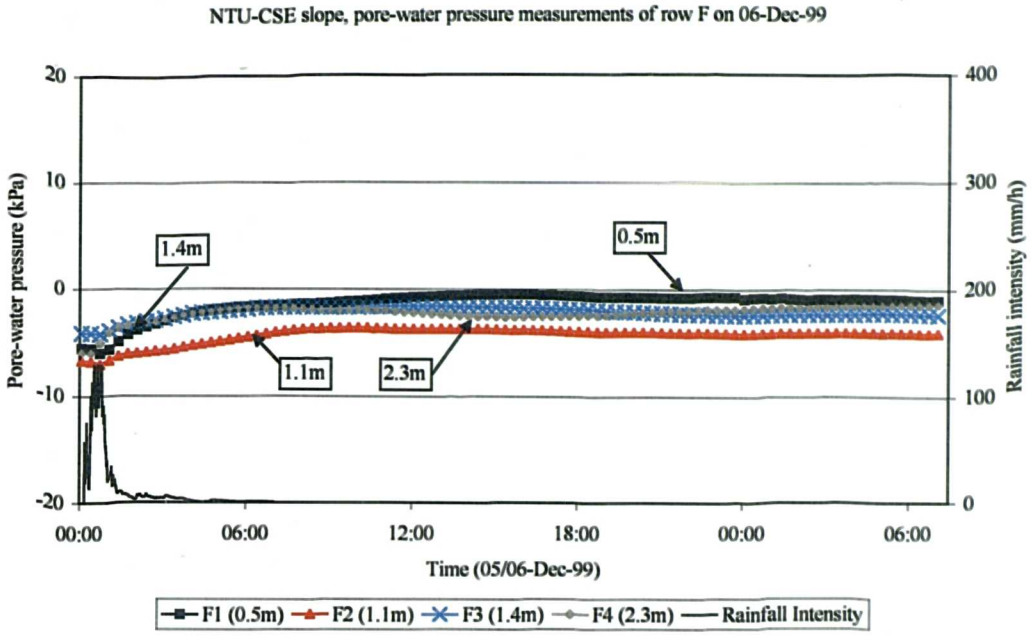

c)

Figure 5.4 Pore-water pressure measurements in the NTU-CSE slope on 06-Dec-99: a) at the crest of the slope (row A), b) at the middle of the slope (row C) and c) at the toe of the slope (row F).

The distribution of pore-water pressures within the slope can also be seen from the pore-water pressure contours (in kPa) of Figure 5.5. The pore-water pressure contours of Figure 5.5a show the initial existence of a zero pressure contour, which defines the border between the zone of negative pore-water pressures (unsaturated zone) and the zone of positive pore-water pressures. The zone of positive pore-water pressures is attributed to the heavy 5-day antecedent rainfall of 98mm. The depth of the zero pressure contour at 00:10 was about 2m from the ground surface at the crest of the slope and about 1 to 1.5m from the ground surface in the rest of the slope.

At 01:03 the pore-water pressures have increased (Figure 5.3) and the zero pressure contour, that defines the limit between the unsaturated and the saturated zone (Figure 5.5b) has risen close the ground surface. However, there was still a small area at the crest of the slope, where negative pore-water pressures were retained near the ground surface (in row A the pore-water pressures at 0.5m deep have increased from –11 to -10kPa as seen in Figure 5.4a).

The comparison of the pore-water pressure contours of Figure 5.5b and Figure 5.5c show that the unsaturated zone near the ground surface at the crest of the slope was

retained after 86mm of rainfall were precipitated on the slope. During the 24 hours after the end of the rainfall pore-water pressures near the ground surface started to recover negative values and an unsaturated zone was developed near the ground surface (Figure 5.5d).

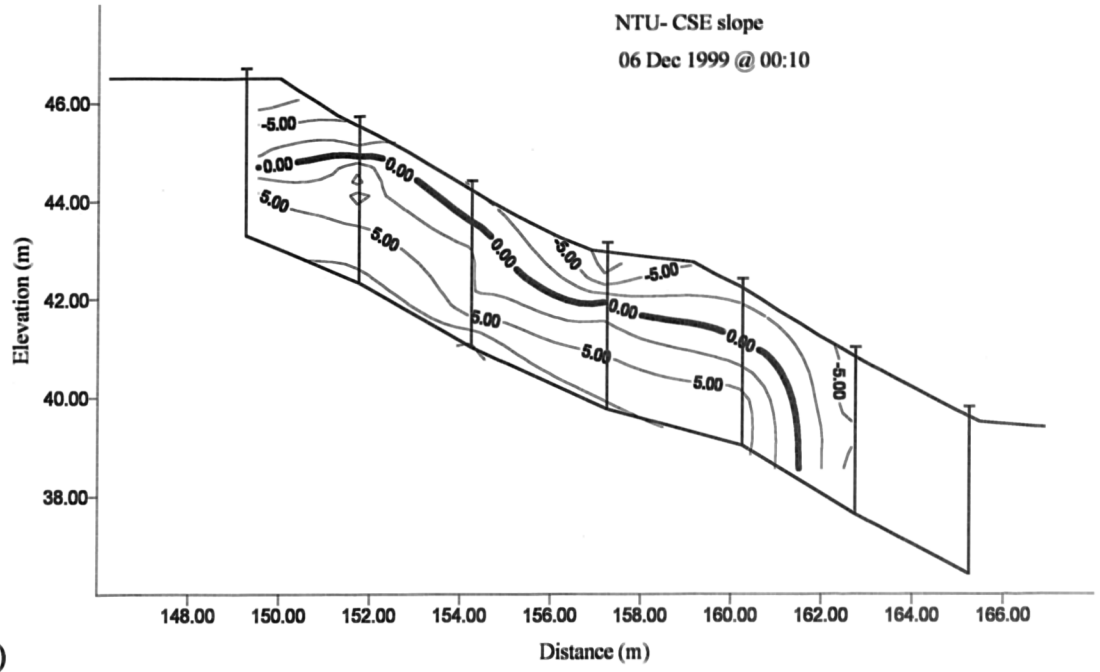

a)

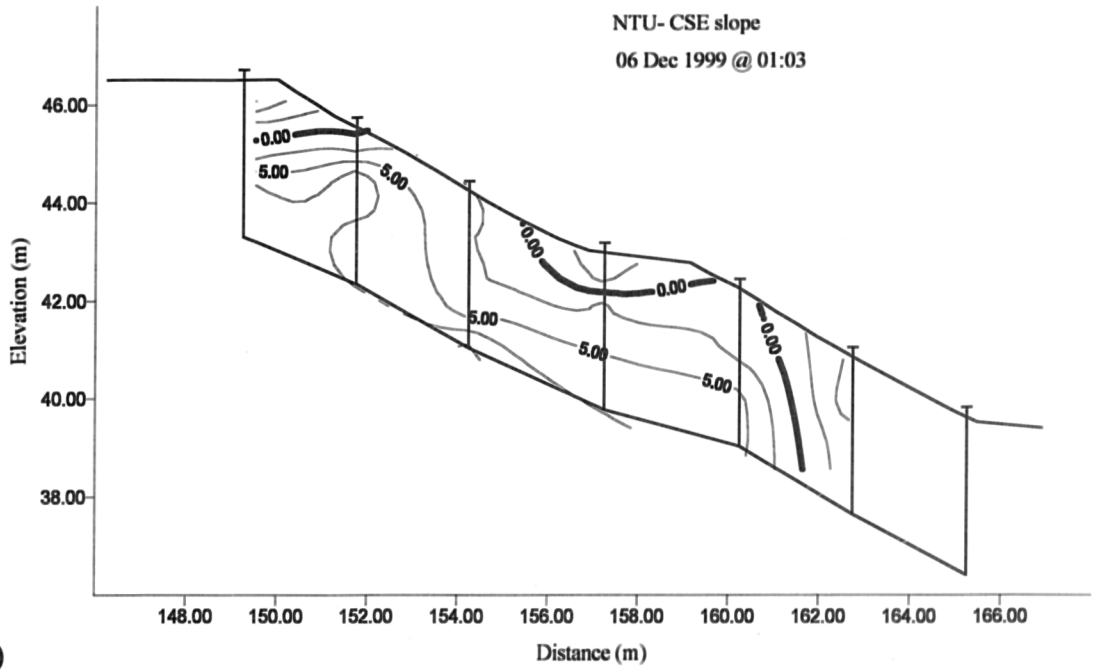

b)

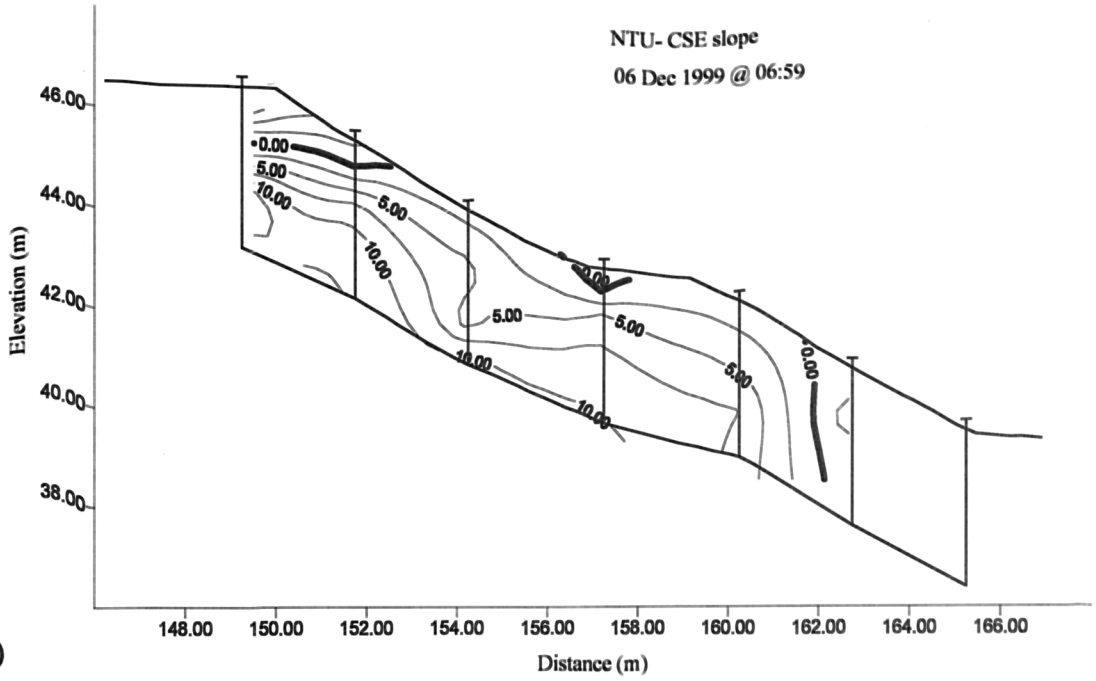

c)

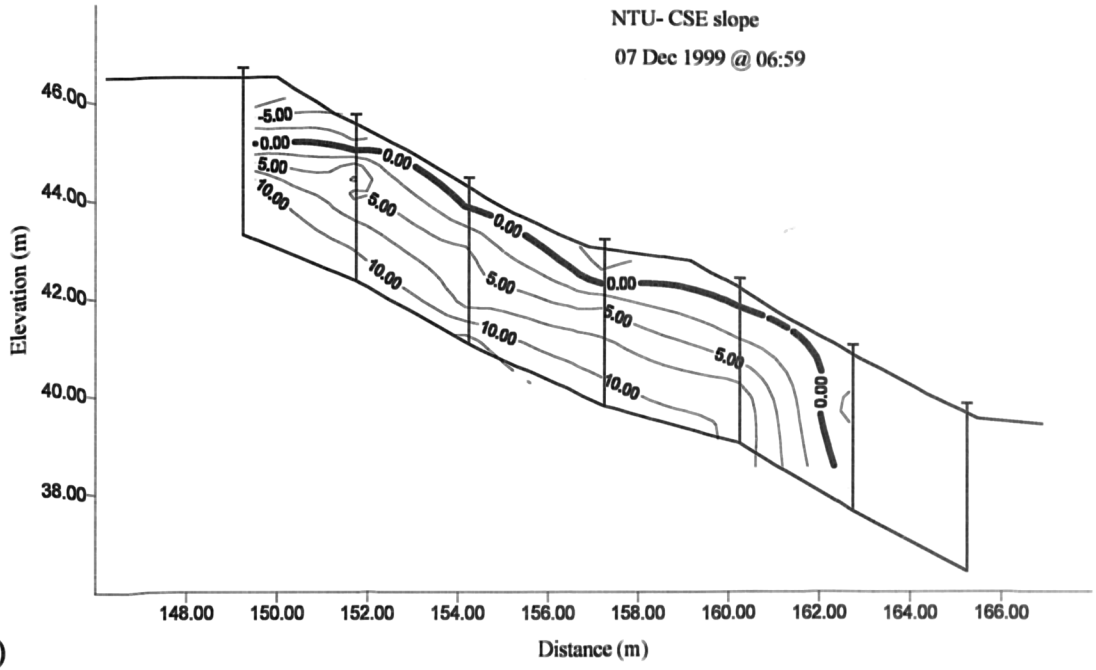

d)

Figure 5.5 Pressure contours (in kPa) of the NTU-CSE slope on a) 06-Dec-99 00:10, b) 06-Dec-99 01:03, c) 06-Dec-99 06:59 and d) 07-Dec-99 06:59.

The pore-water pressure changes caused by the rainfall event of 06 December 1999 can be explained in terms of flow patterns. At 0.5m deep, the pore-water pressure increased during the first hour of the rainfall (from 00:10 to 01:03), when the rainfall intensity was very high. However, especially at the crest of the slope the pore-water pressure near the ground surface increased only by 1kPa and in general remained constant. At the middle of the slope the increase at 0.5m deep was 5kPa. At the

same time, at larger depths the pore-water pressures were not significant. This would mean that the rainwater that infiltrated into the slope started flowing downslope towards the toe where the total heads were smaller. The contours of total head in Figure 5.6a, at the start of the rainfall, are inclined and water flow takes place from a high to a lower total head. The downslope flow is partially due to the difference in total head, but also due to the fact that the permeability with respect to water of the surficial soil is higher than the permeability of the soil at larger depths.

After the first hour of the rainfall, the intensity decreases, the pore-water pressures near the ground surface (0.5m deep) become constant and at the same time pore-water pressures at larger depths start to increase. Figure 5.6b presents the contours of total head of the slope at 01:03 (i.e. at the time the pore-water pressures near the ground surface are at maximum). The contours of total head of Figure 5.6b are almost horizontal indicating that water will be flowing vertically towards larger depths at higher rates than earlier. However, the increase of pore-water pressures is larger downslope than in the areas close to the crest of the slope. In addition, the increase of the pore-water pressures lasts for longer downslope than at the crest of the slope (Figure 5.4). This indicates that during the rainfall event, only small volumes of water reach large depths of the crest and more water will flow down, parallel to the slope.

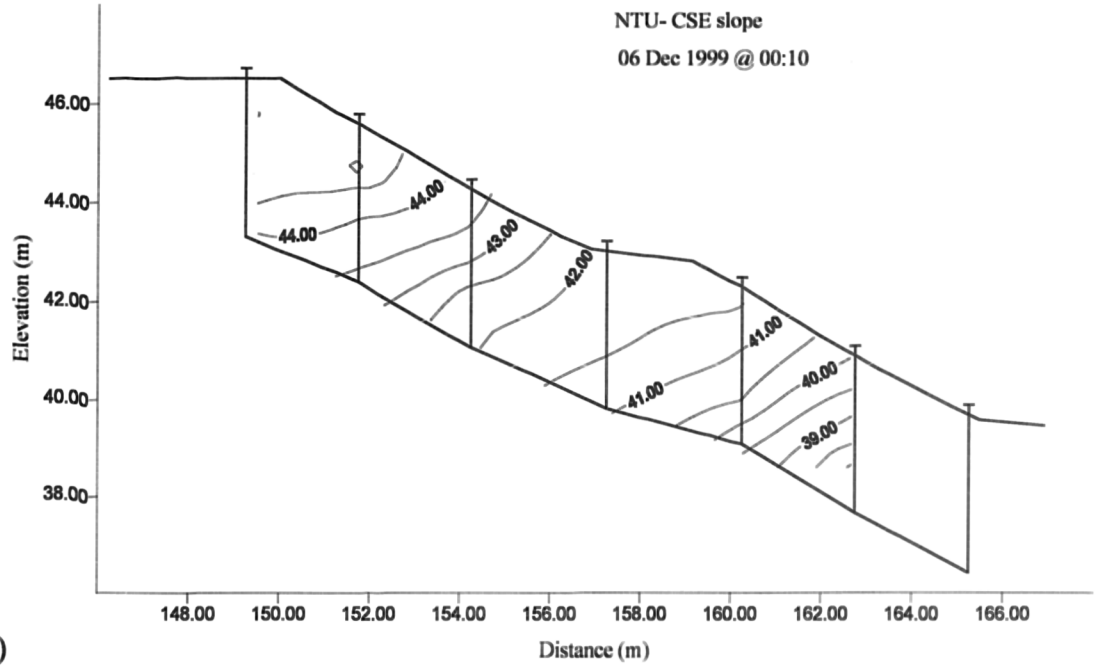

a)

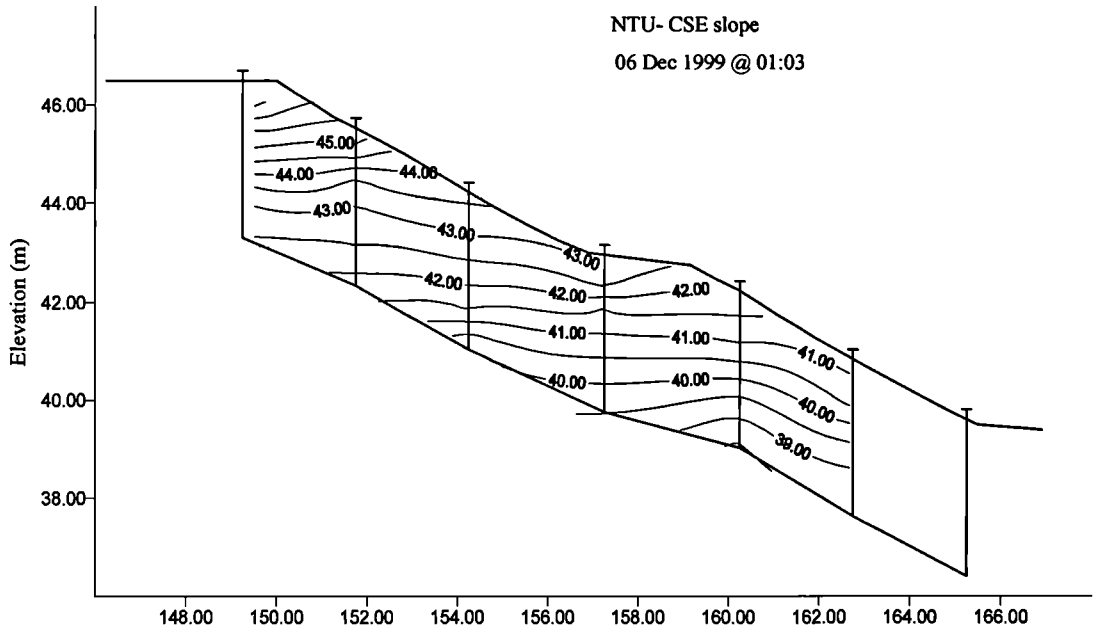
NTU- CSE slope
06 Dec 1999 @ 01:03
Elevation (m)
46.00
44.00
42.00
40.00
38.00
45.00
44.00
43.00
42.00
41.00
40.00
39.00
148.00
150.00
152.00
154.00
156.00
158.00
160.00
162.00
164.00
166.00
Distance (m)

b)

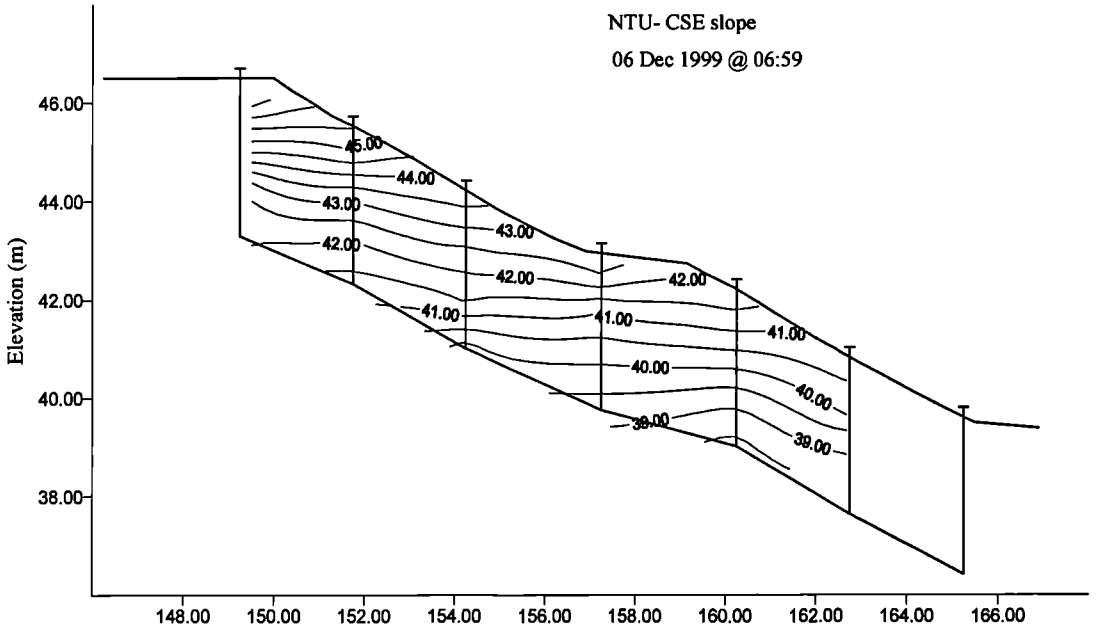
NTU- CSE slope
06 Dec 1999 @ 06:59
Elevation (m)
46.00
44.00
42.00
40.00
38.00
45.00
44.00
43.00
42.00
41.00
40.00
39.00
148.00
150.00
152.00
154.00
156.00
158.00
160.00
162.00
164.00
166.00
Distance (m)

c)

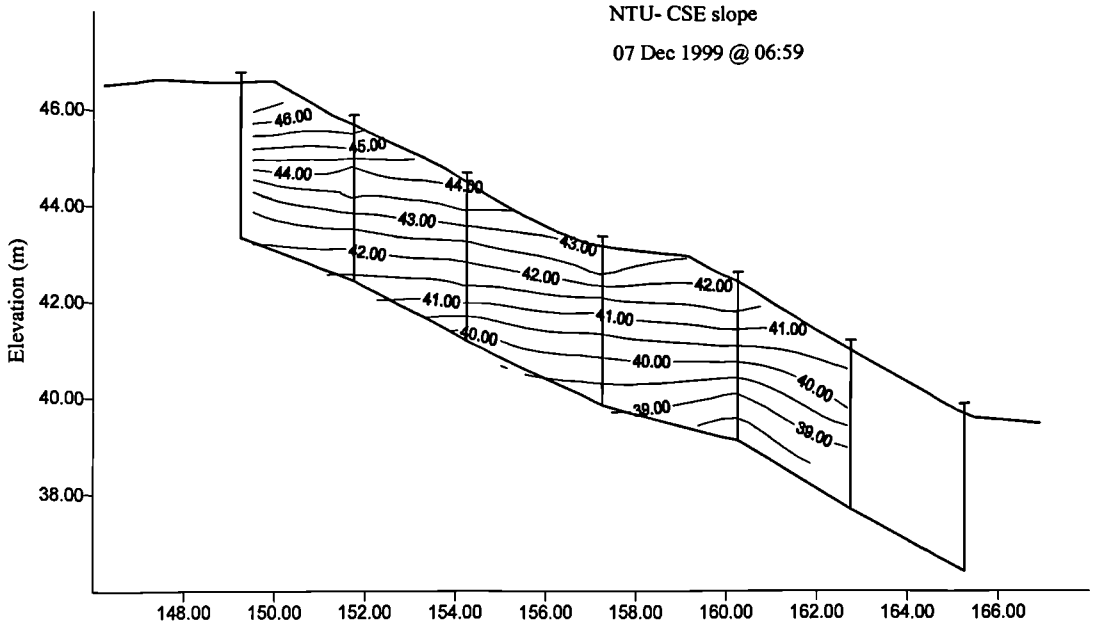

d)

Figure 5.6 Total head contours (in m) of the NTU-CSE slope on a) 06-Dec-99 00:10, b) 06-Dec-99 01:03, c) 06-Dec-99 06:59 and d) 07-Dec-99 06:59.

Analysis of the best (driest) conditions

The measurements of the pore-water pressures at the NTU-CSE site were at minimum on 15-Mar-00 at 15:45. The time steps adopted for the analysis of the pore-water pressures were the following:

1. 15-Mar-00 15:45, when the pore-water pressures were recorded as minimum.
2. 15-Mar-00 16:27, when a minor rainfall started.
3. 15-Mar-00 18:37, when the minor rainfall stopped.
4. 16-Mar-00 18:37, 24 hours after the end of the rainfall event of 15-Mar-00.

Figure 5.3 presents the pore-water pressure profiles of the all rows of tensiometers of the NTU-CSE slope (rows A though F). The pore-water profiles of Figure 5.3 were used for the production of the pressure and total head contours of the slope, which are presented in Figure 5.8 and Figure 5.9. The contour plots were drawn using the commercial software Surfer for Windows (Golden Software Inc.). Figure 5.7 presents the pore-water pressure changes with time, as they were monitored at the crest, the middle and the toe of the slope.

The pore-water pressures at 0.5m deep measured at rows A and C, at the crest and the middle of the slope respectively, are very low before the start of the rainfall (Figure 5.7a and b). In row A, the pore-water pressures, measured at 0.5m, were –81kPa, in Row C –71kPa (Figure 5.3a and c). The small rainfall event of 1mm total rain that started at 16:27 caused a large pore-water pressures increase at these points. At the crest of the slope the increase was from –81kPa to -31kPa, a change of 50kPa (Figure 5.3a and c). The pore-water pressures at the middle of the slope, 0.5m deep, increased from –71kPa to –7kPa an increase equal to 64kPa (Figure 5.3a and c).

At 1.1m deep, at the crest of the slope (row A) there were only small pore-water pressure changes. However, in Row C there was a large pore-water pressure increase but this increase took place over a longer time (from –49kPa at the start of the rain to –30kPa 24 hours later) (Figure 5.7a and b). The pore-water pressures at 1.4m and 2.3m at the crest and the middle of the slope increased slightly, but not significantly and at 3.2m deep no pore-water pressure changes were observed (Figure 5.7a and b).

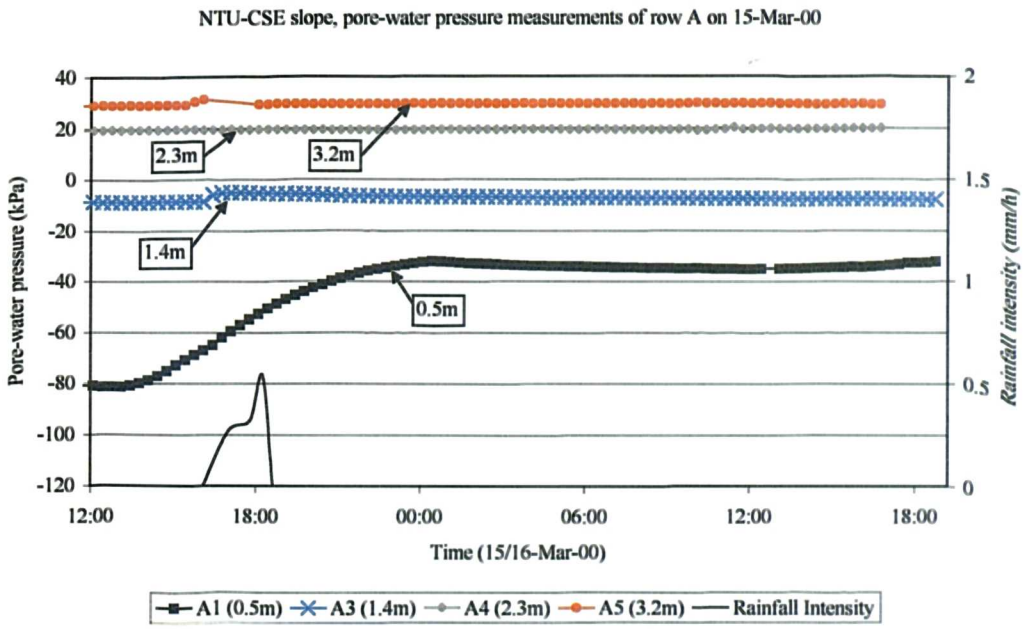

a)

b)

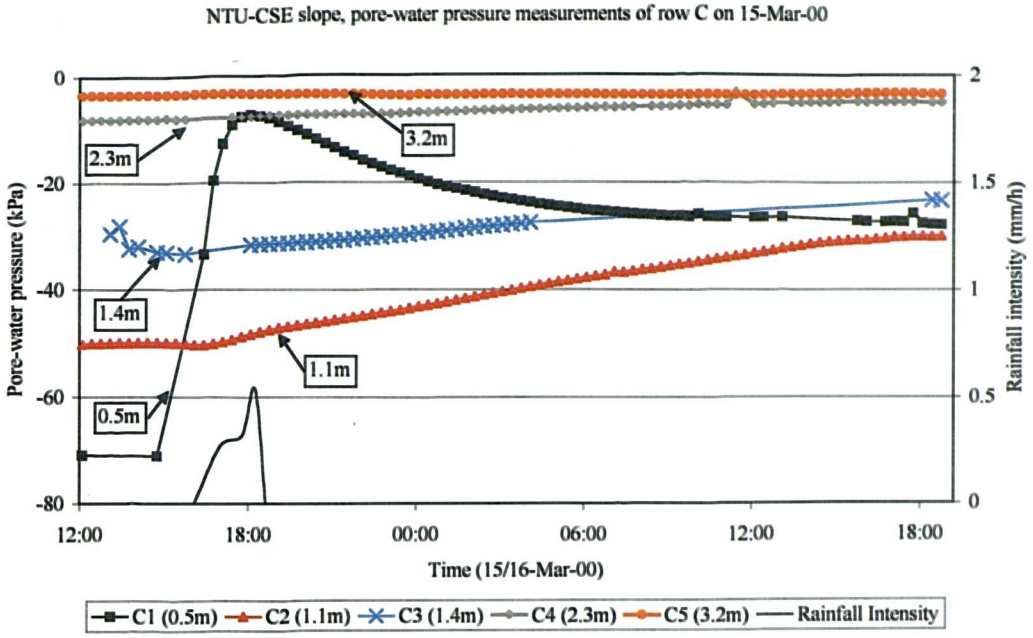

c)

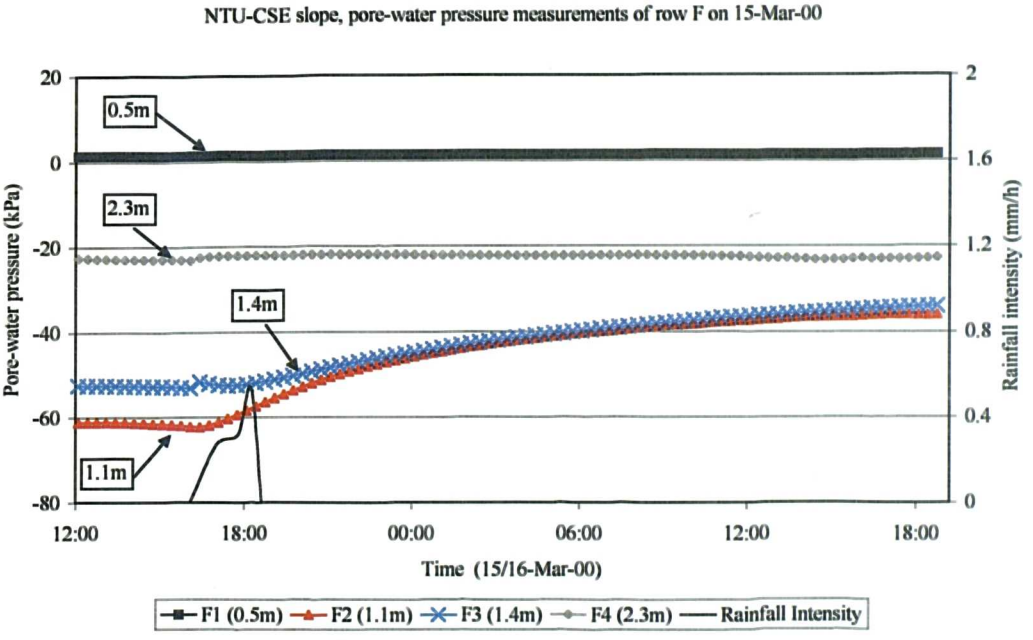

Figure 5.7 Pore-water pressure measurements in the NTU-CSE slope on 15-Mar-00: a) at the crest of the slope (row A), b) at the middle of the slope (row C) and c) at the toe of the slope (row F).

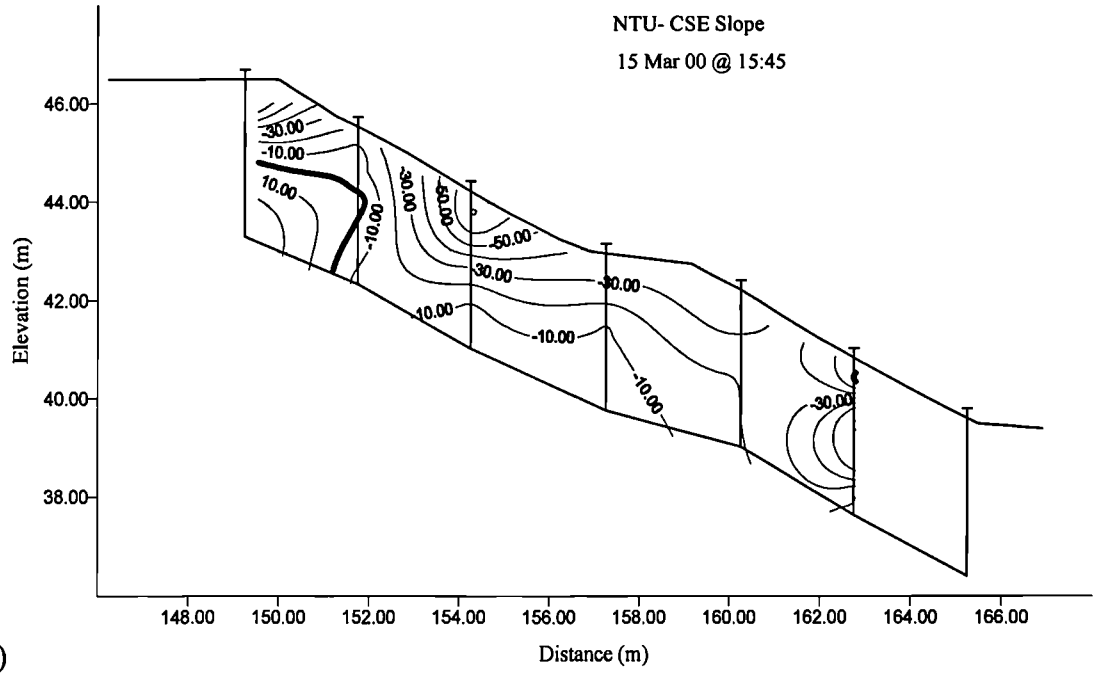
NTU- CSE Slope
15 Mar 00 @ 15:45
Elevation (m)
46.00
44.00
42.00
40.00
38.00
148.00
150.00
152.00
154.00
156.00
158.00
160.00
162.00
164.00
166.00
Distance (m)
-30.00
-10.00
10.00
-50.00
30.00

a)

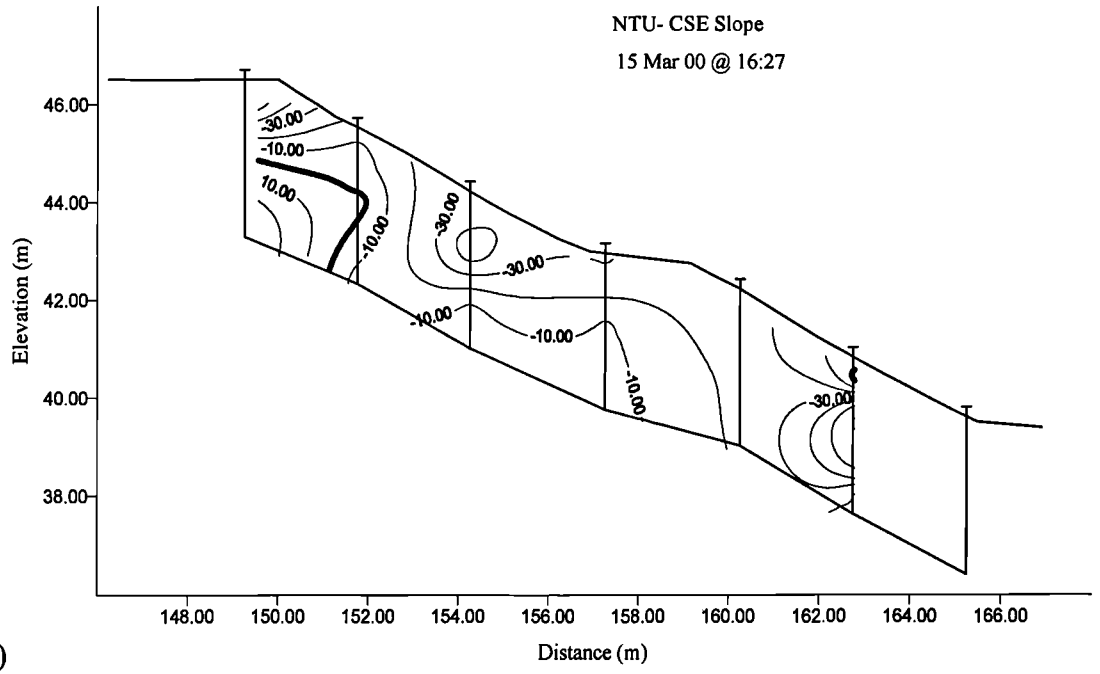
NTU- CSE Slope
15 Mar 00 @ 16:27
Elevation (m)
46.00
44.00
42.00
40.00
38.00
148.00
150.00
152.00
154.00
156.00
158.00
160.00
162.00
164.00
166.00
Distance (m)
-30.00
-10.00
10.00
30.00

b)

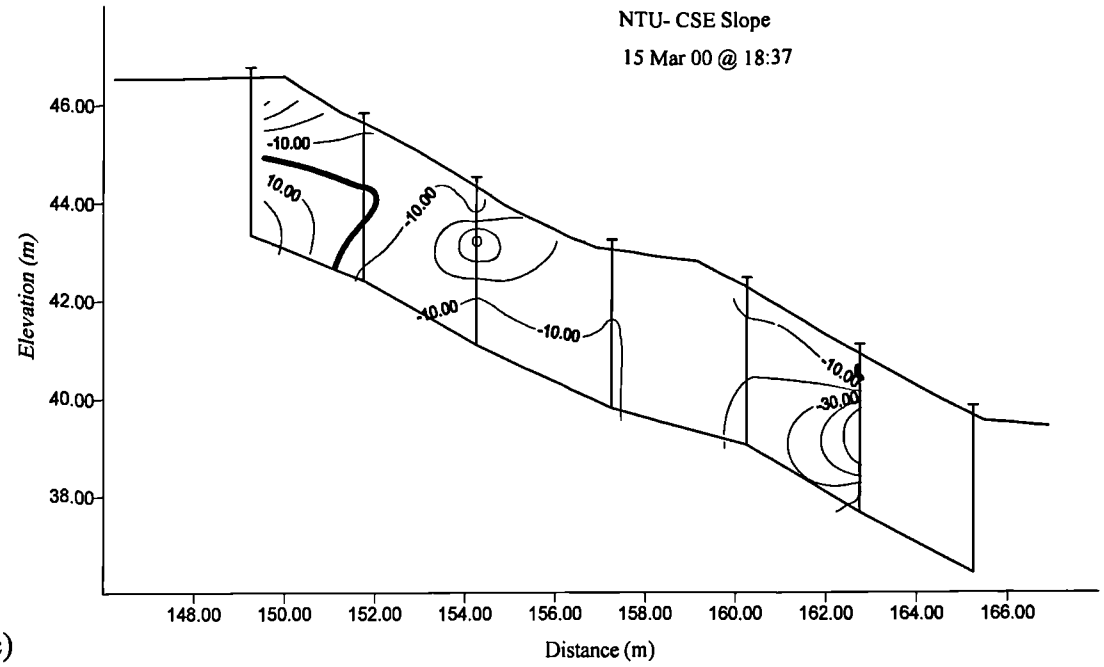

c)

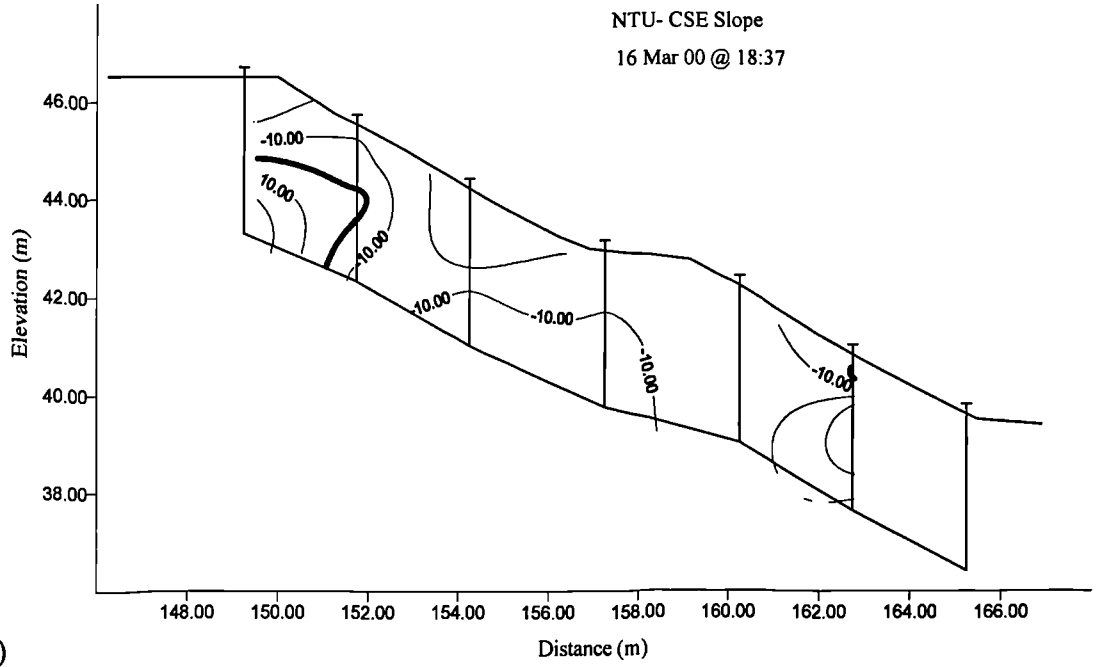

d)

Figure 5.8 Pressure contours (in kPa) of the NTU-CSE slope on (a) 15-Mar-00 15:45, (b) 15 Mar-00 16:27, c) 15-Mar-00 18:37 and (d) 16-Mar-00 18:37.

The pore-water pressures 0.5m deep at the toe of the slope remained constant during the rainfall event and equal to 1kPa (Figure 5.7c). However, significant pore-water pressure changes were observed at 1.1 and 1.4m deep at the toe of the slope. It is likely that the unchanging value of pore-water pressure at 0.5m deep indicates cavitation of the tensiometer measuring at 0.5m deep (Figure 5.3f). The true

pore-water pressure was probably more negative than –80kPa, which could cause cavitation.

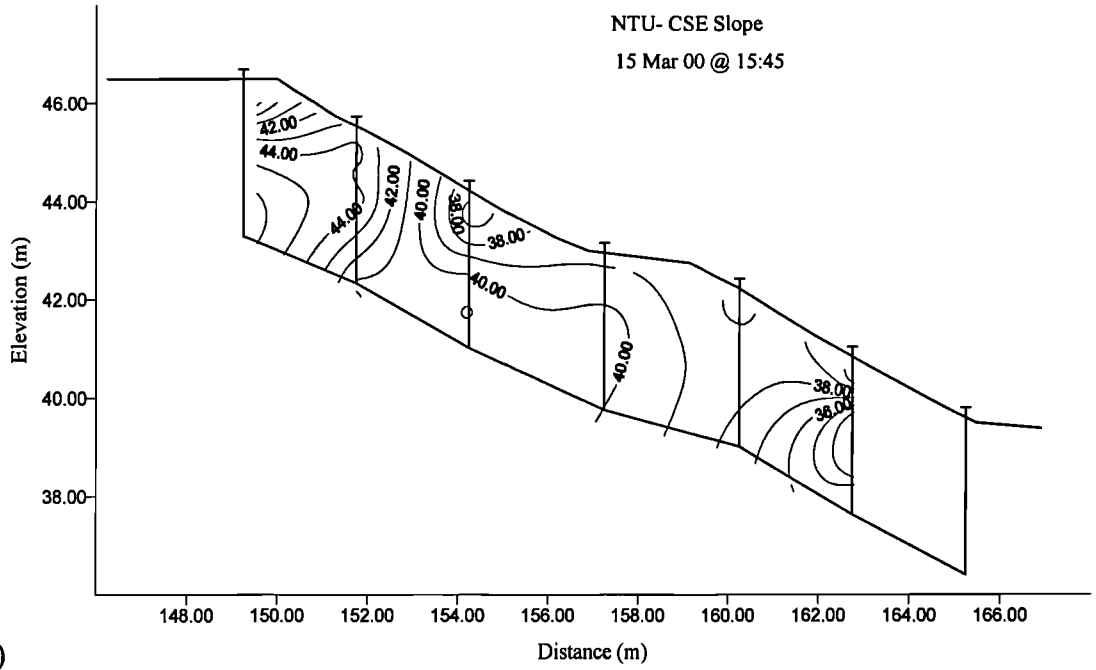

a)

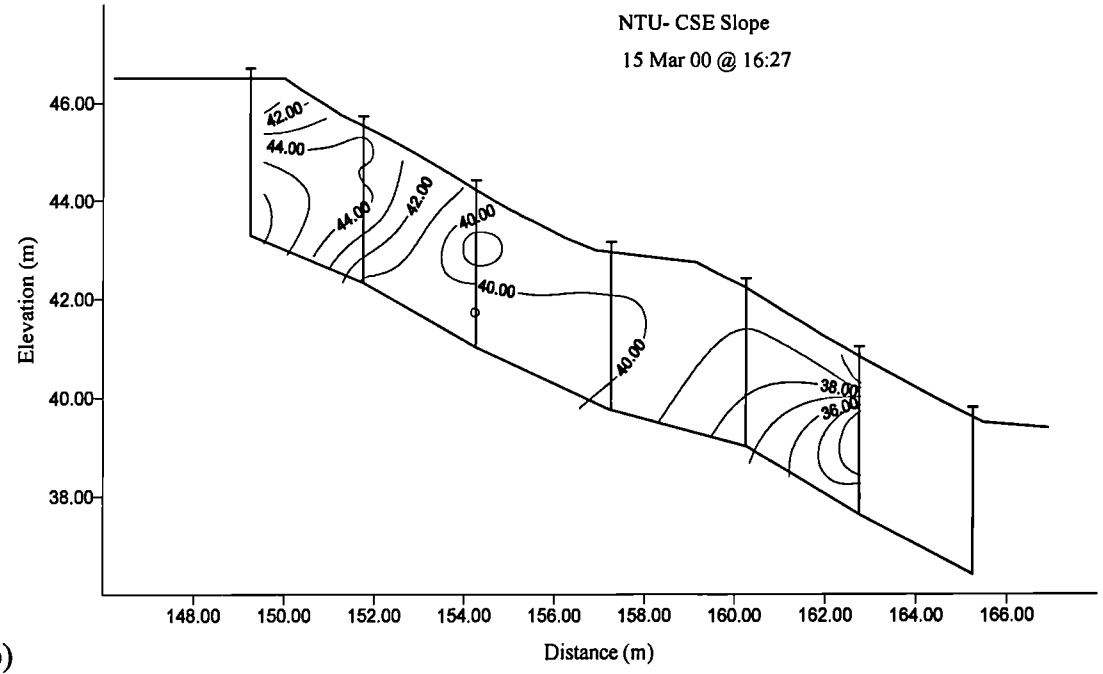

b)

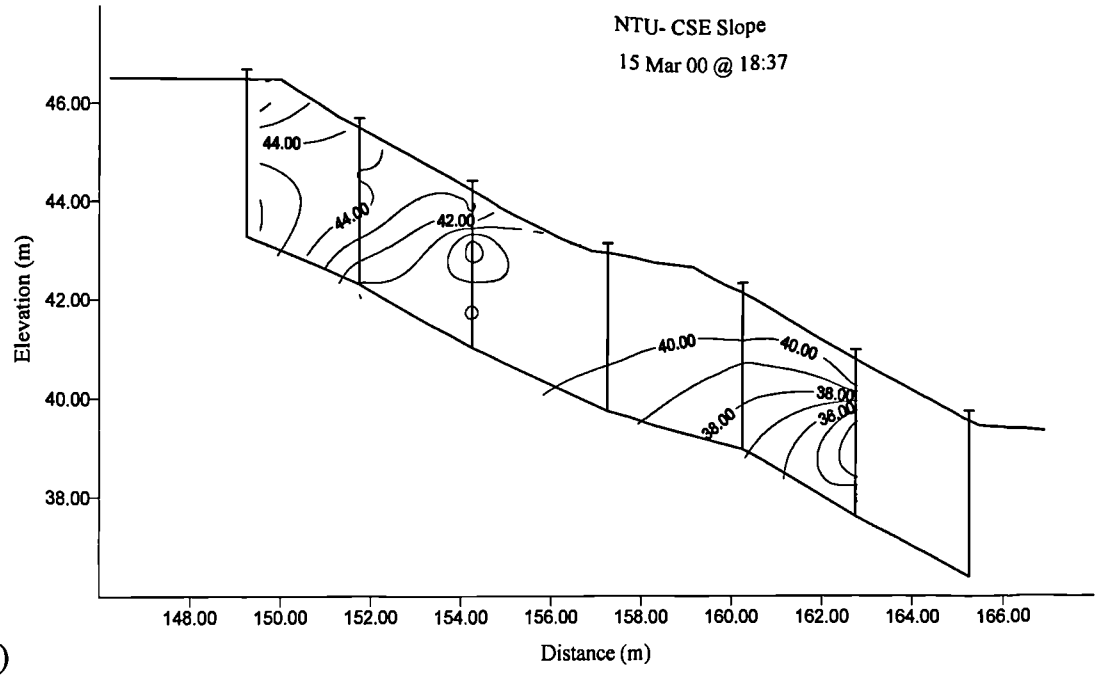

c)

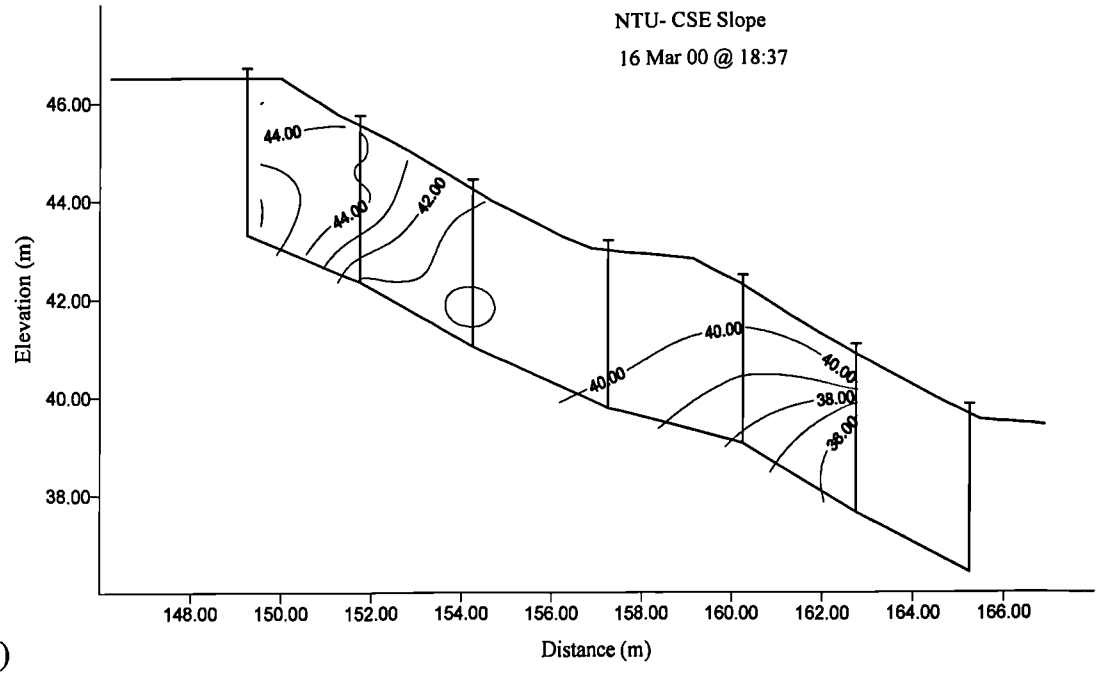

d)

Figure 5.9 Total head contours (in m) of the NTU-CSE slope on (a) 15-Mar-00 15:45, (b) 15 Mar-00 16:27, c) 15-Mar-00 18:37 and (d) 16-Mar-00 18:37.

The pore-water pressures at the toe of the slope, 1.1m and 1.4m deep, increased gradually from the start of the minor rainfall event until 24 hours after the end of the rainfall event. At 1.1m deep the increase was from –62kPa to -38kPa (i.e. an increase equal to 24kPa) and at 1.4m the pore-water pressures increased from –53 to –37kPa, an increase equal to 16kPa. At 2.3m deep the pore-water pressures increased slightly, but not significantly (Figure 5.7c).

The redistribution of the pore-water pressures within the slope, during and until 24 hours after the minor rainfall event of 15 March 2000, can also be seen from the pressure contours of the slope for the each time step of the analysis (Figure 5.8). The pore-water pressures changed significantly between the locations of the slope showing the variability of the soil properties, as was discussed in Section 3.2. The minimum pore-water pressure measurements were made on 15 March 2000 15:45 (Figure 5.8a). The pore-water pressures near the ground surface were lower than -30kPa for most of the locations of the slope. Pore-water pressures significantly higher than –30kPa were observed at row B, which lies immediately below the crest of the slope. The pore-water pressures at row B were measured at 15:45 equal to -7kPa (Figure 5.3b). In the upper half of the slope, the pore-water pressures near the ground surface were as low –80kPa, however in the lower half of the slope the pore-water pressure were about –40kPa (Figure 5.3 and Figure 5.8a). The minor rainfall event of 1mm caused large pore-water pressure changes near the ground surface of the upper half of the slope (Figure 5.8b and c) and minor changes in the pressure contours can be observed at higher depths. For the lower part of the slope, there was some increase observed at greater depths (Figure 5.8).

The flow patterns of the minor rainfall event cannot easily be identified from the total head contours of Figure 5.9. This can be attributed to the fact that the rainfall event is too small and with a very low intensity and also to the fact that the slope is not homogenous and thus the drying process varied considerably at different locations during the dry period prior to the rainfall event. Initially (Figure 5.9a), there is a high decrease of the total heads near the ground surface at the upper half of the slope. By the end of the rainfall event, the soil near the ground surface has increased its moisture content, resulting in an increase of the pore-water pressure. Therefore, by the end of the rainfall event (Figure 5.9c) the total head increased more gradually with depth. The shape of the total head contours at the middle of the slope is almost perpendicular to the ground surface (Figure 5.9c and d), indicating that water flows downslope towards the toe of the slope. At the toe of the slope, the shape of the total head contours is less inclined, than in the middle, and in that area water flowed towards larger depths.

Comparison of the two extreme cases

The analysis of the two extreme cases for the NTU-CSE slope shows that the changes in the pore-water pressures are not only dependent on the rainfall patterns but also on their initial values. When the pore-water pressures were at maximum (06-Dec-99) and the rainfall event was of a long duration and intensive, only limited changes were observed, especially near the ground surface, although the soil was not saturated (Figure 5.3). In the same case it was found that the pore-water pressures at 0.5m deep remained constant and slightly decreased after they have reached a peak value during the rainfall. At greater depths it was also found that it took a long time before the pore-water pressures started to increase due to the infiltration.

For the case of minimum pore-water pressures (15-Mar-00) it was found that the pore-water pressures near the ground surface are very sensitive even to a very small amount of infiltration, when they are very low (in the range of −30 to −80kPa). In that case the increase of pore-water pressures was significant (Figure 5.3a and c). At the same time, for points in the slope where the pore-water pressures were measured in a usual range of 0 to −15kPa the influence of infiltration was not very significant (Figure 5.3b).

Due to the geological complexity of the NTU-CSE slope, there are locations where pore-water pressures can change significantly and very rapidly as soon as a rainfall event starts (e.g. the difference of the pore-water profiles of rows C as shown in Figure 5.3c). By contrast, at other locations of the slope the changes in the pore-water pressures can be small and can occur after a long time from the start of the rainfall event (e.g. the pore-water pressure profiles of row D in Figure 5.3d). Also, at the toe of the slope, where the tree exists, pore-water pressures are highly influenced by the tree roots, and the pore-water pressure profile of row F (Figure 5.3f) may significantly differ to the pore-water pressure profile of the neighbouring row E (Figure 5.3e). This geological complexity makes a detailed analysis a difficult task.

5.1.2 Effect of rainfall and the initial conditions within the NTU-CSE slope on the pore-water pressures

The previous cases (Section 5.1.1) indicated that the initial conditions within the two slopes at the start of the rainfall events influence the pore-water pressure changes during and after a rainfall event. This is examined further by considering all the rainfall events within the study period. Chapter 4 presents all the significant rainfall events of the study period (August 1999 to August 2000) with total rainfall greater than 5mm. However the pore-water pressure measurements indicate that pore-water pressures may change with total rainfall of less then 5mm. For that reason, the analysis presented in this section, includes all rainfall events (105 in total) of total rainfall greater than 1mm. In the analysis presented in the following paragraphs it is attempted to correlate the final pore-water pressure, resulted by rainfall, with the total rainfall and the initial value of the pore-water pressure. As it will be seen from the following analysis, some useful trends were shown from these correlations. However, it has to be noted that the available data, especially for 0.5m deep, do not cover the full range of initial values of pore-water pressures for all values of total rainfall. Therefore, the conclusions from this analysis are handled with a degree of uncertainty.

The analysis for the effect of rainfall and the initial conditions of the NTU-CSE slope on the pore-water pressure changes is concentrated on the pore-water pressure changes that were monitored at the crest, the middle and the toe of the slope. The analysis adopts the data of row A for the crest of the slope and the data of row C for the middle of the slope. The analysis of the worse (most moist) and best (driest) conditions showed that it very likely that the roots of the existing tree at the toe of the NTU-CSE slope influenced the data of row F (at the toe of the slope), by preserving the pore-water pressure at low values in comparison with other locations of the slope. For that reason, the data of the neighbouring row E were chosen for the analysis. The choice of row E for the analysis is not considered to alter significantly the conclusions of the analysis, as it lies in a horizontal distance of approximately 2.5m from the toe of the slope and at the same time it is unlikely that the data from row E are influenced from the existing tree. Section 3.3.2 describes the location and layout of the tensiometers of rows A, C and E on the NTU-CSE slope.

The contour plots of Figure 5.10 present the final pore-water pressure (caused by a rainfall event), at 0.5m deep, for different total rainfall and initial pore-water pressure, at the crest (row A), the middle (row C) and the toe (row E) of the NTU-CSE slope. The data in Figure 5.10 include all rainfall events, with total rainfall greater than 1mm that were precipitated on the NTU-CSE slope during the monitoring period (from August 1999 to August 2000). From Figure 5.10a can be seen that the contours of the final pore-water pressure at the crest of the slope, 0.5m deep, are almost vertical for rainfall events with total rainfall up to approximately 15mm. In addition, the pore-water pressures at the crest of the slope, 0.5m deep increase largely from their initial value for rainfall events up to 15mm. This means that for rainfall events up to 15mm the pore-water pressure changes are controlled by the amount of rainfall and are largely unaffected by the initial pore-water pressure values. For rainfall events greater than 20mm the contours of Figure 5.10a are almost horizontal (Figure 5.10a). This means that for rainfall events greater than 15mm, the amount of rainfall is unimportant and the pore-water pressure changes are controlled by the initial pore-water pressure conditions. Finally, it has to be noted that no rainfall event that was precipitated on the NTU-CSE slope resulted in positive final pore-water pressures at the crest of the slope, 0.5m deep (Figure 5.10a).

The contours of the final pore-water pressures (caused by rainfall) at the middle of the slope (row C), 0.5m deep, as shown in (Figure 5.10b) show similar trends as for the crest of the slope (Figure 5.10a). The final pore-water pressures at 0.5m deep, at the middle of the slope, (Figure 5.10b) increase significantly for rainfall events up to approximately 15mm. For rainfall events greater than 15mm (Figure 5.10b), the increase of the pore-water pressures occurs with a smaller rate. However, rainfall events greater than 15mm result in positive final pore-water pressure at 0.5m deep, at the middle of the slope. The contour plot of final pore-water pressures (resulted by rainfall) at 0.5m deep for the toe of the slope (row E in Figure 5.10c) show similar behaviour with the plot for the middle of the slope (Figure 5.10b), although not as clear cut. Nevertheless, there is a transition in behaviour around 15mm of total rainfall, as for the crest and the middle of the NTU-CSE slope.

As was seen in section 5.1.1, the pore-water pressure changes during rainfall at great depths in the NTU-CSE slope are smaller than the pore-water pressure changes at

0.5m deep (Figure 5.3). Figure 5.11 and Figure 5.12 presents the contour plots of the final pore-water pressures at 1.1m and 3.2m deep, respectively, at the crest (row A), middle (row C) and toe (row E) of the NTU-CSE slope for different total rainfall and different initial pore-water pressures. Figure 5.11 and Figure 5.12 show that the final pore-water pressures are highly influenced by their initial values at the start of the rainfall event. Especially for the depth of 3.2m of rows A, C and E of the NTU-CSE slope (Figure 5.12), the pore-water pressure changes during rainfall are limited and any significant changes occur only after large amounts of rainfall.

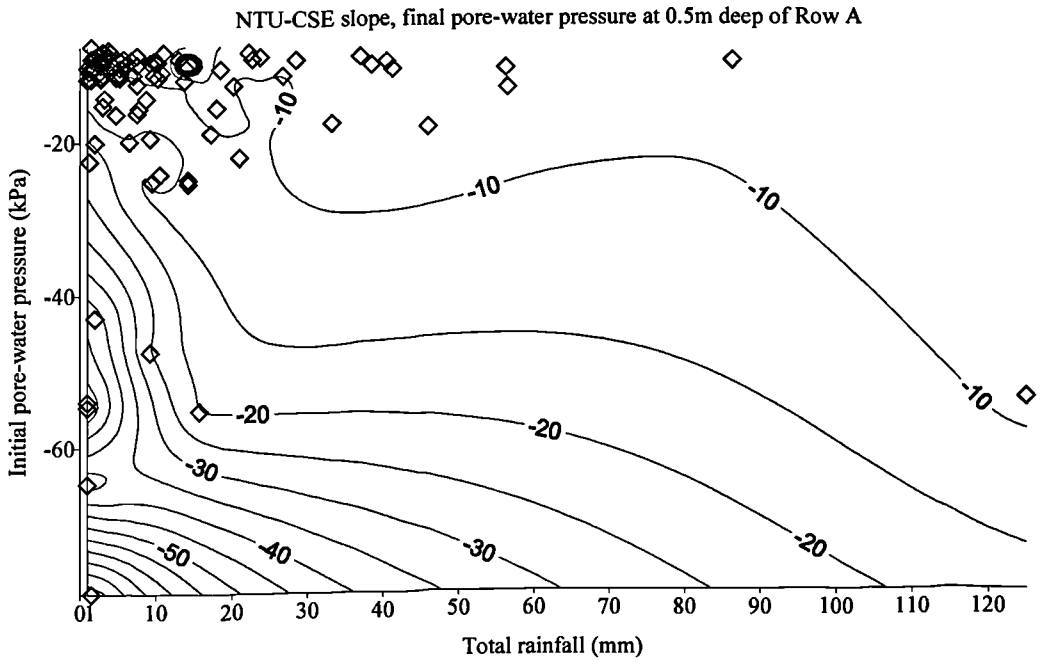

a)

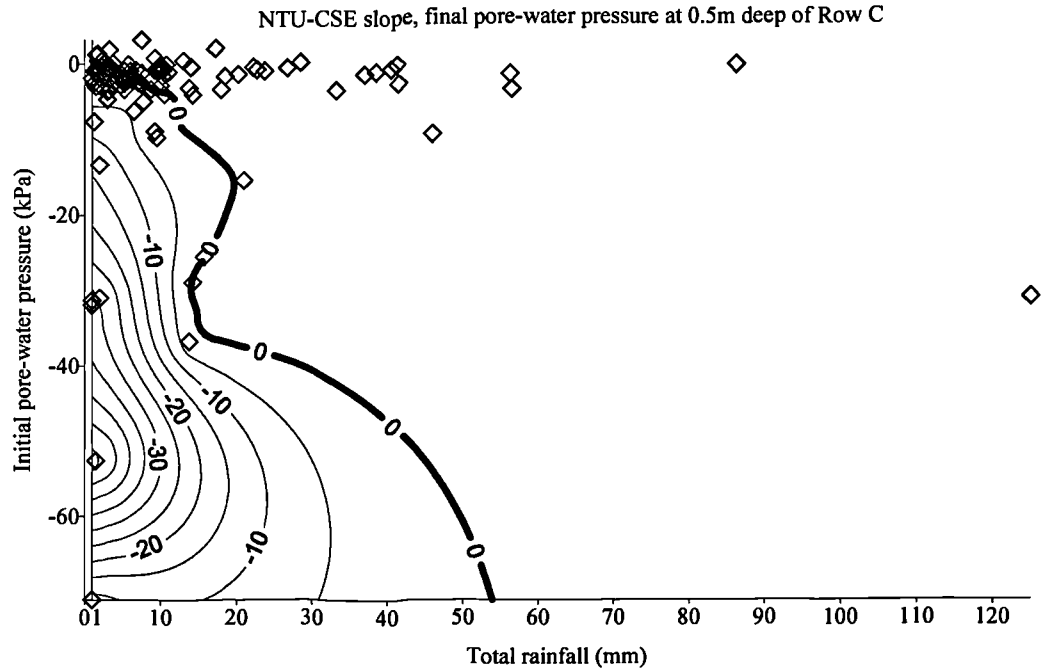

b)

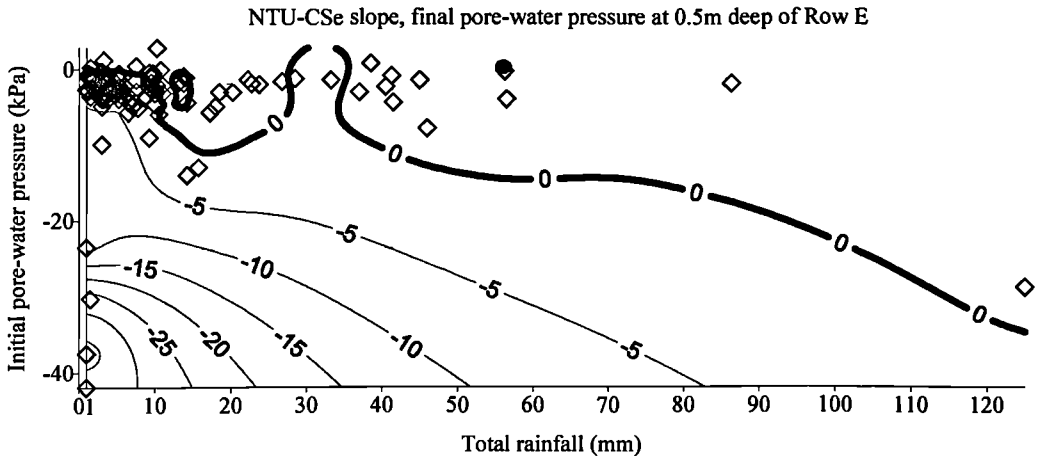

c)

Figure 5.10 Contour plot (in kPa) of the final pore-water pressure (resulted by rainfall) at 0.5m deep at the a) crest (row A), b) middle (row C) and c) toe (row E) of the NTU-CSE slope for different total rainfall and different initial pore-water pressures.

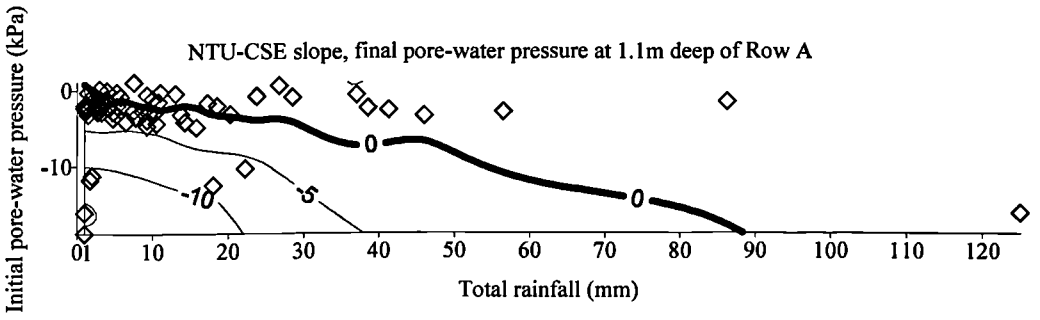

a)

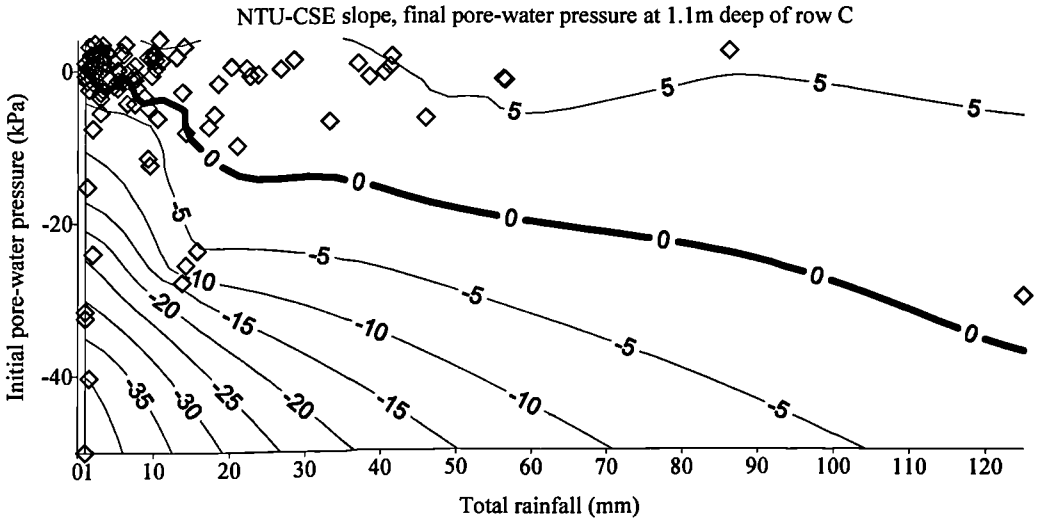

b)

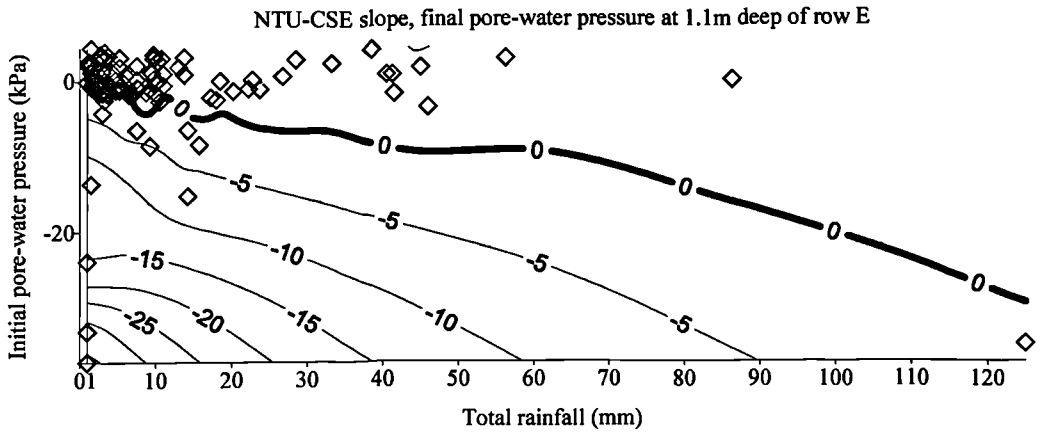

c)

Figure 5.11 Contour plot (in kPa) of the final pore-water pressure (resulted by rainfall) at 1.1m deep at the a) crest (row A), b) middle (row C) and c) toe (row E) of the NTU-CSE slope for different total rainfall and different initial pore-water pressures.

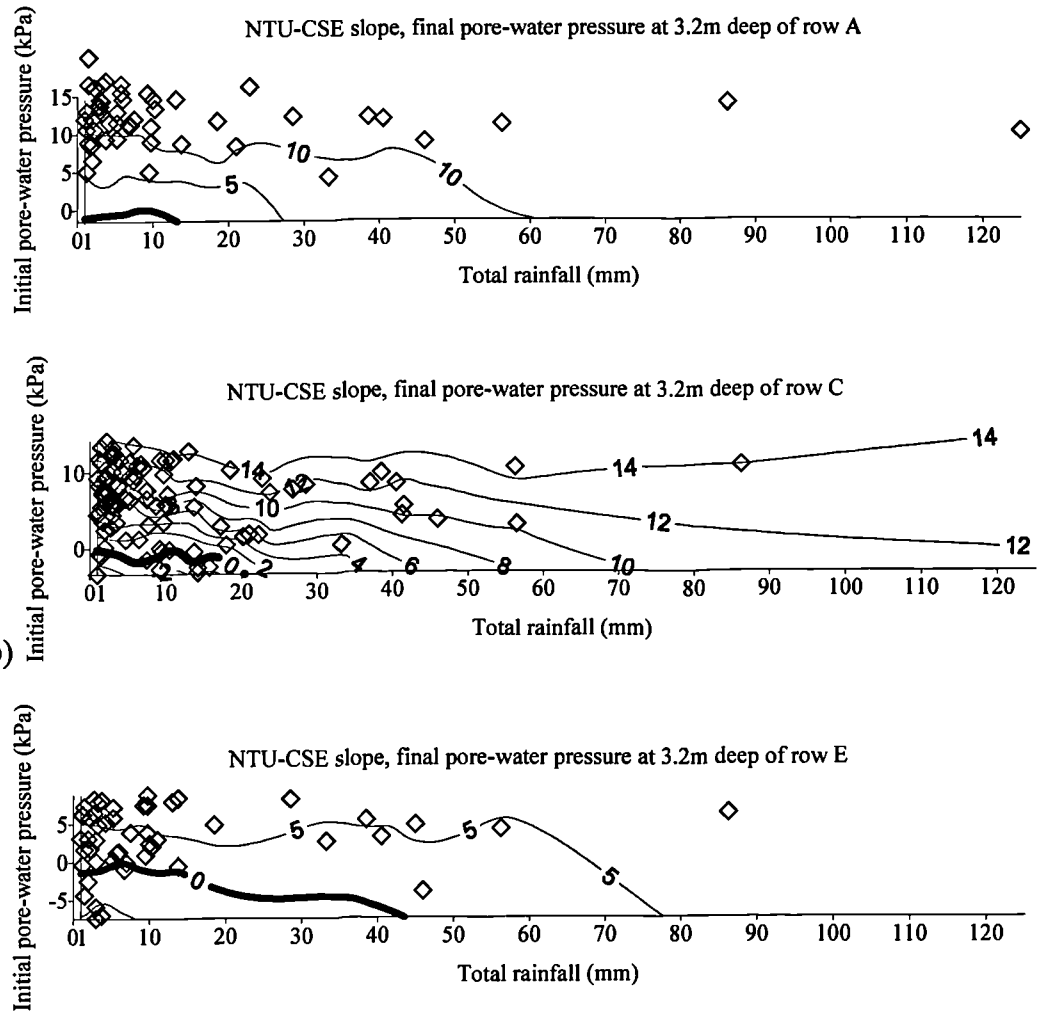

a)

(b)

c)

Figure 5.12 Contour plot (in kPa) of the final pore-water pressure (resulted by rainfall) at 3.2m deep at the a) crest (row A), b) middle (row C) and c) toe (row E) of the NTU-CSE slope for different total rainfall and different initial pore-water pressures.

From the above analysis it can be concluded that at small depths the initial conditions within the slope is an important parameter in the way the pore-water pressures will develop during rainfall. The pore-water pressures near the ground surface (Figure 5.10) are highly influenced by rainfall events of total rainfall less than 15mm. As the total rainfall increases above the limit of 15mm then the pore-water pressure changes are controlled mainly by their initial values. For larger depths (Figure 5.12) the pore-water pressure changes are limited.

5.1.3 Slope stability analysis of the worst (wettest) and best (driest) conditions of the NTU-CSE slope

An analysis on the stability of the NTU-CSE slope was also conducted for the time steps of the analysis as they were described in Section 5.1.1. The methodology of the slope stability analysis is described in Section 2.9 and satisfies moment equilibrium. For the slope stability analysis the commercial software Slope/W (Geo-Slope Int. 1998b) was used. Table 5.1 summarises the strength parameters for each soil layer of the NTU-CSE slope. Gasmo (1997) and Hritzuk (1997) measured the strength parameters of Layer 1 and Layer 2 respectively. Layer 3 is assumed for the analysis to be hard layer and Layer 4 is the bedrock. Since no failure surfaces penetrated Layers 3 and 4 during the analyses, the choice of parameters was unimportant. The properties of soil Layers 1 through 3 and the soil profile of the NTU-CSE slope are documented in Chapter 3 (Section 3.2).

Table 5.1 Summary of the strength parameters used in the slope stability analysis of the NTU-CSE slope.

No.	Friction angle ϕ'	Friction angle ϕ^b	Cohesion c' (kPa)	Unit weight (kN/m^3)
1	26.5°	23°	20	21.00
2	35°	35°	90	22.6

Figure 5.13 presents the results of the slope stability analyses for the major rainfall event of 86mm that took place on 06 December 1999. The times that were chosen are at the start of the rain (i.e. at 00:10), at the moment of the highest pore-water pressures (i.e. at 01:03), at the end of the rainfall (i.e. at 06:59) and finally 24 hours after the end of the rainfall (i.e. on 07-Dec-99 at 06:59).

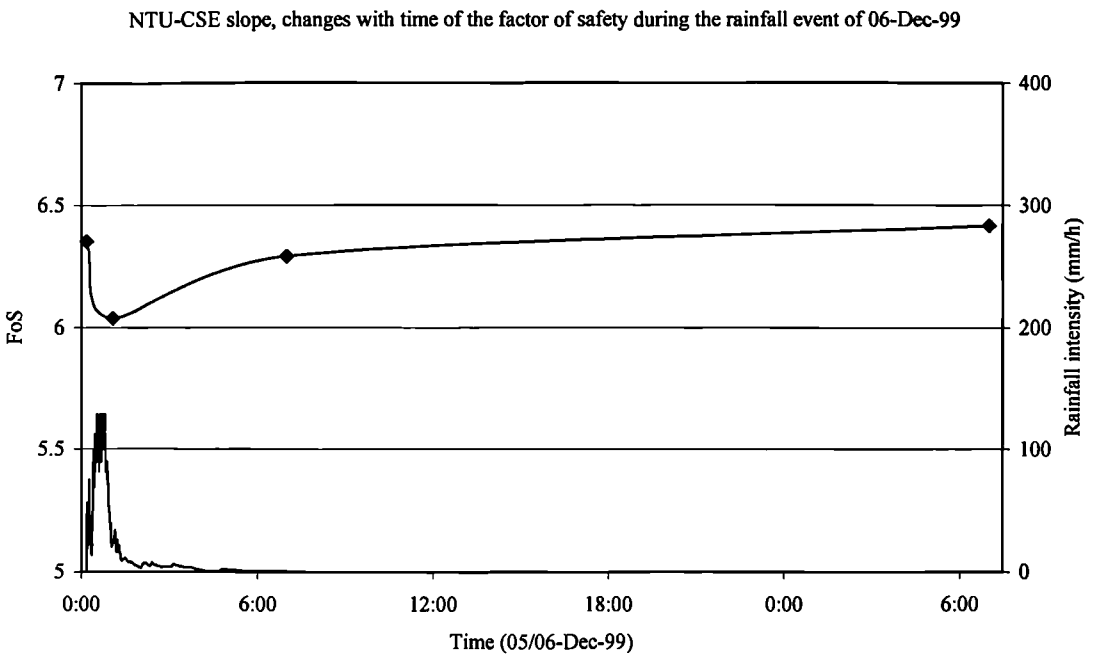

Figure 5.13 Development with time of the factor of safety of the slope for the NTU-CSE slope on 06-Dec-00.

From Figure 5.13 it can be seen that the factor of safety at the start of the major rainfall event is 6.5 and one hour later (at 01:03), when the pore-water pressures near the ground surface were at maximum, the factor of safety drops to 6.04. At the end of the rainfall event the factor of safety has almost recovered to its initial value of 6.3, and 24 hours later it has increased further to 6.4. The trend that the factor of safety of the slope follows is in good agreement with the changes of the pore-water pressures near the ground surface at the crest of the slope.

Figure 5.14 presents the most critical slip surface from the slope stability analysis for 06-Dec-99 01:03. The potential slip surface lies entirely within the weakest material, Layer 1, at the crest of the slope and its depth is shallow, between 0.5m and 1.0m. The potential slips with the 6 lowest calculated factors of safety lay in Layer 1 due to the low strength parameters of that layer (Table 5.1). However, it has to be noted that the location of the critical slip surface of Figure 5.14 does not lie in the zone of the highest pore-water pressures (Figure 5.5b), which were identified at the middle of the slope.

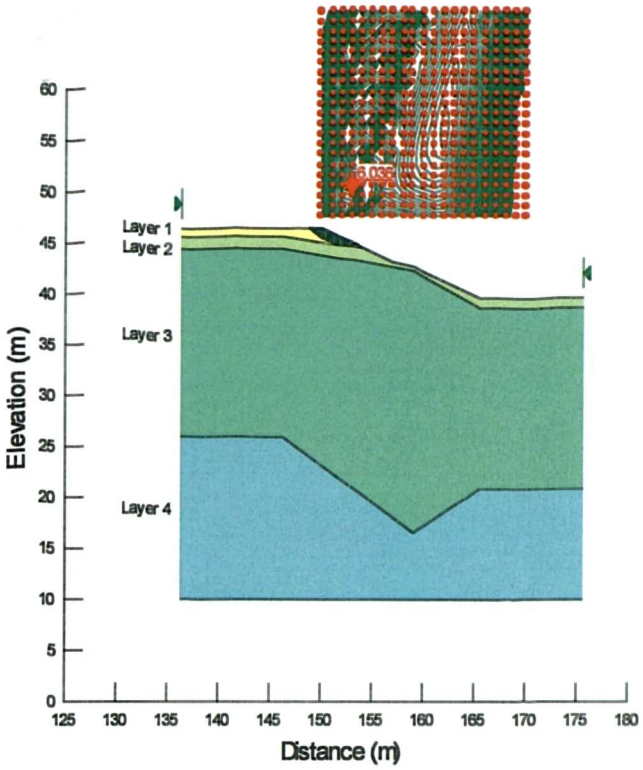

Figure 5.14 Location of the critical slip surface at the NTU-CSE slope for the stability analysis conducted for 06-Dec-99 at 01:03.

Figure 5.15 presents the results of the slope stability analysis for the 15 March 2000, when the pore-water pressures near the ground surface were at minimum and a minor rainfall event of 1mm took place. The times that were chosen for the slope stability analysis are on 15-Mar-00 at 15:45 when the minimum pore-water pressure readings were observed, at 18:37 when the minor rainfall event ended and finally on 16-Mar-00 at 18:37 (i.e. 24 hours after the end of the rainfall event). The factor of safety when the minimum pore-water pressures (i.e. 15-Mar-00 15:45) were observed was 9.1 and at the end of the rainfall it dropped to 8.0. After 24 hours the factor of safety dropped further to 7.8.

Figure 5.16 and Figure 5.17 give the critical slip surface with the lowest and highest factor of safety during the period of 15 and 16 March 2000. The critical slip failure is the same in both cases and it goes through Layer 1. The drop in the calculated factor of safety is caused by the significant increase of the pore-water pressures near the ground surface at the crest of the slope (Figure 5.7a).

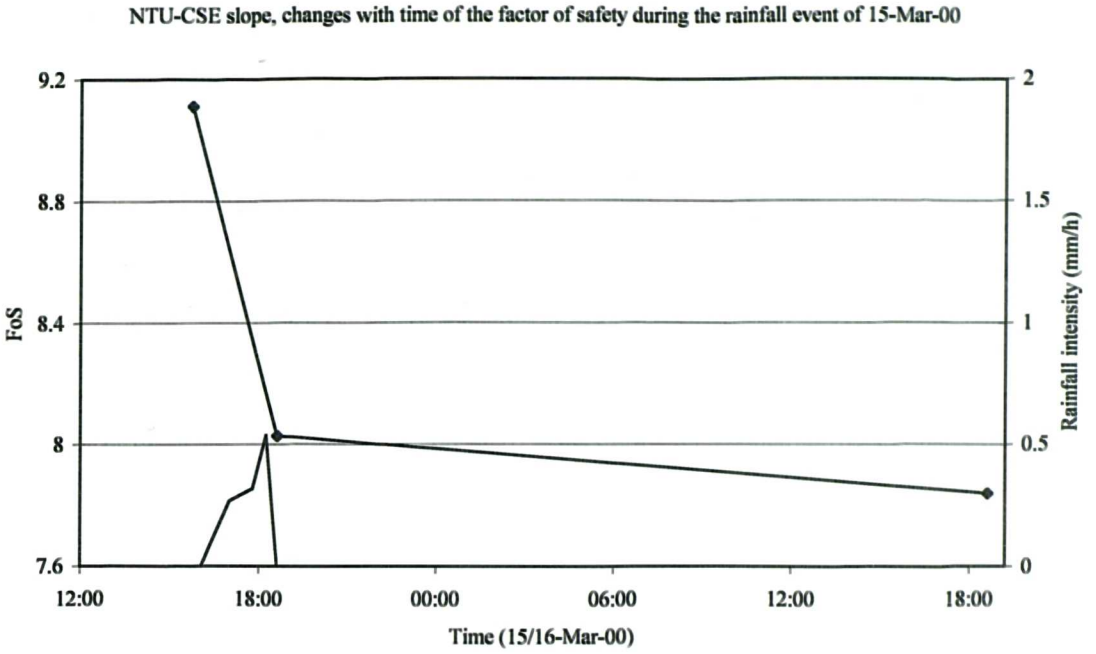

Figure 5.15 Development with time of the factor of safety for the NTU-CSE slope on 15-Mar-00.

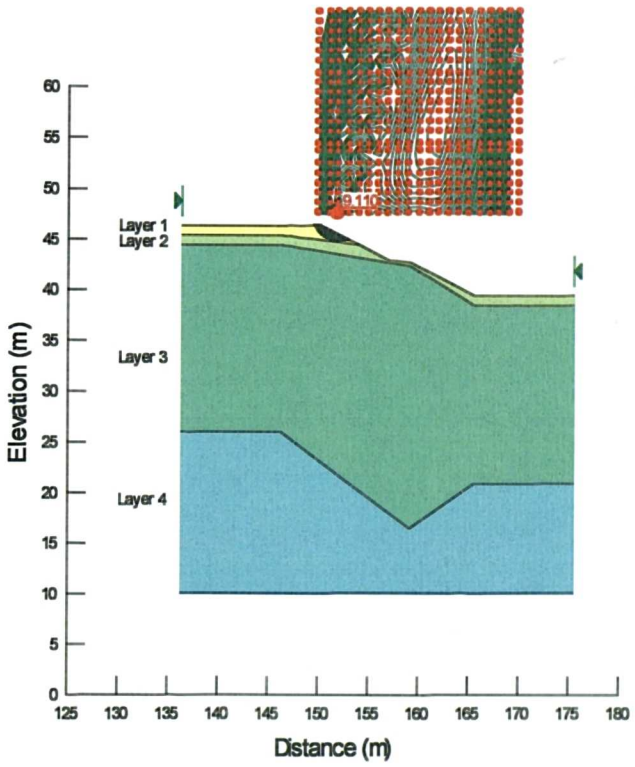

Figure 5.16 Location of the critical slip surface at the NTU-CSE slope for the stability analysis conducted for 15-Mar-99 at 15:45.

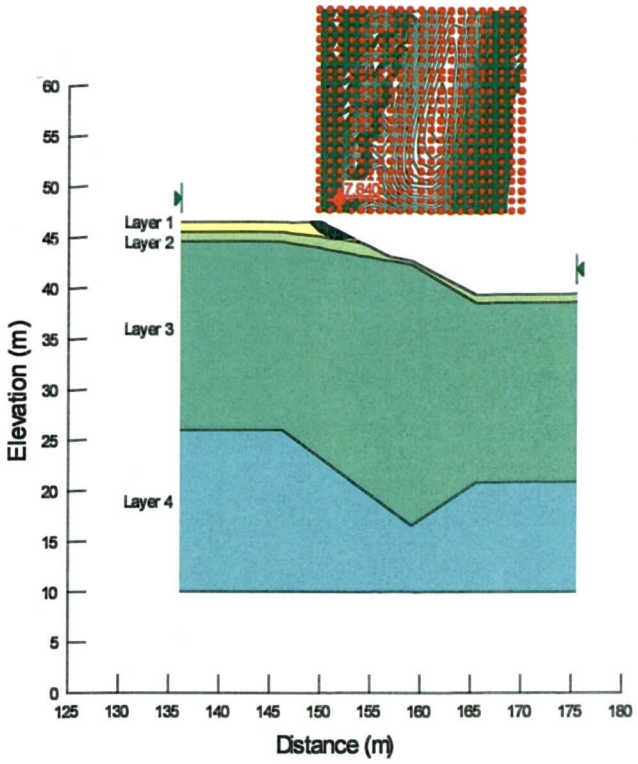

Figure 5.17 Location of the critical slip surface at the NTU-CSE slope for the stability analysis conducted for 16-Mar-99 at 15:45.

The slope stability analysis, which was conducted for the two extreme cases, on 06 December 1999, when the pore-water pressures near the ground surface of the slope were at maximum and on 15 March 2000, when the pore-water pressures near the ground surface were at minimum, show that the critical slip failure lies at shallow depths (about 1m) at the crest of the slope. However, in both extreme cases, the pore-water pressures below the crest of the slope were higher, than near the crest, where the critical slip surface was identified. This is attributed to the low strength parameters of Layer 1, in comparison with the defined strength parameters of Layer 2 (Table 5.1). Nevertheless, the increase of the pore-water pressures due to rainfall along the critical failure surface for both extreme cases has caused a considerable decrease to the calculated factor of safety.

5.2 NTU-ANX slope

This section presents the analysis of the field measurements and field-testing for the NTU-ANX slope. The monitoring period was approximately 6 months, from March to August 2000. The field measurements consist of pore-water pressures, natural rainfall, runoff produced by natural rainfall and depth of the groundwater table. The field-testing consists of simulated rainfall during dry periods. Measurements of runoff produced by the simulated rainfall are also available. The instrumentation of the NTU-ANX slope is described in detail in Chapter 3, while the presentation of the field measurements and the field-testing can be found in Chapter 4. As was seen in Section 4.2.3, the depth of the groundwater table in the NTU-ANX slope lies between 15m and 17m deep from the ground surface. Finally, it has to be remembered that the research area on the NTU-ANX slope is small in comparison with the length of the slope (which is greater than 30m). In addition, the research area on the NTU-ANX lies at great distance from the crest and toe of the slope. For these reasons the research area of the NTU-ANX is considered as an infinite slope.

5.2.1 Magnitude and distribution of pore-water pressures during rainfall for the NTU-ANX slope

For the analysis of the magnitude and distribution of the pore-water pressures in the NTU-ANX slope, the two extreme initial conditions are examined: when the slope was at its most moist (i.e. when the pore-water pressures were observed to be maximum) and when the slope was at its driest (i.e. when the pore-water pressures were observed to be minimum). During the monitoring period (from March to August 2000) the NTU-ANX slope was at its most moist condition on 06 April 2000, when a major rainfall event took place and at its driest on 18 May 2000 after a long dry period. The 5-day antecedent rainfall (i.e. the rainfall which is precipitated prior to the major rainfall event) prior to the rainfall event of 06 April 2000 was 26mm, and the 5-day antecedent rainfall prior to the rainfall event of 18 May 2000 was zero.

On 06 April 2000 a major rainfall event of 49mm took place, which was distributed over 3hours. The average intensity of this rainfall event was 16.5mm/h. Figure 5.18 presents the hyetograph of the natural rainfall event of 06 April 2000 and the measured runoff produced. The data logger installed on the NTU-ANX slope could

provide only 10-minute readings of cumulative rainfall (Section 3.3.1) and for that reason no peak rainfall intensity could be measured. In the first ten minutes of the rainfall the average intensity was 94mm/h and that was the highest 10-minute average rainfall intensity recorded. After that, the rainfall intensity decreased gradually to 78mm/h, 59mm/h, 19mm/h and from 13:59 until the end of the rainfall, when its intensity remained below 10mm/h. For the rainfall event of 06 April 2000 the runoff produced was also measured (Figure 5.18). Table 5.2 summarises the particular rainfall event and the runoff and infiltration characteristics. The infiltration characteristics of the NTU-ANX slope are discussed in the following sections. Runoff started reaching the collection point (below row C) at 13:36; the peak runoff-intensity was 97mm/h and was measured at 13:45 (Figure 5.18). Runoff stopped at 14:32 when the rain intensity was very low (1.4mm/h) and after that and until the end of the rainfall, no more runoff was produced.

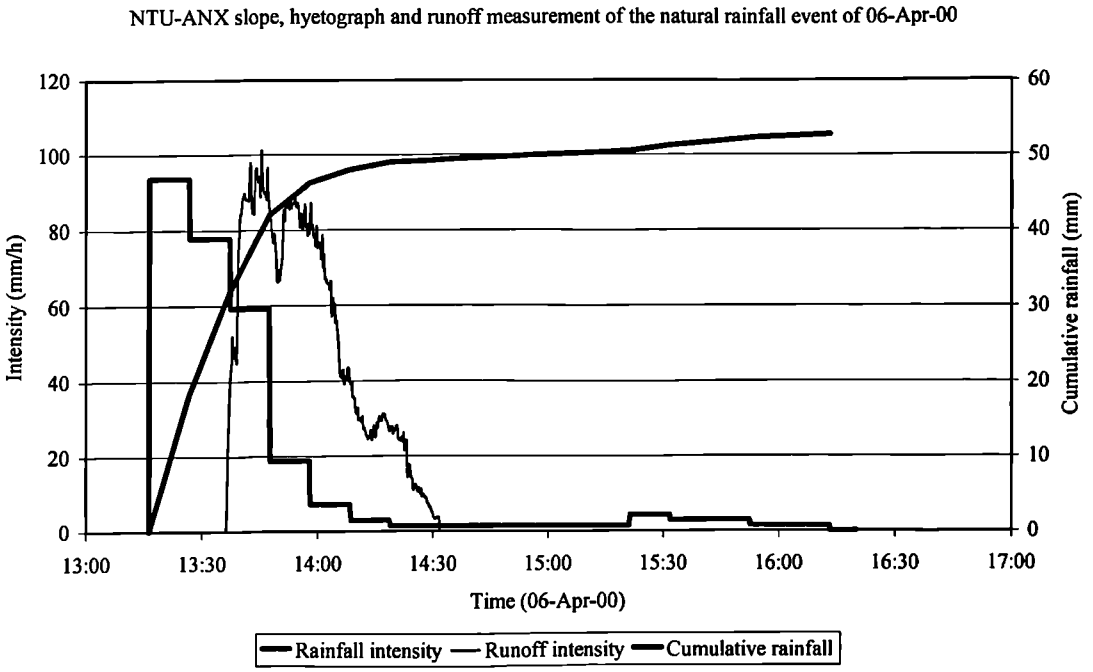

Figure 5.18 Hyetograph of the natural rainfall event of 06-Apr-00 with the runoff measurement, measured on the NTU-ANX slope.

Table 5.2 Summary of rainfall and runoff characteristics of the rainfall event of 06-Apr-00.

Rainfall		Runoff		Infiltration		
Total Rainfall (mm)	Duration (hours)	Average intensity (mm/h)	Total runoff (mm)	Total runoff (%)	Total infiltration (mm)	Total infiltration (%)
48.75	2.95	16.5	45.9	94	2.85	6

On 18 May 2000, 23mm of natural rainfall were precipitated over 1 hour. The average intensity of this rain event was 22mm/h. Figure 5.19 presents the hyetograph of the natural rainfall event of 18 May 2000. In the first ten minutes of the rainfall the average intensity was 50mm/h and during the next 10 minutes the intensity peaked with a 10-minute average of 55mm/h. After that the intensity decreased to 21mm/h, 3mm/h and during the last 20 minutes of the rainfall event the 10-minute average rainfall intensity was reduced to 1.4mm/h. Unfortunately, the runoff produced during the rainfall event of 18 May 2000 could not be measured due to a technical problem with the capacitive water level probe, which was used for the runoff measurements.

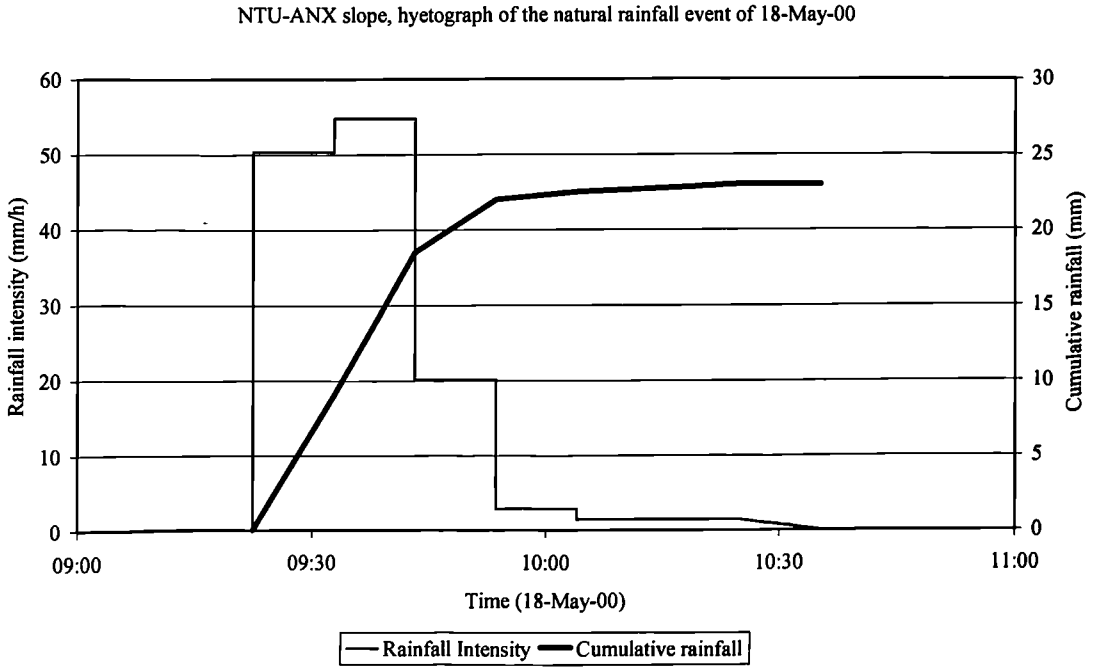

Figure 5.19 Hyetograph of the natural rainfall event of 18-May-00 measured on the NTU-ANX slope.

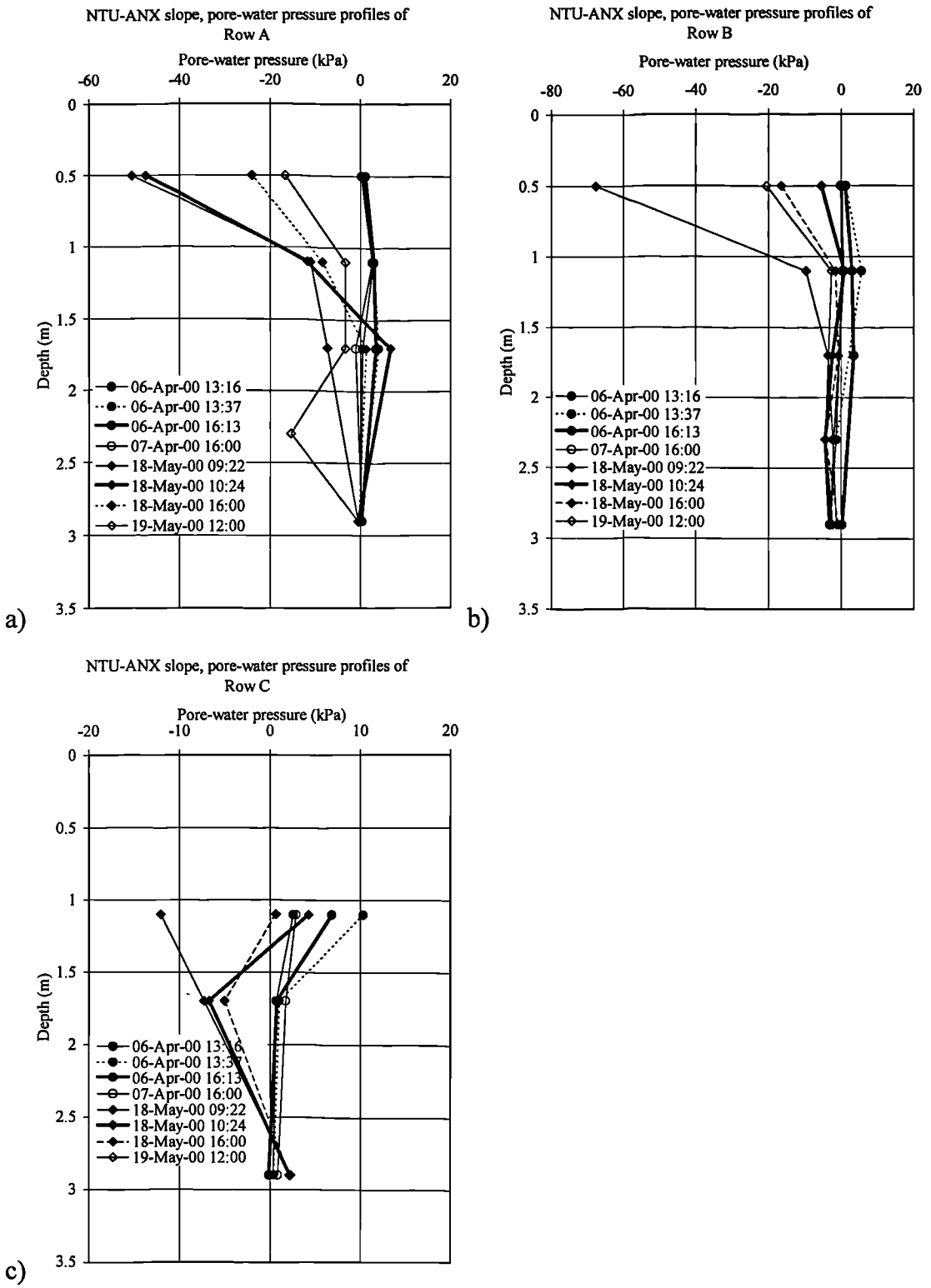

Figure 5.20 Pore-water pressure profiles of the NTU-ANX slope at the analysis time steps during 06-Apr-00 and 18-May-00: a) Row A, b) Row B and c) Row C.

The pore-water pressure distribution with depth at rows A to C for the key times are presented in Figure 5.23. The pore-water pressure profiles in each figure refer to the following times:

Analysis of the worst (wettest) conditions

The measurements of pore-water pressures at the NTU-ANX slope were at maximum on 06 April 2000. The chosen time steps of the analysis of the pore-water pressure changes during and after the rainfall event of 06 April 2000 are the following:

1. 06-Apr-00 13:16, at the start of a long heavy rainfall recorded on that day.
2. 06-Apr-00 13:37, when the pore-water pressures near the ground surface were at maximum.
3. 06-Apr-00 16:13, when the rainfall stopped.
4. 07-Apr-00 16:00, approximately 24hours after the end of the rainfall event of 06-Apr-00.

Figure 5.20 presents the pore-water pressure profiles of rows A through C for the analysis time steps during 06 and 07 April 2000. Figure 5.21 presents the evolution of the pore-water pressures with time during 06 and 07 April 2000 for each row of tensiometers (rows A through C). The rainfall hyetograph of 06 April 2000 with the runoff measurement (Figure 5.18) are also superimposed on Figure 5.21.

The pore-water pressure profiles of 06 and 07 April 2000 (Figure 5.20) show that the rainfall event of 06 April 2000 caused only limited pore-water pressure changes near the ground surface (0.5m deep) and at 3.2m deep. However, some pore-water pressures changes between 1.1 and 1.7m deep were observed. The pore-water pressure changes with time for all depths can be identified in Figure 5.21. In addition, the pore-water pressure profiles of Figure 5.20 were almost vertical at the end of the rainfall event (at 16:13 of 06 April 2000) and a zone of constant pore-water pressure was developed.

The pore-water pressure readings of Figure 5.21 show that almost as soon as the rainfall started there was an increase of the pore-water pressures near the ground surface (0.5m deep), but the increase was small in magnitude. In rows A and B the pore-water pressures at 0.5m depth increased by less than 1kPa, up to 1kPa within the first 20 minutes (until 13:37) of the rainfall. After that they decreased slightly

(by 0.5kPa at 14:38) and then remained constant during the rest of the rainfall event until the next day.

At 1.1m deep the development of the pore-water pressures was similar, but the magnitude of pore-water pressure change was greater than at 0.5m depth. At 1.1m deep, in row A, it was found that pore-water pressures peaked at 13:57 with a value of 3kPa, and reached 6kPa in row B. In row C at 1.1m deep the pore-water pressure was very close to the hydrostatic pressure, as the pore-water pressures at 13:57 were 10.6kPa.

At depths greater than 1.1m the increase of the pore-water pressures occurred with a smaller rate and over a longer time (Figure 5.20 and Figure 5.21). At 1.7m deep, in row A, the increase of the pore-water pressure with time was disproportional in comparison with the increase at smaller depths (i.e. 0.5 or 1.1m deep) or at larger depths (i.e. 2.9m). In row A, at 1.7m deep, at the start of the rainfall (i.e. at 13:16) the pore-water pressures were measured to be 0.5kPa and by 13:47 had increased to 5kPa (Figure 5.21). From that moment and on the pressure-readings show that the pore-water pressures at 1.7m deep, started to decrease and by the end of the rainfall the reading have become 3.5kPa. At row C at 1.7m depth the pore-water pressures at the start of the rain were measured to be 1kPa and an almost linear, but relatively small increase was observed until 20:00 of the same day. At the end of the rain the pore-water pressures at 1.7m deep in row C were measured to be 1.5kPa.

The measurements at 2.9m depth show the same trend as for 1.7m. In row A, the pore-water pressures were measured to be close to zero kPa and no increase were observed during the rainfall event. In row B and C, at 2.9m deep, the behaviour was similar, as the pore-water pressure remained almost constant with a value of –2kPa and 1kPa, respectively.

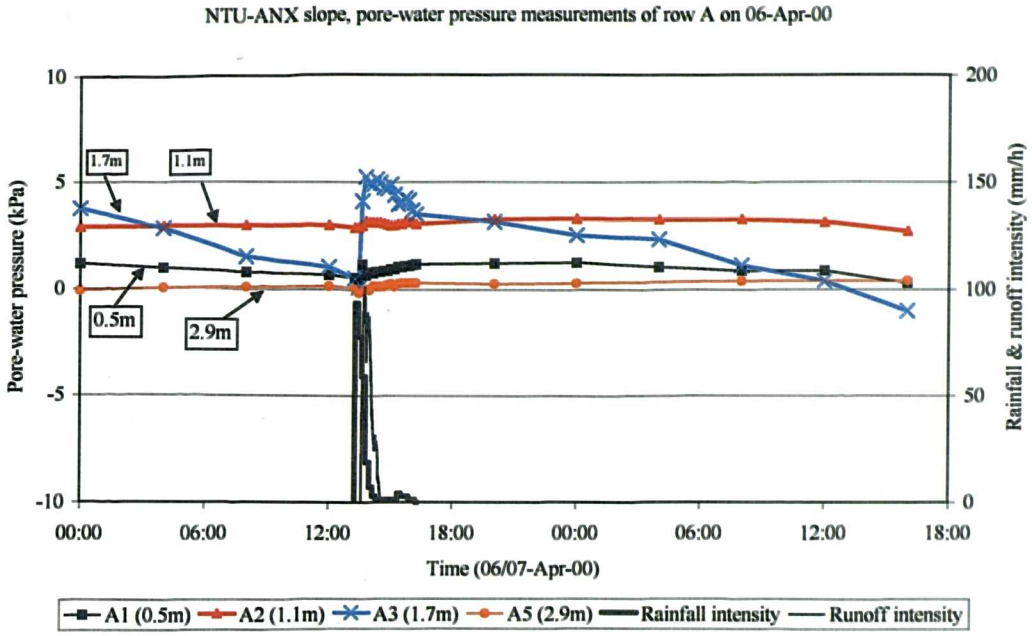
NTU-ANX slope, pore-water pressure measurements of row A on 06-Apr-00
Pore-water pressure (kPa)
Rainfall & runoff intensity (mm/h)
1.7m
1.1m
0.5m
2.9m
Time (06/07-Apr-00)
A1 (0.5m)
A2 (1.1m)
A3 (1.7m)
A5 (2.9m)
Rainfall intensity
Runoff intensity

a)

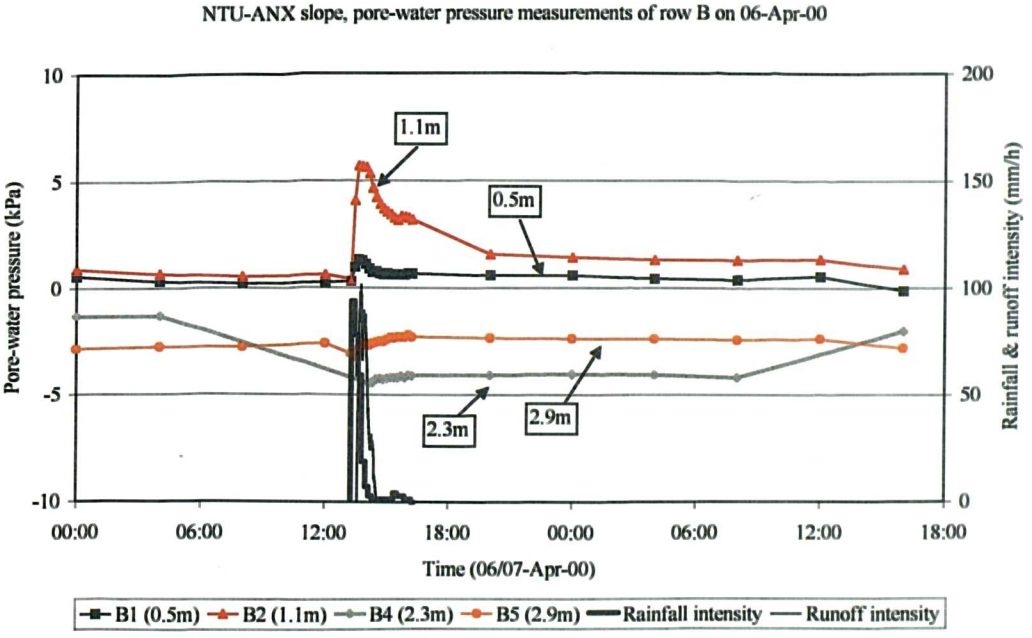
NTU-ANX slope, pore-water pressure measurements of row B on 06-Apr-00
Pore-water pressure (kPa)
Rainfall & runoff intensity (mm/h)
1.1m
0.5m
2.3m
2.9m
Time (06/07-Apr-00)
B1 (0.5m)
B2 (1.1m)
B4 (2.3m)
B5 (2.9m)
Rainfall intensity
Runoff intensity

b)

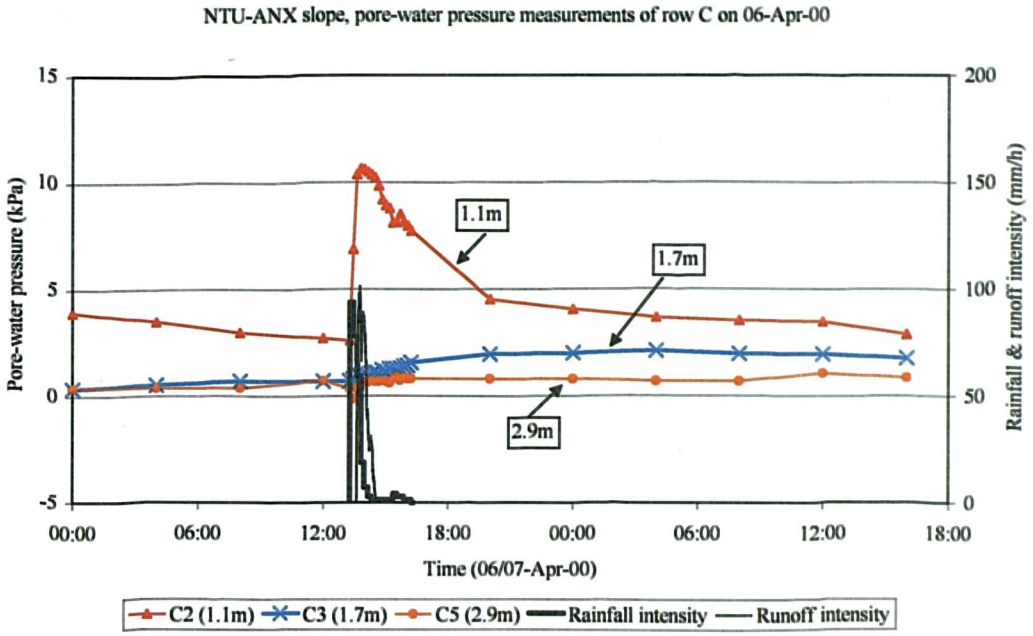

c)

Figure 5.21 Pore-water pressure measurements in the NTU-ANX slope on 06-Apr-00: a) row A, b) row B and c) row C.

Analysis of the best (driest) conditions

The measurements of pore-water pressures at the NTU-ANX slope were at minimum on 18 May 2000. The time steps for the analysis of the pore-water pressure changes during and after the rainfall event of 18 May 2000 are the following:

1. 18-May-00 09:22, at the start of the rainfall event, which was recorded on that day.

2. 18-May-00 10:24, when the rainfall event stopped.

3. 18-May-00 16:00, approximately 6 hours after the end of the rainfall event of 18-May-00.

4. 4 19-May-00 12:00, approximately 26 hours after the end of the rainfall event of 18-May-00.

Figure 5.20 presents the pore-water pressure profiles of the NTU-ANX slope for the chosen time steps of the pore-water pressure analysis. From the pore-water pressure profiles of Figure 5.20 it can be seen that very low pore-water pressures (lower than -30kPa) were developed only close to the ground surface (i.e. 0.5m deep).

Comparing the pore-water pressures at 0.5m deep of row A and B, prior to the rainfall event of 18 May 2000 (Figure 5.20), it can be seen that there is a large difference between the two measurements (0.5m deep in row A the measured pore-water pressure is –52kPa, and in row B, 0.5m deep, the pore-water pressures initially were –68kPa) . At 1.1m deep the initial pore-water pressure (prior to the rainfall event of 18 May) were approximately –10kPa for all rows of tensiometers and at even larger depths the pore-water pressures were greater than –10kPa (Figure 5.20). From the pore-water pressure profiles of Figure 5.20 can also be seen that during the rainfall event and after the end of the rainfall, large pore-water pressure changes occurred only close to the ground surface. This point will be illustrated in greater detail below.

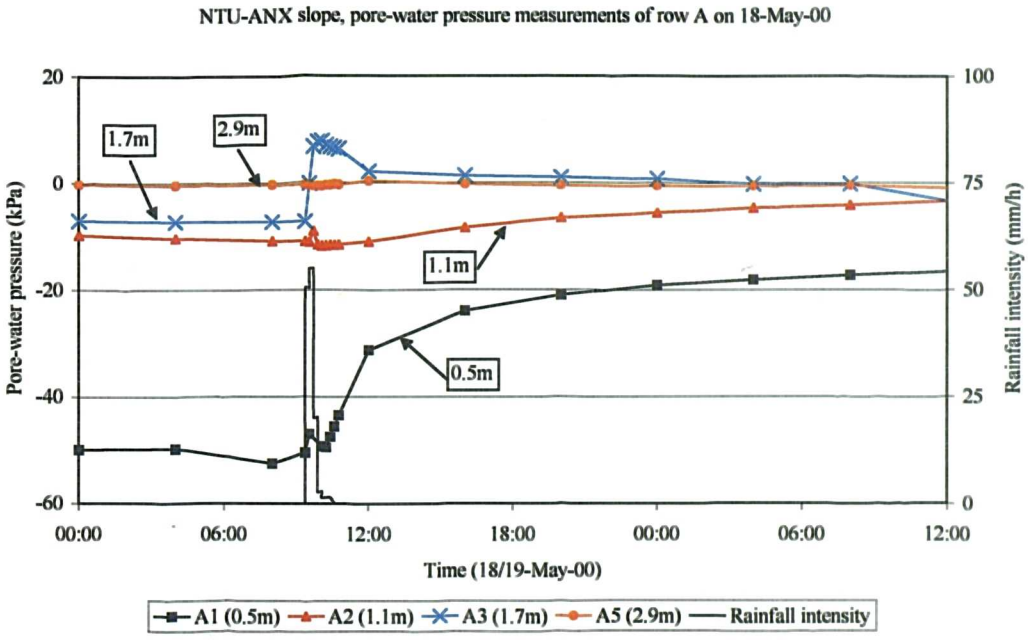

a)

b)

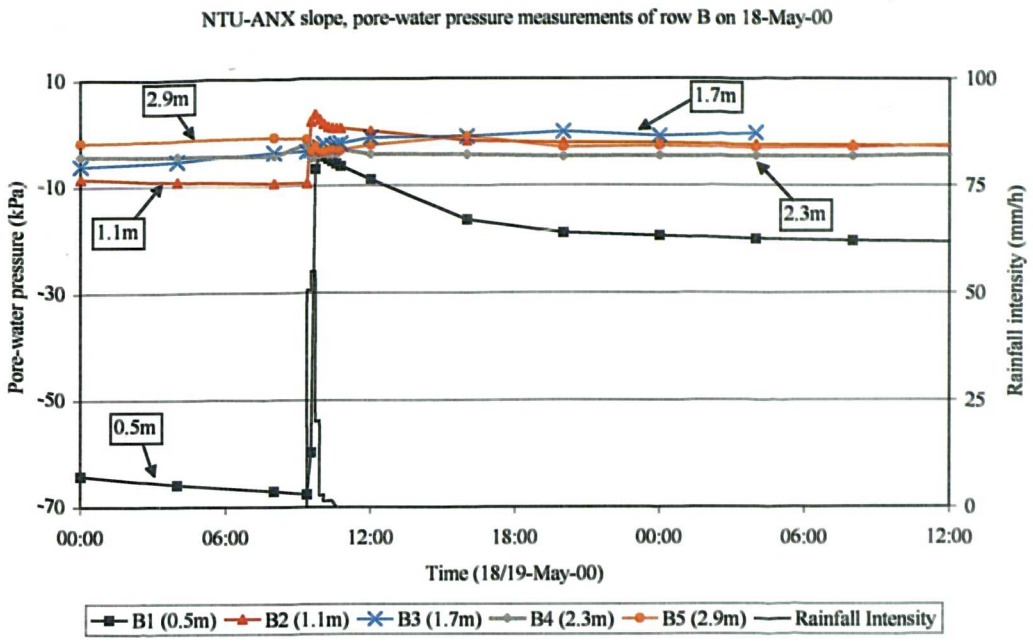

c)

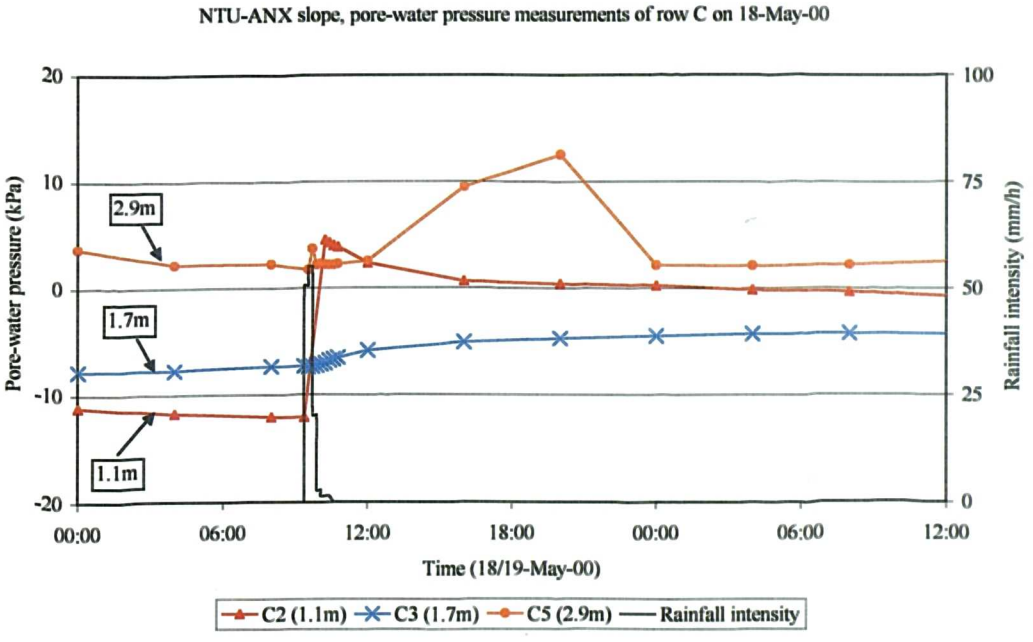

Figure 5.22 Pore-water pressure measurements in the NTU-ANX slope on 18-May-00: a) row A, b) row B and c) row C.

Figure 5.22 presents the evolution of the pore-water pressures with time for each row of tensiometers during the rainfall event of 18 May 2000 and also the hyetograph of that rainfall event. As mentioned above the lowest pore-water pressure readings were taken at 09:22, the moment the rainfall started. Figure 5.22 shows that the effect of the rainfall is significant in the development of the pore-water pressures near the ground surface, where the lower the initial pore-water pressures, the more

significant the pore-water pressure changes were. At 0.5m deep the readings in rows A and B show different behaviour of the pore-water pressures during rainfall (Figure 5.22a and b). In row A, 0.5m deep, the initial pore-water pressure at the start of the rain was –53kPa and during the rainfall the increase was 10kPa (pore-water pressures at the end of the rainfall –43kPa). The increase of the pore-water pressure, at 0.5m of row A, continued for several hours, and after 26.5 hours (until 19-May-00 12:00) the pore-water pressures had increased by 36kPa to a magnitude of –17kPa (Figure 5.22a). At 0.5m deep of row B the pore-water pressures increased significantly during the rainfall and by the end of the rainfall they had already started to decrease again (Figure 5.22b). More specifically, at the start of the rain (i.e. 09:22) the initial pore-water pressures at 0.5m deep of row B were measured as –68kPa. At 10:04 the pore-water pressures (0.5m deep of row B) peaked to a value of –5kPa and after that they started to decrease. On the next day at midday (i.e. 19 May 00 12:00) the pore-water pressures had decreased to –21kPa.

In row A, the pore-water pressures at depth 1.1m (Figure 5.22a) increased gradually from –11kPa at the start of the rainfall event, to –3kPa on the next day at midday (i.e. 19 May 2000 12:00). Downslope in rows B and C, at 1.1m deep, the pore-water pressures increased by larger magnitude than in row A (Figure 5.22b and c). In row B, 1.1m the pore-water pressures increased during the rainfall event from –10kPa to 4kPa, while in row C, at 1.1m the pore-water pressure increased from –12kPa to 5kPa.

At depth of 1.7m, in row A the pore-water pressure readings show that there was a significant increase (from –7kPa to 7kPa) mainly during the rainfall and after the end of the rain the pore-water pressures started to decrease again (Figure 5.22a). At 2.3m and 2.9m deep only small pore-water pressures could be observed (Figure 5.22).

Comparison of the two extreme cases

The analyses of the two extreme cases of the NTU-ANX slope show that the changes in the pore-water pressures are not only a function of the rainfall intensity or of the total rain, but are also dependent on the initial conditions. The lower the pore-water pressures, the higher the changes in the pore-water pressure during rainfall. The

pore-water pressure profiles of Figure 5.20 show that even when the pore-water pressures were very low near the ground surface (0.5m deep), the pore-water pressures at large depths (i.e. 2.3m and 2.9m deep) remained rather high and close to positive values. When the pore-water pressures at 0.5m deep were very low, they had increased by a large amount during a rainfall, but when pore-water pressures at 0.5m deep were positive, only limited changes during a rainfall event were observed. For both cases (06 April 2000 and 18 May 2000) the pore-water pressures at 3.2m deep did not change significantly during rainfall.

In row A, the pore-water pressures at 1.7m deep increased by a large magnitude during the two rainfall events (Figure 5.21a and Figure 5.22a). The increases at 1.7m deep in row A are not in agreement with changes at larger or smaller depths of row A. The development of the pore-water pressures in row A at depths up to 1.7m, during the rainfall event of 18-May-00 did not follow the trend of the Rows B and C (Figure 5.22). This anomaly at 1.7m deep of row A, can be attributed to localised non homogeneity of the soil properties at that depth.

The rainwater did not produce any immediate and rapid changes in the pore-water pressures in row A (Figure 5.22a) as happened at rows B and C (Figure 5.22b and c). The changes took place at a slow rate and continued for a long period after the end of the rain (Figure 5.22a).

5.2.2 Runoff and infiltration characteristics of the natural and simulated rainfall events applied on the NTU-ANX slope

The analysis of the infiltration characteristics of the NTU-ANX slope is based on the assumption that the total rainfall water is divided only into runoff and infiltration. In reality, rainfall water that seeps into a slope is divided into interception by vegetation, depression storage at the ground surface, and infiltration (Premchitt et al. 1986). However, interception by vegetation, and depression storage at the ground surface (their sum is also called initial abstraction) are very difficult to measure and usually are estimated to be minor, relative to the total infiltration.

Figure 5.23 presents the relationship between total rainfall and total runoff for 37 rainfall events falling within the study area of NTU-ANX slope. Details of the

runoff measurements of each individual rainfall event can be found in Chapter 4 (Sections 4.2.5 and 4.2.6). From Figure 5.23, it can be concluded that runoff is directly dependent on the total rainfall, and there is a clear trend that as the total rainfall increases the runoff produced also increases. The correlation between total rainfall and total runoff is good (R^2= 0.93) with a polynomial relationship of second order between the two variables.

The rainfall events that produced no runoff had total rainfall between 5 and 12mm with an average of 8mm. It can therefore, be assumed that a rainfall event greater than 8mm is expected to produce some runoff and any rainfall event of less than 8mm will produce very small amounts of runoff and almost all the rainfall water will infiltrate the slope.

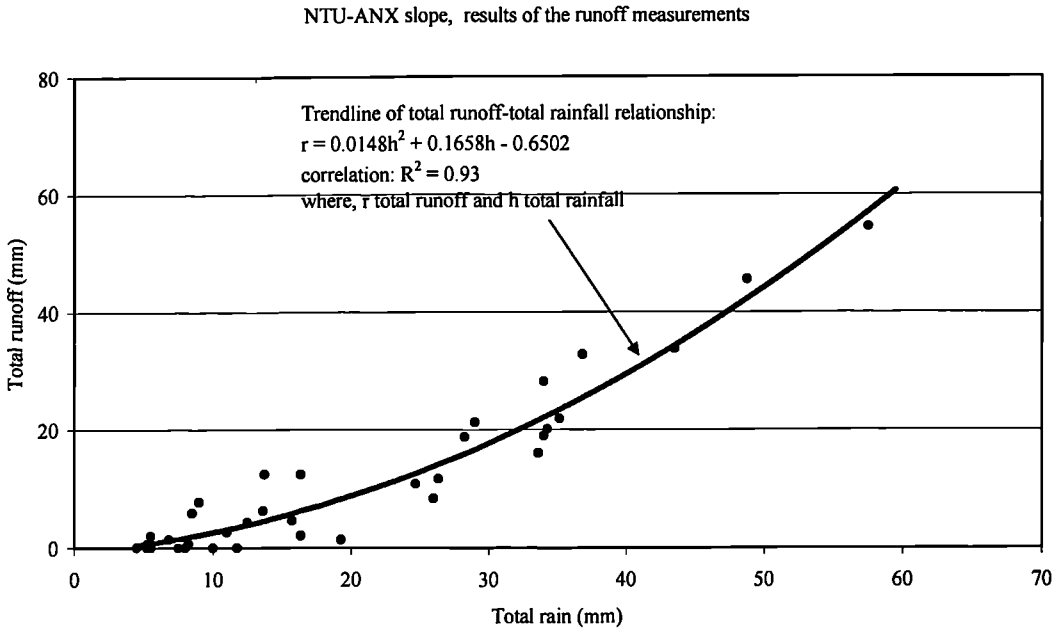

Figure 5.23 Relationship of total runoff with total rainfall for the NTU-ANX slope.

Figure 5.24 presents the average rainfall intensities with total rainfall, with the rainfall events classified into those that did not produce any runoff and into those rainfall events that produced runoff. The average intensity of all data in Figure 5.24 are expressed in m/s for comparison with the coefficient of saturated permeability with respect to water of the surface soil layer of NTU-ANX slope, which was measured to be $6x10^{-7}$m/s. Figure 5.24 also shows the f-index of those rainfall events that produced runoff. The f-index represents the rainfall intensity above

which runoff will be produced and below which all the rainfall water will become infiltration (Premchitt et al. 1986).

The average rainfall intensity of all rainfall events that did not produce any runoff is $2.4x10^{-6}$m/s (Figure 5.24). The average rainfall intensity of the rainfall events that produced runoff on NTU-ANX slope was between $1.4x10^{-6}$m/s and $1.9x10^{-5}$m/s with an average of $6.7x10^{-6}$m/s. The calculated f-index ranges between $1.4x10^{-7}$m/s and $9.8x10^{-6}$m/s, with an average of $3.2x10^{-6}$m/s. The average values of the f-indexes and the average rainfall intensity of those rainfall events that did not produce any runoff are very similar ($2.4x10^{-6}$m/s and $3.1x10^{-6}$m/s, respectively). These numbers indicate that there is a threshold average rainfall intensity of about $2.5x10^{-6}$ m/s; any rainfall events with average rainfall intensity greater than $2.5x10^{-6}$ m/s should produce runoff. However, it has to be noted that this threshold is significantly higher than the coefficient of saturated permeability with respect to water (k_{sat}=$6x10^{-7}$m/s,), which was measured near to the surface of the slope (30cm deep, Section 4.2.7). This difference can be attributed to an underestimation of the k_{sat} or more likely to the existence of vegetation and cracks of the soil on the ground surface of the slope, which may increase the saturated coefficient of permeability with respect to water.

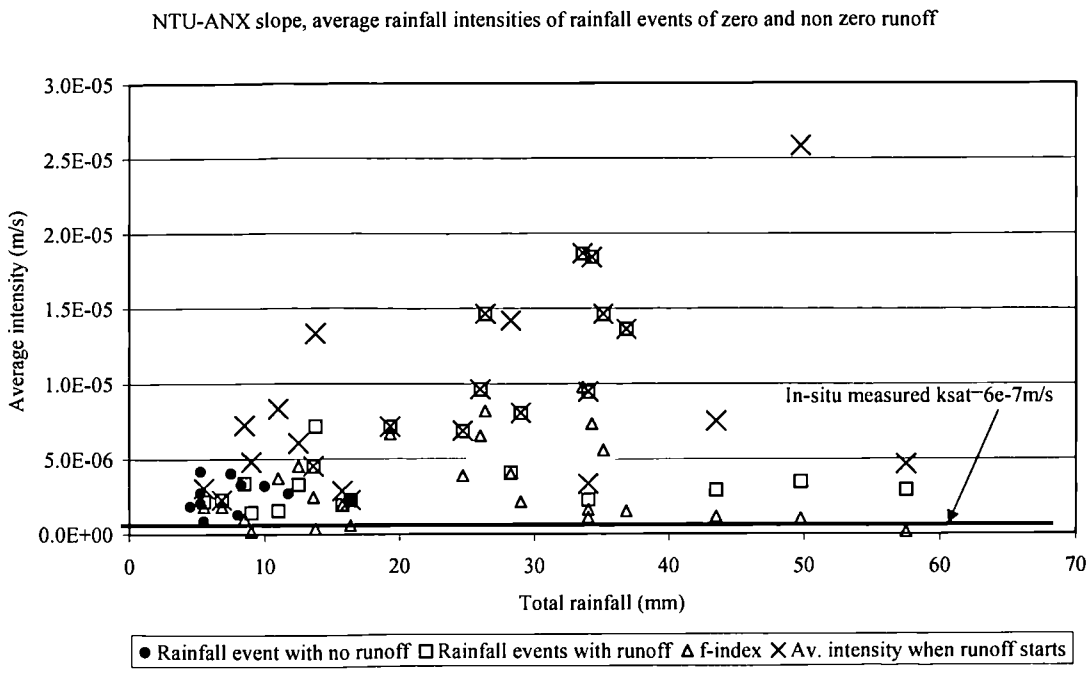

Figure 5.24 Average rainfall intensities and f-index of natural and simulated rainfall events precipitated on the NTU-ANX slope with zero and non-zero runoff.

Figure 5.25 presents the relationship between total rainfall and total infiltration. The relationship of total rainfall and total infiltration shown in Figure 5.25 is derived with the assumption that the initial abstraction at the ground surface of the slope is negligible and infiltration will be the difference between total rainfall and total runoff. The data of Figure 5.25 show that there is a significant scatter in the relationship between total rainfall and total infiltration, despite the good relationship of total rainfall and total runoff (Figure 5.23). The scatter in the relationship between total infiltration and total rainfall indicates that the infiltration characteristics of the NTU-ANX slope are not dependent only on the total amount of rainfall. In addition, the results of a preliminary analysis on the effect of the average rainfall intensity on the total amount of infiltration did not show any clear trends. The complexity of the infiltration characteristics of the NTU-ANX slope is further discussed in the following paragraphs.

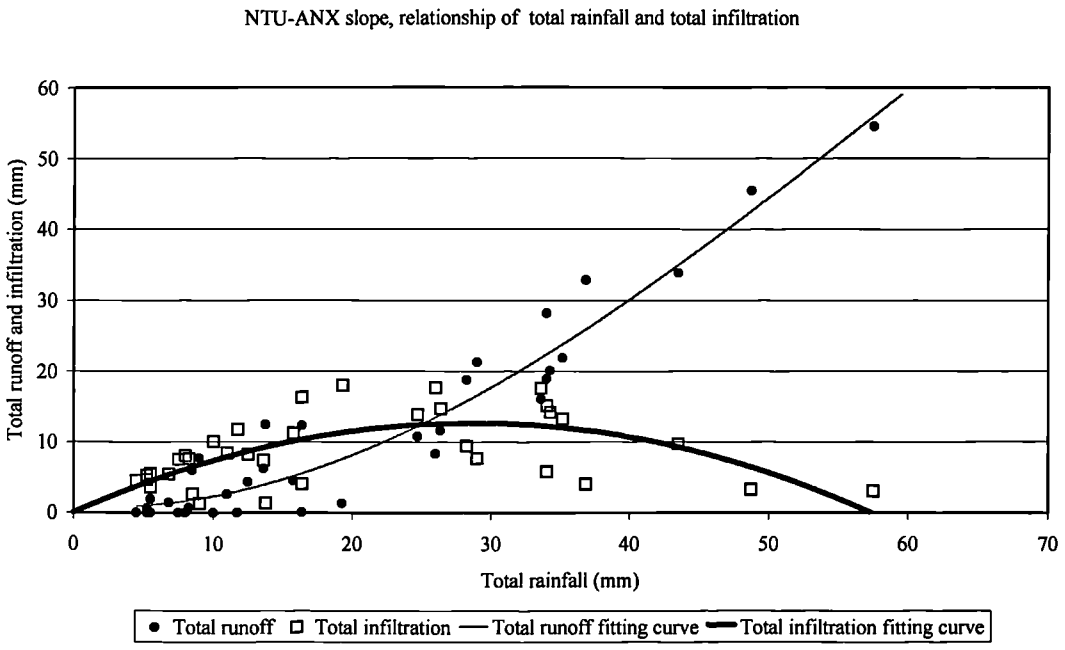

Figure 5.25 Relationship of total infiltration with total rainfall for the NTU-ANX slope.

Despite, the scatter in the relationship between total infiltration and total rainfall, the data of Figure 5.25 shows a general trend. As total rainfall increases from zero to 25mm the infiltration also increases. Further increase of the total rainfall from 25mm shows a decline in total infiltration and when the total rainfall exceeds the 50mm then infiltration is less than 5mm. From this observation an upper limit line on the total infiltration can be drawn as shown in Figure 5.26.

During the study period, two simulated rainfalls were applied on the NTU-ANX slope with the same rainfall pattern. The first rainfall simulation was conducted on 12 July 2000 with a constant rainfall intensity of 8.2mm/h (i.e. 2.3×10^{-6}m/s). The duration of the rainfall simulation was 2 hours resulting in a total rainfall of 16.4mm. The 1-day antecedent rainfall (i.e. the total rainfall precipitated on the slope 1-day prior to the rainfall event) was zero. During the simulated rainfall of 12 July 2000 insignificant amounts of runoff were measured (i.e. 16.3mm of simulated rainfall water became infiltration). The next day, on 13 July 2000 a rainfall simulation with the same rainfall pattern as in 12 July 2000, was applied on the slope. On 13 July 2000 the 1-day antecedent rainfall was 16.4mm. The collected runoff was equal to 10.3mm, or 63% of the total simulated rainfall (6.1mm of simulated rainfall became infiltration). The two examples, described above, indicate that the initial conditions of the slope, expressed as antecedent rainfall, plays a major role on the amount of the rainfall water that will infiltrate the slope.

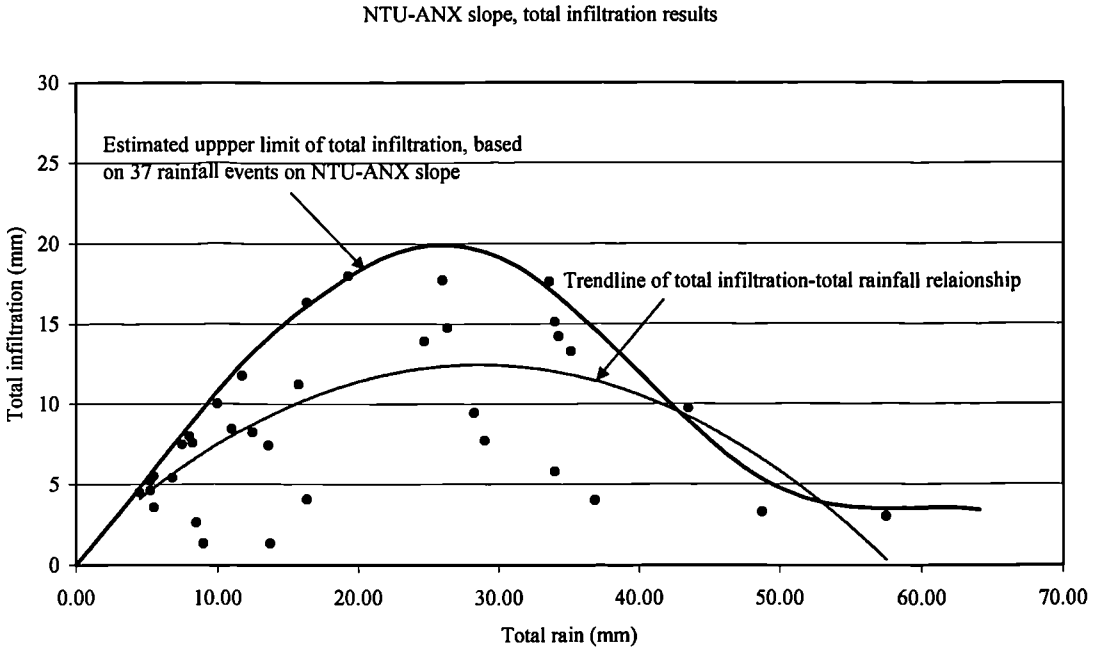

Figure 5.26 Estimated upper limit of the total infiltration for the NTU-ANX slope.

Figure 5.27 presents a contour plot of total infiltration for different total rainfall and for different 1-day antecedent rainfall for the NTU-ANX slope. The contour plot of Figure 5.27 combines the observations of the effect of total rainfall and antecedent rainfall, as were described above. From Figure 5.27, it can be seen that as total

rainfall increases up to 25mm and the 1-day antecedent rainfall is small then infiltration also increases. For total rainfall higher than 25mm then infiltration will be small. At the same time as the 1-day antecedent rainfall increases (such as 60mm of antecedent rainfall) infiltration will decrease. Similar analyses with Figure 5.27 was also conducted using 5-day and 15-day period for the antecedent rainfall (i.e. antecedent rainfall periods that Chatterjea (1989), Rahardjo et al. (2001) and Toll (2001) adopted for rainfall-induced landslides analyses in Singapore). The analyses with 5-day and 15-day periods of antecedent rainfall did not show any trends like in Figure 5.27.

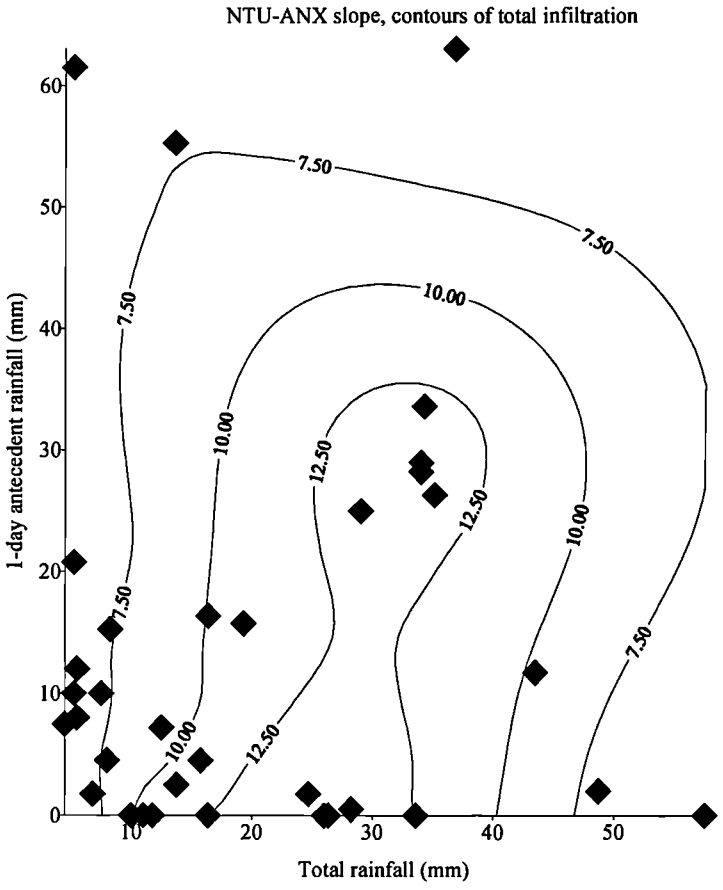

Figure 5.27 Contour plot (in mm) of total infiltration in NTU-ANX slope for different total rainfall and 1-day antecedent rainfall.

The results of Figure 5.27 indicate that the slope has a 'capacity' of how much rainfall water can infiltrate into the slope. In other words, high total rainfall does not automatically result to high infiltration. If the soil near the ground surface of the slope is dry (i.e. low antecedent rainfall) then it is more likely to allow more rainfall water to infiltrate into the slope. However, from the available data it is difficult to

identify the specific conditions under which infiltration will be maximum or minimum.

From all the above it is clear that during a rainfall event, infiltration occurs in a complex way. It was seen that total runoff is directly related to the total rainfall (Figure 5.23). It was also seen that the average rainfall intensity also plays some role on when runoff will be produced, but no clear relation could be established (Figure 5.24). The data also show that total infiltration is a function of total rainfall and the initial conditions of the slope, expressed as 1-day antecedent rainfall. The runoff measurements on the NTU-ANX slope indicate that infiltration increases as total rainfall increases until the total rainfall reaches 25mm. From that point and after, as total rainfall increases total infiltration will start to decrease.

5.2.3 Effect of rainfall and the initial conditions on the pore-water pressure changes of NTU-ANX slope

Section 5.2.1 presented some analysis on the way pore-water pressures changed during rainfall at depths to 2.9m at the NTU-ANX slope. The analysis was based on two occasions, when the NTU-ANX slope was at its most moist conditions and at its driest conditions. Section 5.2.2 presents an analysis of the infiltration characteristics of the NTU-ANX slope and it was seen that infiltration occurs in a complex way. This section attempts to link the pore-water pressures changes with total rainfall as well as with total infiltration. However, it has to be noted that the pore-water pressure measurements during rainfall events (natural or simulated) when runoff was measured (Section 4.2.5 and 4.2.6) were relatively high (close to zero) and only small changes were observed. Therefore, a direct relationship between the pore-water pressure changes and total infiltration could not be established. However, the findings on the relationship between total rainfall and total infiltration, as this discussed in Section 5.2.2, were used in order to explain the mechanism of pore-water pressure changes during rainfall.

The analysis of the pore-water pressure changes during rainfall at the extreme cases of the slope (most moist and driest conditions) indicated that the initial conditions play a significant role for the evolution of the pore-water pressure changes during rainfall. Figure 5.28 presents contour plots (in kPa) of the final pore-water pressure

(resulting from rainfall) at 0.5m, 1.1m and 2.9m deep of row A for different total rainfall and different initial values of the pore-water pressure at the start of each rainfall event. The contour plots of Figure 5.28 were derived using all natural and simulated rainfall events, applied on the NTU-ANX slope, with total rainfall greater than 1mm. It has to be noted that the available data, especially for 0.5m deep, do not cover the full range of initial values of pore-water pressures for all values of total rainfall. Therefore, the conclusions from this analysis are handled with a degree of uncertainty.

Figure 5.28a shows that pore-water pressure changes at 0.5m deep are large when the initial pore-water pressure is low. In addition, pore-water pressure changes at 0.5m deep (Figure 5.28a) become smaller as the initial pore-water pressure increases. From Figure 5.28a can also be seen that for rainfall events smaller than approximately 25mm the final pore-water pressure contours are almost vertical, indicating for rainfall events up to 25mm (approximately) the final pore-water pressure is heavily affected by the total rainfall. There is a transition in behaviour around 25mm of total rainfall, above which the contours of final pore-water pressure become almost horizontal. This indicates that for rainfall events greater than approximately 25mm the final pore-water pressure at 0.5m deep is highly controlled by its initial value. This behaviour of the final pore-water pressure resulted by rainfall is very similar with the findings of NTU-CSE slope (Figure 5.10).

The way pore-water pressure change at 0.5m deep with rainfall, as seen in Figure 5.28a, can be explained in terms of infiltration. As it was shown in Section 5.2.2, total infiltration increases with total rainfall until total rainfall reaches approximately 25mm (Figure 5.26 and Figure 5.27). A rainfall event with total rainfall above 25mm, does not lead to a further increase of total infiltration. The pore-water pressures at 0.5m deep (Figure 5.28a), increase by large amounts for rainfall events that had total rainfall up to approximately 25mm (i.e. when total infiltration was also high). For rainfall events above 25mm of total rainfall, the pore-water pressures will not increase by a significantly larger magnitude than in a case where the total rainfall was up to 25mm, as there is no increase in the total infiltration.

At larger depths the final pore-water pressure contours at 1.1m and 2.9m deep (Figure 5.28 b and c) show that little changes usually occur during rainfall. It can also be noted that at 1.1m and 2.9m deep, the pore-water pressures were usually high and especially for the data at 2.9m deep, the pore-water pressures were usually positive or, if negative, then close to zero.

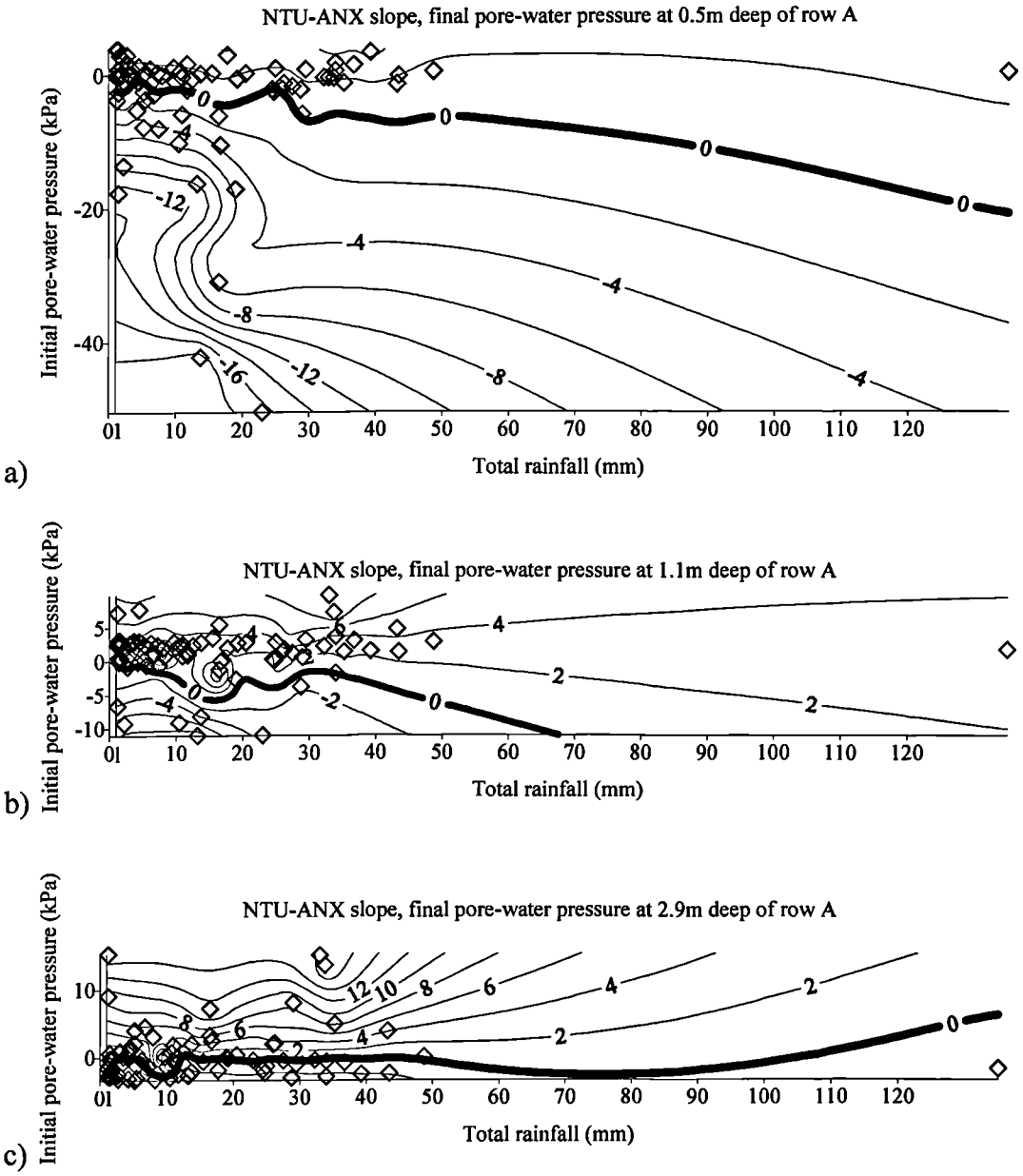

Figure 5.28 Contour plots (in kPa) of the final pore-water pressure at a) 0.5m deep b) 1.1m deep, and c) 2.9m deep, of row A at the NTU-ANX slope for different total rainfall and different initial pore-water pressures.

5.2.4 Slope stability analysis of the worst (wettest) and best (driest) conditions of the NTU-ANX slope

An analysis on the stability of the slope was also conducted for the time steps of the analyses of the two extreme conditions (wettest and driest) of the NTU-ANX slope. The time steps of the two analyses are mentioned above, in Sections 5.1.1 and 5.2.1. The slope stability analyses, presented in this section, use the methodology described in Section 2.9, which satisfies moment equilibrium. For the slope stability analysis the commercial software for slope stability Slope/W (Geo-Slope Inc 1998b) was used. The soil profile that was used in the slope stability analysis is the simplified profile of Figure 3.7. A detailed description of the soil properties of the simplified profile of NTU-ANX slope is presented in Section 3.2. Table 5.3 summarises the strength parameters for each soil layer of the slope. Gasmo (1997) and Hritzuk (1997) measured the strength parameters of Layer 1 and Layer 2 respectively.

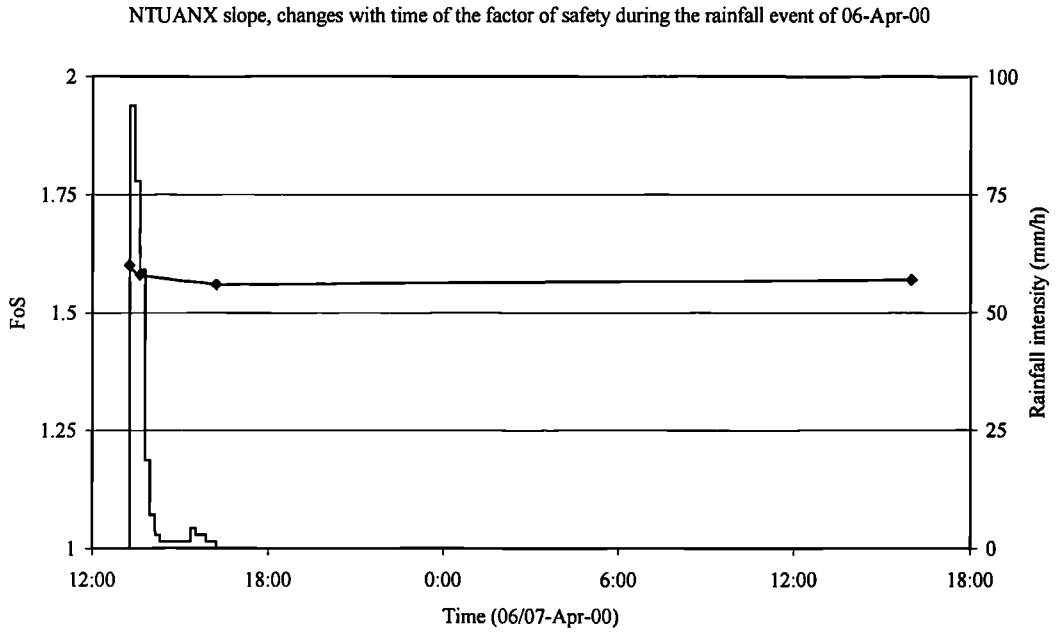

Figure 5.29 Development with time of the factor of safety of the slope for the NTU-ANX site on the 06-Apr-00.

Table 5.3 Summary of the strength parameters used in the slope stability analysis of the NTU-ANX slope.

No.	Friction angle ϕ'	Friction angle ϕ^b	Cohesion c' (kPa)	Unit weight (kN/m^3)
1	30.0°	30.0°	12	19.81
2	31.0°	31.0°	14	19.03

Figure 5.29 presents the results of the slope stability, conducted for the rainfall event of 06 April 2000 (i.e. when the NTU-ANX slope was at its most moist conditions). The chosen time steps of the analysis are at the start of the rain (i.e. at 13:16), at the moment of the highest pore-water pressures (i.e. at 13:37), at the end of the rainfall (i.e. at 16:13) and finally the next day (i.e. 07 April 2000) at 16:00. From Figure 5.29 can be seen that the factor of safety at the start of the rain was 1.6 and 21 minutes later (at 13:37) drops by an insignificant amount to 1.58. At the end of the rain the factor of safety was decreased only slightly more from the initial value to 1.56. The next day at 16:00 (i.e. approximately 24 hours after the end of the rainfall event) the factor of safety of the slope had recovered to 1.57.

The trend shown by the changes in the factor of safety of the slope is in good agreement with the changes of the pore-water pressures near the ground surface (Figure 5.20). The pore-water pressure profiles of Figure 5.20 show that at 0.5m and 1.m deep, the pore-water pressure changes during the rainfall event were small. In addition, after the end of the rainfall event the recovery of the pore-water pressures was slow (Figure 5.20). The small changes of the pore-water pressures near the ground surface of the NTU-ANX slope resulted in limited changes of the factor of safety of the slope. Figure 5.30 presents the most critical slip surface as was predicted by the slope stability analysis for the 06 April 2000 16:13. The potential slip surface lies entirely within the weakest material, Layer 1, and is approximately 20m long and nearly 3.5m deep.

Figure 5.31 presents the results of the slope stability analysis of the NTU-ANX slope during the rainfall event of 18 May 2000 (i.e. when the slope was at its driest). The time steps that were chosen are at the start of the rain (i.e. at 09:22), at the end of the rainfall (i.e. at 10:24) and finally the next day (i.e. 19 May 00) at 12:00. From Figure 5.31, it can be seen that the factor of safety at the start of the rain was 1.81 and by the

end of the rain the factor of safety decreased considerably to 1.68. The next day at midday the factor of safety of the slope recovered considerably to 1.8 (i.e. close to the initial value prior to the rainfall event).

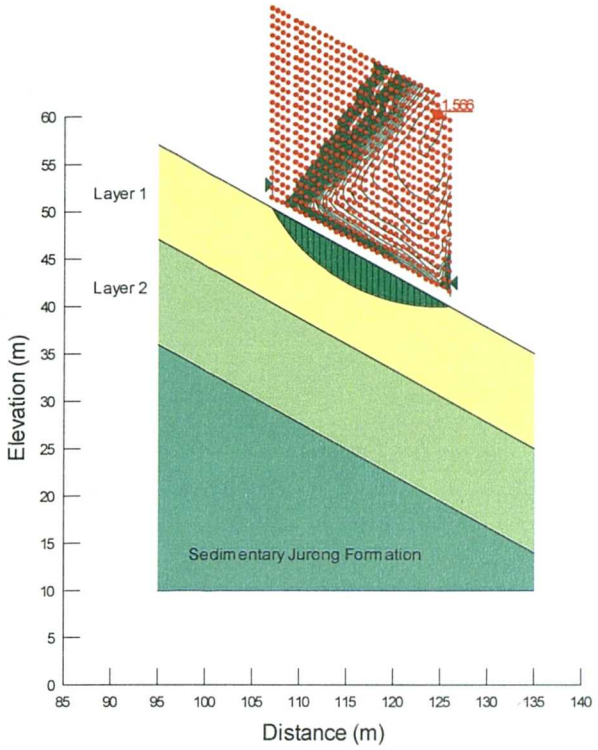

Figure 5.30 Location of the critical slip surface at the NTU-ANX slope for the stability analysis conducted for 06-Apr-00 at 16:13.

Figure 5.32 and Figure 5.33 present the most critical slip surfaces of the slope stability analysis for the 18 May 00 at the start and at the end of the rainfall. The entire potential slip surfaces are located on the weakest material of Layer 1. The most critical slip surface at the start of the rainfall event (Figure 5.32) is up to 6m deep, but the critical slip surface at the end of the rainfall event is only 3m deep. The difference in the depth of the two critical slip surfaces can be attributed to the fact that significant pore-water pressure changes were observed mainly close to the surface and not at large depths.

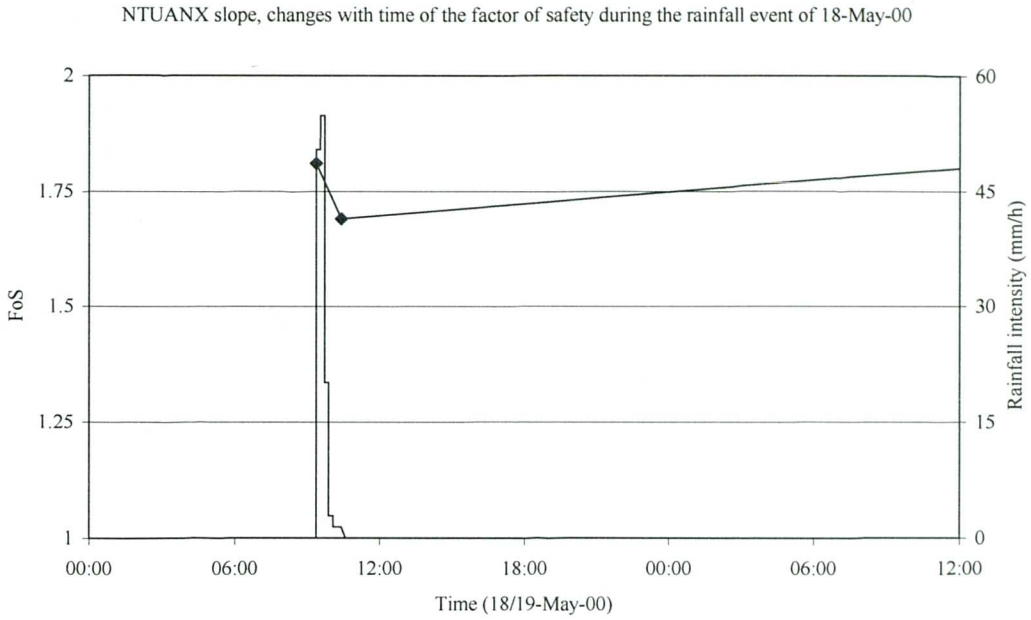

Figure 5.31 Development with time of the factor of safety of the slope for the NTU-ANX site on the 18-May-00.

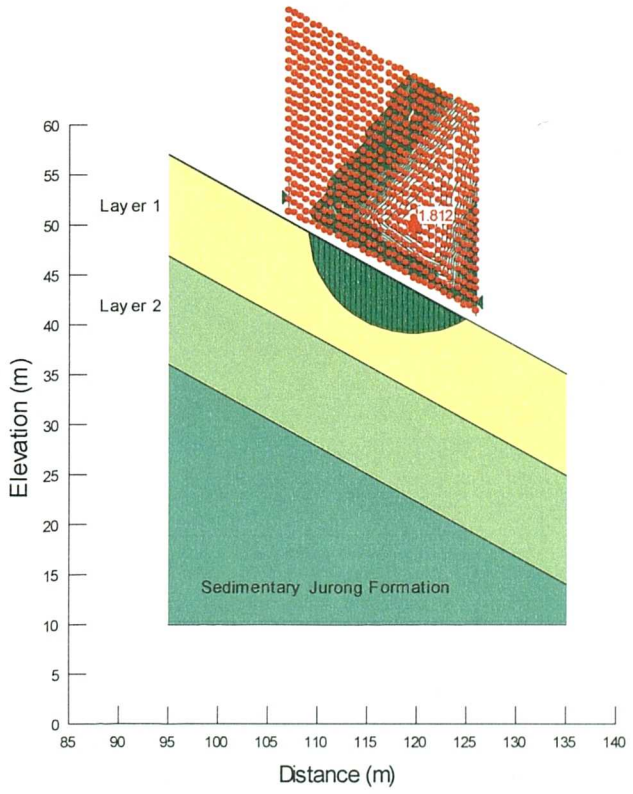

Figure 5.32 Location of the critical slip surface at the NTU-ANX slope for the stability analysis conducted for 18-May-00 at 09:22.

The slope stability analyses of the NTU-ANX slope showed that the factor of safety corresponding to the best and the worst condition differ significantly. The lowest factor of safety was 1.56 when the pore-water pressures were at maximum near the ground surface. The highest factor of safety of the NTU-ANX slope was calculated when the slope was at its driest conditions and was equal to 1.85. Taking under consideration the difference between the lowest and the highest predicted factor of safety of the NTU-ANX slope it can be concluded that negative pore-water pressures play an important role in the stability of the slope.

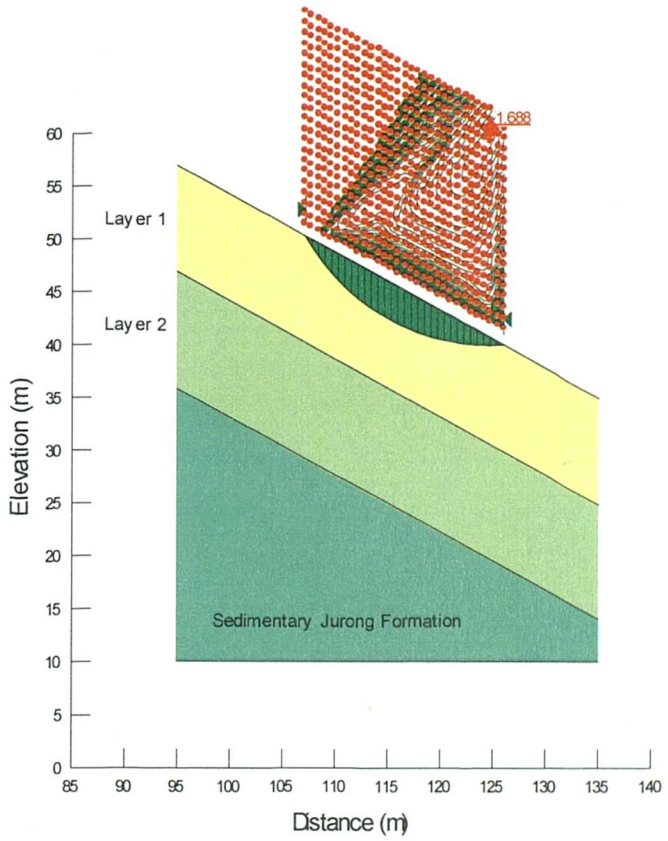

Figure 5.33 Location of the critical slip surface at the NTU-ANX slope for the stability analysis conducted for 18-May-00 at 10:24.

5.3 Comparison between the field observations from the NTU-CSE and the NTU-ANX slopes

The analysis of the pore-water pressure changes at the middle of the NTU-CSE slope (row C) and NTU-ANX slope (row A) (Figure 5.10 and Figure 5.28, respectively) showed that the changes in the pore-water pressures were not entirely dependent on the total rainfall but also on the initial pore-water pressure values. When the

pore-water pressures were high, with positive values, even if the rainfall event was of a long duration and intensive only limited changes were observed (especially near the ground surface). The pore-water pressures close to the ground surface remained constant after they had reached a peak value during a rainfall event (Figure 5.4 and Figure 5.21). At greater depths, it took a longer time before the pore-water pressures started to increase. For the cases of low negative pore-water pressures it was found that the pore-water pressures near the ground surface were very sensitive even to a very small amount of rainfall (Figure 5.10 and Figure 5.28). In the cases of low pore-water pressures the increase of pore-water pressures was significant.

The analysis of the effect of the initial pore-water pressures on the pore-water pressure changes during rainfall showed that the initial conditions play an important role on the development of the pore-water pressures during a rainfall event. For NTU-CSE slope, it was seen that a rainfall event with total rainfall greater than 15mm would produce similar pore-water pressure changes near the ground surface when the initial pore-water pressures were similar (Figure 5.10). For NTU-ANX slope, this change of behaviour in the pore-water pressure changes is identified in rainfall events greater than 25mm (Figure 5.28). This threshold of 25mm was linked to the infiltration characteristics of the slope. It was seen that for rainfall events with total rainfall greater than 25mm, there was no further increase in the total infiltration (Figure 5.26) and consequently the pore-water pressures would not increase significantly more for rainfall events higher than 25mm. The pore-water pressures at large depths (i.e. at 3.2m deep for NTU-CSE slope and 2.9m deep for NTU-ANX slope) showed that increase of the pore-water pressures during rainfall were usually very small (Figure 5.12 and Figure 5.28).

CHAPTER 6

Controlling Parameters for Rainfall-Induced Slope Instability

The numerical analysis of rainfall-induced slope instability requires the definition of various hydrological characteristics of the soil in addition to the climatic information. This chapter presents the results of a parametric study on the effect of different rainfall patterns and different saturated coefficients of permeability on the development of the pore-water pressures within a slope during infiltration and subsequently on the stability of the slope. Attempts have been made to investigate the relationship between the climatic conditions, soil properties and initial conditions within a slope that can lead to slope instability. The situation under which the antecedent rainfall, prior to a major rainfall event can be crucial and needs to be accounted for in the analysis is also investigated. Finally, from the results, the principal parameters that can affect the stability of the slope are identified.

6.1 Description of the parametric study

6.1.1 Objective of the parametric study

The study includes both seepage analyses and slope stability analyses. The seepage analyses are used to investigate how seepage will occur in a slope under different hydrological conditions. For these analyses the commercial finite element software Seep/W (Geo-Slope 1998a) was used. The slope stability analyses were used to study the effect of different seepage conditions (as predicted by Seep/W) on the factor of safety of the slope. For these analyses the commercial software Slope/W (Geo-Slope 1998b) was used. The parameters that were investigated in this study were the distribution of rainfall, the antecedent rainfall prior to the main rainfall event, the saturated coefficient of permeability with respect to water and finally the initial conditions within the slope. Table 6.1 presents the parameters that were varied in the study.

Table 6.1 Summary of variables investigated in the parametric study.

Rainfall patterns	Soil Parameters	Initial Conditions
Distribution of major rainfall	Saturated coefficient of permeability with respect to water	Initial pore-water pressures
Distribution of antecedent rainfall		Initial groundwater level

6.1.2 General geometry of the slope and soil properties

The slope used in this study is 10m high and stands at an inclination of 26.6° (inclination 2H:1V). These are typical dimensions of engineered slopes in Singapore. The slope geometry is presented in Figure 6.1. In order to simplify the problem it is assumed that the slope is composed of a homogenous and isotropic residual soil. The idealised slope isolates the influence of complex hydro-geological conditions on the seepage analysis. The left and right edges are located at a distance of 30m from the crest and the toe respectively in order to avoid any influence of the boundary conditions on the seepage process within the slope area.

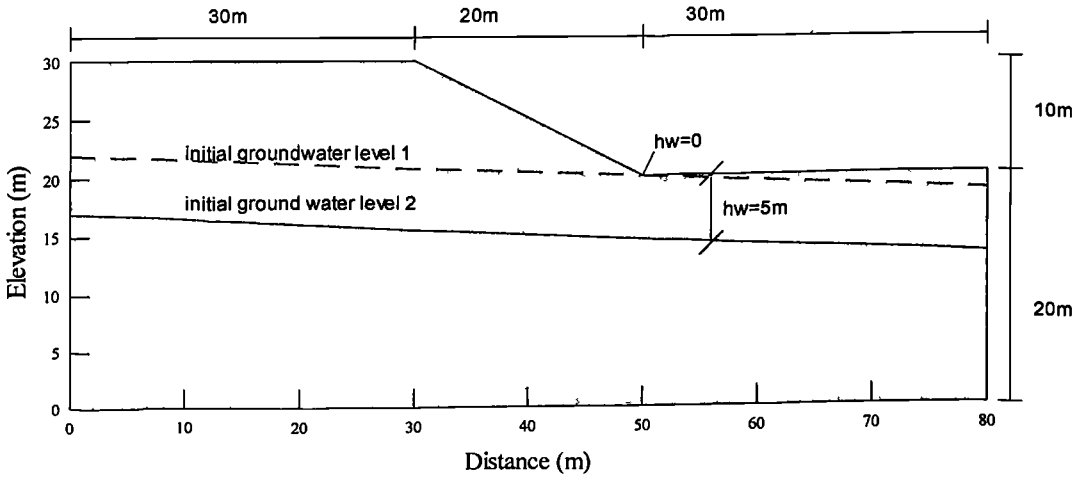

Figure 6.1 Geometry of the homogenous slope used for the numerical analysis.

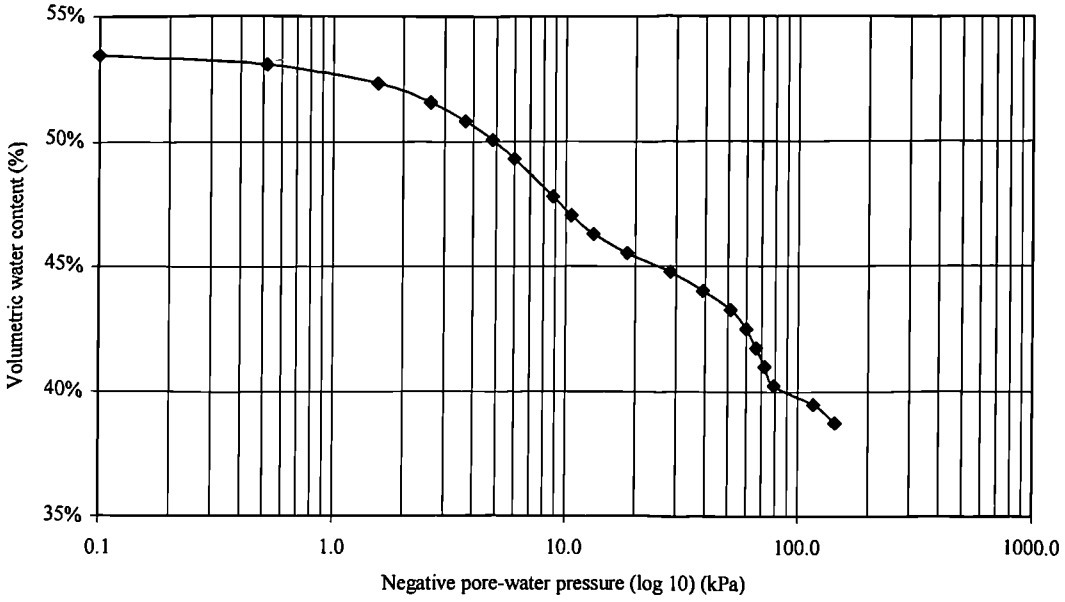

Figure 6.2 Volumetric soil-water characteristic curve for the numerical analysis.

The soil properties adopted in this study are typical of those from the surficial soil layer (Layer 1) of the NTU-ANX slope (Chapter 3, Section 3.2). The soil is silty clay with grade of weathering 6 (residual). The soil-water characteristic curve (swcc) of the soil is shown in Figure 6.2 and was obtained using a volumetric pressure plate in the laboratory (Sections 3.5 and 4.2.1). The volumetric water content at saturation was determined to be 0.53. The curve shows that from zero pore-water pressure to -50kPa (i.e. that is the common range of negative pore-water pressure measured within the field in Singapore) the volumetric water content drops from 0.53 to 0.43. The coefficient of volumetric water change (m_w^2) with respect to changes in negative pore-water pressure (u_a-u_w) from 0 to -20kPa pore-water pressure is 0.004 kPa^{-1} and 0.0007 kPa^{-1} for pore-water pressure from -20kPa to -50kPa. The residual volumetric water content (the volume of water that is held even at low negative pore-water pressures and does not take part in the flow process) is approximately 0.38.

For the slope stability analysis it was assumed that the soil has a very low effective cohesion (c') of 1kPa, an effective angle of internal friction (ϕ') of 25° and a (ϕ^b) angle of 24°. These values of the strength parameters are in agreement with the ones

used in Chapter 5 (Section 5.2.4) for the NTU-ANX slope. All soil parameters used for the slope stability analyses are summarised in Table 6.2.

Table 6.2 Summary of the soil parameters used for the slope stability analysis.

Effective cohesion c' (kPa)	Effective angle of friction ϕ'	ϕ^b angle	Saturated Unit weight (kN/m^3)	Unsaturated unit weight (kN/m^3)
1.0	25.0°	24.0°	20.0	19.0

6.1.3 Description of the finite element mesh design for the seepage analysis

The finite element mesh was designed to overcome problems regarding unstable solutions in transient analyses. These instabilities related mainly to the non-linearity of the water flow equation through unsaturated soil (Chapter 2, Equation 2.29) and to the use of 'steep' permeability functions that caused difficulties associated with convergence in the analysis. The areas of instabilities were mainly located near the ground surface where the pore-water pressures change rapidly during infiltration. It was found that in order to overcome this problem a very fine mesh design was required. However, the use of a uniform, very fine finite element mesh for the entire slope was not possible because of the long computation time required for the solution. The finite element mesh in Figure 6.3 was found to produce satisfactory and stable results and could be used to solve the problem in a reasonable time.

The tolerance of the computed norm of the head vectors between two consecutive iterations was set to 0.05%. Seep/W would continue the iteration procedure at each time step until this requirement was met. Between two consequent iterations, Seep/W changes the value of the coefficient of permeability with respect to water of each node with rate of change 1.1 of orders of magnitude (the value of this rate of change can be set by the user). From one iteration to the next, the minimum change of the initial value of the permeability with respect to water was set to 10^{-4} of order of magnitude and a maximum change of 1 order was allowed. With the use of such requirements a number of iterations (typically around 30) was required. It was possible to check the oscillation of the iteration procedure and this was seen to be stable. The typical duration for each simulation was between four to eight hours on a PC Pentium with a 333 MHz speed. However, there were cases when more than 100 iterations were needed in each time step in order to achieve the necessary

convergence between two iterations and in this case the calculations could take longer than one day. In all cases a detailed check of the results was performed. The results were also compared with field observations from the instrumented slopes on NTU campus for their validity (Chapter 4, Section 4.2.4).

The finite element mesh is a combination of very fine 8-noded quadrilateral elements (0.25m x 0.25m) near the ground surface of the slope to a depth of 3m and fine 4-noded quadrilateral elements (0.5m x 0.5m) from 3m deep and below. At the distance of 15m from the crest and toe of the slope the mesh was designed to be coarser (1m long x 0.5m high) in order to decrease the total number of nodes and hence the required solution time for each simulation. In total this mesh consists of 8260 nodes and 5706 elements.

Along the left and right edges, head boundaries were applied in order to define the initial groundwater level and the initial pore-water pressure profile. It was assumed that there was no slope at the base of the problem and therefore a zero nodal flow boundary (Q) was applied along the base. The precipitation rate was modelled as a unit flux boundary (q) along the nodes at the ground surface and the infiltration and seepage processes within the slope were modelled in two dimensions (x- and y-coordinate). During the solution procedure, Seep/W 'translates' the unit boundary (q) into a nodal boundary (Q) and then calculates the hydraulic head at each node. In order to avoid any ponding phenomenon, that is unlikely to take place in sloping ground, the software performs a check that every node at the ground surface has zero or negative hydraulic head. In case a ground surface node is found with a positive pore-water pressure (greater than zero) at the end of the calculation for each time step then that node is set to have head equal to the elevation and the problem is resolved. In this case the flux boundary is changed to a head boundary and the flux is determined.

The seepage analysis presented in this work has two important limitations. The first limitation is that no evaporation was taken into consideration during the dry periods of each simulation. In reality the actual evaporation rate from a soil surface is a function of the atmospheric demand (potential evaporation) and the available water content of the soil (Wilson et al. 1995). Seep/W can handle an evaporative flux only

by defining a negative flux along the ground surface. Gasmo et al. (2000) attempted to incorporate evaporation as a negative flux in a seepage analysis using Seep/W and concluded that the decrease of the pore-water pressures was unrealistically fast in comparison with field observations in Singapore. Some similar trials were also carried out during the preliminary phase of the analyses and found similar unrealistic results. Therefore, evaporation was not taken into account. Since the focus of this work is the changes in pore-water pressures during a rainfall event (when no evaporation would be occurring) this is not a major limitation to the analyses presented.

The second limitation in this analysis is the assumption that the hysteresis of the soil-water characteristic curve between the wetting and the drying phase is not significant. The soil-water characteristic curves produced in the laboratory from soil samples of the NTU-ANX slope (Section 4.2.1) show that there is some hysteresis between the wetting and trying phase of the soil-water characteristic curve. However, this is a necessary assumption, as Seep/W is not able to determine in every time step which area of the slope is in the drying or the wetting phase so that it can use the appropriate curve and therefore only a single curve can be defined within the software.

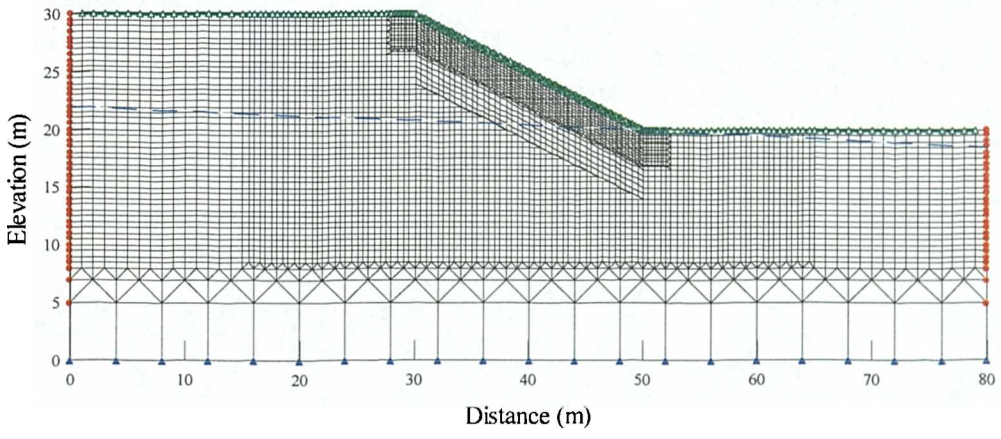

Figure 6.3 Geometry of the finite element mesh used for the seepage analysis.

6.1.4 Description of the slope stability analysis

For the slope stability analyses, the method of slices satisfying moment equilibrium was used (Chapter 2, Section 2.9). The design of the grid of circles centres and the

radius that were used in the analyses are presented in Figure 6.4. The pore-water pressures that were determined in the seepage analysis by Seep/W were used as input data for the slope stability analysis. For this method, Slope/W determines the element that lies closest to the centre of each slice base and computes the pore-water pressure at each location from the nodal pore-water pressure conditions of the element nodes.

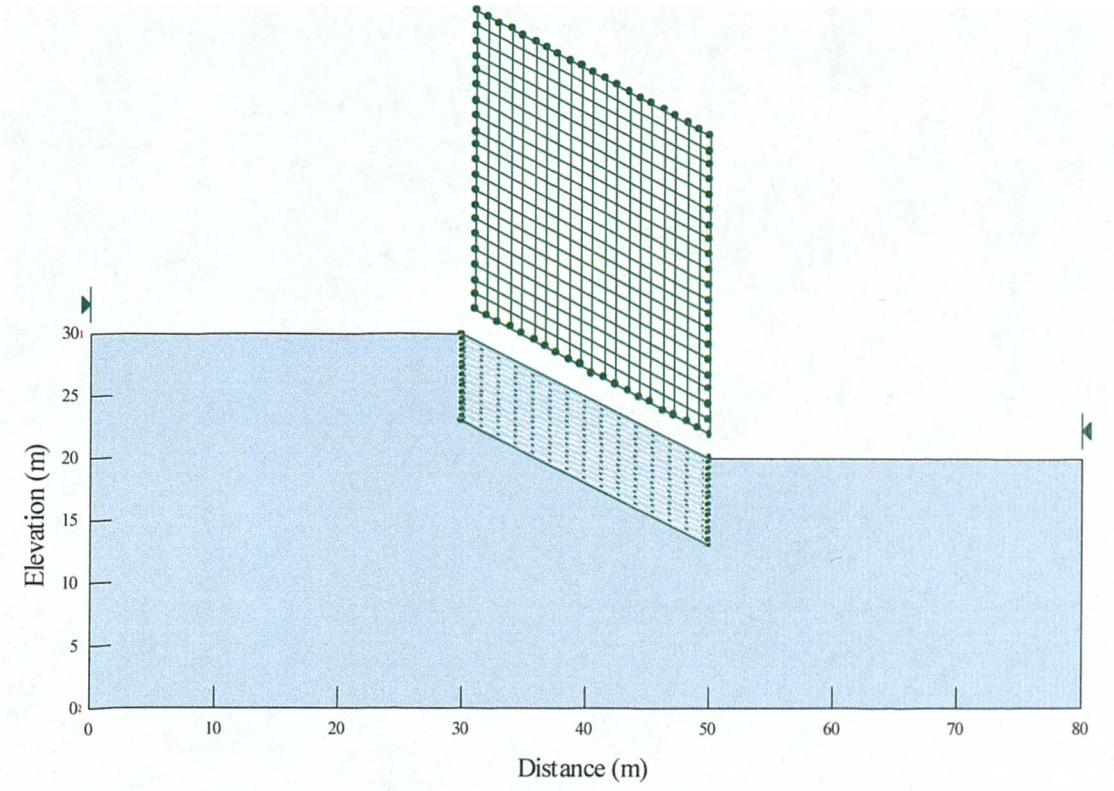

Figure 6.4 Range of possible critical slip surfaces used for the slope stability analysis.

6.1.5 Variable parameters in the analysis

The variable parameters in the analysis were the distribution of the antecedent rainfall, the distribution of the major rainfall event, the saturated coefficient of permeability with respect to water and the initial pore-water pressures and groundwater table.

The precipitation characteristics were divided into 5-day antecedent rainfall (i.e. the rainfall prior to a significant rainfall event) and the major rainfall event itself. The total amount of rainfall of the antecedent rainfall and of the major rainfall was constant and different distributions were examined. The total rainfall for the

antecedent rainfall period was 25mm and the total rainfall of the major rainfall event was 240mm.

Major Rainfall

Different distributions of the major rainfall event were included in the study. The major rainfall event of 240mm total rainfall was distributed over four different periods as shown in Figure 6.5 and also summarised in Table 6.3. These periods were 16 hours, 8 hours, 4 hours, and 2 hours, corresponding to intensities of 15mm/h, 30mm/h, 60mm/h, and 120mm/h accordingly. In order to allow the slope to drain and to study the recovery of the negative pore-water pressures, the simulation lasted for 120 hours, i.e. 5 days. No antecedent rainfall was applied to the slope prior to those four rainfall events.

Table 6.3 Summary of distribution of the major rainfall events applied to the slope.

Major rainfall no.	Total (mm)	Duration (hours)	Intensity (mm/h)
1	240	16	15.0
2		8	30.0
3		4	60.0
4		2	120.0

Antecedent Rainfall

For the antecedent rainfall, four different scenarios were assumed based on a distribution over the 5-day period. In Figure 6.6, the four different rainfall scenarios are presented and in Table 6.4 a summary for each of the scenarios are presented. For scenarios 1 through 3, the total rainfall of the major rainfall event was distributed over 4hours with 60mm/h intensity. The distribution of the antecedent rainfall was varied in three different scenarios. In scenario 1 the antecedent rainfall was distributed into 5 events of 5 hours duration each. In scenario 2 the antecedent rainfall was distributed into 5 events of 1hour duration each and in scenario 3 the antecedent rainfall was distributed in one continuous event that lasted 5 days. Finally a fourth rainfall-scenario, scenario 4, was applied to the slope and the total amount of 265mm (i.e. the equivalent of 25mm of antecedent rainfall and 240mm of the major rainfall from the scenarios 1, 2 and 3) was distributed evenly into 5 days

and 4 hours. In each case the rainfall period was followed by a dry 9-day period to study the negative pore-water pressure recovery process.

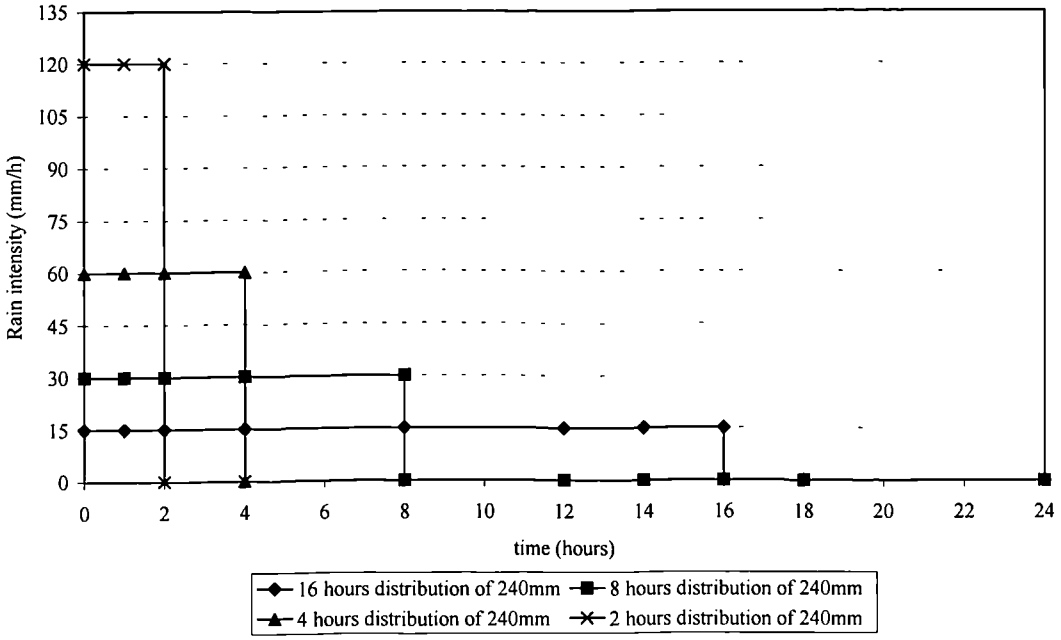

Figure 6.5 Different distributions of the major rainfall event applied in the slope.

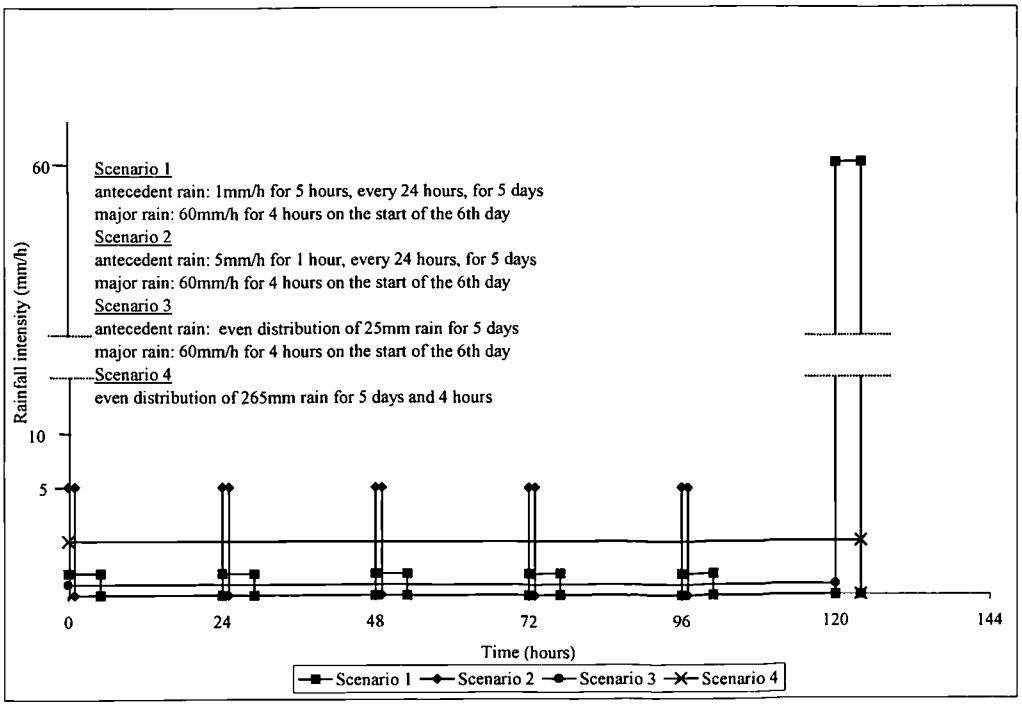

Figure 6.6 Rainfall scenarios applied in the slope for the study of antecedent rainfall.

Table 6.4 Summary of rainfall scenarios for the study of the effect of the antecedent rainfall.

	Antecedent rainfall				Major rainfall		
Scenario no.	Total (mm)	No. of events	Duration (hours)	Intensity (mm/h)	Total (mm)	Duration (hours)	Intensity (mm/h)
1		5	5	1.00			
2	25	5	1	5.00	240	4	60.00
3		1	120	0.21			
4	-	-	-	-	265	124	2.14

Saturated Coefficient of Permeability with Respect to Water

Four different saturated coefficients of permeability with respect to water (k_{sat}) were assumed in order to investigate their effect on the infiltration process and on the development of the pore-water pressures with time. The coefficients that were assumed were 10^{-4}m/s, 10^{-5}m/s, 10^{-6}m/s, and finally 10^{-7}m/s. This range covers all types of soils in terms of permeability, from very permeable soils (10^{-4}m/s), moderately permeable soils (10^{-5}m/s to 10^{-6}m/s) to low permeable soils (10^{-7}m/s). The permeability functions that are presented in Figure 6.7 were predicted from the soil-water characteristic curve of Figure 6.2 using Green and Corey's (1971) equation.

Initial Conditions

The initial depth (h_w) of the groundwater table, at the toe of the slope, was 0 and 5m and its inclination was 12H:1V (inclination angle 5°). Figure 6.1 presents the two initial groundwater levels. For the pore-water pressure profiles within the slope three initial conditions were assumed with minimum pore-water pressure near the ground surface of –25kPa, –50kPa, and –75kPa. Figure 6.8 shows the three initial pore-water pressure profiles of the slope used in the study. The pore-water pressures below the groundwater table are assumed to be hydrostatic. Above the groundwater table the pore-water pressures become negative until they reach the appropriate limiting values (i.e. –25kPa or –50kPa or –75kPa) and after that they remain constant. These minimum values for the pore-water pressures are chosen to represent the typical range of negative pore-water pressures in Singapore. Field measurements from the instrumented slopes on the NTU campus show that negative

pore-water pressures can be as low as –70kPa near the ground surface (0.5m depth) after a long dry period (Chapters 4 and 5).

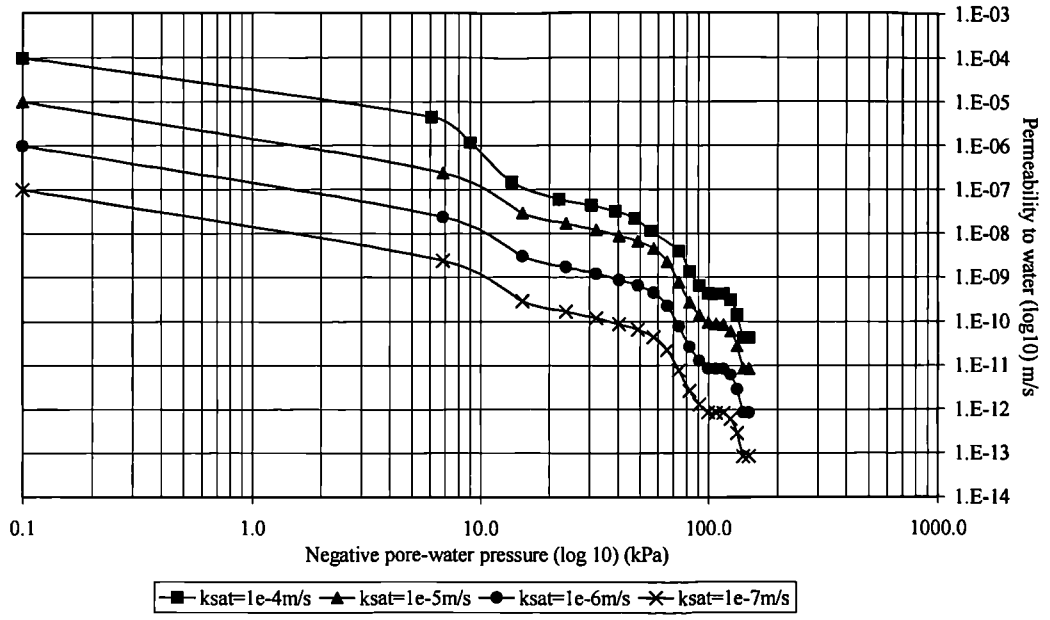

Figure 6.7 Permeability with respect to water for different saturated coefficients of permeability.

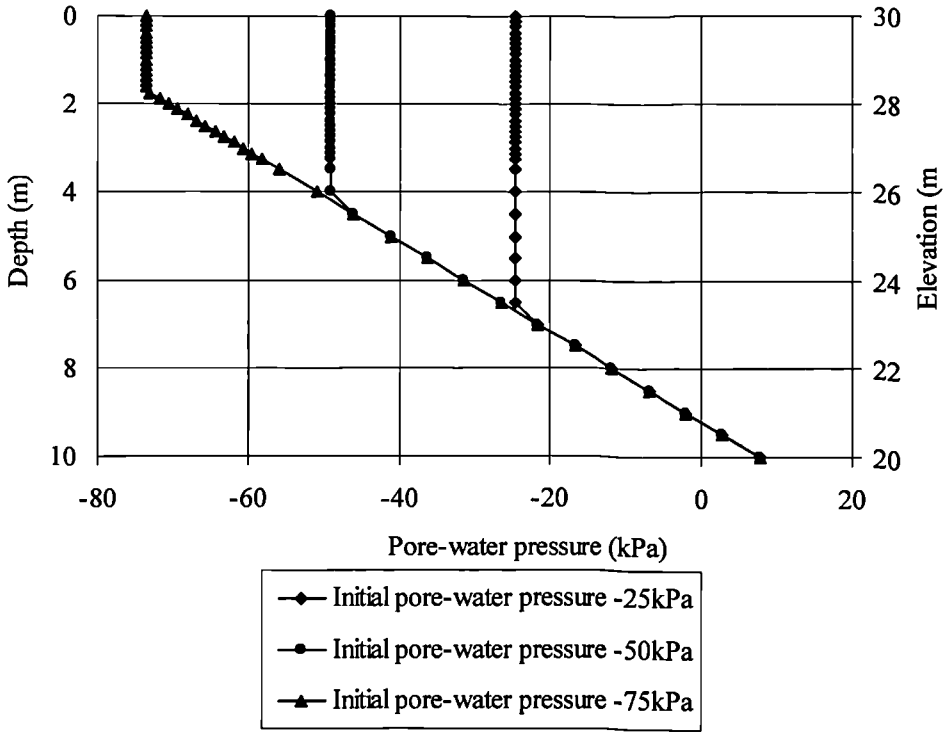

a)

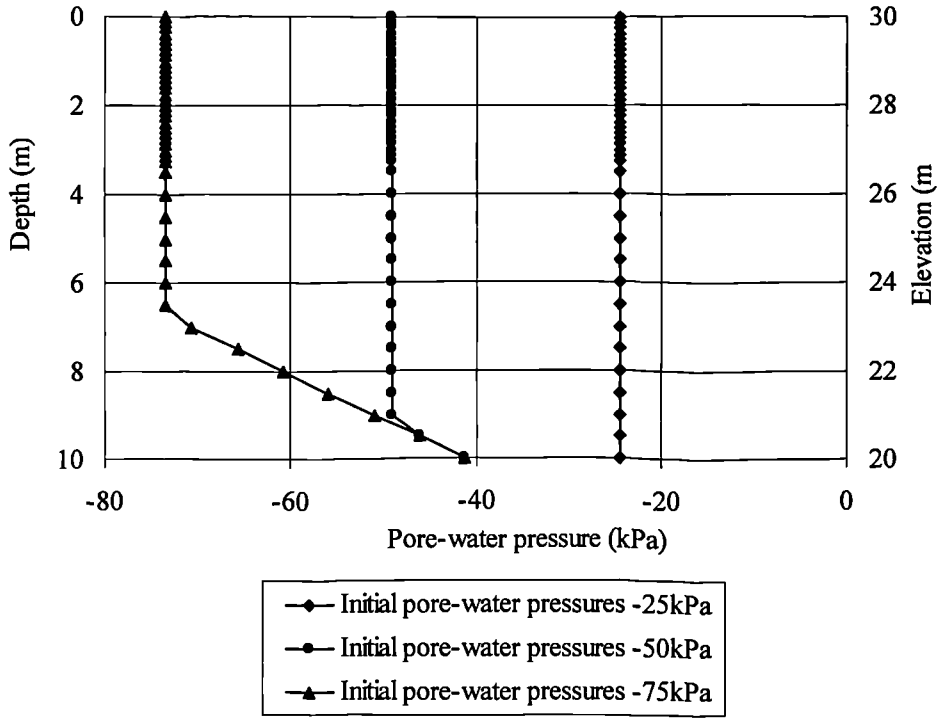

b)

Figure 6.8 Initial pore-water pressure profiles at the crest of the slope used in the study a) for h_w=0 and b) h_w=5m.

6.2 Seepage analysis results

6.2.1 Influence of different rainfall distributions for the major rainfall

The results, presented in Figure 6.9, show that for high and medium values of saturated coefficient of permeability with respect to water (10^{-4}m/s and 10^{-5}m/s) the way in which the same total rainfall is distributed plays a major role in the development of the pore–water pressures during rainfall. Figures 6.9a, 6.9b and 6.9c present the pore-water profiles at the crest of the slope, at the end of the rainfall for the saturated coefficients of permeability with respect to water (k_{sat}) of 10^{-4}, 10^{-5} and 10^{-6}m/s, initial depth of the groundwater table (h_w) of 0 and initial pore-water pressure -25kPa. Figures 6.9a and 6.9b show that the longer the period over which the 240mm of total rainfall is distributed, the deeper will be the movement of the wetting front (line of zero pore-water pressure). For k_{sat}=10^{-4}m/s (Figure 6.9a), if the rainfall is distributed in 16 hours (i.e. 15mm/h intensity) then the wetting front reaches as deep as 3.5m. At the same time for a short and intense rainfall (i.e. 2

hours distribution with intensity of 120mm/h) the wetting front can be as shallow as 0.25m.

The same behaviour can be noticed for the case of $k_{sat}=10^{-5}$m/s (Figure 6.9b). However, the results presented in Figure 6.9c show that with a low k_{sat}, such as 10^{-6}m/s, the pore-water pressure profiles at the crest of the slope at the end of the four different rainfall events are very similar and a very shallow wetting front, around 0.13m, is developed only when the rainfall was distributed in 16 hours. Comparing the pore-water pressure profiles of Figures 6.9a through 9c show that for the same distribution of the 240mm of total rainfall, the depth of wetting front increases as the value of k_{sat} increases. This can be seen more clearly in Figures 6.10a and 6.10b that show the pore-water pressure profiles at the end of the rainfall events for rainfall distributions of 16 hours (intensity 15mm/h) and 2 hours (intensity 120mm/h), respectively. Both figures show that for the same distribution of rainfall, the higher the value of k_{sat}, the greater the increase of the pore-water pressures from the initial conditions and the deeper the wetting front will be. For example, for the lowest rainfall distribution of 2 hours (i.e. rainfall intensity of 120mm/h) the wetting front is 0.25m deep for $k_{sat}=10^{-4}$m/s, 0.13m for $k_{sat}=10^{-5}$m/s and finally it is zero for $k_{sat}=10^{-6}$m/s.

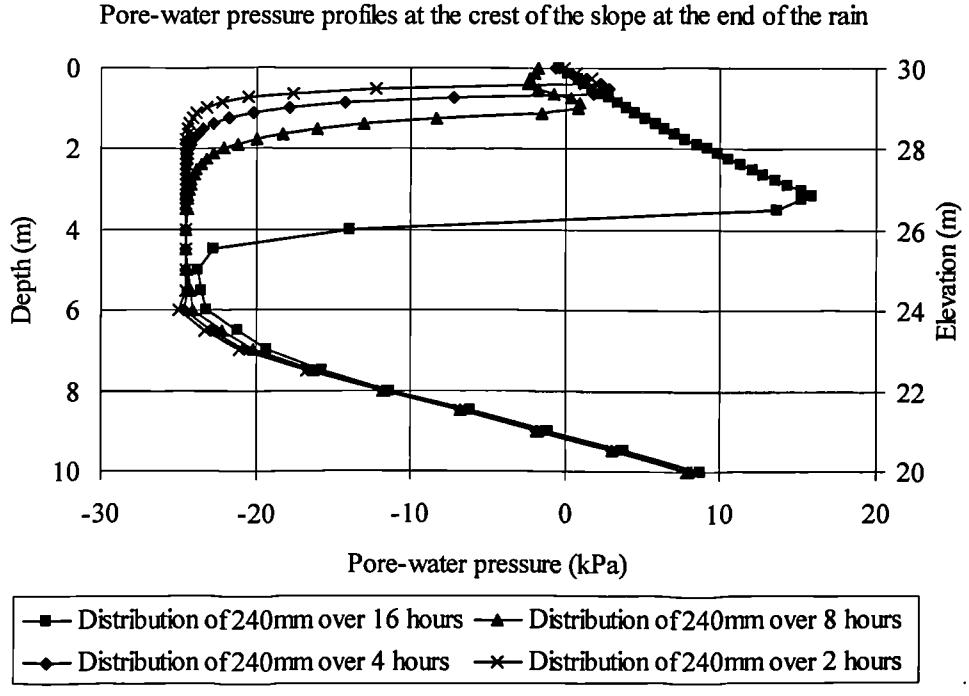

(a)

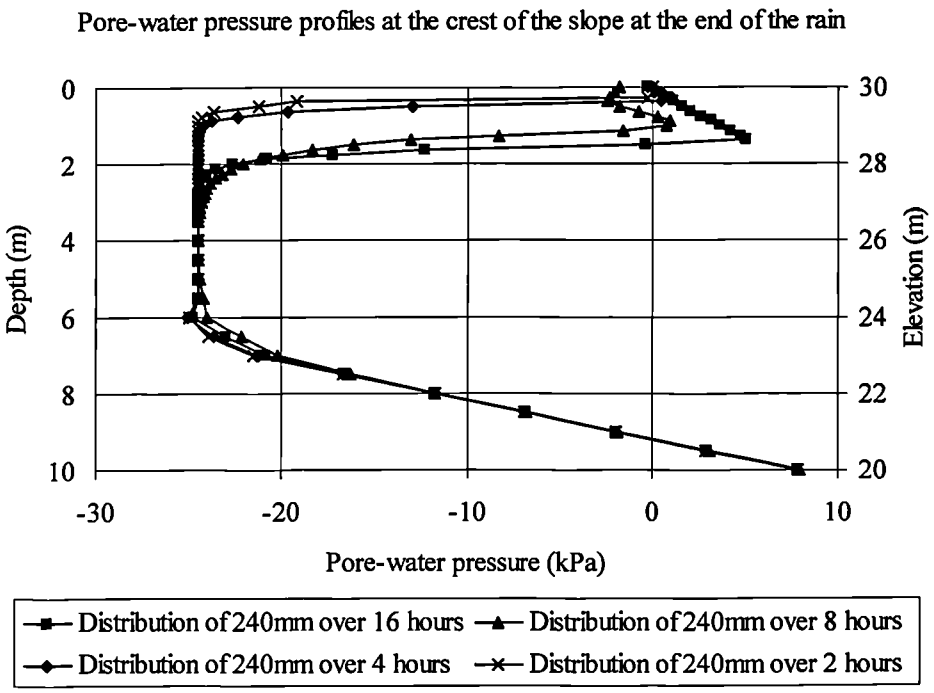

(b)

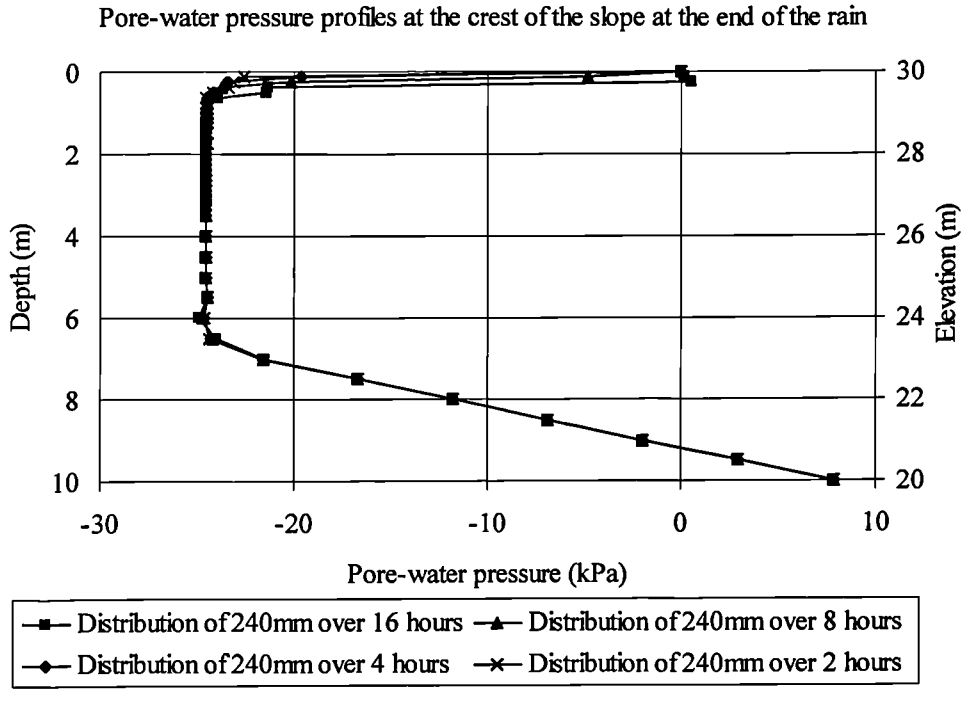

(c)

Figure 6.9 Pore-water pressure profiles at the crest of the slope at the end of the rainfall studying different rainfall distributions for initial pore-water pressures –25kPa, h_w=0 and (a) k_{sat}=10^{-4}m/s, (b) k_{sat}=10^{-5}m/s and (c) k_{sat}=10^{-6}m/s.

The trends shown in Figures 6.9 and 6.10 can be explained in terms of infiltration rate. A soil-surface will allow infiltration to enter at a rate that is controlled by the

saturated coefficient of permeability with respect to water (k_{sat}) and the remaining amount of rainwater will run off. For a highly permeable soil, if the total rainfall is distributed in a long period (i.e. with a low intensity) then a small amount of the rainwater will run off (as the infiltration rate will be low compared to k_{sat}) and most of the rainfall will infiltrate into the soil and build a deep wetting front. On the other hand, a soil with a low k_{sat} will allow only a very small amount of rainwater to infiltrate the ground and most of the rainwater will runoff. As a result of this, in cases of relatively impermeable soils, the changes in the pore-water pressures will be small and the wetting front developed will be shallow. This can also explain why the pore-water pressure profiles of Figure 6.9c are very similar even though the rainfall is distributed differently. The 10^{-6}m/s (equivalent to 3.6mm/h) value for k_{sat} is significantly smaller than the rainfall intensities of all four rainfall events. Therefore in all four cases only a very small amount of rainfall-water will infiltrate the ground and the most of it will disappear as runoff. This is in good agreement with results of similar analyses by Ng (1998a and b) who studied the development of the wetting front and McDougall (1998) who studied the infiltration rate under different precipitation rates.

6.2.2 Influence of antecedent rainfall

The influence of different distributions of antecedent rainfall was studied using a soil of a medium coefficient of permeability with respect to water of 10^{-5}m/s and with different initial conditions. A major rainfall event with an intensity of 60mm/h for 4-hour duration was adopted for the analysis. Three distributions of the antecedent rainfall were examined (Figure 6.5). In scenarios 1 and 2, the 25mm antecedent rainfall was distributed into 5 events of 5- and 1-hour duration, respectively. In scenario 3 the 25mm antecedent rainfall was distributed evenly over the 5-day period. For comparison a fourth scenario was introduced in the study. In scenario 4, the total amount of rainfall (i.e. 265mm) was distributed evenly over the rainy period that lasted 5 days and 4 hours.

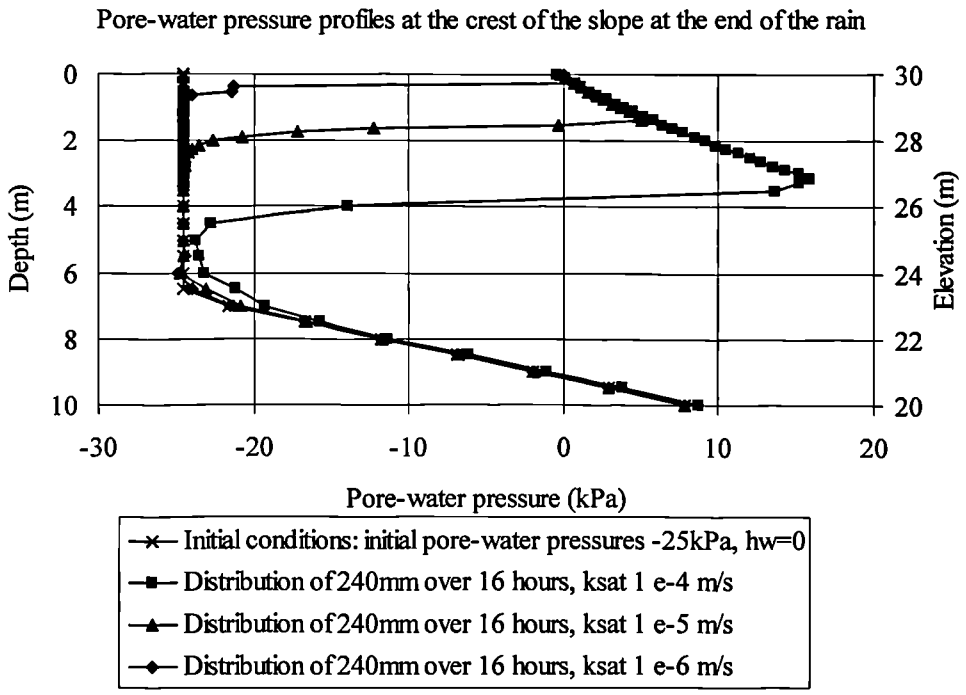

(a)

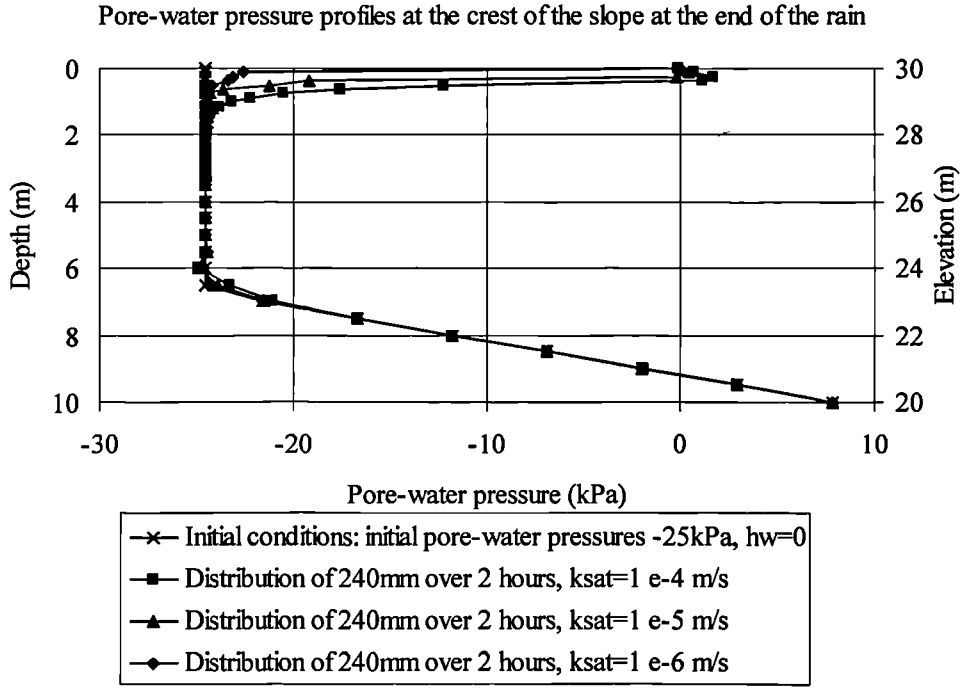

(b)

Figure 6.10 Comparison of the pore-water pressure profiles at the crest of the slope, at the end of the rainfall for initial pore-water pressures –25kPa, h_w=0 and for different saturated coefficients of permeability with respect to water (a) distribution over 16 hours (i.e. intensity 15mm/h) and (b) distribution over 2 hours (i.e. intensity 120mm/h).

Figures 6.11a and 6.11b show the pore–water pressure profiles at the crest of the slope for -25kPa initial pore-water pressures and for an initial groundwater table at the toe of the slope. The pore-water pressure profiles correspond to the conditions at the end of the antecedent rainfall (Figure 6.11a) and at the end of the major rainfall event (Figure 6.11b). From the trials it was found that the distribution of the antecedent rainfall has a significant effect on the changes in pore-water pressures during the major rainfall event and also in the development of the wetting front. Figure 6.11a shows that for scenario 3, the pore-water pressures have increased significantly at the end of the antecedent rainfall. At the ground surface the pore-water pressures have become zero. From the ground surface and down to 3m depth the pore-water pressures have increased considerably from their initial value. The changes of the pore-water pressures in scenarios 1 and 2 are more limited. The pore-water pressures near the ground surface remained negative at the end of the antecedent rainfall. The explanation for the different evolutions of the pore-water pressures near the ground surface is attributed to the difference in the rainfall patterns. In scenarios 1 and 2 the antecedent rainfall is distributed in short events and in between the rainfall events the slope is able to drain, while in scenario 3 (where the antecedent rainfall is distributed in evenly over the whole 5-day period) the infiltrated water does not have sufficient time to percolate.

The different distributions of a small amount of antecedent rainfall (25mm) can affect significantly the final pore-water pressure profile of the slope (Figure 6.11b) and also the final depth of the wetting front. For scenario 3, a wetting front of approximately 1.20m deep has developed at the crest of the slope. The wetting front for scenarios 1 and 2 is quite shallow and is not deeper than 0.5m.

In the case of scenario 4 (where the total amount of rainfall antecedent and major rainfall is distributed over the whole period of 5 days and 4 hours), the soil near the ground surface reaches an almost steady state condition where no significant changes in the pore-water pressure take place (Figures 6.11a and 6.11b). From the ground surface and down to 4m the pore-water pressures remain negative and are approximately –4.5kPa.

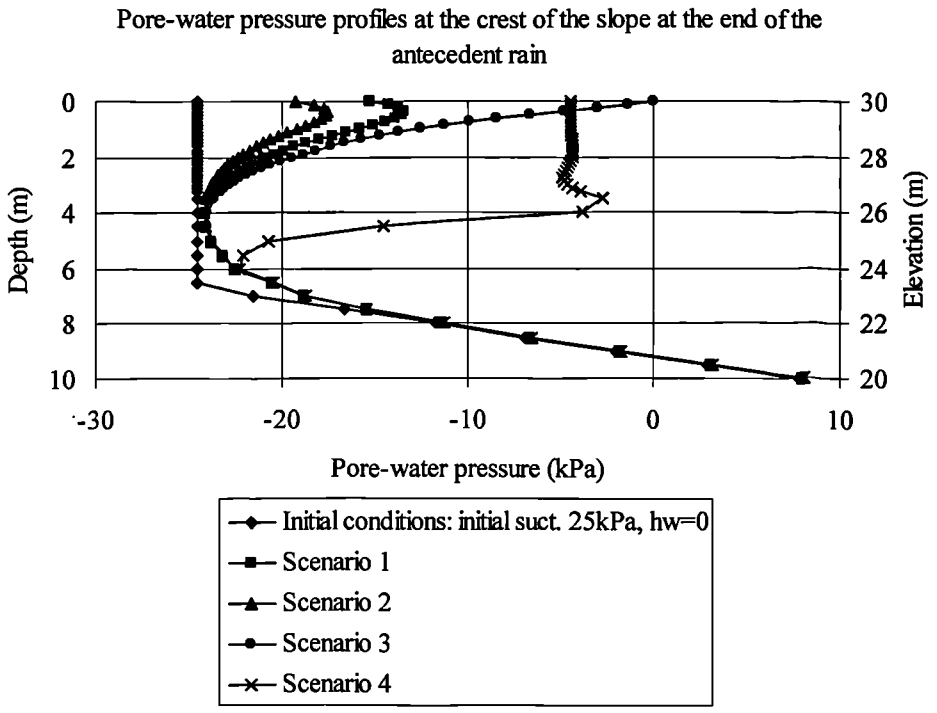

(a)

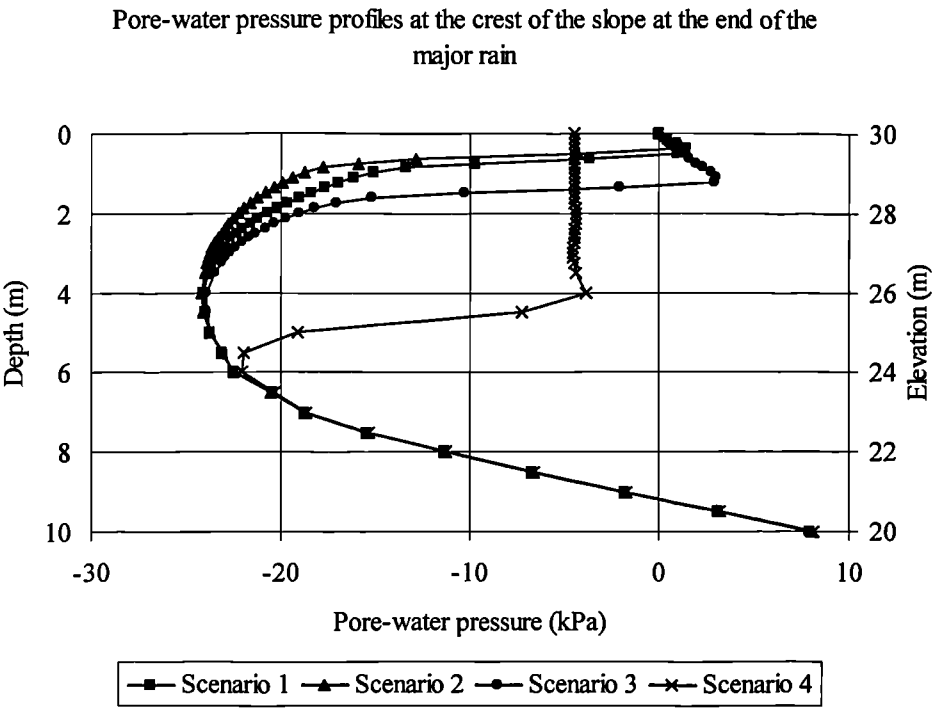

(b)

Figure 6.11 Comparison of the pore-water pressure profiles at the crest of the slope for different distributions of antecedent rainfall for $k_{sat}=10^{-5}$m/s, initial pore-water pressures -25kPa and water level at the toe of the slope (a) at the end of the antecedent rainfall and (b) at the end of the major rainfall event.

The development of the pore-water pressures with time throughout the entire simulation for scenario 3 for all the cases of initial conditions is shown in Figure 6.12a. Figure 6.13 shows the same data as Figure 6.12a but focuses on the major rainfall event. In both figures, the different stages are distinguished as antecedent rainfall, major rainfall, and drainage periods. The figures show that the influence of the initial conditions on the seepage conditions is limited for the case where antecedent rainfall is applied to the slope. It can be seen that for the case of initial pore-water pressures –75kPa (Figure 6.12a) the antecedent rainfall has an important effect as the soil increases its pore-water pressure rapidly and at the start of the major rainfall the pore-water pressures have increased to –31kPa. This means that the pore-water pressures have decreased more than half of their initial value. In the cases of initial pore-water pressure of –25kPa and –50kPa the pore-water pressures at the same time period are equal to –7kPa and –13kPa, respectively. Again the increase of the pore-water pressures is also large and exceeds two thirds of the initial values.

At the end of the major rainfall event in all cases, the pore-water pressures converge into a small range between 1 and 2.5 kPa of positive pressure (Figure 6.13). Of course this behaviour is limited only to a shallow zone close to the ground surface. Figure 6.12b presents the development with time of the pore-water pressures 3.0m deep at the crest of the slope. From the graph it can be seen that for low initial pore-water pressures (–75kPa) the increase is small, while for the cases of initial pore-water pressure –50kPa and –25kPa the changes are significant, but the pore-water pressures still remain negative. It can also be noted that this increase in the pore-water pressures does not start to take place until some hours after the end of the major rainfall. From Figures 6.12a it can also be noted that the depth of the initial groundwater level does not affect significantly the development of the pore-water pressures at shallow depths.

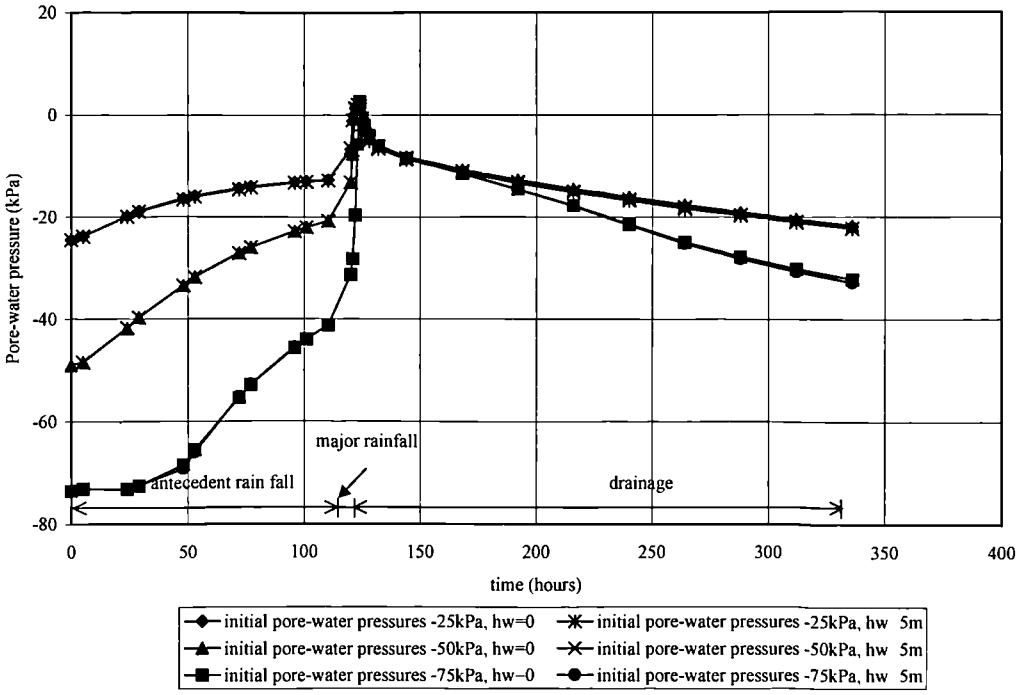

(a)

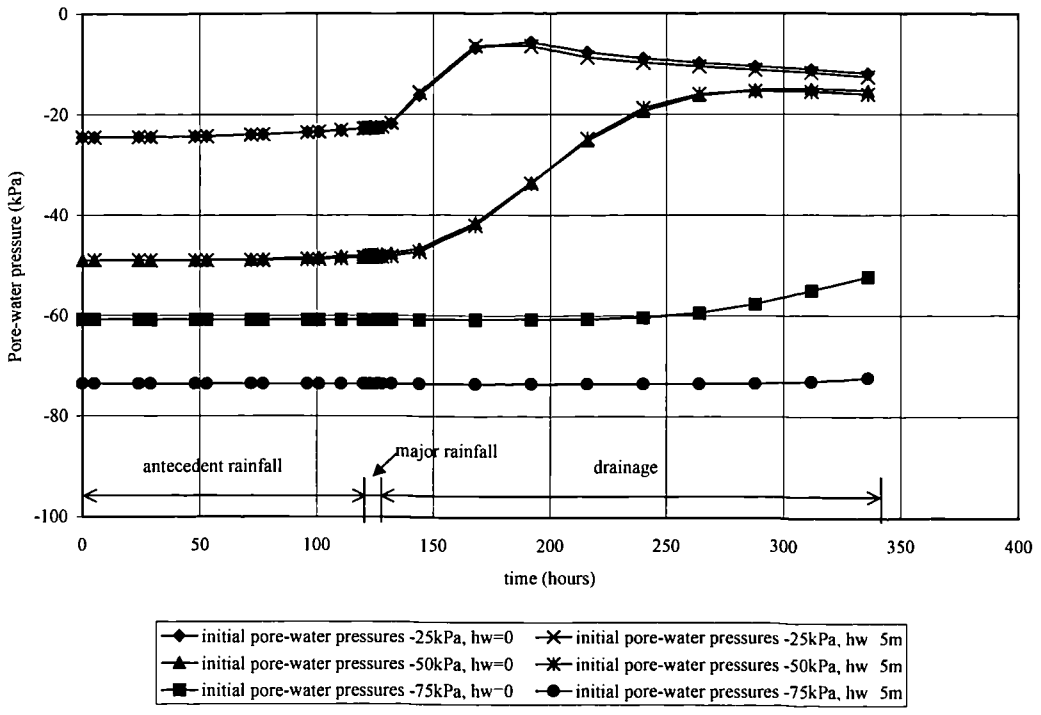

(b)

Figure 6.12 Development with time of the pore-water pressures at the crest of the slope for Scenario 3, $k_{sat}=10^{-5}$m/s and for all sets of initial condition at the crest of the slope (a) at 0.5m deep and (b) at 3m deep.

From the above analysis it is clear that there are large changes in the pore-water pressures in the first 2m from the ground surface where the pore-water pressures

become positive regardless of their initial values. From the above it can be assumed that when antecedent rainfall is taken into consideration in the analysis, then the initial conditions prior to the antecedent rainfall period are not a significant parameter in the development of the pore-water pressures at shallow depths.

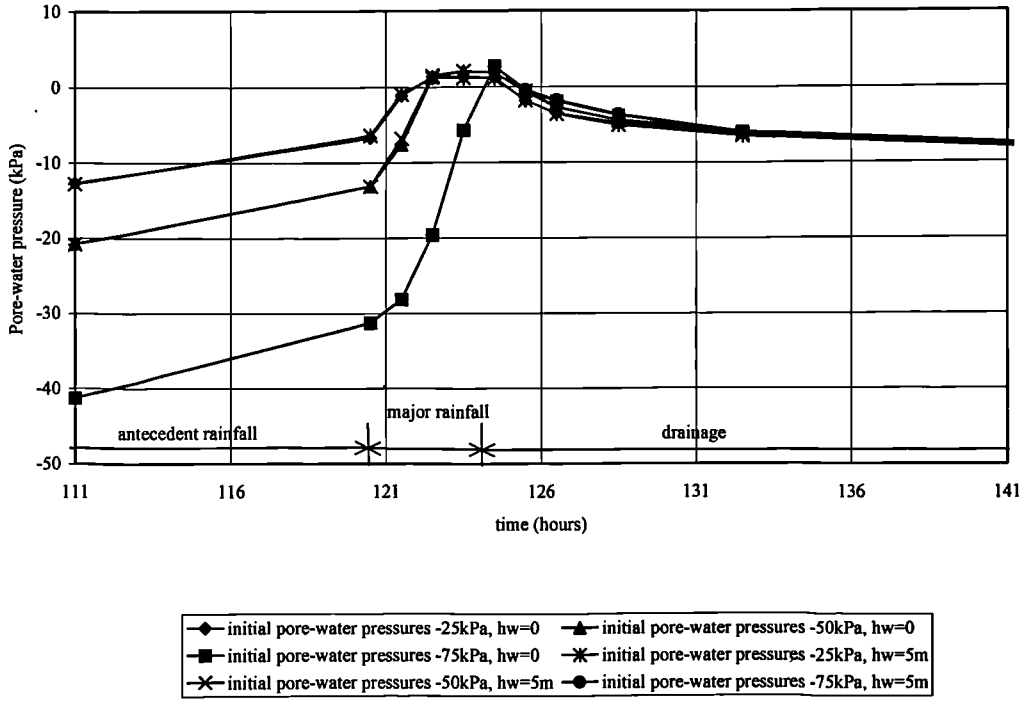

Figure 6.13 Detail of the development with time of the pore-water pressures during the major rainfall event of Scenario 3 at the crest of the slope, 0.5m deep for $k_{sat}=10^{-5}$m/s and for all initial conditions.

6.2.3 Influence of different saturated coefficients of permeability with respect to water

Figures 6.14a and 6.14b present the pore-water pressure profiles at the end of the antecedent rainfall and at the end of the major rainfall respectively, for the case of initial pore-water pressures -25kPa and for the initial groundwater level at the toe of the slope. The saturated coefficient of permeability with respect to water plays a significant role in the infiltration process during rainfall. The results show that the evolution of the pore-water pressures has the same trend as those in Figures 6.10a and 6.10b when the influence of different major rainfall distributions with various k_{sat} was studied. For a low saturated coefficient of permeability with respect to water (i.e. 10^{-7}m/s) the pore-water pressures increase very slowly and any changes can be

noticed only at shallow depths, near the ground surface. During the major rainfall event the changes in the pore-water pressures within the slope are small for $k_{sat}=10^{-7}$m/s (Figure 6.14b). For higher saturated coefficients of permeability with respect to water (i.e. cases of $k_{sat}=10^{-5}$m/s and 10^{-4}m/s), the changes of the pore-water pressures during infiltration become more important, resulting in high positive pore-water pressures at the end of the major rainfall event. In Figure 6.14b, the wetting front for the case of $k_{sat}=10^{-5}$m/s extends to almost the same depth as that for the case of $k_{sat}=10^{-4}$m/s (approximately 1.20m). However, the pore-water pressures for the case of $k_{sat}=10^{-4}$m/s are slightly higher (by about 2kPa). From Figures 6.14a and 6.14b, it can also be concluded that the increase in the pore-water pressures can occur deep within the slope if the soil is moderately to highly permeable.

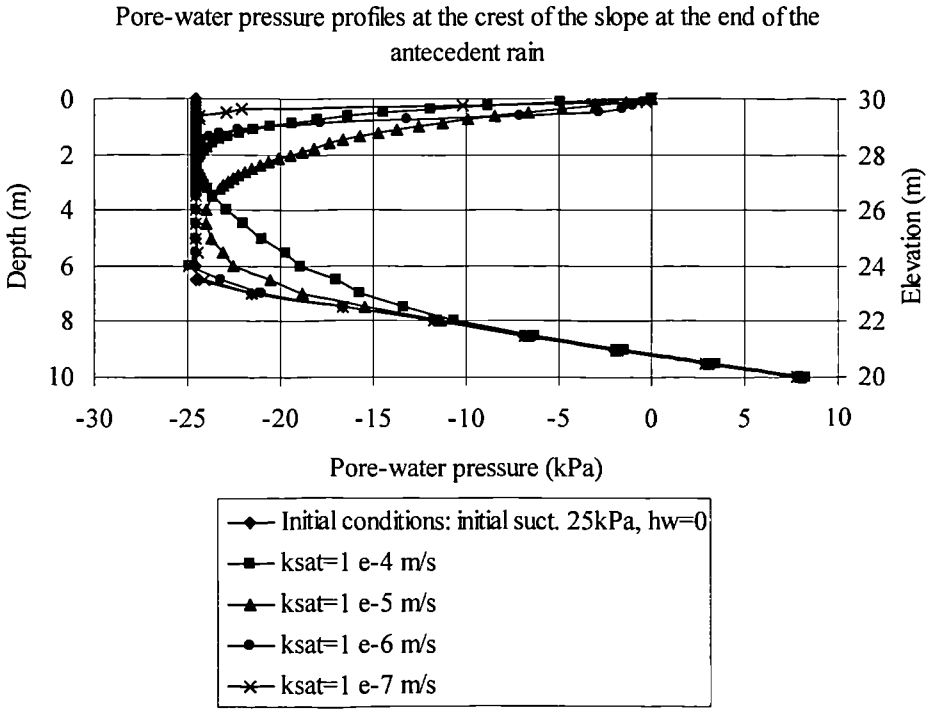

(a)

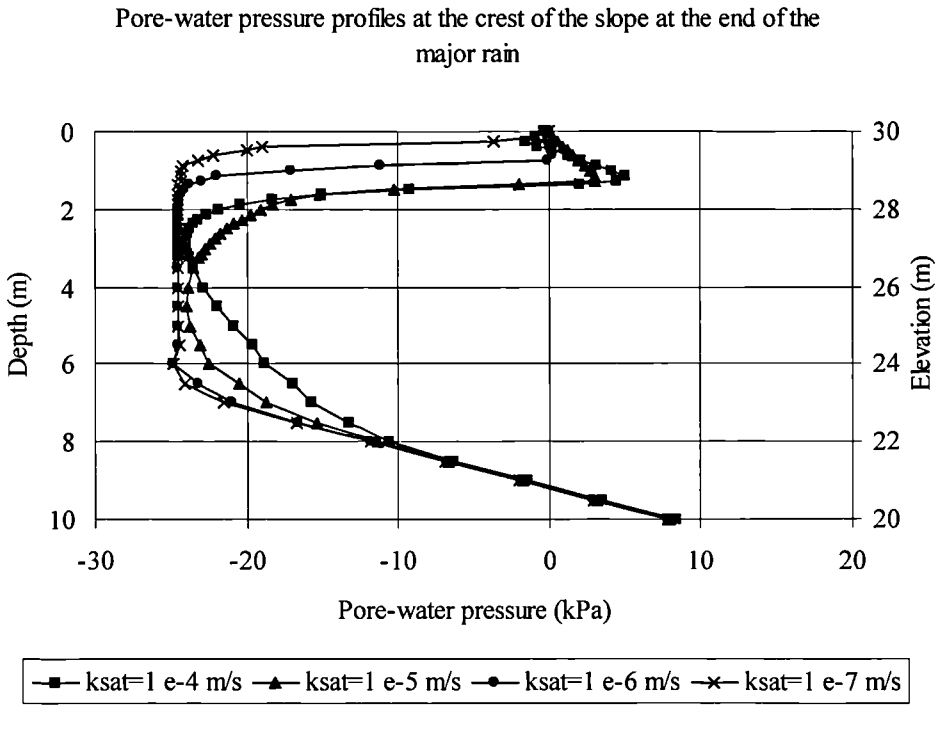

(b)

Figure 6.14 Pore-water pressure profiles for different saturated coefficients of permeability with respect to water at the crest of the slope for Scenario 3, initial pore-water pressures -25kPa and for initial groundwater level at the toe of the slope (a) at the end of the antecedent rainfall and (b) at the end of the major rainfall.

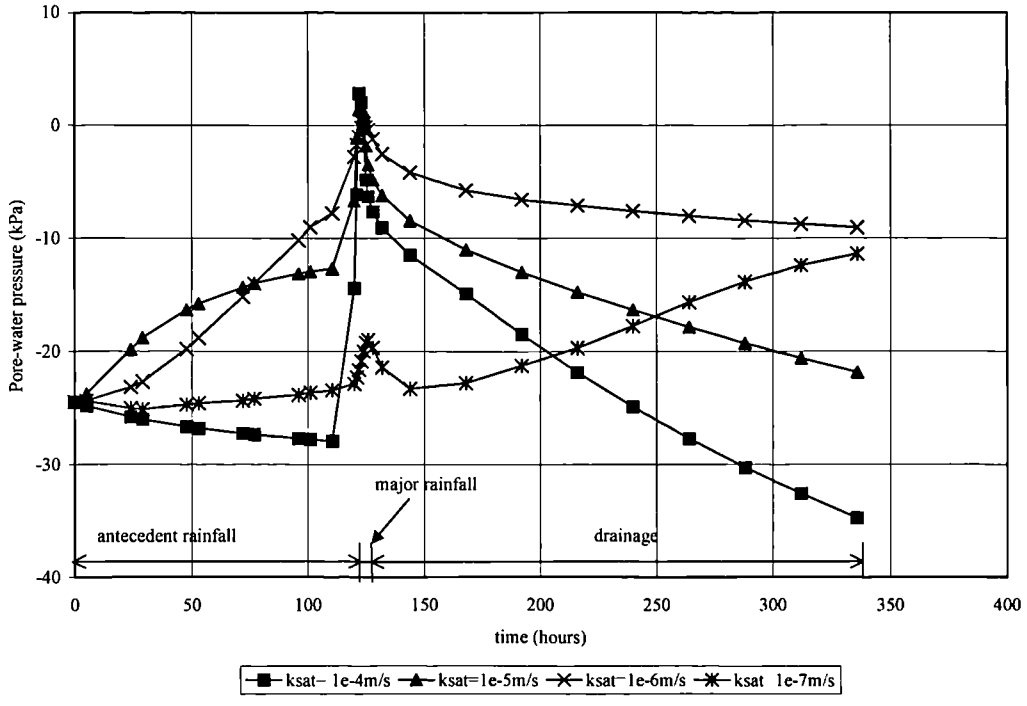

(a)

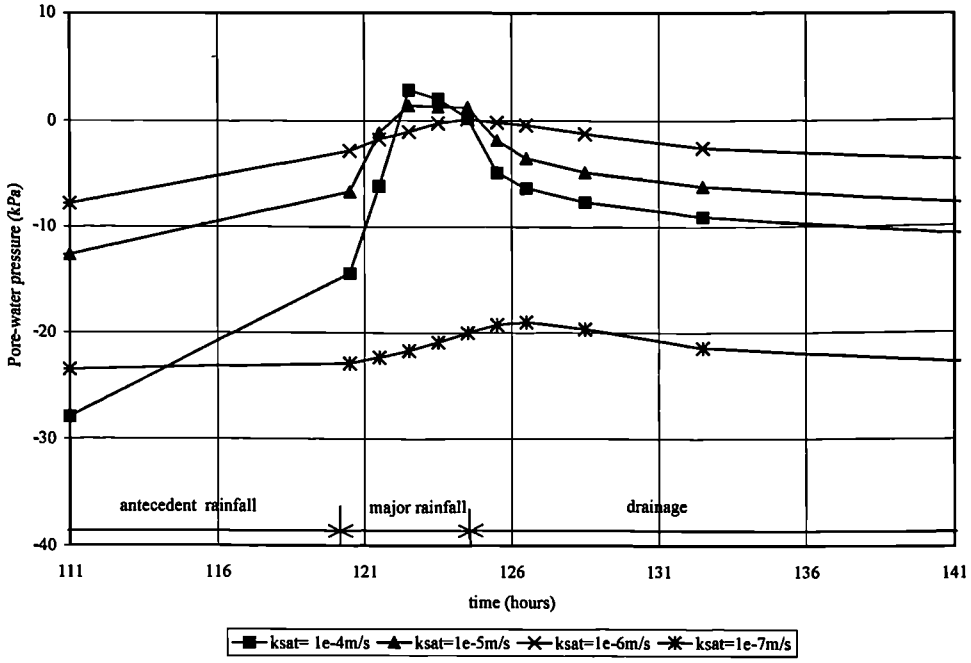

(b)

Figure 6.15 Development with time of the pore-water pressures at the crest of the slope, 0.5m deep, for Scenario 3, initial pore-water pressure -25kPa, initial water table at the toe of the slope and for different saturated coefficients of permeability with respect to water (a) for the whole simulation and (b) during the major rainfall event.

Another important difference in the results with different saturated coefficients of permeability with respect to water is that the higher the value of k_{sat}, the smaller the observed influence of the antecedent rainfall. This difference can be clearly seen in Figures 6.15(a) and 6.15(b), which present the development with time of the pore-water pressures at the crest of the slope, 0.5m deep, for rainfall scenario 3, initial pore-water pressures –25kPa and initial groundwater table at the toe of the slope. For a low k_{sat} such as 10^{-7}m/s the pore-water pressures decrease during antecedent rainfall and increase only by 6kPa during the major rainfall event. However, a long time after the end of the major rainfall the pore-water pressures start to increase again due to the slow rate of drainage closer to the ground surface and because it takes a long time for the rainwater to reach lower depths. For this low permeability (i.e. 10^{-7}m/s) the influence of the rainfall at the level of the groundwater table is insignificant. For $k_{sat}=10^{-6}$m/s the antecedent rainfall causes the pore-water pressure to increase to a value of –3kPa (increase by 22kPa) and during the major rainfall event the pore-water pressures increase slightly more and become positive (a value of approximately 0.5kPa). The pore-water pressures for $k_{sat}=10^{-5}$m/s increase

during the antecedent rainfall by 18kPa and increase by another 9kPa during the major rainfall reaching a positive maximum value of 2kPa. For $k_{sat}=10^{-4}$m/s (Figures 6.15a and 6.15b), the pore-water pressures at 0.5m decrease by 3kPa overall during the antecedent rainfall period. There are slight increases during the minor rainfall events of the 5day period of antecedent rainfall. However, the water infiltrating drains away between these minor rainfall events so that overall a decrease is seen. During the major rainfall the pore-water pressures at 0.5m deep at the crest of the slope for $k_{sat}=10^{-4}$m/s become positive with a value of 3kPa.

6.3 Slope stability analysis

The slope stability analyses for different distributions of the major rainfall show that the longer the period over which the rainfall is distributed, the lower the FoS of the slope will be. Figure 6.16 shows the lowest FoS for all the different distributions of the 240mm of rainfall and for all the saturated coefficients of permeability with respect to water. The initial FoS for all cases is 1.32. In the analysis for the distribution of 240mm of rainfall over 2 hours the lowest FoS that was predicted is 1.28 at the end of the rainfall for $k_{sat}=10^{-5}$m/s. That means that if the total rainfall of 240mm is distributed over 2 hours then the decrease of the FoS at the end of the rainfall is very small. If the rainfall is distributed in 4hours (60mm/h intensity), then the FoS drops to 1.14 at the end of the rainfall. For $k_{sat}=10^{-5}$m/s the FoS of the slope at the end of the 16-hours long rainfall with an intensity of 15mm/h is as low as 0.88.

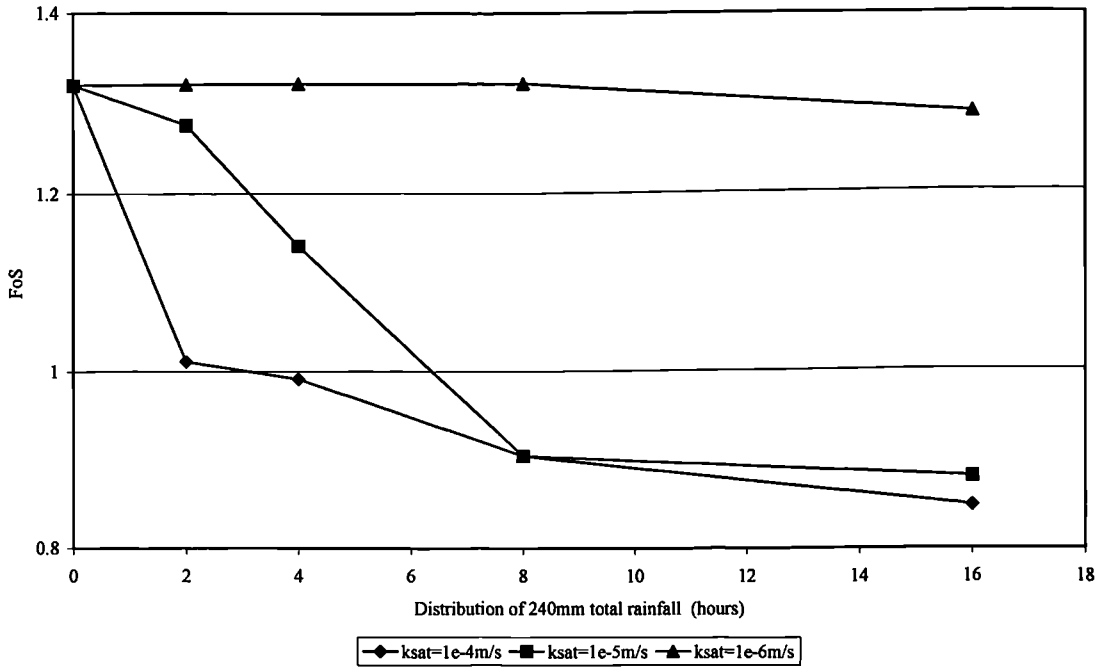

Figure 6.16 Lowest values of the factors of safety for all saturated coefficients of permeability with respect to water k_{sat} and for all distributions of 240mm major rainfall.

Different distributions of the antecedent rainfall can affect significantly the stability of the slope. Figure 6.17 shows the development of the FoS with time for the different rainfall scenarios for $k_{sat}=10^{-5}$m/s, initial pore-water pressure -25kPa and groundwater table at the toe of the slope. From the figure, it can be seen that only in scenario 3 (where the antecedent rainfall was distributed evenly over a 5-day period) does the FoS drop below 1.0. In all other cases the FoS is well above the critical value of 1.0. It must also be noted that for both scenarios 1 and 2 (where the antecedent rainfall was distributed in 5 events) the FoS at the end of the rainfall is equal to 1.17. In scenario 4 at the end of the rainfall the lowest FoS is approximately 1.15. For scenario 4 the lowest FoS is very close to that calculated for scenarios 1 and 2, although in scenario 4 no positive pore-water pressures were developed near the ground surface. However, in scenario 4 at the end of the rainfall the pore-water pressures at greater depths increase from their initial values (Figure 6.11). In scenarios 1 and 2 any increase in the pore-water pressures from their initial values is observed only in shallow depths. The difference in the depth where changes of the pore-water pressures occur between scenario 4 and scenarios 1 and 2 is the reason

why the FoS between these cases is almost the same at the end of the rainy period (Figure 6.17).

For a soil with $k_{sat}=10^{-4}$m/s, it is likely that the slope would become unstable under conditions of heavy rainfall with or without antecedent rainfall. In Figure 6.16 it can be seen that the factor of safety is above 1.0 only for a 2hours long distribution of rainfall. It must also be noticed that for a highly permeable soil ($k_{sat}=10^{-4}$m/s) the effect of the rainfall distribution of the same total rainfall is small on the FoS in comparison with the case of a moderately permeable soil ($k_{sat}=10^{-5}$m/s) (Figure 6.16). Further more, the rainfall distribution does not play a significant role on the FoS of the slope of a moderate to low saturated coefficient of permeability with respect to water of 10^{-6}m/s. For the case of $k_{sat}=10^{-6}$m/s, Figure 6.16 shows that for a 16-hour long distribution of the 240mm total rainfall the FoS is 1.29 and for a 2-hour long distribution of 240mm total rainfall the lowest FoS is 1.32. Since the initial FoS is 1.32 it is clear that for the case of $k_{sat}=10^{-6}$m/s there is no real change in the stability of the slope during a rainstorm of 240mm whether it is a short but very intense event or a more prolonged but less intense event.

Adding antecedent rainfall to the problem (Figure 6.18) the FoS shows the same trend with the results of the rainfall distributions. To be more specific, for initial pore-water pressure -25kPa and initial groundwater table at the toe of the slope, the FoS of the slope before any rainfall is applied is 1.32. If scenario 3 is applied to the slope (Figure 6.18) then for $k_{sat}=10^{-7}$m/s the FoS at the end of the rainfall remains at 1.32 and only at the end of the simulation (9 days of drainage period) the FoS drops slightly to 1.31. With the increase in the saturated coefficient of permeability with respect to water the antecedent rainfall and the major rainfall have a more significant effect on the stability of slope. For $k_{sat}=10^{-6}$m/s the lowest FoS is 1.25 at the end of the major rainfall event and for $k_{sat}=10^{-5}$m/s the FoS at the end of the major rainfall drops below 1.0 to 0.99. Finally for $k_{sat}=10^{-4}$m/s the FoS drops to an even lower value of 0.82 at the end of the major rainfall (Figure 6.18).

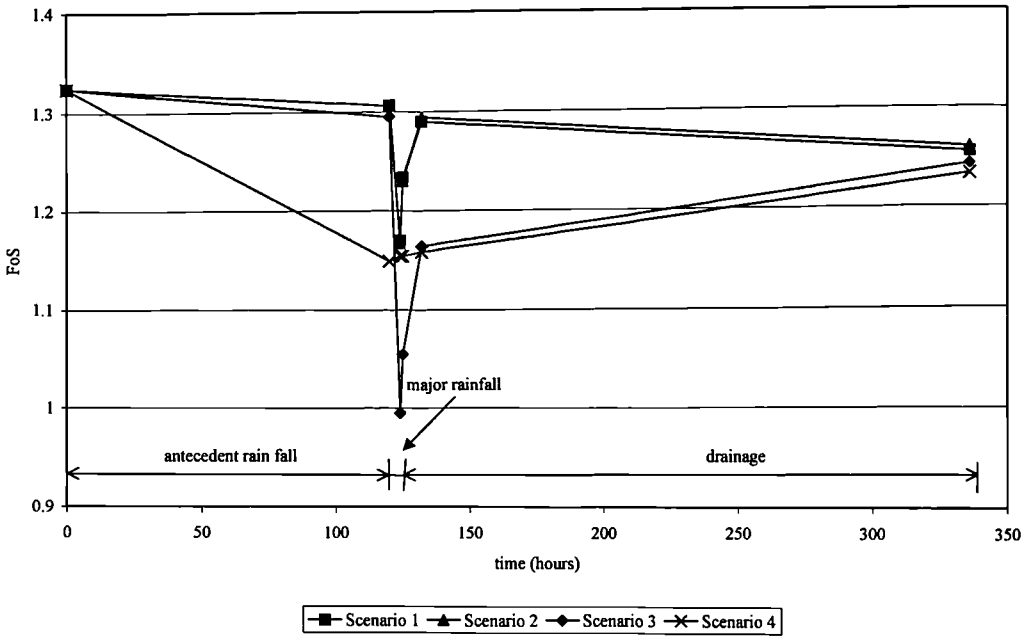

(a)

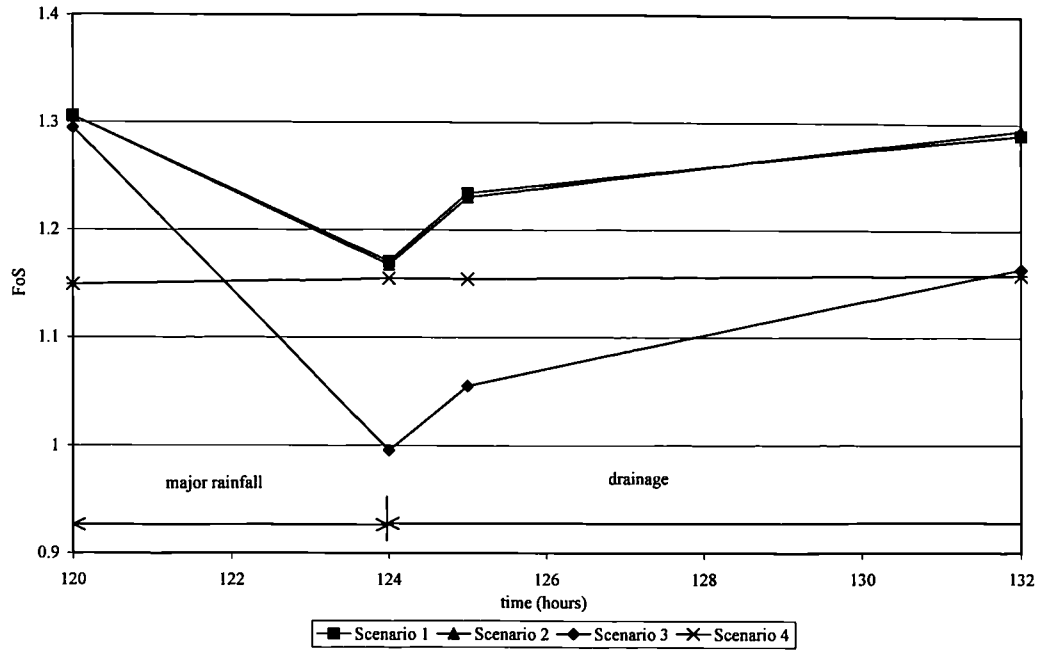

(b)

Figure 6.17 Development of the factor of safety with time for different distributions of antecedent rainfall for the case of $k_{sat}=10^{-5}$m/s, initial pore-water pressure -25kPa and initial groundwater level at the toe of the slope (a) for the whole simulation and (b) during the major rainfall event.

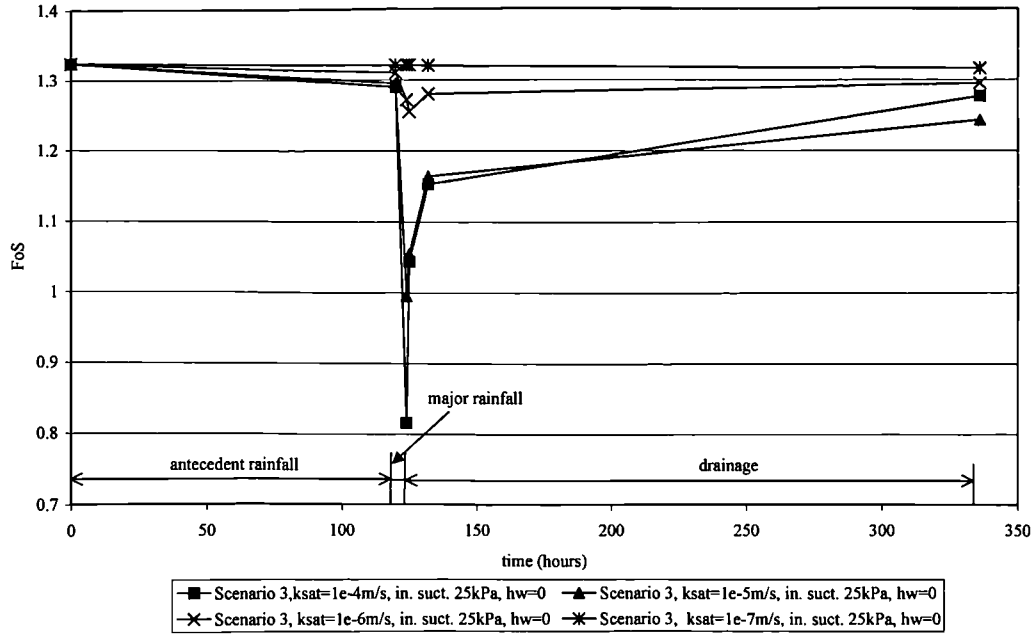

(a)

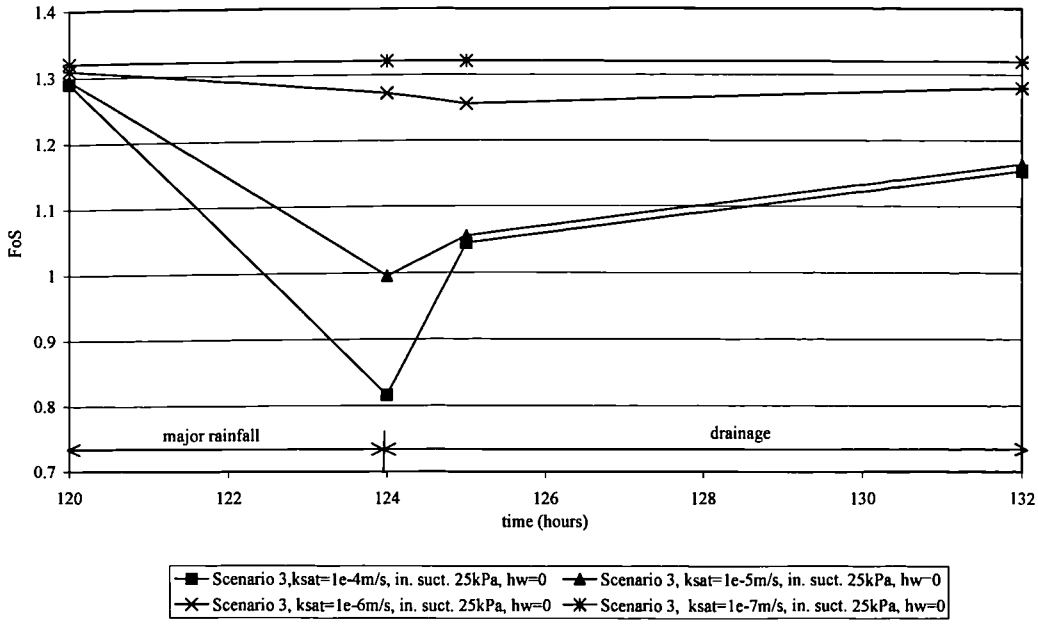

(b)

Figure 6.18 Development of the factor of safety with time for Scenario 3, initial pore-water pressure -25kPa and initial groundwater table at the toe of the slope (h_w=0) for different saturated coefficients of permeability with respect to water (a) for the whole simulation and (b) during the major rainfall.

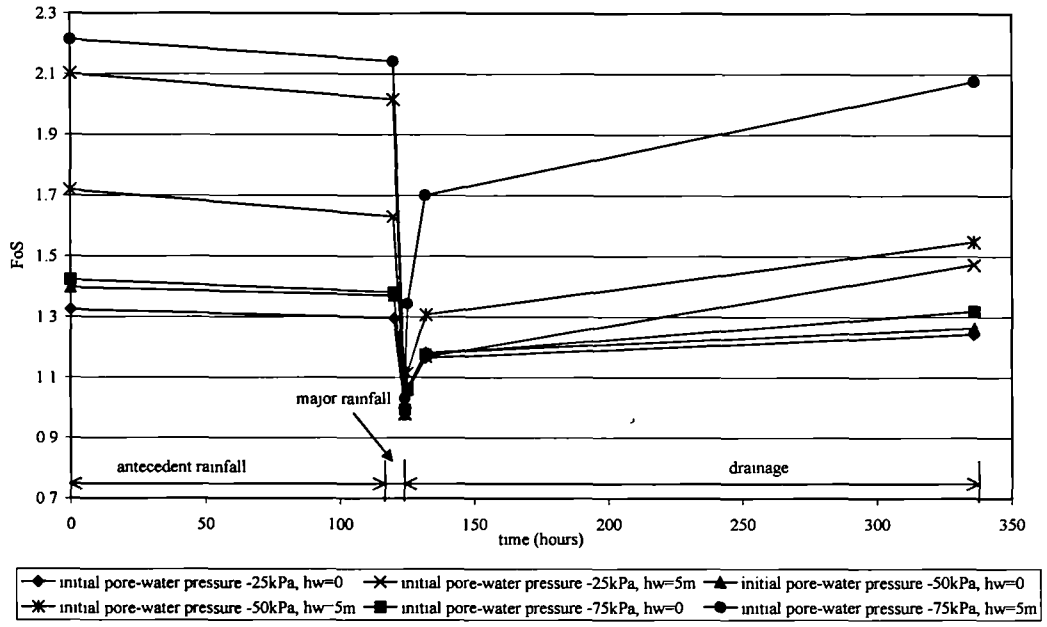

(a)

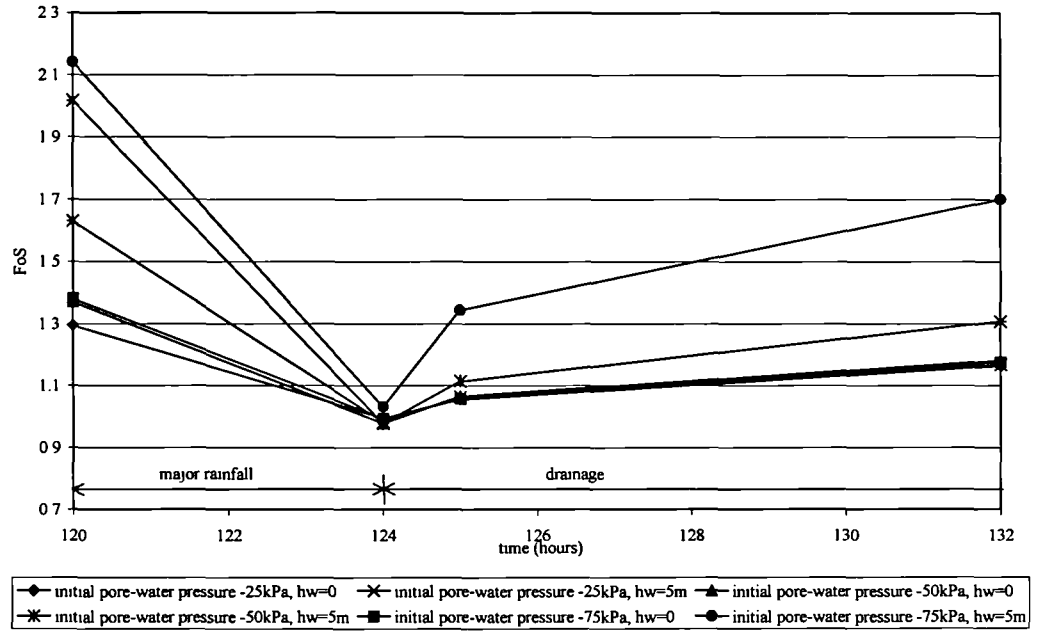

(b)

Figure 6.19 Development of factor of safety (FoS) with time for Scenario 3, $k_{sat}=10^{-5}$m/s and for all initial conditions (a) for the whole simulation (b) during the major rainfall.

Figure 6.19 presents the development of the FoS with time for different initial conditions when rainfall scenario 3 was applied to the slope. From Figure 6.19 it can be seen that in all cases at the end of the major rainfall the FoS is almost the same and close to 1.0. For example for the case of initial pore-water pressures -75kPa and initial groundwater level 5m below the toe of the slope, the initial FoS for the slope is 2.21 and at the end of the rainfall period drops drastically to 1.03. At the same time

assuming initial pore-water pressures of -25kPa and the initial ground water level is at the toe of the slope, the initial FoS is 1.32 and the factor of safety drops to 0.99 at the end of the wetting period. As is shown in Figures 6.12a and 6.12b the pore-water pressures at the end of the major rainfall do not differ significantly at 0.5m deep even if the initial conditions are significantly different. The critical slip surfaces for all cases are shallow and not deeper than 2m. At the end of the major rainfall the pore-water pressures developed along the critical slip surface are very similar for all sets of initial conditions. This is the reason why the FoS at the end of the major rainfall event varies only within a small range of values and is not affected by the initial conditions, if antecedent rainfall is added to the problem.

6.4 Discussion of results

The results show that seepage conditions within the slope are very sensitive to the magnitude of the saturated coefficient of permeability with respect to water. The saturated coefficient of permeability with respect to water controls the rate that precipitation will infiltrate the soil. A highly permeable soil will allow a high rate of flux, theoretically up to a value equivalent to k_{sat}, and rainwater will penetrate deeper into the ground. As the saturated coefficient of permeability with respect to water decreases, the amount of rainwater that can infiltrate the ground reduces. The analysis showed that if the major rainfall event were distributed over a long period then this would have the largest effect on the development of the pore-water pressures (Figure 6.9). The analysis also showed that the loss of negative pore-water pressures cannot be attributed only to the rainfall patterns applied to the slope, but that the relative values of the flux and the saturated coefficient of permeability with respect to water have to be taken into consideration. If the ratio between rainfall intensity and k_{sat} is low then more water will infiltrate the ground and less amount of the rainfall will disappear as runoff. If the ratio is too small then negative pore-water pressures may not even be affected by the infiltration. This can explain why in geographical areas with slopes composed of porous and highly permeable soils, antecedent rainfall is not a significant factor that can cause slope failures. On the other hand a high intensity rainfall applied on a low permeability soil slope can initially have a small impact on the increase of the negative pore-water pressures, but long after the end of the rainy period this effect may become important (Figure 6.15).

In this case antecedent rainfall prior to a major rainfall event can be a significant factor.

The results of the slope stability analysis also show that the relative value of the flux and the saturated coefficient of permeability with respect to water control the FoS. The slope stability analysis showed that for highly permeable soils, the lowest FoS is below the critical value (1.0) regardless of whether antecedent rainfall was applied to the slope or not. For moderately permeable soils, if antecedent rainfall is applied to the slope then the slope may become unstable at the end of the major rainfall. However, if antecedent rainfall is excluded from the analysis, the factor of safety that was predicted only for the major rainfall event was above 1.0.

6.5 Conclusions

Numerical modelling has been used to investigate the influence of several hydrological parameters on the seepage conditions in a typical residual soil slope in Singapore with an inclination of 2H:1V and a height of 10m. These parameters are the rainfall intensity, different distributions of antecedent rainfall, different initial conditions and saturated coefficients of permeability with respect to water.

The analysis showed the worst case occurred when a major rainfall event of 240mm is distributed in a long period of 16 hours. The same amount of rainfall distributed as a very intense rainfall in a very short period does not lead towards a large decrease of the FoS. Different distributions of antecedent rainfall over a 5-day period prior to the major rainfall event can affect the seepage conditions even if its amount is very small in comparison to the major rainfall. It was found that the worst case occurred if antecedent rainfall was distributed evenly over the 5-days.

Several simulations with different saturated coefficients of permeability with respect to water showed that this parameter controls significantly the infiltration process in the slope. Highly permeable soil slopes ($k_{sat}=10^{-4}$m/s), are unlikely to be influenced by small amounts of antecedent rainfall. The infiltration process during a major rainfall event can be affected by antecedent rainfall if a slope is composed of a moderately permeability soil ($k_{sat}=10^{-5}$m/s). Finally if the soil permeability with respect to water is very low ($k_{sat}=10^{-6}$ to 10^{-7}m/s) then the pore-water pressures may

not change significantly during the rainfall, but they can start increasing towards positive values after the end of the wet period.

The strong interaction amongst all these parameters highlights the need for proper and realistic choices of the hydrological properties of the soil when performing transient analysis. It is crucial that the appropriate choice of rainfall patterns to be used for the design on an unsaturated soil slope has to be determined by taking into consideration the characteristics of the soil and not only climatic information.

CHAPTER 7

Numerical Analysis of Infiltration into an Unsaturated Soil Slope

This chapter presents numerical analyses to attempt to simulate the field measurements of the NTU-ANX slope. The field measurements of the NTU-ANX slope consist of pore-water pressures and rainfall data over a period of 6 months (from March 2000 to August 2000). Runoff measurements were also made during natural and simulated rainfall events. The field measurements of the NTU-ANX slope are presented in Chapter 4 (Section 4.2) and are also discussed in Chapter 5 (Section 5.2).

7.1 Description of the numerical model

7.1.1 Objective of the numerical analysis

The objective of the numerical analyses, presented in this chapter, is to bring together all the available information from the field and the laboratory into one realistic numerical model. The numerical simulation of the observed field behaviour of the NTU-ANX slope served towards a better understanding of the mechanism of infiltration and seepage within the NTU-ANX slope. The commercial finite element software Seep/W (Geo Slope Int. Ltd. 1998a) was used for the numerical modelling of the field measurements, adopting a two-dimensional and transient seepage model.

The field data for the NTU-ANX slope were chosen for this numerical analysis, as opposed to the field data for the NTU-CSE slope, for two reasons. The first reason is because the soil profile of the NTU-ANX slope is significantly simpler than the soil profile of the NTU-CSE slope (Chapter 3). The second reason is that runoff measurements of natural and simulated rainfall were made for the NTU-ANX slope and it was possible to estimate the amount of rainfall water that infiltrated the slope during the monitoring period. Thus, the field data for the NTU-ANX slope are more complete than those of the NTU-CSE slope.

Past research work has identified a number of limitations in the modelling of seepage

in the unsaturated zone of a slope (Section 2.11.1). Vargas et al. (1990) limited their seepage analysis only to the wetting period, in order to avoid the effect of evaporation and the hysteresis of the soil-water characteristic curve between the wetting and the drying phase. In their analysis Gasmo et al. (2000) applied some evaporation rates at the ground surface of the slope and concluded that the rate with which the pore-water pressures decreased near the ground surface was unrealistically high compared to actual field observations. Taking these limitations into account, the present work attempts to incorporate the wetting and drying processes in the analysis and compare the results with the available field data.

7.1.2 Description of the slope used in the numerical analysis

The slope being modelled (referred as the slope in this work) was designed to represent the NTU-ANX slope. Figure 7.1 presents the geometry of the slope used in the numerical model. The inclination of the slope was 27° (i.e. approximately 2H:1V). The research area on the NTU-ANX slope is small in comparison with the length of the whole slope and the crest and the toe of the slope are at a distance from the research area. For that reason no crest and toe were defined in the slope of the numerical model. Figure 7.1 also shows the locations of rows A through C, which represent the tensiometer positions where field observations were made (Chapter 3).

During a site investigation of the NTU-ANX slope, Rahardjo et al. (2000) identified two main soil layers, Layers 1 and 2 (Chapter 3, Section 3.2). The field data showed that the seepage conditions of the slope are affected only at depths close to the ground surface (Chapters 4 and 5). In addition the field data of the NTU-ANX slope showed that the groundwater table lies at depths between 15m and 17m from the ground surface (Chapter 4, Section 4.2.3). Therefore, in this numerical analysis attention was given to the proper definition of the parameters especially for the surficial Layer 1. The hydrological properties of Layer 2 were less important.

The surficial layer, Layer 1 extending to 10m deep, was a silty to sandy clay, hard, with orange colour, moderate plasticity and 58% fines. The underlying layer, Layer 2, was clayey silt with siltstone and sandstone fragments and 32% of fines. The interface between the two layers had an inclination parallel to the slope. A more

detailed description of the geology of the NTU-ANX slope can be found in Chapter 3 (Section 3.2).

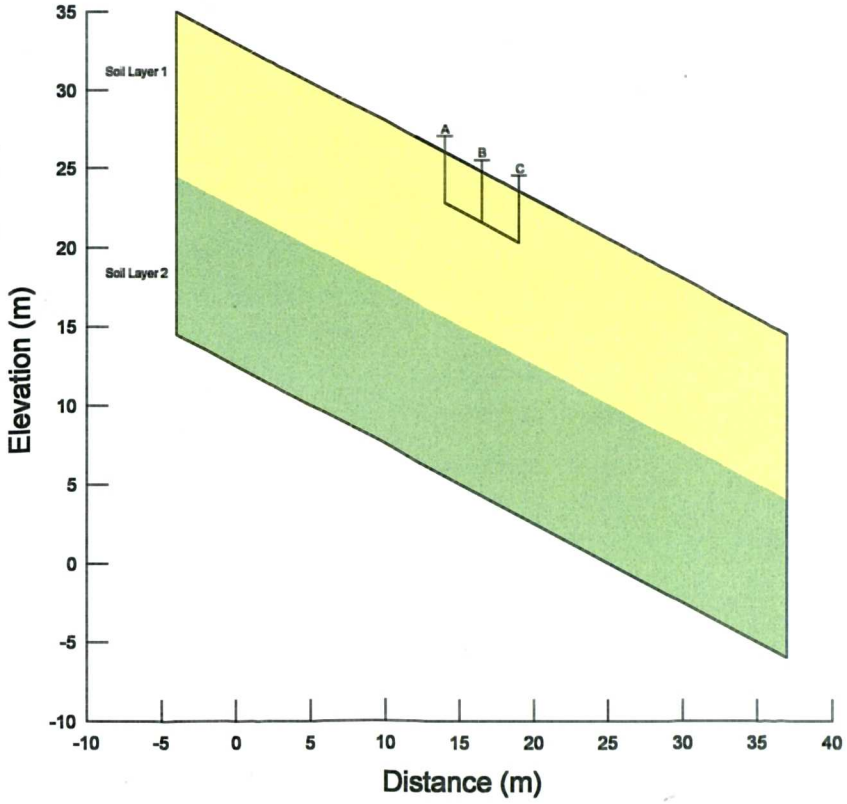

Figure 7.1 Geometry of the slope that was used in the numerical analysis.

Figure 7.2 presents the fitted volumetric soil-water characteristic curve (wetting and drying phase) of a soil sample of Layer 1 from the NTU-ANX slope. The soil-water characteristic curve of Figure 7.2 was used in the numerical analysis. The data points were produced in the laboratory with a pressure plate (Sections 3.5 and 4.2.1). The fitting curve of the data was produced with the RETC code (van Genuchten et al. 1991), using the van Genuchten (1980) equation (Equation 2.22). The saturated volumetric water content (θ_{sat}) was 0.53 and when an applied matric suction of 200kPa was established in the sample, then the volumetric water content reduced to 0.38. The in-situ saturated coefficient of permeability (k_{sat}) was measured to be equal to $6x10^{-7}$ m/s at approximately 0.4m deep, using a Guelph permeameter (Sections 3.4 and 4.2.7). Figure 7.3 presents a predicted permeability function derived from the soil-water characteristic curves of Figure 7.2 using the Green and Corey (1971) equation (Equation 2.27). The permeability function of Figure 7.3 was

defined as the permeability function of the surficial Layer 1.

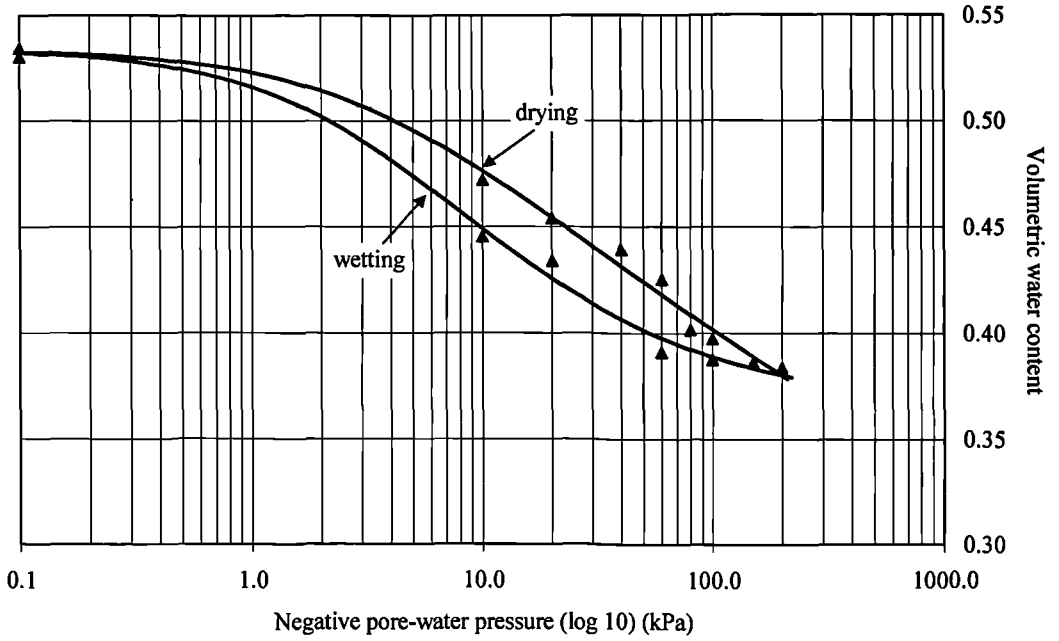

Figure 7.2 Volumetric soil-water characteristic curve for the wetting and drying phase that was used for the surficial soil layer in the numerical model.

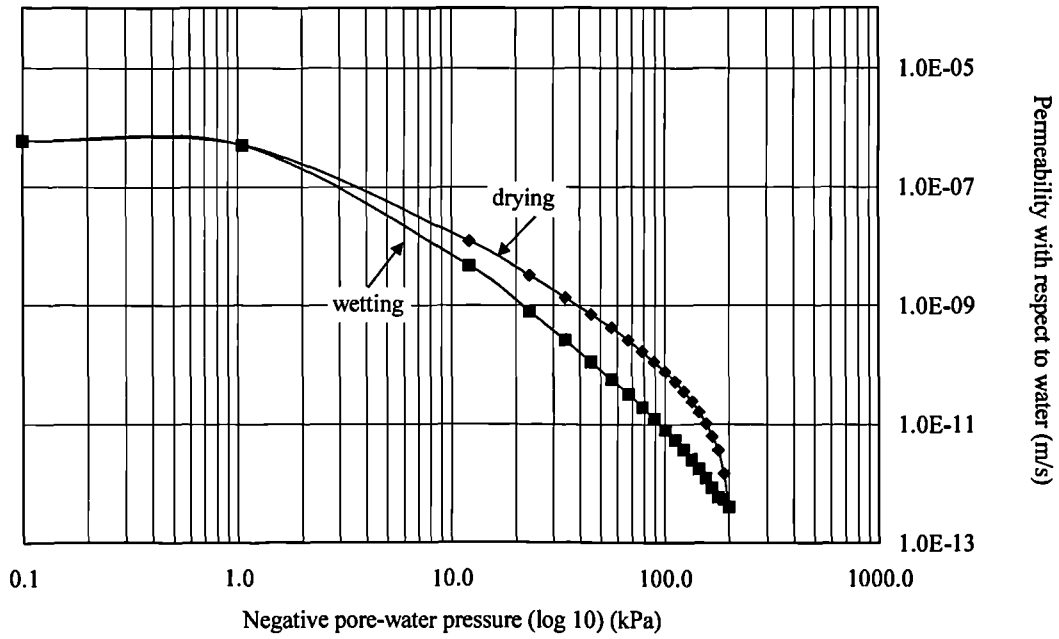

Figure 7.3 Predicted permeability function for the wetting and drying phase that was used for the surficial soil layer in the numerical model.

7.1.3 Description of the finite element mesh for the numerical model

The commercial finite element software Seep/W (Geo Slope Int. Ltd., 1998a) was used for the numerical modelling of the field measurements, adopting a two-dimensional and transient seepage model for the slope. The governing differential equation used for the transient and two-dimensional flow can be found in Section 2.5.2 (Equation 2.29). In a transient analysis the nodal values of head are time-dependent and for an unsaturated soil the coefficient of permeability with respect to water is a function of the volumetric water content. The solution process of the non-linear differential Equation 2.29 is handled with a numerical method, i.e. the finite element method and requires the volumetric soil-water characteristic curve and the permeability function of the soil.

Figure 7.4a presents the finite element mesh, which was used for the numerical modelling of the field data. Figure 7.4b presents a detail of the finite element mesh. The criteria for the design of the finite element mesh are the same as those explained in Chapter 6 (Section 6.1.3). The boundaries of the finite element mesh are at a great distance from the study area (rows A through C in Figure 7.4a), in order to avoid any influence of the boundary conditions on the computed pore-water pressure changes. Near the ground surface of the slope the finite element mesh is very fine with dimensions 0.25x0.25m and with 8-nodal elements, in order to avoid any possible numerical instabilities that may occur in the solution. At larger depths the finite element mesh consists of coarser, 4-nodal elements with dimensions 0.5x0.5m. The finite element mesh of Figure 7.4 consists of 6882 nodes and 4264 elements in total.

The analysis adopted the same convergence criteria with the criteria adopted in Chapter 6 (Section 6.1.3). The tolerance of the computed norm of the head vector between two consecutive iteration was set to the 0.05%. Between two consequent iterations, Seep/W changes the value of the coefficient of permeability with respect to water of each node with rate of change 1.1 orders of magnitude (the value of this rate of change can be set by the user). From one iteration to the next, the minimum change of the initial value of the permeability with respect to water was set to 10^{-4} of order of magnitude and a maximum change of 1 order was allowed.

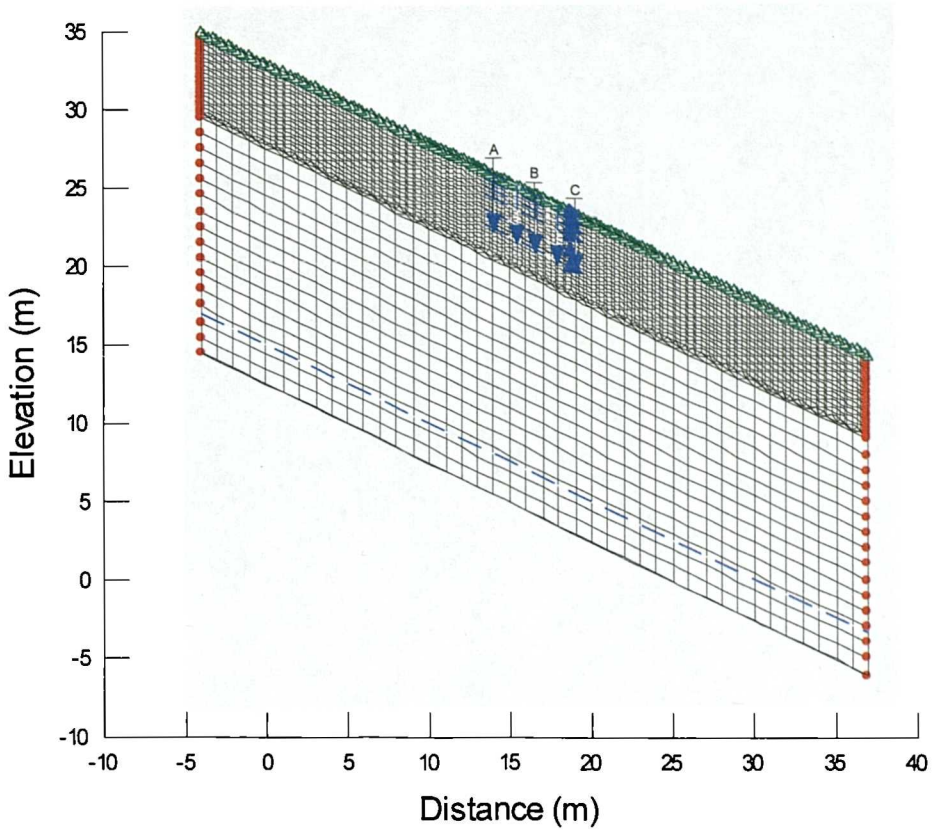

a)

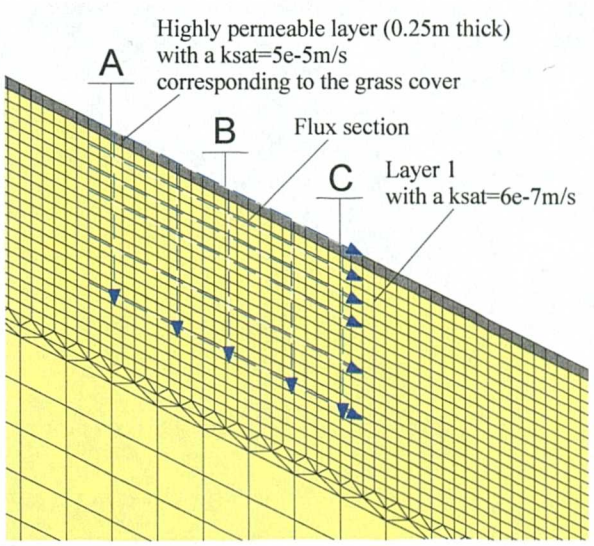

b)

Figure 7.4 a)Finite element mesh for the numerical model of the NTU-ANX slope and b) detail of the finite element mesh showing also the flux sections.

The infiltration was modelled as a unit flux boundary (q) along the ground surface of the whole slope. The unit flux boundary (q) along the ground surface of the slope, was a function of time to simulate the real rainfall distributions as they were recorded in the field (Chapter 4, Section 4.2.2) All the nodes along the slope, to which the

flux boundary was applied, were reviewed by the maximum pressure mode. In order to avoid any ponding phenomenon, that is unlikely to take place in sloping ground (as any ponded water will run off), the software performs a check that every node at the ground surface has zero or negative hydraulic head. In case a ground surface node is found with a positive pore-water pressure (greater than zero) at the end of the calculation for each time step then that node is set to have a head equal to the elevation and the problem is re-solved. Head boundaries were applied along the edges of the slope in order to define the initial pore-water pressure profiles and the initial level of the groundwater table. Immediately under the ground surface a flux section was drawn (Figure 7.4b), across which Seep/W calculated the infiltration rate. Flux sections were also drawn at 0.5m, 1.1m, 2.5m and 3m deep, in order to examine the groundwater flow at larger depths (Figure 7.4b).

7.1.4 Methodology of the numerical analysis

The objective of the present analysis is to combine all the available measurements from the field and the laboratory into a numerical model. That means that using the available hydrological properties of the soils of the NTU-ANX slope (soil-water characteristic curve and saturated coefficient of permeability with respect to water), the model should predict pore-water pressure changes and total amount of infiltration for comparison with the field measurements. Particular attention was given to the proper definition of the hydrological properties of Layer 1 of the NTU-ANX slope, because the pore-water pressure measurements (Sections 5.2.1 and 5.2.3) showed that pore-water pressures change significantly only at small depths (i.e. 0.5m to 1.1m deep). In addition, it was seen that the level of the ground water table lies at great depth (15 to 17m deep) and is not greatly affected by rainfall. Consequently, for this study the pore-water pressures at very large depths are not of particular interest.

Creation of the initial pore-water pressure profile

The monitoring period of NTU-ANX slope started on 17 March 2000. Figure 7.5 presents the pore-water pressure measurements of row A of the NTU-ANX slope between 17 and 22 March 2000. Prior to 17 March 2000 some rainfall was precipitated, which was not recorded by the rainfall gauge of the NTU-ANX slope.

For the creation of the initial pore-water pressure profile, it is essential that the pore-water pressures within the slope do not change significantly (either increase due to infiltration, or decrease due to a high rate of evaporation), but are reasonably constant. Figure 7.5 shows that from 20 to 22 March 2000 the pore-water pressures did not change considerably. For that reason it was decided that the initial pore-water pressure profile, for the numerical simulations of the seepage conditions of the NTU-ANX slope, would correspond to 22 March 2000 at 00:00, after a 2-day period of no rainfall occurring.

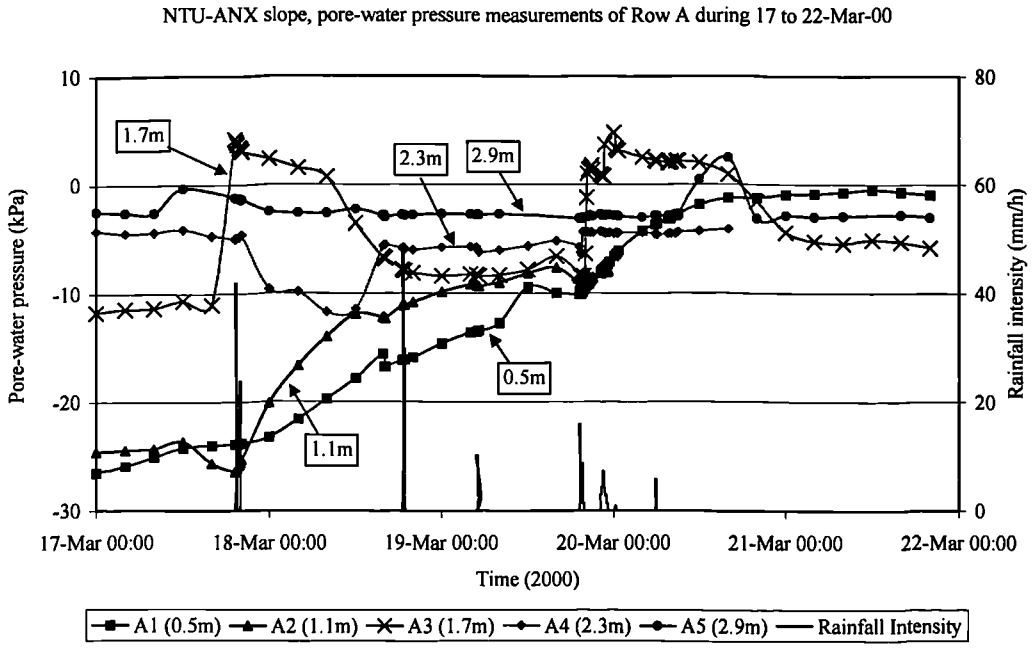

Figure 7.5 Pore-water pressure measurements of Row A in the NTU-ANX slope from 17 to 22-Mar-00.

Figure 7.6 presents the pore-water pressure profile of Rows A and B of the NTU-ANX slope on 22 March 2000, at 00:00. The pore water pressure profile of Figure 7.6 shows that the pore-water pressures for all depths are close to –3kPa with small discrepancies at 0.5m deep (pore-water pressure at 0.5m deep of Row A was equal to -1.4kPa) and at 1.7m deep (pore-water pressure at 1.7m deep of Row A was equal to –4.7kPa). Therefore, the initial pore-water pressure profile, used in the numerical model of the NTU-ANX slope, is defined as a constant pore-water pressure with depth, equal to –3kPa. Figure 7.6 also shows the initial pore-water pressure profile used for the numerical model of the NTU-ANX slope. For the initial

conditions of the numerical model, the groundwater table was defined to be 17m deep from the ground surface (as was measured in the NTU-ANX slope on 22 March 00:00).

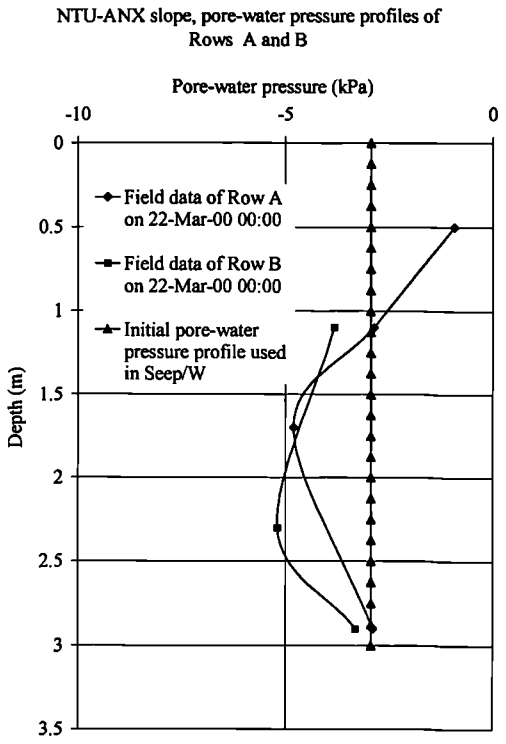

Figure 7.6 Initial pore-water pressure profile, corresponding to the field measurements of 22 March 2000 at 00:00, which was used in the numerical model.

Application of rainfall on the numerical model (wetting process)

The analysis of the seepage conditions of the NTU-ANX slope, used the finite element mesh of Figure 7.4, the soil-water characteristic curve of Figure 7.2 and the permeability function of Figure 7.3. All rainfall events that were measured on the NTU-ANX slope during the monitoring period (from March 2000 to August 2000) were applied on the slope of the numerical model. The available rainfall data of the NTU-ANX slope are presented in Section 4.2.2. Figure 7.7 presents the flux (q) that was applied on the slope of the numerical model, which corresponds to all natural and simulated rainfall events that were recorded on the NTU-ANX slope during the monitoring period.

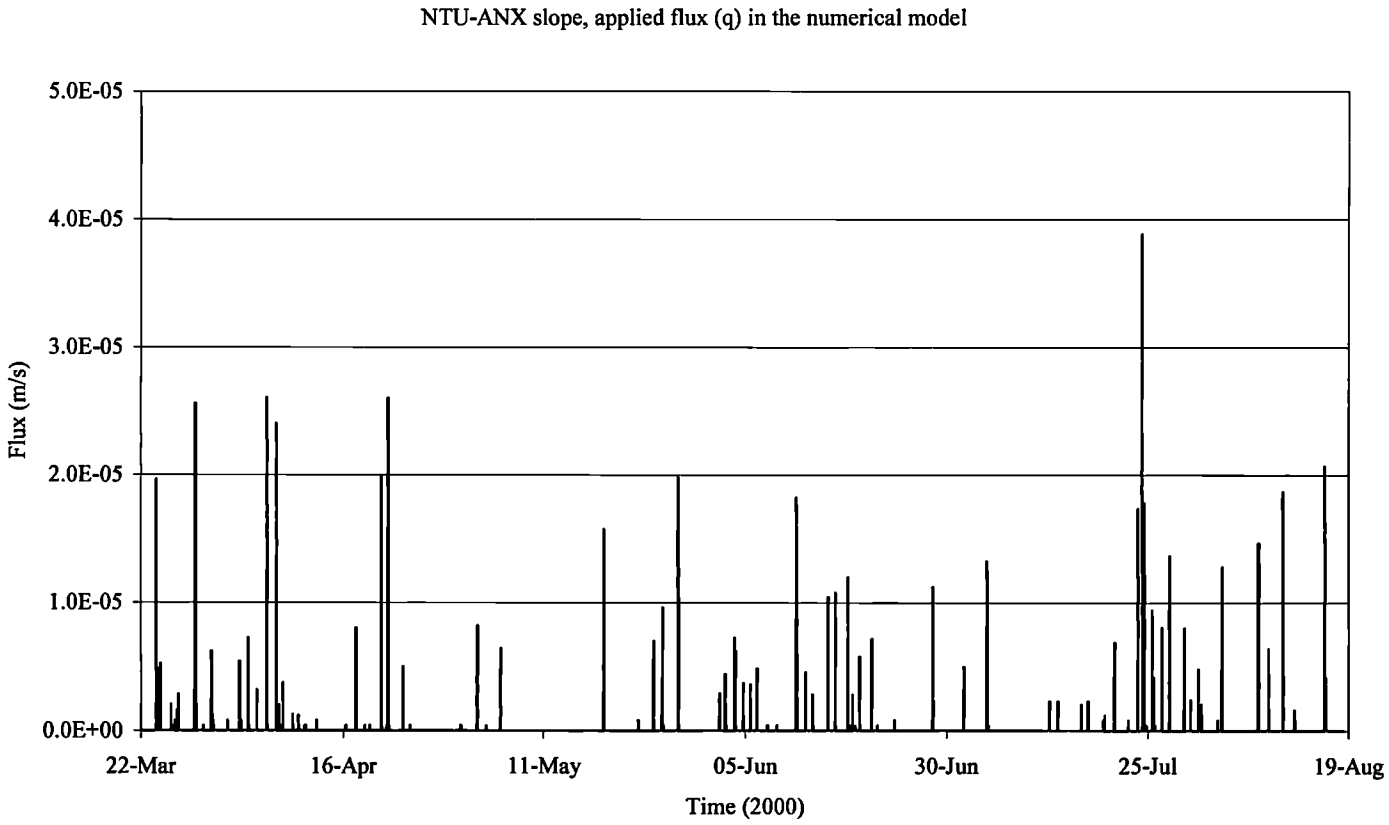

Figure 7.7 Applied flux (q) in the numerical model for the study period.

When rainfall was applied on the slope shown in Figure 7.4 the wetting phase of the soil-water characteristic curve (Figure 7.2) and of the permeability function (Figure 7.3) were initially defined for Layer 1. In the initial stages of the analysis, it was found that there was a discrepancy between the results of the numerical model and the field observations.

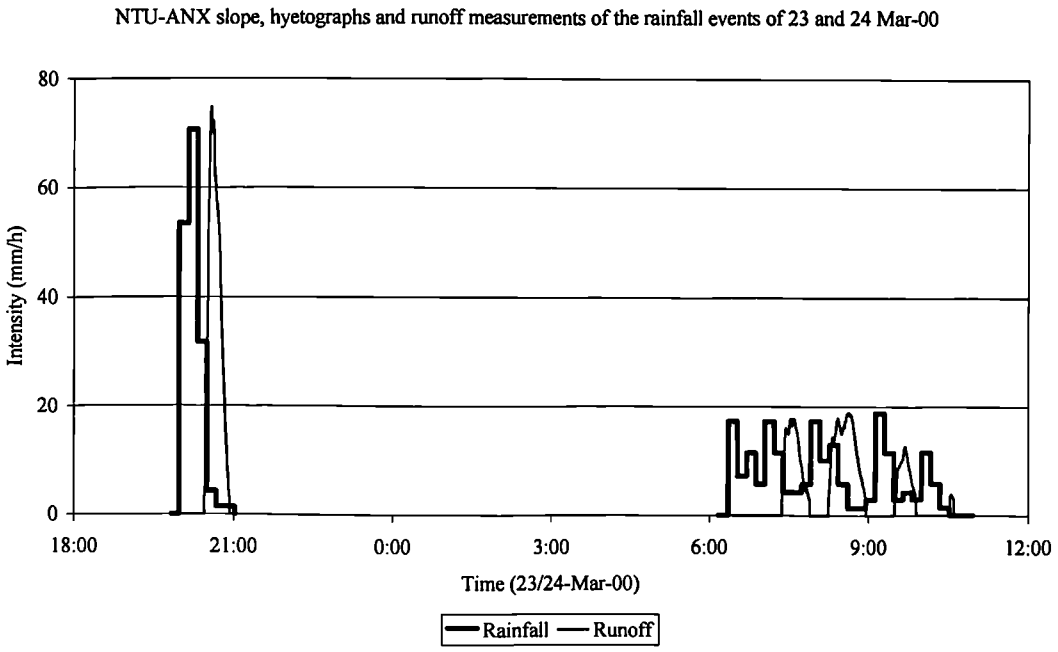

Figure 7.8 Hyetograph of the natural rainfall events of 23 and 24-Mar-00 with the runoff measurement, measured on the NTU-ANX slope.

In order to illustrate the discrepancy between the predictions of the numerical model and the field observation, let us consider the pore-water pressure changes during the period from 22 March 2000 00:00 to 25 March 2000 16:00. During this time period two natural rainfall events were recorded on the NTU-ANX slope and the runoff produced was also measured. Figure 7.8 presents the hyetograph and the runoff measured for the two rainfall events. The first rainfall event took place on 23 March 2000, when 28mm of total rainfall fell with an average intensity of 14mm/h. The runoff produced during this rainfall event was 19mm (i.e. total infiltration equal to 9mm). The second rainfall event took place on 24 March 2000, when 34mm were precipitated with an average intensity of 8.2mm/h. The runoff produced during the rainfall event of 24 March was also 19mm (i.e. total infiltration equal to 15mm).

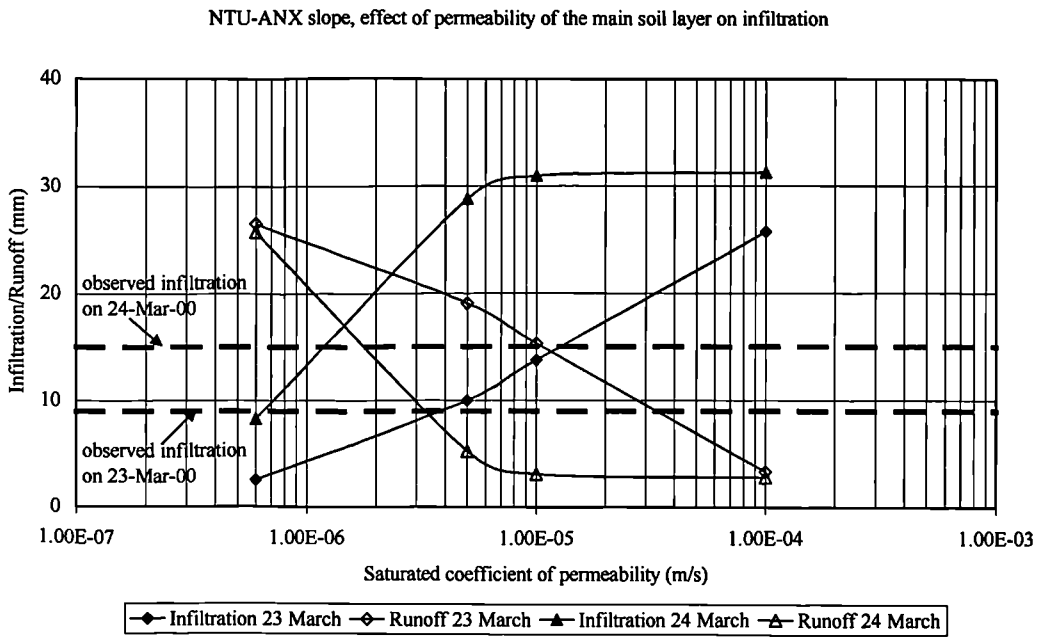

Figure 7.9 Effect of different saturated coefficients of permeability with respect to water of the surficial soil layer on the predictions of total infiltration and total runoff for the rainfall events of 23 and 24 March 2000.

Initially, the permeability function of Figure 7.3 was defined for the surficial soil layer of the slope, with a $k_{sat}=6x10^{-7}$m/s. When the rainfall pattern of Figure 7.8 was applied on the slope of the numerical model, the predicted infiltration for the two rainfall events of 23 and 24 March 2000 was considerably lower than the field observations. The numerical model predicted, with a $k_{sat}=6x10^{-7}$m/s, a total infiltration of 2.5mm for the rainfall event of 23 March 2000 (the field measurements showed a total infiltration of 9mm). In addition, the numerical model predicted also a low total infiltration of 8mm for the rainfall event of 24 March 2000 (the field measurements showed a total infiltration of 15mm). In order to improve the numerical model's prediction of the total infiltration, so that the results would be in agreement with the field observations, a number of trials with different k_{sat} values of the surficial soil layer of the slope were made. Figure 7.9 presents the results of this analysis that were conducted for the rainfall events of 23 and 24 March 2000. From Figure 7.9 it can be seen that with k_{sat} values between $1x10^{-6}$ and $5x10^{-6}$m/s, the numerical model predicts total infiltration (or total runoff) for the rainfall events of 23 and 24 March 2000 that are comparable with the field observations. Further consideration will be given to this issue after a discussion of the pore-water

pressures.

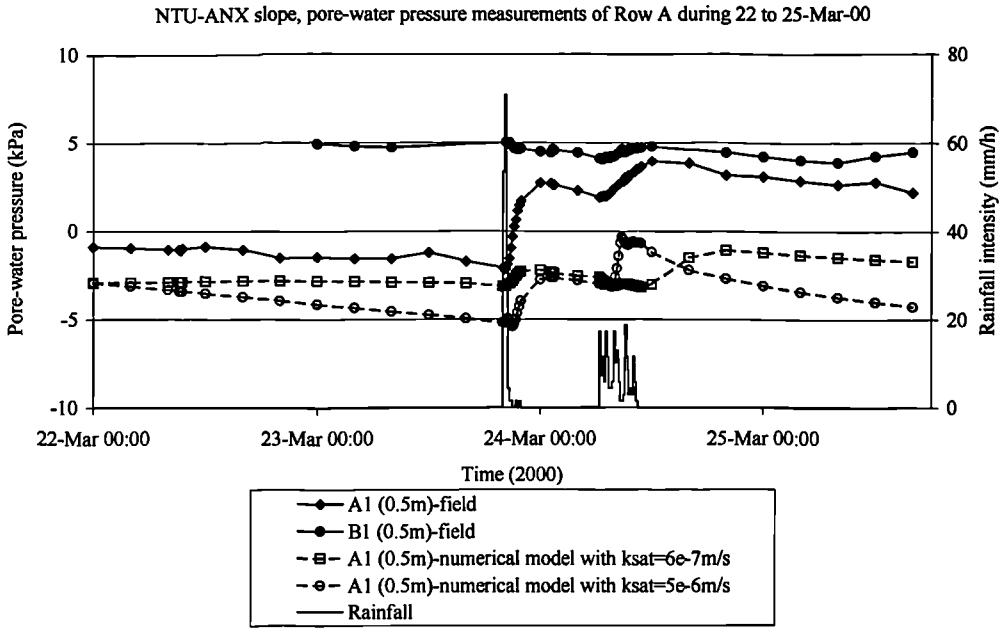

a)

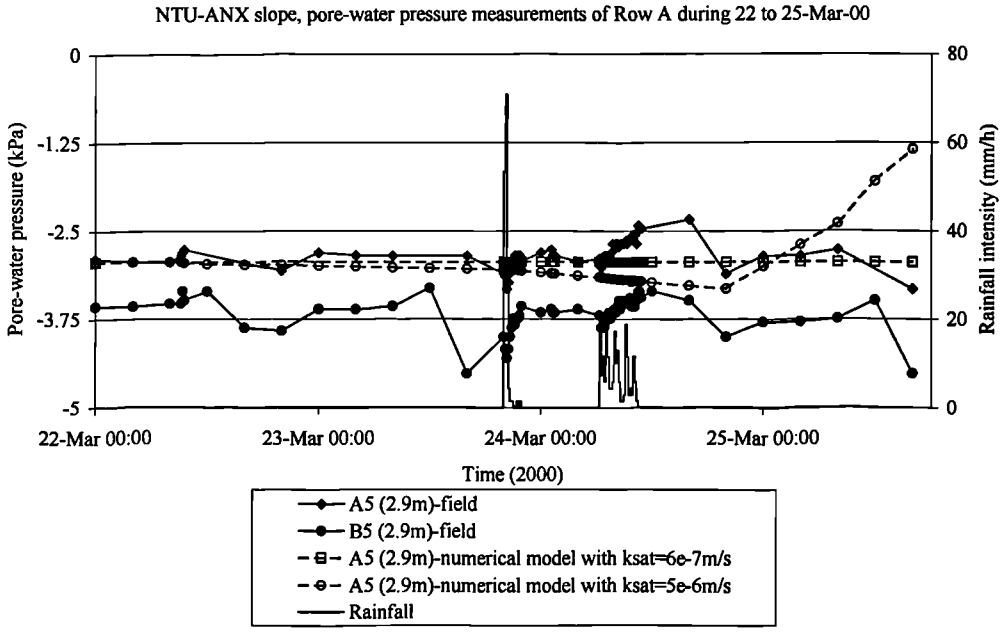

b)

Figure 7.10 Pore water pressure changes a) 0.5m deep and b) 2.9m deep of the NTU-ANX slope from field observations and from the numerical model for different soil properties of the surface soil layer (Layer 1).

Figure 7.10 presents pore-water pressure changes with time from the field measurements of the NTU-ANX slope and from the numerical model for different saturated coefficients of permeability with respect to water (k_{sat}) of the surficial

soil layer (Layer 1). The period of the pore-water pressure changes in Figure 7.10 starts on 22 March 2000, at 00:00 (i.e. start of the numerical simulations) and finishes on 25 March 2000 at 16:00. The pore-water pressure changes of Figure 7.10, from the numerical model, are those predicted using a k_{sat}=$6x10^{-7}$m/s (i.e. as it was measured in the field) and a k_{sat}=$5x10^{-6}$m/s. The value of k_{sat}=$5x10^{-6}$m/s represents the upper limit to the permeability values that gave a closer match to the observed infiltration values for this for this rainfall period.

For k_{sat}=$6x10^{-7}$m/s the numerical model predicted pore-water pressure at 0.5m deep (Figure 7.10a) that change with time in a similar fashion with the field observations, despite the fact that the magnitude of pore-water pressure change during rainfall was not the same as the field observations. More specifically, prior to the rainfall event of 23 March, the predicted pore-water pressures at 0.5m deep decrease with a small rate (similar to the field measurements). After the end of the two rainfall events the pore-water pressures decrease gradually with time following the same pattern as the field observations. However, the absolute increase of the pore-water pressures (for k_{sat}=$6x10^{-7}$m/s) during the two rainfall events is smaller in comparison with the field observations. This is attributed to the fact that only a small amount of water infiltrated the slope of the numerical model (Figure 7.9). On the other hand, using a k_{sat}=$5x10^{-6}$m/s, the predicted pore-water pressures at 0.5m deep (Figure 7.10a) changed rapidly in comparison with the field observations. In addition, at 2.9m deep (Figure 7.10b) some significant changes were predicted with the numerical model if the k_{sat}=$5x10^{-6}$m/s was used (when field observations do not show any significant changes at that depth).

In reality, the ground surface of the NTU-ANX slope is covered by grass (Chapter 3, Figure 3.4) and its roots create small pathways in the soil and therefore the saturated coefficient of permeability with respect to water (k_{sat}) can be significantly higher at the ground surface than at larger depths (Anderson et al. 1996). In order to couple the two sets of field observations from the NTU-ANX slope (runoff/infiltration measurements and pore-water pressure measurements) in the numerical model, a 0.25m thick highly permeable layer was defined at the ground surface to model the grass covering of the slope. Figure 7.4b presents the thin layer at the ground surface,

which corresponds to the grass covering of the slope. The saturated coefficient of permeability with respect to water (k_{sat}) of the thin surficial soil layer, which corresponds to the grass covering of the slope, was determined with trials using several values. For Layer 1, below this thin grass covering, the permeability function of Figure 7.3 was defined with a k_{sat} equal to $6x10^{-7}$m/s (i.e. as was measured in the field). Figure 7.11 presents the relationship between total infiltration (and total runoff) and different values of k_{sat} of the surficial soil layer (i.e. the grass cover of the slope), as was predicted by the numerical model for the rainfall events of 23 and 24 March 2000.

The results of Figure 7.11 show that if a k_{sat} equal to $5x10^{-5}$m/s was used then the numerical model predicted a total infiltration of 5mm for the rainfall event of 23 March 2000. The field observations showed that the total infiltration of the 23 March 2000 rainfall event was 9mm. In Figure 7.9 it was seen that if Layer 1 had a uniform k_{sat} equal to $5x10^{-6}$m/s, then the total infiltration during the rainfall event of 23 March 2000 would have been 10mm. The difference between the results of Figure 7.9 and Figure 7.11 is attributed to the use of the low $k_{sat}=6x10^{-7}$m/s of Layer 1, that affects to a great extent the infiltration rates at the ground surface. This issue will be further discussed in more detail in a later section.

Figure 7.11 shows that the use of a k_{sat} value equal to $5x10^{-5}$m/s predicts total infiltration of the two rainfall events that are in a reasonable agreement with the field observations. More specifically, for the rainfall event of 23 March 2000 the numerical model predicted (with $k_{sat}=5x10^{-5}$m/s of the surficial soil layer that corresponds to the grass cover) a total infiltration equal to 7mm (the field observation for this rainfall event was 9mm total infiltration). For the rainfall event of 24 March 2000 the numerical model (with $k_{sat}=5x10^{-5}$m/s of the surficial soil layer that corresponds to the grass cover) predicted a total infiltration of 17mm (the field observation for this rainfall event was 15mm). Especially for the rainfall event of 24 March 2000, Figure 7.11 shows that total infiltration does not change significantly for k_{sat} greater than $5x10^{-6}$m/s. This can be explained, by the fact that the recorded rainfall intensities of the 24 March 2000 were relatively low and did not exceed at any time the value of $5x10^{-6}$m/s.

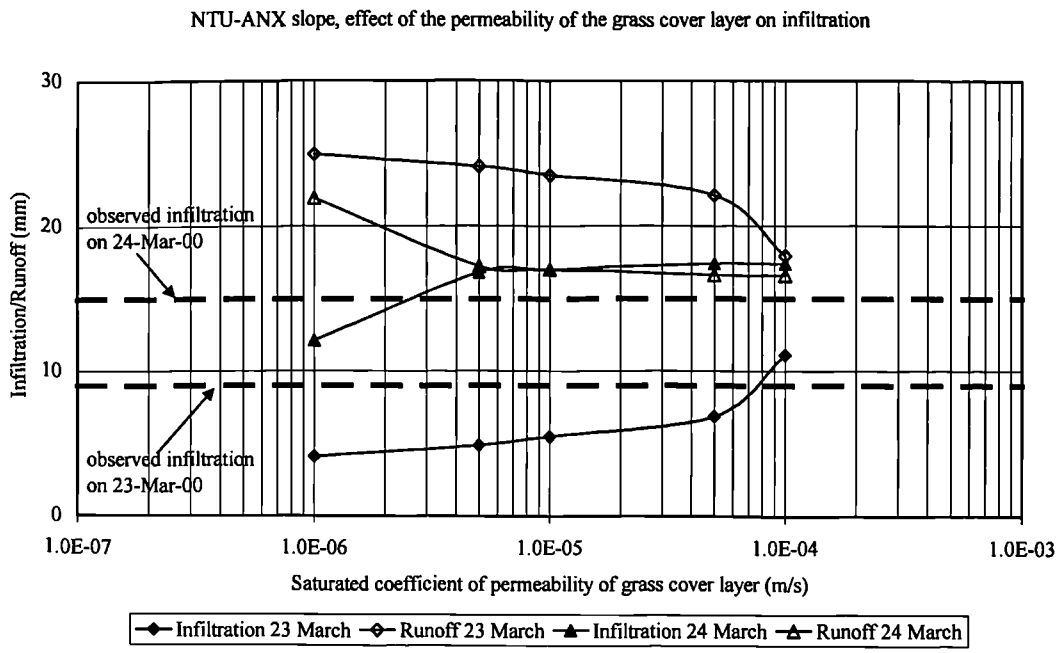

Figure 7.11 Effect of different coefficients of permeability of the thin surficial layer of the slope, which corresponds to the grass covering of the slope, on the total infiltration and total runoff for the rainfall events on 23 and 24 March 2000.

As will be seen in later sections the adjustment to the model, by adding the thin highly permeable surficial layer that corresponds to the grass cover of the slope, made the model performance significantly better, with results comparable to the field observations. The use of the grass cover layer predicted total infiltration that is in reasonable agreement with the field observations and at the same time still gave reasonable pore-water pressure changes that are in agreement with the field measurements.

Application of evaporation in the numerical model (drying process)

As was mentioned in previous sections, the objective of the present numerical analysis is to study the seepage conditions of the NTU-ANX slope during infiltration. Therefore, the drying process of the slope between rainfall events was not the main focus of the study. However, it was necessary to incorporate the draining process into the analysis, in order for the numerical model to predict a realistic decrease of the pore-water pressures during periods of no rainfall, that would be comparable to the field observations.

During dry periods the pore-water pressures in the surficial soil layer decrease as water is removed by evaporation. The volumetric water content decreases following the drying phase of the soil-water characteristic curve of Figure 7.2. Similarly, during dry periods the coefficient of permeability with respect to water will follow the drying phase of the permeability function of Figure 7.3. Seep/W cannot determine automatically whether the soil is in a drying or a wetting phase. Therefore, immediately after the end of a rainfall event the simulation was stopped and the drying phase of the soil-water characteristic curve (Figure 7.2) and of the permeability function (Figure 7.3) was assigned for the surficial soil layer of the NTU-ANX slope (Layer 1). The simulation then continued will these parameters until another rainfall event occurred. The difficulty with this was the fact that after the end of a rainfall event, part of the slope (especially near the ground surface) starts to dry, while other parts of the slope (at larger depths) continue wetting due to percolation of water from smaller depths. However, it was not possible to overcome this, due to the limitations of Seep/W. Nevertheless, it was appropriate to investigate the effect of the hysteresis during the wetting and drying phase of the soil-water characteristic curve on the pore-water pressure changes.

During preliminary analyses, the effect of the hysteresis of the soil-water characteristic curve on the pore-water pressure changes was studied. Figure 7.12 presents the pore-water pressures at 0.5m deep of Row A during the period from 22 to 25 March 2000 as they were measured in the field and as they were predicted by the numerical model. During the period from 22 to 25 March 2000, only two rainfall events took place. The first rainfall event took place on 23 March 2000 and the second rainfall event took place on 24 March 2000 (Figure 7.8). Figure 7.12 shows two sets of data from the numerical model. The first set of data corresponds to predictions of the pore-water pressures at 0.5m deep using both the wetting and the drying phases of the soil-water characteristic curve during the wet and the dry periods of the analysis, respectively. The second set of data corresponds to predictions of the pore-water pressures using only the wetting phase of the soil-water characteristic curve for both the wetting and the drying period.

The two predictions of the numerical model of Figure 7.12 show that the hysteresis

of the soil-water characteristic curve has little effect on the decrease of the pore-water pressures during the drying process. Both sets of results show quite similar trends. For that reason, it was decided to insert the drying phase of the soil-water characteristic curve into the analysis only for dry periods that were longer than 12 hours. This methodology has the advantage that it allowed the study of the increase, during rainfall, of the pore-water pressures at large depths (where the increase of the pore-water pressures may occur long after the end of the rainfall event).

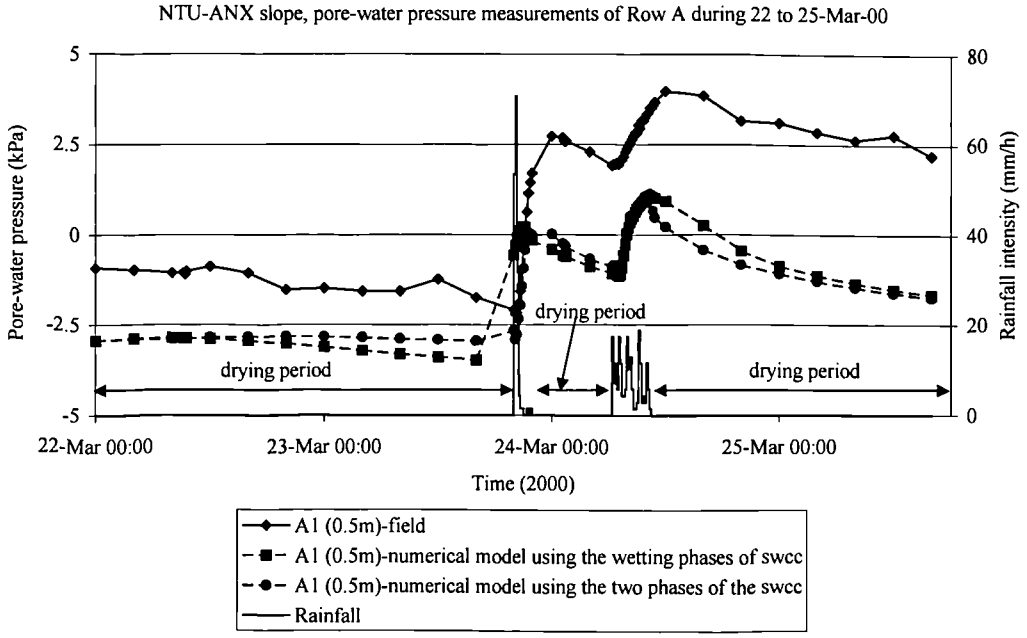

Figure 7.12 Pore-water pressures of Row A of the NTU-ANX slope as they were measured in the field and as they were predicted by the numerical model during the period 22 to 25 March 2000.

Another advantage of the methodology described above, is that possible numerical instabilities in the solution were avoided, as they might have occurred with the change of the soil-water characteristic curve and the permeability function. In practice, when the simulation resumes after changing the soil-water characteristic curve and the permeability function from the wetting phase to the drying phase, Seep/W uses the distribution of total heads within the slope of the previous time step, as the initial conditions. The initial head file is translated into pore-water pressure at each node. The permeability with respect to water at each node is determined from

the pore-water pressure using the permeability function. The permeability function of Figure 7.3 also shows some hysterisis between the wetting and the drying phase. Thus, for the time step when the change takes place from the wetting to the drying phase of the soil-water characteristic curve and the permeability function, it is possible that the permeability values may differ considerably. This difference in the permeability values may cause some numerical instabilities.

Seep/W can model evaporation only by defining a negative flux at the ground surface. As was noted in Chapter 2 (Section 2.11.1), the actual evaporation rate from a soil surface is a function of the potential evaporation and the available water content of the soil (Wilson et al. 1995). Unfortunately, during the monitoring period of the NTU-ANX slope no evaporation was measured. Gasmo et al. (2000) measured evaporation rates on the NTU campus at an earlier time (where the NTU-ANX slope is situated). Gasmo et al. (2000) concluded that on the NTU campus the evaporation rates may vary from $4x10^{-11}$m/s (i.e. 0.004mm/day) to $2x10^{-7}$m/s (i.e. 17mm/day). It should be noted that the pore-water pressures near the ground surface of the NTU-ANX slope (Chapter 4) did not always decrease with the same rate during the dry periods. This indicates that the decrease of the pore-water pressures during the dry periods is not only dependent on the duration of the dry period but also on the atmospheric conditions (temperature, humidity etc.).

For consistency, the following indirect method was adopted for the estimation of the negative flux (i.e. evaporation), which was required for achieving similar trends in the numerical model as were observed in the field pore-water pressure conditions:

- First the lowest field pore-water pressure conditions were noted. The lowest pore-water pressure conditions were recorded on 18 May 2000 (Chapter 5, Figure 5.23) after a 12-day dry period. At 0.5m deep at row A, the total decrease of the pore-water pressure over the 12 days (from 06 April to 18 April 2000) was 44kPa. In order to achieve such pore-water pressure conditions in the numerical model a negative flux of $5x10^{-8}$m/s (i.e. 4.3mm/day) was required. This is within the range quoted by Gasmo et al. (2000).

- The negative flux that was applied on the slope for other drying periods was a proportion of the maximum negative flux of $5x10^{-8}$m/s, according to the total decrease of the field pore-water pressure at 0.5m deep, e.g. for a pore-water pressure decrease of 10kPa the negative flux (q_{neg}) would be:

$$q_{neg} = \frac{10}{44} \cdot 5x10^{-8} \Rightarrow q_{neg} = 1.1x10^{-8} m/s$$

The methodology for the application of the negative flux during the dry periods, as described above takes into consideration the total decrease of the pore-water pressure at 0.5m and the duration of the dry period. As will be seen in the presentation of the results below, the use of this methodology made it possible to predict the decrease of the pore-water pressures at all depths in a way that was comparable with the field measurements. The applied negative fluxes varied between $2.4x10^{-10}$m/s (i.e. 0.02mm/day) and $5x10^{-8}$m/s (i.e. 4.3mm/day). These values fall within the range of observed evaporation rates given by Gasmo et al. (2000).

7.2 Presentation of the results

7.2.1 Infiltration and runoff

All rainfall events that were applied on the slope of the numerical model correspond to the rainfall events (natural and simulated) that took place on the NTU-ANX slope during the monitoring period (from March to August 2000).

The infiltration and runoff predictions of the numerical model were calculated for all rainfall events that were applied on the slope with total rainfall higher than 5mm. Figure 7.13 and Figure 7.14 present the results of three individual rainfall events to compare how the agreement is for predicting runoff and infiltration with the field observations. Figure 7.13 presents the infiltration results for the rainfall events of the 23 and 24 March 2000 (Figure 7.8). Figure 7.14 presents the infiltration results for the rainfall event of 06April 2000 (Chapter 5, Figure 5.18). For comparison, the two figures also present the field measurements of the runoff produced during these rainfall events.

The results of infiltration and runoff predictions for the rainfall events of 23 and 24 March 2000 (Figure 7.14a) show reasonable agreement with the field observations. The total infiltration that the numerical model predicted for the rainfall event of 23 March 2000 was 7mm, leading to a total runoff of 22mm (the field observation was 19mm total runoff). The total infiltration that the numerical model predicted for the rainfall event of 24 March 2000 was 17mm, leading to a total runoff of 17mm (the field observation was 19mm total runoff). These results are in a reasonable agreement with the field observation. In addition, the numerical model predicted the development of runoff during the two rainfall events to be very similar with the field measurements (Figure 7.13), as can be seen by the 'step-like' shape of cumulative runoff predicted for the 24 March rainfall event. The difference in time scales of runoff between the field observations and the numerical predictions (Figure 7.13) are attributed to the fact that in the field some time is needed after the start of the rain for rainwater to reach the collection point. The usual delay in the field for runoff to reach the collection point was usually between 20 and 30 minutes (Chapter 4, Sections 4.2.5 and 4.2.6).

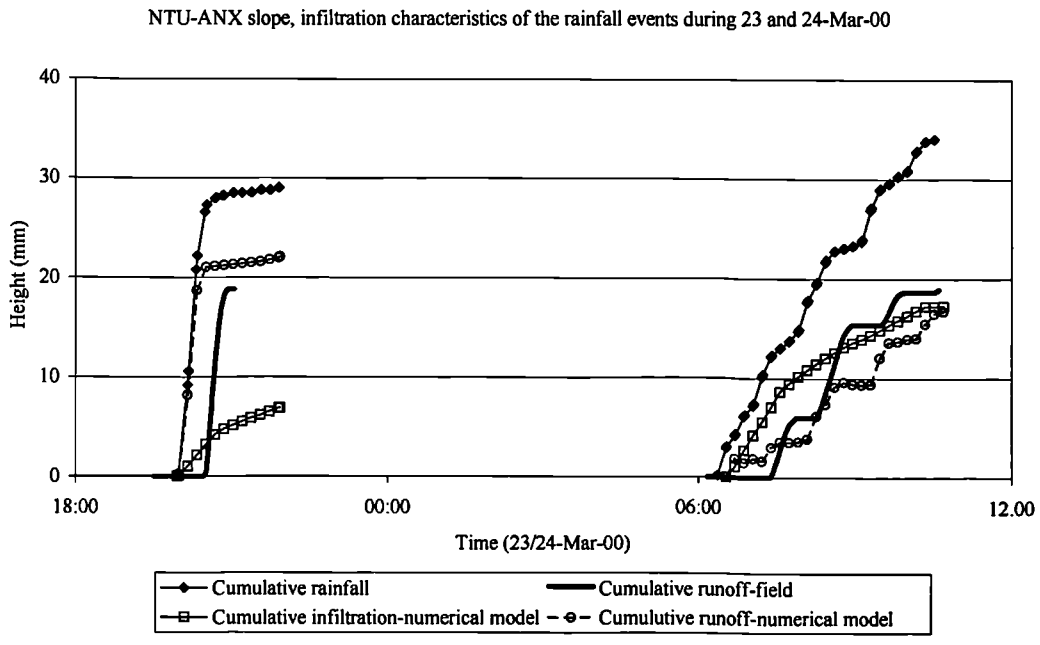

Figure 7.13 Comparison of measured in the field and calculated with the numerical model of natural rainfall events that took place on 23 and 24 March 2000.

The prediction of total infiltration and total runoff for the rainfall event of 06 April

2000 (Figure 7.14) was also in reasonable agreement with the field observations. The total rainfall that was applied on the slope was 49mm and the predicted infiltration was 9mm, leading to a total runoff of 40mm. In the field 46mm of runoff were measured during the rainfall event of 06 April 2000. Although there is some discrepancy in actual numbers between the numerical prediction and the field observation for the rainfall of 06 April 2000 (40mm of runoff compared to 46mm respectively), the numerical model did predict a relatively low total infiltration in comparison with the total rainfall.

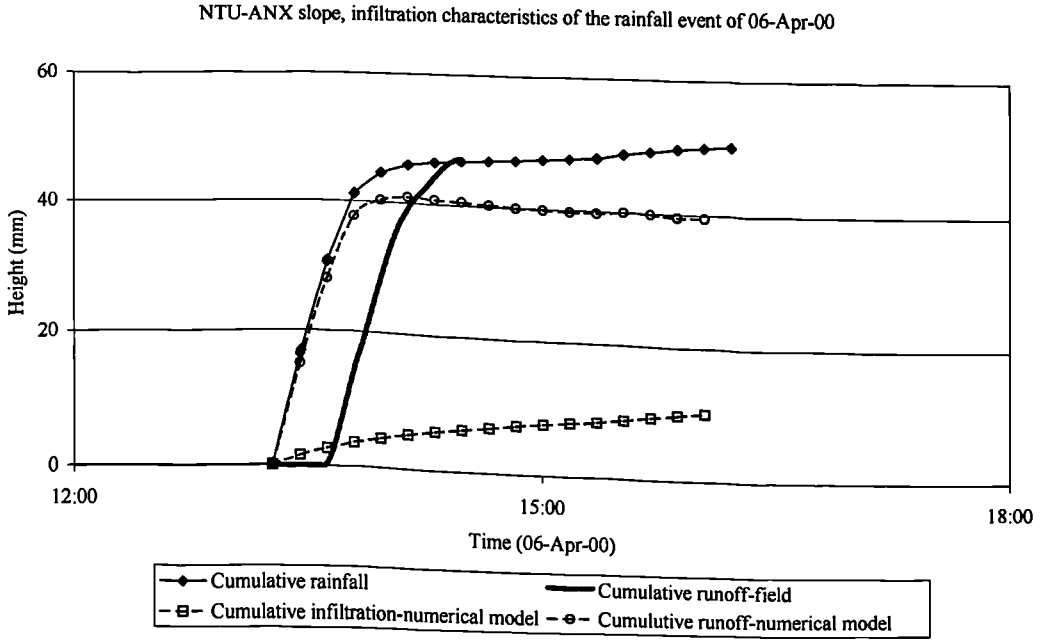

Figure 7.14 Comparison of measured in the field and calculated with the numerical model of natural rainfall events that took place on 06 April 2000.

As it will be seen below, the numerical model overestimated the total infiltration for major rainfall events (with total rainfall greater than 30mm). This discrepancy can be attributed to several factors such the vegetation and the initial abstraction at the ground surface. It is also possible that runoff was also overestimated in the field during such major and very intense rainfall events. For example, it should be remembered that during the first 30 minutes from the start of the rainfall event of 06 April 2000, 42mm out of the 49mm were precipitated on the slope. Under conditions of such intense rainfall the possibility of a small error of the runoff measurement device cannot be omitted. Despite such limited discrepancies the numerical model

generally predicted infiltration characteristics that are in a reasonable agreement with the field observations. This will be discussed in more detail for all rainfall events in the following paragraphs.

Figure 7.15 presents the relationship between total rainfall and total runoff for the NTU-ANX slope, based on the field measurements and on the predictions of the numerical model with the adjustment for the modeling of the grass cover at the ground surface of the slope (Figure 7.4b). Figure 7.16 presents the relationship between total rainfall and total infiltration for the NTU-ANX slope, based on the field measurements and on the predictions of the numerical model. The data of Figure 7.15 and Figure 7.16 correspond to the same rainfall events (natural and simulated) for which runoff was measured on the NTU-ANX slope (Chapter 4, Sections 4.2.5 and 4.2.6).

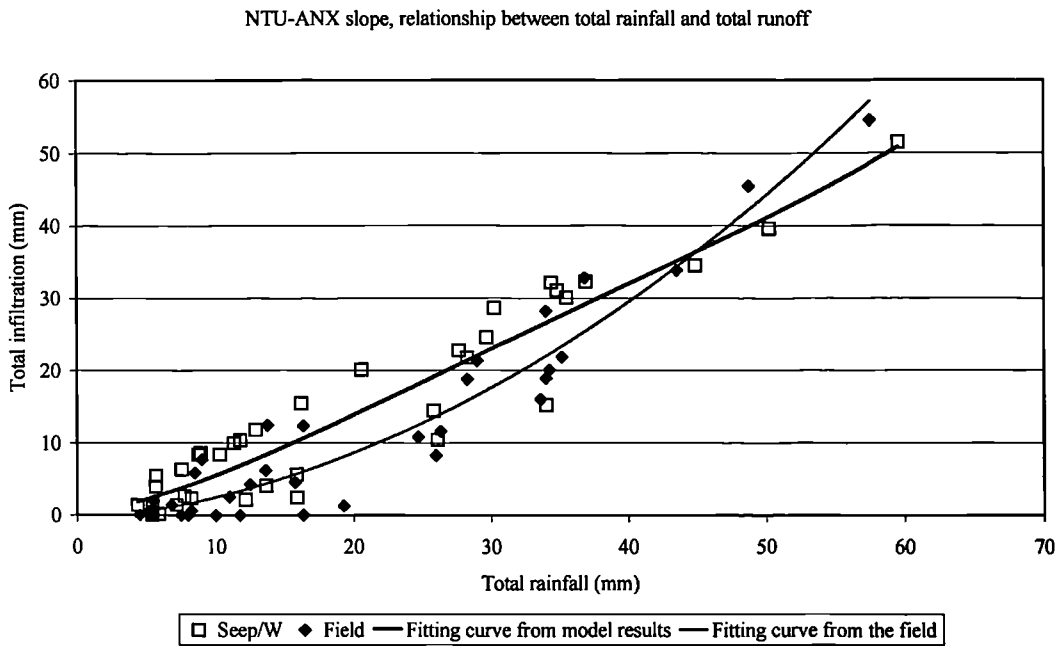

Figure 7.15 Comparison of the total rainfall-total runoff relationships from the field measurements and from the numerical model of 37 rainfall events, for which runoff was measured in the field.

Figure 7.15 and Figure 7.16 show that the results from the numerical model are in good agreement with the field measurements. The fitting curves in the two sets of data of Figure 7.15 are very similar and show the same trend: as the total rainfall

increases the total runoff increases. The estimated upper limit curves of Figure 7.16 based on the field measurements and on the predictions of the numerical model show similar trends. The two curves of Figure 7.16 show that, initially, as total rainfall increases the total infiltration increases too. However as the total rainfall increases beyond a limit of 25 to 30mm then infiltration start to decrease (Figure 7.16). However, some discrepancies can be observed between the two sets of data. The numerical model overestimated the total runoff produced (or underestimated the total infiltration) of rainfall events with total rainfall smaller than 30mm. At the same time, for rainfall events higher than 30mm some underestimation by the numerical model of the total runoff (overestimation of total infiltration) can be observed if compared with the available field data. This phenomenon was clearly seen in the example of Figure 7.14. The differences can be attributed to a number of uncertainties (e.g. initial abstraction, vegetation etc.) that cannot be modeled.

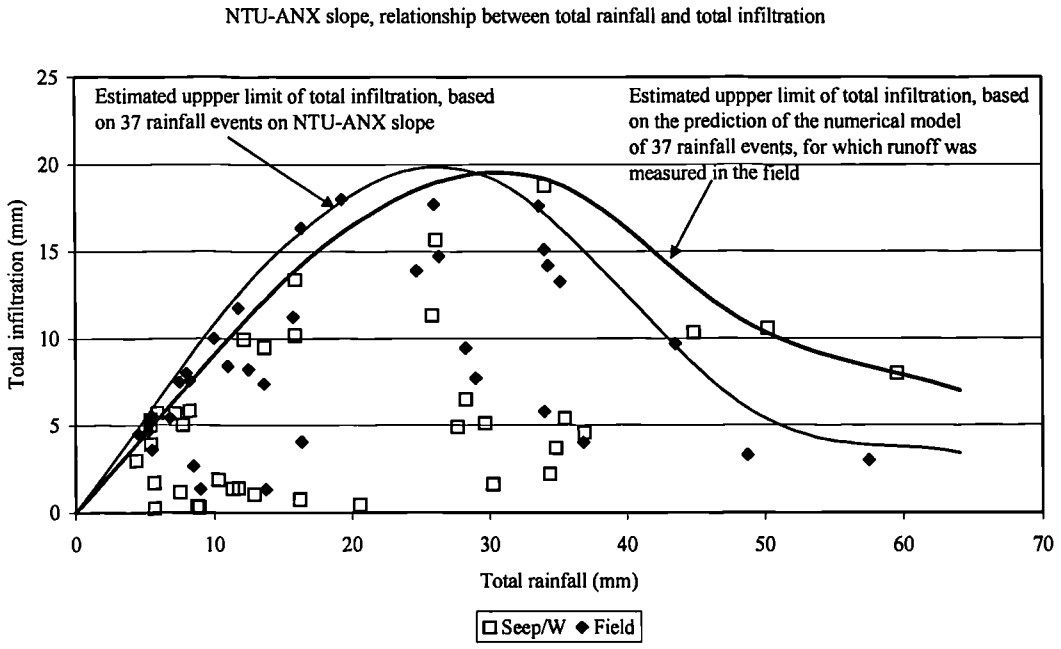

Figure 7.16 Comparison of the total rainfall-total infiltration relationships from the field measurements and from the numerical model of 37 rainfall events, for which runoff was measured in the field.

Figure 7.17 and Figure 7.18 present the relationships between total rainfall and total runoff and total infiltration, respectively, for all rainfall events that were applied on the slope of the numerical model. This includes rainfall events for which no runoff

measurements were made, whereas the previous plots (Figure 7.15 and Figure 7.16) only showed the results of modelling for the rainfall events where runoff measurements were available. The rainfall events that were applied on the slope of the numerical model are the same with the rainfall events that were recorded on the NTU-ANX slope (Chapter 4, Section 4.2.2).

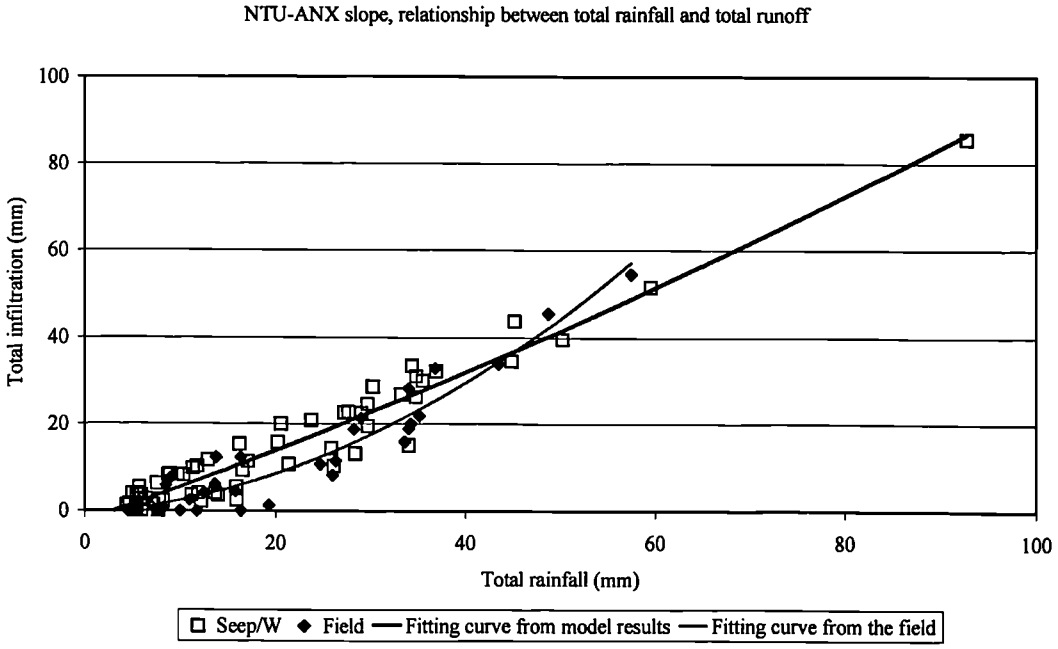

Figure 7.17 Total rainfall – total runoff relationships from the field measurements and from the numerical model for all rainfall events applied on the slope during the monitoring period.

The relationships between total rainfall and total runoff and total infiltration of Figure 7.17 and Figure 7.18. respectively, confirm the field observations of the 37 rainfall events, for which runoff was measured in the field. As total rainfall increases the total runoff increases (Figure 7.17) in a polynomial way. The relationships between total rainfall and total runoff and total infiltration of Figure 7.17 and Figure 7.18. respectively, confirm the field observations of the 37 rainfall events, for which runoff was measured in the field. As total rainfall increases the total runoff increases (Figure 7.17) in a polynomial way.

The results of the numerical model (Figure 7.18) also shows that there is a considerable scatter in the relationship between the total rainfall and total infiltration, which was also seen from the field measurements. The upper limit of the total

infiltration shows that for total rainfall greater than 25mm to 30mm the total infiltration decreases (Figure 7.18). Even for the rainfall event of 93mm that took place on 24 July 2000 the numerical model predicted a relatively small infiltration that amounts to 7mm. In comparison with the field measurements it was seen that for rainfall events greater than 25mm the total infiltration starts to decrease and as total rainfall increases further the total infiltration drops below 5mm.

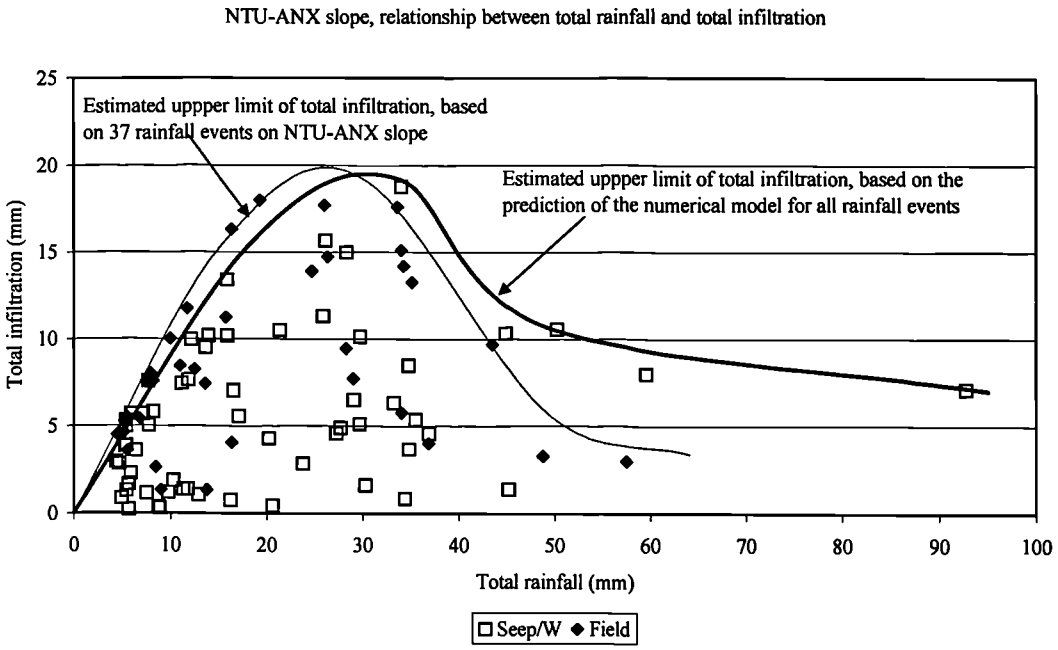

Figure 7.18 Total rainfall – total runoff relationships from the field measurements and from the numerical model for all rainfall events applied on the slope during the monitoring period.

7.2.2 Pore-water pressure changes

Figure 7.19 to Figure 7.22 present the pore-water pressures at 0.5m, 1.1m, 1.7m and 2.9m deep, respectively, of Rows A, B and C of the NTU-ANX slope as they were measured in the field and the pore-water pressures at 0.5m, 1.1m, 1.7m and 2.9m deep of Row A as they were predicted using the numerical model of Figure 7.4. Predicted pore-water pressures of rows B and C are not presented in Figure 7.19 to Figure 7.22. In the slope of the numerical model rows A to C were defined at the middle of the slope in great distance from the left and right boundaries (Figure 7.4). Therefore the predicted pore-water pressure changes between the three rows are the same, as the soil materials of the slope are defined as homogeneous and isotropic.

On the Figure 7.19 to Figure 7.22 the applied daily rainfall is also superimposed.

The numerical model predicted pore-water pressure changes during rainfall at 0.5m (Figure 7.19) that are in good agreement with the pore-water pressures that were measured in the field. However, there are some small differences in the way pore-water pressures decrease during the drying period, which reflects the 'weakness' of the numerical model to handle in a realistic fashion the evaporation during drying. Differences in the recovery of the negative pore-water pressure is mainly identified between the field measurements of row B at 0.5m deep and the results of the numerical model. In general the recovery of pore-water pressures at 0.5m deep of Row B was very sharp during the dry periods of May and July 2000. In order to simulate the decrease of pore-water pressures at 0.5m deep during May 2000 (which was approximately 80kPa decrease within 12 days) with the numerical model a very high negative flux of 10^{-7}m/s (i.e. 9mm/day) would be needed. Such a high negative flux is still within the limits of evaporation rate that Gasmo et al. (2000) quoted. However, the application of such a high negative flux for a long period of time caused major instabilities in the results especially on the ground surface of the slope.

At 1.1m deep (Figure 7.20) the differences in the pore-water pressure changes between the results of the numerical model and the field measurements are more obvious. From 22 March to 04 June the model underestimated the pore-water pressure changes. During the periods from 11 to 17 June 2000 and from 24 to 31 July 2000 (Figure 7.20), which were particularly wet periods (100mm and 290mm of rainfall were distributed over these two periods, respectively), the predicted pore-water pressure increase during rainfall was considerably higher in comparison with the field measurements at 1.1m deep of Row A. However, during these two wet periods (11 to 17 June and from 24 to 31 July 2000) the pore-water pressure changes of the model show a more 'spiky' behaviour and this is in more reasonable agreement with the field measurements of row B and C at 1.1m deep.

At 1.7m deep (Figure 7.21) the field pore-water pressures of Row A were usually increasing during rainfall by large amounts in comparison with the pore-water pressure changes at smaller depths (i.e. 1.1m deep, Figure 7.21) and at larger depths (i.e. 2.9m deep, Figure 7.22). Unfortunately the pore-water pressure measurements a

the same depths for the rows B and C were not very reliable and therefore are not presented in Figure 7.21. The behaviour of pore-water pressures at 1.7m deep of Row A was well documented in Chapter 5 (Section 5.2) and is atributed to the non-homogeneity of the soil material. The numerical model is not capable of predicting such changes, although the general trend of pore-water pressures is reasonable. However, during the periods 11 to 17 June 2000 and 24 to 31 July 2000 (which were periods of very high rainfall) the predicted pore-water pressures at 1.7m deep (Figure 7.21) were higher in comparison with the field observations.

The comparison of the predicted pore-water pressures at 2.9m deep and the field measurements at 2.9m deep (Figure 7.22) also show that during the periods from 11 to 17 June 2000 and from 24 to 31 July 2000, the numerical model predicted highly positive pore-water pressures, in comparison with the field measurements of row A and B. However, pore-water pressure changes at 2.9m of row C show that pore-water pressures at 2.9m went also relatively high during these wet periods. For the rest of the analysis period the prediction of the pore-water pressures at 2.9m (Figure 7.22) deep show similar trends in relation with the field observations of Rows A.

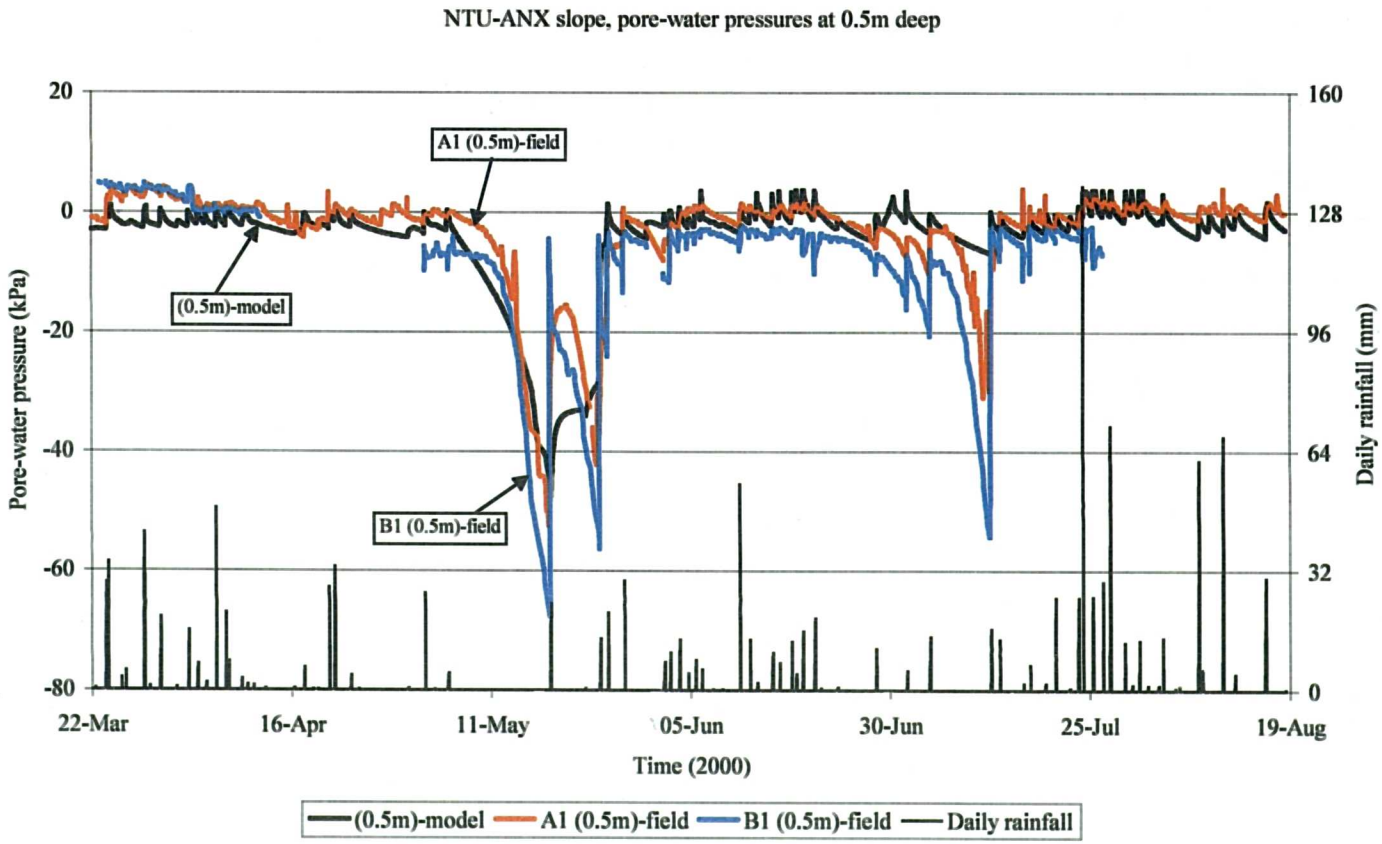

Figure 7.19 Pore-water pressures at 0.5m deep at the NTU-ANX slope as they were measured in the field and predicted with the numerical model.

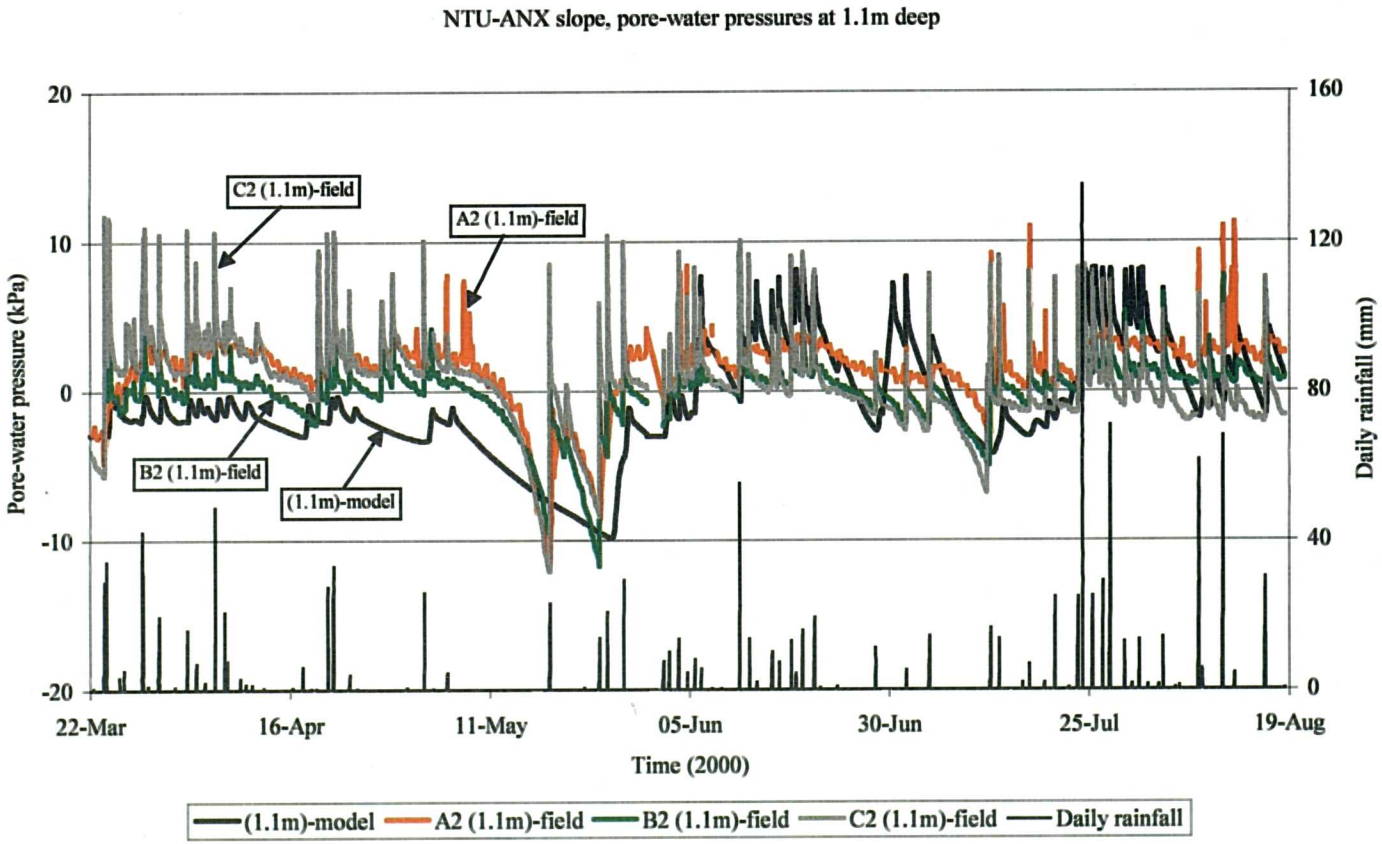

Figure 7.20 Pore-water pressures at 1.1m deep at the NTU-ANX slope as they were measured in the field and predicted with the numerical model.

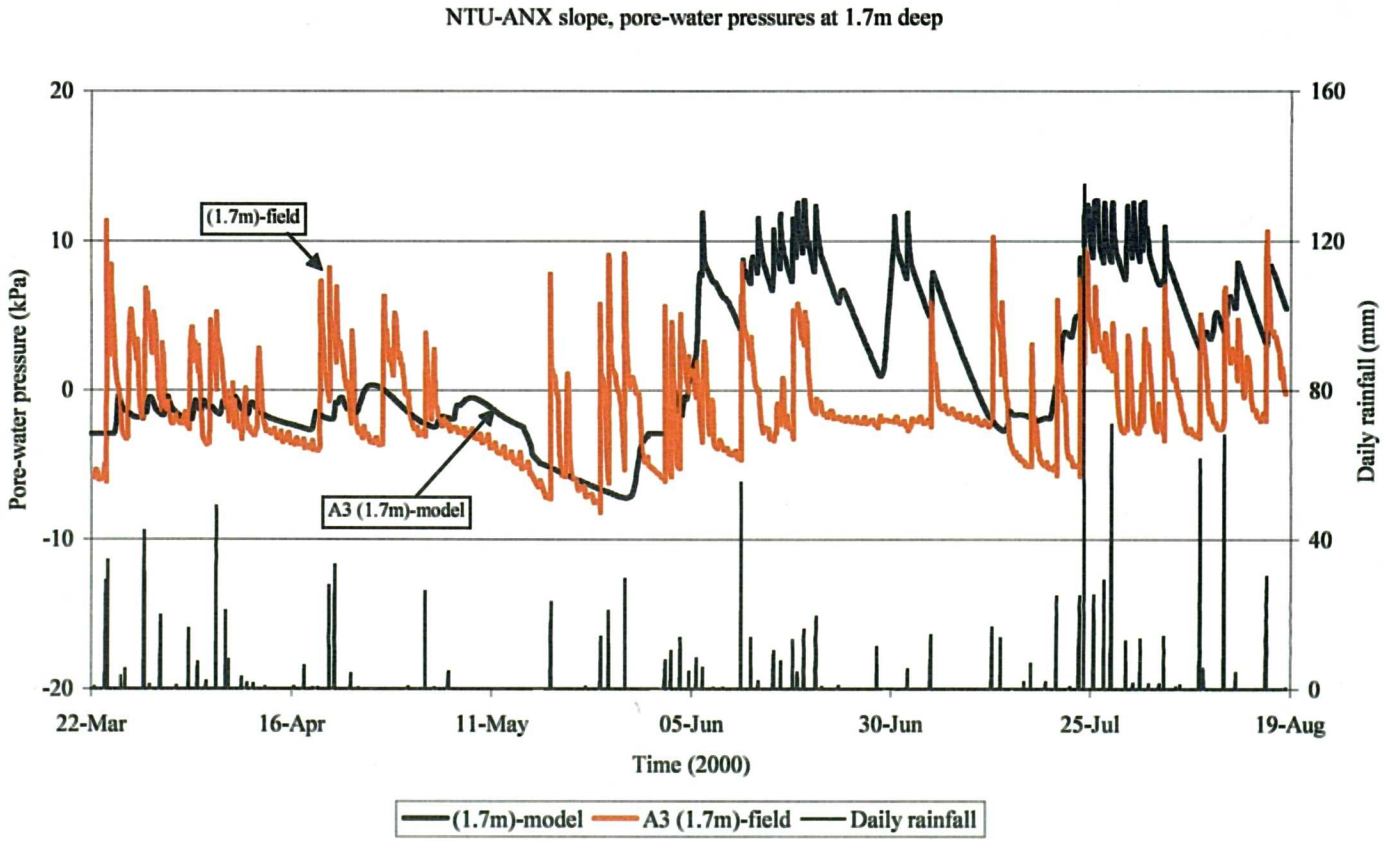

Figure 7.21 Pore-water pressures at 1.7m deep at the NTU-ANX slope as they were measured in the field and predicted with the numerical model.

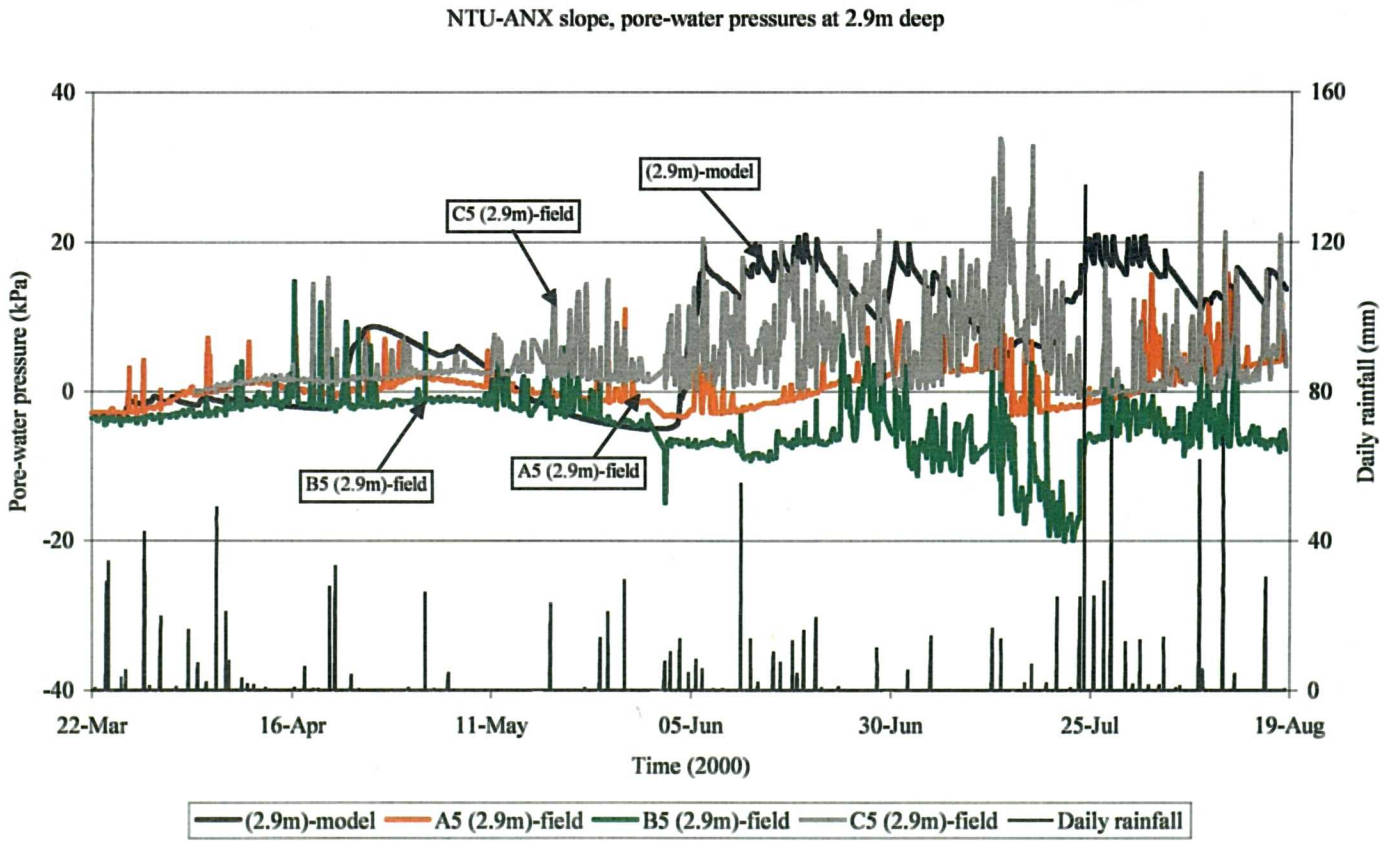

Figure 7.22 Pore-water pressures (Row A), 2.9m deep, at the NTU-ANX slope as they were measured in the field and predicted with the numerical model.

7.3 Discussion of the results

7.3.1 Infiltration characteristics of the slope

The results from the numerical model offer a better understanding of the seepage conditions within the slope. Figure 7.23 presents the pore-water pressure changes with time during the two rainfall events of 23 and 24 March 2000, as they were measured in the field and as they were predicted by the numerical model. Large changes of pore-water pressures towards hydrostatic values are predicted near the ground surface, building a perched water table about 1m deep from the ground surface. As depth increases, only minor pore-water pressure changes are predicted.

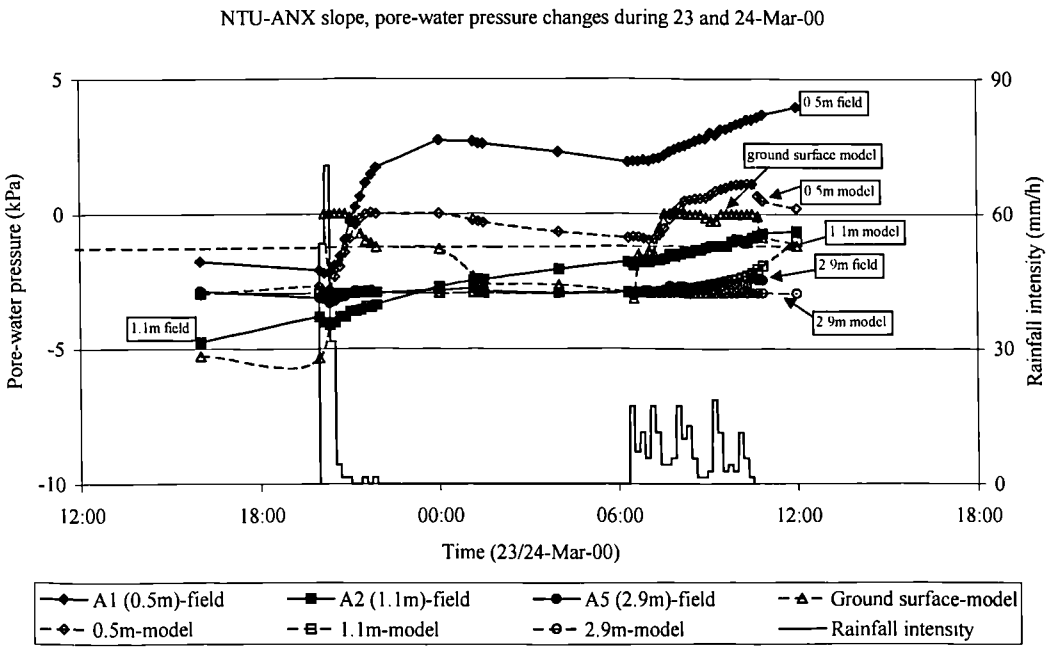

Figure 7.23 Pore-water pressure changes with time during the rainfall events of 23 and 24 March 2000, as predicted by the numerical model.

The pore-water pressure changes of Figure 7.23 suggest that smaller amounts of infiltrated water reach greater depths within the slope and thus the negative pore-water pressures at large depth will not be greately affected. Figure 7.24 presents the calculated infiltration rate with time at the ground surface and the calculated fluxes with time at depth of 0.5m, 1.1m, and 2.9m for the rainfall events of 23 and 24 March 2000. Figure 7.24 also presents the hyetograph of the two

rainfall events.

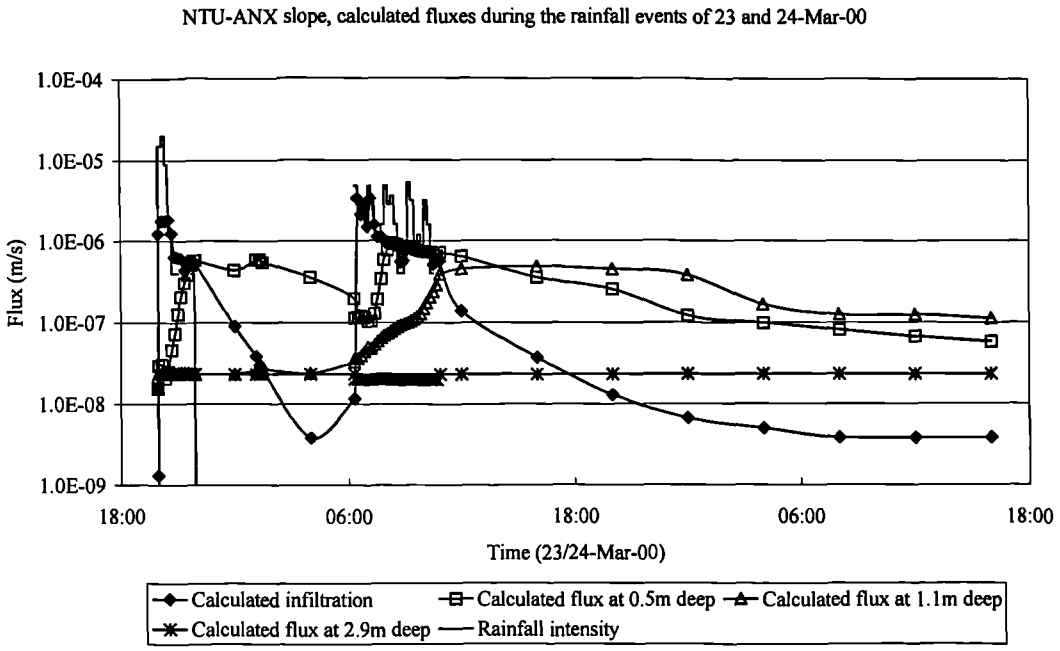

Figure 7.24 Calculated flux during the rainfall events of 23 and 24 March 2000.

From Figure 7.24 it can be observed that at the start of the rainfall the infiltration rate at the ground surface increases up to a maximum rate and then drops sharply very soon after the end of the rainfall, since it is controlled by the rainfall intensity. The flux rates at 0.5m deep show that water movements occur very soon after the start of the rainfall event and continue for some time after the end of the rainfall event, as water flows through the soil which has a low permeability with respect to water. At larger depths water movements, expressed as fluxes, are considerably smaller. The flux at 1.1m deep was unaffected by the first rainfall (intense, short event) and increased only during the second rainfall event, which had longer duration. At 2.9m deep no water movement was predicted.

The results of the numerical model also offer a better explanation of the way infiltration takes place near the ground surface. Figure 7.25 presents the calculated infiltration flux at the ground surface and the calculated flux at 0.5m deep during the rainfall events of 23 and 24 March 2000. Figure 7.25 also presents the permeability changes with time of the surficial layer, which corresponds to the grass covering of the slope and the permeability changes of the main soil layer (Layer 1) of the slope.

Finally Figure 7.25 also presents for comparison the rainfall intensity of the rainfall events that took place on 23 and 24 March 2000 on the same logarithmic scale.

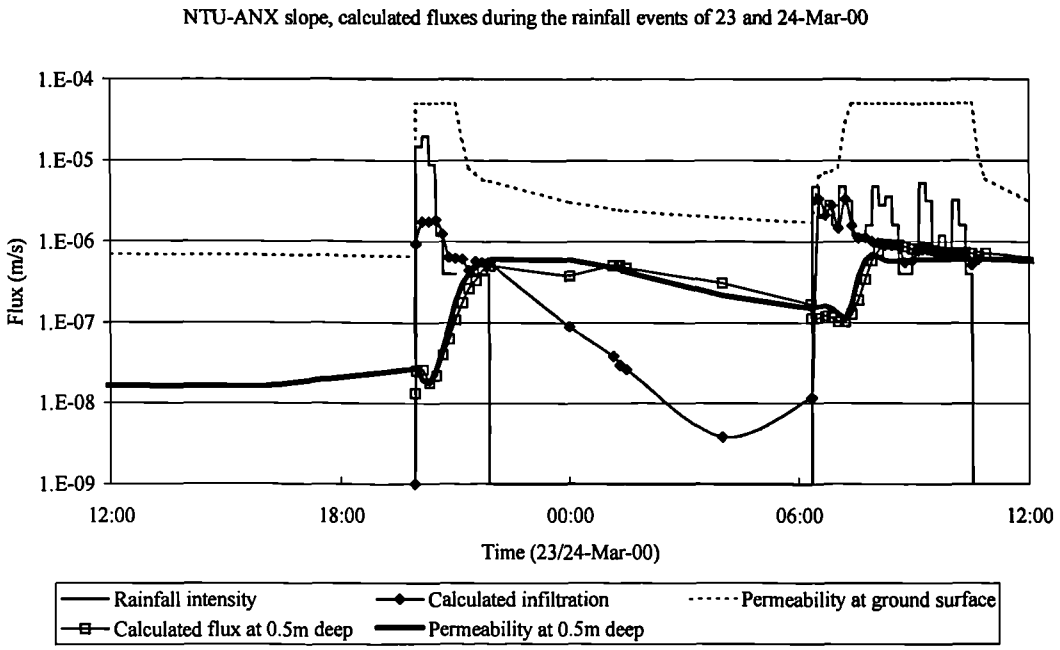

Figure 7.25 Calculated infiltration flux at the ground surface and at 0.5m deep and permeability changes during the rainfall events of 23 and 24 March 2000.

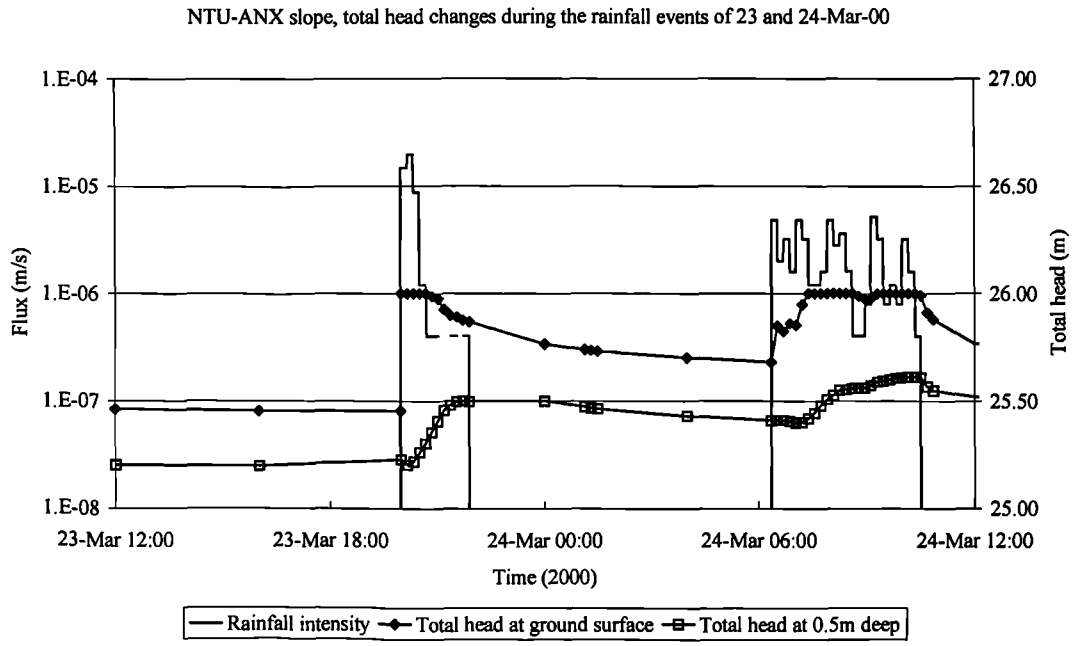

Figure 7.26 Changes of total head at the ground surface and at 0.5m deep during the rainfall events of 23 and 24 March 2000.

From Figure 7.25, it can be seen that at the start of rainfall event the infiltration rate at the ground surface initially was high and with the development of time it decreased. The peak infiltration rate was approximately $2x10^{-6}$m/s. The maximum infiltration rate is considerably lower than the rainfall intensity, which was greater than 10^{-5}m/s. In addition, the maximum infiltration rate and the rainfall intensity of the 23 March 2000 were significantly lower than the saturated coefficient of permeability of the grass cover ($5x10^{-5}$m/s). Theoretically, in this case the infiltration rate could be as high as the rainfall intensity. However, at 0.5m deep the permeability of the soil is low (approximately $5x10^{-8}$m/s) and rainfall water cannot penetrate the soil at that depth with a high rate equal to the rainfall intensity. Thus, a great amount of rainfall water will be forced to runoff from the ground surface.

At the start of the rainfall of 24 March 2000, (Figure 7.25) the permeability of the soil at 0.5m deep is significantly higher (approximately equal to 10^{-7}m/s) due to the high antecedent rainfall of the 23 March 2000 rainfall event. During the rainfall event of 24 March 2000, the model predicted higher infiltration rates than for the rainfall event of 23 March, despite the fact that the rainfall intensity for 24 March 2000 was significantly lower than that for the 23 March 2000 rainfall event. This can be attributed to the fact that at 0.5m deep the soil has a higher permeability and thus allows water to flow towards greater depths at higher rates. Towards the end of the 24 March 2000 rainfall event the infiltration rate at 0.5m deep is slightly higher than the permeability at the depth. This phenomenon was also predicted by Gasmo et al. 2000 and can be justified with the Darcy's law (Chapter 2, Equation 2.15). Darcy's law expresses the flow rate through the soil as the hydraulic gradient (i) multiplied by the permeability of the soil (k). If the hydraulic gradient (i) at a specific point is greater than 1, then it is possible to achieve a flow rate greater than the permeability of the soil.

The above analysis gives some means to justify why the infiltration rate at the ground surface was initially greater during the rainfall of 24 March (when the rainfall intensity was relatively low) than the infiltration rates during the rainfall event of 23 March (when the rainfall intensity was relatively high). This phenomenon is justified due to the relatively high permeability of the soil at 0.5m deep after 28mm of rainfall

were precipitated during the 23 March 2000 rainfall event. However, Figure 7.25 shows that during the rainfall event of 24 March 2000 the infiltration flux starts to decrease after 18mm of rainfall were precipitated on the slope. While the infiltration rate decreases, the rainfall intensity of 24 March 2000 still reaches some peaks, which do not affecting the infiltration rate values at the ground surface. This issue can be explained by taking into consideration the changes of total head at the ground surface and at 0.5m deep.

Figure 7.26 presents the changes of the total head at the ground surface and at 0.5m deep of the slope as they were predicted using the numerical model. At the start of the rainfall event of 23 March 2000, the total head at the ground surface of the slope (Figure 7.26) increased from 25.5m (initial value) to 26m and then remained constant for the rest of the rainfall event. At 0.5m deep the total head increased gradually from 25.2m to 25.5m by the end of the rainfall, as opposed to the immediate increase of the total head at the ground surface (Figure 7.26). The initial high difference of the total head between the ground surface and at 0.5m deep resulted in higher hydraulic gradient and thus to high infiltration rate at the ground surface even with a low permeability at 0.5m. As the total head at 0.5m increased during the rainfall event of 23 March 2000, it caused the hydraulic gradient to decrease and subsequently the infiltration rate decreases. Similar behaviour can be seen for the rainfall event of 24 March 2000. Initially there was a total head difference of 0.5m between the ground surface and at 0.5m deep. As the pore-water pressure at 0.5m increased towards positive values (Figure 7.23) this caused a significant increase of the total head and thus a decrease of the total head difference between the ground surface and at 0.5m deep (Figure 7.26). That lead to a decrease of the hydraulic gradient at the ground surface. The decrease of the hydraulic gradient resulted in the decrease of the infiltration rate of the slope, even when the rainfall intensity was high.

The description of the infiltration mechanism during the rainfall events of 23 and 24 March 2000 (Figure 7.24 to Figure 7.26) showed that infiltration is greatly affected by the initial conditions. This can clearly be seen if the extreme initial conditions of the slope are considered (when the slope was at its most moist and when the slope was at its driest). The slope was at its most moist conditions during 06 of April

2000, when a major rainfall event of 49mm was precipitated on the slope over 3 hours. The slope was at its driest on 18 May 2000, when a major rainfall event of 23mm was precipitated over 1 hour. The discussion of the field observations of the most moist and driest conditions of the NTU-ANX slope (on 06 April and 18 May 2000, respectively) is presented in Chapter 5 (Section 5.2.1).

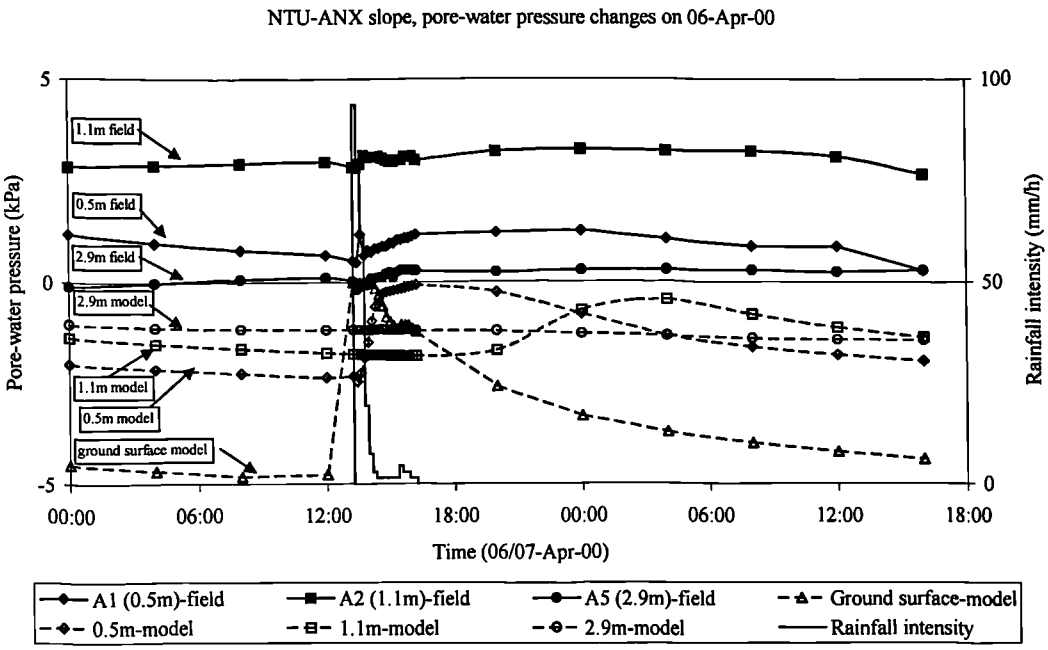

Figure 7.27 Pore-water pressure changes with time during the rainfall event of 06 April 2000, as predicted by the numerical model.

Figure 7.27 presents the prediction of the pore-water pressure changes with time during 06 April 2000 (when the slope was at its most moist conditions). For comparison the field measurements during the same period are also presented. Figure 7.27 also presents the hyetograph of the 06 April 2000 rainfall event. The numerical model predicted a total infiltration of 9mm, while the field observation suggest a total infiltration of 3mm (Figure 7.14). The predicted pore-water pressures of Figure 7.27 during 06 April 2000 are somewhat underestimated in comparison with the field observations. These discrepancies are discussed in more detail in Section 7.2. However, the overall trend of the pore-water pressure changes is similar with the field observations.

From Figure 7.27 it can be seen that initially the pore-water pressures (from the

numerical model) are close to zero (between –2kPa at 0.5m deep and –1kPa at 2.9m deep). During the rainfall event, the predicted pore-water pressures at 0.5m deep increased by 2kPa. The pore-water pressures at 1.1m deep increased at a low rate from –1.5 to -0.5kPa. The predicted pore-water pressures at 2.9m did not change significantly. This behaviour can be explained by consideration of the ground water movements. Figure 7.28 presents the calculated fluxes at the ground surface, at 0.5m, 1.1m and 2.9m deep for the rainfall event of 06 April 2000. From Figure 7.28 it can be seen that the infiltration rate at the ground surface is initially high (up to $2.5x10^{-6}$m/s) and then decreased rapidly to $5x10^{-7}$m/s, despite the fact that the rainfall intensity was considerably higher and also the permeability of the slope was also high (Figure 7.29). The development of the infiltration flux at the ground surface during the rainfall event of 06 April 2000 (Figure 7.28) is similar to the development of the infiltration flux during the rainfall events of 23 and 24 March 2000 (Figure 7.25).

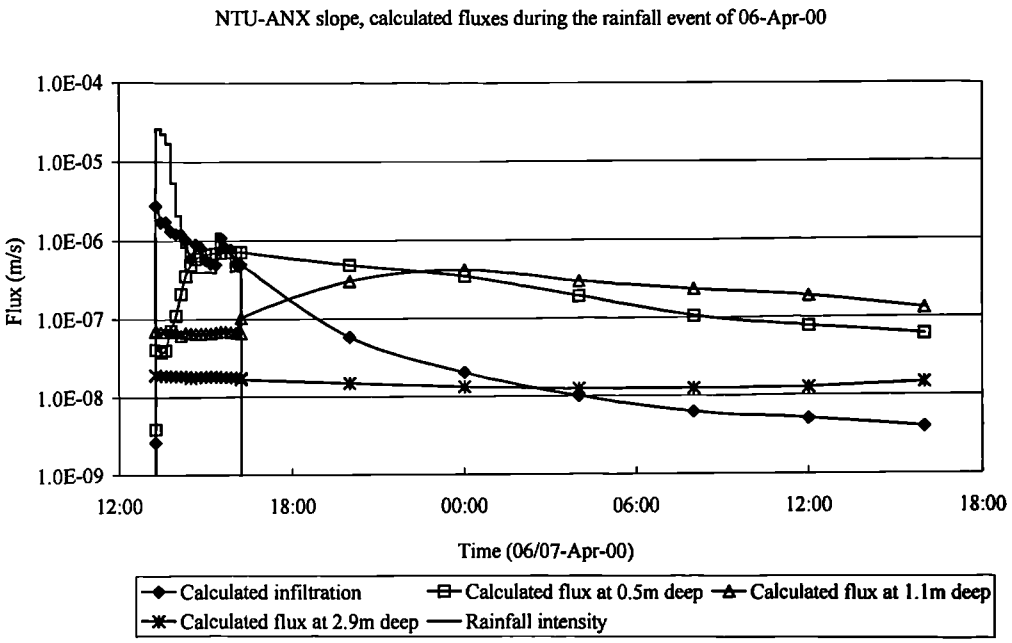

Figure 7.28 Calculated flux during the rainfall event of 06 April 2000.

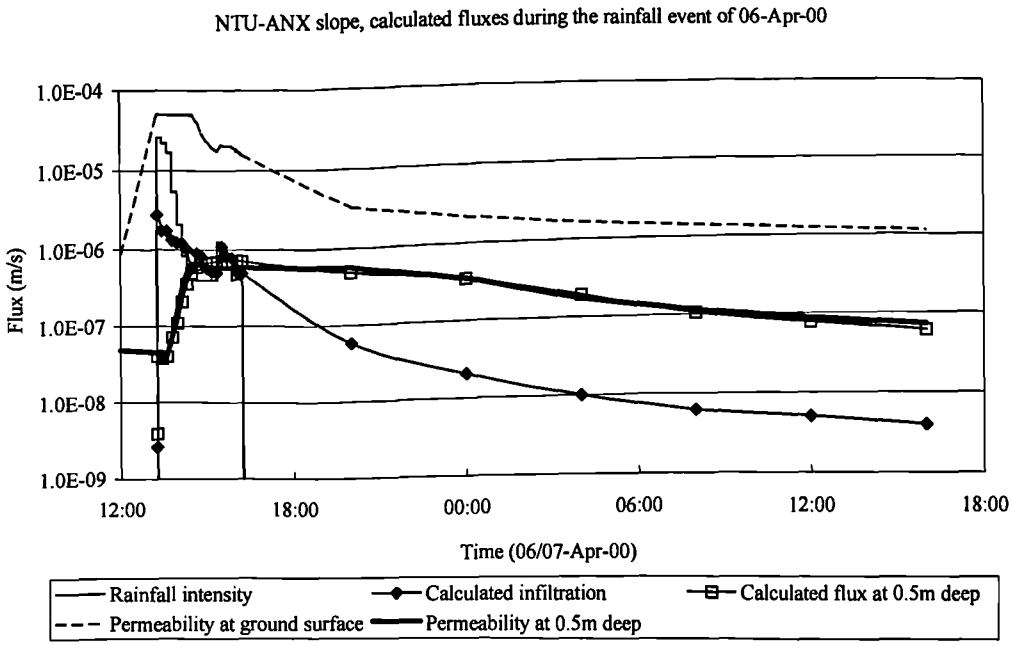

Figure 7.29 Calculated infiltration flux at the ground surface and at 0.5m deep and permeability changes during the rainfall event of 06 April 2000.

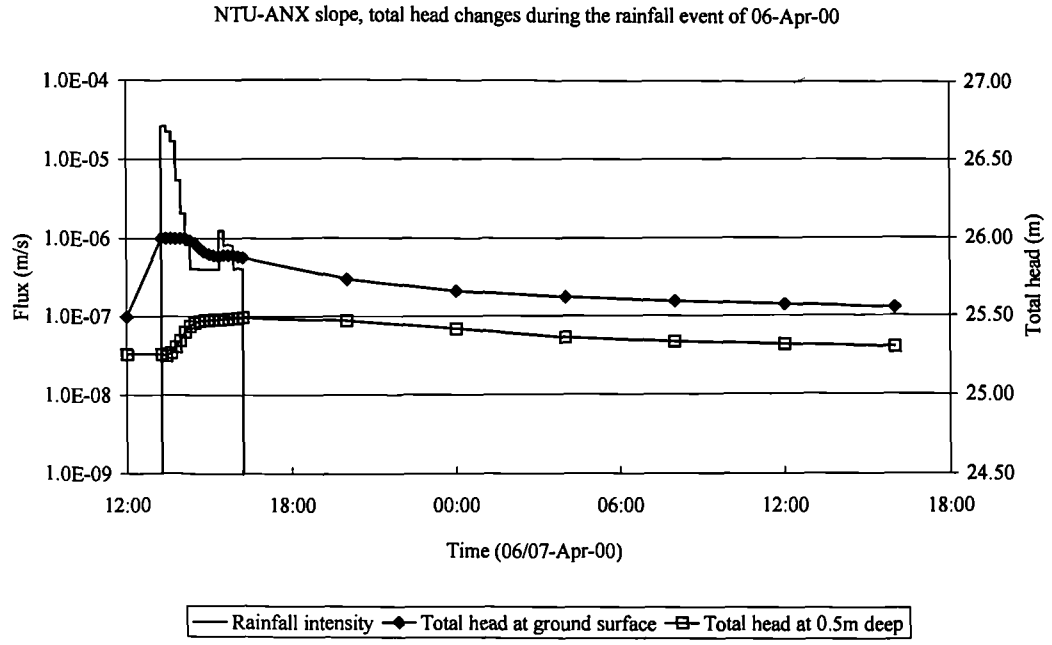

Figure 7.30 Changes of total head at the ground surface and at 0.5m deep during the rainfall event of 06 April 2000.

The sharp decrease of the infiltration rate during the 06 April 2000 rainfall event (Figure 7.28) can be explained by considering the total head changes at the ground

surface and 0.5m deep. Figure 7.30 presents the development of total heads at the ground surface and at 0.5m deep. From Figure 7.30 it can be seen that the total head at 0.5m deep started to increase soon after the start of the rainfall. Since the total head at the ground surface becomes constant and equal to the elevation head (the pore-water pressure at the ground surface becomes zero), then as the total head at 0.5m increases the hydraulic gradient at the ground surface will decrease. Thus the infiltration rate at the ground surface will decrease due to the lack of a significant potential difference (expressed as total head).

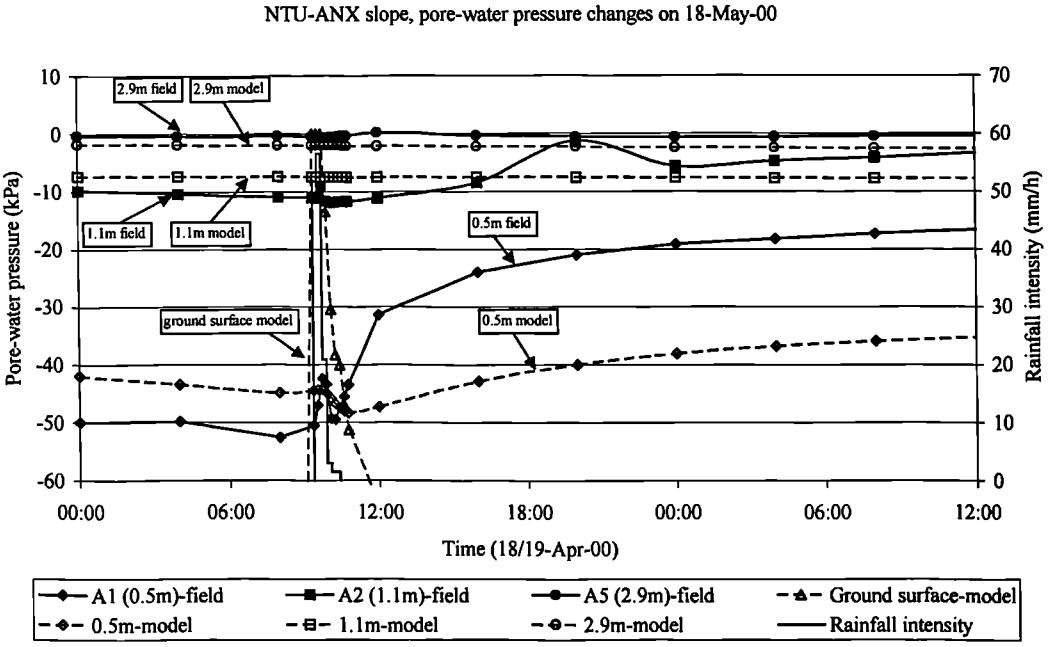

Figure 7.31 Pore-water pressure changes with time during the rainfall event of 18 May 2000, as predicted by the numerical model.

Figure 7.31 presents the predicted pore-water pressure development during the 18 May 2000 rainfall event (when the slope was at its driest conditions). The rainfall event of 18 May was 23mm and the predicted total infiltration was 3mm. Unfortunately for the 18 May 2000 rainfall event no field measurements of runoff are available. During 18 May 2000, the pore-water pressures are very low (Figure 7.31). At the ground surface the numerical model predicted a pore-water pressure approximately –350kPa and at 0.5m deep pore-water pressures were approximately –45kPa. The rainfall event caused the pore-water pressures at 0.5m deep to increase gradually from –45kPa to –17kPa. At the same time pore-water pressures at larger

depths did not increase significantly (Figure 7.31).

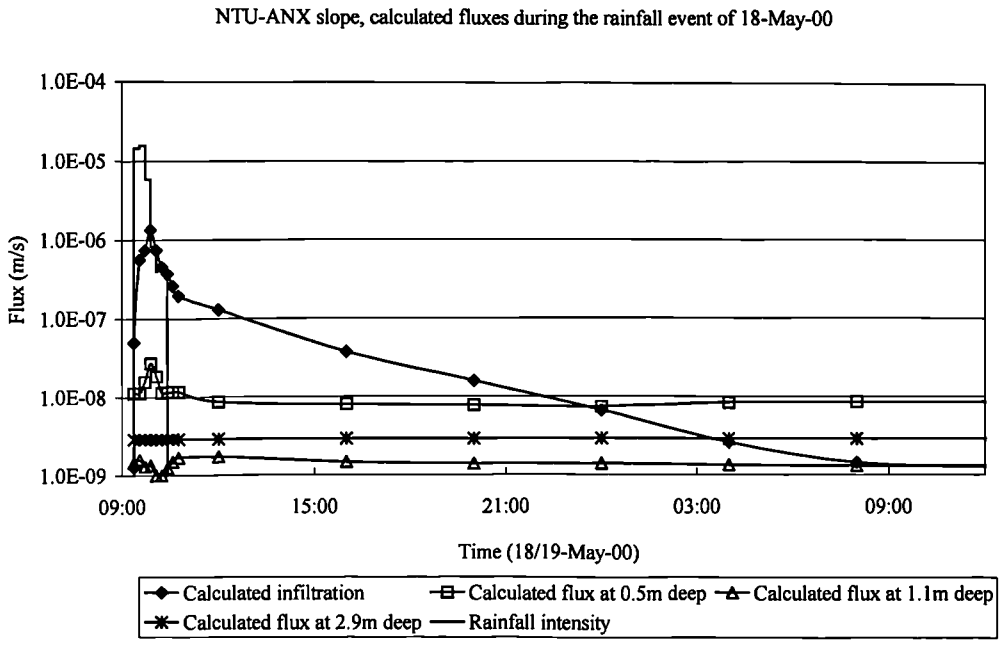

Figure 7.32 Calculated flux during the rainfall event of 18 May 2000.

The pore-water pressure changes of Figure 7.31 also reflect the water movement within the slope, expressed as fluxes in Figure 7.32. At the ground surface high infiltration rates were achieved (Figure 7.32) and some low flux can also be seen at 0.5m deep. At larger depths very low flux were observed. Figure 7.33 presents the development with time of the infiltration rate at the ground surface, the flux rate at 0.5m deep and the changes with time of the permeability at the ground surface and at 0.5m deep. Figure 7.34 presents the changes in total head at the ground surface and at 0.5m deep, as predicted by the numerical model. From Figure 7.33, it can be seen that both at the ground surface and at 0.5m deep the calculated fluxes are significantly higher than the permeability of the soil. That means that the hydraulic gradients are also very high. The high hydraulic gradient during the rainfall event of 18 May 2000 can also be concluded by observing the difference in total head between the ground surface and at 0.5m deep (Figure 7.34). Initially, the total head at the ground surface was negative (Figure 7.34), due to the very low pore-water pressure equal to -350kPa. As rainfall was precipitated on the slope and the pore-water pressure at the ground surface became zero, the total head at the ground surface became to equal to elevation (26m). At the same time the maximum total

head at 0.5m deep, that was predicted was only 24m. The minimum difference of 2m in total head between the ground surface and at 0.5m deep resulted in a high hydraulic gradient and thus in flux rates at 0.5m deep that are significantly larger than the permeability of the soil. Under such conditions it may be possible to achieve flux rates that are great than the permeability of the soil, however a flux rate will still be affected by the permeability values. In other words, if the coefficient of permeability of the soil is very low, then the flux rate will also be relatively low (even if it is somewhat greater than the permeability value). For that reason a large amount of the rainfall water could not infiltrate into the slope, but would run off. In addition, the pore-water pressures at large depths are significantly higher than at 0.5m deep (Figure 7.31). Thus the total head at large depths will not be significantly lower than at 0.5m deep and therefore no conditions for high flow potential existed. This justifies why infiltrated water did not reach large depths within the slope.

Considering the analyses of the infiltration mechanisms during different initial conditions it can be seen that the initial pore-water pressure close to the ground surface is a controlling parameter of the total infiltration. Figure 7.35 presents the contours (dimensionless) of the total infiltration as a ratio of total rainfall for different total rainfall and different initial pore-water pressure at 0.5m deep. The contours of Figure 7.35 are derived for the predictions of the total infiltration generated by the numerical model.

The contours of Figure 7.35 show that the effect of the initial pore-water pressure at 0.5m deep affects the rate of total infiltration versus total infiltration in a complex way. Low initial pore-water pressure at 0.5m deep lead to small amounts of infiltration (as a percentage of total rainfall). As the initial pore-water pressure at 0.5m deep increases then the total infiltration increases. However, for positive initial pore-water pressures only small amount of rainfall water infiltrate the slope.

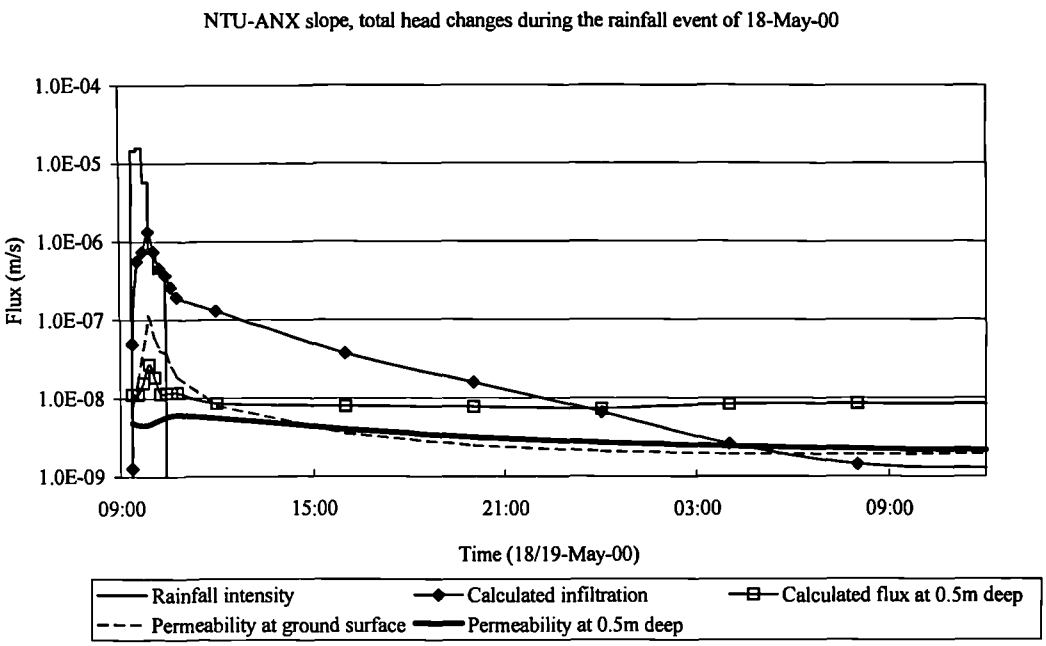

Figure 7.33 Calculated infiltration flux at the ground surface and at 0.5m deep and permeability changes during the rainfall event of 18 May 2000.

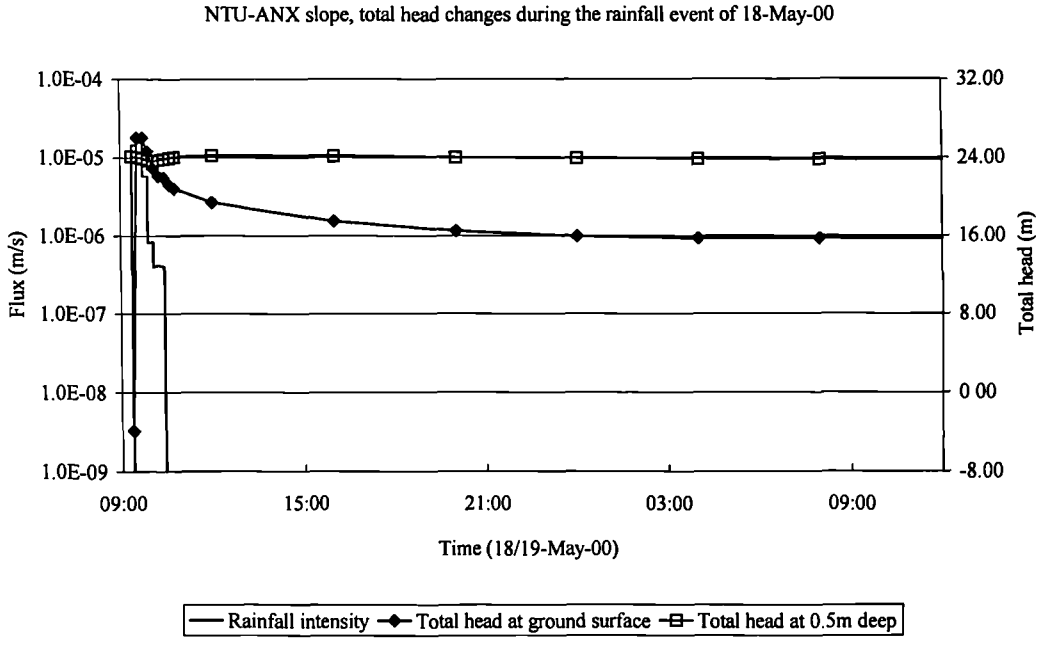

Figure 7.34 Changes of total head at the ground surface and at 0.5m deep during the rainfall event of 18 May 2000.

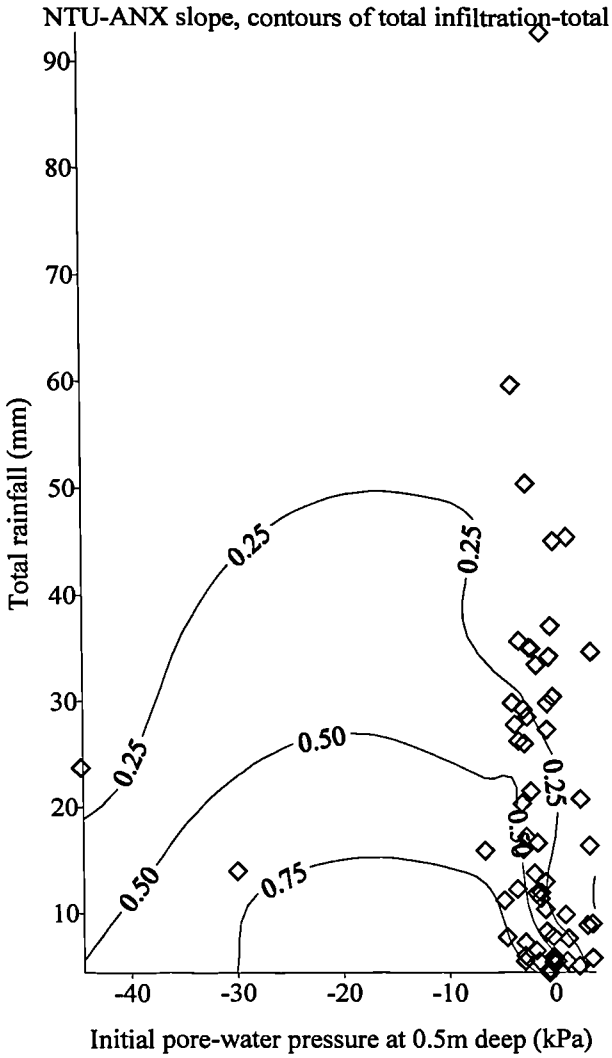

Figure 7.35 Contours of total infiltration-total rainfall ratio for different total rainfall and different initial pore-water pressure at 0.5m deep as predicted by the numerical model.

The above analysis demonstrates that the way infiltration takes place is affected by several parameters. It can be seen that the rainfall intensity affects the rate under which rainwater will infiltrate the slope. At the same time the infiltration rate at the ground surface is also controlled by the permeability of the soil at 0.5m deep. As the permeability of the soil at 0.5m deep increases a higher infiltration rate can be achieved. At the same as the pore-water pressure at 0.5m deep increases the total head at 0.5m deep increases. Since the total head at the ground surface of the slope becomes maximum very soon after the end of the rainfall, then as the total head at 0.5m deep increases the hydraulic gradient at the ground surface will start to decrease. Small differences of total head (i.e. low hydraulic gradient) between the ground surface and 0.5m deep leads to a decrease in groundwater movement from

the ground surface towards larger depths, thus the infiltration rate decreases.

Runoff measurements from the NTU-ANX slope, as they were discussed in Chapter 5 (Section 5.2.2), indicated that the NTU-ANX slope appears to have a 'capacity' of how much rainfall water could infiltrate the slope. The results from the numerical model demonstrate that this apparent 'capacity' of a limiting amount of infiltration can be attributed to the increase of total heads near the ground surface that reduce the infiltration rate to a low level.

7.3.2 The effect of rainfall, infiltration and the initial conditions on the pore-water pressure changes

In Chapter 5 (Section 5.2.3) the pore-water pressure changes at 0.5m, 1.1m, 1.7m and 2.9m deep (as they were measured in NTU-ANX slope) were analysed in terms of total rainfall. The effect of the initial values of the pore-water pressures was also discussed. The analysis in Section 5.2.3 showed that pore-water pressure changes at 0.5m deep were significant for rainfall events up to 25mm (Figure 5.29). As total rainfall increases beyond the 25mm, then the pore-water pressures at 0.5m deep were affected largely by their initial values. At larger depths it was seen that pore-water pressure changes were relatively limited (Figure 5.29). In this section the analysis of pore-water pressure changes, as predicted with the numerical model, are analysed in terms of total rainfall and also in terms of total infiltration for comparison with these field observations.

Figure 7.36 presents the contour plots (in kPa) of the final pore-water pressures at 0.5m deep for different total rainfall (Figure 7.36a) and infiltration (Figure 7.36b) and for different values of the initial pore-water pressure. The contours of Figure 7.36a show that for low initial pore-water pressures, rainfall causes larges changes to the pore-water pressure at 0.5m deep. For high initial values of the pore-water pressure, total rainfall causes less significant changes to the pore-water pressure. In addition, the total rainfall has a major impact on the pore-water pressure changes at 0.5m deep. As total rainfall increases the pore-water pressure changes are not increasing by large amounts. The transition in the behaviour can be identified at approximately 25mm of total rainfall. This behaviour is attributed to the fact that the

amount of rainfall that will infiltrate into the slope is not increasing further as total rainfall exceeds a value between 25mm to 30mm.

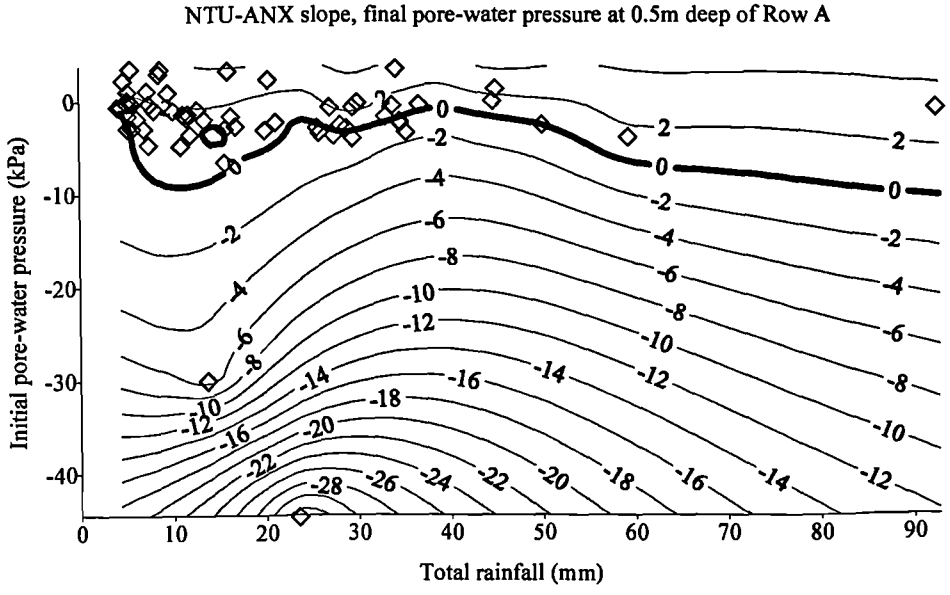

a)

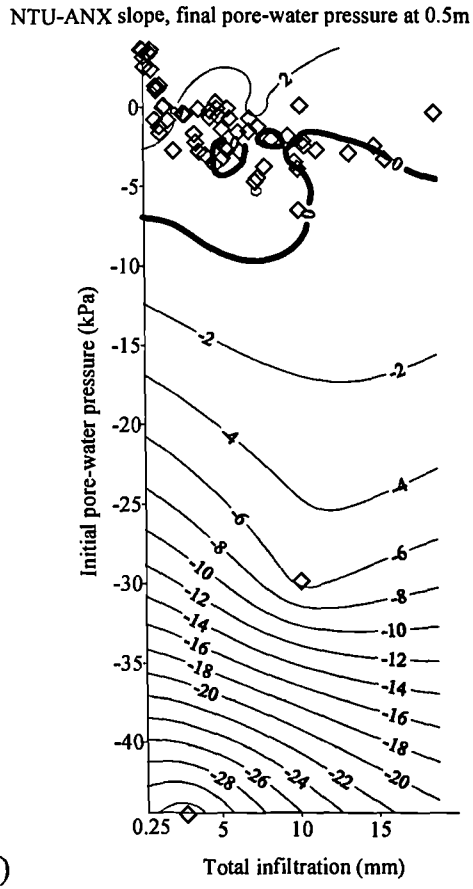

b)

Figure 7.36 Contour plots (in kPa) of the final pore-water pressure at 0.5m deep, of row A of the numerical model for different initial pore-water pressures and a)for different total rainfall and b) for different total infiltration.

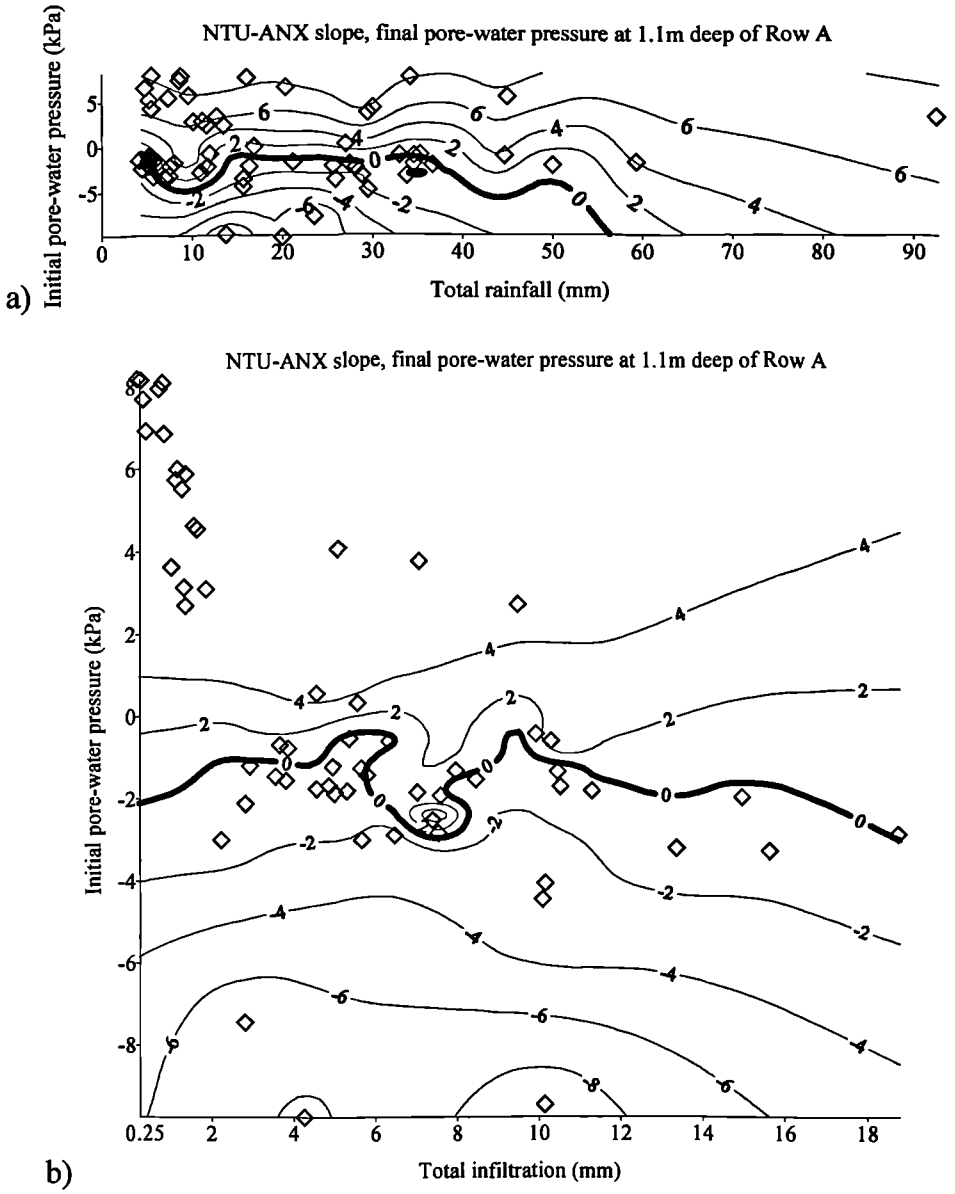

Figure 7.37 Contour plots (in kPa) of the final pore-water pressure at 1.1m deep, of row A of the numerical model for different initial pore-water pressures and a)for different total rainfall and b) for different total infiltration.

The contours of Figure 7.36a show a similar trend with the contours of Figure 5.29. The contours (in kPa) (Figure 7.36b) of the final pore-water pressure at 0.5m deep for different total infiltration and different initial values of the pore-water pressures, show large changes of the pore-water pressures for low initial values and smaller changes as the initial pore-water pressure increases.

The contours of the final pore-water pressure at 1.1m, 1.7m and 2.9m deep (Figure 7.37 to Figure 7.39) show that pore-water pressures at large depths do not change

significantly during rainfall (or infiltration). These results are also in good agreement with the field observations (Figure 5.29).

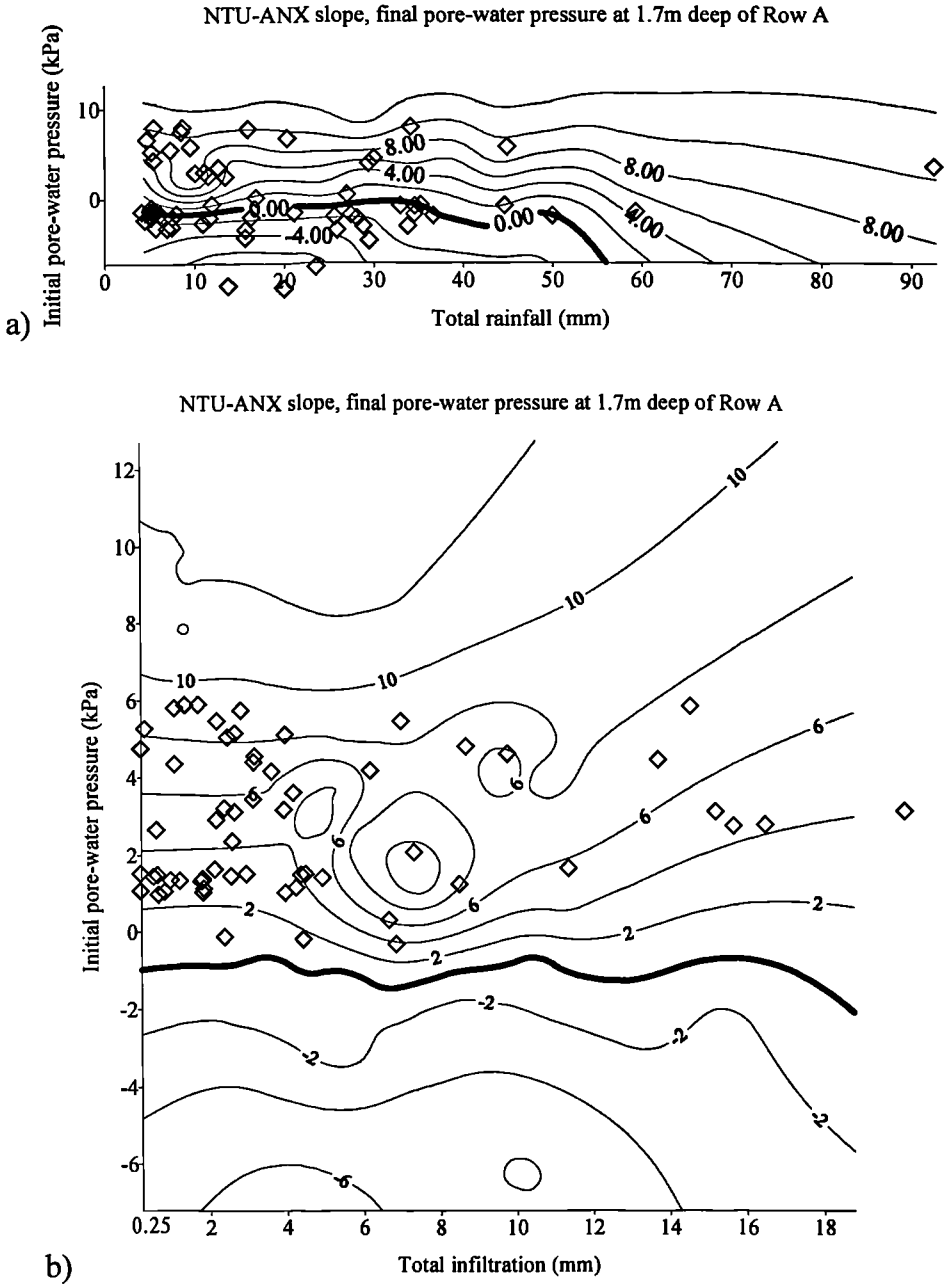

Figure 7.38 Contour plots (in kPa) of the final pore-water pressure at 1.7m deep, of row A of the numerical model for different initial pore-water pressures and a)for different total rainfall and b) for different total infiltration.

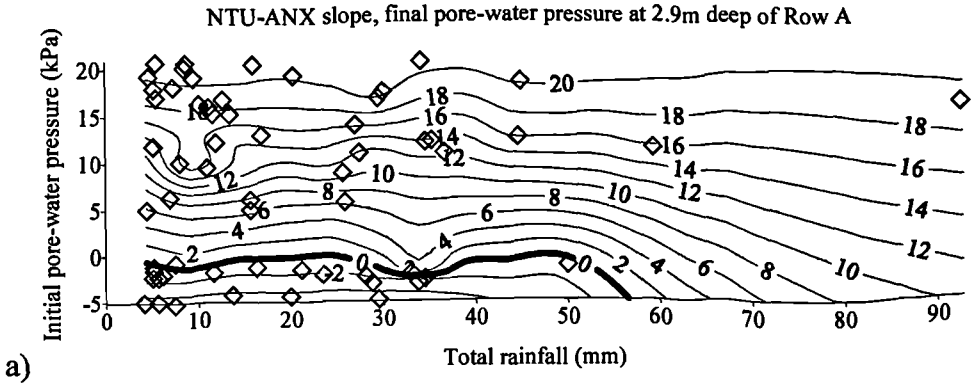

a)

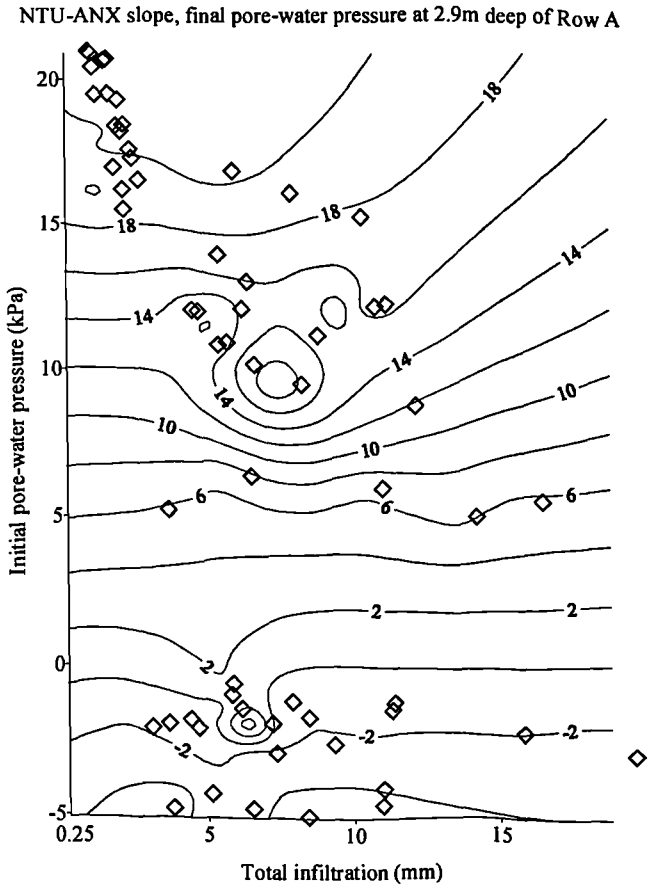

b)

Figure 7.39 Contour plots (in kPa) of the final pore-water pressure at 2.9m deep, of row A of the numerical model for different initial pore-water pressures and a)for different total rainfall and b) for different total infiltration.

7.4 Final remarks of the numerical analysis

The objective of the analysis presented in this chapter was to use a numerical model to simulate the field observations from the NTU-ANX slope (pore-water pressure changes and runoff measurements). The runoff measurements on the NTU-ANX

slope show that a large portion of the rainfall water infiltrates the slope, suggesting that the slope surface is relatively permeable. At the same time, in situ measurements of the saturated coefficient of permeability of the soil with respect to water (k_{sat}) showed that the soil within the slope has a low coefficient of permeability. The difference in the observations is attributed to the surficial vegetation. In order to couple both sets of information in the numerical analysis, a thin permeable soil layer was defined at the ground surface. With this adjustment the model performed well and the infiltration and runoff results were in reasonable agreement with the field data.

The predictions of the pore-water pressure changes are also comparable with the field measurements at the NTU-ANX slope, although there is some discrepancy at large depths (1.7 and 2.9m deep). Overall, the numerical model predicted similar trends in the pore-water pressure changes to the field measurements. Finally, it has to be noted that despite the fact that the overall trends of the field measurements were reproduced with the numerical model in an adequate way, the numerical model cannot fully model a number of variables such as vegetation or initial abstraction.

The analysis is based on the mechanism that rainfall water infiltrates the slope up to a maximum rate, which is controlled by the coefficient of permeability with respect to water and the hydraulic gradient and the excess disappears as runoff. Infiltrated water seeps into the slope causing the pore-water pressures to increase towards positive values. If the initial pore-water pressures near the ground surface are low then initially small amounts of rainfall water will infiltrate the slope. Infiltration rate will increase as the soil near the ground surface gets wet (increase of the permeability). As pore-water pressures near the ground surface increase towards positive values then infiltration rate start to decrease. If pore-water pressures are high then due to lower hydraulic gradients at the ground surface, only small amounts of rainfall water will infiltrate the slope.

CHAPTER 8

Conclusions and Recommendations for Future Work

The study presented in this work was divided in two parts. The first part concerned the presentation of the field monitoring that took place on two instrumented residual soil slopes in Singapore and the discussion of the field measurements (Chapters 3 to 5). The first part also included the presentation of soil-water characteristic curves produced in the laboratory using pressure plates, of soil samples from the two instrumented slopes. The second part of the present work concerned the numerical modelling of the seepage conditions within a residual slope (Chapters 6 and 7).

This chapter presents a summary of the main conclusions of the analyses that were carried out in previous chapters. Some recommendations on where attention should be focused in future research studies are also included in this chapter.

8.1 Conclusions

Two residual soil slopes were instrumented for field monitoring. The two slopes are called NTU-CSE and NTU-ANX slopes and are located on the Nanyang Technological University (NTU) in the west part of Singapore. The slopes are comprised of residual soils from the Jurong Sedimentary Formation. These residual soils are mainly of medium plasticity clayey silt, sandy clay and clayey to silty sand materials.

The monitoring period of the NTU-CSE slope was 12 months long (from August 1999 to August 2000). The monitoring period of the NTU-ANX slope lasted for 6 months (from March to August 2000). Negative pore-water pressures were measured at several locations of the two slopes using jet fill tensiometers installed at various depths to 3.2m deep. Rainfall was recorded on both research slopes using rainfall gauges. Piezometers were installed on the two slopes and the fluctuation of the level of the groundwater table was monitored. On the NTU-ANX slope runoff measurements of natural and simulated rainfalls were also measured.

Generally, the instrumentation and the data acquisition system performed well and at

the end of the monitoring period on both research slopes, consistent sets of data were produced. However, the installation and operation of the instrumentation was a difficult task and continuous maintenance was required.

8.1.1 Field observations at the NTU-CSE slope

The pore-water pressures near the ground surface of the NTU-CSE slope were seen to become very low, during long dry periods, but during rainfall become positive. The minimum pore-water pressures near the ground surface (i.e. 0.5m to 1.1m deep) reduced below –70kPa. During wet periods, the pore-water pressure at NTU-CSE slope often became positive reaching hydrostatic values of pressure. However, pore-water pressures near the ground surface at the crest of the NTU-CSE slope retained negative values during the whole monitoring period. The range of the pore-water pressures measurements at large depths (i.e. 2.3m to 3.2m deep) at the NTU-CSE slope was smaller in comparison with the range of measurements near the ground surface.

The analysis of the pore-water pressure changes at the NTU-CSE slope showed that the changes in the pore-water pressures were not entirely dependent on the total rainfall but also on the initial pore-water pressure values. When the pore-water pressures were high, with positive values, and the rainfall event was of a long duration and intensive, only limited changes were observed (especially near the ground surface). The pore-water pressures close to the ground surface, might remain constant after they had reached a peak value during the rainfall. At greater depths, it took a long time before the pore-water pressures started to increase. For the cases of highly negative pore-water pressures it was found that the pore-water pressures near the ground surface were very sensitive even to a very small amount of rainfall. When pore-water pressures were low the increase of pore-water pressures was significant.

The pore-water pressure changes during rainfall near the ground surface of the NTU-CSE slope showed that for rainfall events up to 15mm pore-water pressures were highly affected by the rainfall. As total rainfall increases beyond 15mm, then pore-water changes near the ground surface did not increase significantly further.

The pore-water pressure increase near the ground surface during rainfall exceeding 15mm was controlled to a great extent by the initial value of pore-water pressure. At larger depths, pore-water pressure changes were generally limited in comparison with the pore-water pressure changes near the ground surface.

The slope stability analyses, which were conducted for the two extreme cases, when the pore-water pressures near the ground surface of the slope were at maximum and when the pore-water pressures near the ground surface were at minimum, show that the critical slip failure lies at shallow depths at the crest of the slope. The location of the predicted critical slip failures is attributed to the low strength parameters of the soil at the crest of the slope in comparison with the defined strength parameters of the soil layers in the rest of the slope. Nevertheless, the increase of the pore-water pressures due to rainfall along the critical failure surface for both extreme cases has caused a considerable decrease to the calculated factor of safety.

8.1.2 Field observations at the NTU-ANX slope

The analysis of the runoff measurements of the NTU-ANX slope, for both natural and simulated rainfall events, showed that infiltration is controlled by the total rainfall, the initial conditions and the average rainfall intensity. On average, rainfall events of total rainfall less than 8mm did not produce any runoff and all the rainfall water infiltrated the slope. As a trend, it was concluded that the higher the total rainfall is the great amount of runoff will be produced.

The runoff measurements on the NTU-ANX slope showed that there is a poor relationship between the total rainfall and total infiltration. However, the runoff data showed that as total rainfall increased from zero to approximately 25mm, total infiltration increased towards a maximum value of 20mm. As total rainfall increased further above 25mm total infiltration started to decrease towards a minimum value of 4mm.

The pore-water pressures near the ground surface (i.e. 0.5m deep) of the NTU-ANX slope could go as low as –65kPa. However, during rainfall such low pore-water pressures could not be sustained, but increased by large magnitudes towards positive

values. When pore-water pressures near the ground surface of the NTU-ANX slope were high then even if an intense, major rainfall event took place, no significant increase of the pore-water pressures was observed. In general, the final pore-water pressure after a rainfall event was highly controlled by total rainfall up to 25mm. For total rainfall greater than 25mm the pore-water pressure changes did not increase significantly more. This behaviour of the pore-water pressures was attributed to the fact that for rainfall events greater than 25mm the total infiltration did not increase any further. At large depths (i.e. 2.9m deep) no significant changes in the pore-water pressures were observed, indicating that only small amounts of rainfall water reach these depths.

The slope stability analyses of the NTU-ANX slope showed that the factor of safety corresponding to the best and the worst conditions differ significantly. The difference in the predicted factor of safety of the NTU-ANX slope between the two extremes was attributed to the existence of the negative pore-water pressures, which play an important role in the stability of the slope. In addition the predicted critical failure surface was shallow where the wetting front during rainfall was developing.

8.1.3 Controlling parameters for rainfall-induced slope failures

As part of the numerical modelling of the seepage conditions within a residual slope, a parametric study was conducted. The objective of the parametric study was to investigate the influence of rainfall intensity, different distributions of antecedent rainfall, different initial conditions and saturated coefficients of permeability with respect to water on the seepage conditions in a residual soil slope in Singapore.

The analyses showed the worse conditions for slope instability occur when a major rainfall event was distributed over a long period. If a major rainfall event was distributed over a short period (i.e. as a very intense rainfall) it was not the worse case. It was also seen that the ratio of rainfall intensity to saturated coefficient of permeability of the soil was a controlling parameter on the evolution of the pore-water pressures. For a given intensive rainfall event, the higher the coefficient of permeability was the more significant the increase of the pore-water pressures would

be.

Several simulations with different saturated coefficients of permeability with respect to water showed that this parameter controls significantly the infiltration process in the slope. Highly permeable soil slopes are unlikely to be influenced by small amounts of antecedent rainfall. The infiltration process during a major rainfall event can be affected by antecedent rainfall if a slope is composed of a moderately permeable soil. For a slope that is composed of a moderately permeable soil, different distributions of antecedent rainfall over a 5-day period prior to the major rainfall event can affect the seepage conditions even if its amount is very small in comparison to the major rainfall. Finally, if the soil permeability with respect to water is very low then the pore-water pressures may not change significantly during the rainfall, but they can start increasing towards positive values after the end of the wet period.

The slope stability analyses for different distributions of the major rainfall showed that the longer the period over which the rainfall is distributed, the lower the FoS of the slope will be. Different distributions of the antecedent rainfall can also affect significantly the stability of the slope. It was seen that in the scenario where the antecedent rainfall was distributed evenly over a 5-day period the FoS drops below 1.0. For a permeable soil, with $k_{sat}=10^{-4}$m/s, it is likely that the slope would become unstable under conditions of heavy rainfall with or without antecedent rainfall. In addition, for a highly permeable soil ($k_{sat}=10^{-4}$m/s) the effect of different distribution of the same total rainfall is small on the FoS in comparison with the case of a moderately permeable soil ($k_{sat}=10^{-5}$m/s). Finally, as the saturated coefficient of permeability with respect to water increases the antecedent rainfall and the major rainfall have a more significant effect on the stability of slope.

8.1.4 Numerical modelling of the infiltration characteristics of the NTU-ANX slope

A numerical model was used to represent the seepage conditions of the NTU-ANX slope. The numerical modelling adopted all the available information from the field (pore-water pressure and runoff measurements) and the laboratory (soil-water

characteristic curve). The preliminary analysis identified the need to represent more realistically the ground surface of the slope, which was expected to be more permeable than the soil at greater depths due to cracks, discontinuities and the surficial vegetation. Therefore, a thin permeable soil layer was defined at the ground surface. With this adjustment, the model performed well and the results were in reasonable agreement with the field data. Overall, the numerical model predicted similar trends in the pore-water pressure changes and the total infiltration to the field measurements.

The results of the numerical model were used in order to describe the infiltration mechanism of the slope. The results of the numerical model showed that infiltration occurs in a complex way. The analysis showed that it is possible to achieve infiltration at rates greater than the coefficient of permeability of the soil. If there is a large difference of pore-water pressure between the ground surface and at depths close to the ground surface (e.g. 0.5m deep) then the hydraulic gradient becomes greater than one and thus an infiltration rate greater than the coefficient of permeability is possible. On the other hand, as the difference of pore-water pressure between the ground surface and at 0.5m deep decreases, the hydraulic gradient will be small. Therefore, infiltration at the ground surface will occur at small rates, even if the rainfall intensity is very high. This means that the slope appears to have a capacity for how much water can infiltrate the slope. A large rainfall will not automatically lead to high infiltration.

The predictions of the pore-water pressure changes are also comparable with the field measurements at the NTU-ANX slope, although there is some discrepancy at large depths. The field observations from the NTU-ANX slope on the effect of rainfall (in terms of total rainfall and total infiltration) on the pore-water pressures near the ground surface of the slope were also verified using the results of the numerical model. In addition, the numerical model predicted similar effects of the initial values of the pore-water pressure changes (i.e. at the start of a rainfall event) on the final pore-water pressures.

Finally, it has to be noted that despite the fact that the overall trends of the field measurements were reproduced with the numerical model in an adequate way, the

numerical model cannot fully model a number of variables such as vegetation or initial abstraction. Problems were also encountered with modelling the decrease of the pore-water pressures during dry periods and a number of simplifications needed to be made.

8.2 Recommendations for future work

Taking into account the conclusions of this work, it is clear that infiltration within a residual soil slope is a complex mechanism. The rainfall pattern, the hydrological properties of the surficial soil of the slope and the initial conditions (expressed either as initial pore-water pressures or antecedent rainfall) interact strongly with each other.

The runoff measurements of natural and simulated rainfall events that were undertaken on the NTU-ANX slope showed that the total rainfall is the most significant parameter that controls both the total runoff and total infiltration. However, it was seen that the direct relationship between total rainfall and total infiltration is poor since it is also dependent on other factors. It was seen that the initial conditions of the slope, expressed as antecedent rainfall, affects the total infiltration. In order to extract more firm conclusions on how other parameters, apart from the total rainfall, affect the total infiltration more data are required over long periods of times.

The field observations of the two research slopes showed that there is an upper limit of the total rainfall above which no more significant changes in the pore-water pressures will be observed. This upper limit was identified to be between 15 and 25mm for the two slopes. The runoff measurements of NTU-ANX slope also showed that total infiltration increases for rainfall up to 25mm. This was also linked with the changes of the pore-water pressure changes near the ground surface of the NTU-ANX slope. The coefficient of permeability of the surficial soil layer of the two slopes were measured to be in the range of $1x10^{-7}$m/s to $1x10^{-6}$m/s. In order to generalise these conclusions pore-water pressure changes and runoff measurements of natural or simulated rainfall events over long periods of time (e.g. 6 months or more) should be studied for more permeable slopes. Of course, for more permeable

slopes, this upper limit of the total rainfall would be expected to be higher than the one established from the present analysis.

The numerical modelling showed that the conditions on the ground surface (vegetation etc.) affect the amount of rainfall that infiltrates the slope. For that reason, runoff measurements should be accompanied with a more detailed description of the initial conditions at the ground surface. Therefore, more information is needed such as the coefficient of permeability and the initial pore-water pressures at the ground surface so as to gain a better understanding of how the infiltration mechanism really works. Despite the fact that, with the definition in the numerical model of a thin permeable soil layer at the ground surface that will represent vegetation, the numerical predictions were comparable with the field measurements, a better justification for the surficial values of permeability is required.

The numerical analysis showed that there are serious limitations in realistically modelling the recovery of the negative pore-water pressure during dry periods. The numerical analysis of the NTU-ANX slope showed that the hysteresis of the soil-water characteristic curve does not significantly affect the recovery of the negative pore-water pressures during the drainage of the slope. Nevertheless, this needs further investigation with different soil-water characteristic curves, as this conclusion may not be true for soils showing greater hysteresis.

In order to establish a numerical model to simulate field pore-water pressure conditions, evaporation needs to be inserted in the analysis. For that reason, evaporation measurements together with weather conditions and soil conditions at the ground surface are required. What is more, inserting evaporation in a numerical model as a negative flux does not represent truly the way in which evaporation really operates. Therefore, more work in developing constitutive models that can properly handle drying conditions is needed.

Finally, the influence of the soil-water characteristic curve on the seepage conditions within a slope should also be investigated. This study has focused on residual soils from Singapore. While some of the conclusions may well be applicable to a wider

range of materials, this should be investigated both experimentally and numerically.

APPENDIX A

Pore-Water Pressures of the NTU-CSE Slope

NTU-CSE slope, pore-water pressures of Row A during August 1999

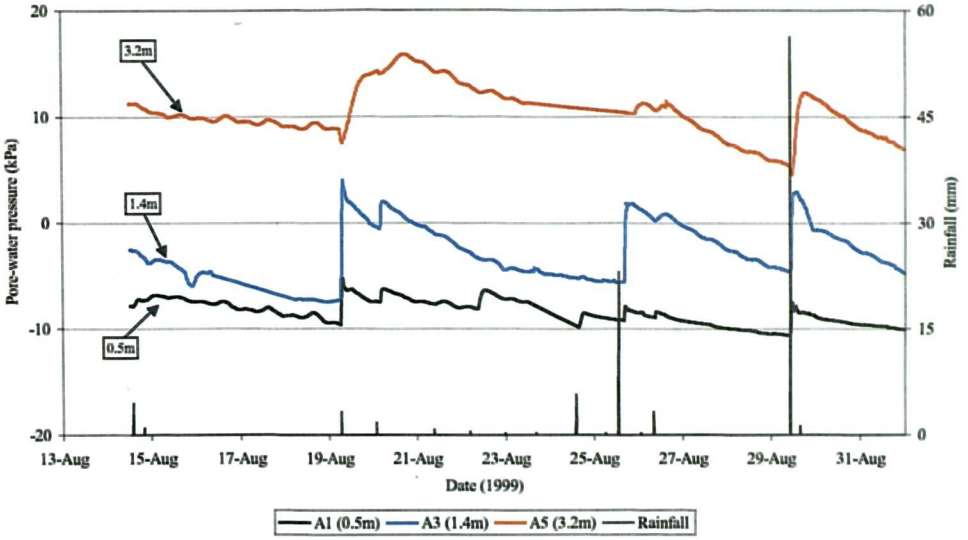

NTU-CSE slope, pore-water pressures of Row B during August 1999

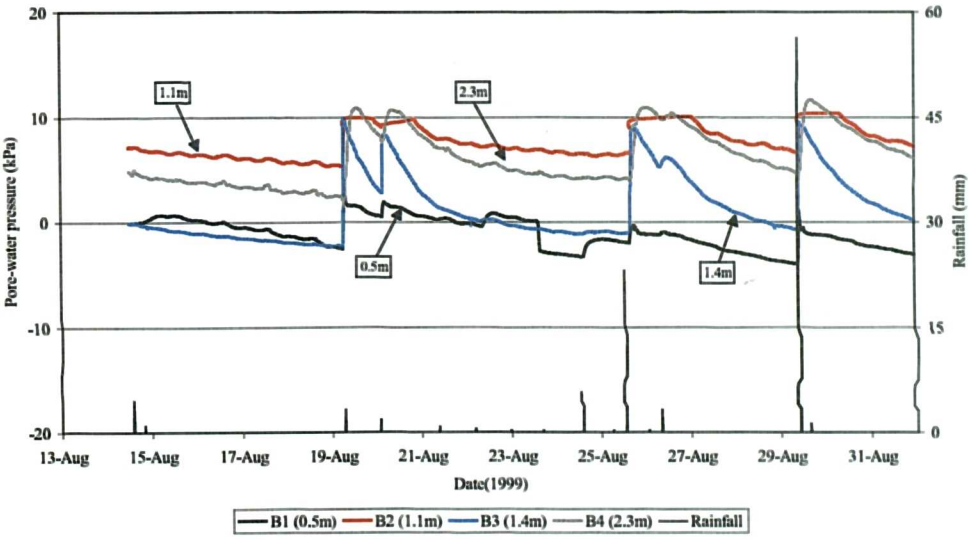

NTU-CSE slope, pore-water pressures of Row C during August 1999

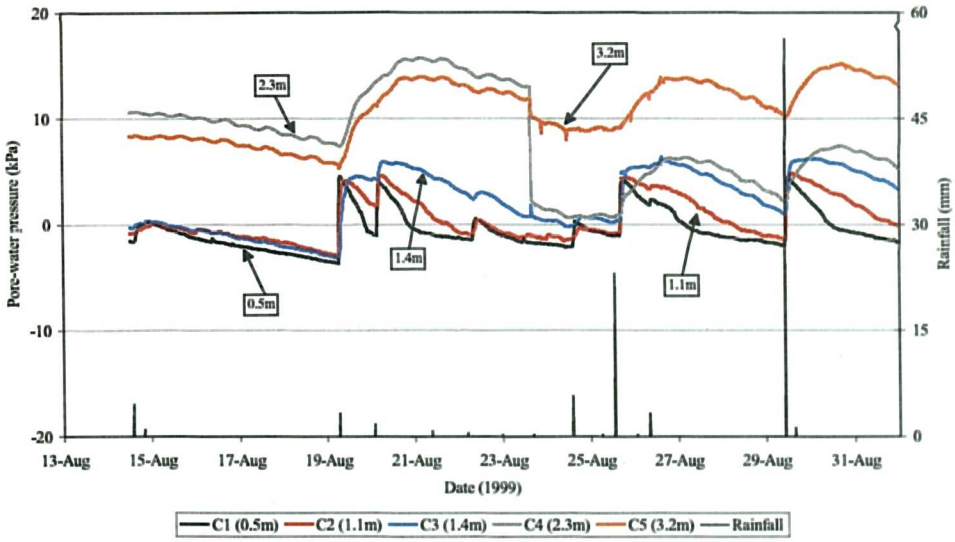

NTU-CSE slope, pore-water pressures of Row D during August 1999

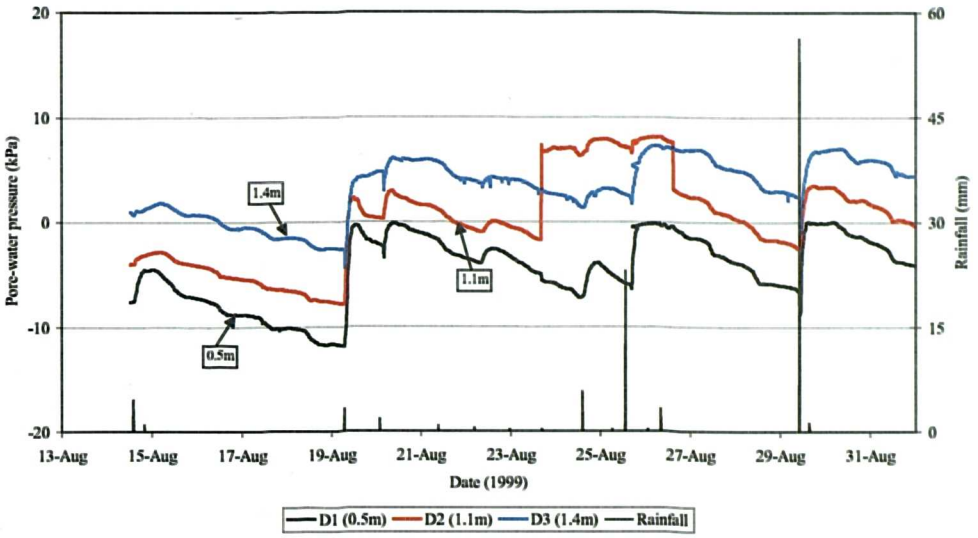

NTU-CSE slope, pore-water pressures of Row E during August 1999

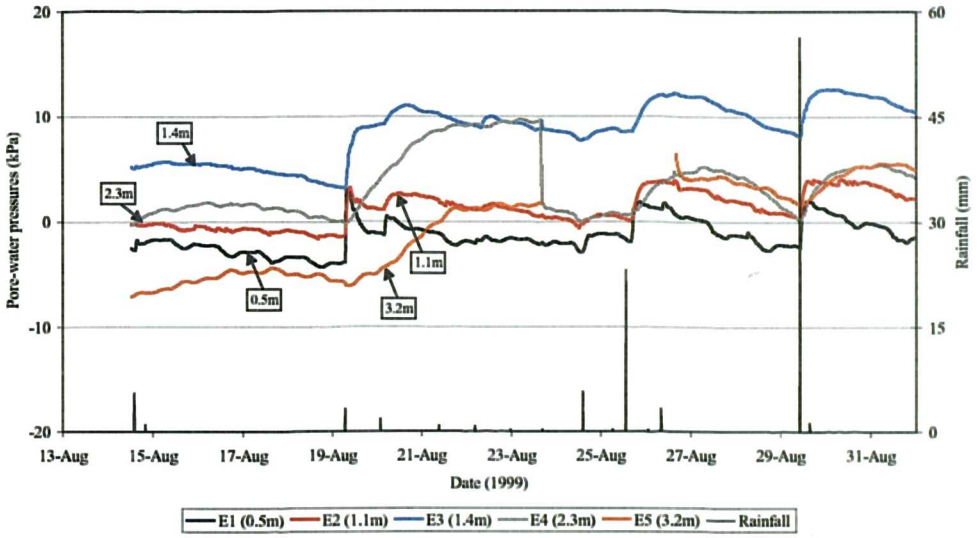

NTU-CSE slope, pore-water pressures of Row F during August 1999

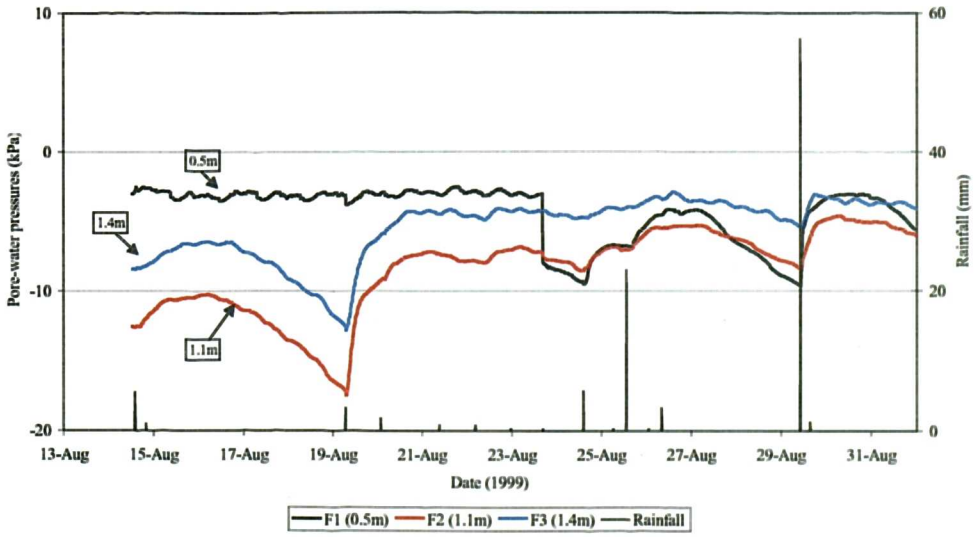

NTU-CSE slope, pore-water pressures of Row A during September 1999

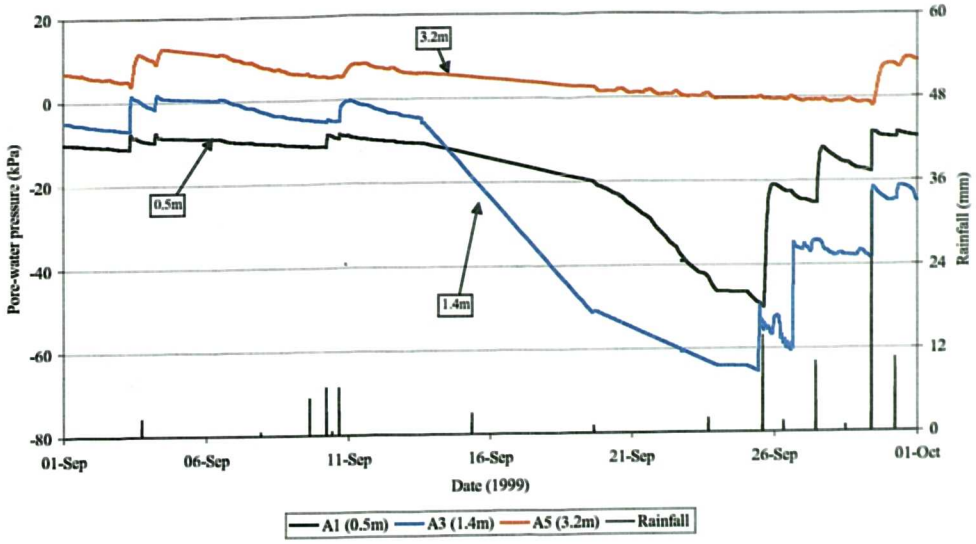

NTU-CSE slope, pore-water pressures of Row B during September 1999

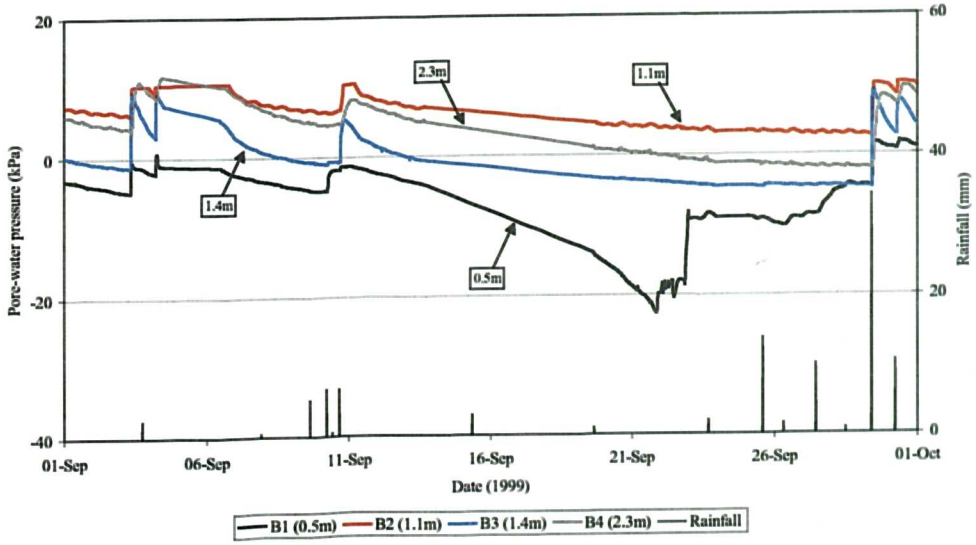

NTU-CSE slope, pore-water pressures of Row C during September 1999

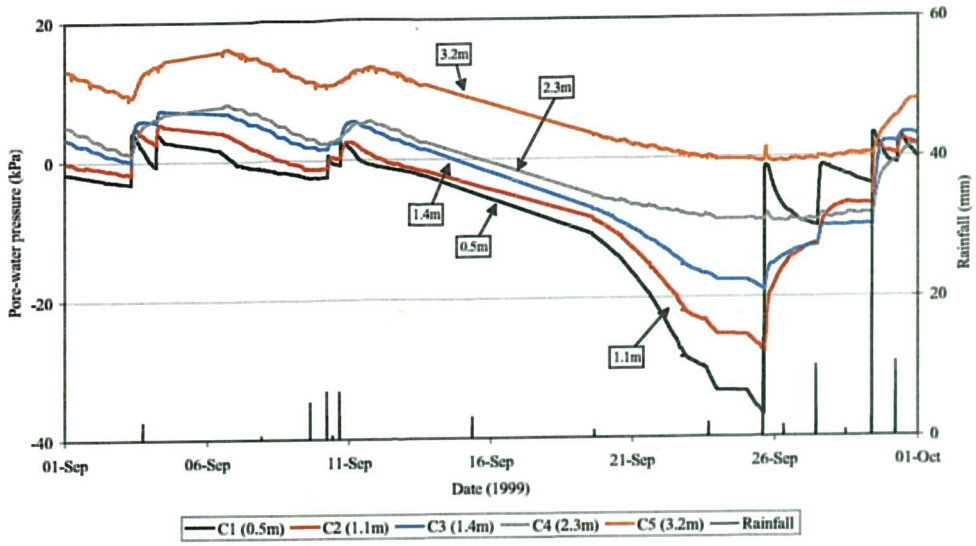

NTU-CSE slope, pore-water pressures of Row D during September 1999

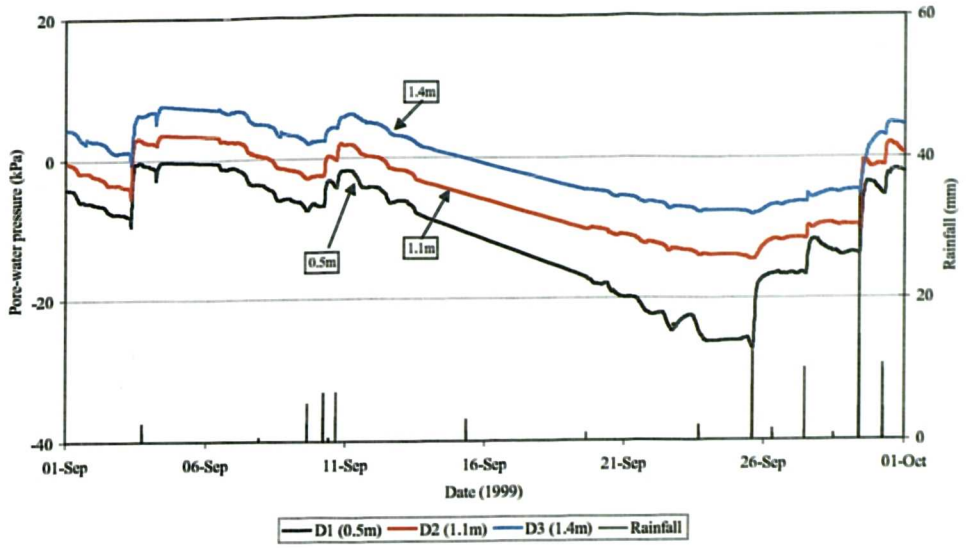

NTU-CSE slope, pore-water pressures of Row E during September 1999

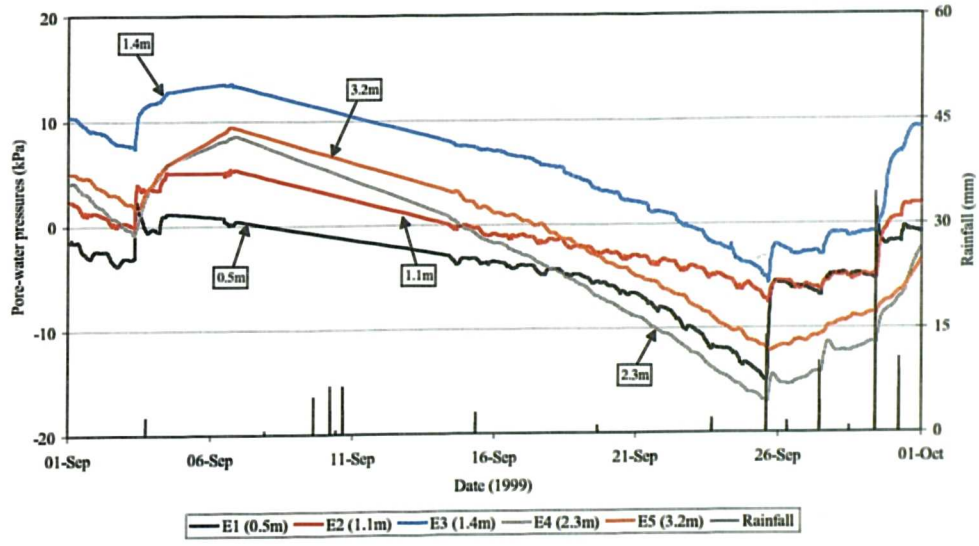

NTU-CSE slope, pore-water pressures of Row F during September 1999

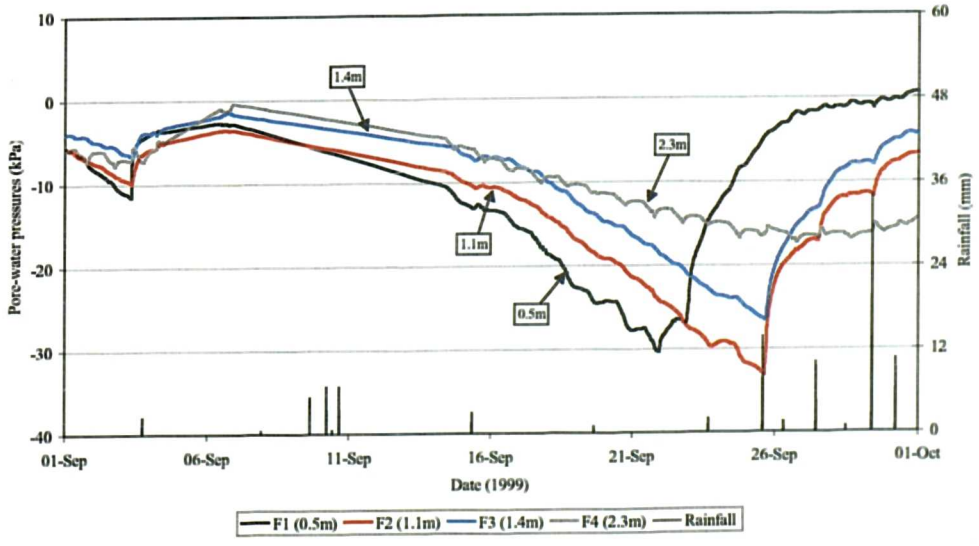

NTU-CSE slope, pore-water pressures of Row A during October 1999

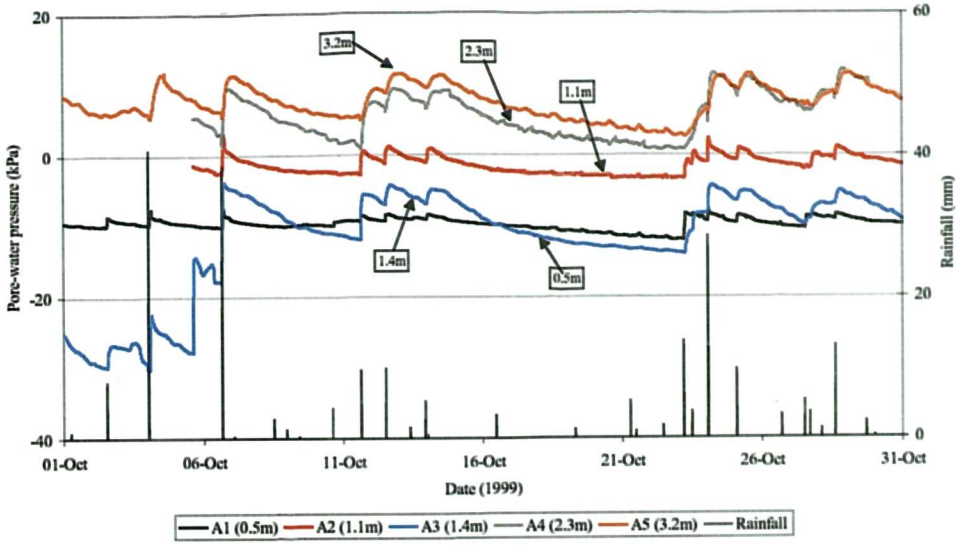

NTU-CSE slope, pore-water pressures of Row B during October 1999

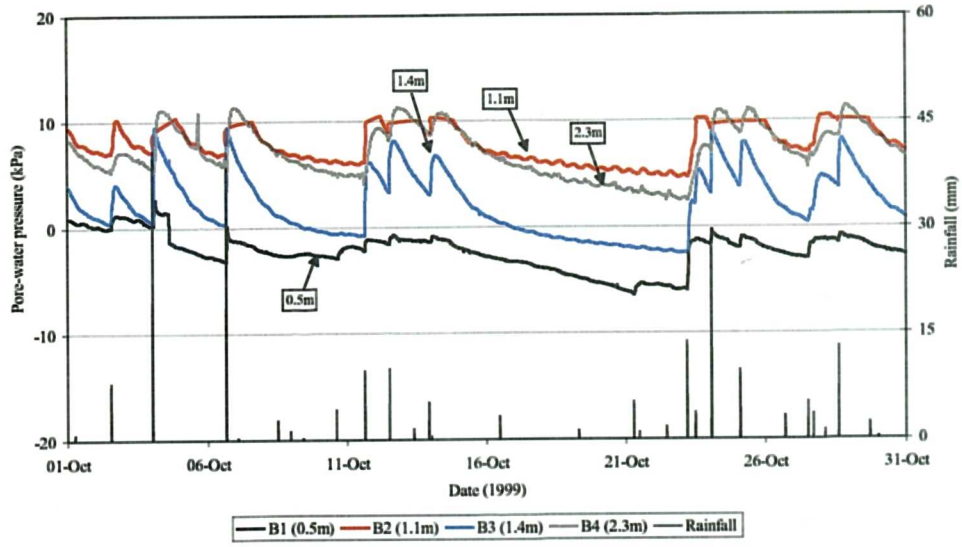

NTU-CSE slope, pore-water pressures of Row C during October 1999

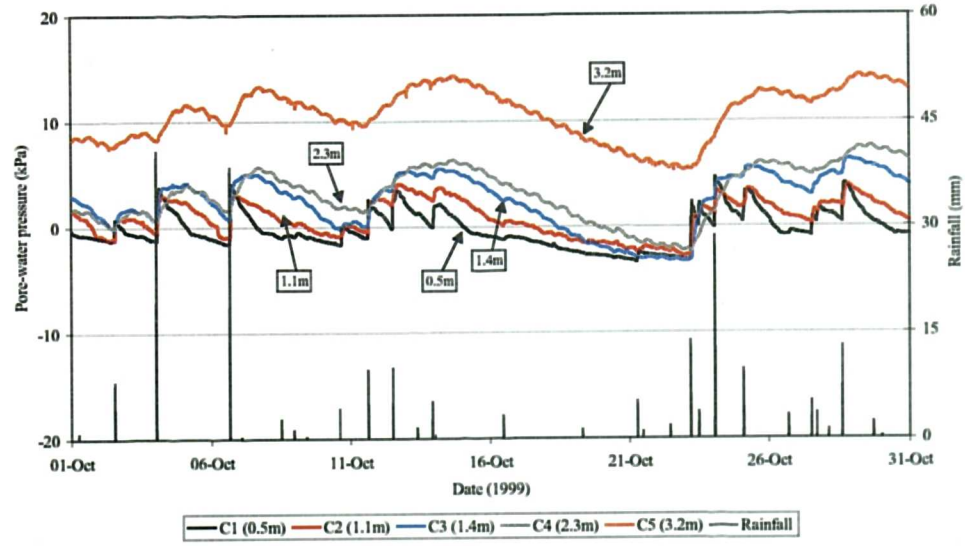

NTU-CSE slope, pore-water pressures of Row D during October 1999

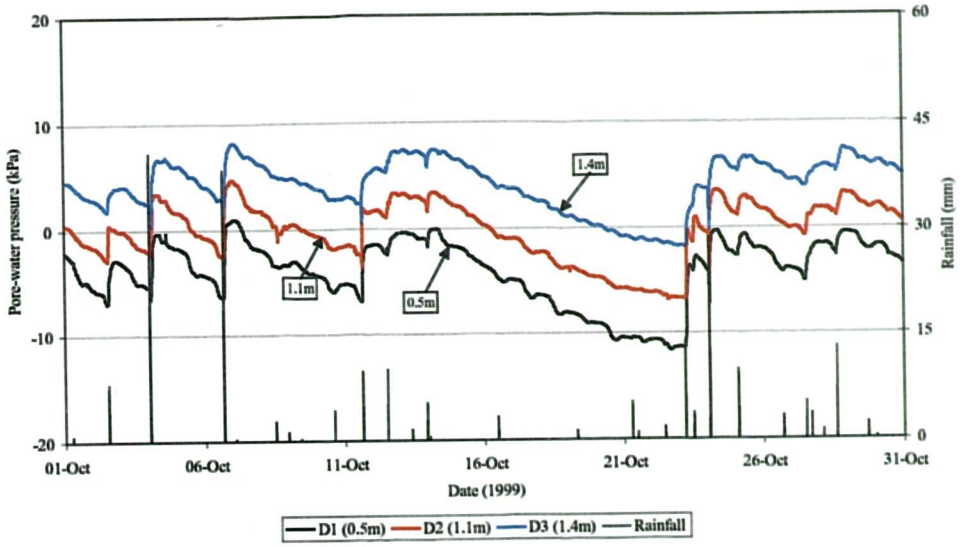

NTU-CSE slope, pore-water pressures of Row E during October 1999

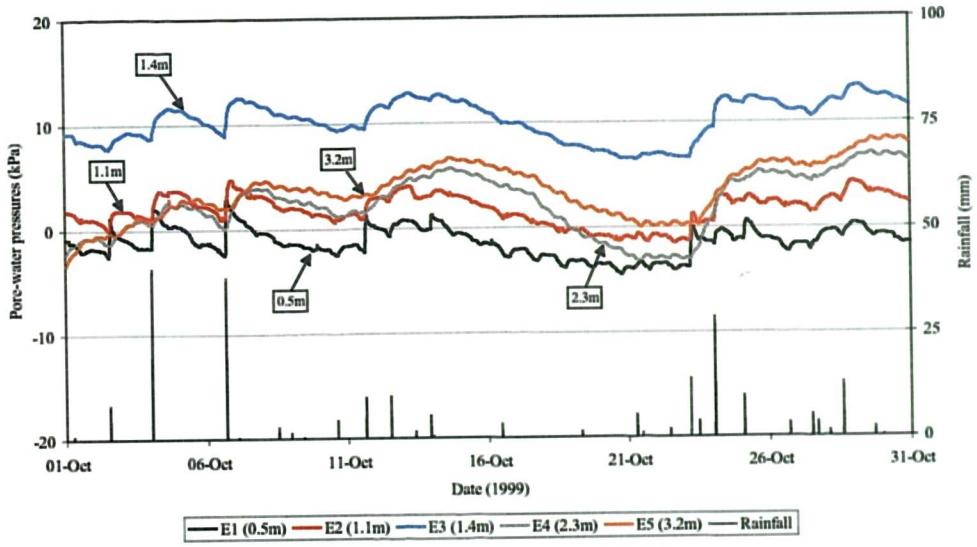

NTU-CSE slope, pore-water pressures of Row F during October 1999

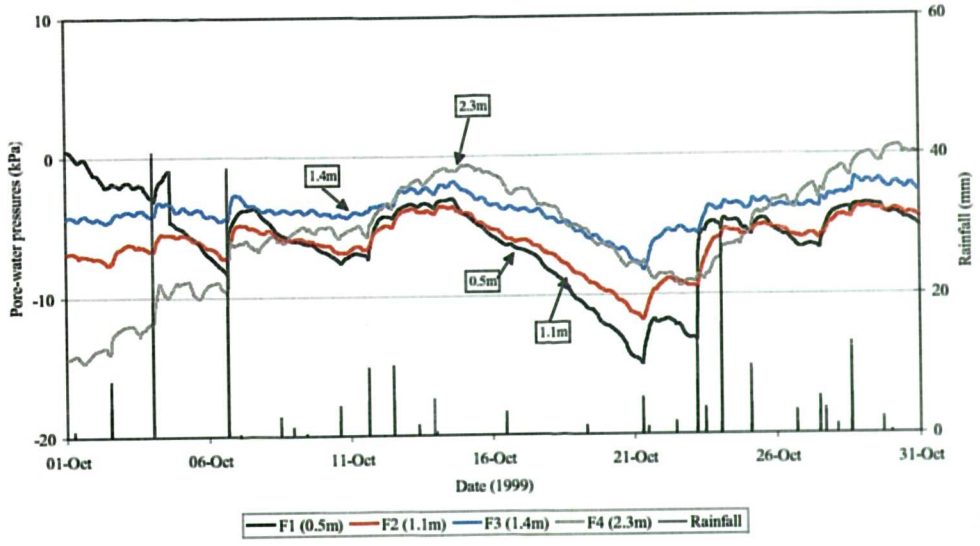

NTU-CSE slope, pore-water pressures of Row A during November 1999

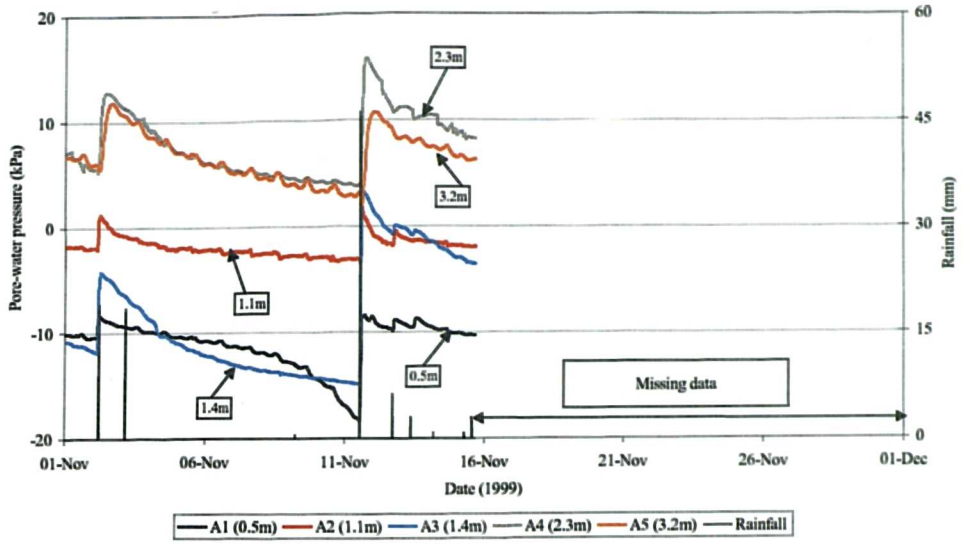

NTU-CSE slope, pore-water pressures of Row B during November 1999

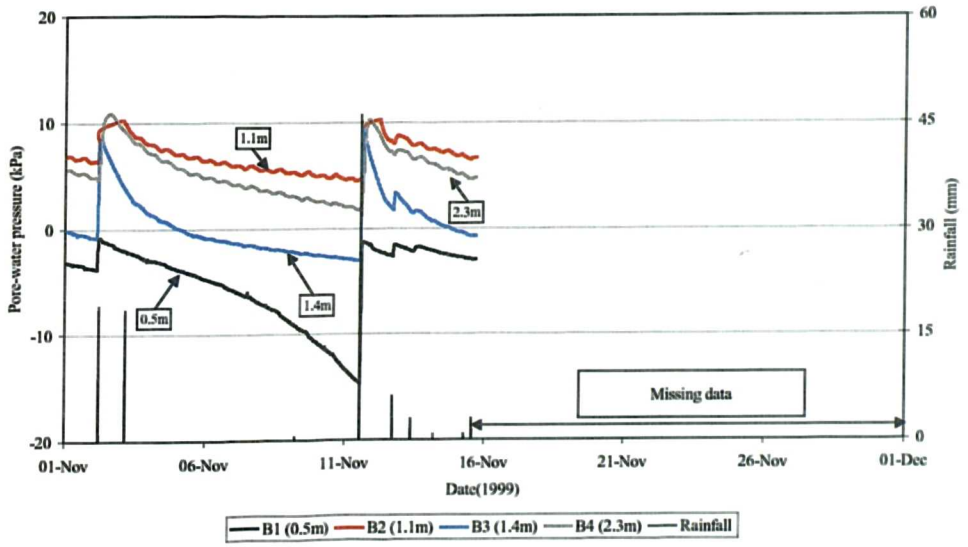

NTU-CSE slope, pore-water pressures of Row C during November 1999

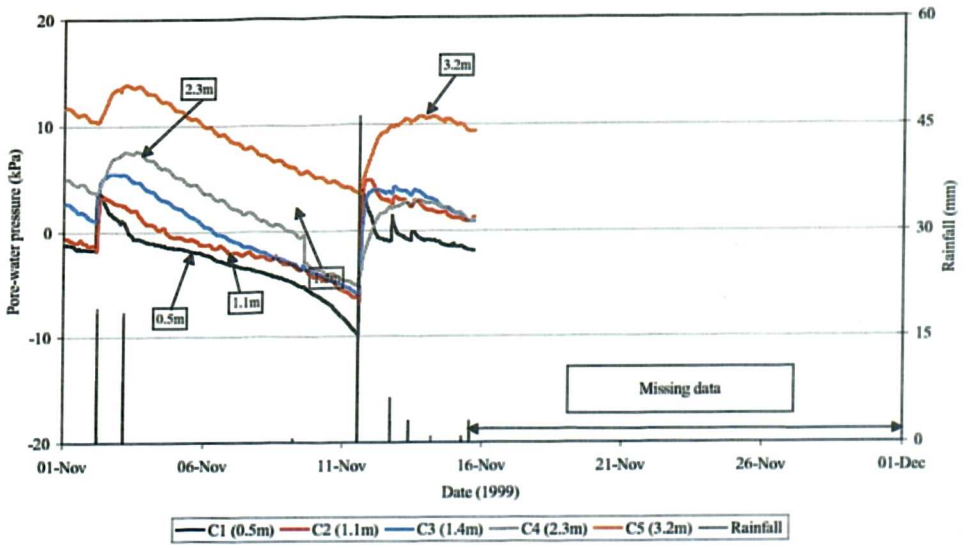

NTU-CSE slope, pore-water pressures of Row D during November 1999

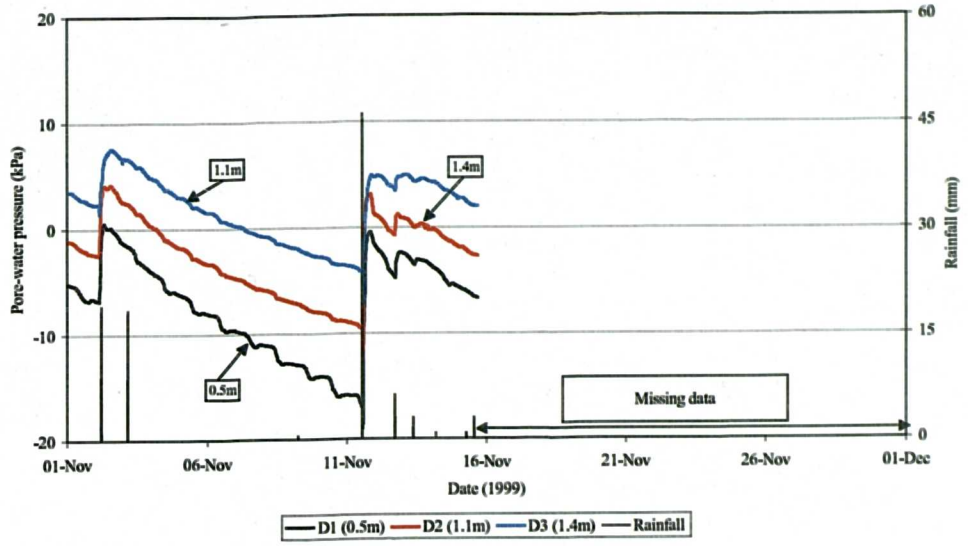

NTU-CSE slope, pore-water pressures of Row E during November 1999

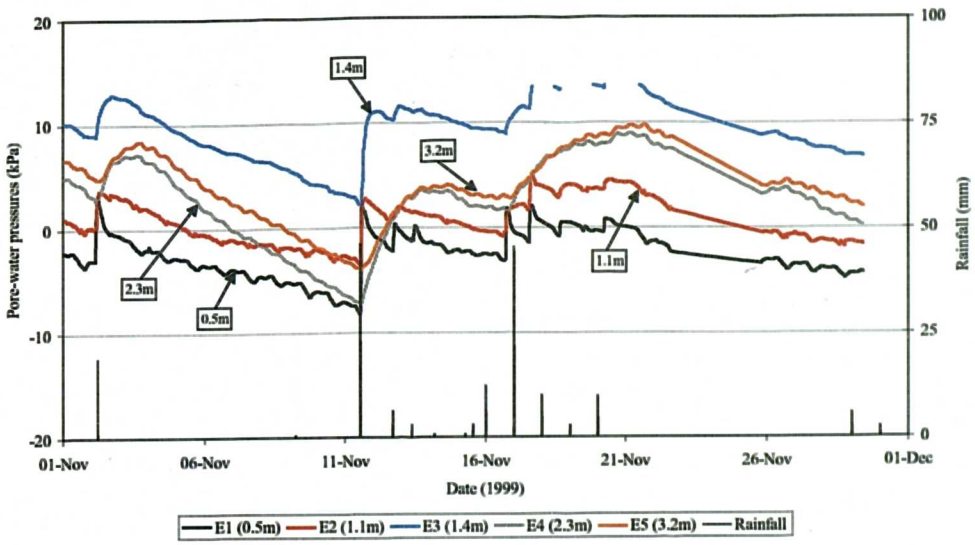

NTU-CSE slope, pore-water pressures of Row F during November 1999

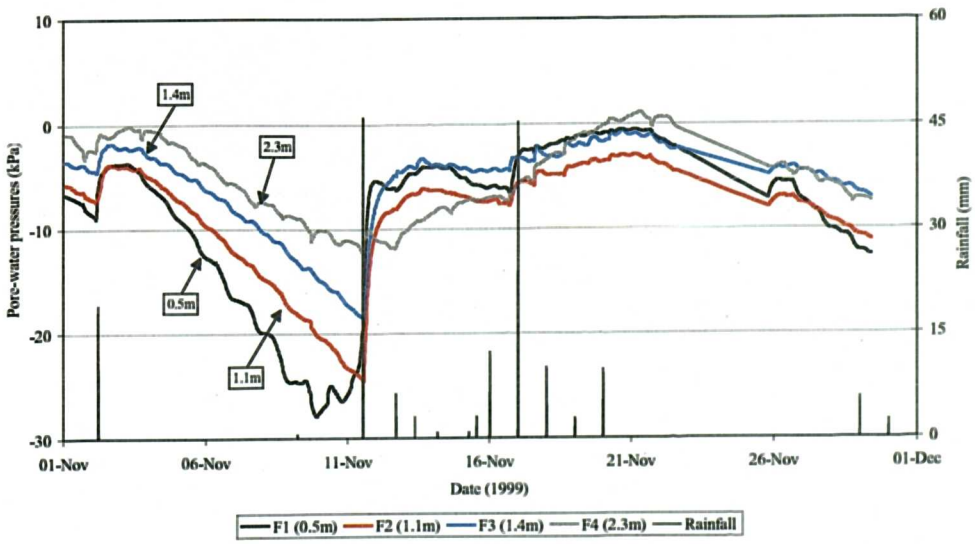

NTU-CSE slope, pore-water pressures of Row A during December 1999

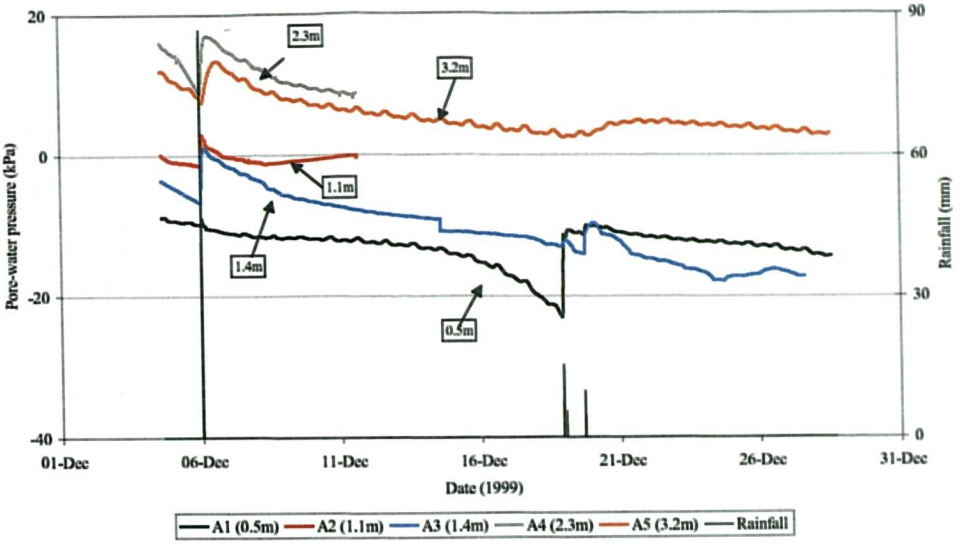

NTU-CSE slope, pore-water pressures of Row B during December 1999

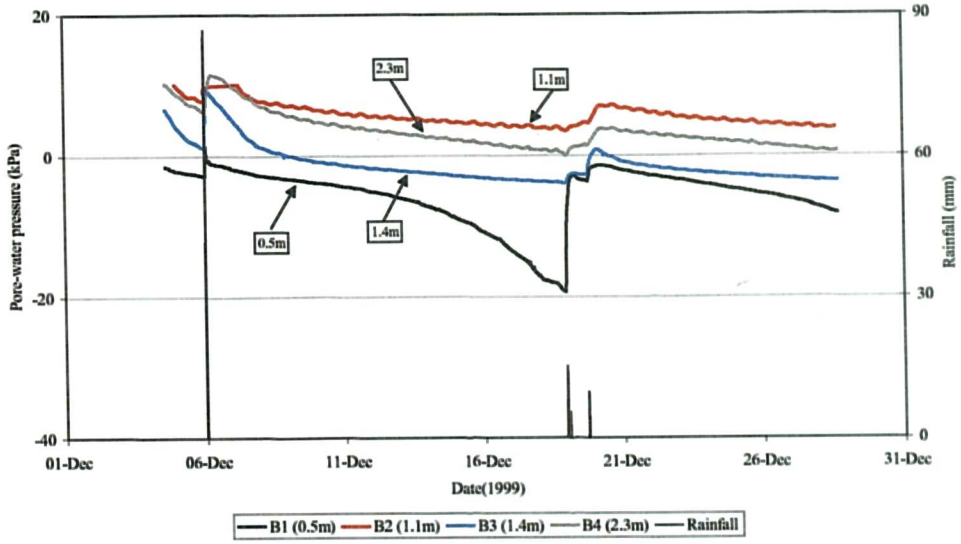

NTU-CSE slope, pore-water pressures of Row C during December 1999

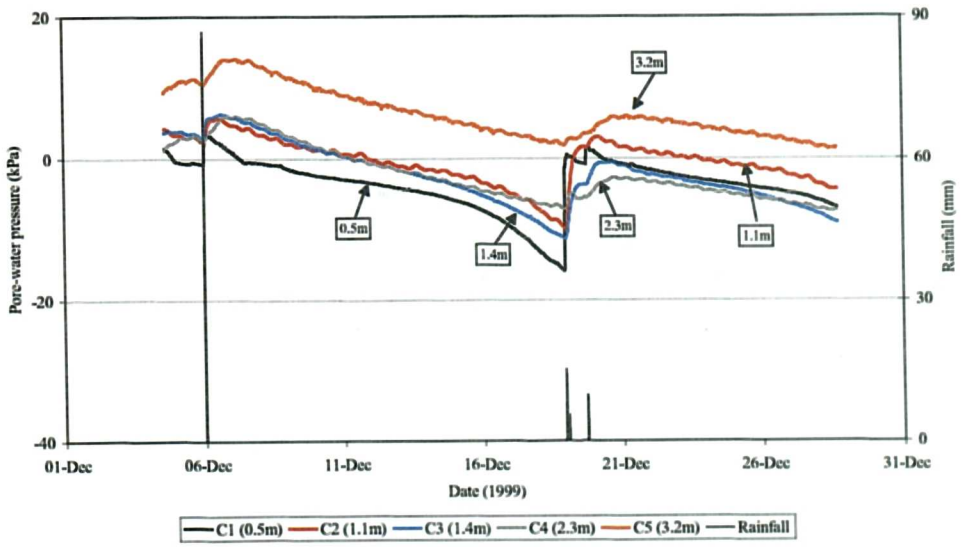

NTU-CSE slope, pore-water pressures of Row D during December 1999

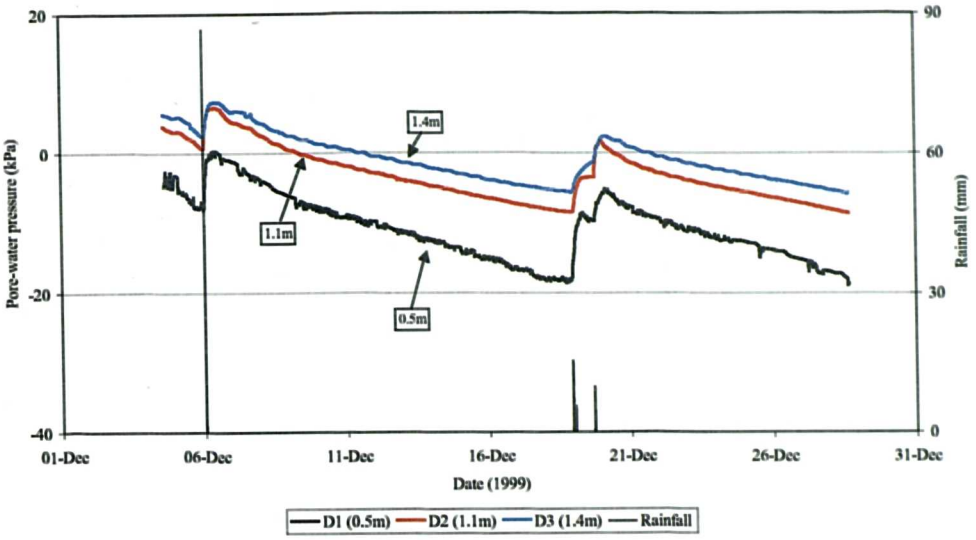

NTU-CSE slope, pore-water pressures of Row E during December 1999

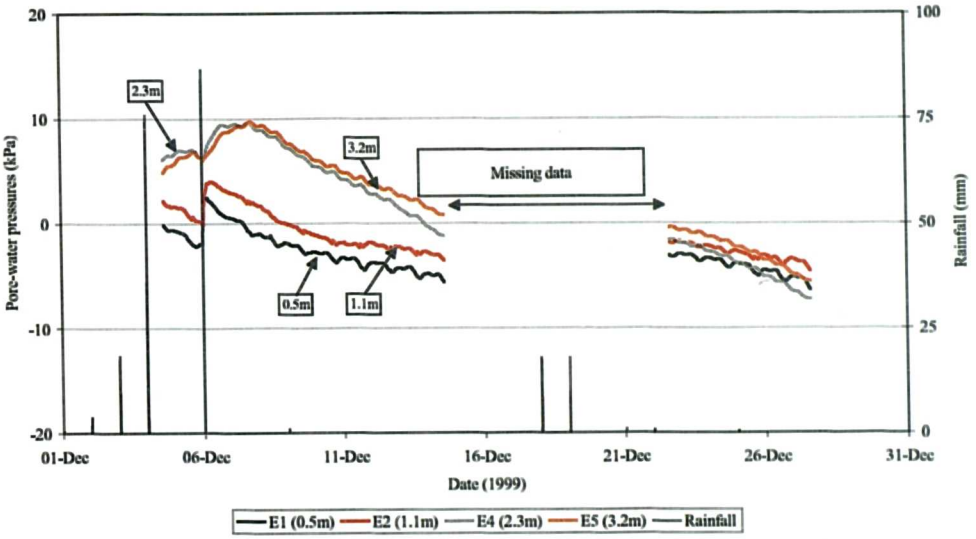

NTU-CSE slope, pore-water pressures of Row F during December 1999

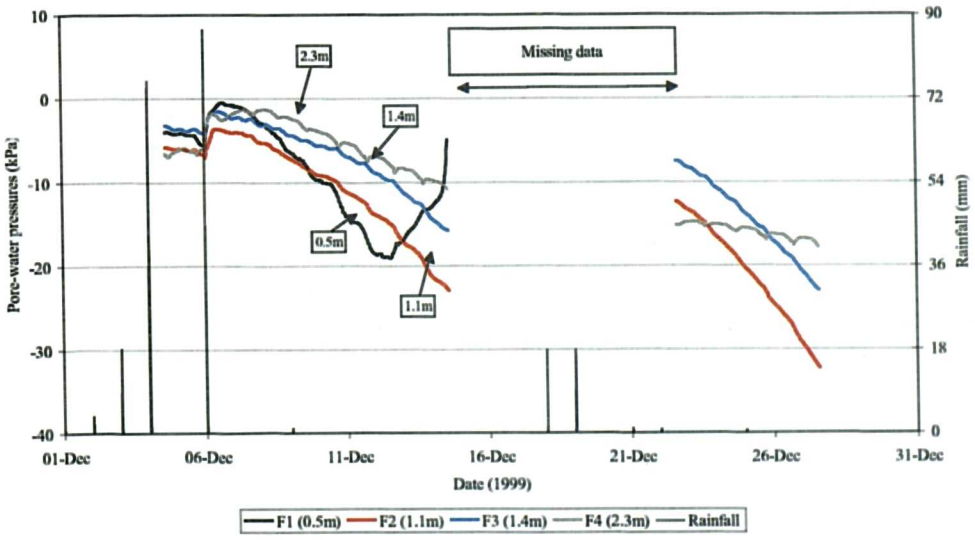

NTU-CSE slope, pore-water pressures of Row A during January 2000

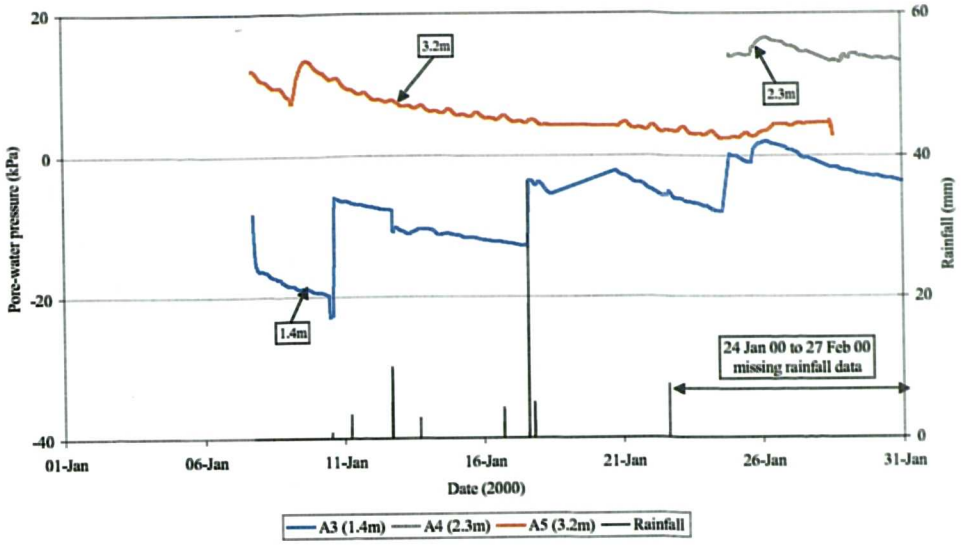

NTU-CSE slope, pore-water pressures of Row B during January 2000

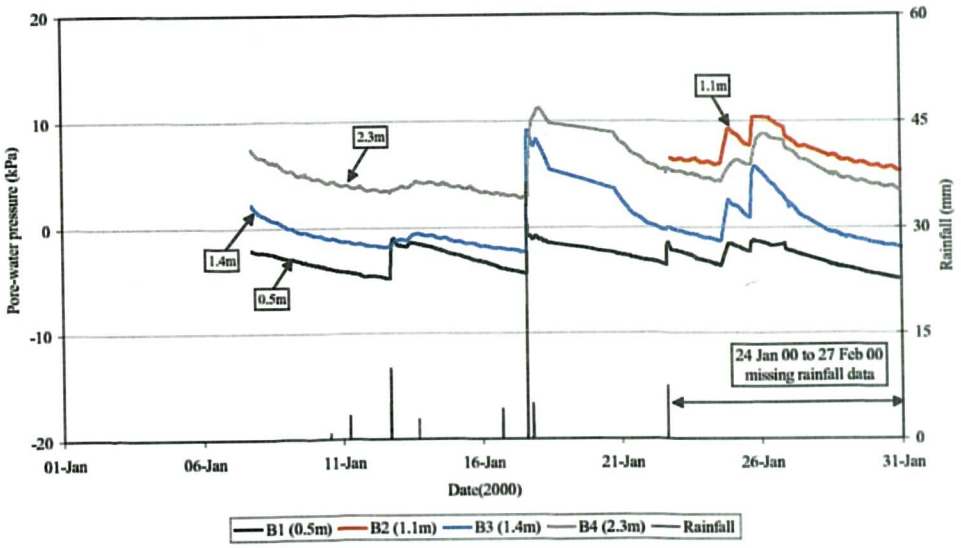

NTU-CSE slope, pore-water pressures of Row C during January 2000

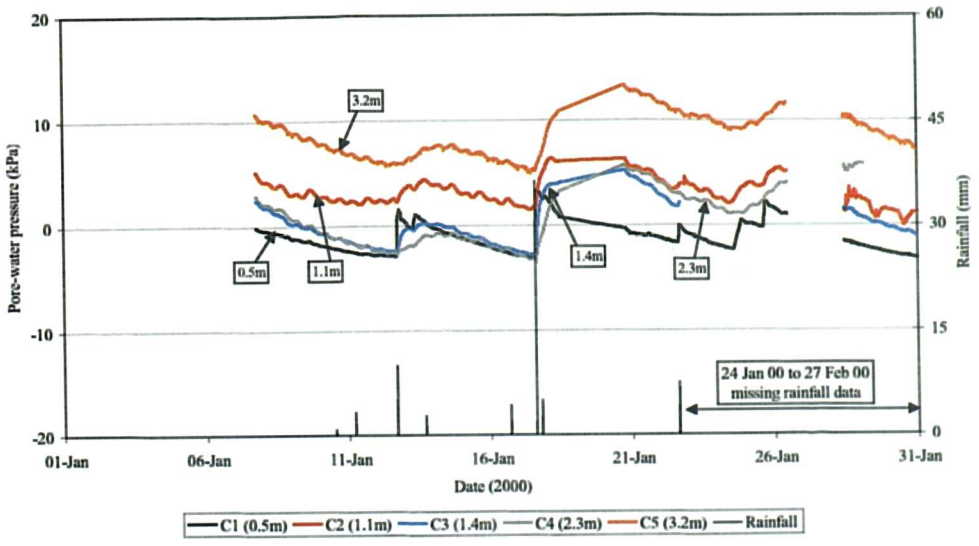

NTU-CSE slope, pore-water pressures of Row D during January 2000

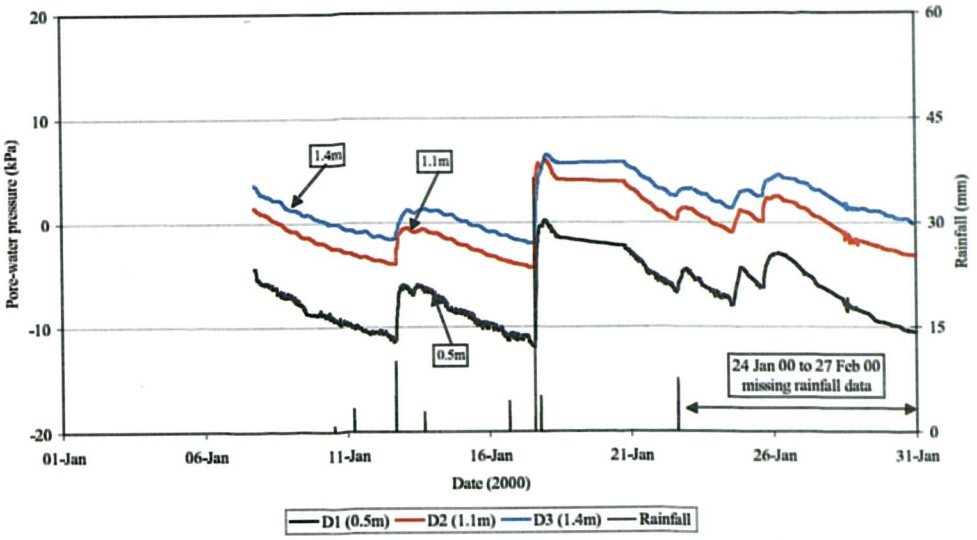

NTU-CSE slope, pore-water pressures of Row E during January 2000

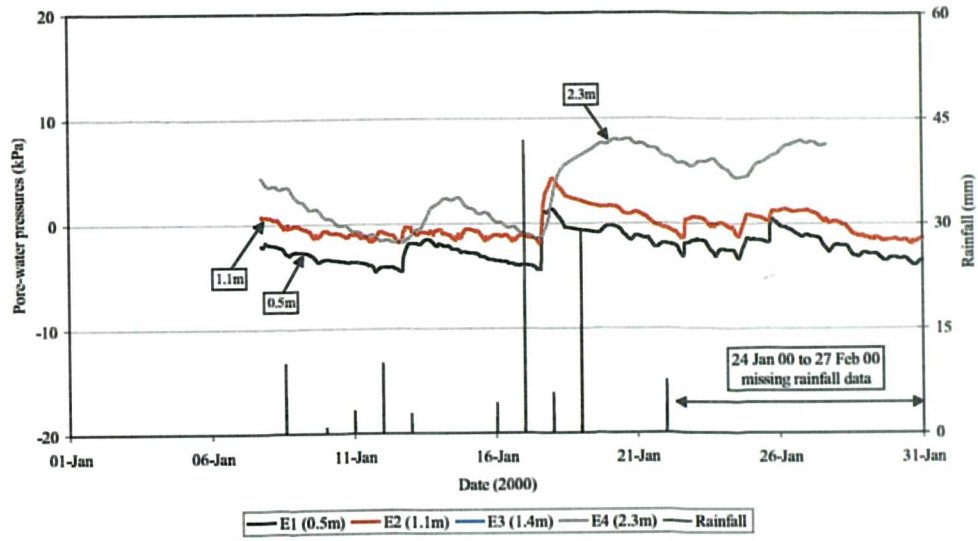

NTU-CSE slope, pore-water pressures of Row F during January 2000

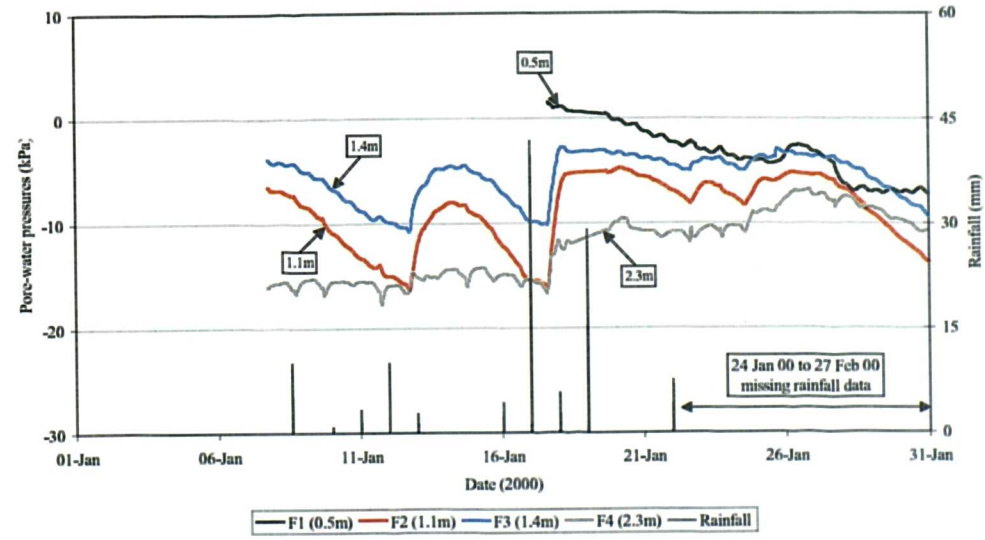

NTU-CSE slope, pore-water pressures of Row A during February 2000

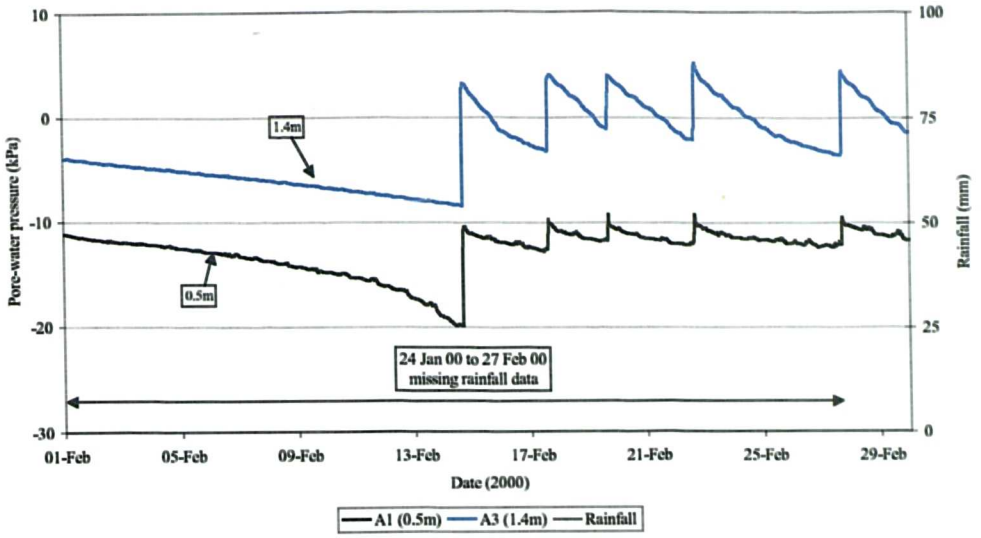

NTU-CSE slope, pore-water pressures of Row B during February 2000

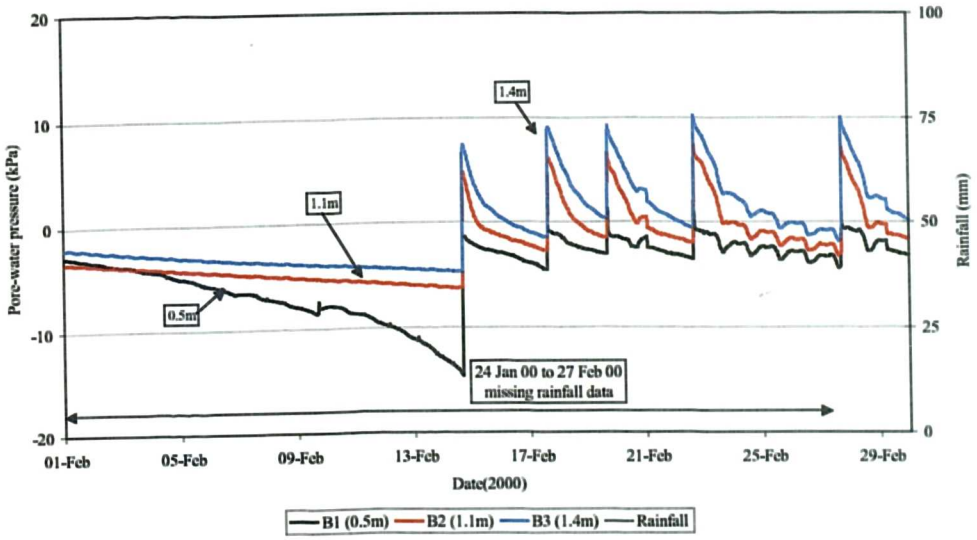

NTU-CSE slope, pore-water pressures of Row C during February 2000

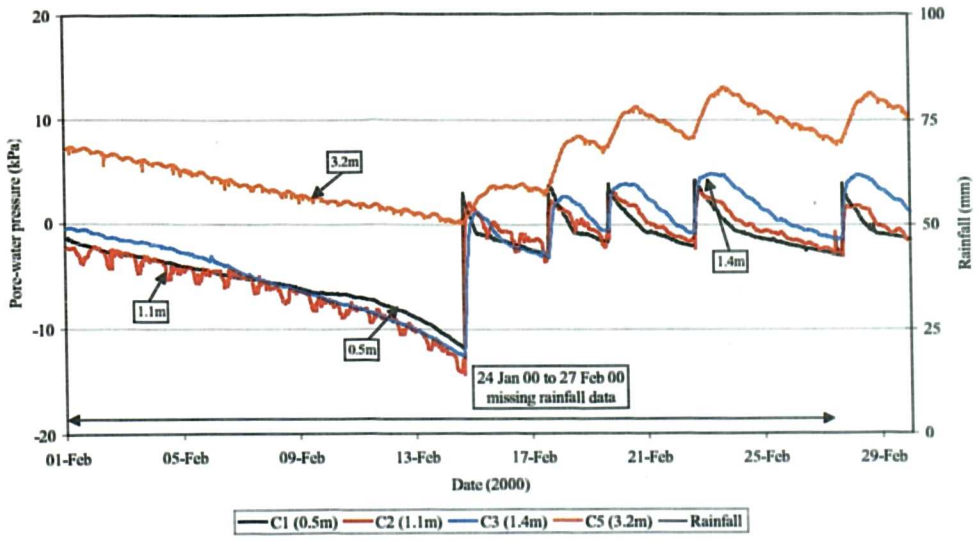

NTU-CSE slope, pore-water pressures of Row D during February 2000

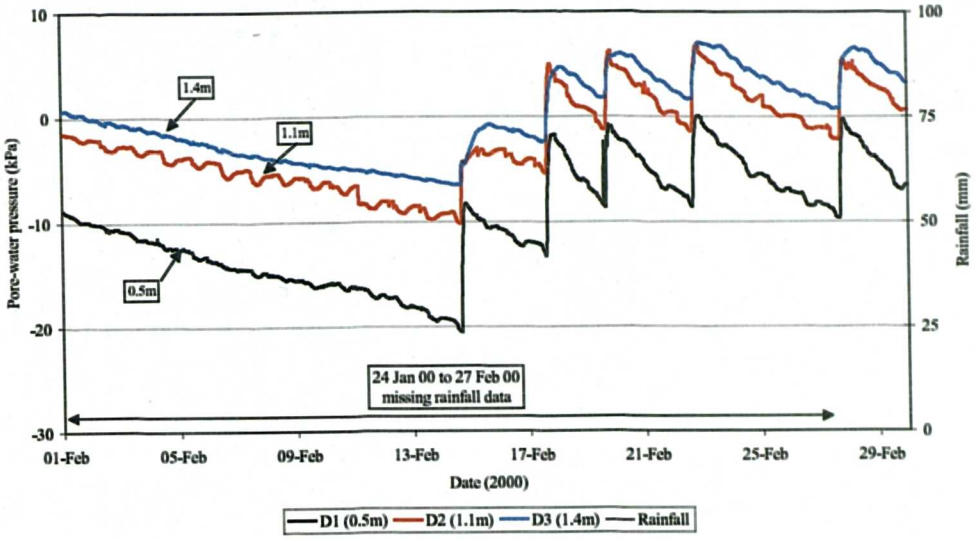

NTU-CSE slope, pore-water pressures of Row E during February 2000

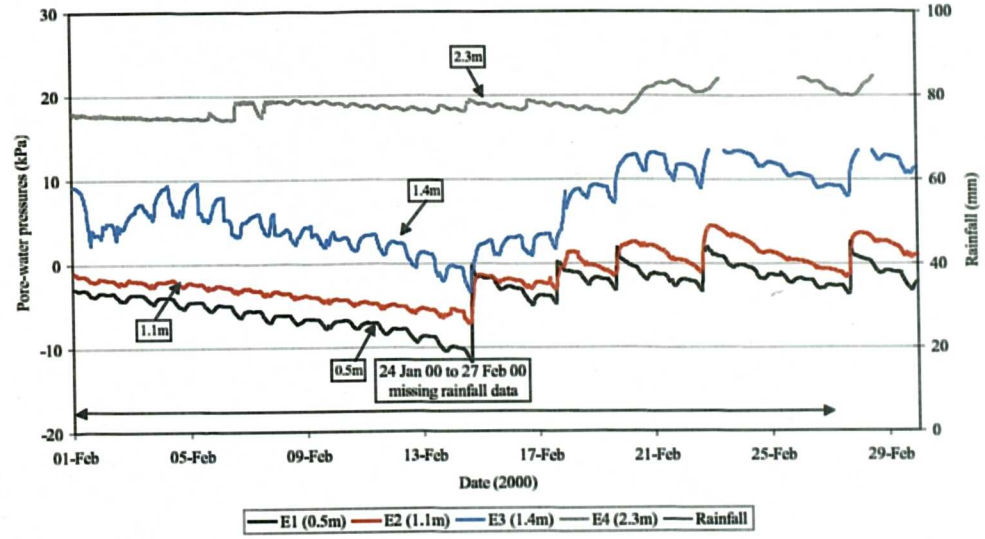

NTU-CSE slope, pore-water pressures of Row F during February 2000

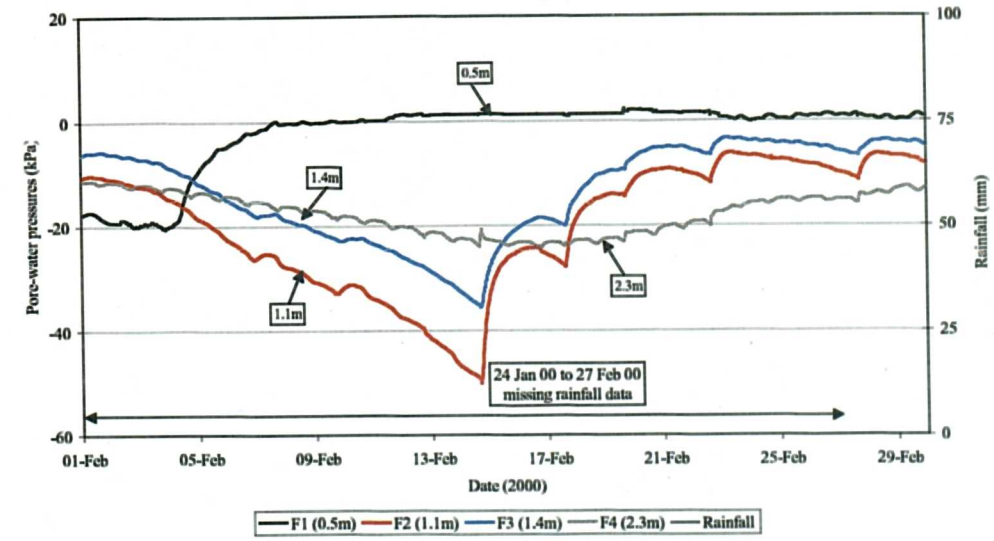

NTU-CSE slope, pore-water pressures of Row A during March 2000

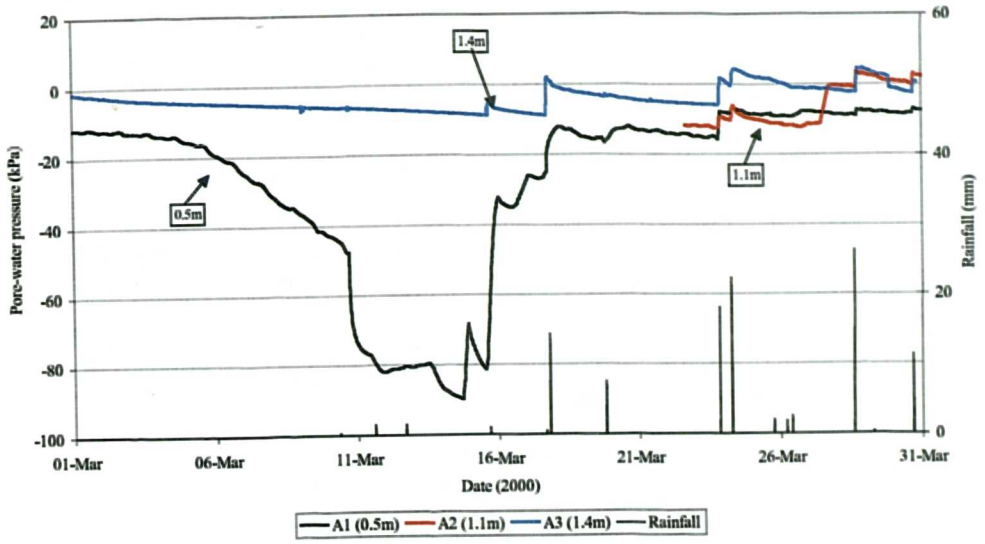

NTU-CSE slope, pore-water pressures of Row B during March 2000

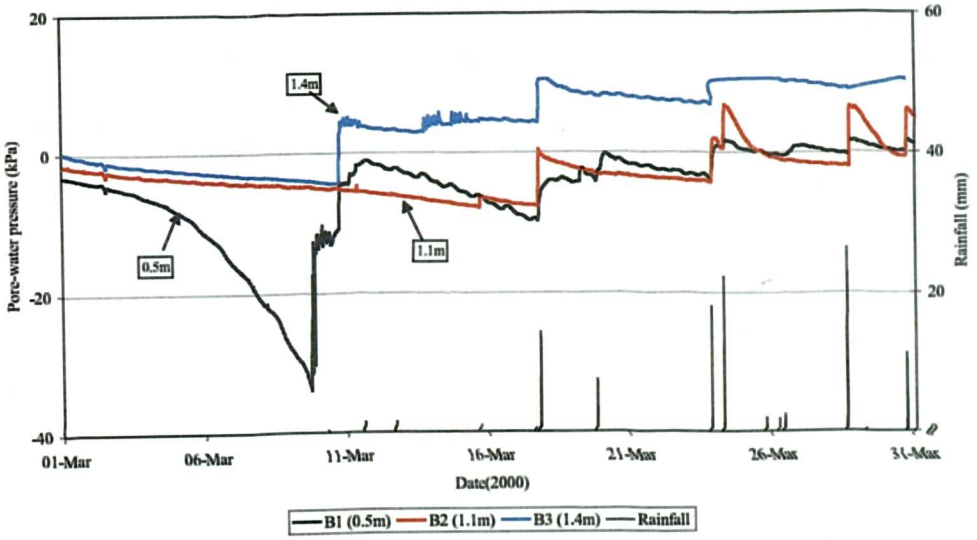

NTU-CSE slope, pore-water pressures of Row C during March 2000

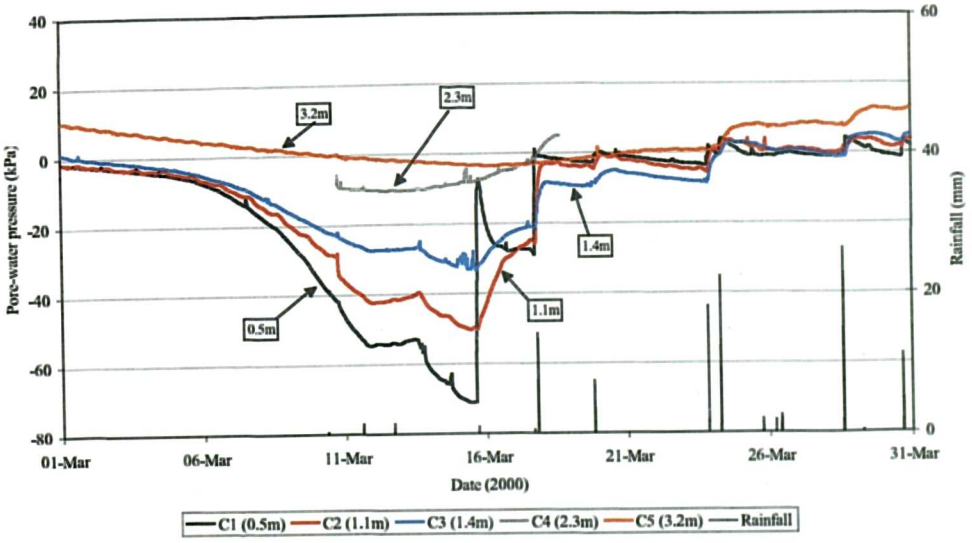

NTU-CSE slope, pore-water pressures of Row D during March 2000

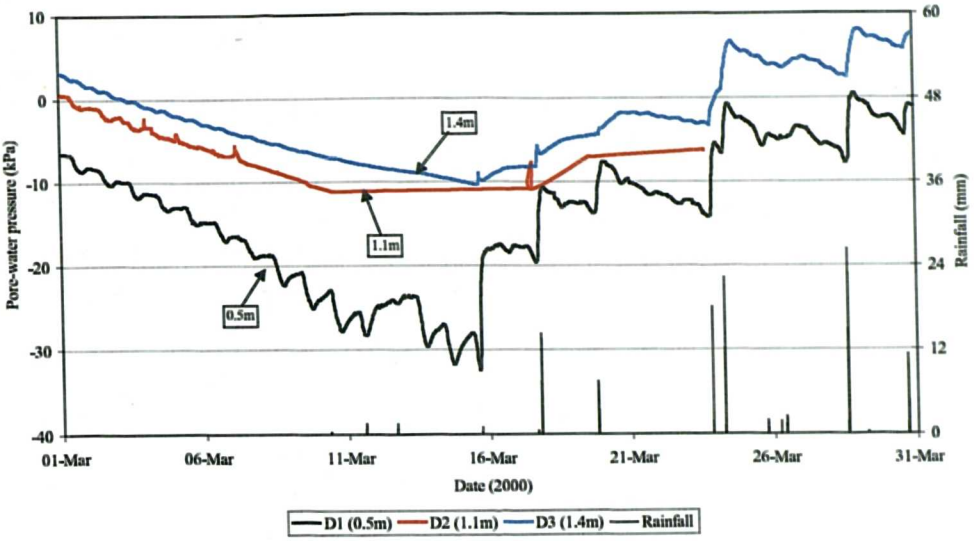

NTU-CSE slope, pore-water pressures of Row E during March 2000

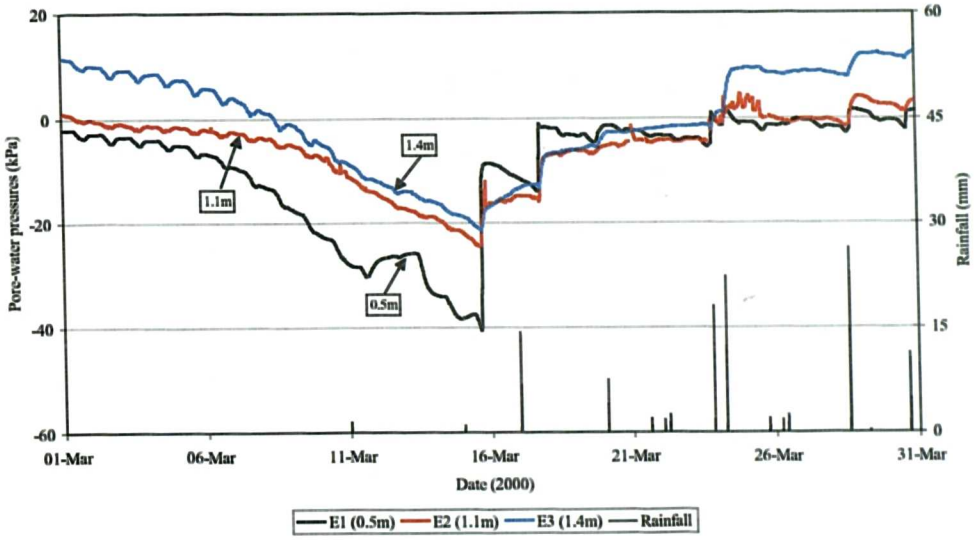

NTU-CSE slope, pore-water pressures of Row F during March 2000

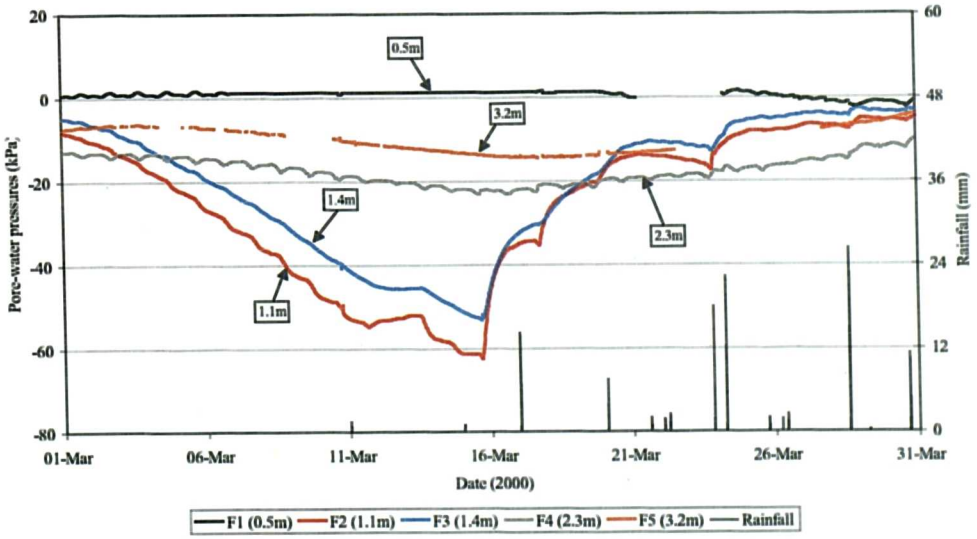

NTU-CSE slope, pore-water pressures of Row A during April 2000

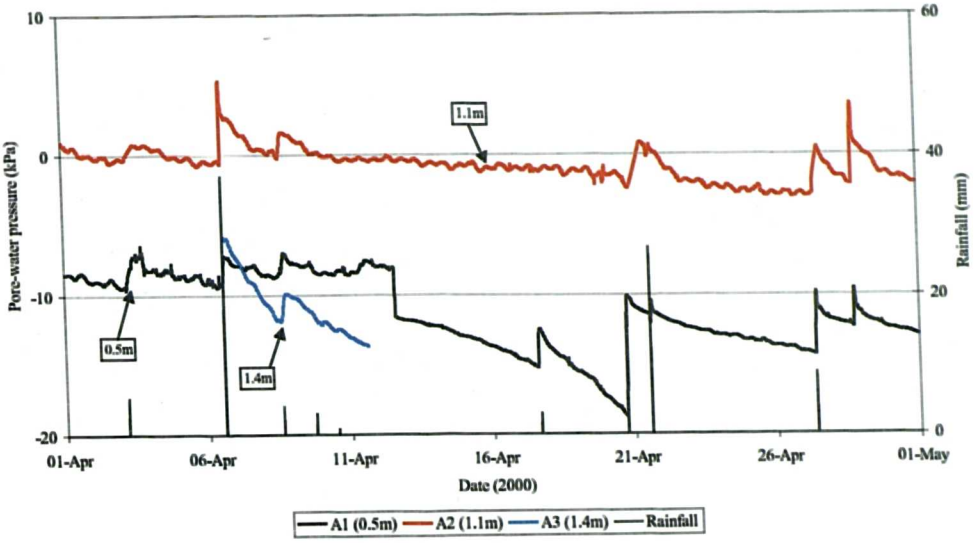

NTU-CSE slope, pore-water pressures of Row B during April 2000

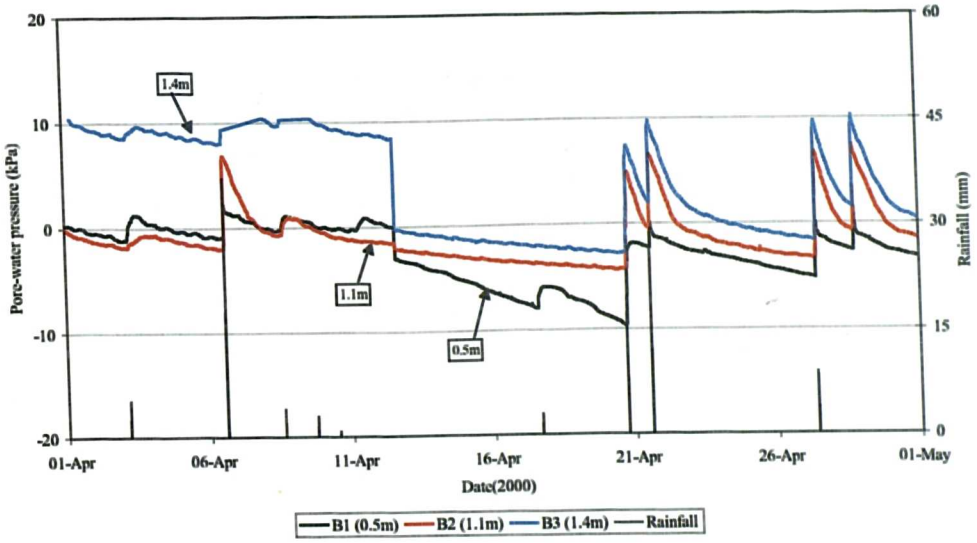

NTU-CSE slope, pore-water pressures of Row C during April 2000

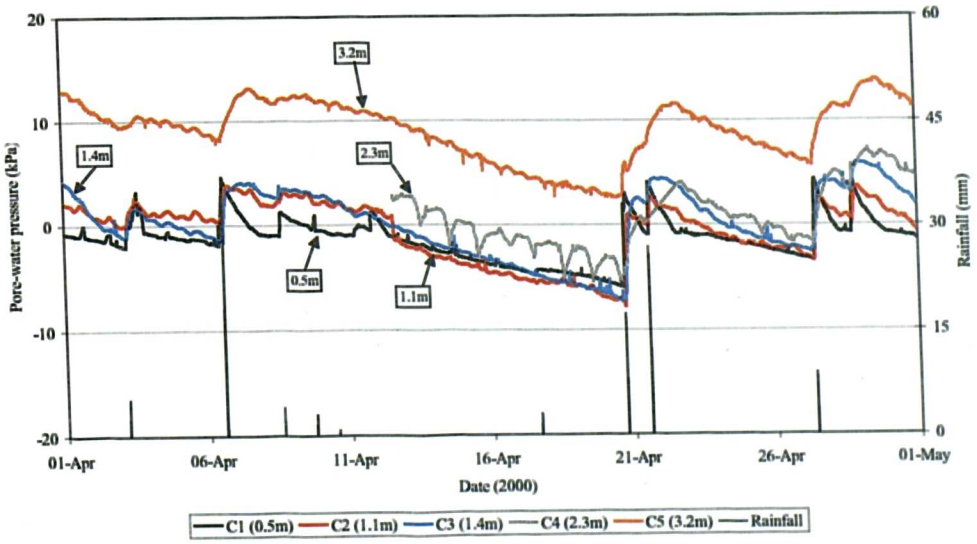

NTU-CSE slope, pore-water pressures of Row D during April 2000

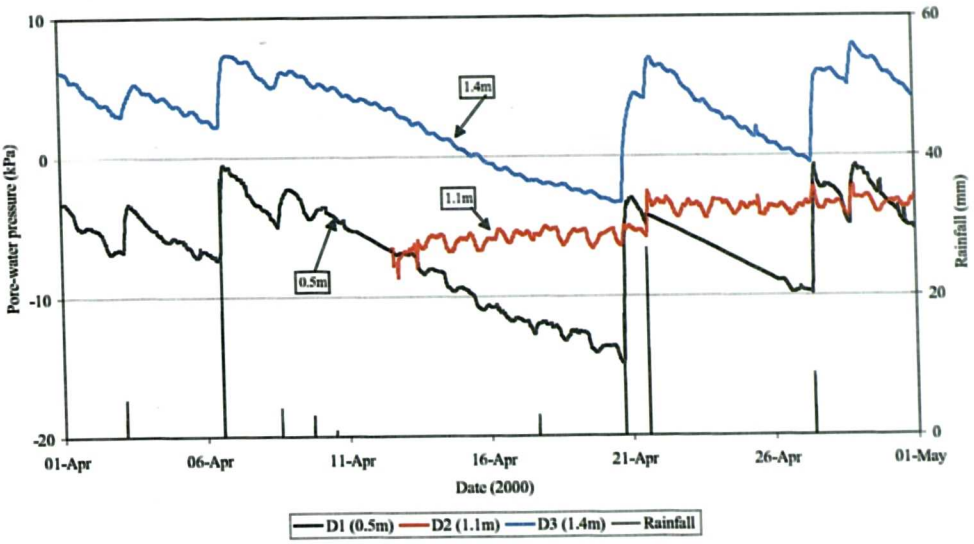

NTU-CSE slope, pore-water pressures of Row E during April 2000

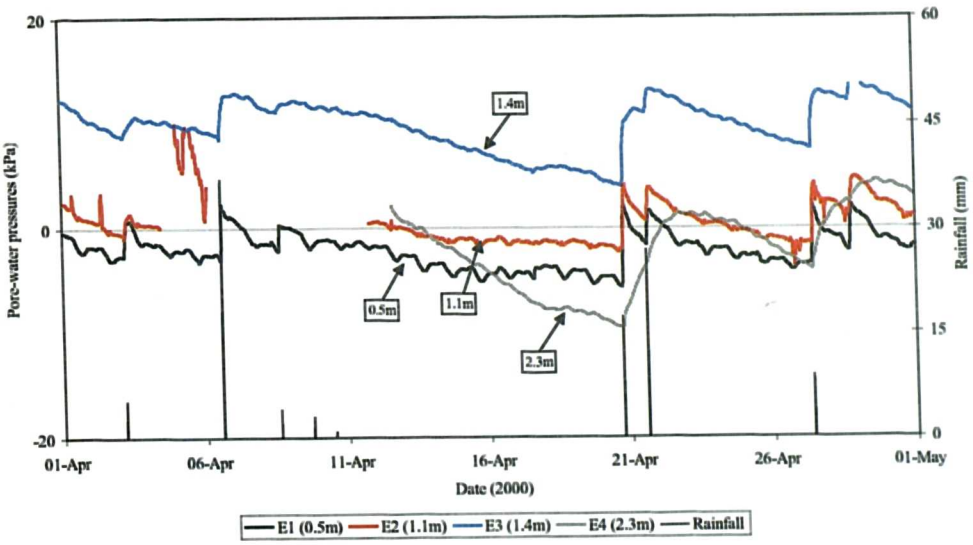

NTU-CSE slope, pore-water pressures of Row F during April 2000

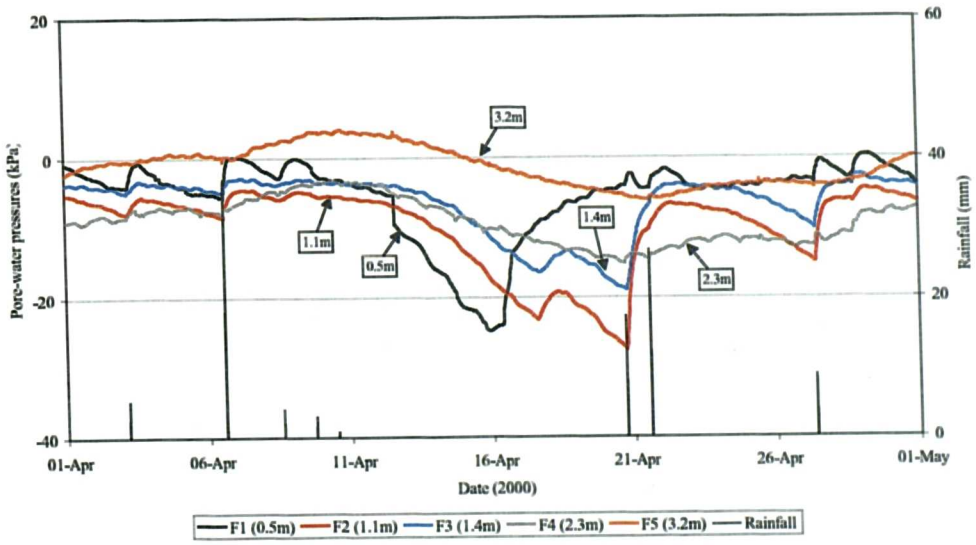

NTU-CSE slope, pore-water pressures of Row A during May 2000

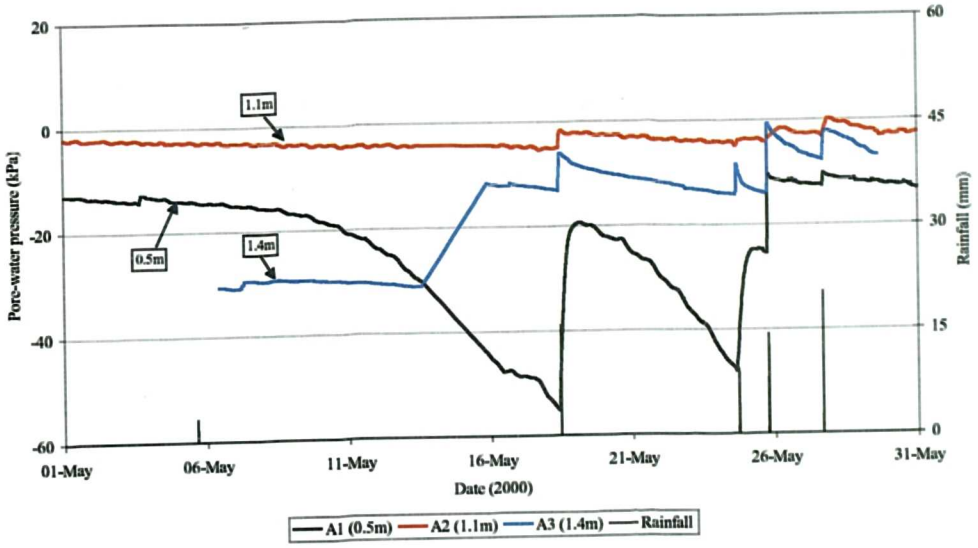

NTU-CSE slope, pore-water pressures of Row B during May 2000

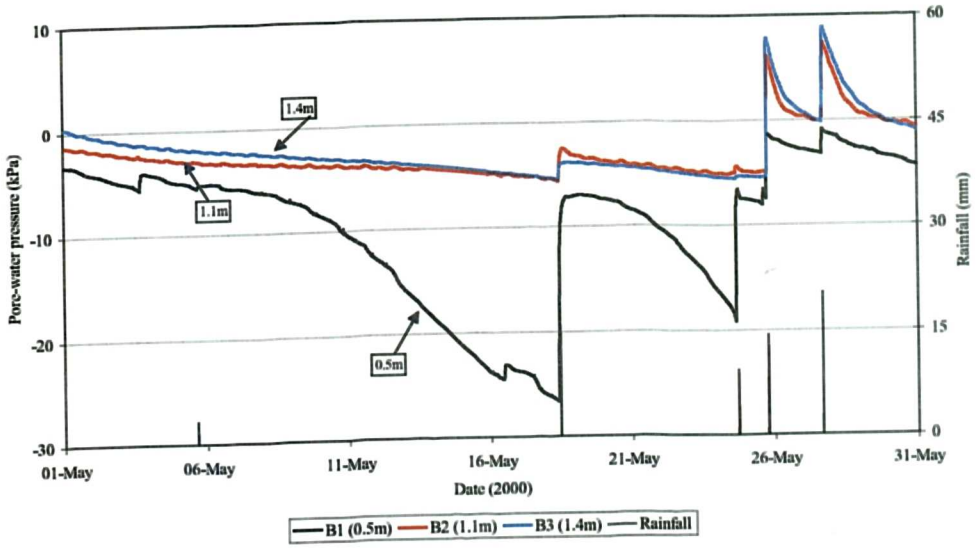

NTU-CSE slope, pore-water pressures of Row C during May 2000

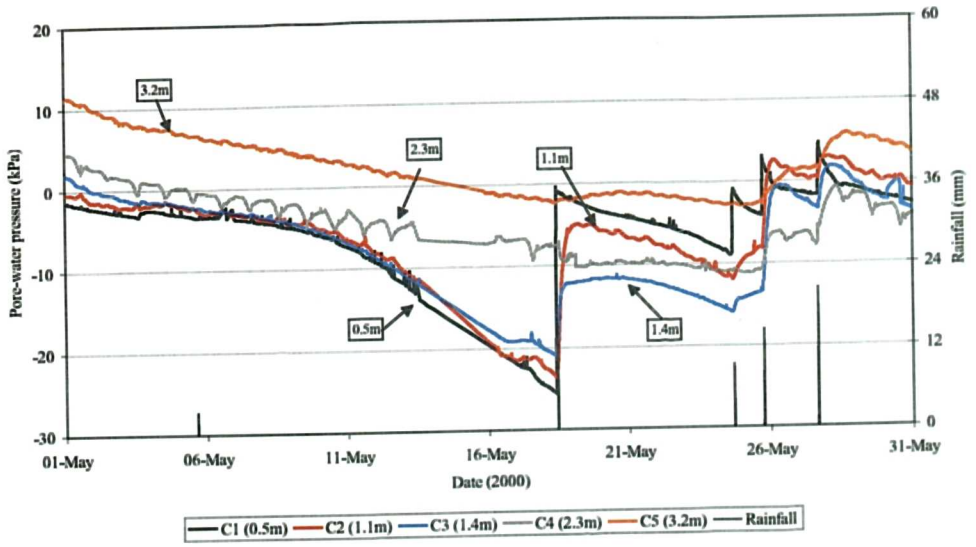

NTU-CSE slope, pore-water pressures of Row D during May 2000

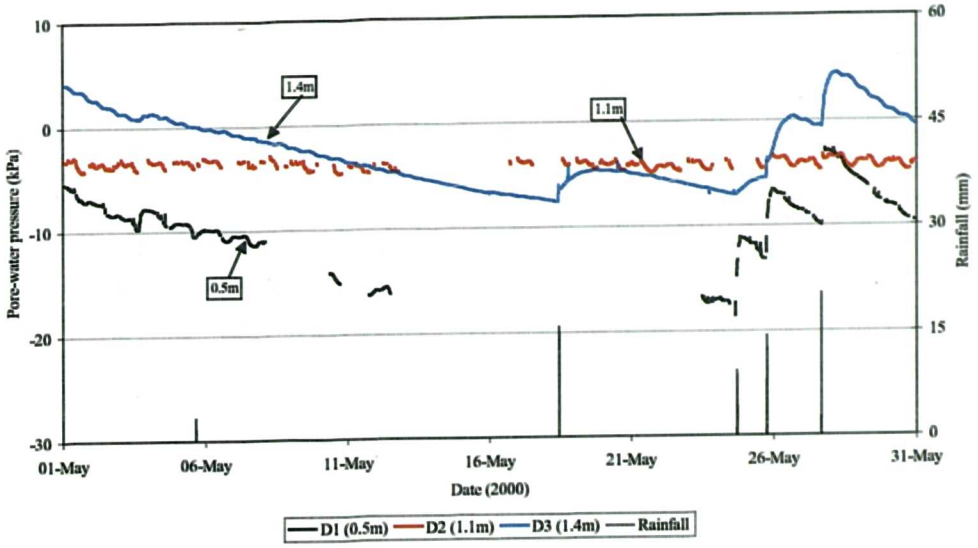

NTU-CSE slope, pore-water pressures of Row E during May 2000

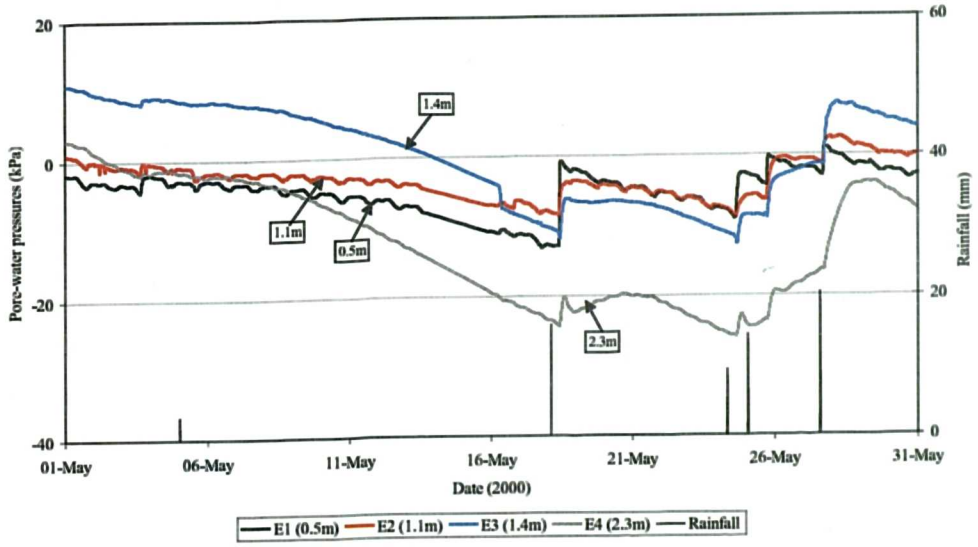

NTU-CSE slope, pore-water pressures of Row F during May 2000

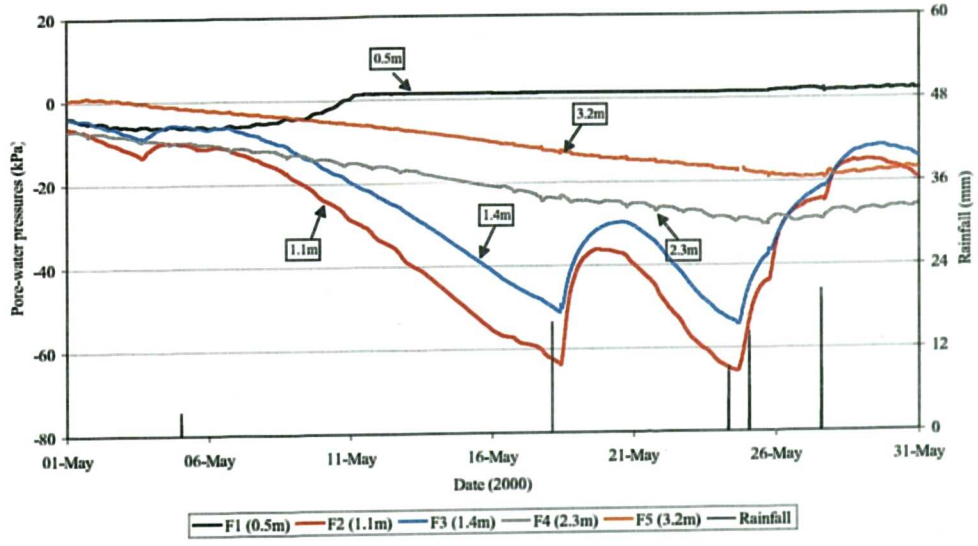

NTU-CSE slope, pore-water pressures of Row A during June 2000

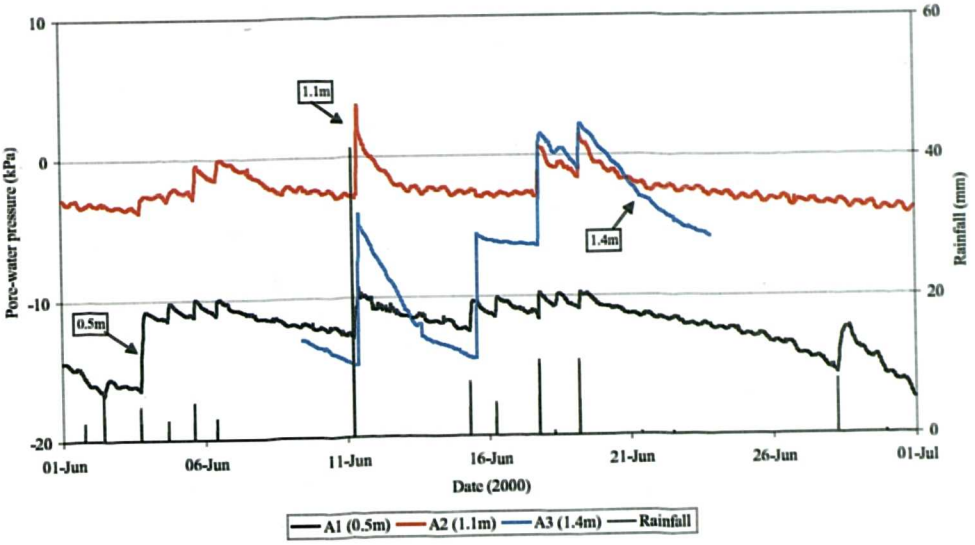

NTU-CSE slope, pore-water pressures of Row B during June 2000

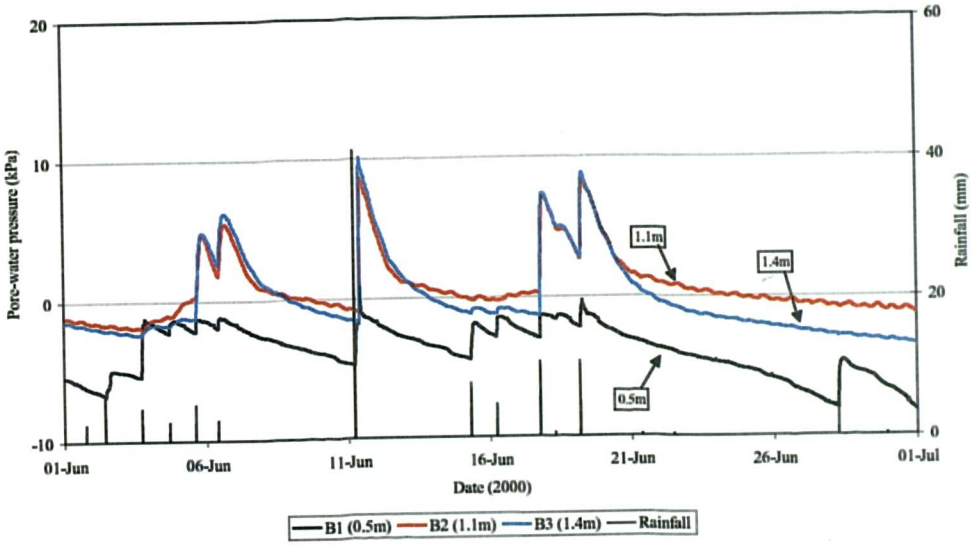

NTU-CSE slope, pore-water pressures of Row C during June 2000

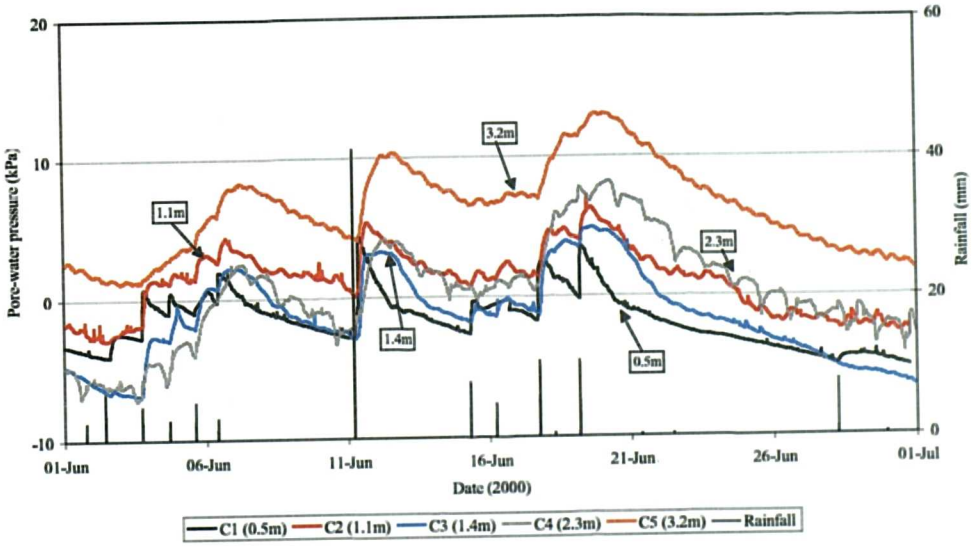

NTU-CSE slope, pore-water pressures of Row D during June 2000

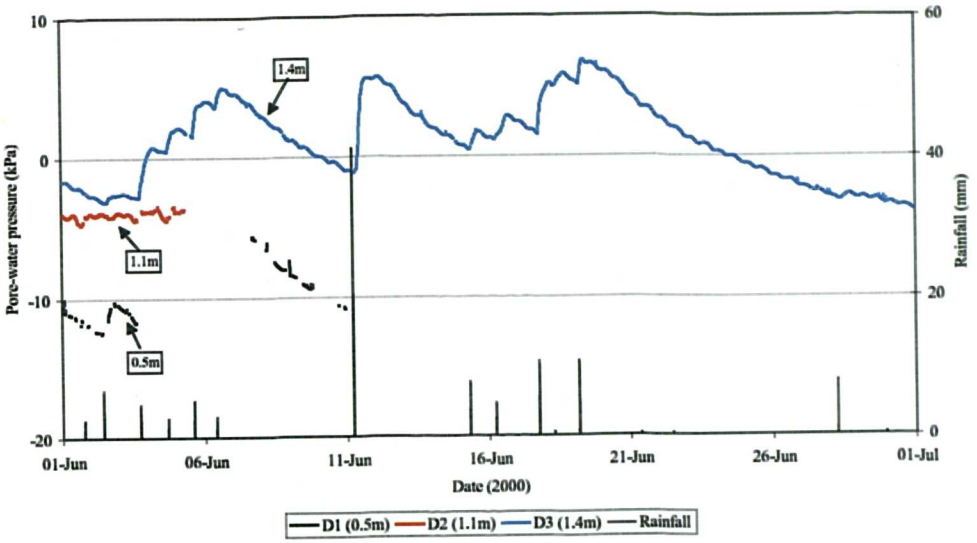

NTU-CSE slope, pore-water pressures of Row E during June 2000

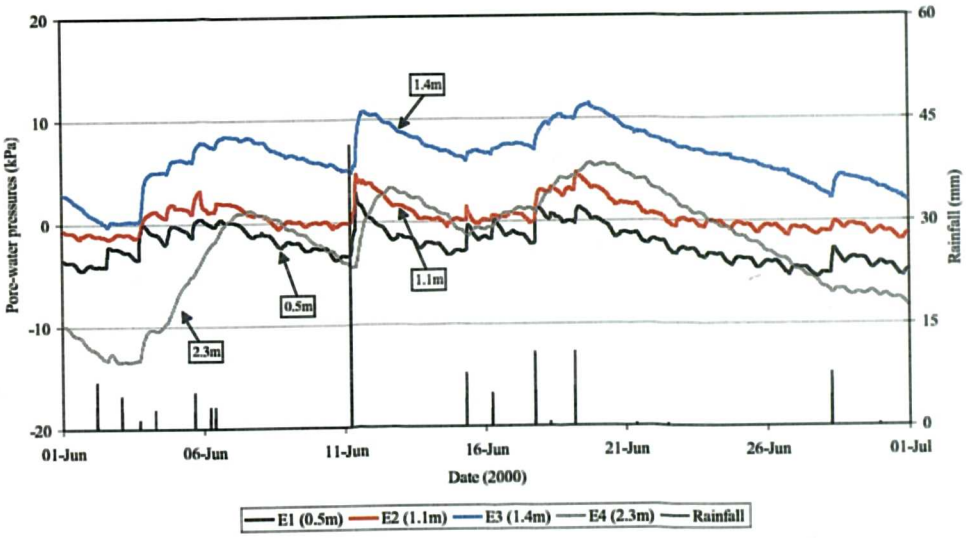

NTU-CSE slope, pore-water pressures of Row F during June 2000

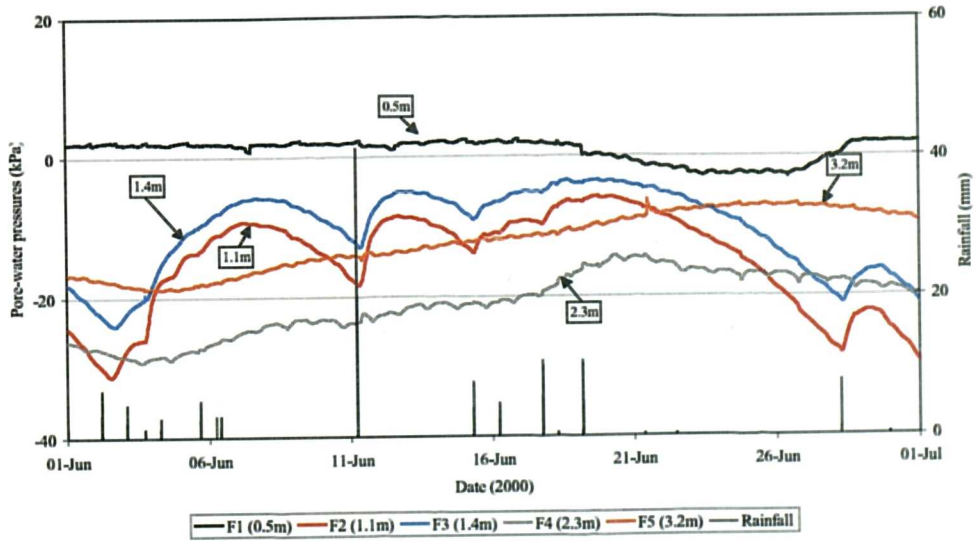

NTU-CSE slope, pore-water pressures of Row A during July 2000

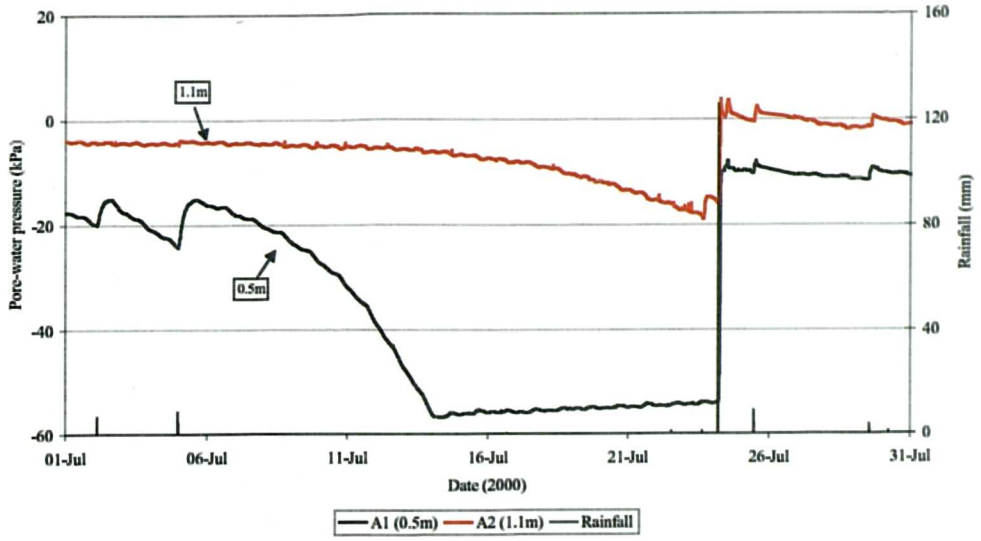

NTU-CSE slope, pore-water pressures of Row B during July 2000

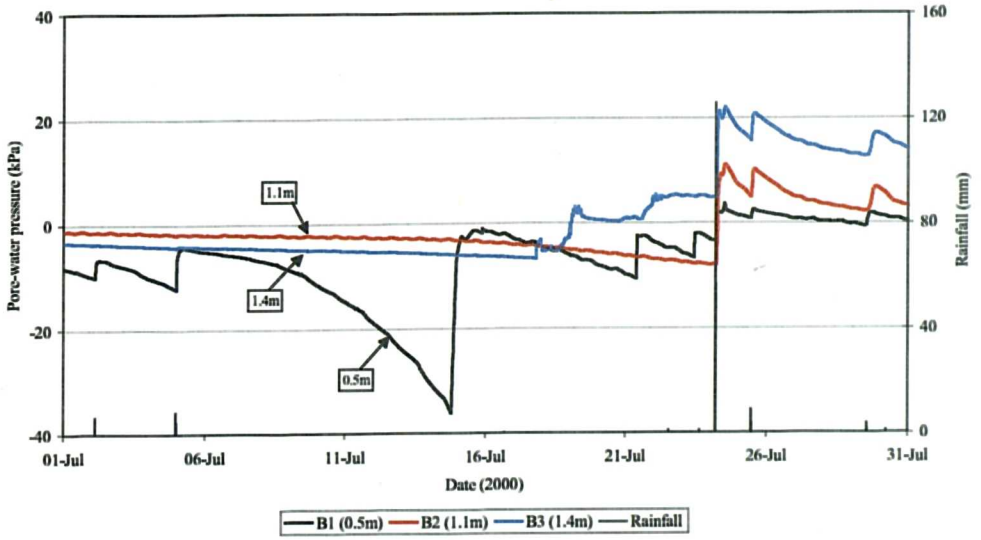

NTU-CSE slope, pore-water pressures of Row C during July 2000

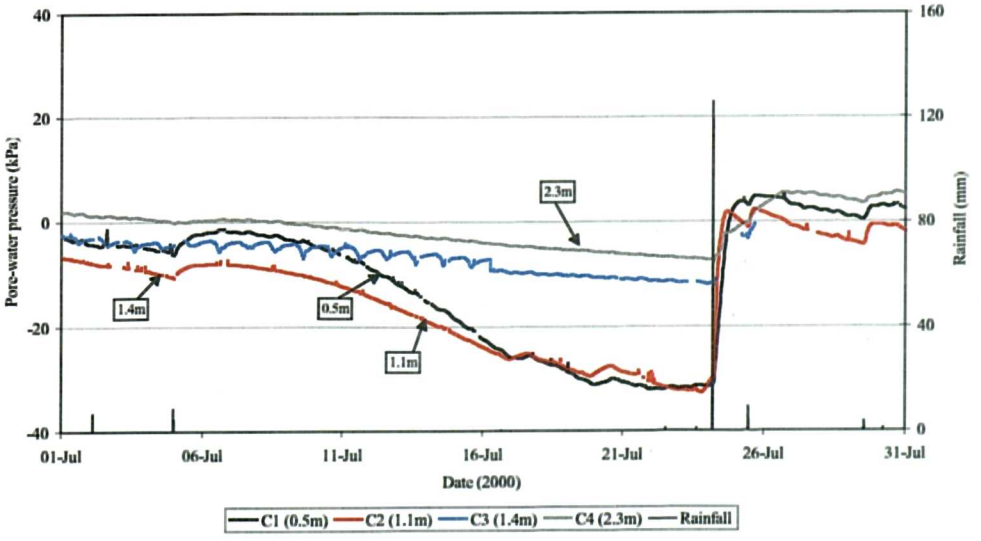

NTU-CSE slope, pore-water pressures of Row D during July 2000

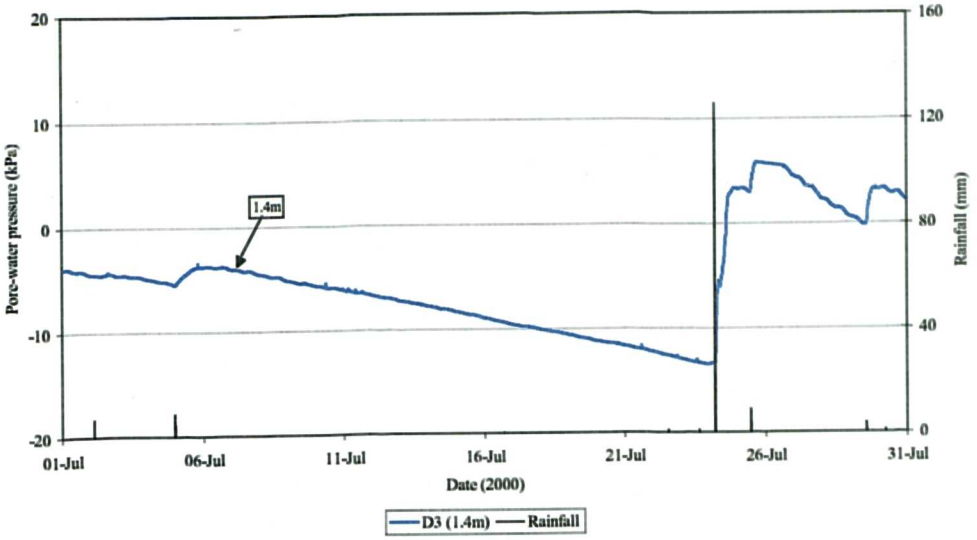

NTU-CSE slope, pore-water pressures of Row E during July 2000

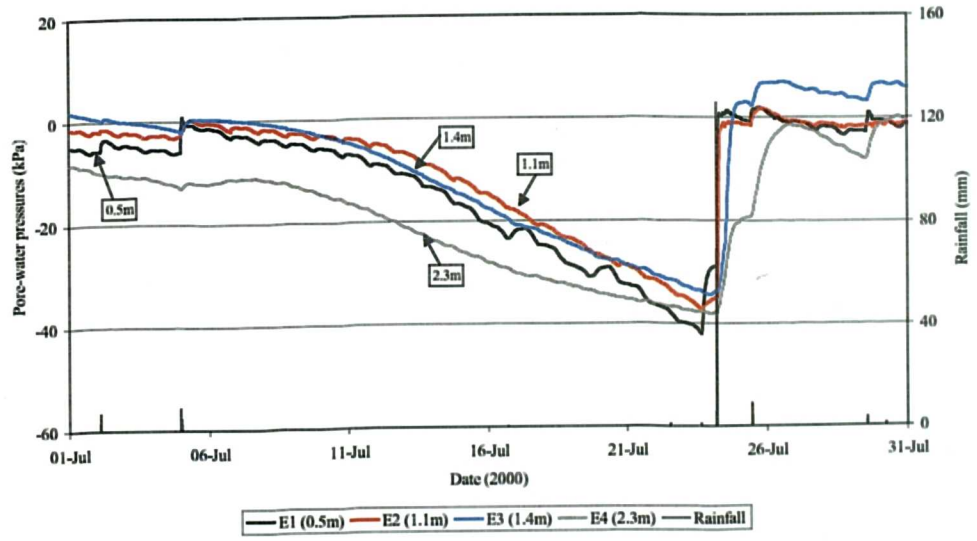

NTU-CSE slope, pore-water pressures of Row F during July 2000

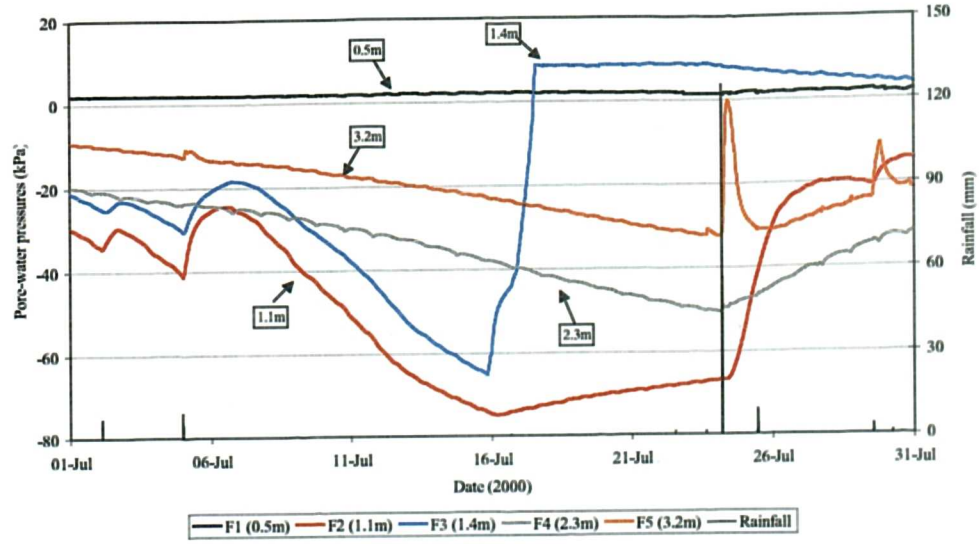

NTU-CSE slope, pore-water pressures of Row A during August 2000

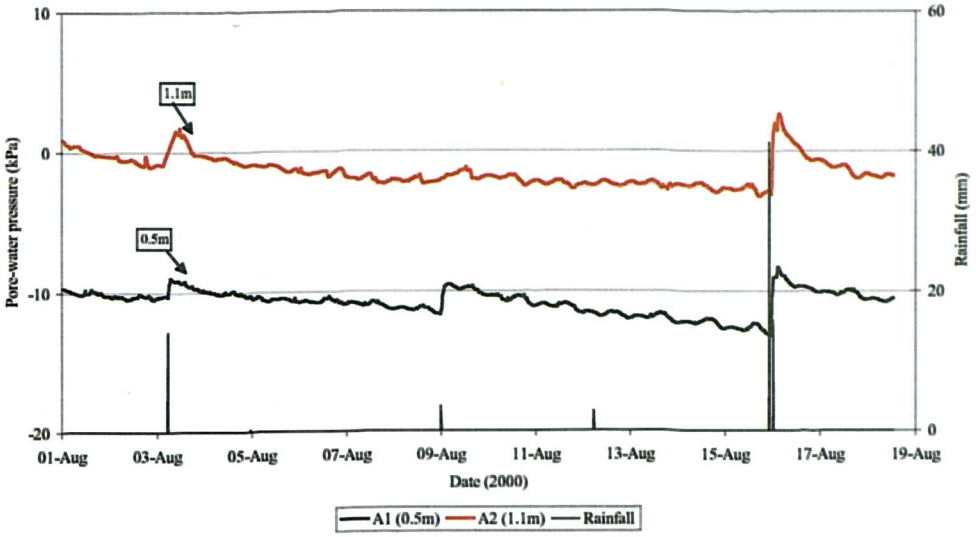

NTU-CSE slope, pore-water pressures of Row B during August 2000

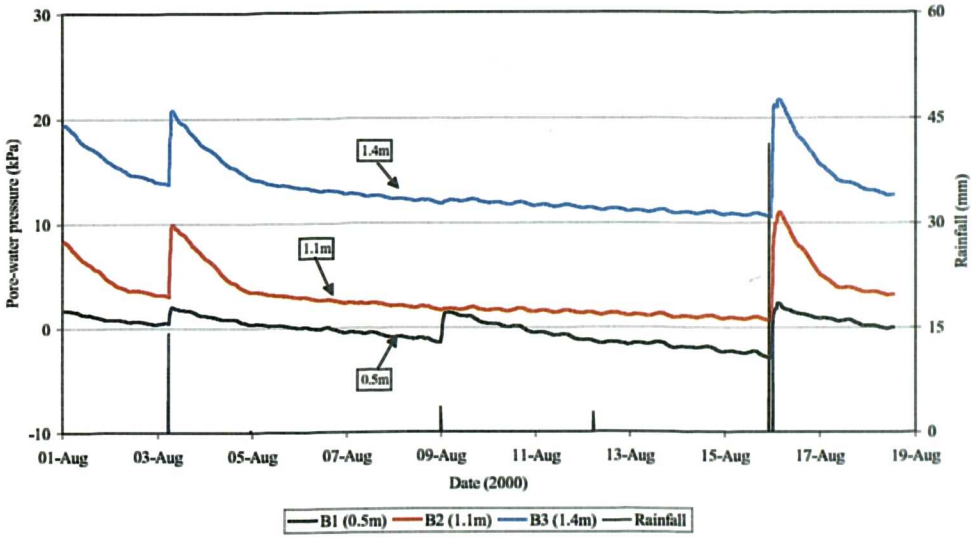

NTU-CSE slope, pore-water pressures of Row C during August 2000

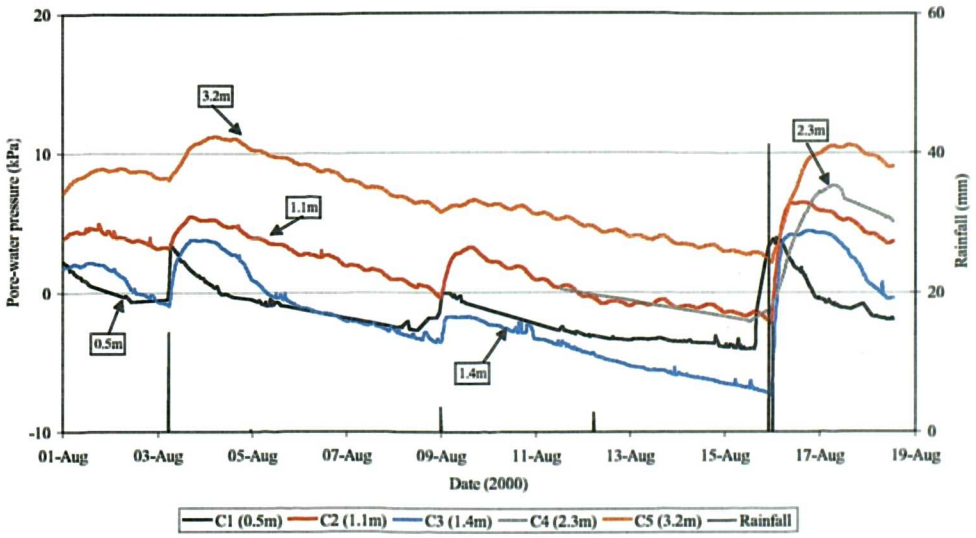

NTU-CSE slope, pore-water pressures of Row E during August 2000

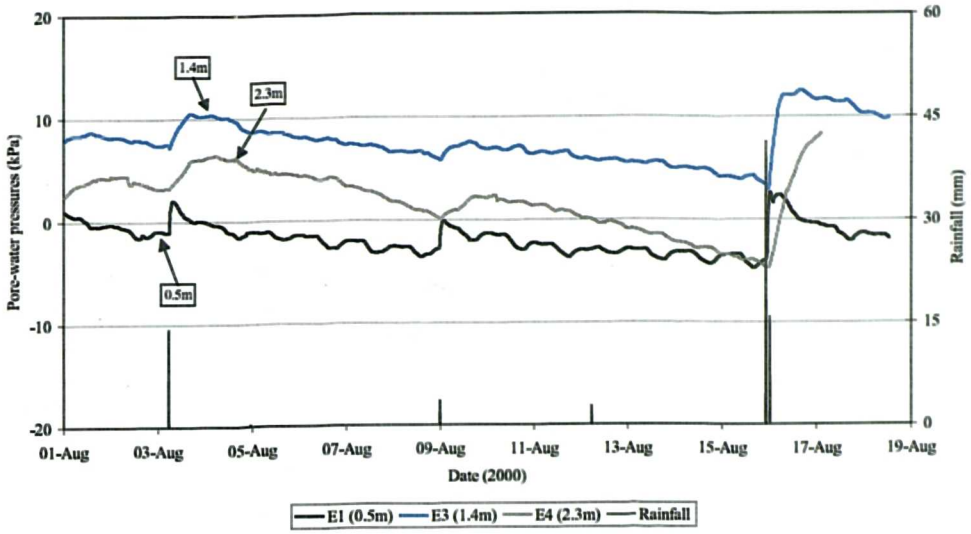

NTU-CSE slope, pore-water pressures of Row F during August 2000

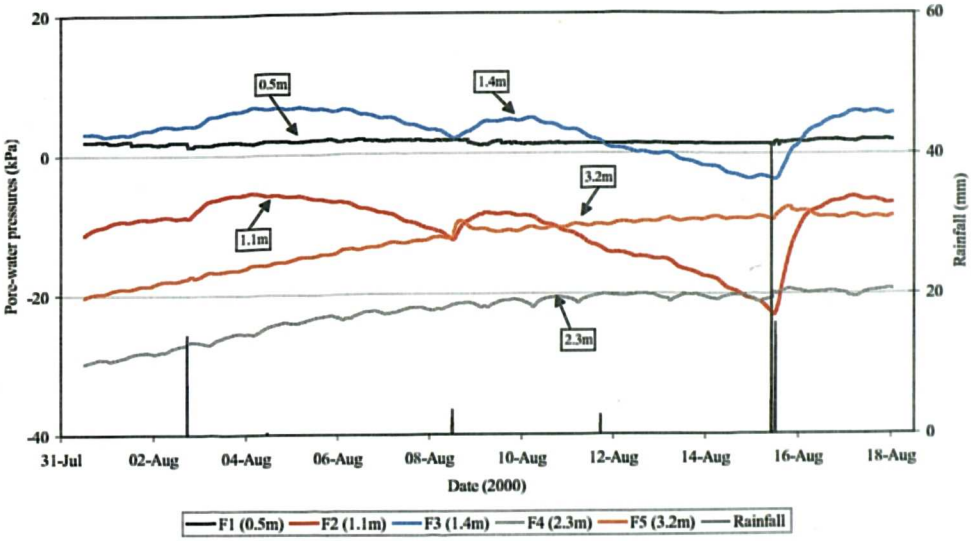

APPENDIX B

Pore-Water Pressures of the NTU-ANX Slope

NTU-ANX slope, pore-water pressures of Row A during March 2000

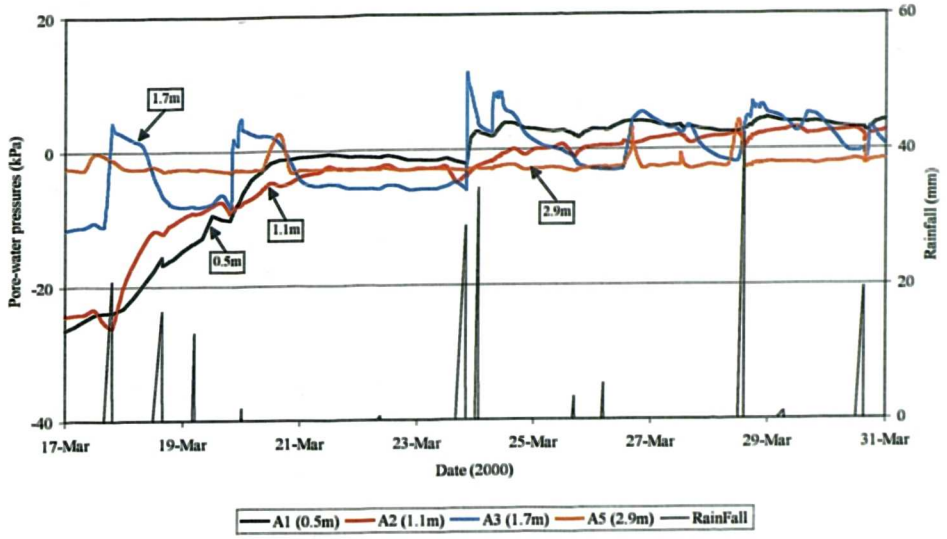

NTU-ANX slope, pore-water pressures of Row B during March 2000

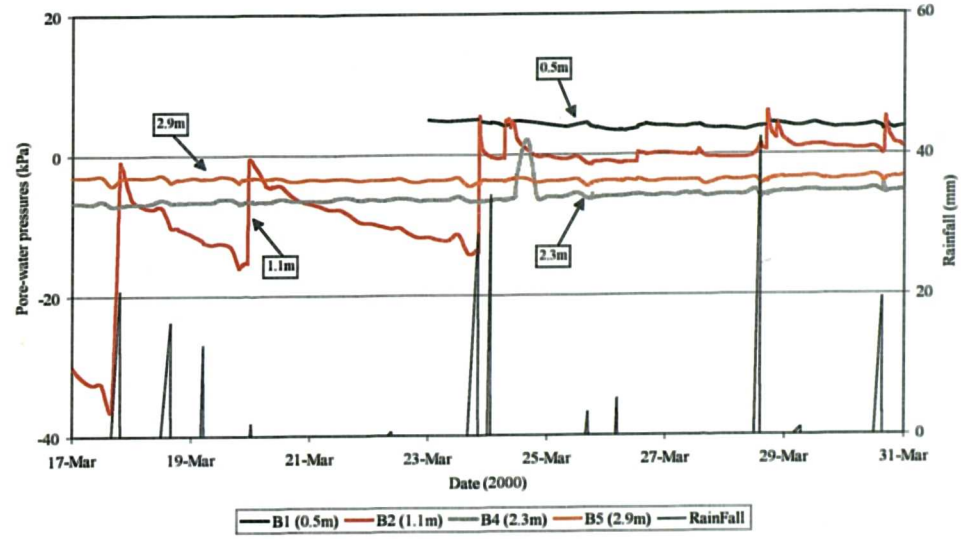

NTU-ANX slope, pore-water pressures of Row C during March 2000

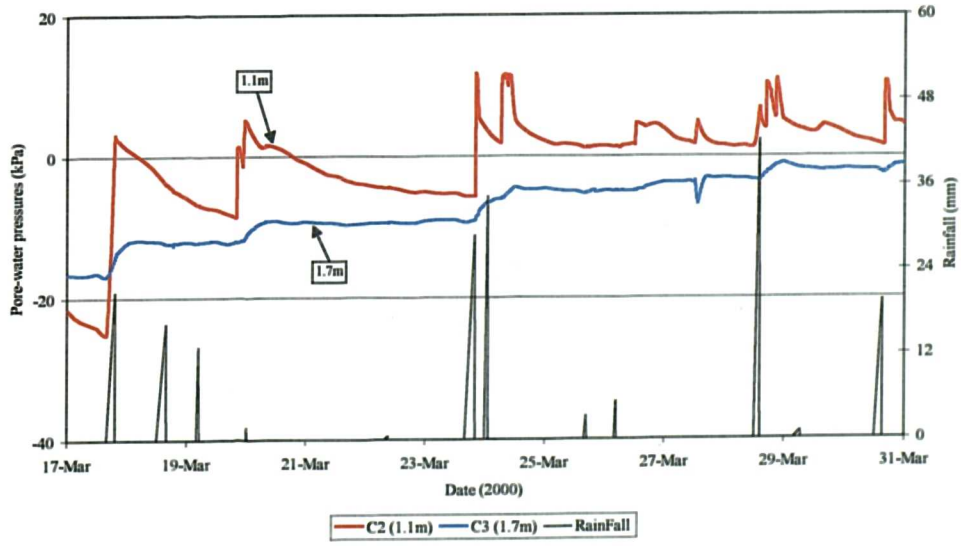

NTU-ANX slope, pore-water pressures of Row A during April 2000

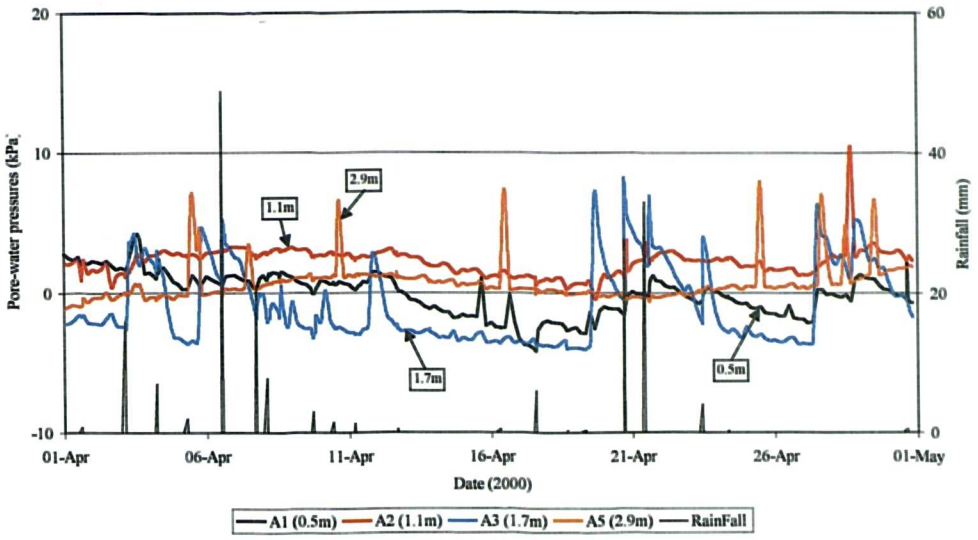

NTU-ANX slope, pore-water pressures of Row B during April 2000

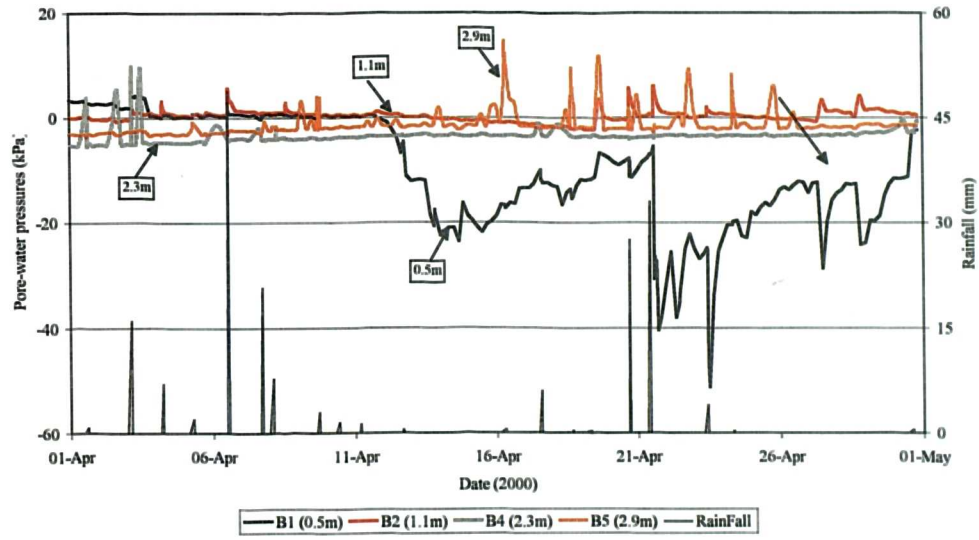

NTU-ANX slope, pore-water pressures of Row C during April 2000

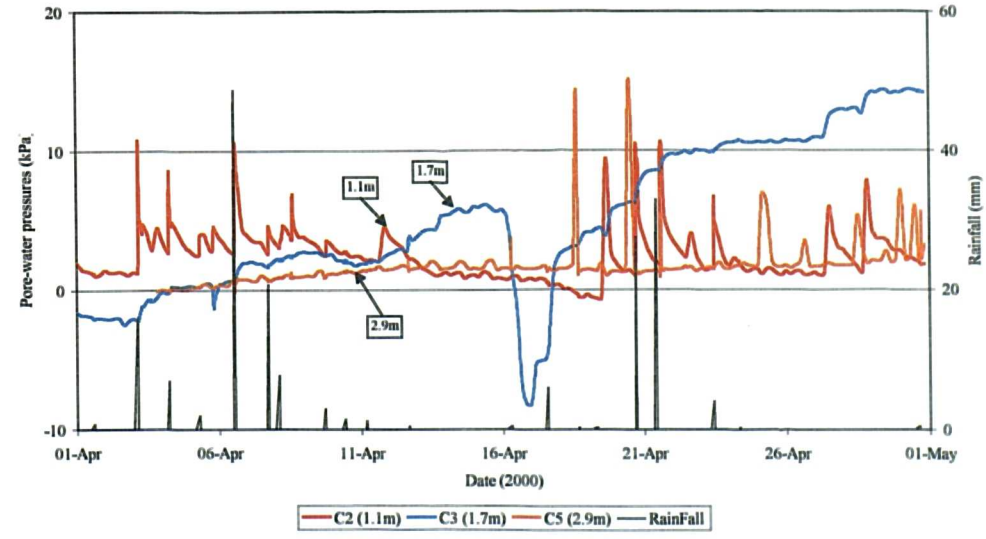

NTU-ANX slope, pore-water pressures of Row A during May 2000

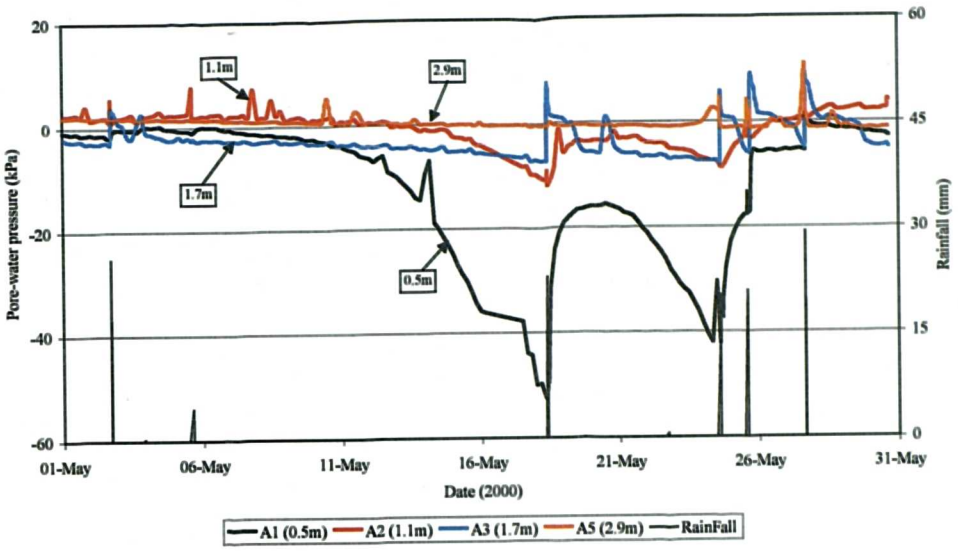

NTU-ANX slope, pore-water pressures of Row B during May 2000

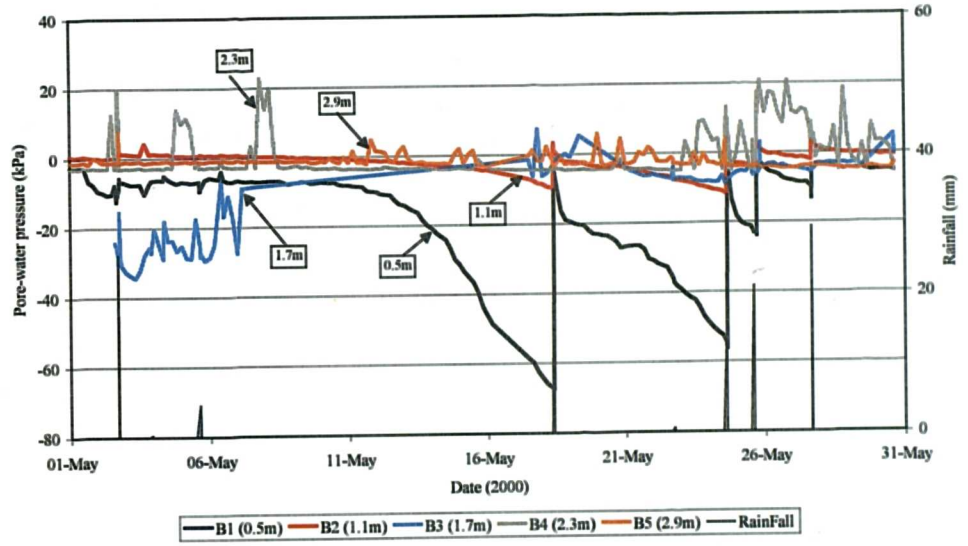

NTU-ANX slope, pore-water pressures of Row C during May 2000

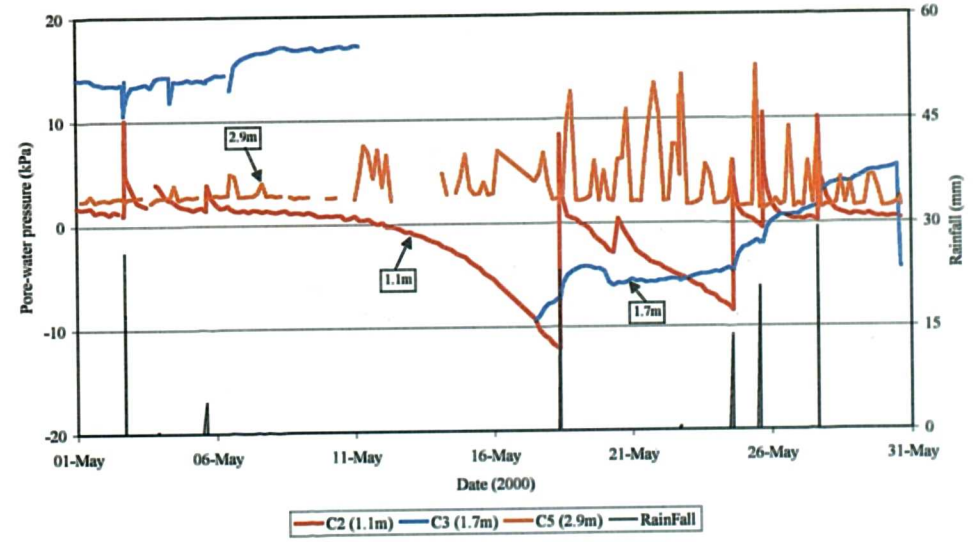

NTU-ANX slope, pore-water pressures of Row A during June 2000

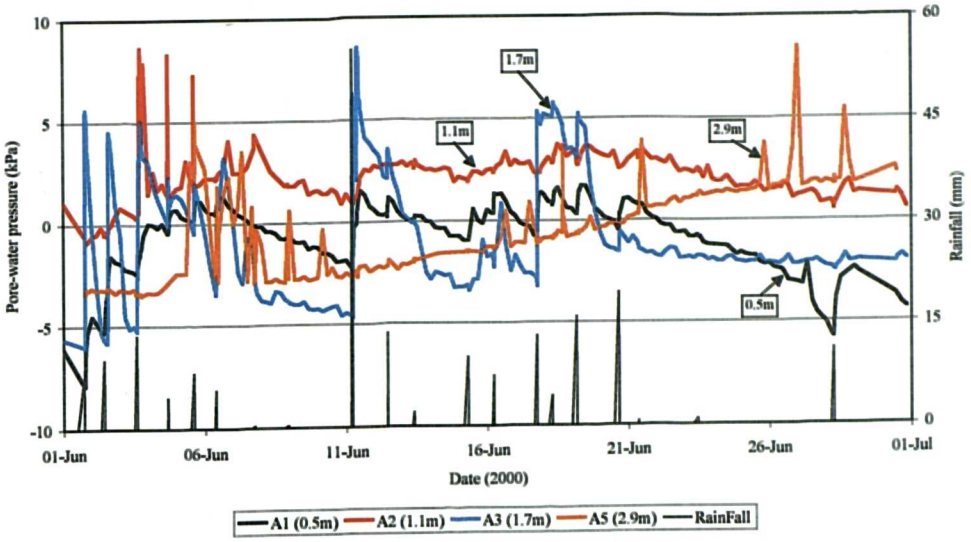

NTU-ANX slope, pore-water pressures of Row B during June 2000

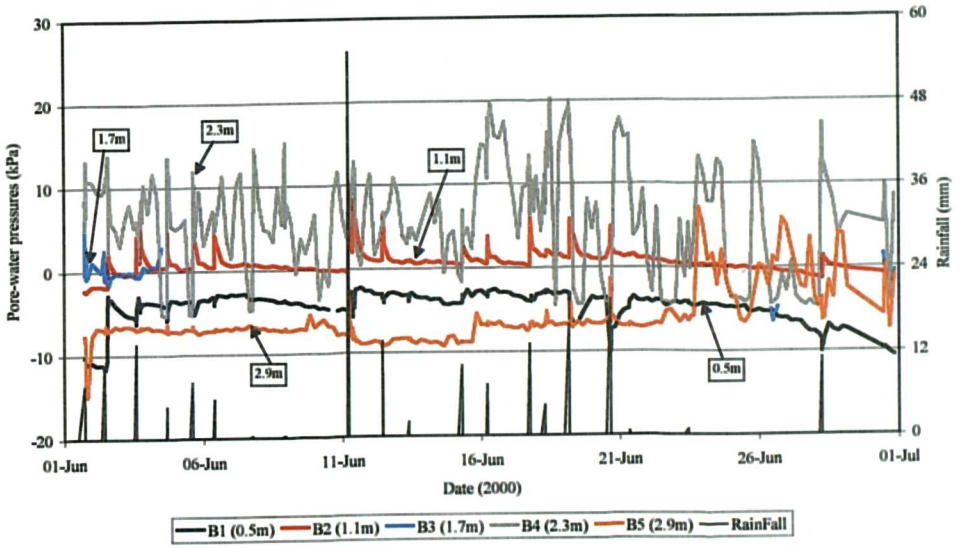

NTU-ANX slope, pore-water pressures of Row C during June 2000

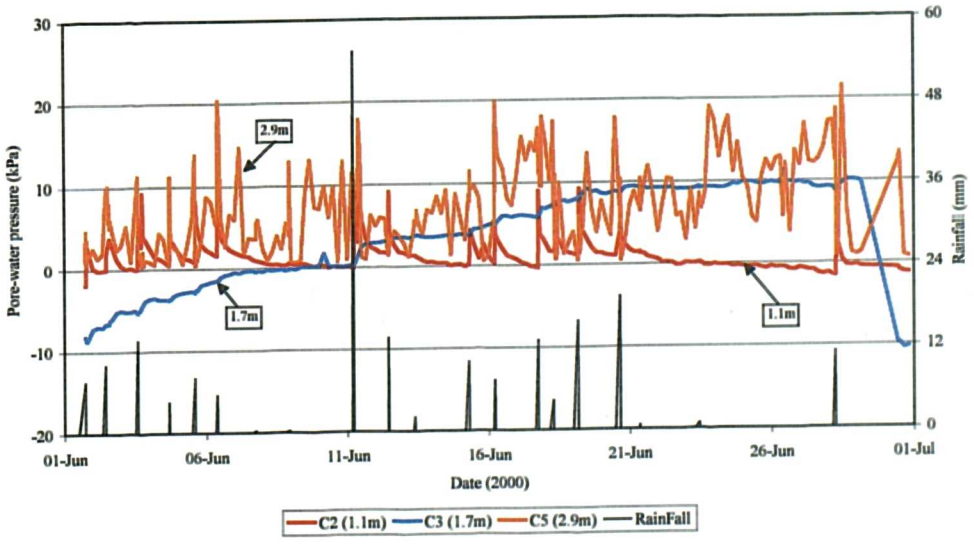

NTU-ANX slope, pore-water pressures of Row A during July 2000

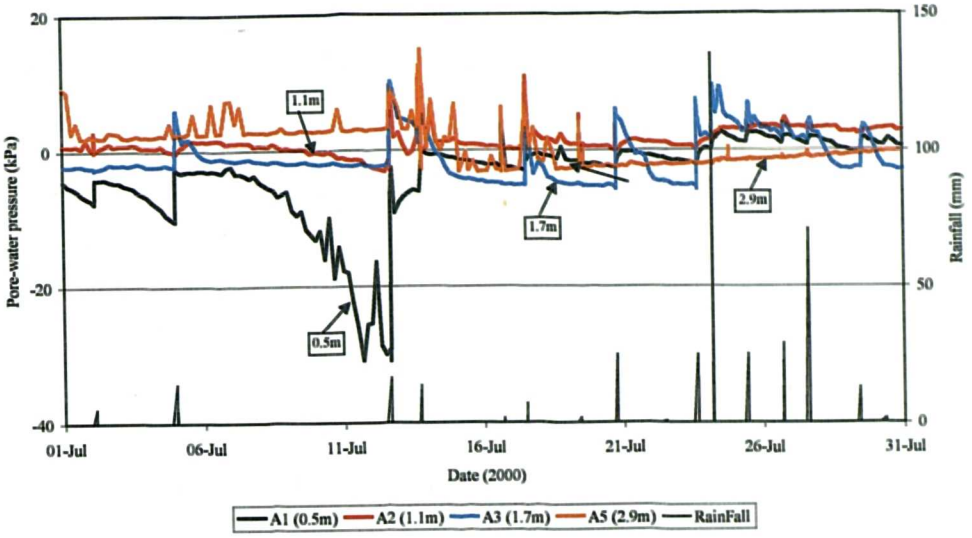

NTU-ANX slope, pore-water pressures of Row B during July 2000

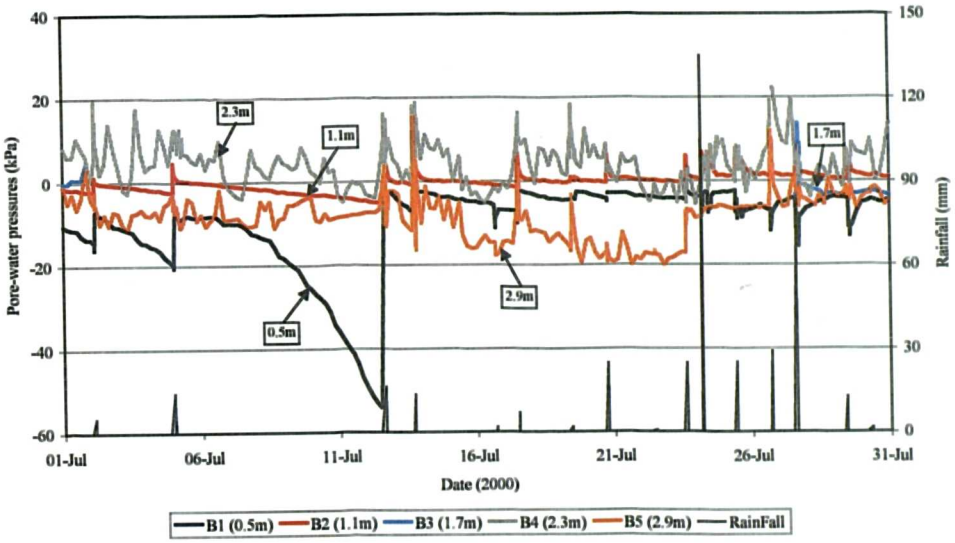

NTU-ANX slope, pore-water pressures of Row C during July 2000

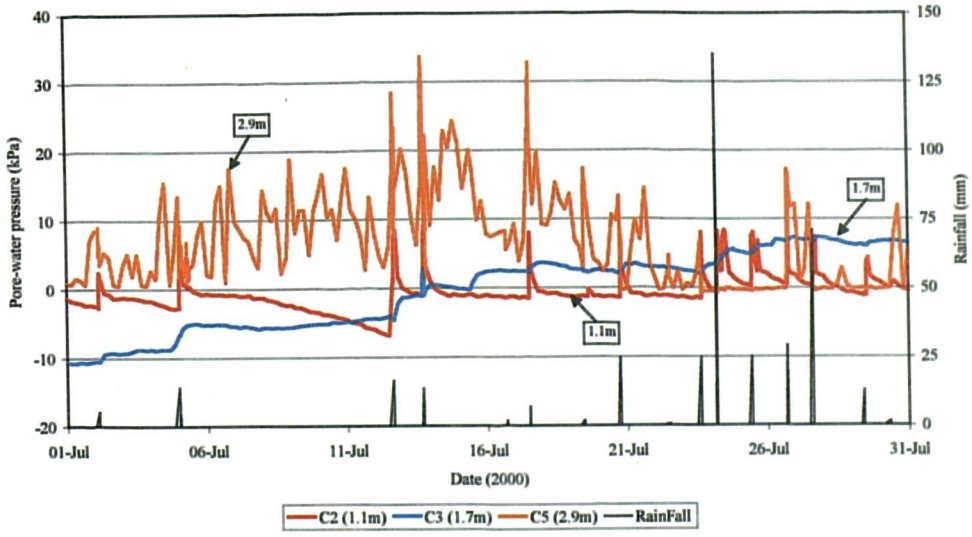

NTU-ANX slope, pore-water pressures of Row A during August 2000

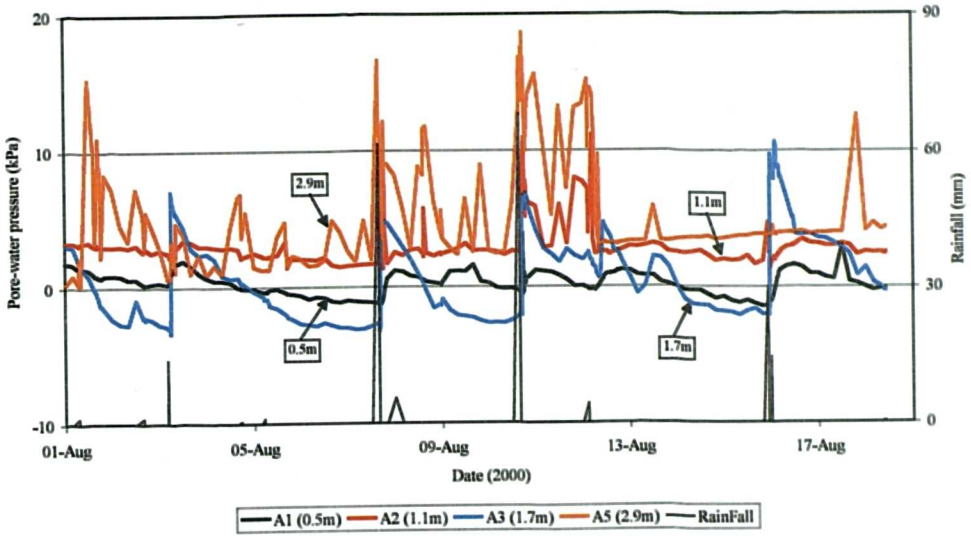

NTU-ANX slope, pore-water pressures of Row B during August 2000

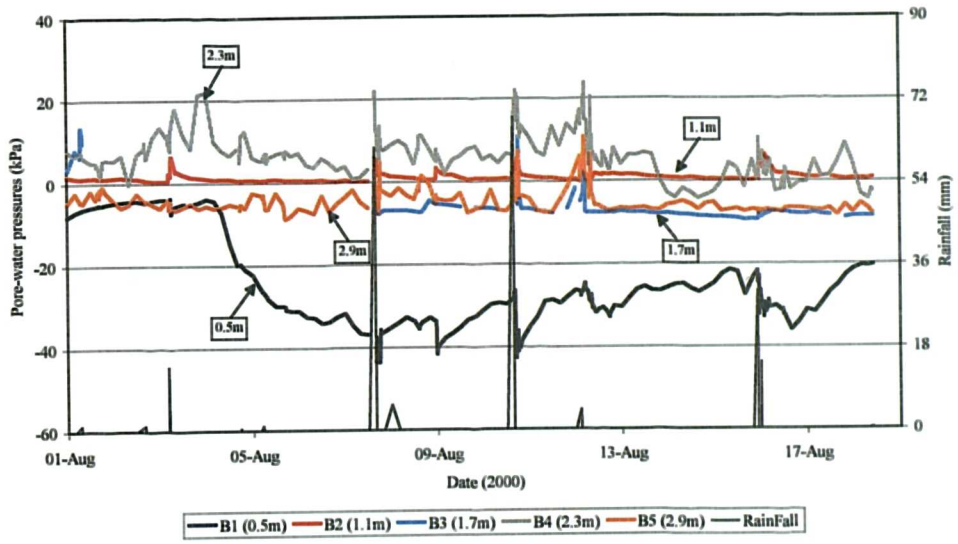

NTU-ANX slope, pore-water pressures of Row C during August 2000

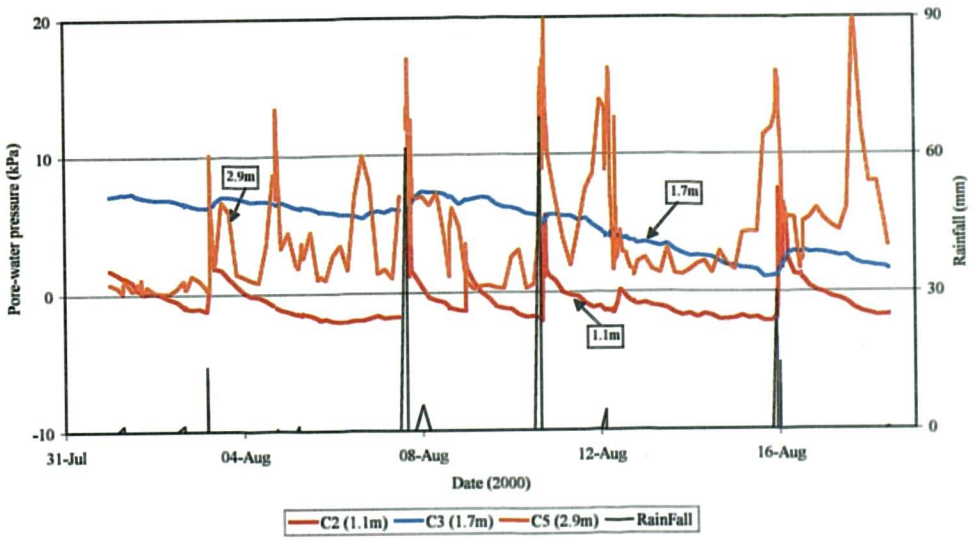

APPENDIX C

Runoff Measurements of Natural Rainfall Events on the NTU-ANX Slope

NTU-ANX slope, hyetographs and runoff measurements of the rainfall event of 23-Mar-00

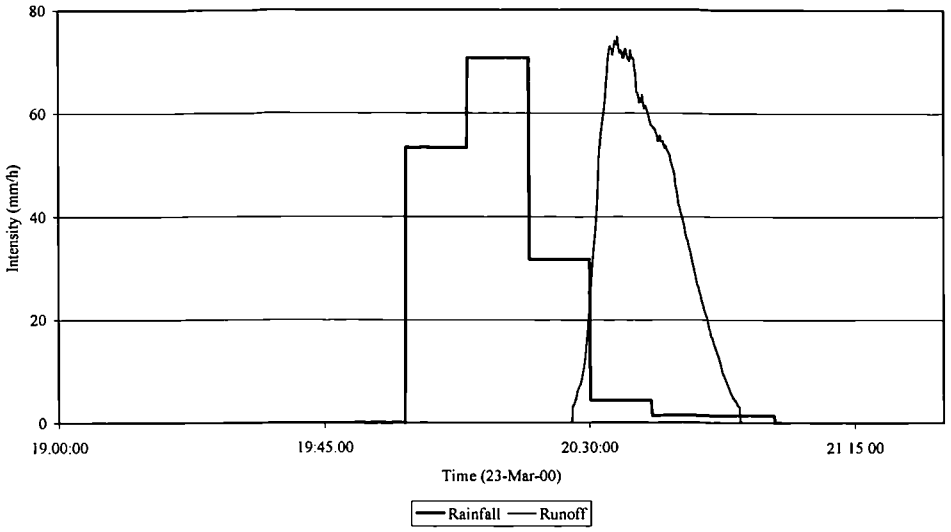

NTU-ANX slope, hyetographs and runoff measurements of the rainfall events of 24-Mar-00

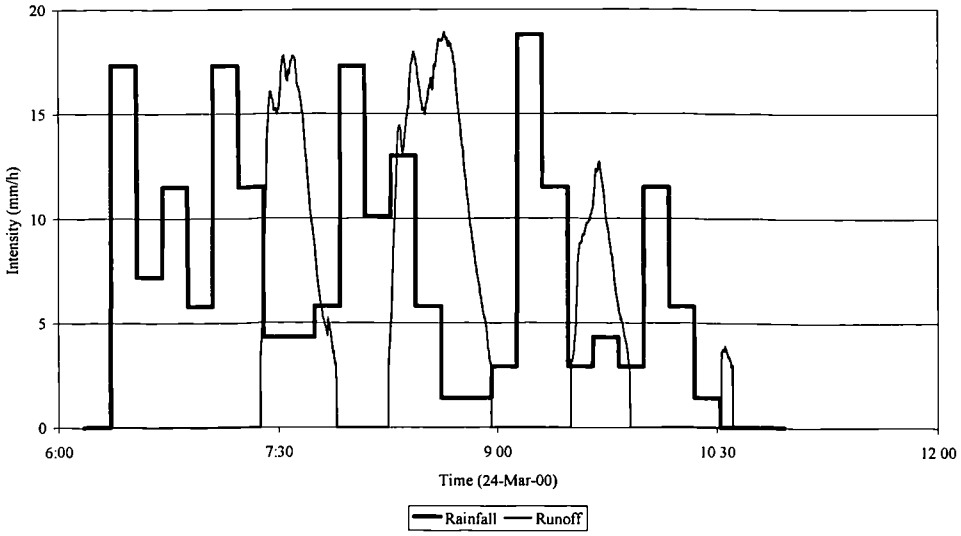

NTU-ANX slope, hyetograph and runoff measurement of the rainfall event of 06-Apr-00

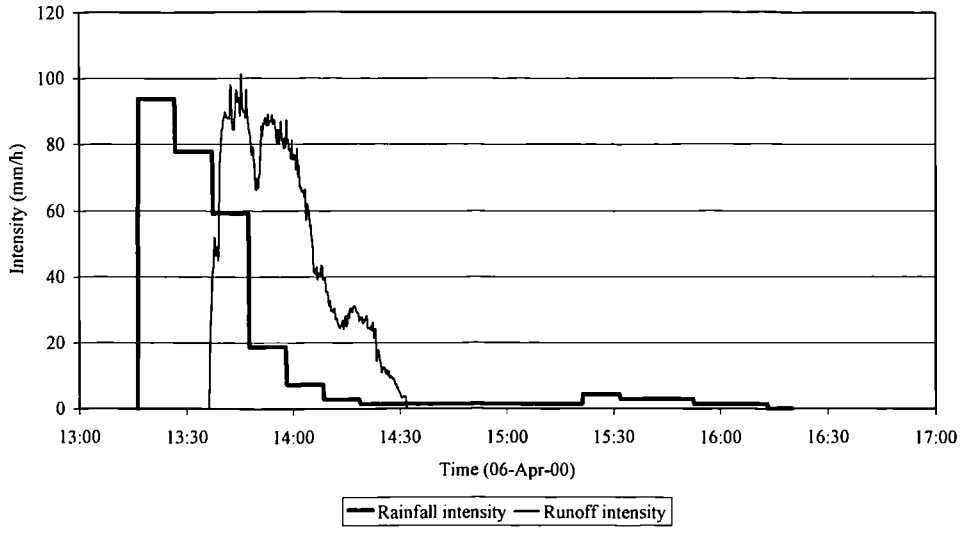

NTU-ANX slope, hyetograph and runoff measurement of the rainfall event of 03-Jun-00

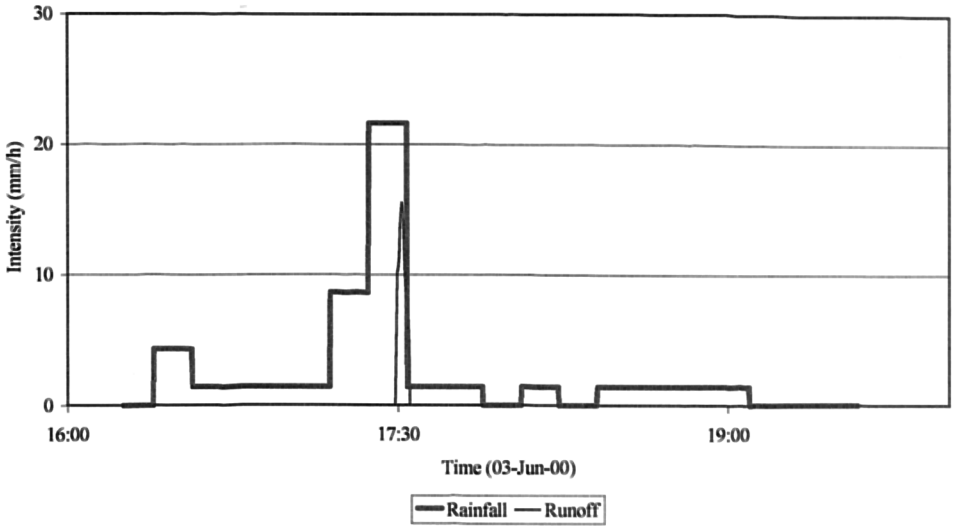

NTU-ANX slope, hyetograph and runoff measurement of the rainfall event of 11-Jun-00

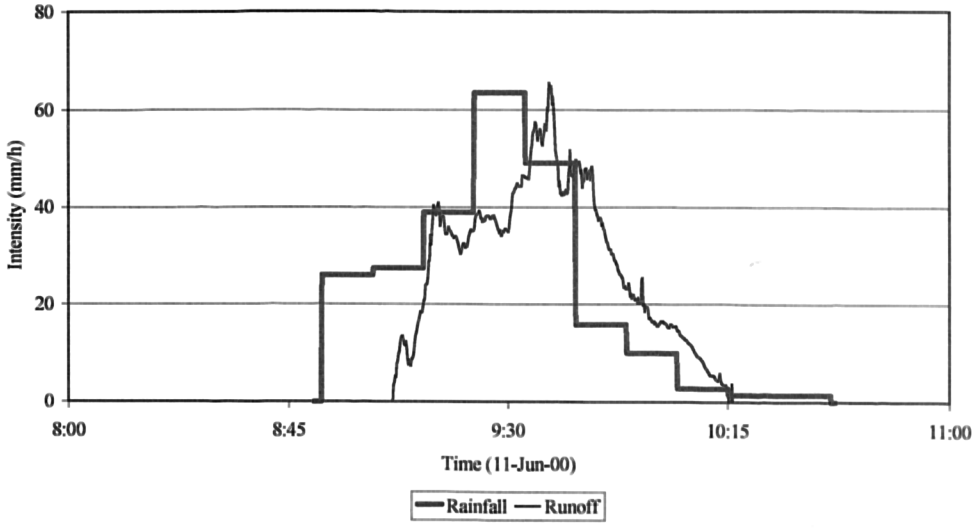

NTU-ANX slope, hyetograph and runoff measurement of the rainfall of 17-Jun-00

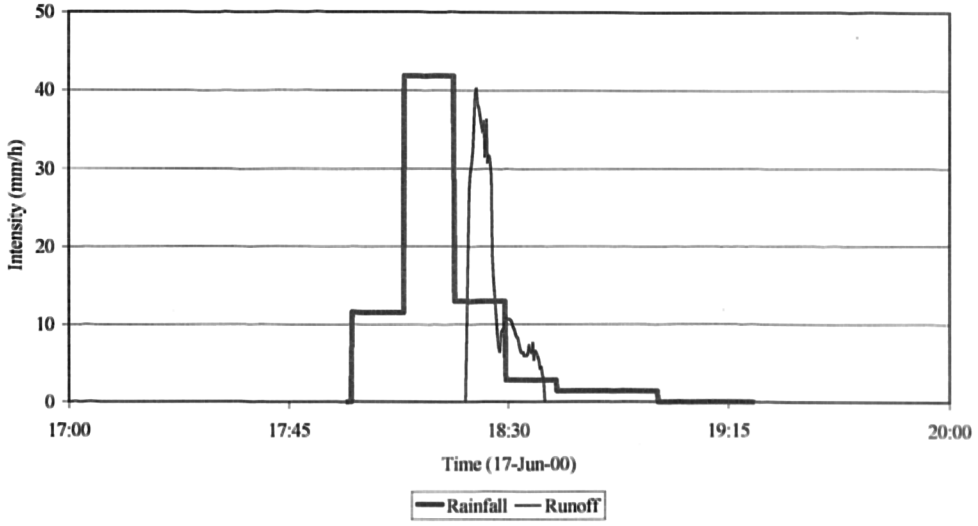

NTU-ANX slope, hyetograph and runoff measurement of the rainfall event of 19-Jun-00

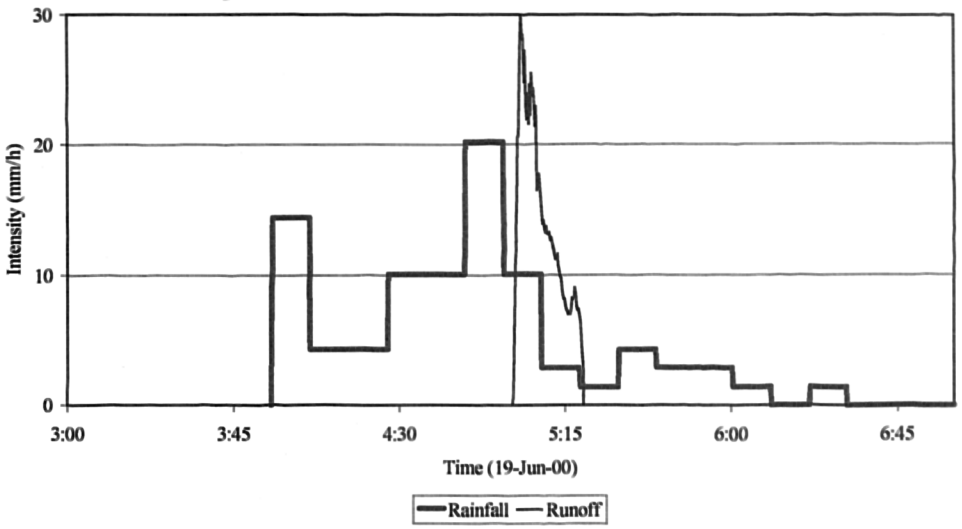

NTU-ANX slope, hyetograph and runoff measurement of the rainfall event of 25-Jul-00

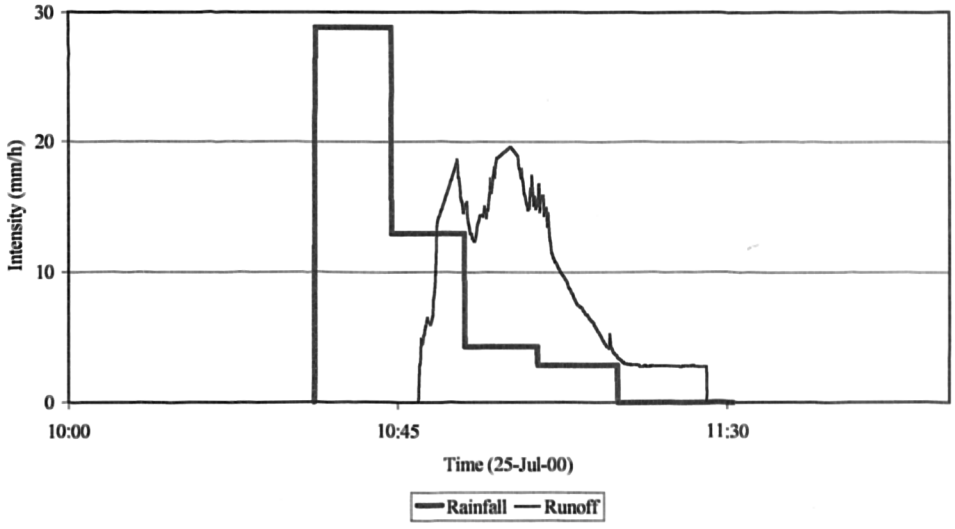

NTU-ANX slope, hyetograph and runoff measurement of the rainfall event of 25-Jul-00

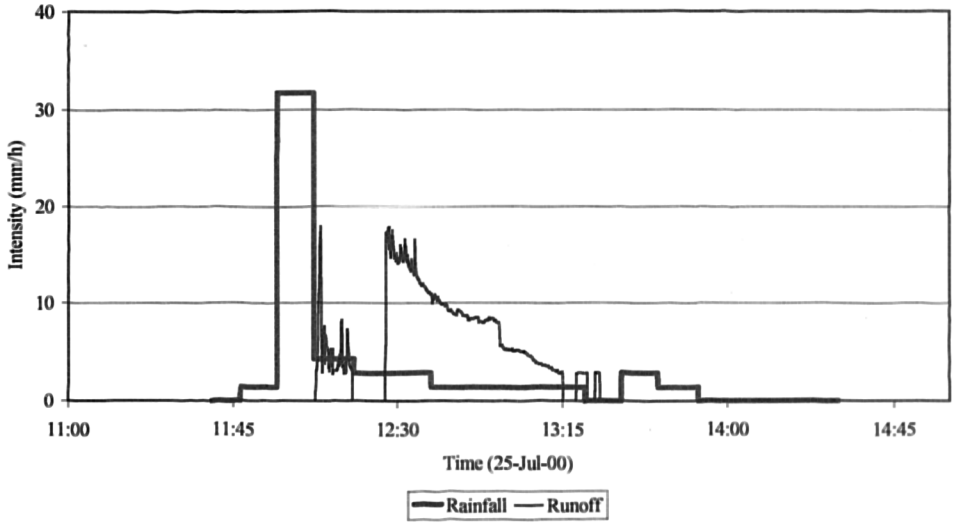

NTU-ANX slope, hyetograph and runoff measurement of the rainfall event of 25-Jul-00

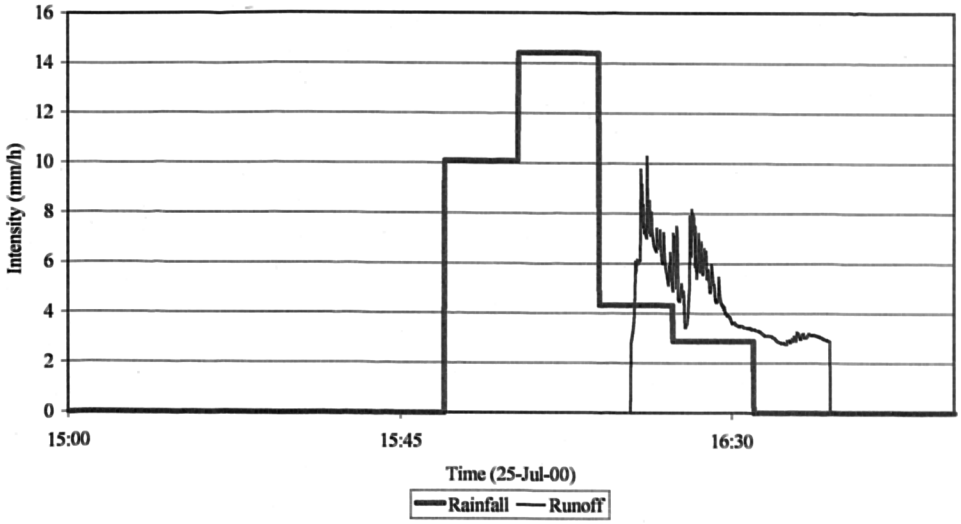

NTU-ANX slope, hyetograph and runoff measurement of the rainfall event of 29-Jul-00

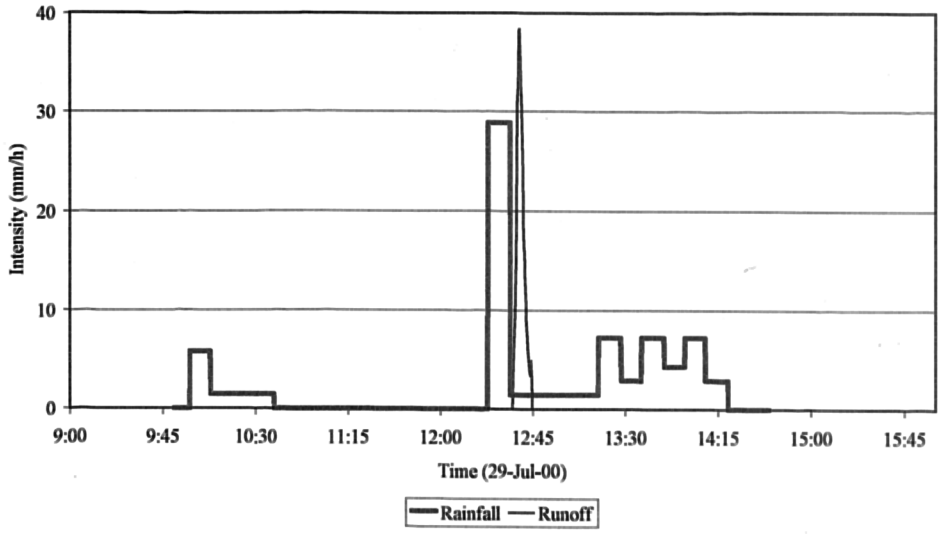

NTU-ANX slope, hyetograph and runoff measurement of the rainfall event of 03-Aug-00

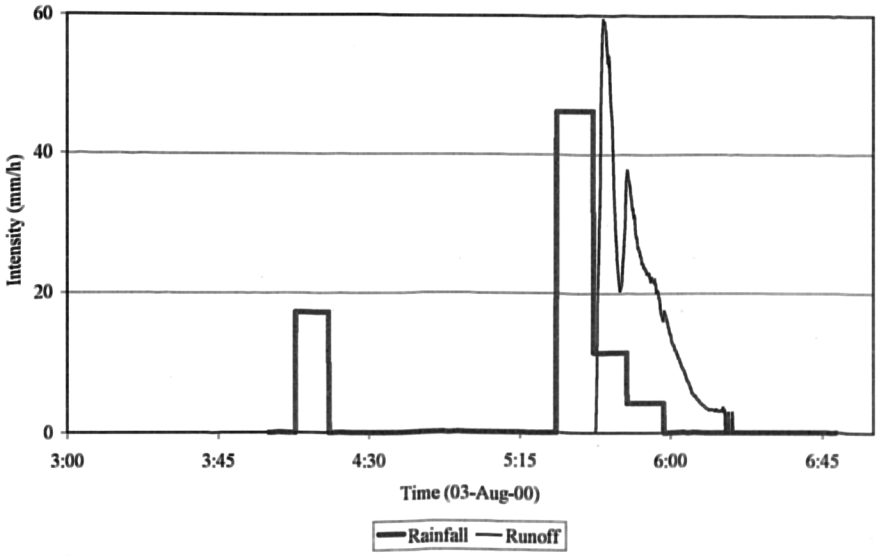

NTU-ANX slope, hyetograph and runoff measurement of the rainfall event of 08-Aug-00

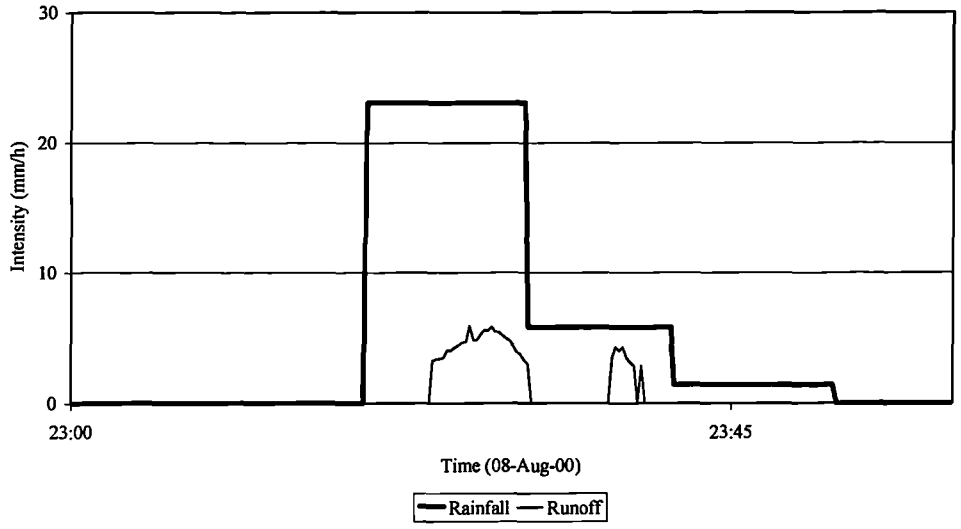

NTU-ANX slope, hyetograph and runoff measurement of the rainfall event of 15/16-Aug-00

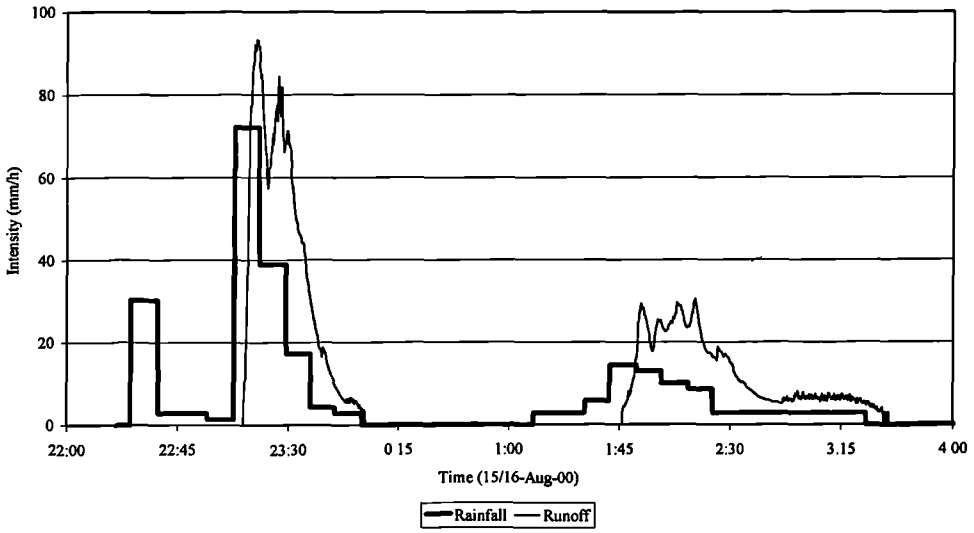

APPENDIX D

Runoff Measurements of Simulated Rainfall Events on the NTU-ANX Slope

NTU-ANX slope, hyetograph and runoff measurement of the simulated rainfall event of 02-May-00

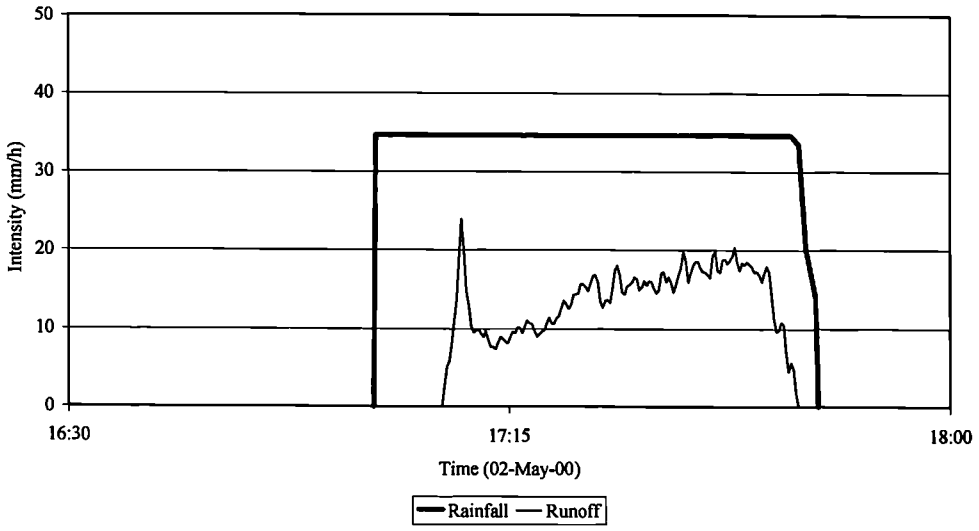

NTU-ANX slope, hyetograph and runoff measurement of the simulated rainfall event of 12-Jun-00

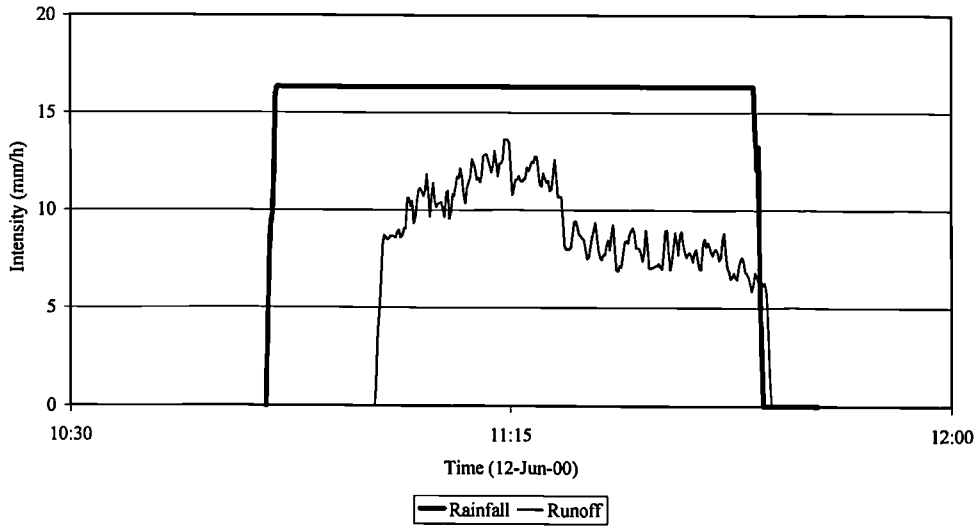

NTU-ANX slope, hyetograph and runoff measurement of the simulated rainfall of 20-Jun-00

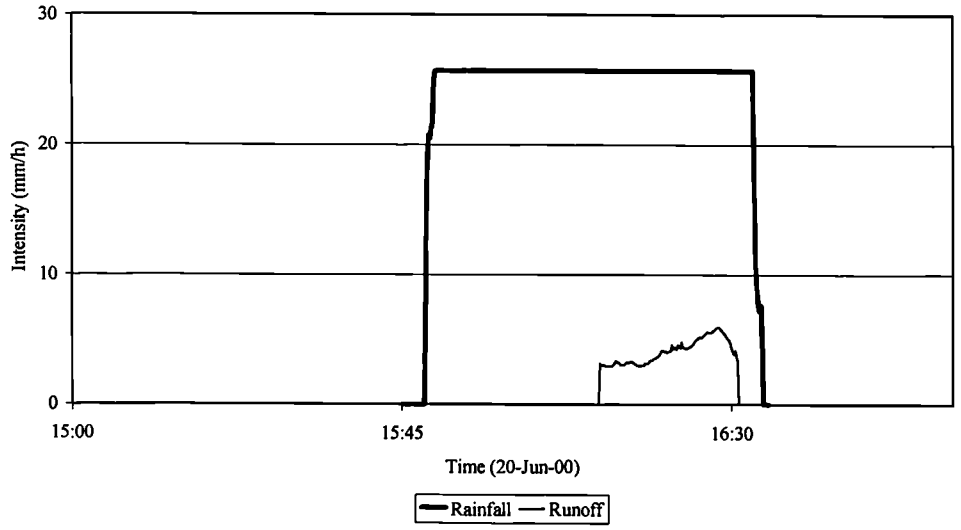

NTU-ANX slope, hyetograph and runoff measurement of the simulated rainfall of 13-Jul-00

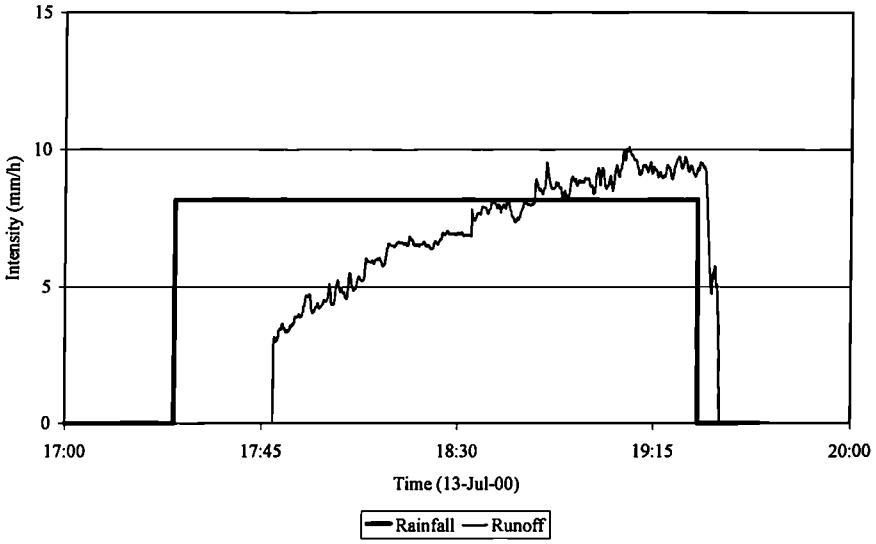

NTU-ANX slope, hyetograph and runoff measurement of the simulated rainfall of 17-Jul-00

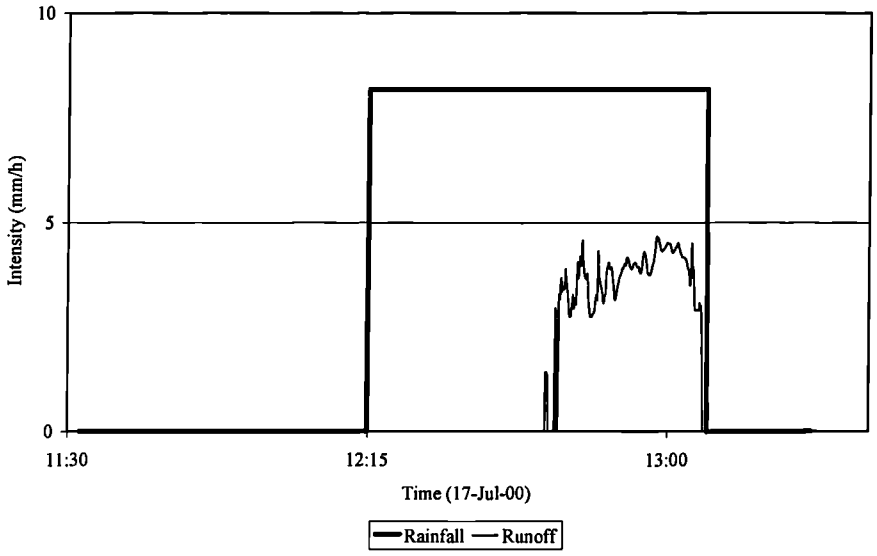

NTU-ANX slope, hyetograph and runoff measurement during the simulated rainfall of 20-Jul-00

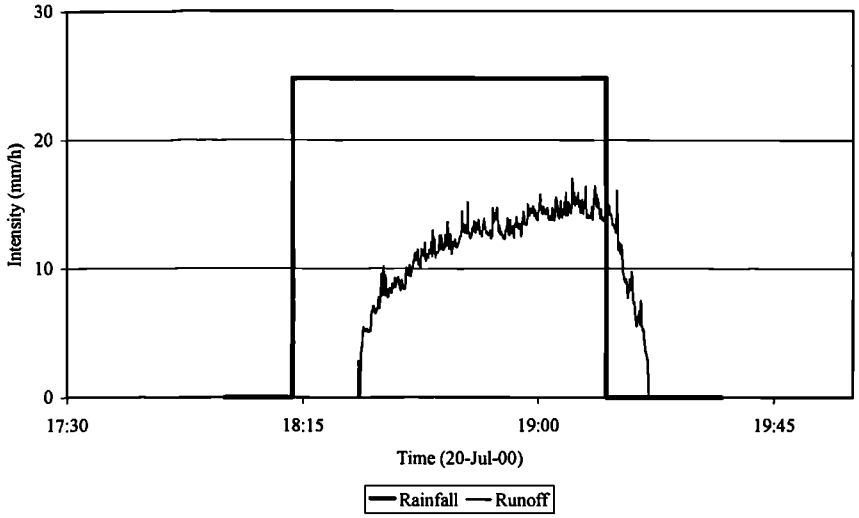

NTU-ANX slope, hyetograph and runoff measurement of the simulated rainfall of 26-Jul-00

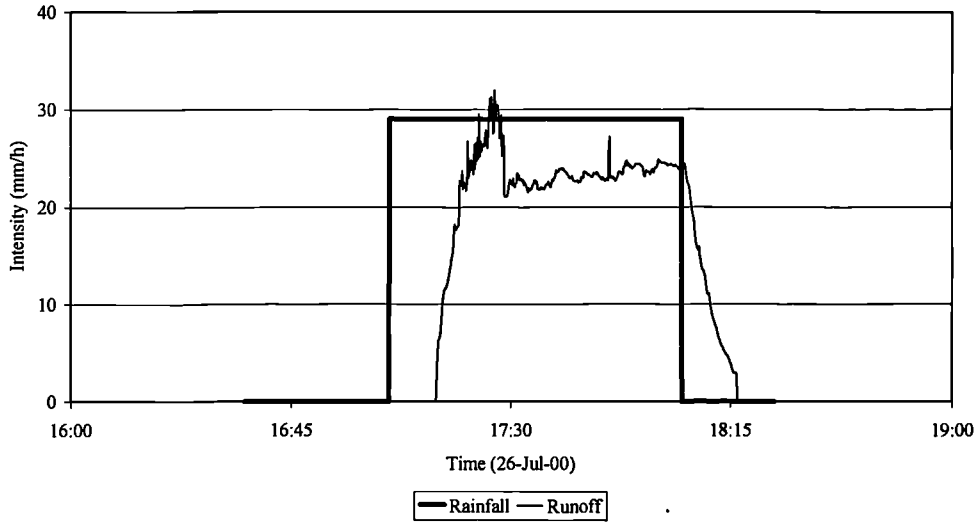

NTU-ANX slope, hyetograph and runoff measurement of the simulated rainfall of 27 Jul-00

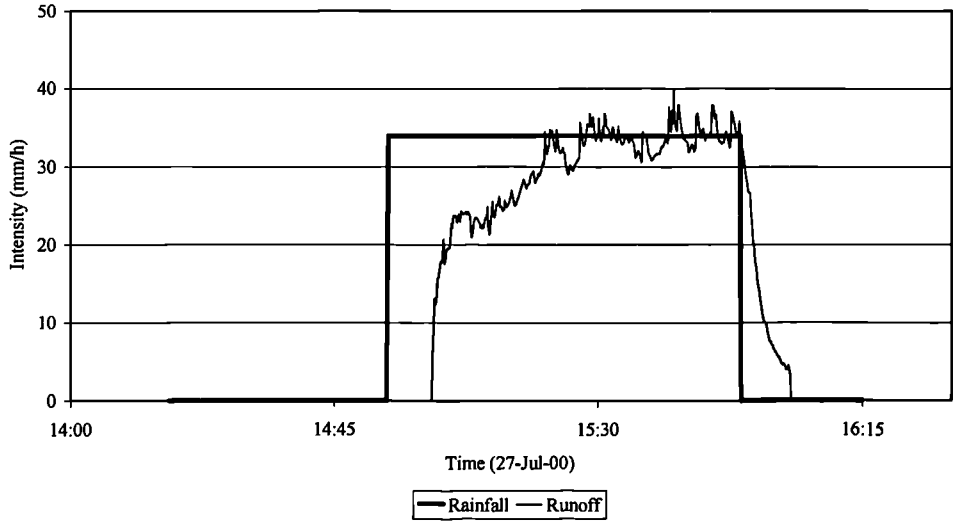

NTU-ANX slope, hyetograph and runoff measurement of the simulated rainfall of 27 Jul-00

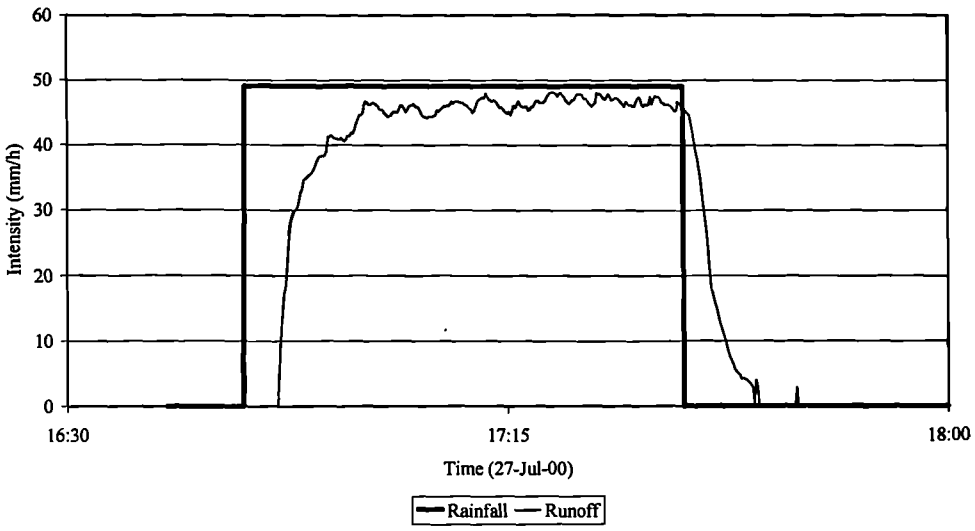

NTU-ANX slope, hyetograph runoff measurement of the simulated rainfall of 07-Aug-00

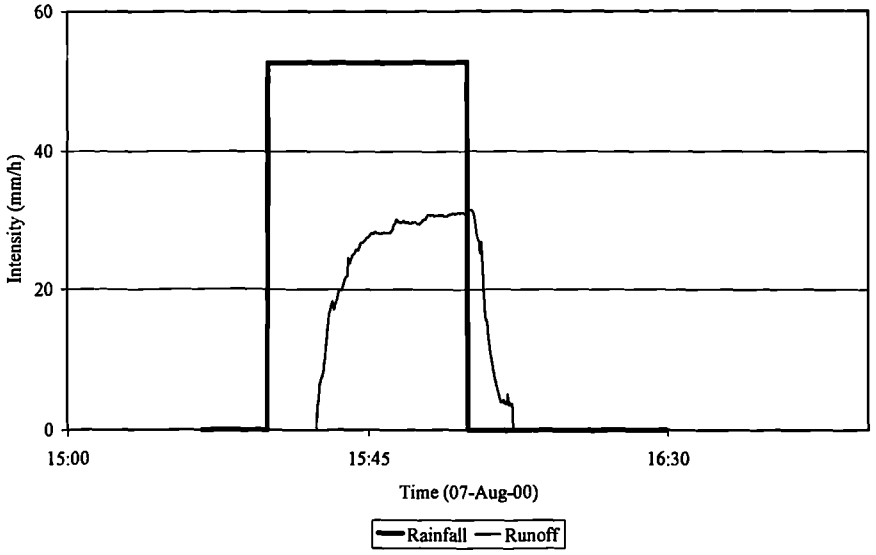

NTU-ANX slope, hyetograph runoff measurement of the simulated rainfall of 07-Aug-00

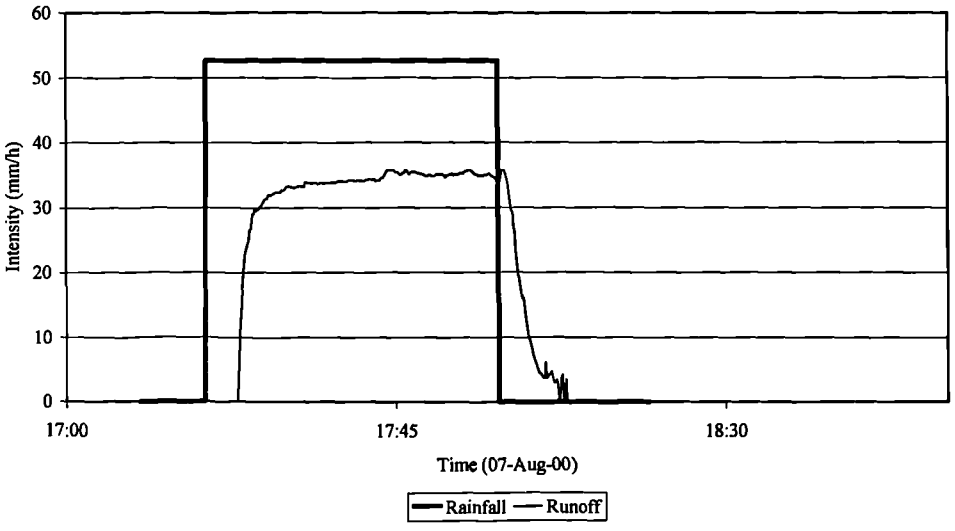

NTU-ANX slope, hyetograph and runoff measurement of simulated rainfall of 10-Aug-00

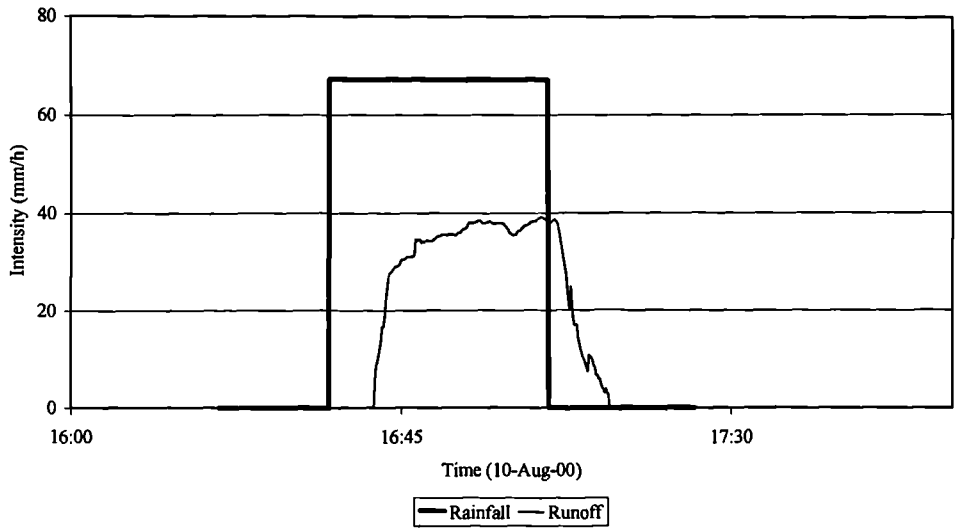

NTU-ANX slope, hyetograph and runoff measurement of simulated rainfall of 10-Aug-00

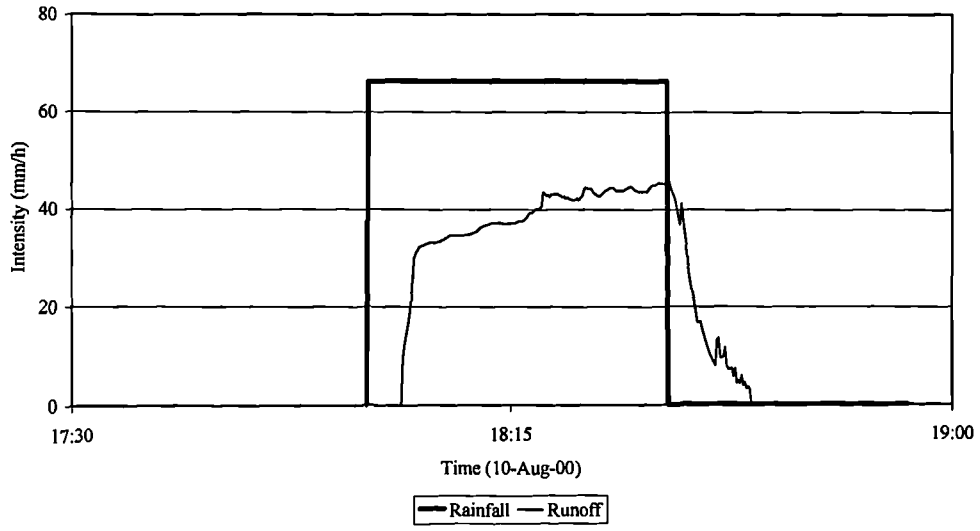

Dissemination

Parts of the analyses related to this work are published in or submitted for publication to International Scientific Journals and in Proceedings of International Conferences. By the date of the submission of this thesis (March 2002) to the School of Engineering of the University of Durham, the references of these publications are:

I. Tsaparas and D.G. Toll. *Numerical Modelling of Infiltration into an Unsaturated Soil Slope,* abstract submitted in February 2002 for review to Geotechnique.

I. Tsaparas, H. Rahardjo, D.G. Toll and E.C. Leong. *Infiltration Characteristics of two Instrumented Residual Soil Slopes,* submitted in January 2002 for review and possible publication to Canadian Geotechnical Journal.

I. Tsaparas, D.G. Toll. (2002) *Numerical Analysis of Infiltration into Unsaturated Residual Soil Slopes,* Proceedings of the International Conference of Unsaturated Soils, UNSAT-2002, Brazil 2002. (in press)

I. Tsaparas, H. Rahardjo, D.G. Toll and E.C. Leong (2002). *Controlling Parameters for Rainfall-Induced Landslides,* Computers and Geotechnics, Vol. 29, pp. 1-27.

D.G. Toll, I. Tsaparas, H. Rahardjo (2001). *The Influence of Rainfall Sequences on Suctions within Slopes*, Proceedings of the XVth International Conference on Soil Mechanics and Geotechnical Engineering, August 2001, Istanbul, Turkey.

I. Tsaparas, D.G. Toll and H. Rahardjo 2000. *Influence of Rainfall Sequences on the Seepage Conditions within a Slope: a Parametric Study*, Proceedings of the Asian Conference on Unsaturated Soils: From Theory to Practise, May 2000, Singapore: 837-842.

References

Agus S.S., Leong E.C. and Rahardjo H. (1999) *Field Measurements of Permeability for Residual Soils*, Proceedings of the 5th International Symposium on Field Measurements in Geomechanics, Singapore, December 1-3, pp. 537-542.

Alonso E., Gens A. & Josa A. (1990) *A Constitutive Model for Partially Saturated Soils,* Geotechnique, Vol. 40, No. 3, pp. 405-430.

Alonso E., Gens A. & Lloret A. (1995) *Effect of Rain Infiltration on the Stability of Slopes,* Proceedings of the 1st International Conference on Unsaturated Soils. UNSAT 95, Paris, pp. 241-249.

Anderson M.G., Collison A.J.C., Hartshorne J., Lloyd D.M. & Park A. (1996) *Developments in Slope Hydrology-Stability Modelling for Tropical Slopes,* Advances in Hillslope Processes, Vol. 2, pp. 799-821.

Bao C.G. & Ng C.W.W. (2000) *Some Thoughts and Studies on the Prediction of Slope Stability in Expansive Soils,* Proceedings of the Asian Conference on Unsaturated Soils, UNSAT-ASIA 2000, Singapore, pp.15-31.

Barden L. (1965) *Consolidation of Compacted and Unsaturated Clays,* Geotechnique, Vol. 15, 267-286.

Bishop A.W. (1959) *The Principle of Effective Stress,* Tecknisk Ukeblad 106, No. 39, pp. 859-863.

Brand E.W. (1981) *Some Thoughts on Rain-Induced Slope Failures,* Proceedings of the 10th International Conference on Soil Mechanics and Foundation Engineering, Stockholm, 1981, Vol. 3, pp. 373-376.

Brand E.W. (1984) *Landslides in Southeast Asia: A State of the Art Report,* Proceedings of the 4th International Symposium on Landslides, Toronto, Canada, Vol. 1, pp. 17-59.

Brand E.W., Premchitt J. & Phillipson H.B. (1984) *Relationship Between Rainfall and Landslides in Hong Kong,* Proceedings of the 4th International Symposium on Landslides, Toronto, Canada 1984; Vol. 1, pp. 377-384.

Brooks R.H. and Corey A.T. (1964) *Hydraulic Properties of a Porous Media,*

Hydrology Paper No.3, Colorado State University, Fort Collins, Colorado.

Campbell G.S. (1974) *A Simple Method for Determining Unsaturated Conductivity from Moisture Retention Data,* Soil Science, Vol. 117, pp. 311-314.

Chang M.F. (1988) *In-Situ Testing of Residual Soils in Singapore,* Proceedings of the 2nd International Conference on Geomechanics in Tropical Soils, Singapore 12-14 December 1988, Vol. 1, pp: 97-108.

Chatterjea, K. (1989) *Observations on the Fluvial and Slope Processes in Singapore and their Impact on the Urban Environment*, PhD Thesis, National University of Singapore.

Chinniah G., Clemence S.P. & Thurairajah A. (1994) *Slope Stability in Residual Soils: an Overview,* Proceedings of the International Conference on Landslides, Slope Stability and the Safety of Infrastructures, Malaysia, 1994.

Collison A.J.C., Anderson M.G. & Lloyd D.M. (1995) *Impact of Vegetation on Slope Stability in a Humid Tropical Environment: a Modelling Approach*, Proceedings of Institution of Civil Engineers, Water, Maritime and Energy, Vol. 112, pp. 168-175.

Corey A.T. (1954) *The Interrelation between Gas and Oil Relative Permeabilities*, Producer's Monthly, Vol. 19, No. 1, pp. 7-10.

Dane J.H. & Klute A. (1977) *Salt Effects on the Hydraulic Properties of a Swelling Soil,* Soil Science Society of America Journal, Vol. 41, pp.1043-1049.

Day R. W. & Axten G.W. (1989) *Surficial Stability of Compacted Clay Slopes*, Journal of Geotechnical Engineering, ASCE, Vol. 115, No. 4, pp. 577-580.

Deutcher M.S., Gasmo J.M., Rahardjo H., Leong E.C. & Tang S.K. (2000) *Field Measurements of Pore-Water Pressure Profiles in Residual Soil Slopes of the Bukit Timah Granite Formation, Singapore,* Proceedings of the Asian Conference on Unsaturated Soils, UNSAT-ASIA 2000, Singapore, pp.777-782.

Dykes A.P. & Thornes J.B. (2000) *Hillslope Hydrology in Tropical Rainforest Steeplands in Brunei,* Hydrological Processes, Vol. 14, pp. 215-235.

Elrick E.D & Reynolds W.D. (1992) *Infiltration from Constant-Head Well Permeameters and Infiltrometers,* Soil Science Society of America Special

Publication, pp. 01-23.

Escario V & Saez J. (1986) *The Shear Strength of Partly Saturated Soils,* Geotechnique, Vol. 36, No. 3, pp. 453-456.

Faisal H.A. (2000) *Unsaturated Tropical Residual Soils and Rainfall Induced Landslides in Malaysia,* Proceedings of the Asian Conference on Unsaturated Soils, UNSAT-ASIA 2000/ Singapore, May 2000, pp 41-52.

Fluke® Co. (1997) *2635A Hydra Series II Data Bucket, Users Manual,* Everett, USA

Fourie A. B. (1996) *Predicting Rainfall-Induced Slope Instability,* Proceedings of Institution of Civil Engineers, Geotechnical Engineering, Vol. 119, pp. 211-218.

Fredlund D. G. (1979) *Appropriate Concepts and Technology for Unsaturated Soils*, Canadian Geotechnical Journal, Vol. 16, pp. 121-139.

Fredlund D. G. & Barbour S.L. (1992) *Integrated Seepage Modelling and Slope Stability Analyses: A Generalized Approach for Saturated/Unsaturated soils*, Geomechanics and Water Engineering in Environmental Management. R. N. Chowdhury (ed.), ISBN 90-5410-112-1, A.A. Balkema, Rotterdam, pp. 3-35.

Fredlund D. G. & Morgenstern R.N. (1977) *Stress State Variables For Unsaturated Soils*, Journal of Geotechnical Engineering, ASCE, Vol. 103, No. 5, pp. 447-466.

Fredlund D. G., Morgenstern N.R. & Widger R.A. (1978) *The Shear Strength of Unsaturated Soils,* Canadian Geotechnical Journal, Vol. 15, No. 3, pp. 313-321.

Fredlund D. G. & Rahardjo H. (1993) *Soil Mechanics for Unsaturated Soils*, Wiley Interscience Publication, ISBN: 0-471-85008-X, p. 517.

Fredlund D.G. & Xing A. (1994) *Equations for the Soil-Water Characteristic Curve*, Canadian Geotechnical Journal, Vol. 31, pp. 521-532.

Gardner W.R. (1958) *Some Steady State Solutions of the Unsaturated Moisture Flow Equation with Application to Evaporation from a Water Table,* Soil Science, Vol. 85, No. 4, pp. 228-232.

Gasmo J. (1997) *Stability of Unsaturated Residual Soil Slope as Affected by Rainfall,* MEng. Thesis, School of Civil and Structural Engineering, Nanyang Technological University, Singapore.

Gasmo J., Hritzuk K.J., Rahardjo H. and Leong E.C. (1999) *Instrumentation of an Unsaturated Residual Soil Slope*, Geotechnical Testing Journal, GTJODJ, Vol. 22, No. 2, pp. 128-137.

Gasmo J.M, Rahardjo H. & Leong E.C. (2000) *Infiltration Effects on Stability of a Residual Soil Slope,* Computers and Geotechnics, 26, pp.145-165.

Geo-Slope International Ltd. (1998a) *Seep/W for Finite Element Seepage Analysis (v.4)*, Users Manual. Calgary, Alberta, Canada.

Geo-Slope International Ltd. (1998b) *Slope/W for Slope Stability Analysis (v.4)*, Users Manual. Calgary, Alberta, Canada.

Grayhill Inc. (1995) *72-UMM-IL, System Configuration, Installation and Troubleshooting Manual*, La Grange, Illinois, U.S.A.

Green R.E and Corey J.C. (1971) *Calculation of Hydraulic Conductivity: a Further Evaluation of some Predictive Methods*, Soil Science Society of America Proceedings, Vol. 35, pp. 3-8.

Hillel D. (1982) *Introduction to Soil Physics*, Academic Press, Inc., New York

Hodge R. A. L. & Freeze A.R. (1977) *Groundwater Flow Systems and Slope Stability,* Canadian Geotechnical Journal, Vol. 14, pp. 466-476.

Hritzuk K.J. (1997) *Effectiveness of Drainage Systems in Maintaining Soil Suction,* MEng. Thesis, School of Civil and Structural Engineering, Nanyang Technological University, Singapore.

Huang S., Fredlund D.G. & Barbour, S.L. (1998) *Development and Verification of a Coefficient of Permeability Function for a Deformable Unsaturated Soil,* Canadian Geotechnical Journal, Vol. 35, No. 3, pp. 411-425.

Hubert M.K. (1940) *The Theory of Groundwater Motion,* Journal of Geology, Vol. 48, pp.785-944.

Jennings J.E.B. & Burland J.B. (1962) *Limitations to the Use of Effective Stresses in*

Partly Saturated Soils, Geotechnique, Vol. 12, pp. 125-144.

Kay J. N. & Chen, T. (1995) *Rainfall-landslide Relationship for Hong Kong,* Proceedings of Institution of Civil Engineers, Geotechnical Engineering, Vol. 119, pp. 242-243.

Khallili N. & Khabbaz M.H. (1998) *A unique Relationship for χ for the Determination of the Shear Strength of Unsaturated Soils,* Geotechnique, Vol. 48, pp. 681-688.

Krahn J., Fredlund D.G. & Klassen M.J. (1989) *Effect of Soil Suction on Slope Stability at Notch Hill,* Canadian Geotechnical Journal, Vol. 26, pp. 269-278.

Kunze R.J., Uehara G., & Graham K. (1968) *Factors Important in the Calculation of Hydraulic Conductivity*, Proceedings of Soil Science Society of America Proceedings, Vol. 32, pp.760-765.

Leach B. & Herbert R. (1982) *The Genesis of a Numerical Model for the Study of the Hydrogeology of a Steep Hillside in Hong Kong,* Quarterly Journal of Engineering Geology, Vol. 15, pp. 243-259.

Lee D.T.T., Rahardjo H. and Leong E.C. (1999) *Simulation and Natural Runoff Measurement on Residual Hillslopes*, Proceedings of the Fifth International Symposium on Field Measurements in Geomechanics, Singapore, December 1-3, pp. 387-391.

Leong E. C. & Rahardjo H. (1997a) *Review of Soil-Water Characteristic Curve Equations,* Journal of Geotechnical and Geoenvironmental Engineering, Vol. 123, No. 12, pp. 1106-1117.

Leong E. C. & Rahardjo H. (1997b) *Permeability Functions for Unsaturated Soils,* Journal of Geotechnical and Geoenvironmental Engineering, Vol. 123, No. 12, pp. 1118-1126.

Lim T. T., Rahardjo H., Chang M.F. & Fredlund D.G. (1996) *Effect of Rainfall on Matric Suctions in a Residual Soil Slope*, Canadian Geotechnical Journal, Vol. 33, pp. 618-628.

Little A.L. (1969) *The Engineering Classification of Residual Tropical Soil,* Proceedings of the 7th International Conference on Soil Mechanics and

Foundation Engineering, Specialty Session on Engineering Properties of Lateritic Soils, Mexico, 1969, Vol. 1, pp. 1-10.

Low T.H., Faisal H.A. & Saravanan M. (2000) *Suction and Infiltration Measurements on Cut Slope in Highly Heterogeneous Residual Soil,* Proceedings of the Asian Conference on Unsaturated Soils, UNSAT-ASIA 2000, Singapore, pp.807-811.

Luckner L.M., van Genuchten M.Th. and Nielsen D.R. (1989) *A Consistent Set of Parametric Models for the Two-phase Flow of Immiscible Fluids in the Subsurface,* Water Resources Research, Vol. 25, pp. 2187-2193.

Lumb P. (1965) *The Residual Soils of Hong Kong,* Geotechnique, Vol. 15, pp. 180-194.

Lumb P. (1975). *Slope Failures in Hong Kong,* Quarterly Journal of Engineering Geology, Vol. 8, pp. 31-65.

Macari E J, Laymon C A and Costes N C (1992) *Hydrologic Field Instrumentation for a Small-Scale Experiment with Implication for Rain-Induced Slope Stability Analysis,* US Brazil NSF Geotechnical Workshop on Applicability of Classical Soil Mechanics Properties to Structured Soils, pp 79-88

Marshall T.J. (1958) *A Relation Between Permeability and Size Distribution of Pores,* Soil Science of America Journal, Vol. 9, pp. 1-8.

Mualem Y. (1986) *Hydraulic Conductivity of Unsaturated Soils: Prediction and Formulas,* In Methods of Soil Analysis, edited by Klute A., American Society of Agronomy, Madison, Wisconsin, Part 1, No. 9, pp. 799-823.

Millington R.J. & Quirk J.P. (1961) *Permeability of Porous Solids*, Transaction of the Faraday Society, Vol. 57, pp. 1200-1207.

McDonell J.J. (1990) *The Influence of Macropores on Debris Flow Initiation,* Quarterly Journal of Engineering Geology, Vol. 13, pp. 325-331.

McDougall J.R. & Pyrah I.C. (1998) *Simulating Transient Infiltration in Unsaturated Soils*, Canadian Geotechnical Journal, Vol. 35, pp. 1093-1100.

Neuman (1973) *Saturated-Unsaturated Seepage by Finite Elements,* ASCE Journal of the Hydraulics Division, Vol. 99, pp. 2233-2250.

Ng C. W. W. & Shi Q. (1998a) *Influence of Rainfall Intensity and Duration on Slope Stability in Unsaturated Soils*, Quarterly Journal of Engineering Geology, Vol. 31, pp. 105-113.

Ng C. W. W., & Shi Q. (1998b) *A Numerical Investigation of the Stability of Unsaturated Soil Slopes Subjected to Transient Seepage,* Computers and Geotechnics, Vol. 22, No. 1, pp. 1-28.

Overton D.E. & Meadows M.E. (1976) *Stormwater Modelling,* Academic Press Ltd, New York, USA, p. 358.

Penman H.L. (1963) *Vegetation and Hydrology,* Commonwealth Agricultural Bureaux, Technical Communication No.53, Farnham Royal, 124 p.

Philip J.R. (1986) *Linearized Unsteady Multidimensional Infiltration,* Water Resources Research, Vol. 22, pp. 1717-1727.

Pitts J. (1984) *A Review of Geology and Engineering Geology in Singapore*, Quarterly Journal of Engineering Geology, Vol. 17, pp. 93-101.

Pitts J. (1985) *An Investigation of Slope Stability on the NTI Campus, Singapore*, Applied Research project RPI/83, Nanyang Technological Institute, Singapore.

Pradel D. & Raad G. (1993) *Effect of Permeability on Surficial Stability of Homogenous Slopes,* Journal of Geotechnical Engineering, ASCE, Vol. 119, No. 2, pp. 315-332.

Premchitt J., Lam T.S.K., Shen J.M. & Lam H.F. (1986) *Rainstorm Runoff on Slopes*, GEO Report No. 12, Geotechnical Engineering Office, Civil Engineering Department, Hong Kong.

Premchitt J., Brand E.W. & Chen P.Y.M. (1994) *Rain-Induced Landslides in Hong Kong, 1972-1992,* Asia Engineer, Journal of Hong Kong Institution of Engineers, June, 43-51.

Public Works Department, Singapore (1976) *Geology of the Republic of Singapore*, Public Works Department, Singapore, p. 79.

Rahardjo, H. 2000. *Rainfall-Induced Slope Failures*, NSTB 17/6/16 Research Report, School of Civil and Structural Engineering, Nanyang Technological University.

Rahardjo H., Leong E.C., Gasmo J.M. & Tang S.K. (1998) *Assessment of Rainfall Effects on Stability of Residual Soil Slopes.* Proceedings of 2nd International Conference on Unsaturated Soils, Beijing, P.R. China 1998, Vol. 1, pp. 280-285.

Rahardjo H., Leong E.C, Deutcher M.S., Gasmo J.M. & Tang S.K. (2000) *Rainfall-Induced Slope Failures*, Geotechnical Engineering Monograph 3, NTU-PWD Geotechnical Research Centre, Nanyang Technological University Singapore, ISBN 981-04-2928-2, p.86.

Rahardjo H., Li X.W., Toll D.G. & Leong E.C. (2001) *The Effect of Antecedent Rainfall on Slope Stability*, Geotechnical and Geological Engineering, Vol. 19, pp. 369-399.

Rahardjo H., Lim T.T., Chang M.F. & Fredlund D.G (1995) *Shear-Strength Characteristics of a Residual Soil,* Canadian Geotechnical Journal, Vol. 32, pp. 60-77.

Rao A.N. & Wee Y.C. (1987) *Singapore Trees,* Singapore Institute of Biology, Jin Jin Printing Industry, Singapore, pp. 287-288.

Reynolds W.D. & Elrick D.E. (1986) *A Method of Simultaneous In-Situ Measurement in the Vadose Zone of Field-Saturated Hydraulic Conductivity, Sorptivity, and the Conductivity-Pressure Head Relationship,* Groundwater Monitoring Review, Vol. 6, pp. 84-95.

Richards L.A. (1931) *Capillary Conduction of Liquids through Porous Medium,* Journal of Physics, No. 1, pp. 318-333.

Rulon J.J., & Freeze R.A. (1985) *Multiple Seepage on Layered Slopes and their Implication for Slope-Stability Analysis,* Canadian Geotechnical Journal, Vol. 22, pp. 347-356.

Soilmoisture™ Equipment Corp. (1997) *Model 2725A Jet Fill Tensiometer Operating Instructions*, Santa Barbara, California, U.S.A.

Spierenburg S.E.J., van Esch J.M. & Koehorst B.A.N. (1995) *Slope Stability during Infiltration,* Proceedings of the 1st International Conference on Unsaturated Soils. UNSAT 95, Paris, pp. 309-314.

Toll D. G. (1990) *A Framework for Unsaturated Soil Behaviour,* Geotechnique Vol. 40, No. 1, pp. 31-44.

Toll D.G. (2001) *Rainfall-Induced Landslides in Singapore,* Geotechnical Engineering (in press).

Townsend F. C. (1985) *Geotechnical Characteristics of Residual Soils,* Journal of Geotechnical Engineering, ASCE, Vol. 111, No. 1, pp. 77-94.

UNIDATA (1990) *Starlog Capacitive Water Depth Probe, Model 6521, User Manual* Supplement, Revision C, U.S.A.

van Genuchten M. Th. (1980) *A Closed-Form Equation for Predicting the Hydraulic Conductivity of Unsaturated Soils,* Soil Science Society of America Journal, Vol. 44, pp. 892-898.

van Genuchten M. Th., Leij F.J. & Yates S.R. (1991) *The RETC Code for Quantifying the Hydraulic Functions of Unsaturated Soils,* Robert S. Kerr Environmental Research Laboratory, US Environmental Protection Agency, USA.

Vargas Jr. E.A., Velloso R.C., de Campos T.M.P. & Filho L.M.C. (1990) *Saturated – Unsaturated Analysis of Water Flow in Slopes of Rio De Janeiro, Brazil,* Computers and Geotechnics, Vol. 10, pp. 247-261.

Vaughan P.R. (1985) *Pore Pressures due to Infiltration into Partly Saturated Slopes,* Proceedings of the 1st International Conference on Tropical, Lateritic and Saprolitic Soils, Brasilia, 1985, Vol. 2, pp. 61-71.

Wang H.F. & Anderson M.P. (1982) *Introduction to Groundwater modelling,* Academic Press Ltd, London, UK, ISBN: 0-12-734585-X, p. 237

Wei J., Heng Y.S., Chow W.C. & Chong M.K. (1991) *Landslide at Bukit Batok Sports Complex,* Proceedings of the 9th Asian Regional Geotechnical Conference, Singapore 1991.

Wesley L.D. (1988) *Engineering Classification of Residual Soils,* Proceedings of the second International Conference on Geomechanics in Tropical Soils, Singapore 12-14 December 1988, Vol. 1, pp. 77-84.

Wesley L.D. (1990) *Influence of Structure and Composition on Residual Soils,* Journal of Geotechnical Engineering, ASCE, Vol. 116, No.4, pp. 589-602.

Wheeler S.J & Sivakumar V. (1995) *An Elasto-plastic Critical State Framework for Unsaturated Soils,* Geotechnique, Vol. 45, pp. 35-53.

Wilson G.W., Barbour S.L. & Fredlund D.G. (1995) *The Prediction of Evaporative Fluxes from Unsaturated Surfaces,* Proceedings of the 1st International Conference on Unsaturated Soils. UNSAT 95, Paris, pp. 423-429.

Wolle C. M. & Hachichi, W. (1989) *Rain-Induced Landslides in Southeastern Brazil,* Proceedings of the 12th International. Conf. on Soil Mechanics and Foundation Engineering, Rio de Janeiro, pp. 1639-1642.